

Dispersive Source Models in Wireless Communications Subscriber Location

**Doctoral Thesis
Written by
René Játiva Espinoza
Directed by
Josep Vidal Manzano
November 2016**

**Department of Signal Theory and Communications
Universitat Politècnica de Catalunya
Barcelona-Spain**

Deo omnis gloria!

To my wife Veronica ... her permanent support has facilitated the culmination of this work. To my children who have forgiven me for taking several hours of my attention. To my parents that taught me the value of dedication and perseverance. To all who want to know a little more about mobile communications from the point of view of statistical signal processing.

Milior est finis quam principium

Acknowledgments

I would like to thank all the people who assisted me along the program with their advice, guide and the good example of an exigent and good performed work. Thanks to all of you, Toni, Gregori and Xavier for your worthy attention during my first steps within the vast fields of communications signal processing. I am especially indebted to you, Josep for you direction along these years. This task is over!

Abstract

Mobile subscriber positioning is an issue in permanent revision due to the new possibilities of relation that the knowledge of the position introduces, among users and an increasing number of devices. Being this a relevant problem, it is frequently boarded under diverse perspectives and contexts. This thesis studies it in the context of wireless communications and from the perspective of the statistical signal processing. This research provides a quite complete description of this task both from the theoretical viewpoint and through intensive simulations, by using stochastic models than conceive signal as a dispersive source characterized for their spatial and temporal probability density functions. These models are justified from experimental measurements and they are very suited for studying the problem of positioning, not just because they reduce the mathematical complexity and use a fewer number of parameters, but also because these parameters are in fact those required for these positioning techniques.

Signal is studied in the framework of Direct Sequence – Spread Spectrum (DS – SS), but once that channel estimation has been performed, the subsequent processes are quite general and could be applied with other infrastructures. This document introduces the positioning technologies, and discusses the problems and possible solutions appearing when these schemes are applied to wireless communications systems, and also some mechanisms for the evaluation of the positioning accuracy. Furthermore, it particularly studies the degradation associated with the Non Line Of Sight (NLOS) condition between the transmitter and the receiver, and possible mechanisms for its mitigation. In order to achieve realistic simulation scenarios, the Greenstein's gain-delay propagation model has been used, and a simulation platform to evaluate positioning accuracy has been developed. Furthermore, the use of some important statistics to perform NLOS mitigation on timing – based positioning algorithms have been proposed. As a result of the derivation of these statistics from the Greenstein's model, it was concluded that the quality of the timing measures decays more strongly with the link distances between transmitter and receiver than the suggested when the propagation model has not been taken account. Therefore, the proper weightings have been provided. Moreover, the weighted linear least squares algorithm has been revisited and a new two-stage solution that includes geometrical restrictions has been proposed and successfully implemented.

Since the signal in a wireless channel is affected by scattering, the use of dispersive models for the theoretical study of these signals in the context of the positioning problem is justified. Therefore the use of Cramer-Rao bounds derived from these models is proposed to extract pondered conclusions about the quality of timing estimates. This research includes a detailed description of Cramer-Rao Bounds derivation for Time of Arrival estimation for both Rice and Rayleigh propagation. Particularly, to the best of our knowledge, it is in fact the most complete model of its kind in the literature, since it incorporates a way to take into account spatial and temporal correlation among channel estimates, the impact of the roll-off factor, the number of sensors and the number of channel estimates, and also because it assumes an

exponential dispersion from delays, which it is characteristic of mobile channels, instead of two or three paths, typical in literature. Moreover, this information model that provides the lower limits of the error variance in the estimation of the first arrival has been integrated to the simulation platform providing a useful approach to evaluate both qualitative and quantitative the benefits of using space-time diversity in terms of the positioning accuracy.

Finally, this thesis proposes a two-stage procedure to acquire the required improved timing estimates for enhancing the positioning accuracy of the wireless mobile subscribers. Therefore, signal is discriminated from noise at the first stage using a Generalized Likelihood Ratio Test (GLRT) derived from notions of the Statistical Theory of Decision. Signal detectability is evaluated using a novel model developed to put in evidence the optimum operation point from the viewpoint of the quality of the timing detection. This model has been used to evaluate different configurations of the proposed GLRT, but it can be used to evaluate other detectors once provided their receiver operating characteristics. Moreover, a high resolution timing estimation has been proposed for the second stage to reduce timing uncertainty from a chip time at the first stage to a small fraction of this value. From the two candidates methods proposed to be part of this second stage, this research has shown that the NMV approach is suitable to perform this task. Eventually, the operational results from this two-stage detection-estimation approach have been incorporated to the simulation platform to assess their application to the subscriber positioning problem in realistic conditions. The final results show the benefits of using this two-stage procedure, as well as the advantage of counting with space-time diversity in the solution of the positioning problem. Furthermore, they show as subscriber location may be performed with a high degree of accuracy from network-based architectures.

Resumen

El posicionamiento de abonado móvil es un tópico en permanente revisión debido a las nuevas posibilidades de relación que el conocimiento de la posición introduce entre usuarios y un creciente número de dispositivos. Siendo éste un problema relevante, se aborda con frecuencia bajo diversas perspectivas y contextos. Esta tesis lo estudia en el contexto de comunicaciones inalámbricas y desde la perspectiva del procesamiento estadístico de la señal. Esta investigación provee una descripción bastante completa de esta tarea tanto desde el punto de vista teórico como a través de simulaciones intensivas, usando modelos estocásticos que conciben la señal como una fuente dispersiva caracterizada por sus funciones de densidad de probabilidad en los dominios de espacio y tiempo. Estos modelos se justifican de mediciones experimentales y son muy adecuados para el estudio del problema de posicionamiento, no sólo porque reducen la complejidad matemática y usan un número más pequeño de parámetros, sino también porque estos parámetros en efecto son los requeridos por estas técnicas de posicionamiento.

La señal se estudia en el marco de trabajo del Espectro Disperso de Secuencia Directa, pero una vez que la estimación de canal se ha realizado, los procesos subsiguientes son bastante generales y podrían aplicarse con otras infraestructuras. Este documento presenta las tecnologías de posicionamiento, y discute los problemas y posibles soluciones que aparecen cuando estos esquemas se aplican a sistemas de comunicaciones inalámbricas, así como también algunos mecanismos para la evaluación de la precisión del posicionamiento. Adicionalmente, estudia particularmente la degradación asociada con la condición de ausencia de línea de visión entre el transmisor y receptor, y los posibles mecanismos para su mitigación. Con el objeto de conseguir escenarios de simulación realistas, se ha usado el modelo de propagación de ganancia-retardo de Greenstein, y se ha desarrollado una plataforma de simulación para evaluar la precisión del posicionamiento. Aún más, se ha propuesto el uso de algunos estadísticos importantes para conseguir la mitigación de la condición de ausencia de visión usando algoritmos de posicionamiento basados en la temporización. Como resultado de la derivación de estas estadísticas a partir del modelo de Greenstein, se ha concluido que la calidad de las medidas de temporización decae más fuertemente con las distancias de los enlaces entre transmisor y receptor que la sugerida cuando el modelo de propagación no se ha tomado en cuenta. Consecuentemente, se han proporcionado las ponderaciones adecuadas. Adicionalmente, el algoritmo de mínimos cuadrados lineales ponderados se ha revisado y una nueva solución de dos pasos que incluye restricciones geométricas se ha propuesto e implementado.

Puesto que la señal en un canal inalámbrico está afectada por dispersión, se justifica el uso de modelos dispersivos para el estudio teórico de estas señales en el contexto del problema de posicionamiento. Por consiguiente, se propone el uso de cotas de Cramer-Rao derivadas a partir de estos modelos para extraer conclusiones ponderadas al respecto de la calidad de las estimaciones de temporización. Esta investigación incluye una descripción detallada de la derivación de las cotas de Cramer-

Rao en la estimación del Tiempo de Arribo tanto para propagación Rice como propagación Rayleigh. Particularmente, y hasta donde conocemos, éste es en efecto el modelo más completo de su clase en la literatura, puesto que incorpora una forma de tomar en cuenta la correlación espacial y temporal entre las estimaciones de canal, el impacto del factor de roll-off, el número de sensores y el número de estimaciones de canal, y también porque asume una dispersión exponencial de retardos, la cual es característica de los canales móviles, en lugar de dos o tres trayectos, típico en la literatura. Más aún, este modelo de información que provee los límites inferiores de la varianza del error en la estimación del primer retardo se ha integrado a la plataforma de simulación proveyendo un enfoque útil para evaluar tanto cualitativamente como cuantitativamente los beneficios del uso de la diversidad espacio-temporal en términos de la precisión del posicionamiento.

Finalmente, esta tesis propone un procedimiento de dos etapas para adquirir las estimaciones mejoradas de temporización y enriquecer de esta forma la precisión del posicionamiento de los abonados móviles inalámbricos. Por consiguiente, la señal es discriminada del ruido en la primera etapa usando una prueba del cociente de máxima verosimilitud (GLRT de sus siglas en inglés) derivada de nociones de la Teoría Estadística de la Decisión. La capacidad de detección de la señal se evalúa usando un nuevo modelo desarrollado para poner en evidencia el punto de operación óptimo desde el punto de vista de la calidad de la detección de la temporización. Este modelo se ha usado para evaluar diferentes configuraciones del detector GLRT propuesto, pero puede usarse en la evaluación de otros detectores siempre y cuando se proporcionen sus características de operación de recepción. Adicionalmente, se ha propuesto para la segunda etapa una estimación de temporización de alta resolución para reducir la incertidumbre en la temporización desde un tiempo de chip en la primera etapa hasta una pequeña fracción de este valor. De los dos métodos candidatos propuestos para ser parte de esta segunda etapa, esta investigación ha mostrado que el enfoque de Mínima Varianza Normalizado (NMV de sus siglas en inglés) es adecuado para llevar a cabo esta tarea. Finalmente, los resultados operacionales de este enfoque de dos etapas de detección-estimación se han incorporado a la plataforma de simulación para evaluar su aplicación al problema de posicionamiento de abonado en condiciones realistas. Los resultados finales muestran los beneficios de usar este procedimiento de dos etapas, así como también las ventajas de contar con diversidad espacio-temporal en la solución del problema de posicionamiento. Más aún, éstos muestran que la localización de abonado puede realizarse con un alto grado de precisión a partir de arquitecturas basadas en red.

Table of Contents

Acronyms	I
Chapter 1	1
Introduction	1
1.1 Mobile Communication Systems and Services	1
1.1.1 Mobile Location Services	2
1.1.2 Classification of Mobile Location Services	4
1.1.3 Importance of Positioning Systems	8
1.2 Location Service Standards	9
1.3 Positioning Systems and the Emergency Service	17
1.3.1 Classification	18
1.3.2 The Positioning Systems and the Emergency Service	18
1.4 Research Objectives	22
1.5 Thesis Structure and main contributions	23
1.6 List of Publications	26
1.7 References	28
Chapter 2	31
Wireless Communications Signals and Positioning Technologies	31
2.1 Communications Signals and the Wireless Channel	31
2.1.1 Some Relevant Functions and Parameters in Wireless Channels	32
2.1.2 Channel Models	37
2.1.3 Fundamentals of Wideband Code Division Multiple Access (WCDMA)	42
2.2 Positioning Technologies: A Subscriber Location Overview	45
2.2.1 Positioning Principles	47
2.2.2 Positioning Accuracy	57
2.2.3 Positioning Technologies and 3G Mobile Communication Systems	59
2.2.4 The NLOS issue and its mitigation	61
2.3 Simulations and Results	70
2.3.1 Simulation platform for assessing positioning	70
2.3.2 Experiments and results	71
2.4 Summary and Discussion	84
2.5 Annex A2.1 A Linear Least Squares Received Signal Strength (LLS-RSS) based Positioning Algorithm	87
2.6 Annex A2.2 Derivation of the first two moments for the RMS Delay Spread defined as the Greenstein Model	88
2.7 Annex A2.3 Derivation of the first two moments for TDOA measures for environments described by the Greenstein model	89
2.8 Annex A2.4 Signals required for Greenstein Model	91
2.9 References	92
Chapter 3	98
Dispersive Source Models and Cramer-Rao Bounds	98
3.1 Why to use a Dispersive Source Model	99
3.1.1 Overview of Direction Of Arrival Estimation	100
3.1.2 Overview of Time Of Arrival Estimation	101
3.1.3 Overview of Joint Estimation of Time Delays and Direction of Arrival	102

3.1.4	Dispersive Source Models and Direction of Arrival Estimation	102
3.2	Dispersive Source Models and Cramer-Rao Bounds	103
3.2.1	Considerations in the Propagation channel model	105
3.2.2	Coherence Time and Delay Dispersion	107
3.2.3	Channel Model	109
3.2.4	Computing the Cramer Rao Bounds for Delay Estimates	114
3.2.5	Model for angular dispersion	122
3.3	Simulations and Results	124
3.3.1	Performance of Asymptotic Expressions	124
3.3.2	Performance of CRBs for timing and normalized coherence bandwidth for the NLOS Rayleigh fading model	126
3.3.3	Performance of CRBs for timing and normalized coherence bandwidth for the LOS Rice fading model	136
3.3.4	Positioning Accuracy for Location Determination Technologies	141
3.4	NLOS Condition and Positioning	145
3.5	Summary and Conclusions	146
3.6	Recommendations	149
3.7	References	151
Chapter 4		159
Timing and Direction of Arrival Estimation		159
4.1	Timing detection and estimation scheme	160
4.2	Assessing positioning performance bounds using CRB with antenna arrays	161
4.2.1	Antenna Arrays and Quality of the First Arrival Estimation	162
4.2.2	Simulations for Subscriber Positioning based on TDOA	165
4.3	Discriminating Signal from Noise: The Detection Problem	174
4.3.1	Statistical Fundamentals	175
4.3.2	Composite Hypothesis Testing	177
4.3.3	The Generalized Likelihood Ratio Test (GLRT)	178
4.3.3.1	Channel model	178
4.3.3.2	Deriving an Unstructured GLRT Detector	179
4.3.3.3	False alarm and detection probabilities	182
4.3.3.4	A simplified model for detectability in a coarse timing estimator	188
4.3.3.5	Summary and Conclusions	194
4.4	High Resolution Timing and Direction of Arrival Estimation	195
4.4.1	Performing High Resolution Timing Estimation	195
4.4.1.1	Minimum variance timing estimation	196
4.4.1.2	Normalized minimum variance estimation (NMV)	197
4.4.1.3	Use of antenna arrays for enhanced timing estimation	199
4.4.1.4	Reduction of source coherence	199
4.4.1.5	Spatial Filtering	200
4.4.1.6	Timing estimation results using MV approaches	201
4.4.2	Performing High Resolution AOA Estimation	209
4.4.2.1	Normalized Minimum Variance AOA Estimation	209
4.4.2.2	Simulations and Results for AOA Estimation using the NMV Approach	211
4.4.3	Summary and Conclusions	218

4.5	Positioning Accuracy when using a two stage detection and estimation approach	219
4.5.1	General Conclusions	222
4.6	Annex 4.1 Proportion of cases where the error variance as predicted by CRB is higher than a predefined threshold.	224
4.7	Annex 4.2 A basic approach to false alarm and detection probability at the GLRT detector	228
4.8	Annex 4.3: Characterization of the MV and NMV timing estimates	231
4.9	References	235
	Conclusions, Recommendations and Future Research Topics	239
	Conclusions	239
	Recommendations and Future Research Topics	244
Appendix	Published papers	247
	NLOS Mitigation Based on TOA for Mobile Subscriber Positioning Systems by Weighting Measures and Geometrical Restrictions	247
	Cramer Rao Bounds in Time Of Arrival Estimation for a Distributed Source	255
	Positioning accuracy when tracking UMTS mobile in delay and angular dispersive channels	266
	Estimación del Tiempo de Llegada en un canal Rayleigh desde una perspectiva de la Cota Inferior de Cramer-Rao	272
	Cota Inferior de Crámer-Rao en la Estimación del Tiempo de Llegada en un Canal Rice	279
	GLRT detector for NLOS error reduction in wireless positioning systems	289
	First Arrival Detection for Positioning in Mobile Channels	295
	First Arriving Path Detection for Subscriber Location in Mobile Communication Systems	302
	Coarse First Arriving Path Detection for Subscriber Location in Mobile Communication Systems	307
	High resolution time-of-arrival detection for wireless positioning systems	313
	Space-Time Diversity for NLOS Mitigation in TDOA-Based Positioning Systems	320
	Selection of the reference anchor node by using SNR in TDOA-based positioning	327
	Fast Computation of Cramer-Rao Bounds for TOA – An application to network-based positioning simulations	333

Acronyms

2G Second Generation of Mobile Systems

3G Third Generation of Mobile Systems

3GPP Third Generation Partnership Project

3GPP2 Third Generation Partnership Project 2

4G Fourth Generation of Mobile Systems

A

ADT Abstract Data Types

ALI Automatic Caller Identifier

AMPOA AMPLitude Of Arrival

ANSI American National Standards Institute

AOA Angle Of Arrival

AP Access Point

API Application Programming Interface

APP Angular Power Profile

AR Augmented Reality

ARIB Association of Radio Industries and Businesses

ARML Augmented Reality Markup Language

ATCK Angular-Temporal Correlation Kernel

ATIS Alliance for Telecommunications Industry Solutions

A-SCM Analytical SCM

B

BB Barakin Bound

BLUE Best Linear Unbiased Estimator

BS Base Station

BU Bad Urban

C

CAGR Compound Annual Growth Rate

CCD Charge-Couple Device

CCSA China Communications Standards Association

CDMA Code Division Multiple Access

CEP Circular Error Probability

CFAR Constant False Alarm Rate

CID Cell Identifier

CLOP Circular Line Of Position

CN Core Network

CODIT Code Division Testbed

COMET Covariance Matching Estimators

COMPASS

COST-259 DCM COST-259 Directional Channel Model

CyberGIS GIS based on cyber infrastructure

D

DCH Dedicated Channel

DFE Decision Feedback Equalizer

DL-OTDOA Down Link OTDOA

DML Determined Maximum Likelihood

DOA Direction Of Arrival

DOP Dilution of Precision

DPCH Dedicated Physical Channel

DPS Doppler Power Spectrum

DRS Dead Reckoning Systems

DSP Doppler Spread Profile

DS/SS Direct Sequence Spread Spectrum

E

E911 Enhances 911

E-CID Enhanced CID

EGNOS European Geostationary Navigation Overlay Service

EKF Enhanced Kalman Filter

EM Expectation Maximization algorithm

E-OTD Enhanced OTD

ESPRIT Estimation of Signal Parameters by Rotational Invariance Techniques

ETSI European Telecommunications Standards Institute

E-UTRA Evolved UMTS Terrestrial Radio Access

EXIP

F

FACH Forward Access Channel

FCC Federal Communications Commission

FCD Fully Coherently Distributed

FIM Fisher Information Matrix

G

GAA Gaussian Angle of Arrival

GAGAN GPS Aided Geo Augmented Navigation

GALE Geometry-Assisted Location Estimation

GBSB Geometrically Based Single-Bounce Statistical Channels

GBCMCM Geometrically Based Single-Bounce Statistical Circular Model

GBCMEM Geometrically Based Single-Bounce Statistical Elliptical Model

GERAN GSM EDGE Radio Access Network

GDOP Geometric Dilution of Precision

GIS Geographic Information System

GLONASS GLObal'naya Navigatsionnay Sputnikovaya Sistema

GLR Generalized Likelihood Ratio

GLRT Generalized Likelihood Ratio Test

GML Gaussian Maximum Likelihood

GML Geography Markup Language

GMLC Gateway Mobile Location Center

GNSS Global Navigation Satellite Systems

GPS Global Positioning System

GTU Generalized Typical Urban

GWSSUS Gaussian Wide Sense Stationary Uncorrelated Scattering

H

HBR High Bit Rate

HLOP Hybrid Line Of Position

HSDPA High Speed Downlink Packet Access

HSPA High Speed Packet Access

HSPA+ Evolved HSPA

HSUPA High Speed Uplink Packet Access

HVAC Heating, Ventilation and Air Conditioning

I

ICD InCoherently Distributed

IETF Internet Engineering Task Force

IMEI International Mobile Equipment Identity

IMSI International Mobile Subscriber Identity

IMT2000 International Mobile Telecommunications 2000

INS Inertial Navigation Systems

IPDL Idle Period in Down Link

IQML Iterative Quadratic Maximum Likelihood algorithm

ISDN Integrated Services Digital Network

ITU International Telecommunication Union

K

KF Kalman Filter

KML Keyhole Markup Language

L

LBS Location Based Services

LBSN Location Based Social Networks

LCAF Location Client Authorization Function

LCCF Location Client Control Function

LCCTF Location Client Coordinate Transformation Function

LCS Location Services

LCZTF Location Client Zone Transformation Function

LDT Location Determination Technologies

LIF Location Interoperability Forum

LLOP Linear Line Of Position

LLS Linear LS

LS Least Squares

LSAF Location Subscriber Authorization Function

LSBF Location System Billing Function

LSCF Location System Control Function

LSML Least Squares Maximum Likelihood

LSOF Location System Operation Function

LSPF Location Subscriber Privacy Function

LTE Long Term Evolution

M

MAP Maximum A Posteriori

MCRB Modified CRB

METRA Multi-Element Transmit and Receive Antenna

MIMO Multiple Input Multiple Output

ML Maximum Likelihood

MLM Maximum Likelihood Methods

MLP Mobile Location Protocol

MLS Mobile Location Server

MLSE Maximum Likelihood Sequence Estimator

MMAE Minimum Mean Absolute Error

MMSE Minimum Mean Square Error

MS Mobile Station

MSAS Multi-functional Satellite Augmentation System

MSE Minimum Square Error

MSISDN Mobile Station ISDN

MODE Method Of Direction Estimation

MPC Multi-Path Component

MVU Minimum Variance Unbiased

MUSIC Multiple Signal Classification

MZZB Modified ZZB

N

NA-ESRK North America Emergency Services Routing Key

NAVSTAR NAVigation System Timing And Ranging

NENA National Emergency Number Association

NLOS Non Line Of Sight

NLS Nonlinear Least Squares

NOLA Non Overlapping Assumption

O

OFDM Orthogonal Frequency Division Multiplexing

OFDMA Orthogonal Frequency Division Multiplexing Access

OGC Open Geospatial Consortium

OGC KML OGC Keyhole Markup Language

OMA Open Mobile Alliance

OpenLS OGC Open Location Service

OTD Observed Time Difference

OTDOA Observed Time Difference Of Arrival

P

PADS Power Angular Delay Spectrum

PAS Power Angular Spectrum

PCD Partially Coherently Distributed

PCF Position Computing Function

PCH Physical Channel

PDA Personal Digital Assistant

PDDP Power Delay-Direction Profile

PDF Probability Density Function

PDOP Positional Dilution of Precision

PDP Power Delay Profile

PDS Power Delay Spectrum

PF Particle Filter

PLMN Public Land Mobile Networks

PRCF Positioning Radio Control Function

PRRM Positioning Radio Resource Management

PSAP Public Safety Answering Point

PSMF Positioning Signal Measurement Function

PUB/SUB Publish/Subscribe

Q

QZSS Quasi-Zenith Satellite System

R

RFID Radio Frequency Identification

RMS Root Mean Square

RMSE Root Mean Square Error

RMSPE Root Mean Square Position Error

RNSS Regional Navigation Satellite Systems

RSA Range Scaling Algorithm

RSRP Reference Symbol Received Power

RSS Received Signal Strength

RSSI RSS Indicator

RTT Round Trip Time

S

SATURN Smart Antennas UMTS Radio Networks

SBAS Satellite Based Augmentation systems

SCM Spatial Channel Model

SCP Service Control Point

SDP Service Data Point

SINR Signal to Interference Noise Ratio

SIP Session Initiation Protocol

SML Stochastic Maximum Likelihood

SNR Signal to Noise Ratio

SGML Stochastic Gaussian Maximum Likelihood

SS Signal Strength

SVG Scalar Vector Graphics

T

TA Timing Advance

TDOA Time Differences Of Arrival

TDOP Time Dilution Of Precision

TOA Time Of Arrival

TTA Telecommunications Technology Association

TTC Telecommunication Technology Committee

TU Typical Urban

U

UE User equipment

UKF Unscented Kalman Filter

ULA Uniform Linear Array

UMTS Universal Mobile Telecommunications System

URA UTRAN Registration Area

URL Uniform Resource Locator

UTM Universal Transverse Mercator

UTRAN UMTS Terrestrial Radio Access Network

U-TDOA Uplink TDOA

UWB Ultra Wide Band

UWCC Universal Wireless Communications Consortium

V

VGI Volunteered Geographic Information

W

W3C World Wide Web Consortium

WAAS Wide Area Augmentation System

WCDMA Wideband Code Division Multiple Access

WiFi Wireless Fidelity

WiMAX Worldwide Interoperability for Microwave Access

WLAN Wireless Local Area Network

WLLS Weighted Linear Least Squares

WMS Web Map Services

WNLS Weighted Nonlinear Least Squares

WSF Weighted Subspace Fitting

Z

ZZB Ziv Zakai Bound

Chapter 1

Introduction

Positioning of a mobile subscriber is a complex task with the capability of adding value to services and applications. It is undeniable that the knowledge of the position of a certain device is important, but the applications and services provisioned from the awareness of that position will probably be more useful from the perspective of the user, and consequently more impacting to our society. Therefore, it is relevant in a research work, relative to mobile subscriber positioning for wireless communications, to locate our issue and its research viewpoint in a wider framework. It will help the reader to understand its importance within the positioning systems and its relation to Location-Based Services (LBS).

Under this premise, the importance and development of Location-Based Services and their interrelation with mobile communications systems will be treated in the following sections. Further, in order to easily read and follow the topics boarded along this document, the objectives of this research will be outlined and the thesis structure will be summarized, in the last section of this chapter.

1.1 Mobile Communication Systems and Services

The mobile communication systems have experienced a great growth in the last decades, and it is not unusual nowadays that mobile penetration may be even higher than 100% [1][2]. The development of new technologies, the implementation of politics of aggressive introduction, and the possibility of a permanent communication with independence of user location, have enabled this fast evolution. Furthermore, the upcoming of new services of public and private interest seems to provide this sector with its peculiar dynamism, and for sure, LBS are a very important part of this dynamism [17]-[21], not just because LBS are hungry of more resources from network devices but also because they take advantage of the virtuosities of new communication technologies to construct new possibilities of relation among users, between users and service providers, and also between providers and third parties such as contents' providers.

Nowadays, the third generation (3G) of mobile communications systems is part of the daily lives of millions of people not just in the first world countries but also in developing countries. Their specifications were covered under the name proposed by the International Telecommunication Union (ITU) of International Mobile Telecommunications 2000 (IMT2000), and it included the work of several organisms such as the Third Generation Partnership Project (3GPP), the Third Generation Partnership Project 2 (3GPP2), the Universal Wireless Communications Consortium (UWCC) and the European Telecommunications Standards Institute (ETSI) [3]-[11].

Among these groups of specifications, those related to the Terrestrial Interface gained a special interest due to the possibility of interacting with a larger number of end users. Moreover, the incorporation of Code Division Multiple Access (CDMA), as part of these specifications, was favored by the steady state of the art of the technology, and the possibility to use advanced techniques of transmission and reception such as turbo-codes, multi-user detection and adaptive antennas. All these characteristics contributed to dole 3G with higher data rates. IMT-2000 which employs Wideband Code Division Multiple Access (W-CDMA), achieves a transmission rate of 2 Mbit/s with 5 MHz frequency bandwidth, and with the addition of High Speed Packet Data (HSPA) transmission features, current 3G speeds are topped out at 14Mbps downlink and 5.8Mbps uplink [12][14]. Besides these important characteristics, 3G also includes a wider range of positioning technologies with a higher accuracy than those associated with 2G mobile communication systems which in most of the cases just located the subscriber within the cell radius of the serving station.

Initiatives beyond 3G include High Speed Downlink Packet Access (HSDPA), High Speed Uplink Packet Access (HSUPA), HSPA+, WiMax, and Long Term Evolution (LTE) [12][14]. However the coming of the Fourth Generation of Mobile Systems (4G) is expected to provide a widespread solution to deliver voice, data and streamed multimedia to users on an “anytime, anywhere” basis, with higher data rates than previous generations. 4G is expected to have a high network capacity in terms of simultaneous users per cell, spectrally efficient; with a data rate of at least 100 Mbps for outdoors and 1Gbps indoors, a high quality service for next generation multimedia support (real time audio, high speed data, HDTV video content, mobile TV, tele-existence, etc.), and all IP packet switched network with the capacity to dynamically share and use network resources to meet the minimal requirements of all the 4G enable users [12]-[15]. These objectives may be achieved using advanced communications techniques which involve the use of smart antennas based in Multiple Input – Multiple Output (MIMO) technologies, turbo-codes and OFDM modulation. MIMO helps to get ultra-high spectral efficiency and spatial diversity, turbo-codes aids to minimize the SNR at the receptor, and OFDM exploits the frequency selective channel properties [15][16]. Note that these highly developed technologies work together to get the best of communications and cover users’ expectations in terms of reliability and new services. In addition, 4G is also expected to provide enhanced GPS services that might let people be virtually present in many places [15]. It is tele-presence. Lately, it is perhaps LTE-Advanced which looks like the true 4G because it can theoretically achieve data download rates as high as 3 gigabits per second and upload rates as high as 1.5 Gb/s because carrier aggregation, but it will still take some years for operators to deploy the more sophisticated features of LTE, such as voice services and “self-organizing” software, which would let base stations adapt to new network conditions on their own or heal themselves after disruption [16]. However, the entrance of LTE-Advanced certainly will mean the possibility of new developments in LBS.

1.1.1 Mobile Location Services

In the context commented above, where mobile market penetration is currently in most cases above the 90% at world scale [1][2], with increasing data rates’ and

processing possibilities, mobile location services (MLS) have acquired without a doubt, a greater relevance, since they have opened to researchers, business men, and the general public of end users a new set of possibilities of relations and opportunities. Notwithstanding recent forecasts from Pyramid Research and Bergh Insight when they are compared to those of STRATEGYANALITIC in 2007 reveals lower growth rates for revenues of LBS in Europe and United States; they also confirm the great increase of LBS revenues in the last decade. In fact, STRATEGYANALITIC reported that total end-user spending on location aware mobile services in North America would expand from U.S.D. \$110 million at the end of 2006 to U.S.D. \$2,220 million by the end of 2011 at a growth rate of 72%; while it previewed a growing from U.S.D. \$ 191 million to U.S.D. \$1,243 million in Europe for the same period [17][18]. Furthermore, the new Bergh Insight report discloses that mobile LBS market in North America is forecasted to grow at a compound annual growth rate (CAGR) of 16.1 percent from \$1.8 billion in 2013 to reach \$3.8 billion in 2018, and those revenues in Europe would grow from € 735 million (\$1.01 billion) in 2013 at a CAGR of 25.8 percent to reach €2.3 billion (\$3.1 billion) in 2018 [19]. On the other hand, Pyramid Research forecasted that global location-based services market revenues were expected to reach a very high growth in 2015, up from \$2.8 billion in 2010 [21].

It is very possible that diffusion of LBS has been slower than forecasted due to the implementation of more accurate localization techniques, such as Enhanced Observed Time Differences (E-OTD), Uplink Time Differences Of Arrival (U-TDOA) or Assisted GPS (A-GPS), has been taken longer by providers, because they have been more costly than expected, and also because LBS exhibited long response times, often too long for users to handle [32]. However, Berg Insight [19][20] estimates that about 50 percent of all mobile subscribers in Europe were frequent users of at least one location-based service at the end of 2013. Furthermore, in North America, where adoption of GPS-enabled handsets is still higher, an estimated 60 percent of all handset users now access location-based services at least monthly. Mapping and navigation is still the leading segment in terms of revenues, and the second largest in terms of number of active users. Berg Insight also estimates that the number of active users of LBS and apps more than doubled in 2011.

Seven years ago, 31 - 32% of revenues occurred in the car navigation service [17][18], and navigation applications were already the largest LBS revenue generators [21]. Therefore, it is not strange that various business models are being established in this segment, and a range of different players are focusing their efforts on it, creating a dynamic and fast-changing market segment [21]. Besides, other services such as people finding and local search are increasing with GPS and smartphone adoption.

Some navigation service providers are focusing on apps where the core turn-by-turn navigation service is free and users have the option to purchase additional content and features. Ad-funding is already the main source of revenues in many consumer LBS categories, with the exception of mapping and navigation as well as tracking service categories where ad revenues now account for less than 10 percent of total revenues [20]. Many operators are now opening their location platforms to third party developers

and location aggregators that play an important role as intermediaries between mobile operators and developers. It is an important opportunity to expand LBS but it is also a thread for operators which are losing the monopoly of the access to the location information. In fact, operators gained around 80% of all LBS revenue in 2008, and this gain reduced to around the half, three years later; but the total market grew more than fivefold [20][21]. Relatively high prices are being charged nowadays for each location look-up. This is a justifiable cost for services where a successful location look-up adds significant value and the developer can charge their customers accordingly. This is the case for a range of enterprise and Business to Business (B2B) services including asset tracking, workforce management, authentication and fraud prevention [20]. However user privacy concerns and pricing of location data are issues to be resolved before location-based ad campaigns can contribute significantly to overall revenues. Indeed, a study measured the level of enjoyment of participants when using technology innovation providing LBS as extremely high (88%), but the same participants expressed their concerns about privacy [32].

1.1.2 Classification of Mobile Location Services

What Mobile Location Services (MLS) really are? Mobile Location Services are also known as Location Based Service (LBS), and in the broadest sense, are services or applications that extend spatial information processing, or GIS (Geographic Information Systems) capabilities, to end users via wireless network to provide value-adding services to them [23][26]. Some examples include the Emergency response services such as E-911 in the U.S.A., the E-112 in Spain [24], and the American Automobile Association's roadside assistance service [25].

Gravitate Inc. [26] identified three generations of location services in 2002. Second generation services available a decade ago provided rough locations typically at the postal code level. Therefore, a mobile user for i.e. might find the nearest restaurants or gas stations. Applications of this kind associated with the cell id parameter that identified the service base station with its position. The third generation services are currently available, and they supply with more precise positional information and are able to initiate services proactively based on location. Three triggers mode services are mentioned: Object triggers that notify the mobile user when entering within a predefined distance of a facility, Object-temporal triggers that add the temporal dimension, and Affinity triggers that allow one mobile device to know the location of another mobile device. In addition, a new fourth generation of LBS is expected to emerge. I referred to those related to the notion of tele-presence with applications in telemedicine, high-risk exploration, etc.

There is no single winner application, but each industry sector embraces services that significantly change the way information is gathered, maintained, and distributed. When Geographic Information Systems (GIS) are integrated to the field force automation or to the customer relationship management, very promising location service applications appear [26].

Table 1.1 above exhibits some examples of LBS for different categories, their accuracy needs and their application environments.

SERVICES	EXAMPLES	ACCURACY NEEDS	APPLICATION ENVIRONMENT
EMERGENCY	Emergency calls	Medium/High	Indoor/Outdoor
	Automotive Assistance	Medium	Outdoor
	Emergency Alert Services	Medium	Outdoor
NAVIGATION	Directions	High	Outdoor
	Traffic Management	Medium	Outdoor
	Indoor Routing	High	Indoor
	Group Management	Low/Medium	Outdoor
INFORMATION	City sightseeing	Medium/High	Outdoor
	Mobile Yellow Pages	Medium	Outdoor
	Infotainment Services	Medium/High	Outdoor
	Localized Advertising	Medium/High	Indoor/Outdoor
	Weather	Medium	Outdoor
	Asset and Service Finding	Medium/High	Indoor/Outdoor
ADVERTISING	Banners, Alerts, Advertisements	Medium/High	Outdoor
TRACKING	Person tracking	High	Indoor/Outdoor
	Fleet Management	Low/Medium	Outdoor
	Personnel Tracking	Medium	Outdoor
	Asset Management	High	Indoor
BILLING	Location-sensitive charging	Low/Medium	Indoor/Outdoor
ENTERTAINMENT AND COMMUNITY SERVICE	Gaming	Low/Medium	Outdoor
	Find Your Friend	Low/Medium	Indoor/Outdoor
	Dating	Medium/High	Indoor/Outdoor
	Chatting	Low/Medium	Outdoor
	Route Finding	Medium/High	Outdoor
SERVICE PROVIDER	Specific Services	Low/High	Indoor/Outdoor

Table 1.1: Classification of Location Based Services

Therefore, it is not difficult to see from a business perspective, why some consultants believe that the “location information comprises the first major slice of the value pie for location services” while “it is the integration of GIS, Internet and wireless

technologies that comprises the second major slice” [26][27]. These services may be categorized as follows: Emergency services, Navigation services, Information services, Advertising, Tracking and Billing services [23]; however they have been standardized by 3GPP in a slightly different way as: Public Safety Services, Location Sensitive Charging, Tracking, Traffic Monitoring, Enhanced Call Routing Services, Location Based Information Services, Entertainment and Community Services and Service Provider Services.

In addition to this classification, the Location Based Services (LBS) accordingly to the way they are provided may be divided in three types: Pull, Push and Telemetry. Pull type LBS are able to provide their users with worth information associated with their position whenever and wherever it is required. Push type LBS otherwise use wireless user position to qualify the holder as a potential customer or recipient of a service. And, finally Telemetry LBS refer to devices that automatically notify service providers of their location and status. This category includes for i.e. to vending machines, heating, ventilation and air conditioner (HVAC) systems, alarm systems, and mobile assets such as trucks, rail cars, etc.

Emergency services are a kind of public safety services that include Alert services and Emergency call services related to security and some emergency situations where a person requires help, but he/she doesn't know where he/she is. Emergency call services were regulated for the US Federal Communications Commission (FCC) in 1999 in the sense that, by October 2001, emergency services should be able to automatically position any citizen dialing 911 to within 125 meters in two thirds of cases. This mandate put up the initial impulse for the development of LBS [22][23]. Positioning for Emergency services shall be supported for all user equipment where coverage is provided, included stolen UEs and UEs without a SIM/USIM [31].

Navigation services solve users' needs for directions within their current geographical location. From user position, operators are able to inform him/her how to get to a defined destination; and if they have also the ability to monitor traffic conditions, they can even suggest alternative routes to their users. Moreover, travel assistant applications may form part of this category. These applications would perform tasks such as edge matching: multiple map area files would be combined into a seamless map coverage that enables routing across multiple geographic data files. Furthermore, traffic aids could pick up live traffic data from vehicle sensors (mobile speed, direction, etc.) and combine it with incident reports for spreading through Internet or mobile devices. Therefore, people would be able to dynamically evaluate a planned itinerary and, if needed, select an alternative route to avoid problems.

It is not unlikely to think that these services could be extended to support indoor routing, if we consider the introduction and eventually growth of femtocells [23][28][29]. In this case, a new kind of navigation services would assist users to locate products, exhibition stands, and so on. Moreover, new group management applications would be developed to create virtual communities of people with similar interests and social networks based on location and mobility patterns.

Information services refer to the digital distribution of content to mobile terminals based on their location, schedule specifications and user preferences. These services may include travel services such as guided tours and transportation services for tourists; mobile yellow pages, information about local events, location for multimedia contents, and so on.

Advertising Services may have an important development due to their relation with mobile commerce, and their capacities of personalization, that offer new opportunities to place effective and efficient promotions on mobile environments. These services include mobile banners, alerts and proximity triggered advertisements. Due to the potential disturbs of this kind of services [30][32], user authorization is required to receive this information, and some mechanisms such as special offers, discounts or reduced call rates, are being developed to make them attractive for the potential consumers. Concerns about privacy are still limited the development of certain LBS, especially those related with advertising [20].

Tracking Services refer to the possibility to know permanently where vehicles and people are. Corporate segment requires them to know where their goods are at any time, and may use this information to improve their relations with customers and providers: They can also use this information for sending adequate help in an emergency situation, and for tracking their field and sales personnel. On the other hand, families could use these services to track children and elderly people.

Billing Services refer to the possibility of the service provider to reduce fares in relation to spatial and temporal triggers to optimize its network resources.

New LBS are permanently being explored. It is for i.e. the case of the Touring service evaluated in Lukang, a historical town in central Taiwan. The application was retrieved on powerful handheld devices with the goal to guide 42 participants through 258 Point Of Interest (POI), collecting information about tourist satisfaction, and testing algorithms provided to content retrieving to the device and triggering of content presentation to the user [36]. The tested algorithm is called Demodulating and Encoding Heritage (DEH) and it tries to optimize spatial and theme dimensions to give the user the best guiding experience. Spatial dimension leads people to the POI while theme dimension is related to the management of content retrieving and presentation along the Line Of Interest (LOI). LOI is defined previously to the guiding, but it can be changed during the activity. This LBS application turned out worthy but not enough to replace human guiding.

Due to the increasing complexity of new LBS, new techniques are being implemented to optimize resources and improve performance. One of them aims to improve the coarse granularity of the pushed information in current LBS systems [37] by using the PUB/SUB Paradigm instead of the check-in model. In this way the user receives certain subscribed events of interest and his/her information delivery takes less time. This paradigm includes a Universally Unique Identifier (UUID) as a Message

Identifier (MID) to mark an event, and a zone manager. Another interesting work suggests the substitution of the Scalar Vector Graphics (SVG) format recommended by W3C for implementation of online map service for a novel mobile map format, Byte-Map [38]. The basic cell of Byte-Map is a block of 255x255 that can be encoded with only two bytes. In this way, the online map service requires a LBS-p Server and a LBS-p Mobile. PKGML data in GIS platform is encapsulated in Byte-Map format and returned to LBS-p mobile. Experimental results for a seven layers Beijing map in GML format when Byte-map with two levels is used reduced to about 10MB, which is 2.5% of the original data volume. SVG is based on XML and therefore it uses too much data space. Byte-Map request message consists of 3 parts: range description, level ID and block description. Range description includes the left-bottom coordinates, the width and the height of the requested range, Level ID describes the level of the needed map data, and Block description is an optional part which includes marks of every block within the requested range. Each block mark is described by a bit, 1 for including data of the block in response message, and 0 for excluding it [38].

As LBS increase in complexity, some efforts are being developed to ease services composition modeling that includes factors related to location context. It is the case of Timing Constraint Petri Nets (TCPNs) which include a timing constraint to solve the problem of model's time control and dynamism description [39].

1.1.3 Importance of Positioning Systems

The potential spread and richness of LBS, some of them briefly commented above, does reveal the enormous importance of location information, because of the transforming impact over people relationship, interaction and communication that these services offer. In fact, LBS software records person's footprint, and new relationship chains may be shaped based on hobbies, spending habits and geographical characteristics [35]. All this information makes easier initiate group activities. It is certainly seen that this relevance is transferred to the positioning systems which provide user location and, due to the tendency for high mobility, especially to the mobile positioning systems.

With an automated location system for i.e., it is feasible to track any type of vehicle or mobile object, emergency response personnel can find victims of accidents, contractors can track construction equipment, and police can find stolen property. Early implementations based on short message services (SMS), deployed in Japan and Finland, have experienced surprising popularity of friend finder services. Further developments include the GeoLife project in China, a GPS-data-driven social networking service where people can share life experiences and connect each other with their location histories [36]. Due to some markets are more tolerant to user interface limitations and because the emergence of more powerful technologies, a wide spread of location services may be rapidly introduced.

In addition, as more of the work force goes mobile, business men will need help in finding the location of people, objects, facilities, or customers, and to relate those

locations to the organization’s data resources. It would be the work of the proximity searcher type applications.

It is evident that cited examples are not exhaustive, but they provide an idea of the widespread of possibilities that LBSs offer and why they are gaining so great relevance.

1.2 Location Service Standards

Because LBSs require subscriber position and GIS services to provide added value, cooperation between different parts of the network is required. Therefore, standardization efforts were made since early stages of LBS rising. Due to mobility, subscriber position might be enabled by processes related to the access network, while implementation of LBS also required from GIS and other platforms owned by the service provider. In this context several standardization organizations emerged, such as Open Geospatial Consortium (OGC), the Location Interoperability Forum (LIF), the Third Generation Partnership Project (3GPP), and the Internet Engineering Task Force (IETF) among others. Figure 1.1 illustrates this standard framework.

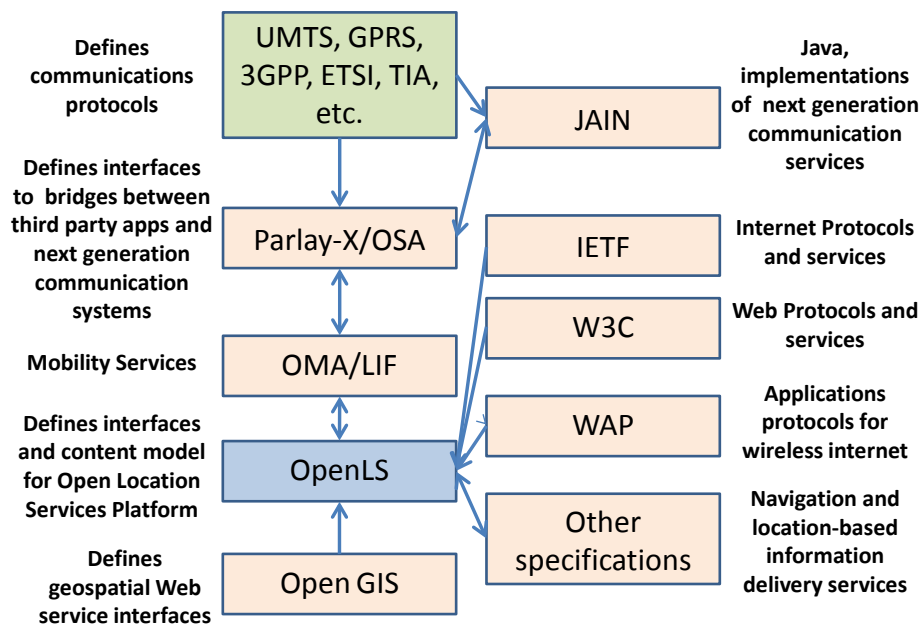


Figure 1.1: Location Services and Standard Framework [33].

The Open Geospatial Consortium (OGC) began its location-based standards work on 1999, and since then it has come enhancing the range of standards to be used in Location Services applications. These standards include Open GeoSMS, the Geography Markup Language (GML), and the OGC sensor standard among others. Most recently, OGC activities have included some standardization work for augmented reality

applications. Some short descriptions of key OGC standards that have been developed and used in Location Services industry are listed below.

- Geography Markup Language (GML) is an XML grammar for expressing geographical features. GML serves as a modeling language for geographic systems as well as an open interchange format for geographic transactions on the Internet. There are two parts for the grammar: the schema that describes the document and the instance document that contains the actual data. Elements of GML have incorporated in dozens of other standards with the goal of having common and consistent mechanisms for expressing and communicating location. GML is also an ISO (International Organization for Standardization) standard [33].
- OGC KML (Keyhole Markup Language) is an XML language focuses on geographic visualization, including annotation of maps and images. It includes also the control of the user's navigation in the sense of where to go and where to look. It was submitted by Google in 2006 and approved as an OGC standard in 2008 [33].
- Web Map Service (WMS) provides a simple HTTP interface for requesting geo-registered map images from one or more distributed geospatial databases. A WMS request defines the geographic layer(s) and area of interest to be processed. The WMS Interface standard is available as an app for Android and iPhone operating systems. WMS is also an ISO standard [33].
- Sensor Observation Services (SOS) define an interface and operations that when implemented enable access to observations from sensors and sensor systems in a standard way that is consistent for all sensor systems including remote, in situ, fixed and mobile sensors [33].
- OGC Open Location Service (OpenLS) Core – Core services, parts 1-5, also known as the GeoMobility Server (GMS), defines an open platform for location-based services. The primary objective of OpenLS is to define access to the core services and abstract data types (ADTs) that comprise the GeoMobility Server, an open location services platform. The GeoMobility Server uses open interfaces to access network location capacity (provided through a GMLS for i.e.) and provides a set of interfaces allowing applications hosted on this server, or on another server, to access to the OpenLS core services. This server puts up content such as maps, routes, addresses, points of interest, and traffic. It can also access other local content databases via the Internet. Figure 1.2 exhibits the relations of GeoMobility Server with other network elements and servers.

The OpenLS Core Services exchange content in the form of well-know OpenLS ADTs. ADTs are data types and structures defined as application schemas that are encoded in XML for location Services. Collectively these ADTs comprise the OpenLS Information Model.

The OpenLS Core Server includes the Directory Service, the Gateway Service, the Location Utility Server, the Presentation Service and the Route Determination Service [33].

- **The Directory Service** provides subscribers with access to an online directory to find the nearest, or a specific, place, product or service. Through an OpenLS application, the subscriber sets the search parameters in the service request, identifying the place, product or service that they seek by entering the name, type, category, keyword, phone number, or some other “user-friendly” identifier. The position required may be the current mobile terminal position, as determined through the Gateway Service (this service translates MLP into an OpenLS “position”) or a remote position determined in some other manner. The service returns one or more responses to the query in ranked order, based on the search criteria.

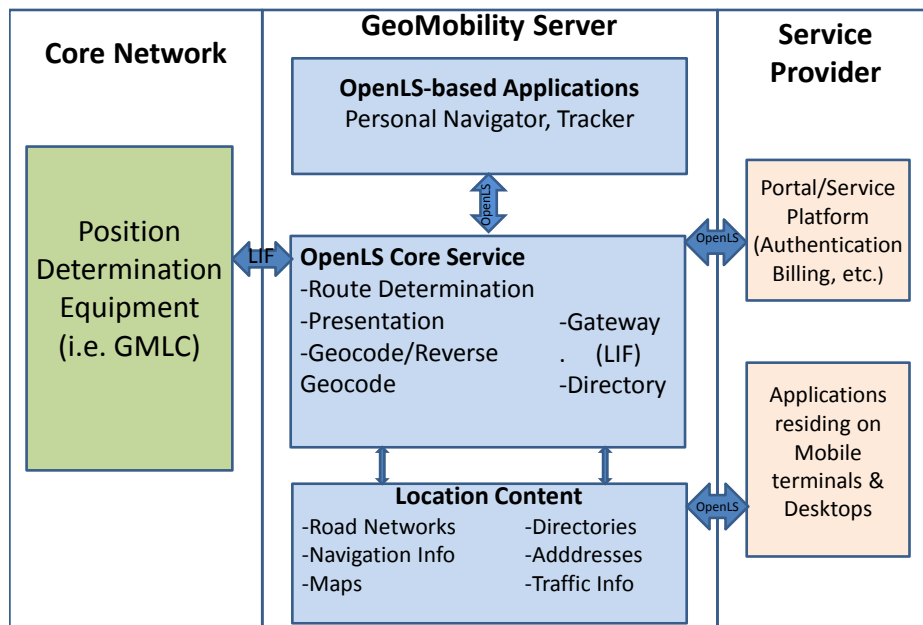


Figure 1.2 : The GeoMobility Server [33].

- **The Gateway Service** is the interface between the GeoMobility server and the location server that resides in the Gateway Mobile Location Center (GMLC) or Mobile Phone Center (MPC) through which OpenLS Services obtain position data for mobile terminals.
- **The Location Utility Server (Geocoder/ Reverse Geocoder)** performs as a geocoder by determining a geographic position, given a place name, street address, or postal code. It also performs as reverse geocoder by determining a complete, normalized place name/street address/ postal code, given a geographic position. The

number of responses to a service request may vary in relation to the algorithm being employed, and the match criteria.

- **The Presentation Service** provides geographic information to display on a mobile terminal. This service may also render route directions and/or route instructions.
- **The Route Determination Service** determines a route for a subscriber. The subscriber must use a navigation application to set up the use of the service. They must indicate the start point and they must enter the endpoint (any location, like a place for which they only have the phone number or an address, or a place acquired through a search to a Directory Service). The subscriber may optionally specify waypoints, in some manner, the route preference (fastest, shortest, least traffic, most scenic, etc.), and the preferred mode of transport. The subscriber may optionally store a route for as long as needed, thus requiring the means to also fetch a stored route.

OpenLS interfaces are not complex but they are not lightweight. Hence, in 2009 the OGC members began to consider a much more light weight consumer-facing location service standards. The first version of Open GeoSMS standard was released in January 2012, and there is already extensive implementation of this standard. It provides developers with an extended SMS encoding and interface to facilitate communication of location content between different LBS devices or applications. Open GeoSMS is already use in deployed commercial applications in Taiwan as well in several disaster response applications. ITRI, for i.e., is an Open GeoSMS based application donated to the Sahana Disaster Management System for providing location updates to Sahana for relief and rescued coordination among several mobile devices [33].

More recent OGC standardization work includes Augmented Reality (AR), IndoorGML and Internet of Things.

Augmented Reality allows the user to see the real world with virtual objects superimposed upon or composited with the real world. AR applications have emerged in the last years on mobile devices equipped with sensors for orientation and location (iPhones, Android devices, etc.). Certain monopoly games where users buy virtual estate and props in real locations, and consumer interaction are proposals for this sort of AR applications [35]. Since 2010, the OGC has a focused AR standards development activity known as “ARML, Augmented Reality Markup Language”. ARML focuses on mapping geo-referenced POIs and their metadata, as well as mapping data for the POI content providers publishing the POIs to the AR application. Due KML and ARML 1.0 are purely descriptive formats, ARML 2.0 will allow dynamic parts to modify the properties defined in the descriptive part, it will extend the rather basic POI presentation options (visual representation) to more sophisticated visualizations like 3D objects, lines, and polygons; and it will provide connecting ports to other widely used AR tracking methods (mainly visual tracking, but also audio tracking) [33]. Request of comments for ARML 2.0 is currently closed, and final version is planned to be released after editing and revision.

Indoor location services such as indoor navigation are a very interesting research topic, not just because the issue of locating a mobile device in an indoor environment, but also because the indoor environment provides a complex set of standards requirements, such as how navigation directions are supplied (go to the second floor and turn right), semantics (my first floor is not your first floor), special zones (heating, security, WiFi, etc.) as well as the lack of a standard for modeling and encoding floor plans; and because indoor navigation needs to be 3D. In January 2012, OGC started an IndoorGML standards activity with the purpose of establishing a common model and schema framework for indoor navigation applications. IndoorGML will provide an essential model and data for important applications like building evacuation, disaster management, personal indoor navigation, indoor robot navigation, indoor spatial awareness, indoor location-based services, and the support for tracking of people and goods. IndoorGML provides a framework for the flexible integration of different localization technologies and allows the ad hoc selection of the appropriate navigation data according to the capabilities of the mobile device and the offered localization technologies of a building.

A very recent activity in the OGC is to consider how OGC standards may contribute to the development and evolution of the Internet of Things. The Internet will be augmented with mobile machine-to-machine communications and ad hoc local network technologies. At the network nodes, information about objects will come from bar-codes, radio-frequency identifiers (RFIDs), and sensors. The location of all objects will be known and the objects will interact extensively with fixed and mobile clients. The OGC initiated an OGC Web of Things (WoT) standardization activity suitable for consumer IoT. The first meeting of OGC Standards Working Group (SWG) for “Sensor Web for the IoT/WoT” was on June 2012.

The Location Interoperability Forum (LIF) was established in 1999 with the goal of delivering LBS providers with a standard set of interfaces that hide the different implementations of the location server. LIF approached location interoperability from the wireless network viewpoint. The result of LIF’s effort was the Mobile Location Protocol (MLP), which is an application-level protocol for getting the position of mobile stations (mobile phones, wireless personal digital assistants, etc.) independent of the underlying network technology, that is, independent of location derivation technology and bearer. The MLP serves as the interface between a Location Server and a Location Service (LCS) Client. This specification defines the core set of operations that a Location Server should be able to perform. The first version of this standard was approved in 2002 by the LIF membership. OGC actively participated in the LIF activity, and focused on the application, data, and presentation layers of the standards stack. Both OGC staff and a number of OGC member organizations participated in the definition and approval of the MLP API. As expected, there was considerable overlap between LIF and OGC concerning wireless location interoperability. Therefore, LIF incorporated the location requirements of 3GPP, OpenLS would include the MLP by reference, and the LIF community determined that various existing OGC standards, such as the GML and standard mechanisms for encoding coordinate reference information, were well suited to modeling and encoding location payloads as part of the

MLP API. Version 3.2 of the MLP Specification was approved by the OMA in July 2011. The current version uses OGC reference for all coordinate reference system (CRS) elements and GML for encoding CRS references and complex geometries [33].

The Third Generation Partnership Project (3GPP) unites six telecommunications standard development organizations: The Association of Radio Industries and Businesses (ARIB) from Japan, the Alliance for Telecommunications Industry Solutions (ATIS), the China Communications Standards Association (CCSA), the European Telecommunications Standards Institute (ETSI), the Telecommunications Technology Association (TTA) from South Korea, and the Telecommunication Technology Committee (TTC) from Japan. This organization provides its members with a stable environment to produce Reports and Specifications. 3GPP includes the following Technical Specification Groups (TSG): Radio Access Networks (RAN), Service and System Aspects (SA), Core Network and Terminals (CT), and GSM Edge Radio Access Networks (GERAN) [4]. 3GPP RAN specifications ensure that 3GPP systems are capable of rapid development and deployment with the provision of global roaming. 3GPP work has provided a high degree of continuity in the evolving systems, improving quality of service and cost efficiencies. 3GPP Release 99 referred to W-CDMA, Release 5 to HSDPA, Release 7 to HSPA+, Release 8 to LTE, and Release 10 to LTE – Advance. From 3GPP Release 10, LTE – Advance was approved by ITU as an IMT-Advanced Radio Interface Technology. The LTE standard provides for peak speeds of 100 Mbps for high mobility and 1 Gbps for low mobility communications. 3GPP Release 12 is expected to be frozen by September 2014 and includes 60 new studies. An important part of 3GPP’s recent work includes carrier aggregation, and improvement of spectral efficiency. Future work will address energy saving, cost efficiency and backhaul enhancements [4].

Due to mobility, subscriber positioning has to be supplied from the access network. 3GPP considers Location Services (LCS) as a network provided enabling technology consisting of standardized service capabilities which enable the provision of location based applications. LCS can be offered without subscription to basis telecommunications services to the following categories of clients: Value Added Services LCS Clients, PLMN Operator LCS Clients, Emergency Services LCS Clients and Lawful Intercept LCS Clients. LCS Clients interacts with a LCS Server for the purpose of obtaining location information for one or more Mobile Stations. The LCS server consists of LCS components which are distributed to one or more PLMNs and/or service providers [31].

3GPP standard Release 9 supports Evolved UMTS Terrestrial Radio Access (E-UTRA), GSM EDGE Radio Access Network (GERAN) and UMTS Terrestrial Radios Access Network (UTRAN) to ease the determination of the location of a mobile station; and it considers accuracy, coverage, privacy and transaction rate as the primary distinguishing attributed that define a value-added service. Transaction rate denotes how frequently network messaging is required to support the service. High level requirements also include [31]:

- Modularity and open interfaces in supporting mechanisms;
- Network flexibility to accommodate evolving enabling technologies and service requirements to provide new and improved services;
- Provision of multiple layers of permissions to comply with local, national, and regional privacy requirements.
- Support of multiple positioning methods in the different Access Networks: Modernized GPS; Satellite Based Augmentation Systems (SBAS): European Geostationary Navigation Overlay Service (EGNOS), Wide Area Augmentation System (WAAS), GPS Aided Geo Augmented Navigation (GAGAN), Multi-functional Satellite Augmentation System (MSAS); Quasi Zenith Satellite System (QZSS); GLONASS; Uplink-TDOA (U-TDOA); Enhanced Observed Time Difference (E-OTD); Idle Period in Down Link – Observed Time Differences Of Arrival (IPDL-OTDOA); Network Assisted GNSS (Network Assisted GPS or Network Assisted GALILEO); methods using cell site or sector information and Timing Advance (TA) or Round Trip Time measurements (RTT).
- Combining of diverse positioning techniques and local knowledge when considering quality of service parameters to provide an optimal positioning request response.
- Provision of position information to location services applications existing within the PLMN, external to the PLMN, or in Mobile Equipment.
- Support to networks based on Intelligent Network architecture.
- Support may optionally be provided to enable the routing of emergency calls based on the geographic coordinates (latitude and longitude) of the calling party.
- Provision of the originating party's serving cell id to the LCS client.

Figure 1.3 shows the logical reference model for LCS in 3GPP whereby an LCS Client is enabled to request location information for one or more certain target user equipment (UE) from the LCS Server supported by a PLMN.

The LCS Server employs a positioning function to obtain the location information and supply the information to the LCS Client. The particular requirements and characteristics of an LCS Client are made known to the LCS Server by its LCS Client Subscription Profile. The particular LCS-related restrictions associated with each Target UE are detailed in the Target UE Subscription Profile. The LCS feature allows a Target UE to be positioned within a specified Quality of Service. The LCS feature allows the location of a Target UE to be determined at any time whilst the UE is attached. For network based positioning methods, no support for LCS is required by the target UE. For mobile assisted and mobile based positioning methods, the target UE actively supports LCS. For all positioning methods, the ability to control privacy may be required to be given to the UE for each location request and/or to the UE through the UE subscription profile to satisfy local regulatory requirements [31].

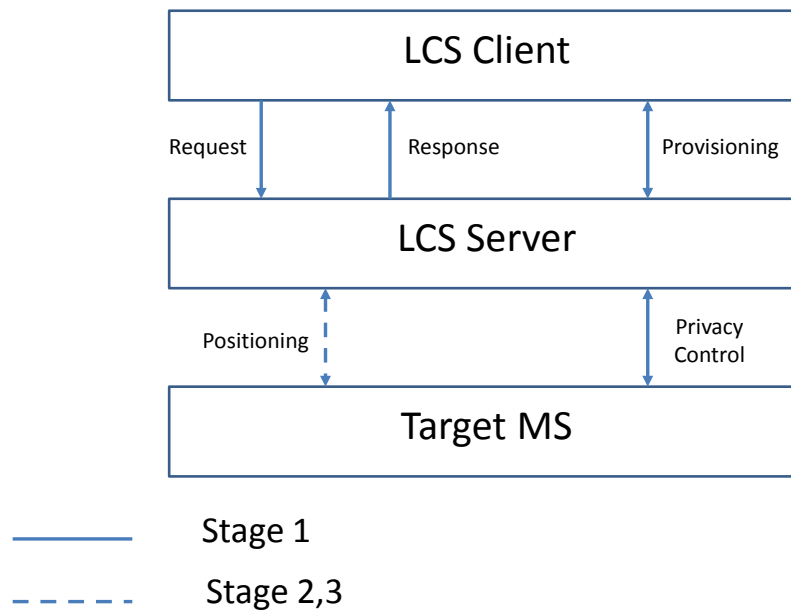


Figure 1.3: LCS Logical Reference Model ETSI 3GPP TS 22.071 v9.1.0 (2010-09)

3GPP has established that for value added services, the LCS client shall identify a target UE using the MSISDN or Session Initiation Protocol (SIP) URL, and that the LCS client shall be able to identify the target UE using IP addressing. For PLMN operator services, the LCS client may identify a target UE using any of the following: MSISDN, SIP URL, International Mobile Subscriber Identity (IMSI), or an identifier internal to the PLMN. In case of emergency services, the LCS client may identify a UE target using anyone of the following: MSISDN, SIP URL, IMSI, North America Emergency Services Routing Key (NA-ESRK) + (optionally) IMEI (ANSI standards) and IMEI (ETSI standards). Furthermore, it is possible for the mobile's user target to hide her true identity from the requestor and the LCS client and replace it with an alias. The alias is a unique identification that has a one-to-one relationship to the true identity of the subscriber and may be permanent or temporary. The target mobile user is able to know her own alias so that it can pass the alias to the LCS client, e.g. when invoking a location-based service. The Privacy attributes consist of: Code-word, Privacy Exception List, Service Type Privacy, and Privacy Override Indicator [31].

It is possible for a Requestor and an LCS client to request location information by indicating a code-word associated with the Target UE. The code-word is either checked by the Target UE/user or by the LCS server in the home network. In the former case, the code-word is forwarded to the Target UE/user for verification and acceptance. In the latter case, the code-word is registered with the LCS server by the Target UE user (or subscriber) in advance. The UE and/or network has the option of being capable to generate and/or distribute code-words. A comparison of the code-word sent by the

Requestor and the registered code-word is performed. A location request is only accepted if this comparison is successful [31].

The Internet Engineering Task Force (IETF) through its IETF GEOPRIV Working Group has been developing and refining representations of location in Internet protocols since 2004. It analyzes the authorization, integrity, and privacy requirements that must be met when these representations of location are created, stored, and used. The IETF developed a concept known as “location object.” There are two types: civic and geodetic. The geodetic location object type is encoded using the GML application schema [33]. On the other hand the civic location objects include categories such as Building, Room, P.O. Box, Road Section, among others [34]. Additionally, the geodetic location (GML) object is now incorporated into a number of Internet standards including HTTP Enabled Location Delivery (HELD), LoST—A Location-to-Service Translation Protocol, Filtering Location Notifications in the Session Initiation Protocol (SIP), and others.

The World Wide Web Consortium (W3C) Point Of Interest Working Group develops technical specifications for the representation of “Point of Interest” information on the Web. Its current draft utilizes the OGC/ISO geometry model and states that GML is the preferred encoding language for POI location elements.

The National Emergency Number Association (NENA) - Next Generation 911 “serves the public safety community as the only professional organization solely focused on 9-1-1 policy, technology, operations, and education issues.” Next Generation 9-1-1 (NG 911) is a system comprised of Emergency Services IP networks (ESInets), IP-based software services and applications, databases, and data management processes that are interconnected to public safety answering point (PSAP) premise equipment. The system provides location-based routing to the appropriate emergency entity. The system uses additionally available data elements and business policies to augment PSAP routing. The system delivers geodetic or civic location information and the call back number. The NENA NG 911 community has determined that GML is a preferred mechanism for sharing GIS data between PSAPs and counties. Besides, other OGC standards have been identified as potentially important to the NG 911 activity, including CityGML, Geosynchronization, and the OGC Web Feature Service [33].

1.3 Positioning Systems and the Emergency Service

It has been shown before that the high dynamism of wireless communications is related to the possibility offered by current and future technologies to provide new services of public and private interest. One of the most relevant communication services is precisely the Subscriber Location, which is in the core of LBS. The called Emergency Service has a particular relevance because it was the engine of those which have appeared later. In the following, a deeper insight in positioning systems and in the emergency service will provide.

1.3.1 Classification

Positioning systems are in the core of LBS providing objects location. In self-positioning, it is the object which provides its own position; while in remote positioning, it is an external center or device which computes where the object is located. GPS is a good example for the first category and radar for the latter.

These systems may be classified into three groups: signpost, wave-based and dead reckoning [25]. Signpost systems are the simplest of them and use a large number of reliable reference points where mobile unit registers or that are used by mobile units to compute its position. The New South Wales government's Road and Traffic Authority's Automatic Network Travel Time Measurement System (ANTTS) is a system of this kind.

Wave based systems use propagation characteristics of signal to determine mobile position for i.e. GPS, radar and wireless communications positioning systems.

Dead reckoning systems use devices to measure speed of acceleration which is used to track mobile location. These systems require an initial position as a reference and are quite autonomous but inaccurate, unless the reference position is being updated regularly or mobile counts with very sophisticated measurement systems.

1.3.2 The Positioning Systems and the Emergency Service

The idea of using a single phone number to attend emergency calls is not new and it was originated in Britain. This concept extended to other countries shortly thereafter. The United States of America adopted the 911 as the only "Universal Emergency Number" for public use to request emergency assistance, and the first 911 call was made in 1968. In this system, all 911 calls arriving at a telephone exchange would automatically route it to the connected emergency communication center.

The original 911 system evolved to Enhanced 911 (E911) in 1980s and it is still in use today. Therefore, 911 calls go currently to a designated telephone switch called a selective router. Each selective router serves several telephone exchanges and it directly connects to the emergency communication centers in the region [41].

By November 1999, nearly 92% of the population in the United States was covered by some type of 911 systems, and due to the wireless subscriber growth; the provision of the E-911 (Enhanced 911) service to wireless users becomes a necessity. Around the 25% of all 911 calls in the U.S. in 1999 were originated from mobile phones, and generally the caller could not state his/her exact position [40].

On June 12, 1996, the Federal Communication Commission (FCC) established performance goals and timetables for the identification of the wireless caller's phone number and physical location when dialing the 911 emergency services telephone. In Phase I, which began on April 1, 1998, wireless operators were required to forward the 911 calls from mobile phones to a Public Safety Answering Point (PSAP) without any

interception for any validation procedure or credit checks. In Phase II, they were required to provide more precise location identification according to the Location Determination Technologies (LDT) used, as it is shown in Table 1.2 [40].

E-911 Phase II Accuracy Requirements		
Percent of calls	Network solution	Handset solutions
67%	100 m	50 m
95%	300 m	150m

Table 1.2: E-911 Phase II Accuracy Requirements

By December 31, 2004 wireless operators were required to ensure that 100% of their total subscriber bases were capable of providing Automatic Caller Identifier (ALI). It meant the provision of caller's name, phone number and address.

Deployment of E-911 service in the precise way specified by FCC would require very huge costs. Less precise solutions such as cell ID were available and had been set up in Europe and Japan, but U.S. carriers had preferred to be cautious because of the potential public backlash against them. Perhaps, they were trying to avoid public perception that carriers were interested in offering consumer LBS to generate money, rather than to aid emergency services and at the same time they were trying to provide a high accuracy positioning service as a core of more developed LBS with the quality degree they perceived it was required by the American market [40].

The 112-Emergency Service is the Spanish analogue to the E-911, and it was originally deployed by *Telefónica*. It used a cell ID positioning technique and included some proprietary network elements. It was designed to evolve from the GSM network to UMTS [24], and it currently supports LTE too. The GSM system just enabled the positioning of a mobile unit when it had originated the call (Mobile Originated), and when the positioning requirement was initiated by an element that did not own to the core network (CN). It is called Mobile Terminated. Moreover, an UMTS system enables positioning when requirement is initiated by the CN. It is called Network Initiated. Spain regulated telecommunication access to 112-Emergency Service in 1997, and currently, all enterprises that provide electronic communication services to final users for calling to numbers that belong to a Telephone Numbering National Plan, with independence of technology, and including VoIP, are obligated to provide the access to this service. Regulation specifies this access is free for users calling from any telephone terminal, and that location information must be provided for free to the PSAP accordingly with accuracy and reliability established criteria. Location information must be provided within network technical possibilities, and in case of mobiles, it must include Cell ID/ Sector ID and contract domicile registered in database [40][42].

Telephone Mobile Operators developed a location information protocol called POSIC112. It establishes a corona from the circular sector defined accordingly to ETSI TS 101.109 V7.1.0 standard to settle where mobile subscriber probably is. Position

definition includes UTM zone and Universal Transverse Mercator (UTM) coordinates, Azimuthal angle, Aperture angle, and inner and uncertainty radiuses. The likelihood that the subscriber is within the defined area is also provided, as well as a temporal mark [42].

Positioning System Architecture for UMTS

Within UMTS, there is a clear division between the functions related to CN and those assigned to the Radio Access Network (RAN). Furthermore, the Positioning Signal Measurement Function (PSMF) belongs to the RAN, while the Location System Operations Function (LSOF) belongs to the CN.

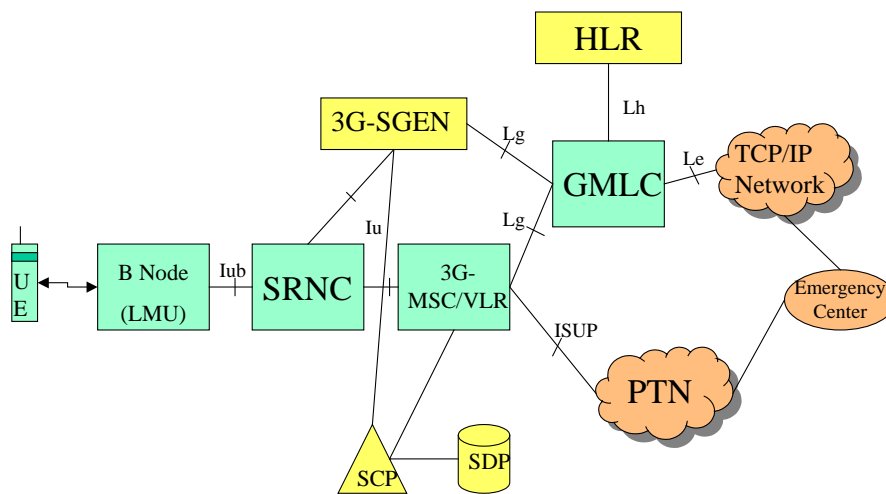


Figure 1.4: Positioning System Scheme for UMTS [3].

The Figure 1.4 shows a diagram of the Positioning System for UMTS. The two nodes related to positioning are the Global Mobile Location Center (GMLC) and the Serving Radio Network Controller (SRNC). The GMLC belongs to the CN and holds data for a set of external LCS clients that may make call related or non-call related requests to this GMLC. This data include the type of LCS client, a list of one or more identifiers for external or internal LCS clients, a logical name associated with LCS client's external identity, the default Quality of Service (QoS) requirements for the LCS client, among others [44]. On the other hand, the SNRC is part of UMTS Terrestrial RAN (UTRAN) and contains the functions related to data acquisition from radio interface and those related with the management of the positioning computing [43].

The functional components associated with the client handling are exclusive of the GMLC. These include the Location Client Control Function (LCCF), the Location Client Authorization Function (LCAF), the Location Client Coordinate Transformation

Function (LCCTF), and the Location Client Zone Transformation Function (LCZTF). The GMLC may also include the Location System Billing Function (LSBF) and the Location System Operation Function (LSOF) [44].

The UTRAN includes three functional groups: the internal client group, the UTRAN System Handling group and the UTRAN Positioning group. The first group is constituted only by the Internal UTRAN Location Client Function (U-LCF); the second one is constituted by the UTRAN Location System Control Function (U-LSCF) and the UTRAN Location System Operations Function (U-LSOF); and the last group is constituted by the UTRAN Position Radio Co-ordination Function (U-PRCF), the UTRAN Position Radio Resource Management (U-PRRM), the UTRAN Position Calculation Function (U-PCF) and the UTRAN Position Signal Measurement Function (U-PSMF). The PCF belongs to SMLC whilst the PSMF belongs to LMU or Node-B. The other UTRAN LCS entities belong to the SRNC [43].

U-LCF represents a logical interface between the internal UTRAN LCS's applications and the LCS RNC handling entities. It can be used for i.e. to interchange positioning information to perform location assisted handover. U-LSCF is responsible for coordinating UE positioning request within the RNC handling entity. It separates the Location clients in the Core Network from the UTRAN positioning methods. In this way several types of core network may be used. U-LSCF provides flow control between simultaneous UE positioning requests, and selects the appropriate positioning method, and when the method requires the broadcast of system information, it initiates and maintains this activity through the U-PRCF. This information may be the spreading codes of neighboring Node Bs, Relative Time Difference (RTD) between Node Bs, the local time-of-day, etc. The U-LSOF is responsible for provisioning of data, positioning capabilities, data related to clients and subscription, fault management of LCS within the RNC [43].

U-PRCF manages a UE positioning for a UE through overall co-ordination and scheduling of resources to perform positioning measurements. This function interfaces with U-PSMF, U-PRRM and U-PCF. U-PRCF determines the positioning method to be used in relation to UE's requirements and capabilities, and it also manages radio resources through U-PRRM. It forwards the signal measurements data to the U-PCF. U-PSMF is responsible for performing and gathering uplink or downlink radio signal measurements for use in the calculation of a UE position. U-PCF computes the final position estimate and accuracy from collected signal measurements.

Sequence of a 112-Emergency Service Call from a mobile terminal

When a user performs a 112 call within the mobile network two tasks are concurrently performed: voice call routing and transmission of location data. A 112-call goes forward to the MSC where it is tagged as an emergency call. There, the MSC sends the Cell ID (CID) and caller identity (subscriber MSISDN/INSI or terminal IMEI) to the Service Control Point (SCP). The SCP consults to the Service Data Point (SDP) for the identification (IP and port number) of the corresponding PSAP where the mobile

position must be transferred and the number of the local emergency center. The SDP looks up the required number in its database and delivers it to the SCP. The SCP informs to the MSC where the call must be transferred, and the necessity of consulting the SRNC for the caller positioning. User position is computed from CID or other enhanced accuracy algorithms. The MSC completes the voice call, and it also transfers the caller location and the emergency center identification to the positioning server from the mobile network (GMLC). The GMLC opens a socket and performs a TCP connection for sending the positioning information along with the caller identity (MSISDN/IMSI or IMEI) to the corresponding PSAP. Finally, the PSAP synchronizes the voice call and the associated Positioning data through the caller identity sent by both the voice call and the signaling data [42].

New trends in the 911/112-Emergency Service

Despite that around the year 2000, most emergency communications systems in U.S. were able to locate mobile callers reasonably well; the fast increase in voice over IP (VoIP) technology imposed a giant step back. A VoIP service knows only caller's IP addresses, not their locations, and internet calls may suffer from delays (in U.S. one in a thousand), and the 20 extra minutes may be an eternity in emergency situations. The only way to fix this mess is to replace the whole systems and starts again [41]. This initiative is known in the United States as Next Generation 911 (NG911) and in Europe as NG112. The core of NG911 is the Emergency Services IP Network (ESInet). This network uses the standard Session Initiation Protocol (SIP), common in VoIP services and 4G mobile networks, to define the data messages that must be sent to begin and end calls, along with data to initiate other calling features like Caller ID and call forwarding.

Because the calling device is connected to both the access network which does not know there is an emergency and to the origination network which does not know the caller location, the calling device can query the access network to get its own location and then send that location data through the origination network to the emergency communications center as part of the data that signals the start of a call. The caller's location is sent to a local server based on the Location-to-Service Translation (LoST) protocol, defined by IETF in 2008 [41]. Call can contain any mix of voice, video, and text media as long as the calling device supports it. This richer information may be completed by relevant information provided by the emergency centers to improve assistance, or even notify or add third parties to the call.

NG911 benefits are indubitable but its implementation involves a greater grade of cooperation among several parties such as: emergency communications center, calling networks, IP networks and also standardization and regulatory organisms.

1.4 Research Objectives

Positioning a device through the use of a sensors' network is a complex issue to be boarded from a system perspective, and whose solution necessarily involves a work in various fronts such as: knowledge of nature of signals transmitted from devices and

received by the sensors; some aspects inherent to the environment geometry where the device is going to be located, which besides of affecting the accuracy in the calculation of the position in relation to the nature of the used measures, they may also introduce severe signal degradation in relation with propagation conditions.

Additionally, when the device to be located is a mobile subscriber that operates on a wireless network, signals that would be collected should be also related to the system for which they were designed, since the taking of measures is necessarily related to the system network procedures. It is therefore useful to have a look at mobile systems, positioning systems, and their possibilities and limitations; but it should be emphasized that the perspective of the research described in this paper corresponds precisely to signal processing, and therefore these topics have been accentuated along the document taking care of delineating their interfaces to other system elements. Thus, the objectives to be covered throughout the research are the following:

- Definition and evaluation of positioning systems for mobile subscriber in multipath environments for both, LOS and NLOS environments.
- Proposing a scheme for delay estimation in two stages: a first gross estimation and a posterior fine estimation.
- Evaluation of proposed schemes within realistic environments.

1.5 Thesis Structure and main contributions

In the following paragraphs, the thesis structure is briefly commented. This document includes four chapters, and each one pretends to be auto content. In this way, the interested reader may begin the appraisal of his/her topic of interest in the corresponding chapter.

Chapter 1 has a descriptive nature, and particularly introduces the notion of Location Based Services, their importance and classification, and their relation with wireless communication networks. It also describes the 911-Emergency Service, and provides a vision of the evolution of these LBS. It addresses to clarify why wireless subscriber positioning is important and it places this issue within the larger scope of the multidisciplinary work where this problem belong. Furthermore, in the last part of this chapter the structure of this document and the main objectives for each chapter are summarized.

Chapter 2 introduces the topics relative to the nature of the wireless communication signal, and the particularities of the mobile channel. It also studies the fundamentals of Direct Sequence – Spread Spectrum (DS –SS), and their relation with the positioning enable technologies. It also introduces the positioning technologies, the problems and possible solutions when these schemes are applied to wireless communications systems, and some mechanisms for accuracy evaluation. Furthermore, it particularly studies the accuracy degradation associated with the Non Line Of Sight

(NLOS) condition and its mitigation. This section justifies the choice of the models used along this research, and develops a simulation platform to evaluate positioning accuracy. Furthermore, the use of some important statistics to perform NLOS mitigation on timing – based positioning algorithms have been proposed. The main contributions in this chapter are the following:

- Derivation of these statistics from the Greenstein’s model, and therefore concluding that the quality of the timing measures decays more strongly with the link distances between transmitter and receiver than the suggested when the propagation model has not been taken account. Therefore, the proper weightings have been provided.
- The weighted linear least squares algorithm has been revisited and a new two-stage solution that includes geometrical restrictions has been proposed and successfully implemented.

Chapter 3 presents the available channel models, and justifies the use of dispersive models for the theoretical study of the positioning problem. It includes a detailed description of Cramer-Rao Bounds derivation for Time Of Arrival (TOA) estimation from these models for both Rice and Rayleigh propagation. Moreover, the simulations provided at the end of this chapter show the benefit of space-time diversity for improving timing and therefore positioning estimates.

- The main contribution of this chapter is precisely the derivation of this model based on CRBs, since that to the best of our knowledge, it is in fact the most complete of its kind in the literature, since it incorporates a way to take into account spatial and temporal correlation among channel estimates, the impact of the roll-off factor, the number of sensors and the number of channel estimates, and also because it assumes an exponential dispersion from delays, which it is characteristic of mobile channels, instead of using two or three paths, a typical approach in literature.

The chapter 4 integrates the information model for the lower limits of the error variance in the timing estimation of the first arrival based on Cramer Rao Bounds to the positioning simulation platform developed in chapter 2 providing a useful approach to evaluate both qualitative and quantitative the benefits of using space-time diversity in terms of the positioning accuracy. Moreover, it introduces the proposed two-stage procedure to acquire the required improved timing estimations for enhancing the positioning accuracy of the wireless mobile subscribers. Therefore, some notions related to the Statistical Theory of Decision are introduced and the problem of discriminating signal from noise is commented, and a Generalized Likelihood Ratio Test (GLRT) is derived. Moreover, this chapter also presents some high resolution schemes to be used at the second stage for the estimation of the first delay, and reduce timing uncertainty from a chip time at the first stage to a small fraction of this value. It also describes some ways to improve estimation using spatial diversity. Eventually, the operational results from this two-stage detection-estimation approach have been incorporated to the simulation platform to assess their application to the subscriber positioning problem in

realistic conditions. The final results show the benefits of using this two-stage procedure, as well as the advantage of counting with space-time diversity in the solution of the positioning problem. Furthermore, they show as subscriber location may be performed with a high degree of accuracy from network-based architectures. The main contributions of this chapter are:

- The derivation of a Generalized Likelihood Ratio Test (GLRT) to perform signal detection in a noisy environment.
- Evaluation of signal detectability using a novel model developed to put in evidence the optimum operation point from the viewpoint of the quality of the timing detection. This model has been used to evaluate different configurations of the proposed GLRT, but it can be used to evaluate other detectors once provided their receiver operating characteristics.

Finally, the last piece of this document exhibits the main observations and conclusions from the whole research, pointing out possible topics for future study.

1.6 List of Publications

In the following, the whole list of publications related to this thesis research is presented:

Chapter 2

- Paúl Prócel, Luis Prócel, René Játiva, Julio Arauz, “Desarrollo de una Aplicación de Servicios Basados en Localización para Redes de tipo Global System for Mobile (GSM) y Universal Mobile Telecommunications System (UMTS) usando el emulador Mobile Positioning System 6.0.1 provisto por la empresa ERICSSON”, *Revista Avances en Ciencias e Ingenierías*, Vol. 1, No. 1, 2009.
- René Játiva, David Sánchez, Josep Vidal, “NLOS Mitigation Based on TOA for Mobile Subscriber Positioning Systems by Weighting Measures and Geometrical Restrictions”, *IEEE Asia-Pacific International Conference on Computer Aided System Engineering*, pp. 325-330, July 2015. DOI: 10.1109/APCASE.2015.64.

Chapter 3

- René Játiva E., Josep Vidal and Margarita Cabrera, “Cramer Rao Bounds in Time Of Arrival Estimation for a Distributed Source”, *Mobile Communications Summit, IST2001*, pp. 236-244, September 2001.
- Josep Vidal, Montse Nájjar, Margarita Cabrera, René Játiva, “Positioning accuracy when tracking UMTS mobile in delay and angular dispersive channels”, *IEEE Vehicular Technology Conference, VTC 2001 Spring*, Vol. 4, pp. 2575-2579, May 2001. DOI: 10.1109/VETECS.2001.944066.
- René Játiva E., Josep Vidal, “Estimación del Tiempo de Llegada en un canal Rayleigh desde una perspectiva de la Cota Inferior de Cramer-Rao”, *Revista Avances en Ciencias e Ingenierías*, pp. 5-10, Abril 2009.
- René Játiva E., Josep Vidal, “Cota Inferior de Crámer-Rao en la Estimación del Tiempo de Llegada en un Canal Rice”, *Revista Avances en Ciencias e Ingenierías*, pp. C14-C21, Julio 2012. ISSN 1390-5384.
- René Játiva E., Josep Vidal, “Cramer-Rao Bounds in the estimation of Time Of Arrival in fading channels”, *EURASIP Journal on Advances in Signal Processing*, submitted on June 2016.

Chapter 4

- René Játiva, Josep Vidal, “GLRT detector for NLOS error reduction in wireless positioning systems”, *IST Mobile and Wireless Telecommunications Summit*, June 2002.
- René Játiva, Josep Vidal, “First Arrival Detection for Positioning in Mobile Channels”, *IEEE International Symposium on Personal, Indoor and Mobile*

Radio Communications, PIMRC 2002, Vol. 4, pp. 1540-1544, September 2002. DOI: 10.1109/PIMRC.2002.1045437.

- Josep Vidal, René Játiva, “First Arriving Path Detection for Subscriber Location in Mobile Communication Systems”, IEEE International Conference on Acoustics, and Statistical Signal Processing, Vol. 3, pp. III-2733 – III-2736, May 2002. DOI: 10.1109/ICASSP.2002.5745213.
- René Játiva, Josep. Vidal, “Coarse First Arriving Path Detection for Subscriber Location in Mobile Communication Systems”, XI European Signal Processing Conference (EUSIPCO 2002), September 2002.
- Josep Vidal, Montse Nájjar, René Játiva, “High resolution time-of-arrival detection for wireless positioning systems”, IEEE Vehicular Technology Conference, VTC-2002-Fall, Vol. 4, pp. 2283-2287, 2002. DOI: 10.1109/VETEFCF.2002.1040627.
- René Játiva, E. Garzón and J. Vidal, “Space-Time Diversity for NLOS Mitigation in TDOA-Based Positioning Systems”, IEEE International Engineering Summit, II Cumbre Internacional de las Ingenierías, March 2016. DOI: 10.1109/IESummit.2016.7459771.
- René Játiva E., Diego Ortiz, Pablo Venegas and Josep Vidal, “Selection of the reference anchor node by using SNR in TDOA-based positioning”, IEEE Ecuador Technical Chapters Meeting (ETCM 2016), October 2016.
- Esteban Garzón, Santiago Valdiviezo, René Játiva E. and Josep Vidal, “Fast Computation of Cramer-Rao Bounds for TOA – An application to network-based positioning simulations”, Latin American Conference on Computational Intelligence, November 2016.

1.7 References

- [1] Alex Moskalyuk, “US Wireless penetration reaches 70%, 200mln subscribers”; available on line at <http://blogs.zdnet.com>
- [2] PRLog.org, “New Report Says Wireless Penetration en the U.S. Mobile Market Will Reach 92.5% By 2010”, December, 2007; available on line at <http://www.prlog.org/10040705-new-report-says-wireless-penetration-in-the-mobile-market-will-reach-92-9-by-2010.html>
- [3] Francisco José Herrera Gálvez, et al, “Panorámica Actual de la Estandarización de los Sistemas Celulares de Tercera Generación”, Comunicaciones de Telefónica I+D, Number 21, June, 2001.
- [4] <http://www.3gpp.org>
- [5] <http://www.3gpp2.org>; <ftp://ftp.3gpp.org/specs/latest>
- [6] <http://www.etsi.org>
- [7] <http://www.uwcc.org>
- [8] José María Hernando Rábanos, Cayetano Lluch Mesquida, “Comunicaciones Móviles de Tercera Generación - UMTS”, Telefónica Móviles España, S.A., 2001.
- [9] Harry Holma, Antti Toskala, “WCDMA FOR UMTS. Radio Access for Third Generation Mobile Communications”, John Wiley & Sons, Ltd, West Sussex, PO19 1UD, England, June, 2000.
- [10] TIA/EIA/IS-2000-2, “Physical Layer Standard for cdma2000 Spread Spectrum Systems”, August, 1999.
- [11] Samuel C. Yang, “CDMA RF System Engineering”, Artech House Inc, Norwood, 1998.
- [12] Kuramavel, K., “Comparative Study of 3G and 4G in Mobile Technology”, International Journal of Computer Sciences Issues (IJCSI), Vol. 8, 5, 3, 2011. ISSN (on line) 1694-0814; available on line at www.IJCSI.org.
- [13] Miki T., Ohya T., Yoshino H. and Umeda N., “The Overview of 4th Generation Mobile Communication System”, IEEE International Conference on Information, Communications and Signal Processing, 2005, DOI: 10.1109/ICICS.2005.1689329.
- [14] Mudit Ratana Bhalla and Anand Vardhan Bhalla, “Generations of Mobile Wireless Technology: A Survey”, International Journal of Computer Applications, Vol. 5,4, 2010. 0975-8887.
- [15] Khan A.H., Qadeer M.A., Ansari J.A., and Waheed S., “4G as a Next Generation Wireless Network” IEEE International Conference on Future Computer and Communication (ICFCC), 2009, DOI: 10.1109/ICFCC.2009.108.
- [16] Ariel Bleicher, “4G gets Real”, IEEE Spectrum, Volume 51, 1, 2014, DOI:10.1109/MSPEC.2014.6701430.
- [17] Nitesh Patel, “North America Consumer Location Based Services (LBS) Forecast”, STRATEGYANALITICS, August, 2007; available at www.strategyanalytics.net.
- [18] Nitesh Patel, “Western Europe Consumer Location Based Services (LBS) Forecast”, STRATEGYANALITICS, August, 2007; available at www.strategyanalytics.net.

-
- [19] Nathan Eddy, “Location-Based Service Market to Reach Nearly \$4 billion by 2018”, e-week, march 28, 2014; available at <http://www.eweek.com/mobile/location-based-service-market-to-reach-nearly-4-billion-by-2018.html#sthash.NN9un4xS.dpuf>.
- [20] André Malm, “MLB Services – Business Models for LBS shift to freemium and advertisement”, Bergh Insight Report, 2014; available at <http://www.berghinsight.com/ReportPDF/ProductSheet/bi-lbs6-ps.pdf>
- [21] “Location Based Services – Market Forecast 2011-2015”, Pyramid Research Report, 2011; available at <http://www.pyramidresearch.com/store/Report-Location-Based-Services.htm>
- [22] “Ranking of Top 3G Services”, UMTS Forum Position Paper #2, August, 2001 available on line at www.umts-forum.org.
- [23] George M. Giaglis, Panos Kourouthanassis, Argirios Tsamakos, “Towards a Classification Framework for Mobile Location Services”, Mobile Commerce: technology, theory and applications, ISBN: 1-59140-044-9, 2003; available on line at <http://portal.acm.org>.
- [24] Ernesto Aranda Almansa et al, “Sistemas de localización en redes móviles: el servicio de emergencias 112”, Comunicaciones de Telefónica I+D, Number 21, June 2001.
- [25] Chris Drane, Chris Rizos, “Positioning Systems in Intelligent Transportation Systems”, Artech House Inc., Norwood, 1998.
- [26] Harry Niedzwiadek, “Where’s the Value in Location Services?”, Image Matters LLC, USA, 2002.
- [27] www.jlocationsservices.com; www.esri.com
- [28] Arantxa Herranz, “Femtocell, oscuro nombre, futuro brillante”, September, 2007; available on line at <http://www.idg.es/pcworldtech>.
- [29] Andy Tiller, “The Case for femtocells”, IP Access Ltd., May, 2007; available on line at <http://www.ipaccess.com/femtocells/femtocell.php>
- [30] Shereen Fink, “Location Based Services and Privacy”, Sun Microsystems, Radio Resource Magazine, Englewood, U.S.A, 2002.
- [31] “Technical Specification Group Services and System Aspects; Location Services (LCS); Service Description; Stage 1 (Release 9) – 3GPP TS 22.071 V9.1.0 (2010-09)”, 3RD Generation Partnership Project, 2010.
- [32] Iris A. Junglas and Richard T. Watson, “Location –Based Services – Evaluating user perceptions of location-tracking and location – awareness services”, Communications of the ACM, Vol. 51, No.3, 2008.
- [33] Harin A. Karini, “Advanced Location-Based Technologies and Services”, CRC Press, 2013, ISBN: 9781466518186.
- [34] M. Thomson and J. Winterbottom, “IETF RFC5139 – Revised Civic Location Format for Presence Information Data Format Location Object (PIDF-LO); available on line at <http://tools.ietf.org/html/rfc5139>
- [35] Pegang Qiu, Jing Zhang, and Jianqiu Zeng, “Study on the Mobile LBS Development Model”, International Conference on Computer Science and Service Systems, 2012, DOI: 10.1109/CSSS.2012.271.

-
- [36] Chung-Ming Huang and Shang-Chun Lu, “DEH: A ubiquitous Heritage Exploring System using the LBS Mechanism”, International Conference on Network-Based Information Systems, 2011, DOI: 10.1109/NBiS.2011.54.
 - [37] Wang Guoshi, Zhao Fang and Wang Rui, “Design and Implementation of an LBS Application Server Software Based on the PUB/SUB Paradigm”, International Conference on Business Computing and Global Informatization, 2012, DOI: 10.1109/BCGIN.2012.171.
 - [38] Xiaolin Wang, Xiao Pang and Yingwei Luo, “LBS-p: A LBS Platform Supporting Online Map Services”, IEEE 72nd Vehicular Technology Fall (VTC 2010-Fall), 2010, DOI: 10.1109/VETEFCF.2010.5594114.
 - [39] Weimin Li and Xiaohua Zhao, “Modeling and Simulation for Dynamic Services Composition of LBS Based on TCPN”, IEEE 14th International Conference on Commerce and Enterprise Computing, 2012, DOI: 10.1109/CEC.2012.34.
 - [40] M. Oğuz Sunay, “Evaluation of Location Determination Technologies Towards Satisfying the FCC E-911 Ruling”, Bell Labs, Lucent Technologies, USA, 2001.
 - [41] Richard Barnes and Brian Rosen, “911 for the 21st century”, IEEE Spectrum, Vol. 51, 4, 2014, DOI: 10.1109/MSPEC.2014.6776307.
 - [42] Manuel Abeijón, “La experiencia española de implantación del número europeo de emergencias 112”, Foro Multisectorial sobre el papel de las telecomunicaciones/TIC para el Manejo de los Desastres”, 2012; available on line at <http://www.itu.int/ITU-D/emergencytelecoms/events/bogota2012>.
 - [43] “Technical Specification Group Radio Access Network; Stage 2 functional specification on User Equipment (UE) positioning in UTRAN (Release 6) – 3GPP TS 25.305 V6.1.0 (2004-06)”, 3RD Generation Partnership Project, 2004.
 - [44] “Technical Specification Group Services and System Aspects; Functional stage 2 description of Location Services (LCS) (Release 4) – 3GPP TS 23.271 V4.13.0 (2004-12)”, 3RD Generation Partnership Project, 2004.

Chapter 2

Wireless Communications Signals and Positioning Technologies

Positioning technologies refer to the ways in which the measured signals from network and/or a mobile subscriber are treated to compute the position of this latter. Therefore, this chapter provides enough information concerning to the solution of the positioning problem with the use of a group of measurements extracted from signals exchanged in a wireless communications system. At first instance, valuable information is presented in section 2.1 in the most general possible way, to clarify properly the nature of the signals used in wireless communications systems and the effects introduced by the mobile channel which potentially disturb the subscriber's positioning. This description is useful as a reference in other application contexts, and eventually is specified for wireless systems that use Direct Sequence-Spread Spectrum (DS/SS) modulation, according to the whole chapters of this document. Indeed, the introduction of these concepts eases the comprehension of the contents described in the next two chapters.

Moreover, the section 2.2 of this chapter introduces an overview of the principles of positioning technologies, describes the issue of the Non Line Of Sight (NLOS) condition on positioning, and discusses possible solutions to mitigate this problem that strongly degrades the location accuracy. Furthermore, in the section 2.3 with the goal of evaluating several positioning technologies and methods, this chapter also describes the process followed in the implementation of a link level simulation platform used to incorporate, in realistic conditions, the main channel effects concerning to signals propagating between the transmitter and the receiver. Results from these simulations provide interesting guidelines that must be considered in the mitigation of the NLOS condition, and they are summarized in section 2.4. This simulation platform and several of the most relevant algorithms discussed in this chapter are also used as part of the study of the final solution proposed at chapter 4 to mitigate the NLOS condition in the mobile subscriber positioning.

2.1 Communications Signals and the Wireless Channel

Communications signals are affected in many ways by the physical propagation channel. Therefore, they must be prior processed in order to become useful for any application. The signal power received from a mobile emitter is not only attenuated by terrestrial propagation in a way worse than free-space (excess path delay), but it also drops along many wavelengths of the carrier due to obstacles that partially block the signal paths arriving to the receiver (slow fading, long term fading or shadowing), and the multiple echoes (multipath) observed in the scenario [1]-[5]. A typical fading signal is shown in Figure 2.1.

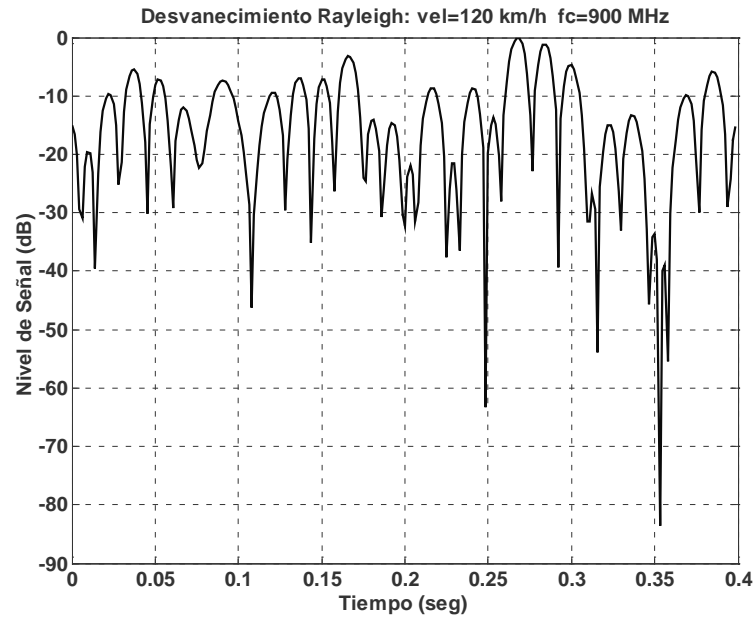


Figure 2.1. Typical Rayleigh Fading Channel for a mobile subscriber running to 120km/h and receiving at a carrier frequency of 900 MHz.

Due to multipath and the relative displacement of the emitter from the receiver, some short-term fading effects are registered such as: rapid changes in signal strength along small distances or time intervals, Doppler shifts on different paths and time dispersion. In a Non Line-Of-Sight (NLOS) case, RF energy travels from the transmitter to the receiver by diffraction, and this small-scale fading is also called Rayleigh fading because if the multiple reflective paths are large in number and there is no a line of sight signal component, the envelope of the received signal is statistically described by a Rayleigh probability density function (pdf). On the other hand, when there is a line of sight (LOS) component, the envelope of the received signal is statistically described by a Ricean pdf. [1]-[5].

2.1.1 Some Relevant Functions and Parameters in Wireless Channels

Due to time dispersion from multipath and temporal variability from Doppler shifts, scattered signal must be treated statistically in the time, the frequency and the spatial domains. Moreover, the concepts of Delay Spread, Doppler Spread and Angular Spread, are those which allow the wireless channels to be classified as time-selective, frequency selective and space selective.

In order to study these channels properly, two different variables must be introduced to describe the channel: its temporal variability (t) and its temporal dispersion (τ), despite the fact that they work simultaneously because the time is unique, due to the mobile channel is time variant. Figure 2.2 exhibits channel evolution with temporal variability expressed in terms of slots and temporal dispersion in terms of lags.

Analogously, two different variables must be defined to describe the channel spectral behavior: frequency (f) and the Doppler shift (f_d).

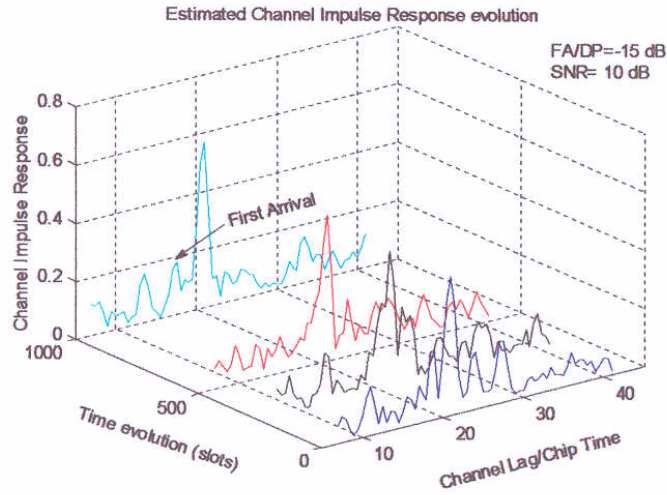


Figure 2.2. Time Evolution of Mobile Channel Impulse Response Estimates

Consequently, four system functions are defined to characterize the channel behavior [5]:

1. $P_h(u, \tau)$: Correlation Function for the temporal variability $u=t_2-t_1$, and Power Density function for the temporal dispersion τ .
2. $R_T(u, \nu)$: Correlation Function for the temporal variability $u=t_2-t_1$ and frequency variability $\nu=f_2-f_1$.
3. $P_H(f_d, \nu)$: Power Density Function for Doppler dispersion f_d and Correlation Function for frequency variability $\nu=f_2-f_1$.
4. $P_S(f_d, \tau)$: Power Density Function for Doppler dispersion (f_d) and for temporal dispersion (τ).

The system functions above are used for computing the Power Delay Profile (PDP), the Doppler Spread Profile (DSP), the Frequency Coherence Function and the Temporal Coherence Function of the channel, respectively.

The PDP $P(\tau)$ results from $P_h(0, \tau)$ and measures the power distribution as a function of the temporal dispersion, when a narrow impulse is transmitted through the channel. The DSP $P_S(f_d)$ results by averaging in τ the function $P_S(f_d, \tau)$ and it is the analogue of PDP in the frequency domain.

The Temporal Coherence Function $R_T(u)$ may be computed from $R_T(u, \nu)$ by averaging on ν , and it is a measure of the variability among different instants. When the value of $R_T(u)$ is small, the channel is time-selective which means that the channel response is very different for the two considered instants (t_1 and t_2). The Frequency Coherence Function $R(\nu)$ is obtained from $R_T(u, \nu)$ for $u=0$. When $R(\nu)$ is small, the

frequencies f_1 and f_2 are seen independently by the channel and hence they also fades autonomously. If it is the case, the channel is frequency selective. When $R(\nu)$ is very high, both considered frequencies fades in the same way, and it is called “flat fading”.

The Temporal Coherence Function and the Doppler Spread Profile (DSP) are a Fourier Transform Pair. Similarly, the PDP and the Frequency Coherence Function form another Fourier Transform pair [5]:

$$\begin{aligned} R(\nu) &= \mathcal{F}[P(\tau)] \\ R_T(u) &= \mathcal{F}^{-1}[P_S(f_d)] \end{aligned} \quad (2.1)$$

Since diverse paths arrive from different directions, an Angular Power Profile (APP) may be defined to describe the space-temporal behavior of the channel. Furthermore, angular and delay information may be integrated in a Power Angular-Delay Spectrum (PADS) as shown in Figure 2.3. The PADS in this figure is certainly simplified but it contains the main typical information of this kind of functions.

The severity of the fading is generally described by several statistical measures such as: the coherence bandwidth, the coherence time and the coherence distance. They are directly related to the temporal dispersion, the Doppler and the angular spreading respectively [6].

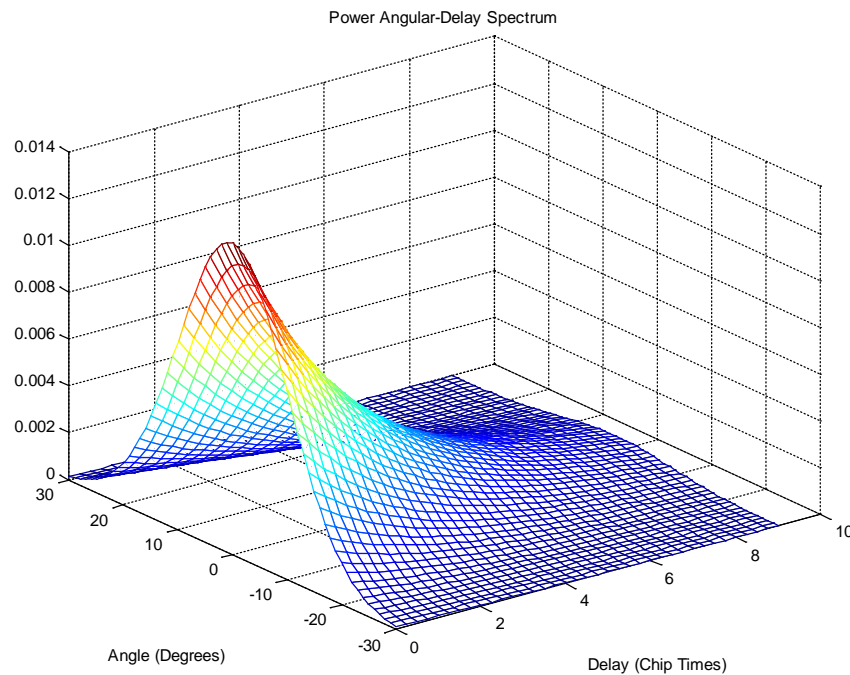


Figure 2.3. Idealized Power Angular-Delay Spectrum of a mobile Channel. Angular spread is set to 10° and Delay spread is set to $3T_c$.

Coherence bandwidth B_C , represents the range of frequencies where the channel approximately passes all spectral components with equal gain and linear phase, and hence the frequency range over which frequency components have a strong potential for amplitude correlation. Coherence time T_c , represents the time interval within the channel impulse response is essentially invariant, and quantifies the similarity of the channel response at different times. Finally, the coherence distance represents the spatial separation between two antennas in a way that the received amplitudes are similar [3][4][6]

Coherence time increases inversely to the Doppler frequency and it is usually computed as in (2.2), while the coherence distance reduces as angular spread increases.

$$T_c = .423 / f_d \quad (2.2)$$

The capricious factor in (2.2) results from the geometrical mean of the intervals u for which $R_T(u)$ takes values of 0.5 and 0.9 respectively [3]. Similarly, the Coherence bandwidth corresponds to the value v for which $R(v)$ is equal to 0.5 or 0.9 of its maximum [3][4]. The exactly way these coherence values are computed may differ in relation to the purpose of the application but they are really useful in the characterization of mobile channels.

For a single transmitted impulse, the time, T_m , between the first and the last received component in the PDP represents the maximum excess delay, during which the multipath signal power falls to some threshold level (10 dB or 20 dB) below that of the strongest component. On the other hand, the RMS Delay Spread is computed as the square root of the second order central moment of the excess delay, when a normalized version of the PDP is chosen as the weighting function.

Expression (2.3) corresponds to the classic Doppler spectrum when a dense-scatterer model is used, for a vertical receive antenna with a constant azimuthal gain, and a uniform distribution for signals arriving between 0 and 2π , and an un-modulated CW signal [4] [7][8].

$$S(v) = \frac{1.5}{\pi f_d \sqrt{1 - \left(\frac{v}{f_d}\right)^2}} \quad (2.3)$$

The equality above holds for frequency shifts of v that are in the range $\pm f_d$ about the carrier frequency f_c , and would be zero outside that range, and it may be regarded as the dual of the multipath intensity profile, $S(\tau)$, since the latter yields knowledge about the time spreading of a transmitted impulse in the time-delay domain. This spectrum exhibits sharp peaks in $v=\pm f_d$ but it is quite flat within this range, especially at indoors; therefore, it is usually modeled as a uniform distribution in these environments [9].

The width of the Doppler Power Spectrum (DPS) is referred to as the spectral broadening or Doppler spread, denoted by f_d , and sometimes called the fading bandwidth of the channel [8]

When the signal bandwidth W , is larger than the channel coherence bandwidth B_C , it suffers a frequency selective fading, and if the transmitted symbol lasts more than the

channel coherence time T_c , it experiences a time-selective fading. It must be noted that if the symbol rate $1/T_s$ is approximately equal to the bandwidth or signaling rate, a channel is frequency selective when B_C is lower than $1/T_s$, being T_s the symbol time. When the opposite is true, and B_C is higher than the signaling rate (or $T_m < T_s$), the channel is flat-fading; however, even these channels may endure frequency-selective distortion whenever a channel null appears at the band center.

A channel is referred to as fast fading if the symbol rate $1/T_s$ is less than the fading rate $1/T_c$ (approximately equal to f_d). In other words when $W < f_d$ or $T_s > T_c$. Thus, in order to avoid signal distortion caused by fast fading, the channel must be made to exhibit slow fading by ensuring that the signaling rate $1/T_s$, exceeds the channel fading rate f_d . Most present terrestrial mobile radio channels can generally be characterized as slow fading.

The time spreading mechanism is characterized in the time-delay domain by a multipath delay spread and in the frequency domain by a channel coherence bandwidth. The channel coherence bandwidth B_C sets an upper limit on the transmission rate that can be used without incorporating an equalizer in the receiver, while f_d sets a lower limit to it, in order to avoid the fast fading.

Fading mitigation is an important issue in order to achieve reliable wireless communications. For instance, an increase in E_b/N_0 of 26 [dB] is required in a Rayleigh channel in case of flat and slow fading, when it is compared to a Gaussian channel to achieve a bit error probability of 10^{-4} . The situation is especially severe in case of frequency-selective or fast fading distortion, where this probability degrades to 0.5 even with the high E_b/N_0 of 35 [dB] [10]. Mitigation method depends on the kind of distortion, and it should follow two steps: first of all, provision of distortion mitigation to combat fading, and then, provision of “diversity” to combat loss in Signal to Noise Ratio (SNR). The term “diversity” denotes the various methods available for providing the receiver with uncorrelated versions of the signal. Distortion may be reduced using adaptive equalizers, such as the decision feedback equalizer (DFE) or the Maximum Likelihood Sequence Estimator (MLSE), accounting with a Viterbi algorithm [10]. It also can be reduced with the use of OFDM [10][11] in case of frequency selective fading, or by using a robust non-coherent or differentially coherent modulation scheme in case of fast fading distortion. It is also advisable the use of error-correction coding and interleaving.

Spatial diversity is usually accomplished through the use of multiple receive antennas separated by a distance of at least 10 wavelengths for a base station and much less for a mobile station. Polarization diversity is another way to achieve additional uncorrelated samples of the signal, and path diversity may be achieved in case of a Direct Sequence/Spread Spectrum (DS/SS) scheme used with a RAKE receiver. Spread spectrum is a form of bandwidth expansion that excels at rejecting interfering signals. Power loss by the rejection is recovered by the RAKE receiver [10].

2.1.2 Channel Models

A large number of channel models have been proposed in the literature, especially for modeling signal fading, path-loss, multipath and Doppler spread. A very complete summary may be found in [7]. Some of them were conceived for macro-cells, and others for microcells, several for outdoors and others for indoors. These models may be classified in four main groups:

- Firstly, those models which trust on distributing scatterers about the mobile with a determined geometry to predict the correlation coefficients. It is the case of Lee's Model that places the scatterers evenly on a circular ring centered at the MS, and the called Discrete Uniform Distribution Model that places the scatterers evenly within a narrow angle centered about the LOS to the MS.
- Secondly, those models defined by a spatial scatterer density function used to place the scatterers within a determined region. It is the case of the Geometrically Based Single-Bounce Statistical Channels (GBSB), the Typical Urban (TU) and the Bad Urban (BU) models. GBSB channels include the circular model (GBCMCM) developed for modeling macrocells and that uses a circular region centered in the BS, the elliptical model (GBCMEM) developed for modeling microcells and that places the BS and the MS in the foci of an elliptical region, and possibly also to the more complex Elliptical Sub-regions Model. On the other hand, the Typical Urban (TU) model also uses a circular region centered in the BS to model the cluster of scatterers, but it introduces large-scale fading effects, and re-computes scattering configuration at intervals of 5m. The Bad Urban model adds a second 120-scatterers cluster to the TU model offset 45° from the first.
- When the number of scatters is large, the Angle Of Arrival (AOA) statistics is approximately Gaussian and therefore a third group of models based on statistics emerges. It includes the Gaussian Wide Sense Stationary Uncorrelated Scattering (GWSSUS) model which takes account of several clusters in the geometry, the Gaussian Angle of Arrival (GAA) model when just one cluster centered on a certain AOA is considered, the Uniform Sectorized Distribution Model, the Modified Saleh-Valenzuela's Model developed for indoor environments based on clustering phenomenon, and CoDIT initially proposed for WSSUS channels and for mobile displacements between 10 and 40 wavelengths among others.
- The fourth group refers to Ray tracing models where geometric theory and reflection, diffraction and scattering models and site-specific information such as building databases or architecture drawing are used to model the channel [7][9][12]. And finally, we have the measurement-based channel models which parameters are based on measurements and characterize the propagation environment in terms of scattering points [7].

However, the tendency in the last years is the migration from simple models to more realistic but complex ones. These models include the joint spatial-temporal behavior [12][13], the electromagnetic coupling among antenna elements [14][15], path gain dependence with frequency [12] and so on. Some of these new models add geometrical considerations to the stochastic ones, or even include stochastic information derived from measurement campaigns with the goal to achieve a better adjusting to technology evolution which it is displaced to higher frequencies, to multi-element antennas, and it is hunger of higher data rates and improved spectral efficiencies [15] [16].

Some measurements campaigns have been carried out to characterize spatio-temporal behavior of radio channel [12][13],[17]-[20], and useful models have been proposed to take account delay-DOA-power information [19][21]. Especially relevant is the Greenstein model [18] which studies the behavior of several measurement-based models and incorporates their information into a small number of parameters to characterize the path-gain/delay spread propagation channel, and suggest the values for these parameters. This model was incorporated to COST-231 and eventually to COST-259 [16][22]. Some of the most recent models include the 3GPP empirical spatial channel model (SCM), the multi-element transmit and receive antenna (METRA) analytical spatial channel model (A-SCM), the COST-259 Directional Channel Model [16], and the correlation-based long-term evolution (LTE) channel model [15]. Particularly, the COST-259 Directional Channel Model (DCM) considers a quite complete Power Delay-Direction Profile (PDDP) for modeling the signal clusters. It may be factored in five terms: the Power Delay Profile, the BS Power Azimuth Profile, the BS Power Elevation Profile, the MS Power Azimuth Profile and the MS Power Elevation Profile. MS Elevation Profile in this model is a function of the average building height, the street width and the excess delay. COST-259 DCM also considers the Ricean-fading statistics by adding a single coherent, Multi Path Component (MPC) to the first cluster. This model also includes a 2x2 polarimetric matrix to take account of polarization.

It is evident that the current trend for modeling the channel; is based on the approaches from groups 3 and 4, discussed above. Models from group 4 have been conceived to reproduce the signal's propagation conditions, in specific environments, require big computational capacities, and they are appropriate for the construction of designing tools and the planning of communication systems. On the other hand, approaches from group 3 describe the channel's behavior in a more general way, using stochastic models with a reduced number of parameters that permit the description of diverse typical environments as long as they are tuned correctly. This approach obviously requires much less computational effort, and it is suitable for academic research in order to extract interesting conclusions based on a general but rigorous characterization of reality.

Since the final objective of this research is to achieve a more accurate subscriber's positioning in a wireless communication environment; and recognizing that small scale

fading effects due to the multipath, especially when there is no a line of sight between the transmitter and the receiver, certainly degrade and even spoil the positioning algorithms as it is shown in the section 2.3, the proper models must include pathloss, as well as the temporal and spatial signal characterization. For this reason, the Greenstein model [18] results the most suitable at the moment of simulating the signal propagation process in our platform; as it is capable of characterizing rigorously the channel's behavior with only a few parameters, and it also permits its integration within a set of more complex models.

2.1.2.1 The Greenstein Model

NLOS environments are modeled using an exponential distribution for the excess delay for a particular location as it is shown in (2.4):

$$f_{\tau}(\tau) = \frac{1}{\tau_{rms}} \exp\left(-\frac{\tau}{\tau_{rms}}\right) u(\tau) \quad (2.4)$$

Moreover, the Greenstein model [18] characterizes the required RMS Delay Spread τ_{rms} required in (2.4). In fact, the Greenstein model is a path-gain/delay spread propagation model well suit for urban, suburban, and rural areas. However, it provides the RMS Delay Spread as a random variable and as a function of the distance between emitter and receiver, as it is shown in (2.5):

$$\tau_{rms} = T_1 d^{\varepsilon} \xi \quad (2.5)$$

Where, ξ is a lognormal random variable, and therefore $\Xi = 10\log(\xi)$, is a zero mean Gaussian variable over the terrain, with a standard deviation σ_{ξ} that lies between 2 and 6 [dB]. Furthermore, T_1 corresponds to the median value of random variable τ_{rms} at $d=1\text{km}$ and characterizes the type of environment; and ε is an exponent that quantifies the depth of the relation of the scattering with the distance, and lies between 0.5-1.0.

The Greenstein model also includes the gain path \mathbf{g} as a random variable. This gain is computed with the use of the expression in (2.6):

$$\mathbf{g} = \frac{G_1}{d^{\beta}} \mathbf{x} \quad (2.6)$$

Where d is the distance in kilometers, G_1 is the median value of \mathbf{g} at $d=1$ km, β is the path loss propagation factor which lies between 3 and 4, and \mathbf{x} is a lognormal random variable. Therefore, $\mathbf{X}=10\log(\mathbf{x})$ is a zero mean Gaussian variable with a standard deviation $\sigma_{\mathbf{x}}$ between 6 and 12 [dB].

Finally, the Greenstein model suggests the setting of the correlation factor between \mathbf{X} and Ξ as $\rho=-0.7$. Therefore $E\{\mathbf{X}\Xi\}=\rho\sigma_{\mathbf{x}}\sigma_{\xi}$.

Figure 2.4 and Figure 2.5 use Greenstein model to illustrate the correlation between delay spread and shadow fading when $\varepsilon=0.5$, $\beta=3.7$, $\rho=-0.75$, $T_1=0.7$ us, $\sigma_{\mathbf{x}}=8.0$ dB, and $\sigma_{\xi}=4.0$ dB. These values are adequate for an urban environment, and expressions used to perform these simulations are part of Annex A2.4.

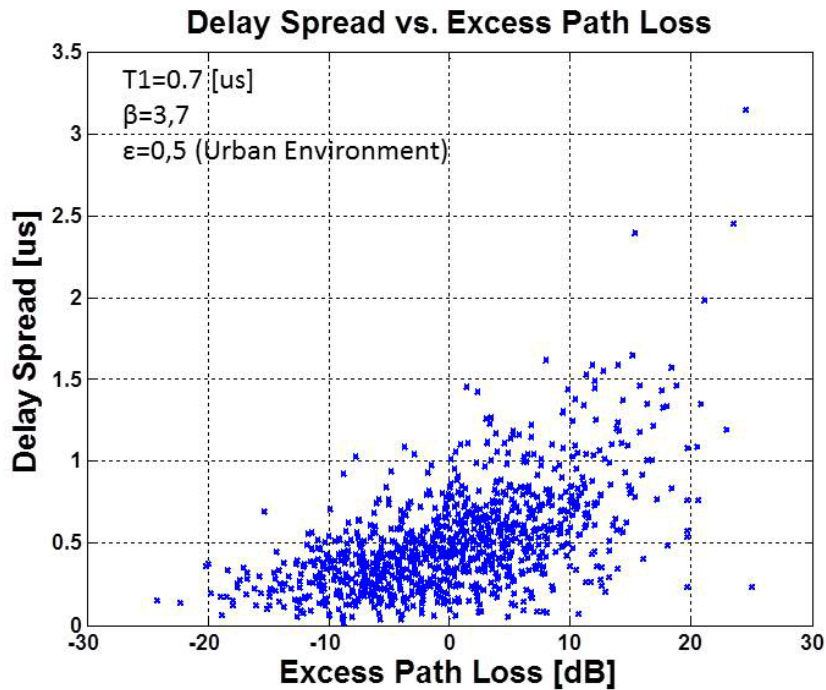


Figure 2.4: Delay Spread vs. Excess Path Loss for an Urban Environment using the Greenstein Model for a range between 0 and 1 km.

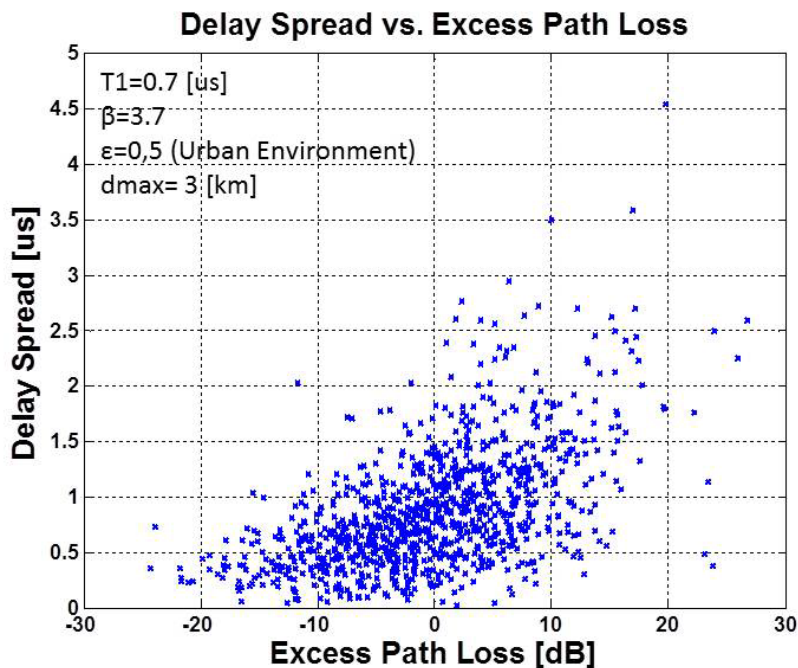


Figure 2.5. Delay Spread vs. Excess Path Loss for an Urban Environment using the Greenstein Model for a range between 0 and 3 km.

Figure 2.4 is adequate for distances between transmitter and emitter below 1 km; whilst Figure 2.5 is adequate for distances below 3 km. The mean RMS Delay Spread

for the first scenario is approximately 0.52 μs and its standard deviation reaches 0.32 μs . These values increase to 0.91 μs and 0.56 μs respectively for the second scenario due to this model predicts a variation proportional with the square root of the distance.

In order to gain a deeper appreciation of the behavior of Greenstein model, Figure 2.6 exhibits the distribution functions constructed from 10 thousand uniform distributed simulated points within four scenarios with radiuses of 0.2 km, 0.6 km, 1.0 km and 3.0 km.

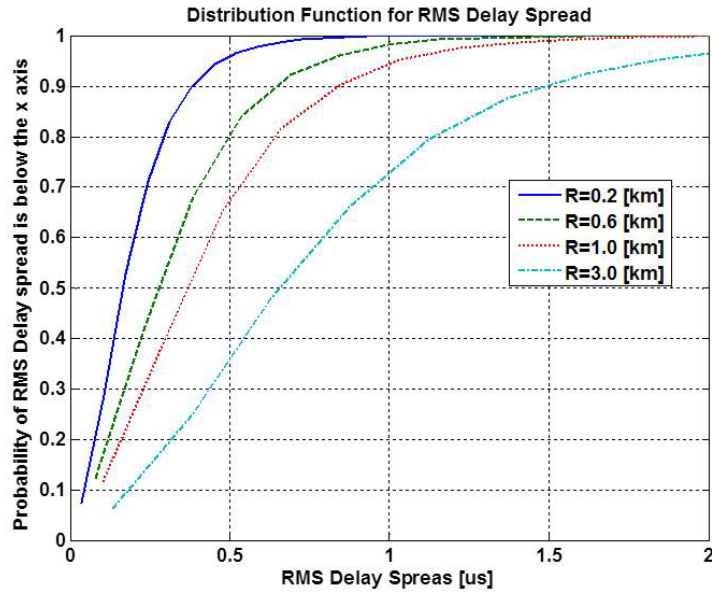


Figure 2.6. Distribution Function for RMS Delay Spread in relation with the cell radius for a uniformly distributed subscriber within the cell.

It is interesting to note that the CDF plot in Figure 2.6, when the cell radius is set to 0.2 km, practically matches with the corresponding results provided from a measurement campaign performed over a medium European city, as it may be easily probed comparing our results with data provided by Ericsson for a WCDMA system [22]. This observation validates the suitability of Greenstein model to apprehend the characteristic of real environments.

Moreover, as a reference, Table 2.1 shows the behavior of the mobile channel in terms of Delay Spread and Coherence Bandwidth for a synthetic model [5], and Table 2.2, shows the behavior of a wideband channel in terms of the angular spread for a measurement campaign made for France Télécom R&D [20] for a carrier frequency of 2.2 GHz in terms of the angular spread, and the distance between mobile and base.

Table 2.1. Typical values of Delay Spread and Coherence Bandwidth for different outdoors environments [5].

Environment	Delay Spread (us)	B_c (kHz)
Rural	0.2	796
Suburban	0.5	318
Urban	3	53

Table 2.2. Moments for AOA distribution according to the distance from a measurement campaign for outdoors and for a carrier frequency of 2.2 GHz[20].

Distance	0-200 m	200-400 m	400-600 m	600-800 m
Average	20.4°	13.9°	9.7°	7.0°
Std. dev.	8.6°	5.5°	4°	2.5°
Ratio	2.4	2.5	2.4	2.8

Furthermore, in case of indoors some measurements performed on different frequencies show that there is no significant difference in delay spread in the frequency range of 800 MHz to 6GHz. The delay spread is related to the building size, and largest delay spreads up to 270 ns were measured in large buildings such as shopping centers and factories. For most office buildings, the maximum delay spread is in the range of 40 to 70 ns. However larger spreads are possible in larger offices of tens of meters of diameter, or for metal walls [11].

Doppler shift and multipath channel dispersion not only impairs the recovery of the transmitted data at the receiver, but also the accurate positioning as it is commented later.

2.1.3 Fundamentals of Wideband Code Division Multiple Access (WCDMA)

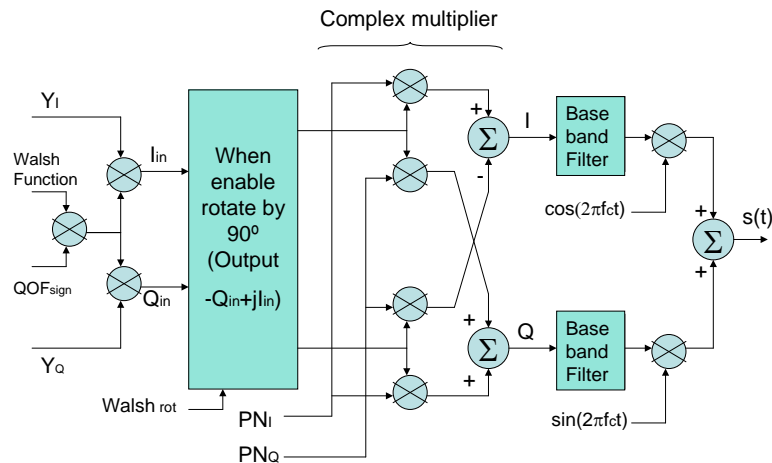
Since Spread Spectrum (SS) uses a larger transmission bandwidth than the modulating signal bandwidth, and therefore it offers opportunities for fading mitigation and protection against jamming and interference, it is not surprising DS-SS is currently in the core of wireless 3G communications systems. Moreover DS-SS provides with means to measure the range between transmitter and receiver. Therefore it is important to provide with fundamentals of Code Division Multiple Access (CDMA) and its relation with subscriber positioning systems.

In fact, CDMA is a scheme by which multiple users are assigned radio resources using Direct Sequence – Spread Spectrum (DS-SS) techniques. All users are transmitting in the same RF band, but each is separated from the others by using orthogonal codes. In case of 3G Wideband CDMA (WCDMA) the final spreading rate corresponds to 3.84 Mcps, and to a RF bandwidth of 5 MHz, where the “chip duration”

corresponds to the clock period of the pseudo-random sequence generator used for spreading signals, and the term “chip” refers to the signal corresponding to an individual term of the random sequence. In general, when all the chips are within a bit interval, we are trying with a short code spreading sequence, and on the contrary, when the spreading sequence is several data bits long, it is a long spreading sequence. The relation between the spreading sequence rate and the symbol data rate is known as the processing gain or the coding gain for DS-SS.

There can be many 5 MHz signals present in the same RF band, and the performance of a CDMA system is interference-limited. It means that the capacity and quality of the systems are limited by the amount of interference power present in the band. Capacity is defined as the total number of simultaneous users the system can support, and quality is related to the probability of bit error, or bit error rate (BER), as a measurement of the perceived condition of the radio link.

Figure 2.7 shows as reference, the scheme for the modulator specified for the Direct Sequence Non-Orthogonal Transmit Diversity (DS Non-OTD) in cdma2000 [23], as well as the corresponding signal mapping.



- Walsh Function = ±1 (Mapping: ‘0’ → +1, ‘1’ → -1)
- QOF_{sign} = ±1 Sign Multiplier QOF Mask (Mapping: ‘0’ → +1, ‘1’ → -1)
- Walsh_{rot} = ‘0’ or ‘1’ 90°-Rotation-Enable Walsh Function
- Walsh_{rot} = ‘0’ means no rotation
- Walsh_{rot} = ‘1’ means rotate by 90°
- The NULL QOF has QOF_{sign} = +1 and Walsh_{rot} = ‘0’
- PN_I and PN_Q = ±1 I-Channel and Q-Channel PN sequences
- QOF (Quasi Orthogonal Function)

Figure 2.7. Spread Spectrum Modulator for the DS Non-OTD Mode of cdma2000 at downlink [23].

From a physical layer perspective, the differences with UTRA-FDD are not really relevant, since many features like Orthogonal Variable Spreading Factors (OVSF)

codes; dedicated control channels in the uplink, common pilot channel in the downlink; packet access; fast power control, among others are shared with UTRA-FDD [24].

Figure 2.7 also helps to identify the common elements to all spread spectrum modulators. Firstly, the channelization codes which are orthogonal functions or quasi-orthogonal functions used to differentiate channels received from the same user; and secondly, the scrambling code or the pseudo random sequences required for separating terminals or base stations from each other. For the case used as example, the first group corresponds to Walsh Functions, while for the Universal Terrestrial Radio Access (UTRA) WCDMA they correspond to Orthogonal Variable Spreading Factors (OVSF) [25]. It must be mentioned that after applying spreading sequences, neither channelization neither scrambling codes provide further spreading.

In fact, the DS-SS signal may be expressed as in (2.7):

$$x(t) = s(t) \sum_{m=0}^{N_c-1} g_p(t-mT) p(m) \quad (2.7)$$

$$s(t) = s(kT_s) = s_k \quad \text{for } kT_s \leq t \leq (k+1)T_s$$

Where s_k refers to the data symbol, $g_p(t)$ to the pulse shape, $p(m)$ to the pseudo-noise spreading sequence, N_c to the number of chips within the sequence, T to the chip time interval, and T_s to the symbol time.

Signal at the receiver $y(t)$, suffers from multipath propagation, and it is also infected with noise as it is shown in (2.8):

$$y(t) = \sum_i^{N_p} \gamma_i x(t - \tau_i) + n(t) = \sum_i^{N_p} \gamma_i s(t - kT_s - \tau_i) \sum_m^{N_p} g_p(t - \tau_i - mT) p(m) + n(t) \quad (2.8)$$

Where, N_p refers to the number of paths, and γ_i and τ_i respectively to the corresponding path gain and delay introduced by the channel due to propagation. This signal is matched filtered to the pulse shape, and is sampled at the chip time as it is shown in (2.9):

$$z(n) = z[t = (n+1)T] = \int_{-\infty}^{\infty} y(\lambda) h(t - \lambda) d\lambda \quad (2.9)$$

with $h(t) = g_p^*(T - t)$

Therefore, the samples $z(n)$ takes the form in (2.10) when (2.8) is introduced at (2.9):

$$z(n) \cong \sum_i^{N_p} \gamma_i s(kT_s - \tau_i) f(\tau_i) p(n) + w(n) \quad (2.10)$$

Where $f(\tau_i)$ refers to the integration of the pulse shape in (2.11), and results in a number between 0 and 1 as it is shown in (2.12), whilst $w(n)$ refers to the filtered noise.

$$f(\tau_i) = \int_{-\infty}^{\infty} g_p(\lambda - \tau_i) g_p^*(\lambda) d\lambda \quad (2.11)$$

$$f(\tau_i) = \begin{cases} 1 & \text{for } \tau_i = 0 \\ 0 & \text{when } \tau_i = nT; n \neq 0 \end{cases} \quad (2.12)$$

$$|f(\tau_i)| \in [0, 1]$$

Sequence $z(n)$ is eventually dispread by applying the pseudo-noise sequence as it is shown in (2.13) to estimate the transmitted symbol, being w_k defined in (2.14).

$$\hat{s}_k = \frac{1}{N_c} \sum_n^{N_p} z(n) p^*(n) = \sum_i^{N_p} \gamma_i s(kT_s - \tau_i) f(\tau_i) + w_k \quad (2.13)$$

$$w_k = \frac{1}{N_c} \sum_n^{N_c} w(n) p^*(n) \quad (2.14)$$

Expression (2.13) shows that the dispread signal contains information not just about the transmitted symbol but also about the traveling time between emitter and receiver for each path. When path delays in (2.13) are separated beyond the chip time T , and one of the delays is selected as the first, estimated symbol is a scaled version of the original one plus some noise, but when several paths are present within the chip time, interference appears, and both symbol and timing information degrades. Furthermore, the first arrival may be strongly degraded due to NLOS, and the achieved delay information could be even biased beyond the chip time.

2.2 Positioning Technologies: A Subscriber Location Overview

Some technologies have emerged for accurate location determination of mobile subscribers based on transmitted signals. These methods may be grouped based on where the measurements for positioning are made within the system. Therefore, Location Determination Technologies (LDT) are classified in mobile station based methods, when measurements are collected exclusively by the mobile unit, network based methods, when measurements are only performed for the base stations (BS), and hybrid methods when radiolocation signals are performed at both the mobile station (MS) and the BS. When the location solution is independent of the underlying network type, it is a U-plane Locations Service (LCS) solution, and Open Mobile Alliance (OMA) has specified the Secure User Plane Location (SUPL) protocol based on IP tunnels to provide information required by the SUPL Positioning Center (SPC) and the SUPL Location Centre (SLC). The first is related to the position enabling technology and the latter is responsible of the location services. On the other hand, when the location solution is dependent of the underlying network type, it is a C-plane LCS solution. The Standalone Serving Mobile Location Center (SAS) is the key functional resource to support LCS in the Universal Mobile Telecommunication System (UMTS) C-Plane. It manages the overall co-ordination and scheduling of resources required for the subscriber location, and it also estimates its position and the achieved accuracy [26]. Moreover, the LDT used along this research belong to the two types discussed above:

mobile station based methods and network based methods. The location is also dependent of the underlying network type.

MS based methods may be classified as those which use just wireless system signals, those which use just Global Navigation Satellite Systems (GNSS) signals, and finally, those using both GNSS and wireless system signals [27]-[29] to perform positioning. Mobile stations detect and process signals arriving from various emitters when any of these methods is used. Furthermore, even when mobile stations incorporate a GNSS/GPS receiver, they will have problems to determine their locations in shadowed areas such as indoors and buildings, and will also suffer of the same problems of high power consumption associated with these systems. Therefore, taking advantage of the wireless network to achieve the subscriber positioning is an important alternative.

Subscriber location technologies that use only the wireless network signals are of interest for this research, and they will be commented in section 2.2.1. These technologies use signal strength, timing, and angular information measurements to achieve the positioning. These technologies include Cell Identification (CID), Enhanced Cell ID (E-CID), Time Of Arrival (TOA), Time Differences Of Arrival (TDOA), Observed Time Difference Of Arrival (OTDOA), Time Advance (TA), Angle Of Arrival (AOA), Received Signal Strength Indicator (RSSI) and Reference Signal Received Power (RSRP) based positioning. Let us briefly describe them.

CID technique estimates subscriber position with the knowledge of its serving Node B (eNode B) and cell, and its accuracy depends on the cell size; therefore, a poor accuracy is achieved for large cells when this method is used. E-CID refers to positioning techniques which use additional User Equipment (UE) and/or network radio resources and other measurements to improve the UE location estimate of CID. These additional measurements include carrier RSSI, RSRP both measured at the UE, and Round Trip Time (RTT), TA and AOA which are measured at the network. Moreover, RSSI, RSRP, RTT and TA provide a range around the BS within the subscriber is located, whilst AOA provides with an angular sector instead.

On the other hand, time-based positioning systems include TOA, TDOA and OTDOA techniques. TOAs of signal transmitted by the MS are measured at multiple BSs, and distances between the subscriber and these BSs are estimated. The subscriber position corresponds to the intersection of the loci of the circumferences centered at the BSs with the estimated radiuses. TDOA and OTDOA use the measurements of the time difference of arrival from signals taken from multiple BSs. Whilst TDOA is a more general term that may be tracked even up to the 2G wireless systems, OTDOA was first standardized in 3GPP Release 9 for UMTS, and it is currently part of 3GPP LTE, as well as of OMA [30]. OTDOA is a downlink positioning method in which the UE measures the TOA of signals received from multiple BSs. Eventually, the TOAs from several neighbor BSs are subtracted from the TOA of a BS taken as the reference to form the OTDOA measures. Although OTDOA refers to the downlink, some literature prefers the use of DL-OTDOA for referring to this method. On the other hand, when TDOA measures are taken at the network, the method is known as UL-TDOA or more recently simply by UTDOA [31]. The BSs have to be time synchronized in order to

support the required precision in the measurements when these latter techniques are used [26][32][33]. The accuracy of these techniques may be degraded due to multipath and shadowing, as it was shown before. It is especially relevant the case of NLOS condition, which will be treated in detail in section 2.2.4.

LDT may be evaluated in terms of accuracy, latency, capacity, reliability and the impact of these technologies on the wireless network [27]. The accuracy is a measure of how close the location estimation is to the true location of the mobile station, and it is the only criteria explicitly stated by the E911-FCC ruling. It may be presented graphically as a probability density function or a cumulative distribution function for the individual test scenarios. Latency is the time needed from the instant of mobile station call origination to the instant the location report is sent. This criterion is very important since many technologies use post-processing to improve their accuracy, increasing their latency figures. Capacity is defined as the maximum number of independent, simultaneous location determinations the technology can sustain for a given wireless system load. Capacity may affect the accuracy, and indeed a large capacity for all different network loads is desirable. Reliability is a measure of the LDT coverage for a specific LBS, and corresponds for instance to the rate between the E911 calls that result in a location report and the whole number of E911 calls. And finally, the impact on the wireless network concerns to changes or adjustments made in network configuration, software, and equipment due to the implementation of a given LDT. Information relative to this latter topic may be found in [34].

2.2.1 Positioning Principles

Torrieri [35] establishes the statistical principles for passive location systems, and generalizes this problem assuming that the measurement vector \mathbf{m} is a function of the position vector \mathbf{x} , plus additive noise \mathbf{n} , as in (2.15):

$$\mathbf{m} = \mathbf{f}(\mathbf{x}) + \mathbf{n} \quad (2.15)$$

Where \mathbf{m} , \mathbf{n} , are the vectors in (2.16), and $\mathbf{f}(\mathbf{x})$ is also a vector function with L elements corresponding to the available measures involved in positioning.

$$\mathbf{m} = [m_1, m_2, \dots, m_L]^T; \quad \mathbf{n} = [n_1, n_2, \dots, n_L]^T \quad (2.16)$$

The nature of $\mathbf{f}(\mathbf{x})$ depends on the type of measurements used, and in the case of range-based methods such as TOA, TDOA, DOA, and RSSI, it is a nonlinear function related to the range among the subscriber position and those BS's participating in the positioning. The expressions for TOA, TDOA and RSSI measurements correspond respectively to (2.17), (2.18) and (2.19) for the two dimensional case;

$$f_{TOA_i}(\mathbf{x}) = \sqrt{(x - x_i)^2 + (y - y_i)^2}; \quad \forall i = 1, 2, \dots, L \quad (2.17)$$

$$f_{TDOA_{i-1}}(\mathbf{x}) = \sqrt{(x - x_i)^2 + (y - y_i)^2} - \sqrt{(x - x_1)^2 + (y - y_1)^2}; \quad \forall i = 2, 3, \dots, L \quad (2.18)$$

$$f_{RSS_i}(\mathbf{x}) = -\beta \ln \left(\sqrt{(x-x_i)^2 + (y-y_i)^2} \right); \quad \forall i = 1, 2, \dots, L \quad (2.19)$$

Where L refers to the number of BSs, $\mathbf{x}=(x,y)$ to the true coordinates of the subscriber position, $\mathbf{r}_i=(x_i,y_i)$ denotes to the position of BS _{i} used as reference, and β is related to the path loss coefficient β' in the signal propagation model, since the received power is proportional to $\|\mathbf{x}-\mathbf{x}_i\|^{-\beta'}$ [36][37]. These expressions may be easily extended to the three-dimensional case by adding a new coordinate for the z axis, but the analysis will remain in 2 dimensions without missing of generality.

Further, when a DOA positioning technique is used, $\mathbf{f}(\mathbf{x})$ is also nonlinear, and each one of their elements f_{DOA_i} takes the form:

$$f_{DOA_i}(\mathbf{x}) = \tan^{-1} \left(\frac{y-y_i}{x-x_i} \right); \quad \forall i = 1, 2, \dots, L \quad (2.20)$$

2.2.1.1 Nonlinear solutions of the Positioning Equation

The solution for \mathbf{x} can be obtained from different criteria: using maximum likelihood (ML), nonlinear least squares (NLS) or the weighted nonlinear squares (WNLS) approach. In case of ML, the solution is estimated as the position vector \mathbf{x} , which maximizes the log-likelihood of the measurements $\ln[p(\mathbf{m})]$, where $p(\mathbf{m})$ refers to the probability density function (PDF) of the measurement noise. On the other hand, the WNLS solution requires minimization of the cost function in (2.21),

$$\hat{\mathbf{x}} = \underset{\mathbf{x}}{\operatorname{argmin}} J_{WNLS}(\mathbf{x}) \quad (2.21)$$

Where the actual function J_{WNLS} depends of the type of measurements employed and its general form is

$$J_{WNLS}(\mathbf{x}) = [\mathbf{m} - \mathbf{f}(\mathbf{x})]^T \mathbf{C}_n^{-1} [\mathbf{m} - \mathbf{f}(\mathbf{x})] \quad (2.22)$$

with $\mathbf{C}_n = E\{\mathbf{nn}^T\}$

Furthermore, the cost function J_{NLS} for NLS is exhibited in (2.23) where L refers to the number of BSs involved in the positioning computation.

$$J_{NLS}(\mathbf{x}) = \sum_{i=1}^L [m_i - f_i(\mathbf{x})]^2 = [\mathbf{m} - \mathbf{f}(\mathbf{x})]^T [\mathbf{m} - \mathbf{f}(\mathbf{x})] \quad (2.23)$$

Obtaining a ML solution for this estimation problem requires noise statistics, and when the measurement noise \mathbf{n} in (2.15) is zero-mean and Gaussian distributed with covariance matrix \mathbf{C}_n , its PDF $p(\mathbf{m})$ takes the form

$$p(\mathbf{m}) = \frac{(2\pi)^{-L/2}}{|\mathbf{C}_n|^{1/2}} \exp \left[-\frac{1}{2} (\mathbf{m} - \mathbf{f}(\mathbf{x}))^T \mathbf{C}_n^{-1} (\mathbf{m} - \mathbf{f}(\mathbf{x})) \right] \quad (2.24)$$

$\mathbf{C}_n = E\{\mathbf{nn}^T\}$

And therefore, ML problem reduces to the WNLS solution, and finally to NLS when measurement noise samples are statistically independent and identically distributed since in this case $\mathbf{C}_n = \sigma_n^2 \mathbf{I}$. The ML approach requires a high complexity when grid search is adopted, and therefore global solution is only guaranteed within the grid, but in general its accuracy is the highest, especially when \mathbf{C}_n is also a function of subscriber position because if it is the case, the cost function includes the term $\ln[\det(\mathbf{C}_n)]$ that avoids selecting positions with large uncertainty [38]. On the other hand, NLS does not require noise statistics but also involves the same issues as ML [37].

The vector function $\mathbf{f}(\mathbf{x})$ in (2.15), which relates the position \mathbf{x} , to the measurement space \mathbf{m} is nonlinear in general, but it becomes linear if approximated through a Taylor series expansion around the point \mathbf{x}_0 , as it is shown in (2.25), where \mathbf{G} is the Jacobian matrix for $\mathbf{f}(\mathbf{x})$ and it contains the set of derivatives evaluated in \mathbf{x}_0 , for the L measurements and n coordinates.

$$\mathbf{f}(\mathbf{x}) \approx \mathbf{f}(\mathbf{x}_0) + \mathbf{G}(\mathbf{x} - \mathbf{x}_0) \quad (2.25)$$

Assuming a zero mean Gaussian distribution for the noise vector \mathbf{n} , the linearized least squares position estimator proposed by Torrieri [35][38] is expressed as in (2.26):

$$\hat{\mathbf{x}} = \mathbf{x}_0 + (\mathbf{G}^T \mathbf{C}_n^{-1} \mathbf{G})^{-1} \mathbf{G}^T \mathbf{C}_n^{-1} [\mathbf{m} - \mathbf{f}(\mathbf{x}_0)] \quad (2.26)$$

Being \mathbf{C}_n the noise covariance matrix, and \mathbf{G} the Jacobian matrix of $\mathbf{f}(\mathbf{x})$ evaluated in a point near to the position to estimate \mathbf{x}_0 , as it is shown in (2.27):

$$\mathbf{G} = \left. \begin{array}{cc} \frac{\partial f_1(\mathbf{x})}{\partial x} & \frac{\partial f_1(\mathbf{x})}{\partial y} \\ \frac{\partial f_2(\mathbf{x})}{\partial x} & \frac{\partial f_2(\mathbf{x})}{\partial y} \\ \vdots & \vdots \\ \frac{\partial f_L(\mathbf{x})}{\partial x} & \frac{\partial f_L(\mathbf{x})}{\partial y} \end{array} \right|_{\mathbf{x}=\mathbf{x}_0} \quad (2.27)$$

This estimator is affected by the linearization error and the noise, and it is unbiased only when $\mathbf{f}(\mathbf{x})$ is linear and $E[\mathbf{n}] = \mathbf{0}$.

The operative form of \mathbf{G} in (2.27) depends on the kind of measurements used for the positioning. In case of a TDOA scheme for example, the derivatives are taken from (2.18), \mathbf{G} becomes \mathbf{G}_{TDOA} and takes the form in (2.28):

$$\mathbf{G}_{TDOA} = \frac{1}{2} \begin{bmatrix} \frac{x-x_2}{f_{TOA_2}(\mathbf{x})} - \frac{x-x_1}{f_{TOA_1}(\mathbf{x})} & \frac{y-y_2}{f_{TOA_2}(\mathbf{x})} - \frac{y-y_1}{f_{TOA_1}(\mathbf{x})} \\ \frac{x-x_3}{f_{TOA_3}(\mathbf{x})} - \frac{x-x_1}{f_{TOA_1}(\mathbf{x})} & \frac{y-y_3}{f_{TOA_3}(\mathbf{x})} - \frac{y-y_1}{f_{TOA_1}(\mathbf{x})} \\ \vdots & \vdots \\ \frac{x-x_L}{f_{TOA_L}(\mathbf{x})} - \frac{x-x_1}{f_{TOA_1}(\mathbf{x})} & \frac{y-y_L}{f_{TOA_L}(\mathbf{x})} - \frac{y-y_1}{f_{TOA_1}(\mathbf{x})} \end{bmatrix} \quad (2.28)$$

Where $f_{TOA_i}(\mathbf{x})$ for $i=1,2, \dots, L$ refers to (2.17) as it may be easily verified performing the derivative procedure. The appearing of two subtracted terms for each element within \mathbf{G}_{TDOA} reflects the structure of TDOA measures conceived as the difference of two TOA measures.

Torrieri solution in (2.26) uses the iterative Gauss-Newton method for reaching the cost function minimum, but others methods such as Newton-Raphson or Steepest Descent may be used instead. Simulations exhibited in [37] show that Gauss-Newton and Newton-Raphson methods converge very quickly, but Newton-Raphson requires the computation of a Hessian matrix and a gradient vector at each iteration, and therefore is significantly more complex. Therefore, another option is the use of the steepest descent method, which may be considered as an approximation of Newton-Raphson that assumes the Hessian matrix as being the identity, but that converges much more slowly.

The iterative expression for the Gauss-Newton method is described in (2.29):

$$\hat{\mathbf{x}}^{k+1} = \hat{\mathbf{x}}^k + \left[\left(\mathbf{G}^T \mathbf{G}^{-1} \right) \mathbf{G}^T \right]_{\hat{\mathbf{x}}^k} (\mathbf{m} - \mathbf{f}(\hat{\mathbf{x}}^k)) \quad (2.29)$$

The corresponding expression for Newton-Raphson method is exhibited in (2.30):

$$\hat{\mathbf{x}}^{k+1} = \hat{\mathbf{x}}^k - \mathbf{H}^{-1} \left(J(\hat{\mathbf{x}}^k) \right) \nabla J(\hat{\mathbf{x}}^k) \quad (2.30)$$

Where the Hessian matrix $\mathbf{H}(J(\mathbf{x}))$ is computed as in (2.31):

$$\mathbf{H}(J(\mathbf{x})) = \frac{\partial^2 J(\mathbf{x})}{\partial \mathbf{x} \partial \mathbf{x}^T} = \begin{bmatrix} \frac{\partial^2 J(\mathbf{x})}{\partial x^2} & \frac{\partial^2 J(\mathbf{x})}{\partial x \partial y} \\ \frac{\partial^2 J(\mathbf{x})}{\partial y \partial x} & \frac{\partial^2 J(\mathbf{x})}{\partial y^2} \end{bmatrix} \quad (2.31)$$

The iterative expression for the Steepest Descent method is shown in (2.32):

$$\hat{\mathbf{x}}^{k+1} = \hat{\mathbf{x}}^k - \mu \nabla J(\hat{\mathbf{x}}^k) \quad (2.32)$$

Being μ is a positive constant that controls the convergence rate and stability; and the gradient vector is described in (2.33):

$$\nabla J(\mathbf{x}) = \begin{bmatrix} \frac{\partial J(\mathbf{x})}{\partial x} \\ \frac{\partial J(\mathbf{x})}{\partial y} \end{bmatrix} \quad (2.33)$$

Moreover, the cost function $J(\mathbf{x})$ is chosen as (2.22) or (2.23) in relation with the selected approach. Note also that the noise covariance \mathbf{C}_n may be reasonably considered as diagonal for TOA, RSS and DOA based enabling positioning technologies, but not for TDOA since in this latter case all the measurements are taken in relation to a BS taken as reference [37].

2.2.1.2 Linear Solutions of the Positioning Equation Principles

In addition to the nonlinear approaches commented above, it is also possible to convert the nonlinear formulation in (2.15) into a set of linear equations with the form in (2.34) after performing some algebraic manipulations under the assumption that measurements errors are small enough.

$$\mathbf{Ax} = \mathbf{b} \quad (2.34)$$

The actual form of matrix \mathbf{A} and vector \mathbf{b} depends on the kind of measurements chosen by the enabling technology. Linear procedures include to linear least squares (LLS), weighted LLS (WLLS) and the subspace estimators [37]. LLS and WLLS are the linear counterparts of NLS and WNLS respectively.

For example, if it is assumed that the position of the nearest BS to the mobile unit, which it is usually the service BS that provides network access and resources to the subscriber is located at the coordinates origin (0,0), and also that a TOA based positioning is performed; by squaring these measures and subtracting them from those referred to the service BS, it is easy to show as (2.15) becomes (2.34). \mathbf{A} becomes \mathbf{A}_{TOA} and includes the positions of BSs involved in positioning, and \mathbf{b} turns into \mathbf{b}_{TOA} and includes some metrics related with the measurements [37][39], as it is shown in (2.35),

$$\mathbf{A}_{TOA} = \begin{bmatrix} x_2 & y_2 \\ x_3 & y_3 \\ \vdots & \vdots \\ x_L & y_L \end{bmatrix} \quad \mathbf{b}_{TOA} = \frac{1}{2} \begin{bmatrix} r_2^2 - m_2^2 + m_1^2 \\ r_3^2 - m_3^2 + m_1^2 \\ \vdots \\ r_L^2 - m_L^2 + m_1^2 \end{bmatrix}$$

$$\text{with } r_i^2 = x_i^2 + y_i^2 \quad \forall i = 1, 2, \dots, L \quad (2.35)$$

$$\text{and } m_i = c\tau_i \quad \forall i = 1, 2, \dots, L$$

Where, time measures τ_i are transformed into range measurements through the light speed factor c , and the coordinates of service BS (x_1, y_1) do not appear due to their null value.

The corresponding forms of \mathbf{A} and \mathbf{b} for TDOA, RSS and DOA based positioning are exhibited within (2.36) through (2.39), being r the distance between the subscriber and its service BS, as it is shown in (2.37).

$$\mathbf{A}_{TDOA} = \mathbf{A}_{TOA}$$

$$\mathbf{b}_{TDOA} = -r \begin{bmatrix} m_2 \\ m_3 \\ \vdots \\ m_L \end{bmatrix} + \frac{1}{2} \begin{bmatrix} r_2^2 - m_2^2 \\ r_3^2 - m_3^2 \\ \vdots \\ r_L^2 - m_L^2 \end{bmatrix} \quad (2.36)$$

$$\text{with } m_i = c\tau_{i,1}; \quad \forall i = 2, 3, \dots, L$$

$$r^2 = x^2 + y^2 \quad (2.37)$$

$$\mathbf{A}_{RSS} = \begin{bmatrix} x_2 & y_2 \\ x_3 & y_3 \\ \vdots & \vdots \\ x_L & y_L \end{bmatrix}; \quad \mathbf{b}_{RSS} = -5r \begin{bmatrix} r_2 \\ r_3 \\ \vdots \\ r_L \end{bmatrix} + \begin{bmatrix} r_2^2 \left[-\frac{1}{\beta}(m_1 - m_2) + 1 + \ln(5) \right] \\ r_3^2 \left[-\frac{1}{\beta}(m_1 - m_3) + 1 + \ln(5) \right] \\ \vdots \\ r_L^2 \left[-\frac{1}{\beta}(m_1 - m_L) + 1 + \ln(5) \right] \end{bmatrix} \quad (2.38)$$

$$\text{with } m_i = RSS_i \quad \forall i = 1, 2, \dots, L$$

$$\mathbf{A}_{AOA} = \begin{bmatrix} \sin(m_1) & -\cos(m_1) \\ \sin(m_2) & -\cos(m_2) \\ \vdots & \vdots \\ \sin(m_L) & -\cos(m_L) \end{bmatrix}; \quad \mathbf{b}_{AOA} = \begin{bmatrix} \sin(m_1)x_1 - \cos(m_1)y_1 \\ \sin(m_2)x_2 - \cos(m_2)y_2 \\ \vdots \\ \sin(m_L)x_L - \cos(m_L)y_L \end{bmatrix} \quad (2.39)$$

$$\text{with } m_i = DOA_i$$

Furthermore, since measures in (2.15) include errors due to noise and signal propagation, (2.34) turns into (2.40):

$$\mathbf{e} = \mathbf{Ax} - \mathbf{b} \quad (2.40)$$

Where \mathbf{e} includes the discrepancies introduced at the model during the linearization procedure. In fact, these errors depend not just from noise \mathbf{n} , but also of the true values of the set of measures. From the expression above, the subscriber position \mathbf{x} may be estimated using a simple LS technique, or a more refined WLS method.

The LS approach requires minimizing the mean error power in (2.41):

$$J_{LLS} = E \{ \mathbf{e}^T \mathbf{e} \} = E \{ (\mathbf{Ax} - \mathbf{b})^T (\mathbf{Ax} - \mathbf{b}) \}$$

$$= E \{ \mathbf{x}^T \mathbf{A}^T \mathbf{Ax} - \mathbf{x} \mathbf{A}^T \mathbf{b} - \mathbf{b}^T \mathbf{Ax} + \mathbf{b}^T \mathbf{b} \} \quad (2.41)$$

Resulting in the expression in (2.42)

$$\nabla_{\mathbf{x}^T} J_{LLS} = \mathbf{0} = \mathbf{A}^T \mathbf{A} \hat{\mathbf{x}} - \mathbf{A}^T \mathbf{b} \rightarrow \hat{\mathbf{x}} = (\mathbf{A}^T \mathbf{A})^{-1} \mathbf{A}^T \mathbf{b} \quad (2.42)$$

On the other side, the WLLS approach emerges from including a weighting matrix \mathbf{W} , within the cost function in (2.41) as it is shown in (2.43):

$$J_{WLLS} = E \left\{ (\mathbf{A}\mathbf{x} - \mathbf{b})^T \mathbf{W} (\mathbf{A}\mathbf{x} - \mathbf{b}) \right\} \quad (2.43)$$

Where, this assessment matrix \mathbf{W} is precisely the inverse of the covariance noise matrix. Therefore, after cost function minimization, the WLLS estimator is achieved in(2.44):

$$\nabla_{\mathbf{x}^T} J_{WLLS} = \mathbf{0} = \mathbf{A}^T \mathbf{W} \mathbf{A} \hat{\mathbf{x}} - \mathbf{A}^T \mathbf{W} \mathbf{b} \rightarrow \hat{\mathbf{x}} = (\mathbf{A}^T \mathbf{W} \mathbf{A})^{-1} \mathbf{A}^T \mathbf{W} \mathbf{b} \quad (2.44)$$

Note as in case of TDOA and RSS based positioning, the LLS procedure leads to an intermediate result which replaced within (2.37) becomes a quadratic equation in r . Hence, by taking the positive root solution back to (2.42) for the corresponding term \mathbf{b} , the final result is achieved [39]. It is worth to note as these two linear methods are quite simpler and reduce considerably the computational burden respect to the nonlinear approaches commented in the section above. However, since LLS techniques dismiss the noise statistics, they will achieve their most performance in case of low noise patterns. Particularly, LLS-RSS in (2.38) is adequate for mobile station positions near to the serving BS due to restrictions introduced within the linearization process as it is shown in annex A2.1; it means positions within 20%-60% of the cell radius closest to the serving BS. A more general LLS-RSS estimator is also possible assuming Gaussian noise of known variance, and performing an exponential transform from the RSSI measures to have a problem structure more alike to TOA. This procedure is described in more detail within [37].

The particular weighting matrix \mathbf{W} required in (2.44) depends on the type of measurements, and it is usually dependent of the distances between subscriber and BSs due to transformations performed during formulation of the linear system. In case of Gaussian measurement noise, these WLS solutions are also the ML solutions. Therefore, WLS approaches are in general much better than LLS methods, and their computational load is not really much heavier. The form of these matrices for positioning technologies based on TOA, TDOA and DOA are respectively exhibited in (2.45), (2.46), and (2.47) [37].

$$\mathbf{W}_{TOA} = \left[E \{ \mathbf{e} \mathbf{e}^T \} \right]^{-1} = \frac{1}{4} \text{diag} \left(\frac{1}{\sigma_{TOA,2}^2 d_2^2}, \frac{1}{\sigma_{TOA,3}^2 d_3^2}, \dots, \frac{1}{\sigma_{TOA,L}^2 d_L^2} \right); \quad (2.45)$$

$$\text{with } d_i^2 = \|\mathbf{x} - \vec{\mathbf{r}}_i\|^2; \quad \forall i = 2, 3, \dots, L$$

$$\mathbf{W}_{TDOA} = \left[4 \text{diag}(d_2, d_3, \dots, d_L) \mathbf{C}_{n,TDOA} \text{diag}(d_2, d_3, \dots, d_L) \right]^{-1};$$

with $d_i = \|\mathbf{x} - \vec{\mathbf{r}}_i\|$; $\forall i = 2, 3, \dots, L$ (2.46)

where $\mathbf{C}_{n,TDOA} = E\{\mathbf{nn}^T\}$

$$\mathbf{W}_{DOA} = \text{diag} \left(\frac{1}{\sigma_{DOA,1}^2 d_1^2}, \frac{1}{\sigma_{DOA,2}^2 d_2^2}, \dots, \frac{1}{\sigma_{DOA,L}^2 d_L^2} \right)$$

with $d_i^2 = \|\mathbf{x} - \vec{\mathbf{r}}_i\|^2$; $\forall i = 1, 2, \dots, L$ (2.47)

It must be noted that the weighting matrix requires the knowledge of distances between subscriber and BSs. In case of a TOA based positioning scheme, this set of distances may be efficiently replaced for the set of measurements m_i , but in case of TDOA or AOA, a LLS procedure should be firstly performed to estimate subscriber position to properly figure out the distances required within \mathbf{W} , and a second step is also required to achieve the refined WLLS position estimation. Furthermore, an iterative process may be performed in order to minimize the function cost in (2.43) and achieve the maximum accuracy, and consequently the Best Linear Unbiased Estimator (BLUE) algorithm, but in general a two-step LS algorithm is adequate [37][40]. Alternative formulations for the positioning problem are possible, but accuracy gains are not important [41].

Finally, subspace-based methods, also known as multidimensional scaling (MDS) –based methods [37][42] provide a computationally simple localization solution, robust even for large measurement noise. This approach trust on the construction of an adequate function related to the available measurements and to the subscriber position to fill a multidimensional similarity matrix \mathbf{D} as in (2.48):

$$\mathbf{D} = \mathbf{X}\mathbf{X}^T \quad (2.48)$$

Where \mathbf{X} relates the positions of the known BSs \mathbf{r}_i and that of the subscriber \mathbf{x} , and takes the form in (2.49) in case of TOA-based positioning:

$$[\mathbf{X}]_i = \mathbf{r}_i^T - \mathbf{x}^T; \quad \forall i = 1, 2, \dots, L \quad (2.49)$$

By inserting (2.49) into (2.48), it is easy to show as the similarity matrix \mathbf{D} becomes (2.50), where $\|\cdot\|$ denotes the Euclidian norm of the vector:

$$[\mathbf{D}]_{i,j} = \frac{1}{2} \left(d_i^2 + d_j^2 - \|\mathbf{r}_i - \mathbf{r}_j\|^2 \right) \quad (2.50)$$

with $d_i^2 = \|\mathbf{r}_i - \mathbf{x}\|^2$

Furthermore, since the elements of this matrix depend on the unknown distances between subscriber and each BS, these values are estimated by scaling the TOA measures using light speed, and therefore expression (2.50) becomes as in (2.51):

$$[\mathbf{D}]_{i,j} = \frac{1}{2} \left(m_i^2 + m_j^2 - \|\mathbf{r}_i - \mathbf{r}_j\|^2 \right); \quad \forall i, j = 1, 2, \dots, L \quad (2.51)$$

The similarity matrix is factorized using Eigen-Value Decomposition (EVD), and since the rank of this matrix is known, it may be rewritten in terms of just signal eigenvectors and eigenvalues as it is shown in (2.52):

$$\mathbf{D} = \mathbf{U}\mathbf{\Lambda}\mathbf{U}^T = \mathbf{U}_s\mathbf{\Lambda}_s\mathbf{U}_s^T \quad (2.52)$$

with $\mathbf{U}_s = [\mathbf{u}_1, \mathbf{u}_2]$

Where \mathbf{U} is an orthonormal matrix whose columns contain the eigenvectors associated with the eigenvalues contained in the diagonal matrix $\mathbf{\Lambda}$, and where \mathbf{U}_s and $\mathbf{\Lambda}_s$ refer to corresponding matrices related just to signal subspace. Indeed, $\mathbf{\Lambda}_s$ is a diagonal matrix of dimension 2 for the two dimensional positioning case, as it is easily seen from inspection of expressions (2.48) and (2.49). The idea behind subspace methods is to perform a position estimator with the knowledge of the noise subspace since $\mathbf{U}_s\mathbf{U}_s^T = \mathbf{I} - \mathbf{U}_n\mathbf{U}_n^T$, and the position is eventually estimated from the expression within (2.53) where $\mathbf{1}$ is an all-ones vector [37].

$$\hat{\mathbf{x}} = \frac{\mathbf{Y}^T \mathbf{U}_n \mathbf{U}_n^T \mathbf{1}}{\mathbf{1}^T \mathbf{U}_n \mathbf{U}_n^T \mathbf{1}}; \quad \text{with } \mathbf{Y} = [\mathbf{r}_1, \mathbf{r}_2, \dots, \mathbf{r}_L]^T \quad (2.53)$$

$$\text{and } \mathbf{U}_n = [\mathbf{u}_3, \mathbf{u}_4, \dots, \mathbf{u}_L]$$

The MDS procedure may be also applied to TDOA-based positioning [42], but in this case a complex space is used since that an extra pure imaginary dimension for the subscriber range respect to the reference BS has to be included in order to construct the similarity matrix. Moreover, in this case the procedure requires two or three iterations to achieve the desired positioning. Results in [42] also show that this method is robust to large measurement noise, since the dimension knowledge and the Eigen-structure information of the similarity matrix are exploited.

Whichever is the positioning technique employed, it should be kept in mind that every set of measurements performed by a sensor reduces the positioning to a region shaped in a way related to the nature of the measurements. Therefore, positioning systems may also be classified as circular-circular systems, hyperbolic-hyperbolic systems, angular-angular systems and angular-circular systems.

Circular-circular systems result from measurement sets where data is related to the distance between emitter and receiver, such as the case of signal Time Of Arrival. The name of circular refers to the fact that in absence of perturbations or noise, TOA measurements are related to the distance between transmitter and emitter through the signal propagation speed, and therefore the positioning locus is a circumference centered at the receiver, and with a radius equal to this distance, as it is easily shown in (2.17). At least three stations are required for positioning systems of this kind in order to remove the sign ambiguity for 2D positioning and one more in case of 3D positioning.

Hyperbolic-hyperbolic systems result from measurements such as the Time Difference Of Arrival (TDOA). System equation is formed using a station as a reference point, and making the differences respect to it as it is shown in (2.18). The focuses of the hyperbolic loci correspond to the stations. At least four stations are required for a 2D TDOA based system.

On the other hand, Angular-angular systems use exclusively measurements associated with signal bearing, as it is exhibited in (2.20), but their performance is poor

when it is compared to TOA or TDOA based positioning methods, as it is shown from simulations using a GBSB scattering model. These simulations show that TOA approach outperforms AOA method by around 100 m in absolute position error when three BS are used for location [32]. Furthermore, an angular-circular systems result from measurements related to the signal bearing and the distance between transmitter and receiver. It is a hybrid system since it uses different nature measurements. A system which uses Angle Of Arrival besides TOA information owns to this category. Subscriber positioning in this case, is possible by using just one BS equipped with an antenna array, but the resulting accuracy is poor when compared to TOA, TDOA or even AOA based positioning systems due to limitations in the array resolution and to the accuracy degradation when the subscriber departs from the BS. In effect, AOA estimation does require a very precise calibration of the antenna array at the base station.

However, it must be noted that hybrid techniques [43]-[46] exhibit a better behavior than homogeneous ones since it is a well-known principle that errors achieved from a particular positioning technique may be overcome with the application of another one. In fact, different techniques lead to different systematic errors, and therefore combining techniques may result in partial compensation and possible smaller overall errors than either technique applied separately. For example, [44] studies a hybrid TOA-TDOA method and notes that especially outside the central coverage the uncertainty region shapes associated with these two techniques are not just different but complementary. It means that uncertainty provided by TDOA is high where TOA technique provides low uncertainty and vice versa; and simulations, in fact, support the premise that positioning error reduces when this hybrid technique is applied. It must be noted however that the advantages provided by this method may be reduced when TOA and TDOA measurements are correlated. Furthermore, some simulations also show as the use of an AOA-TOA-TDOA based positioning procedure achieves a positioning error below 30m in the 90% of the cases, in comparison with the more than 150 m achieved by the simpler TOA-based technique in the same conditions [43]. Furthermore, the use of Best Linear Unbiased Estimators (BLUE) both for homogeneous and hybrid approaches and the accuracy limits on positioning for UMTS is studied in [47], and this work confirms that better accuracies are achieved by hybrid techniques such as TOA-TDOA or AOA-TOA. Analogously, [45] shows that SS measures may provide higher accuracy to TOA based positioning systems, and [46] shows that a hybrid AOA/TDOA scheme outperforms the simpler TDOA, especially when angular spread is lower than 4° and it is able to perform the subscriber position with a more reduced number of BSs.

On the other side, some results for direction finding systems when LS are used to solve the linear equation systems are compared with Torrieri's method in [48] and [49], and the LS approach is recommended for raw positioning and for providing the initial value required by Torrieri's method, since LS shows a better performance around BS and do not suffer from convergence problems, and it helps Torrieri's approach in terms of bias and standard deviation.

An important issue that affects the positioning systems is multipath. This problem is especially relevant in AOA based techniques. Therefore and due to the increased number of local scatterers within microcells, this method is useful for macrocells, and it may become impractical for microcells. Although multipath affects principally to AOA and signal strength based positioning systems, it also affects systems based on timing, especially when the reflected rays arrive within a chip period of the first arriving path, since multipath biases the tracking of the Delay Lock Loop (DLL). Therefore, some refinements to the basic positioning approach commented above are possible and [32] also suggests to weight the measured signal by reliability factors, to form a new function to minimize as it is shown in (2.22) or in (2.43). Furthermore, various techniques have been developed to mitigate these effects, such as Root-MUSIC, TLS-ESPRIT and some kind of delay estimators based on the Extended Kalman Filter (EKF) [32][43][50]. Moreover, positioning systems may acquire a better accuracy from user dynamic by using adaptive filters such as Least Mean Squares (LMS), Root Least Squares (RLS), Extended Kalman Filter or Particle Filters (PF) [38][51]. In fact, simulation from [51] shows that positioning errors reduce to the half when Kalman filtering is performed for LOS conditions when error statistics are Gaussian and known.

In real systems, multiple access interference also affects dramatically the coarse timing acquisition and DLL of spread spectrum signals, and therefore the capacity of a receiver to estimate TOA and TDOA. Power control schemes are used to combat it, trying to ensure that signal strength will be the same at BS for different users, but it is not always true in location application where various BS are used and some of them do not have any control on the signal transmitted power. This near-far effect may be reduced with MS transmitting to its maximum power. This solution is feasible for emergency calls, but it will not be convenient for other applications, since multiple simultaneous requests for location might lead to system instability [33]. Many of the near-far resistant delay estimators are based on subspace techniques such as MUSIC. Other estimators have been produced in conjunction with multi-user detectors and interference cancellation techniques [32].

In order to get high accurate location estimates, all the arguments above suggest that methods based on delays such as TOA and TDOA are the most adequate, and when poor accuracy is permitted, signal strength or cell identification (CID) based methods may be used. However, TDOA is preferred over TOA since TDOA discards clock offset errors and it is the single robust approach in terms of clock drift under hardware constraints [52]. Furthermore, [52] proposes the use of an uncorrelated TDOA method to achieve the optimum performance by choosing the reference station as that with the minimum timing error variance.

Since timing based positioning systems are the most reputed for getting high-accurate-location estimates, these are the interest of this research.

2.2.2 Positioning Accuracy

When the measurement vector \mathbf{m} has a Gaussian distribution, the position estimator in (2.26) is also Gaussian, and a region where the estimate will probably lie may be defined. This locus of constant density function values is described by equation (2.54):

$$\begin{aligned} (\mathbf{x} - E[\hat{\mathbf{x}}])^T \mathbf{P}^{-1} (\mathbf{x} - E[\hat{\mathbf{x}}]) &= \kappa \\ \text{with } \mathbf{P} &= E\left\{(\hat{\mathbf{x}} - E[\hat{\mathbf{x}}])(\hat{\mathbf{x}} - E[\hat{\mathbf{x}}])^T\right\}; \quad \mathbf{x} = [x, y]^T \end{aligned} \quad (2.54)$$

Where \mathbf{P} is the covariance matrix of the estimator, and its associated probability $P_e(\kappa)$, for two and three dimensional cases are defined by (2.55) and (2.56) respectively:

$$\begin{aligned} P_e(\kappa) &= 1 - \exp(-\kappa/2); \quad \text{for 2-D positioning} & (2.55) \\ P_e(\kappa) &= \text{erf}\left(\sqrt{\kappa}/2\right) - \sqrt{2\kappa}/\pi \exp(-\kappa/2); \quad \text{for 3-D positioning} \\ \text{with } \text{erf}(x) &= \frac{2}{\sqrt{\pi}} \int_0^x \exp(-v^2) dv & (2.56) \end{aligned}$$

Where, κ corresponds to the size of the region enclosed by the ellipse (ellipsoid in the 3-D case). If a probability P_e is specified, κ may be found numerically and the corresponding ellipsoid is defined. This concentration ellipsoid is a multidimensional measure of accuracy for an unbiased estimator [35].

A scalar measure of the estimator accuracy is the Root-Mean Square Position Error (RMSPE) ε_r defined by (2.57), where $\text{tr}(\cdot)$ denotes the trace of the matrix, and $\text{bias}(\cdot)$ denotes the bias of the vector:

$$\begin{aligned} \varepsilon_r^2 &= E\left\{\|\hat{\mathbf{x}} - \mathbf{x}\|^2\right\} = \text{tr}(\mathbf{P}) + \|\text{bias}(\hat{\mathbf{x}})\|^2 \\ \text{with } \text{bias}(\hat{\mathbf{x}}) &= E[\hat{\mathbf{x}}] - \mathbf{x} & (2.57) \\ \text{RMSPE} &= \varepsilon_r \end{aligned}$$

Moreover, another scalar measure of the estimator accuracy is known as the circular error probable (CEP), and it is defined as the radius of the circle centered at the mean value of the estimator that contains half of the realizations of the random estimates [35][40]. These measures may be complemented with the eccentricity of ellipse E , as it is shown in (2.58), where λ_{\max} and λ_{\min} refer to the largest and smallest eigenvalues of matrix \mathbf{P} [43]:

$$E = \log(\lambda_{\max}/\lambda_{\min}) \quad (2.58)$$

Another way to characterize the positioning error introduced by the mapping from the measurement space to the real world is the called dilution of precision (DOP), and it applies to systems which use the same coordinate units. DOP represents the ratio between the root-mean square of the position error and the root-mean square of the

measurement error under the assumption of independent and identically distributed errors [35][53][54]. This measure is especially worth since provides the best case error estimation and it is not affected for the presence of multiple solutions. However, DOP does not say the best way to use the data in order to achieve this goal. The positional dilution of precision (PDOP) corresponds to the case of a three spatial dimension system (x, y and z coordinates), and it is computed as it is shown in (2.59), where \mathbf{C}_n and \mathbf{G} were defined in (2.22) and (2.27) respectively, and σ_m^2 refers to the error variance of the measures over all the BSs participating in the positioning. Furthermore, the Geometric Dilution of Precision (GDOP) defined in (2.60) also includes the temporal coordinate variation due to clock offsets, where σ_τ^2 refers to the clock error variance expressed in length terms.

$$PDOP = \sqrt{\text{tr}(\mathbf{P})} / \sigma_m = \sqrt{\text{tr}([\mathbf{G}^T \mathbf{C}_n^{-1} \mathbf{G}]^{-1})} / \sigma_m = \sqrt{\sigma_x^2 + \sigma_y^2 + \sigma_z^2} / \sigma_m \quad (2.59)$$

$$\text{with } \sigma_m^2 = \frac{1}{L} \sum_{i=1}^L \sigma_{m,i}^2$$

$$GDOP^2 = PDOP^2 + TDOP^2; \quad \text{with } TDOP = \sigma_\tau / \sigma_m \quad (2.60)$$

With the tools above, characterizing the performance of a positioning system is reasonable; but comparing two different methods in order to establish which one is strictly better, requires the comparison of their covariance matrices \mathbf{P} . Hence, a positioning method A is said to be strictly superior to a method B when their respective covariance matrices realize the following relation $\mathbf{P}_A \leq \mathbf{P}_B$, for any geometry or noise profile. However, when this condition cannot be guaranteed, the comparison should be performed in terms of their averages as follows: $E\{\mathbf{P}_A\} \leq E\{\mathbf{P}_B\}$. In this case, method A is said to be superior to the method B [52].

From the whole set of possible accuracy figures commented above, the most suitable for the evaluation of the quality of the positioning methods along this document is precisely the RMSPE, since it includes the overall effect of the bias associated with NLOS condition besides the scattering associated with multipath propagation and that degrade the estimation procedure. Moreover, this figure is not just convenient due to the nature of the problem at hand but also requires less computational burden than the others.

2.2.3 Positioning Technologies and 3G Mobile Communication Systems

The subscriber location problem is not new, and due to its relevance was studied in the framework of second generation systems such as the Advanced Mobile Phone Systems (AMPS) and GSM [28][55]. The CAPITAL system, based on AMPS, claimed achieving an average positioning error of around 108m, and even some research work suggested an average error of around 95 m for GSM with the use of TOA or TDOA measures. However a Time Advance (TA) positioning technique was preferred to provide localization based services within this system due to its simplicity, so average errors were slightly higher than 300 m [55].

On the other hand, 3GPP specifications [56] include three standard positioning methods for UMTS: Cell ID, OTDOA, and network-assisted GPS. However, TOA may be derived from RTT and Rx-Tx Time Difference type2 measures as it is shown in [34]; and therefore these TOA measures may be used to perform enhanced- CID [57] and OTDOA [34] positioning. OTDOA measures are performed by using the SFN-SFN time difference type 2 measurements. Enhanced methods include CID+RSCP, CID+RTT, OTDOA-IPDL, and OTDOA+TOA [34][57]. Idle Period DownLink (IPDL) refers to methods for improving hearability at the UE of the pilot signals from neighboring BSs. IPDL approaches include Time Aligned – IPDL (TA-IPDL), Positioning Elements – IPDL (PE-IPDL), and Cumulative Virtual Blanking (CVB)[57]. The TA-IPDL defines a specific configuration of idle periods. Within these periods, all the signals transmitted at the downlink will be shut down, avoiding that signals transmitted from distant BSs are masked by local transmissions. For example, each involved BS will transmit just 30% of the time, and will cease its transmission during the 70% left. On the other side, PE-IPDL includes some additional network elements which transmit, in a synchronized way, DL sequences that the UE can use to complement OTDOA measures. And finally, CVB is a software-based technique that reduces unwanted interference with the application of signal processing techniques. The use of TA-IPDL leads to an estimation error between 30 m and 100 m in the 67% of the cases. The use of PE-IPDL involves an improvement of almost 15% in the attainable position, whilst the CVB method claims to achieve more reduced errors between 12 m and 24 m in the 67% of the cases. However, the final improvement associated with the application of PE-IPDL depends on the number of the available positioning elements. Furthermore, since the Rx-Tx Time Difference type2 measurement is optional for the UEs, those terminals which do not support this feature will not support the TOA-based positioning methods either.

Prior to apply positioning algorithms, measures must be collected. If mobile unit is working at the Idle mode, only the OTDOA (Observed Time Differences of Arrival) method may be implemented by using the BCCH (Broad Cast Channel), and positioning will be mobile based. CID technique may be used by forcing the mobile to change to the Connected mode via a paging. Within the Connected Mode, four states are possible in UTRA: CELL_DCH, CELL_FACH, CELL_PCH and URA_PCH. The first state corresponds to a dedicated radio link with power control provided, the second corresponds to a non-dedicated channel with no power control available (FACH), and the two last states corresponds to the mobile listening to the Paging Channel. Within these two latter states MS may make measurements but they cannot report to the network unless reenter to CELL_FACH or CELL_DCH states. Within the CELL_FACH state, the mobile makes random access using the Random Access Channel (RACH) for uplink transmissions and listens to the Forward Access Channel (FACH) on downlink. Moreover, in UMTS, user data and signaling are transmitted over logical links between the mobile and the Radio Network Controller (RNC). These links are known as Radio Bearers (RAB). A RAB used for signaling is called Signaling Radio Bearer (SRB). Within the CELL_DCH state, the signaling data use the Dedicated Control Channel (DCCH); whilst within the CELL_FACH state, the signaling is sent over the Common Control Channel (CCCH). The SRB#2 is used for the transport of the messages of MEASUREMENT CONTROL and MEASUREMENT REPORT related to

each LDT. Furthermore, since a maximum measurement reporting rate of 250 [ms] has been standardized for these SRB, several measures may be performed to take advantage of the system dynamics, as studied in the following chapters of this document. Moreover, signaling bandwidth is enough for the application of timing positioning methods studied along this document [34]. However the AOA-based positioning method is not part of the standard for UMTS; and the application of space diversity as it is commented in chapter 3 also requires the use of adaptive antenna-arrays; and therefore physical modifications that should be performed at the BSs as well as at UEs. These two issues limit the application of this important technique, analogously to the way as the necessity of Location Measurement Units (LMU) has limited the application of OTDOA-based positioning.

In the case of CDMA systems such as IS-95A CDMA, cdma-2000, and also UTRA-FDD, soft handoffs can be used to get information about vicinity of the MS. However, reverse traffic is only active when a call is in progress so its use is not possible in some applications [23] [32]. Furthermore, the access channel transmissions originated by the mobile may be used for wireless location when the MS is idle in IS-95A and cdma-2000 since these two systems perform a timer-based registration procedure, and this timer may be properly set. However no measurements may be performed on UTRA at the IDLE state. Both of these systems trust in a system wide time that uses the GPS time scale, and it is suitable for TOA- and OTDOA- based positioning. However synchronization is not a requirement for UMTS networks, so the use of LMUs is mandatory to perform OTDOA measures in this case.

The forward link of a CDMA system can also be used to get location. The idea is to use the RAKE receiver included on the mobile unit to get timing synchronization from the pilot pseudo-noise sequence from different nearby BS. With this information the network may compute a measurements' set from which location may be estimated. This technique has been tested on IS-95 [28] and is particularly interesting because no new signaling message is required. However, this approach also requires a GPS/GNSS referential time along the system wide for improving the positioning accuracy.

2.2.4 The NLOS issue and its mitigation

Due to the presence of obstacles between receiver and transmitter, received signal is scattered in space and time, and the LOS path may be strongly degraded or even completely shadowed. This NLOS condition also disturbs the positioning systems since it is related not just with longer paths and greater angular spreads, but also to signal fading. Therefore the NLOS degrades the whole set of measures required to perform the positioning. For example, reports from field measurements performed for Global Systems for Mobile (GSM) communications show average errors within 400-700 m due to the TOA and TDOA measures are biased [32][58]. For this reason, it is relevant to develop methods for NLOS condition identification and NLOS error mitigation, being this problem treated in this section.

In case of a CDMA system where the transmission channel bandwidth is much higher than the information bandwidth, a rake receiver is used to recover the multipath signal avoiding the use of an equalizer. However, this receiver generally uses the most powerful arriving components and therefore, in case of shadowing, the LOS component is eventually discarded, and measurements are recorded under NLOS condition. It is easy to understand that NLOS multipath signal travels a longer distance than the LOS component to reach the receiver and consequently the timing measures and the estimated position are biased. Therefore, expression in (2.15) should be corrected to include this effect as it is shown in (2.61), where \mathbf{q} is the vector which contains biases due to NLOS.

$$\mathbf{m} = f(\mathbf{x}) + \mathbf{n} + \mathbf{q}; \quad \text{with} \quad \mathbf{q} = [q_1, q_2, \dots, q_L]^T \quad (2.61)$$

It should be mentioned that these biases are positive random variables, and hence, $q_i=0$ refers to a LOS condition, whilst $q_i \gg \sigma_{ni}$ refers to a strong NLOS condition, being σ_{ni} the standard deviation of the noise component n_i . Field measurements in IS-95 systems show that the NLOS condition introduces a mean error of around 589 m in range terms [59].

2.2.4.1 NLOS discrimination

Some research studies have been performed to achieve a better understanding of the NLOS condition, its discrimination and mitigation [33], [59]-[70]. Some approaches prefer to discriminate between LOS and NLOS conditions from received signals, and use this information to acquire a better positioning accuracy. It may be made by discarding NLOS measurements from the equation set, weighting the cost function properly in relation to the LOS/NLOS condition [59], or exploiting the fact that NLOS error range is always positive to ensure the solution will be within the feasible region [58][60].

Ideally, NLOS statistics may be known, and when it is the case, the joint PDF of error conditioned to the observed measurement may be computed, and therefore numerical methods can be performed to find the location which maximizes this conditional PDF [59]. However, it is extremely difficult to characterize NLOS error because they vary with time and also are location specific [60]. A Maximum a Posteriori (MAP) probability criterion to discriminate between a LOS/NLOS condition is proposed in [59] for this ideal case, and the decision rule is shown in (2.62):

$$\frac{f_{\varepsilon_i}(m_i - f(\mathbf{x}) | NLOS) P_{NLOS_i}^{LOS}}{f_{\varepsilon_i}(m_i - f(\mathbf{x}) | LOS) P_{LOS_i}^{NLOS}} < 1 \quad (2.62)$$

Making a decision about BS_i requires the knowledge of the prior probability P_{NLOS_i} and the conditional probability $f_{\varepsilon_i}(m_i - f(\mathbf{x}) | NLOS)$, which in turn requires the knowledge of the true MS location. In case of having just one NLOS BS, the intermediate MS location estimate using all BSs except BS_i can be used to approximate the true MS location. When there are multiple NLOS BSs, the number of possible states is 2^L , and the task of NLOS detection is to correctly determine the right system state. The NLOS State Estimation (NSE) algorithm in [59] proposes to estimate the location using the known NLOS information. This estimate is used instead of the true location to calculate the weighted a posteriori probability for each possible state, P_s . Then, the ratio

P_S/P_{S0} is computed for each of the 2^L-1 NLOS states. P_{S0} correspond to the probability of all BS are in LOS. For a hard decision, the state which has the largest ratio is selected, and the corresponding ML estimate is the output location. For a soft decision, those states whose ratio is above a certain threshold are selected, and the magnitude of the ratio corresponds to the relative likelihood of that NLOS state. Since minimum location error is the final goal, a cost/reward function can be formulated which includes the penalty of a false alarm and the reward of a correct detection in terms of RMS error. The optimal values of the weights are the values that minimize the cost function.

The LOS/NLOS discrimination problem can also be treated as a composite hypothesis problem. Since the mean of the LOS distribution is unknown while the variance is known, H_0 is called the composite hypothesis. On the other hand, the parameters of the alternative hypothesis are completely unspecified. Under certain conditions, errors of Type 1, where H_0 is wrongly rejected when it is true, are acceptable, while an error of Type 2, where H_0 is wrongly accepted when it is false, may lead to poorer performance comparable to LOS based location algorithms. It could be for example the case of a configuration with a scarce number of BS or anchor nodes. Therefore, several tests have been formulated for the acceptance or rejection of the null hypothesis at some significance level such as skewness and kurtosis or Modified Shapiro-Wilk (W) and the Anderson-Darling (A2) statistics. However, if there is no information about the proportion of LOS and NLOS components in an observed range series, then treating NLOS corrupted range values as outliers is not possible. W and A2 statistics are relatively more powerful compared to other test of normality [60]. In fact, for the case of W statistic, and normal samples, the numerator and the denominator of W are both, up to a constant, estimating the same quantity, whereas for non-normal populations, this would not be the general case. Therefore, the mean value of W tends to be smaller and the variance is larger for the non-normal case as compared to the normal case. Moreover, if historical observations indicate that the NLOS error has a particular non-Gaussian distribution without the parameters of the distribution being known, then a generalized likelihood ratio test (GLRT) may be used to test for the distribution of the measurements [60]. Another scheme to discriminate NLOS BSs for TOA-based positioning systems has been proposed in [62]. This approach uses a set of measures, recorded in an observation period for each BS, to achieve a ML estimation of the position using the BSs which are assumed to be in LOS, and by using a hypothesis-ratio metric eventually selects the group of BSs that will be used to estimate the final position. This algorithm exhibits very good performance when NLOS bias is high and measurement errors are low since these conditions simplify the discrimination of NLOS BSs.

Furthermore, LOS/NLOS discrimination may be made using side information. For example, the technical report in [54] suggests the periodical monitoring of the Rice factor defined as the ratio between the mean and the variance of the amplitude for each path to discriminate between LOS and NLOS conditions.

2.2.4.2 Statistical approach to NLOS mitigation

The NSE algorithm commented in the section above is not the single approach that takes advantage of the prior knowledge of the ranging statistics. Method in [61] also does. It is applied to mitigate NLOS ranging errors for indoor UWB Ad-Hoc Networks, and models NLOS range PDF as composed by both a Gaussian and an Exponential distribution. For example, in case of severe blockage, the Gaussian weights 26% whilst the exponential 74% and the resulting PDF is alike a Gaussian centered on 20m. This algorithm performs a cooperative maximization of the global likelihood among the network and it preserves a reasonable level of complexity in each node by adopting a distributed and asynchronous approach for the maximization process. This approach exhibits a good behavior for typical 3D environments especially when the number of anchor nodes and the connectivity increase.

In spite of a perfect statistical characterization would lead to an optimal mitigation of the NLOS condition in the positioning problem, a much more realistic assumption is that for each BS, just the mean of the NLOS error and the prior probability that BS_i is an NLOS BS is known. If it is the case, and in order to approximate $f_{ei}(m_i-f(\mathbf{x})|NLOS)$, [59] treats the NLOS error as a constant bias superimposed to the zero mean Gaussian noise and the NSE algorithm is used again with the difference that before to make the position estimation for each state, NLOS errors are compensated by subtracting the NLOS bias from the measurements of BS_i when it is in NLOS. Moreover, a more interesting case is when we know nothing about the NLOS error except its bound of magnitude. For example, the NLOS error for BS_i , if present, is greater than 300 m. These cases may be addressed using the generalized likelihood ratio (GLR) criteria, but it demands a large number of equations and therefore a larger number of BSs. In case of the empirical value of P_{NLOS_i} is not available, a blind estimator can be used which arbitrarily sets the value of P_{NLOS_i} . The value of P_{NLOS_i} can be selected based on the SINR and/or desired robustness to the NLOS error [59].

Furthermore, the worst case appears when we do not have any prior knowledge about the NLOS error. If a limited number of BSs is available, and the majority of them are in NLOS, little can be done to reduce errors. However, a greater number of NLOS BSs does not necessarily mean a larger bias in the final MS location estimate when TOA measures are used, due to more NLOS BSs increase the chance of NLOS errors cancelling each other. Since nothing is known about NLOS errors, NLOS corrupted measurements may be treated as outliers. NLOS stations may be discarded using the “ 3σ edit rule” since the knowledge of the Gaussian measurement noise variance is usually satisfied in practice. A residual algorithm for outlier detection is also proposed in [59]. This approach rely on the conditional probability $f_{ei}(m_i-f_i(\mathbf{x})|LOS)$ instead of $f_{ei}(m_i-f_i(\mathbf{x})|NLOS)$, and since it is Gaussian its cumulative function may be computed to be used as the new residual. Hence, the higher the new residual is, the more likely the BS is biased by NLOS error, and on the contrary, a very small residual indicates a high probability of BS being in LOS, provided that the reference location is close to the true value.

When NLOS BSs removal is not possible, a simple approach is using an asymmetric PDF to model the effect of NLOS and noise. The variance increase at the right side is called a tuning constant. Its value should be chosen to give a reasonably high efficiency in the LOS case and still offer protection against NLOS errors [59]. From simulations performed when NLOS bias is set to 300m, [59] reports accuracy improvements especially when accurate priors are available. If it is the case, a root mean square error lower than 55m is performed for the 60% of the cases, but when limited information is available and the residual weighting algorithm is performed, this error increases to 230 m.

When measurements are only available from three BSs and at least one of them is NLOS, then algorithms such as the Range Scaling Algorithm (RSA) have to be used to mitigate the errors. In case of RSA, the estimation of the true ranges for all BSs is formulated as a constrained minimization problem. RSA and Recursive Weighting Algorithm (RWA) benefit from knowledge of the LOS/NLOS status of the range measurement [60].

An improved MLE algorithm is also proposed in [70]. This approach assumes that the NLOS error \mathbf{q} in (2.61) has an exponential distribution, and modifies the weight matrix \mathbf{W}_{TOA} in (2.45) accordingly as it is shown in (2.63) to include this effect:

$$\mathbf{W}_{TOA,NLOS} = \left[E \{ \mathbf{e} \mathbf{e}^T \} \right]^{-1} = \frac{1}{4} \left[\mathbf{B} \left\{ \text{diag} \left(\sigma_{TOA,2}^2, \sigma_{TOA,3}^2, \dots, \sigma_{TOA,L}^2 \right) + \sigma_{TOA,NLOS}^2 (\mathbf{I} + \mathbf{1}) \right\} \mathbf{B} \right]^{-1}$$

$$\mathbf{B} = \text{diag} \left(d_2, d_3, \dots, d_L \right) \quad (2.63)$$

$$d_i^2 = \|\mathbf{x} - \mathbf{r}_i\|^2 \quad \forall i = 2, 3, \dots, L$$

$$\mathbf{1}_{i,j} = 1 \quad \forall i, j = 1, 2, \dots, L-1$$

Where $\sigma_{TOA,i}^2$ refers to the measurement noise variance, and $\sigma_{TOA,NLOS}^2$ to the timing error variance (Delay spread) introduced by NLOS condition when it is modeled as exponentially distributed; being the left sided term essentially the same as in (2.45) and therefore takes account of the Gaussian noise. On the other hand, the term to the right incorporates the correlation among measures due to the bias introduced by the NLOS condition.

The positioning solution is also achieved as in the LOS case with the ranges in \mathbf{B} replaced by the timing measures, being the light speed the scale factor as before.

In order to provide further enhancing of the positioning accuracy, a location technique that estimates the LOS distance between the MS and the BS based on the NLOS measurements has been proposed in [64]. The suggested algorithms make use of well-known multipath scattering models (ring/disk of scatterers and Gaussian distributed scatterers) in order to incorporate the effects of NLOS propagation. From PDFs for the TOAs derived using these models, maximum likelihood expectation-maximization (ML-EM) and Bayesian estimators are applied to multipath TOA measurements at each BS to estimate the LOS distance between the MS and the BS. Simulated results, assuming that measurements are taken from the three nearest BSs,

show that these algorithms provide considerable improvement over the traditional LLS location algorithm [64].

Moreover, the model in [64] trust on the computation of the probability distribution functions for the paths arriving at each BS. These PDFs are functions of the range between subscriber and each BS, and also from the radius parameter of the ring/disk of scatterers R_s . Furthermore, joint PDFs are computed assuming statistical independence, and since the multipath TOA measurements are also corrupted by zero-mean white noise with known variance, the overall TOA PDF is given by convolving the Gaussian measurements noise with the TOA PDF from the scattering model. The problem is the estimation of LOS ranges between subscriber and BSs from observed data vector, \mathbf{m} , and eventually performing the positioning using these estimated ranges and a traditional algorithm such as in section 2.2.1. Parameter estimation from realizations of an observed random variable admits Bayesian and ML methods. Bayesian estimation includes three criteria: Minimum Mean Square Error (MMSE), Minimum Mean Absolute Error (MMAE) and Maximum a Posteriori (MAP); and all of them require finding the probability of the parameter vector given the observation vector \mathbf{m} , $p([\mathbf{d}, R_s]|\mathbf{m})$, where $\mathbf{d}=[d_1, d_2, \dots, d_L]$, being d_i , the distance between MS and BS_{*i*}. A way to get the MMSE is to use the following iterative algorithm:

- Step 1: Assume the scattering disk/ring radius, R_s .
- Step 2: Estimate the distances between subscriber and BSs from $p(d_i|m_i, R_s)$
- Step 3: Estimate the radius of scatterers from $p(r|m_i, \text{estimation of } d_i)$
- Step 4: Repeat steps 2 and 3 until convergence.

Some further details related to the proper computations and integration limits are developed in the reference [64].

Simulations in [64] use the Nedler-Mead algorithm to solve the search procedure for maximizing the PDF. Furthermore, both Bayesian and ML-EM algorithms require a complicated integration which is replaced by numerical integration using the Riemann summation, the precision which is one meter for d_i and 10 m for r . Noise variance was assumed of 50 m. Results show better behavior as the number of measured multipath TOAs increases. The algorithm outperforms the LLS algorithm when the minimum received multipath TOA was used, at the expense of computational complexity. The Bayesian algorithm exhibits a better performance than ML-EM due the PDF has a peak at the LOS and $E\{d_i|m_i, R_s\}$ is expected to be close to the true LOS d_i . However, the ML-EM algorithm is less complex due to the fact that when estimating d_i in the maximization step, the calculation of the mean is not required. It means that the numerical integration performed in the Bayesian estimator to compute the mean is omitted in the ML-EM algorithm.

Moreover, both algorithms outperform LLS which uses the minimum received TOA of the N_m measured TOAs, especially when just a single TOA measurement is available for the LLS algorithm. Simulations show that an average location error of 250m is achieved for LLS when $N_m=1$; and it reduces to around 115 m for both LLS and ML-EM when $N_m=8$; and near to 60 m for the Bayesian technique and the Ring Of

Scatterers (ROS) model. On the other hand, when the Disk Of scatterers (DOS) model is used, the average location error reduces to 175m for LLS with $N_m=1$, and to 80m for LLS when $N_m=8$, to 60m for ML-EM and to 30m for the Bayesian proposed technique.

Method in [65] also trusts in the identification of NLOS BSs and modifies the two steps-least squares method to introduce position refinement to the Chan procedure in [40] applied to TDOA-based hyperbolic location scheme. This technique essentially includes correction factors to the TDOA range measurements for the NLOS BSs. As these factors are known to be between zero and one, this approach uses an iterative process to estimate such factors by minimizing the error residuals in successive iterations. Once the correction factors have been estimated, these are applied to the range measurements, and refined position is recalculated. Simulations performed in [65] for an urban environment show that this new algorithm outperforms Chan solution. In fact, RMS error reaches 300m for Chan algorithm and reduces to 67.7 m with the application of this algorithm. Since minimization of the residual involves the use of a gradient step, it must be selected carefully to avoid unnecessary computational burden.

2.2.4.3 Geometrical approach to NLOS mitigation

Another approach to NLOS mitigation identifies restraints imposed by the problem geometry, and uses this information to improve positioning. For example, [33] observes as $m_i - f_i(\mathbf{x}) > 0$ in case of NLOS condition and TOA measures. Therefore, proposes the introduction of a penalty function $g_i(\mathbf{x})$ in (2.22) as it is shown in (2.64):

$$J_{WNLS}(\mathbf{x}) = \sum_{i=1}^L w_i^2 [m_i - f_i(\mathbf{x})]^2 - \lambda \sum_{i=1}^L [g_i(\mathbf{x})]^{-1} \quad (2.64)$$

Where $g_i(\mathbf{x}) = -m_i + f_i(\mathbf{x})$; λ is a positive parameter used for minimization; and the initial value should be chosen within the feasible region. This method enables the replacement of a constraint minimization problem for a sequence of unconstrained optimizations where λ decreases in successive iterations.

Furthermore, among the range-based algorithms designed to mitigate NLOS, it is quite interesting one proposed in [63] since it is a non-iterative estimator that does not require knowledge of NLOS error statistics. Moreover, simulation results indicate that the proposed algorithm can restrain the NLOS errors and improve location accuracy and it may be even improve in some cases to the performance of Chan's method in [40] and Caffery's LLS method[71] described by equations (2.35) and (2.42). The closed-form position estimator provided by this estimator is described in (2.65):

$$\hat{\mathbf{x}} = \mathbf{G}(\boldsymbol{\eta})^T \left(\mathbf{G}(\boldsymbol{\eta}) \mathbf{G}(\boldsymbol{\eta})^T \right)^{-1} [\mathbf{m} - f_{TOA}(\boldsymbol{\eta})] + \boldsymbol{\eta} \quad (2.65)$$

with $\boldsymbol{\eta} = \frac{1}{K} \sum_{i=1}^K \boldsymbol{\gamma}_i$

Where $\mathbf{G}(\boldsymbol{\eta})$ corresponds to matrix \mathbf{G} in (2.27) evaluated at $\mathbf{x}_0 = \boldsymbol{\eta}$, being $\boldsymbol{\eta}$ the geometric center of all K points of intersection of Circular Lines Of Position (CLOP) described by the set of equations in (2.15)-(2.17), and $\boldsymbol{\gamma}_i$ is the position vector for each intersection point i . Clearly, solution in (2.65) trusts in that the subscriber position is

within the feasible region. Therefore, it estimates the subscriber position by displacing from the geometrical center of this region, using a correcting factor derived from the Jacobian matrix of $\mathbf{f}(\mathbf{x})$.

A Geometry-Assisted Location Estimation (GALE) algorithm is proposed in [58]. This scheme suggests the incorporation of geometric constraints within the formulation of the two-step LS method in order to estimate the positions of a mobile device by preserving the computational efficiency from the two-step LS algorithm and also achieving precise location estimation under NLOS environments. Essentially, GALE includes a new equation to the system in (2.35), estimating the subscriber position within the feasible region as in (2.66):

$$\mathbf{x}_c = \sum_{i=1}^K w_i \boldsymbol{\gamma}_i \quad (2.66)$$

Where $\boldsymbol{\gamma}_i$ refers to any of the position vectors resulting of the intersection of the CLOP defined by (2.15)-(2.17), and where w_i is a weighting coefficient related to the metric in (2.67):

$$w_k = \frac{\sigma_k^2/d_k}{\sum_{i=1}^K (\sigma_i^2/d_i)}; \quad \forall k = 1, 2, \dots, K \quad (2.67)$$

$$\text{with } d_k = \sum_{j=1, j \neq k}^K \|\boldsymbol{\gamma}_k - \boldsymbol{\gamma}_j\|$$

Being, σ_i the standard deviation of the range measure m_i .

To configure the constrain equation, a virtual range m_γ is incorporated by computing the root mean square distance between the estimated subscriber position in (2.66) and the CLOP intersection points $\boldsymbol{\gamma}_i$, as it is shown in (2.68):

$$m_\gamma = \left[\frac{1}{K} \sum_{i=1}^K \|\mathbf{x}_c - \boldsymbol{\gamma}_i\|^2 \right]^{1/2} \quad (2.68)$$

And also a mean square distance of these CLOP intersection points as it is shown in (2.69):

$$r_\gamma^2 = \frac{1}{K} \sum_{i=1}^K \|\boldsymbol{\gamma}_i\|^2 \quad (2.69)$$

Once the constraint equation is incorporated to the system, the two-steps LS algorithm is performed as usual. It means that subscriber position is firstly estimated using the WLLS method as described within (2.44) following the procedure commented in section 2.2.1.2. Later, by introducing the dummy variable R as in (2.70):

$$R = \|\mathbf{x}\|^2 = x^2 + y^2 \quad (2.70)$$

And the new vector \mathbf{h} in (2.71):

$$\mathbf{h} = [\hat{x}, \hat{y}, \hat{R}]^T \quad (2.71)$$

Vector \mathbf{z} containing the square subscriber position coordinates is estimated applying a second WLLS step as in (2.72):

$$\hat{\mathbf{z}} = (\mathbf{B}^T \Phi \mathbf{B})^{-1} \mathbf{B}^T \Phi \mathbf{h} \quad (2.72)$$

Being the matrices \mathbf{B} and Φ as defined within (2.73) [37][40][58]:

$$\mathbf{B} = \begin{bmatrix} 1 & 0 & 1 \\ 0 & 1 & 1 \end{bmatrix}^T \quad (2.73)$$

$$\Phi = \left[4 \text{diag}(\hat{x}, \hat{y}, 1/2) (\mathbf{A}_{TOA}^T \mathbf{W}_{TOA} \mathbf{A}_{TOA})^{-1} \text{diag}(\hat{x}, \hat{y}, 1/2) \right]^{-1}$$

Finally, subscriber position is re-estimated by rooting values within \mathbf{z} vector and choosing the signs achieved in the first step as it is shown in (2.74):

$$\hat{\mathbf{x}} = \left[\text{sgn}(\hat{x}) \sqrt{[\mathbf{z}]_1}, \text{sgn}(\hat{y}) \sqrt{[\mathbf{z}]_2} \right]^T \quad (2.74)$$

Furthermore, results in [58] show that the TOA-based GALE approach can provide around 50 m lower estimation error compared to the two-step LS scheme and around 25m lower error in comparison with the Range Scale Algorithm (RSA) and the LLS methods. In addition, TOA/AOA-based GALE algorithm can provide around 25 m and 45 m fewer estimation errors in comparison with the two-step LS and the Hybrid Line Of Position (HLOP) schemes respectively. Moreover, when parameters for GALE approach are estimated from measurements, slight error deviations around 8 to 10 m are achieved in comparison with the use of the current parameters. For the 3D case, TOA-based GALE algorithm outperforms the two-step LS and the LLS methods with around 252 m and 1,962 m of estimation errors respectively, under 80 percent of average position errors. Furthermore, the z-direction-position errors of the MS can be reduced as the horizontal relative distances between the BSs decrease (that is, lowered to the range of meter scale). Therefore, it can be suggested that the 3D GALE algorithm is especially feasible to be adopted in the scenarios of microcell layouts. For the 3D case, TOA/AOA based GALE approach can provide around 10 m and 200 m fewer estimation errors, in the position error in comparison to the two-step LS and HLOP schemes.

Subscriber mobility can help to perform NLOS mitigation. In fact, the Kalman Filter has been used to mitigate positioning errors due to NLOS [66]-[69], and has been successfully used in [66] for tracking devices operating in 2.4 GHz when NLOS weakly appears for a TDOA-based scheme. Moreover, modified Kalman filter in [67] [68] uses the Greenstein model in [18] to achieve the bias and variance of NLOS errors, and therefore it uses this information to refine TDOA-based positioning accuracy. Results exhibited in [68] show the best behavior for rural environments in comparison with suburban, urban and bad urban localities. In fact these simulations achieve accuracy better than 60 m in the 67% of the cases, and better than 100 m in the 95% of the cases. The worst case corresponds to the bad urban scenario where accuracy is better than 175 m in the 95% of the cases.

2.2.4.4 Final considerations

Understanding the complexity of the wireless subscriber positioning problem, and in order to evaluate possible methods to perform an accurate positioning, in the following section a simulation platform based on Greenstein propagation model has

been built to test relevant approaches related to timing based positioning methods. Furthermore, since the propagation model statistic is clearly defined, its main statistics have been derived in *Annex A2.2*, and final results are shown below in this section.

Particularly, the mean and the standard deviation for the RMS Delay Spread modeled as in (2.5) are presented as a function of distance within (2.75) and (2.76) respectively:

$$E\{\tau_{rms}\} = T_1 d^\varepsilon e^{m_z + \sigma_z^2/2} \quad (2.75)$$

$$\sigma_{\tau_{rms}} = \sqrt{\text{var}\{\tau_{rms}\}} = T_1 d^\varepsilon \sqrt{e^{2m_z + \sigma_z^2} (e^{\sigma_z^2} - 1)} \quad (2.76)$$

Being m_z and σ_z the mean and standard deviation of the scaled random variable $Z = \Xi \ln(10)/10$.

However, a group of more suitable expressions is achieved recognizing d in (2.5) also as a random variable uniformly distributed between 0 and D . In this way, the mean and the standard deviation for the RMS Delay Spread become as in (2.77) and (2.78) respectively.

$$E\{\tau_{rms}\} = \frac{T_1 D^\varepsilon}{1 + \varepsilon} e^{m_z + \sigma_z^2/2} \quad (2.77)$$

$$\sigma_{\tau_{rms}} = \sqrt{\text{var}\{\tau_{rms}\}} = T_1 D^\varepsilon \sqrt{e^{2m_z + \sigma_z^2} \left(\frac{e^{\sigma_z^2}}{1 + 2\varepsilon} - \frac{1}{(1 + \varepsilon)^2} \right)} \quad (2.78)$$

Moreover, when TDOA measurements are used, the expected value and a bound for the dispersion of these measures may be computed as in (2.79) and (2.80); being “ i ” the subscript that identifies the BS associated with the measure. Note as $i=1$ is reserved for the subscriber’s reference BS.

$$E\{\tau_{i,1}\} = E\{\tau_i - \tau_1\} = T_1 e^{\sigma_z^2/2} (d_i^\varepsilon e^{m_{zi}} - d_1^\varepsilon e^{m_{z1}}) \quad (2.79)$$

$$\text{var}\{\tau_{i,1}\} < T_1^2 e^{2m_z} (2e^{2\sigma_z^2} - e^{\sigma_z^2}) (d_i^{2\varepsilon} + d_1^{2\varepsilon}) \quad (2.80)$$

Expressions (2.75) - (2.78) have been used to validate Greenstein model simulations prior to their inclusion in the simulation platform. Furthermore, these results will be used to characterize the weighting matrices in (2.45) and (2.46) required to perform WLLS positioning as described in section 2.2.1.2.

2.3 Simulations and Results

This section includes simulations that evaluate several relevant positioning algorithms and their capabilities to mitigate the NLOS condition in realistic environments. With this purpose a simulation platform has been developed, and its main characteristics are commented below.

2.3.1 Simulation platform for assessing positioning

The simulation environment corresponds to a group of $N_{BS}=7$ hexagonal cells of radius R . The control BS is supposed to be the central one, and it is located at (0,0) coordinates in the Cartesian plane. The remaining six BSs are located surrounding this.

For simulation purposes, the subscriber will be located anywhere within the central cell since these results would characterize any cell in the system. For the whole set of experiments in this section, the absolute positioning error is computed comparing the true position with the estimated location provided by the positioning algorithm under test. True positions are distributed along a 100x100 grid within the cell of radius R . Moreover, to achieve the average error for each position within the grid, 1000 realizations have been performed for each experiment. Furthermore, the average positioning error is associated with a color to have a visual representation of its distribution within the cell. Dark blue represents the lowest errors and dark brown the highest ones.

Furthermore, since BSs in LOS are just affected by measurement noise, this error is modeled as a Gaussian variable. On the other hand, NLOS environments are modeled using an exponential distribution for the excess delay for a particular location as it is shown in (2.5), being the Greenstein propagation model [18] in (2.5) used to characterize the required RMS Delay Spread τ_{rms} at each position and realization within the simulation platform. Moreover, the SNR received at each BS is computed with the help of the same propagation model using (2.6), reminding that the SNR in the central site is controlled to keep the link quality and hence the SNR in the other stations may be computed from the problem geometry in relation to this goal.

Precisely, expression (2.81) relates the SNR received at BS_i with the SNR received at the control site (BS_1), when measures are taken from the uplink; where $\mathbf{G}(d_i)$ refers to the path gain provided by the Greenstein model using (2.6) in terms of the distance d_i , between the subscriber and the base station BS_i . Therefore, d_1 refers to the distance between the subscriber and the central site.

$$SNR|_i = SNR|_1 + \mathbf{G}(d_i) - \mathbf{G}(d_1) \quad \forall i = 2, 3, \dots, N_{BS} \quad (2.81)$$

The path gain decays with the distance and is related to the lognormal random variable \mathbf{x} as it is shown in (2.6), where G_1 is the median value of $\mathbf{G}(d)$ when $d=1$ km. Analogously, the RMS delay spread τ_{rms} is related with the lognormal random variable ξ . Furthermore, the path gain $\mathbf{G}(d)$ and the RMS delay spread τ_{rms} random variables are correlated, and Greenstein model suggests a correlation coefficient $\rho = -0.75$ for the two Gaussian variables, $\mathbf{X}=10\log(\mathbf{x})$ and $\Xi=10\log(\xi)$. Furthermore, G_1 may be found applying the COST231-Hata model for $d=1$ km, and the path loss coefficient β has been set as $\beta=3.7$ according to the COST 231-Walfisch-Ikegami model [16].

2.3.2 Experiments and results

Since, the interest of this research is achieving low complex efficient methods for performing accurate subscriber positioning in NLOS environments, the algorithms that shall be tested include the WLLS based methods and the geometrical approaches. WLLS methods provide a good balance between accuracy and complexity and do not have the convergence problems reported in the literature for the NLS approaches. Also the application of geometric restrictions seems to be suitable as complementary mitigation methods. The behavior of these methods will be contrasted with that of the traditional Torrieri's algorithm in (2.26).

Moreover, this simulation platform will be used again in chapter 4 to show the effect of incorporating space and time diversity, as a mean to mitigate the NLOS condition and improving the subscriber positioning.

Experiment 2.1: TOA measures provided from 7 LOS BSs – A utopian LOS environment

First of all, Figure 2.8 and Figure 2.9 illustrate the idealistic case of having all the seven BS's in LOS when TOA measures are used for the positioning. To simulate the LOS condition, a zero mean Gaussian distribution for delays is performed with variance provided by the Greenstein model when the distance is uniformly distributed within the cell radius. It corresponds approximately to 0.32 [us] for a cell radius $R=1$ km, and it reduces to 0.15 [us] for $R=0.2$ km as it can be easily shown from expression when $D=R$. Figure 2.8 exhibits the average positioning error when $R=1$ km when Least Squares in (2.42) and Torrieri's in (2.29) methods are performed. Analogously, Figure 2.9 exhibits the results when $R=200$ m.

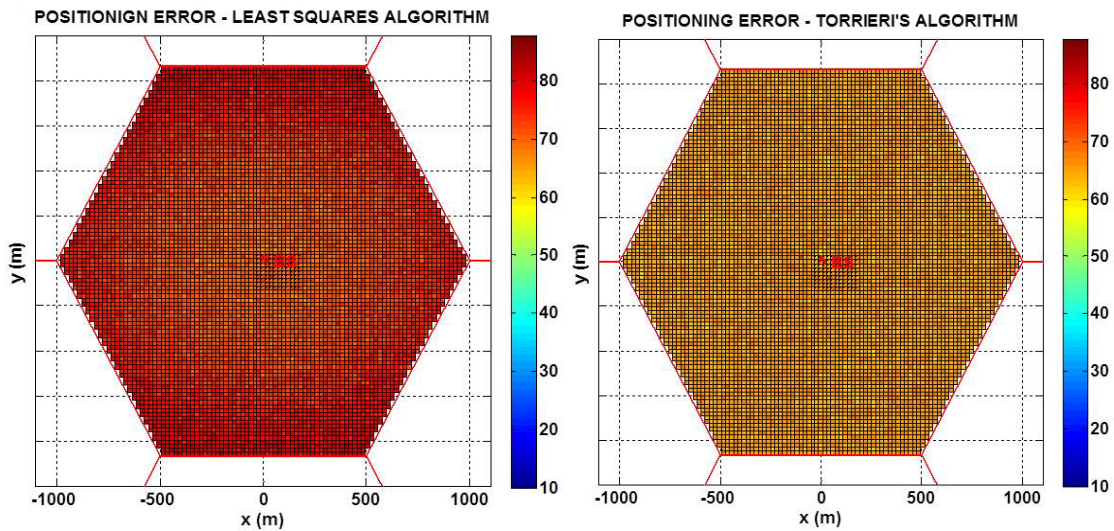


Figure 2.8. Average Positioning Error in case of 7 LOS BS's involved in subscriber positioning based on TOA when the cell radius $R=1000$ m. A) Left: LLS Algorithm. B) Right: Torrieri's Algorithm.

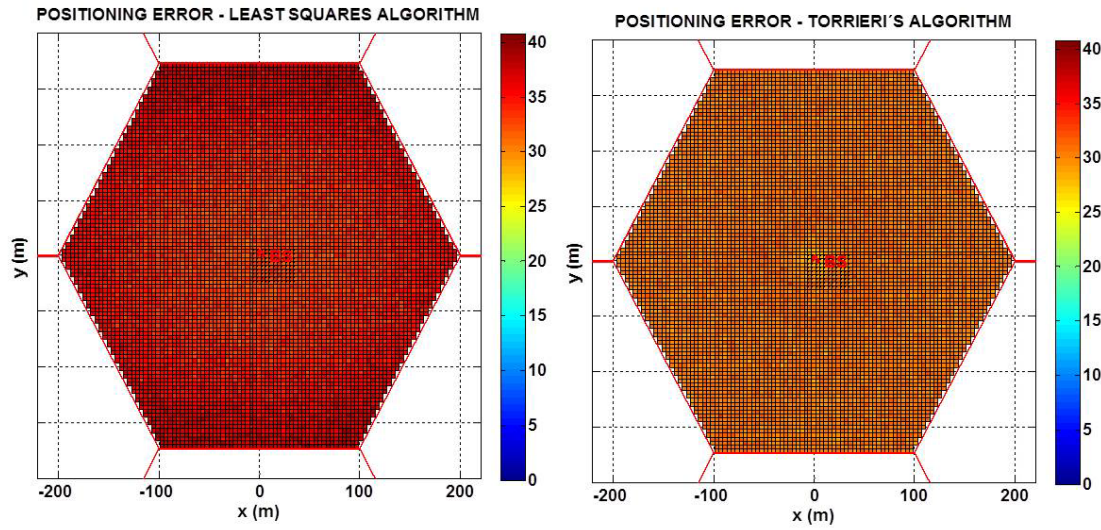


Figure 2.9. Average Positioning Error in case of 7 LOS BS's involved in subscriber positioning based on TOA when the cell radius $R=200$ m. A) Left: LS Algorithm. B) Right: Torrieri's Algorithm.

Not surprisingly, Torrieri's method outperforms LS, especially for higher cell sizes since smaller cells imply a relatively more dispersive environment. Note for i.e. as the mean positioning error reduces from around 73 m to around 65 m when the cell radius $R=1\text{km}$, and from 34 m to 30 m when $R=200$ m. Torrieri's algorithm achieves more uniform results whilst LS degrades with the distance to the control BS. Figure 2.10 exhibits the CDF for the positioning error for this experiment.

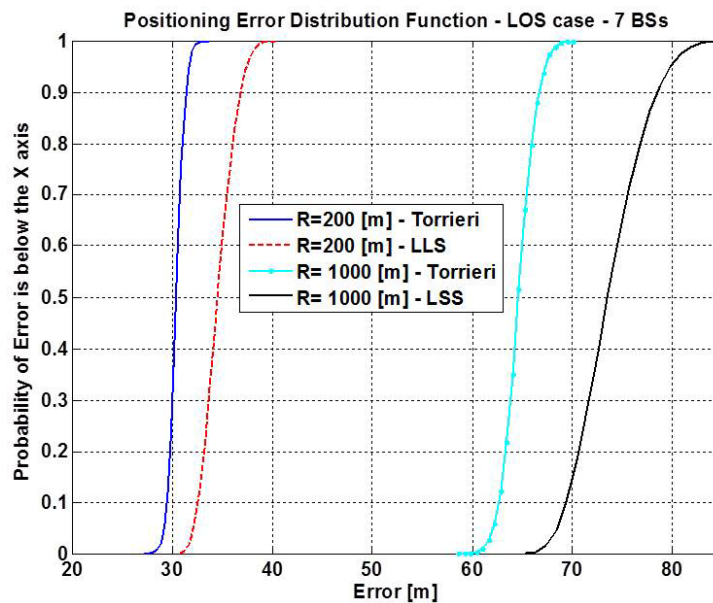


Figure 2.10. CDF for the subscriber positioning error when 7 BSs in LOS are available, and a TOA based scheme is used for different cell sizes.

For this ideal case, the expected error within the cell when $R=200$ m results below 31 m for the 70% of the cases, and below 32 m for the 95% of the cases when Torrieri's algorithm is used, and respectively below 36 m and 38 m when the LLS algorithm is performed. Similarly, for a larger cell with $R=1000$ m, positioning error is below 66 m for the 70% of the cases, and below 68 m for the 95% of the cases when Torrieri's algorithm is employed, and it increases respectively below 76 m and 80 m when LLS algorithm is used instead. Despite the fact that these results exhibit an excellent behavior; the true is they are too optimistic since probability of having a BS in LOS is currently very low.

Experiment 2.2: TOA measures provided from 7 NLOS BSs in a moderate dispersive environment – Introducing the NLOS Problem

A much more realistic scenario is considered in this second experiment. It assumes that NLOS condition is present in the seven BS's. However, NLOS is assumed to be more moderated for the communications between subscriber and the control site. For this latter BS, the Greenstein model is used as in the rest of sites with the only difference that the propagation losses factor β is reduced from 3.7 to 2.5. Particularly, the required parameters for the Greenstein model take the following values suitable for the urban case [18]: $T_1=0.4$ [us], $\varepsilon=0.5$, $\sigma_x=8.0$ [dB], $\sigma_\xi=4.0$ [dB], and $\rho=-0.75$. Particularly, T_1 has been set in agree to the GTU COST 259 model [16][65][68] and it may be considered a moderate dispersive environment. Torrieri's algorithm and LLS method are performed to achieve subscriber positioning. Average positioning errors for the cell radius $R=1000$ m are exhibit in Figure 2.11.

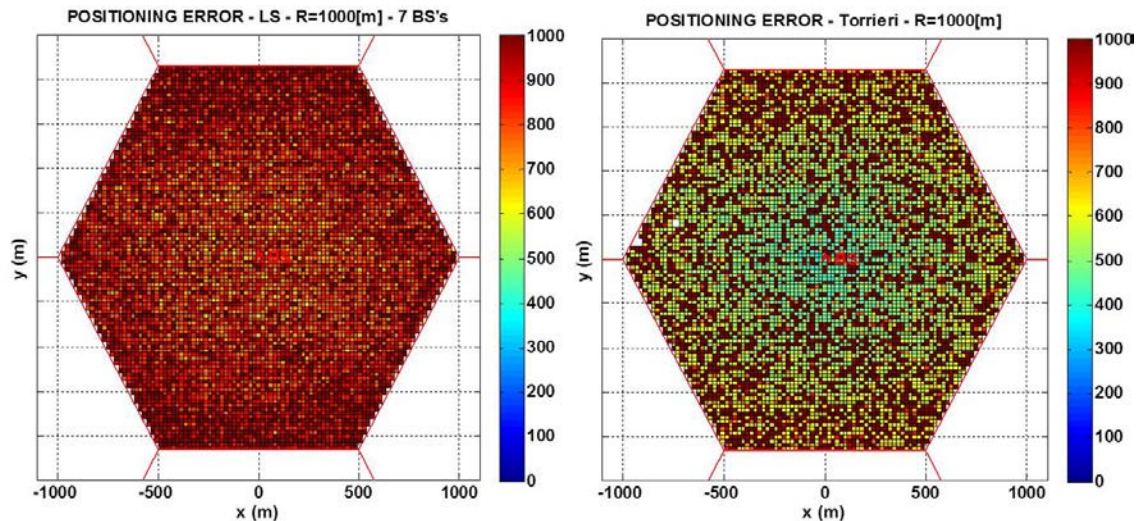


Figure 2.11. Average Positioning Error in case of 7 NLOS BS's involved in subscriber positioning based on TOA when the cell radius $R=1000$ m. A) Left: LLS Algorithm. B) Right: Torrieri's Algorithm.

Clearly, results from this experiment for both techniques are not just poor but completely inadequate. Both methods fail in estimate subscriber positioning. LLS achieves errors between 550 m and 1000 m and Torrieri's algorithm errors slightly

lower between 450 m and 1000 m. Practically, these values just tell us that subscriber is in any place within the cell. Furthermore, the results above reveal that Torrieri's algorithm is unable to converge. Results are even worse for a smaller cell radius, and therefore results for $R=200$ m are not presented in this document. However, these results worthily introduce the harmful effect of NLOS condition.

Experiment 2.3: TOA measures provided from NLOS BSs in a moderate dispersive environment – Mitigating NLOS condition by weighting measures

The current simulation scenario is the same as the precedent experiment, but the WLLS method described in (2.44) is used to perform the NLOS mitigation with two different weighting matrices referred respectively as WLLS and NLOS WLLS.

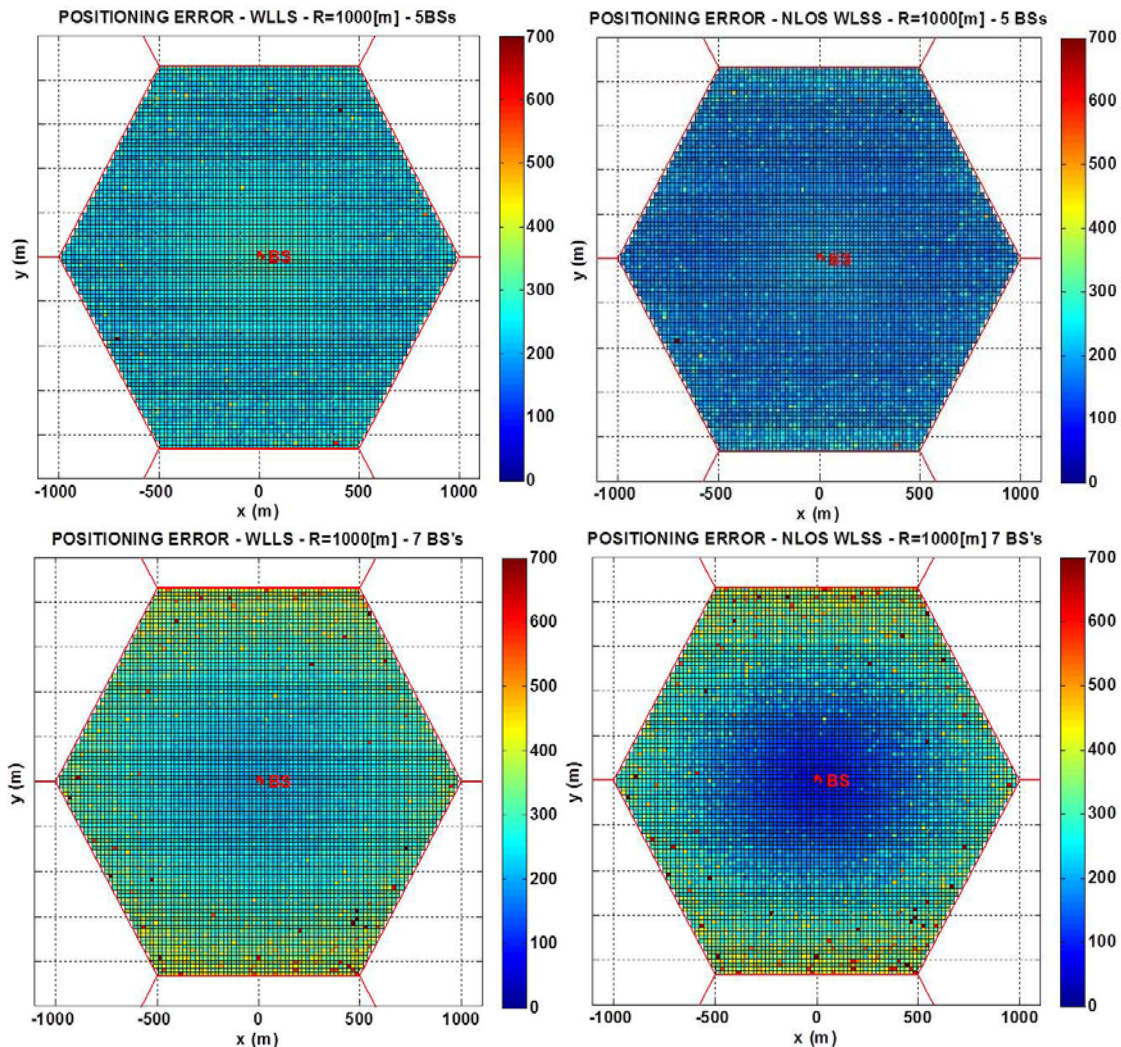


Figure 2.12. Average Subscriber Positioning Error for a NLOS moderate dispersive scenario based on TOA when the cell radius $R=1000$ m. A) Top Left: WLLS Algorithm and 5BSs. B) Top Right: NLOS WLLS ($\epsilon=1$) and 5 BSs. C) Bottom Left: WLLS and 7BSs. D) Bottom Right: NLOS WLLS ($\epsilon=1$) and 7 BSs.

The weighting matrix for WLLS algorithm is described in (2.45) and our NLOS WLLS variant modifies it to emphasize the dependence of timing error with distance as it is easily perceived from (2.75) and (2.76), especially in case of highly dispersive environments where ε is approximately equal to one. The weighting matrix for this NLOS WLLS algorithm is described within (2.82).

$$\mathbf{W}_{NLOS,TOA} = \frac{1}{4} \text{diag} \left(\frac{1}{T_1^2 d_2^{2(1+\varepsilon)}}, \frac{1}{T_1^2 d_3^{2(1+\varepsilon)}}, \dots, \frac{1}{T_1^2 d_L^{2(1+\varepsilon)}} \right); \quad (2.82)$$

with $d_i^2 = \|\mathbf{x} - \vec{\mathbf{r}}_i\|^2$; $\forall i = 2, 3, \dots, L$

Figure 2.12 shows the results of weighting the measures related to each BS. At the top, both methods use just five out of seven available BS's. The five nearest stations to the subscriber have been chosen. It is equivalent to put a null weight to the farther stations. On the other side, the results from using the whole set of measures are appreciated at the bottom. From a visual inspection, it is easy to understand that NLOS WLLS (with $\varepsilon=1$ in this case) outperforms to WLLS for both cases, but it is not so easy to judge if the soft weighting exhibited at the bottom makes in fact a better job since elimination of the farther stations contributes to reduce errors at the boundaries of the cell but also to miss accuracy near to its center.

Figure 2.13 exhibits the CDF's for the subscriber positioning error in this NLOS moderate dispersive scenario. These results confirm that NLOS WLLS outperforms WLLS since their weighting factors better describe the NLOS behavior. In addition, these results also reveal as the soft weighting makes an overall better job that the hard elimination of measures.

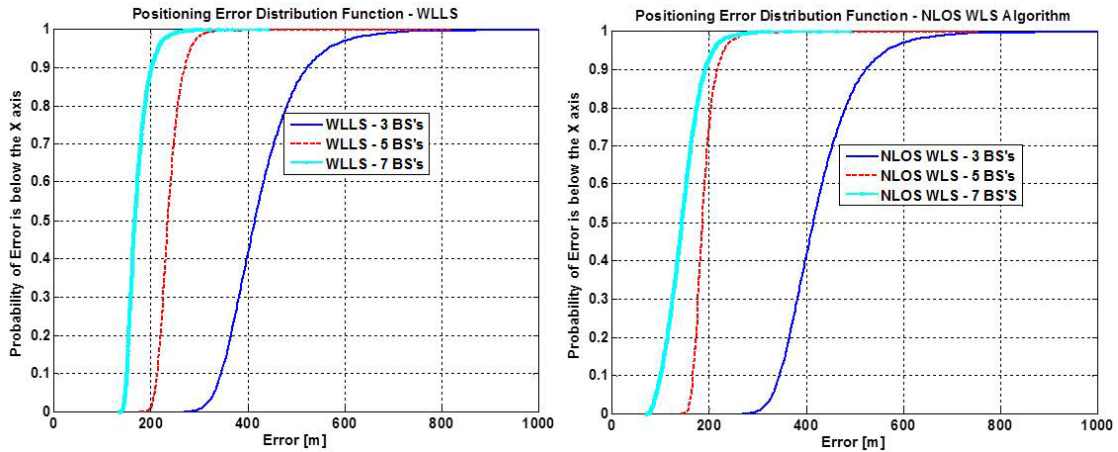


Figure 2.13. CDF for the subscriber positioning error within a NLOS moderate dispersive scenario and a TOA based scheme. A) Left: WLLS method using a different number of BSs. B) Right: NLOS WLLS method ($\varepsilon=1$) using a different number of BSs.

In fact, WLLS achieves a positioning error below 180 m for the 70% of the cases and below 240 m for the 95% of the cases for a soft weighting of the 7 BSs. On the other hand the NLOS WLLS ($\varepsilon=1$) algorithm achieves average errors below to 162m and 208 m respectively for the same events. Moreover, when just the information related to the three nearest BSs is used, the positioning is very poor: below to 460 m for the 70% of the cases and below to 560 m for the 95% of the cases.

In addition, Figure 2.14 shows the results of performing NLOS mitigation with two new different sets of weights: the first set computes the weights again as in (2.82), but currently with $\varepsilon=1/2$; and the second one as in (2.63) by suppressing the first term related to the Gaussian measurement noise and just keeping the term associated with NLOS. Our results favor again to our proposed algorithm over Yi Long NLOS mitigation scheme [70]. In fact, Yi long version achieves a positioning error below 200m for the 70% of the cases and below 229 m for the 95% of the cases for a soft weighting of the 7 BSs, whilst our NLOS WLLS ($\varepsilon=1/2$) version achieves average errors below to 160 m and 202 m respectively for the same thresholds. These latter results are even slightly better than those performed by our last version with $\varepsilon=1$ due to the better adjustment with the signal generation statistics.

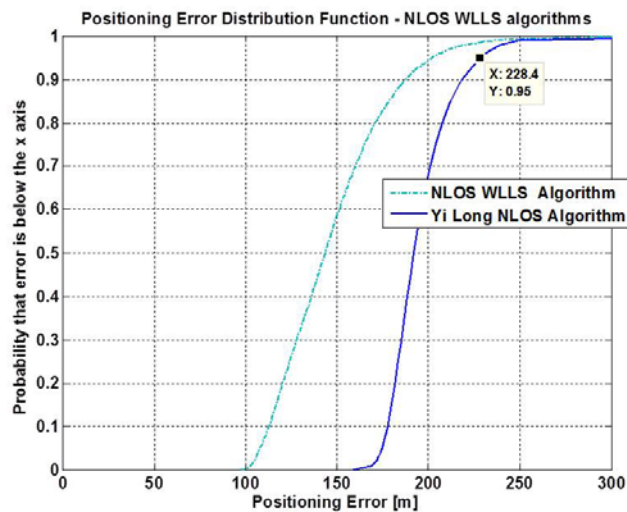


Figure 2.14. CDF for the subscriber positioning error within a NLOS moderate dispersive scenario and a TOA based scheme for two different NLOS WLLS methods and 7 BSs.

Experiment 2.4: TOA measures provided from NLOS BSs in a moderate dispersive environment – Mitigating NLOS condition using geometrical restrictions

This simulation scenario is the same as the two precedent experiments, but algorithms performed to achieve positioning include geometrical considerations. In fact, three algorithms are being considered within this section: a Geometrical estimator,

a One Step LS GALE and the Two Steps LS GALE. Our first Geometrical algorithm identifies the feasible region from the intersection of the CLOPs related to the three nearest BS's to the subscriber and associates the subscriber position to the centroid of these boundary points. Error results for this algorithm are show in Figure 2.15 for both cell radiuses $R=1000$ m and $R=200$ m.

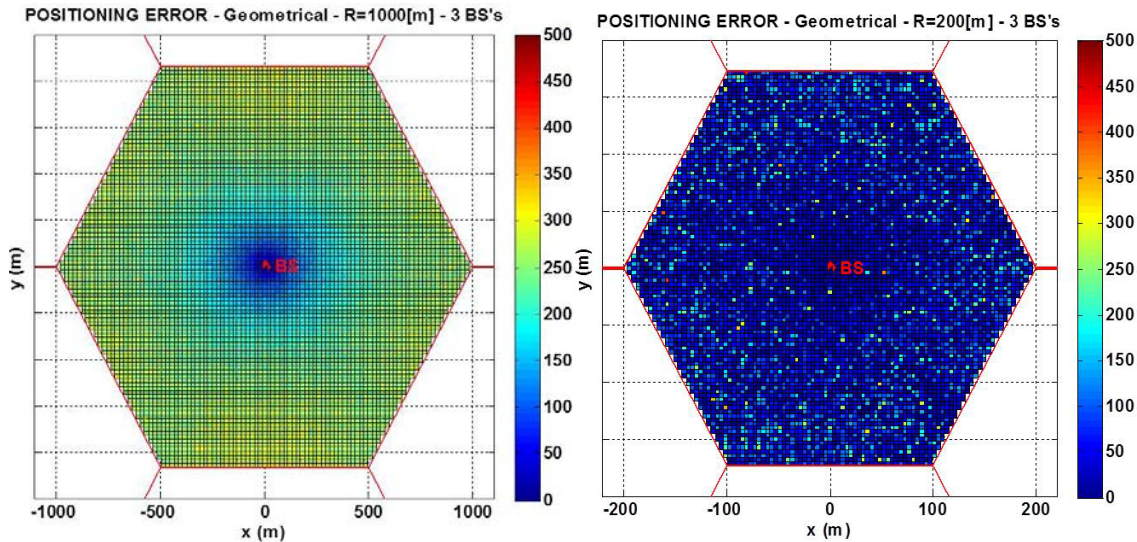


Figure 2.15. Average Subscriber Positioning Error for a NLOS moderate dispersive scenario based on TOA when using a Geometrical based algorithm and the measures from the 3 nearest BS's. A) Left: $R=1000$ m. B) Right: $R=200$ m.

Both graphics show that the positioning accuracy degrades when the subscriber goes further from the control BS and closer to the cell boundaries.

On the other hand, Figure 2.16 exhibits positioning errors for a One LS step GALE algorithm. It corresponds to add a new virtual BS equation to the WLLS system in (2.44) with the results of GALE equations in (2.68) and (2.69). This figure shows the results of using this method in two different cases: the first when just the 3 nearest BS's measures are being employed and the second using the whole set of measures from the 7 BS's. The benefit of using all the available data is evident by comparing these two graphics. In fact, this algorithm completely fails for the lower number of BS's.

Figure 2.17 shows the CDF's for the positioning error of algorithms in this experiment. It is clear that the Geometrical algorithm makes a better work than the One Step GALE method. Note for i.e. as the error is below to 176 m for the 70% of the cases, and below to 188 m for the 95% of the cases when the Geometrical estimator is used, whilst these values degrade below to 213 m and below to 254 m respectively in case of One Step GALE algorithm using the whole set of measures.

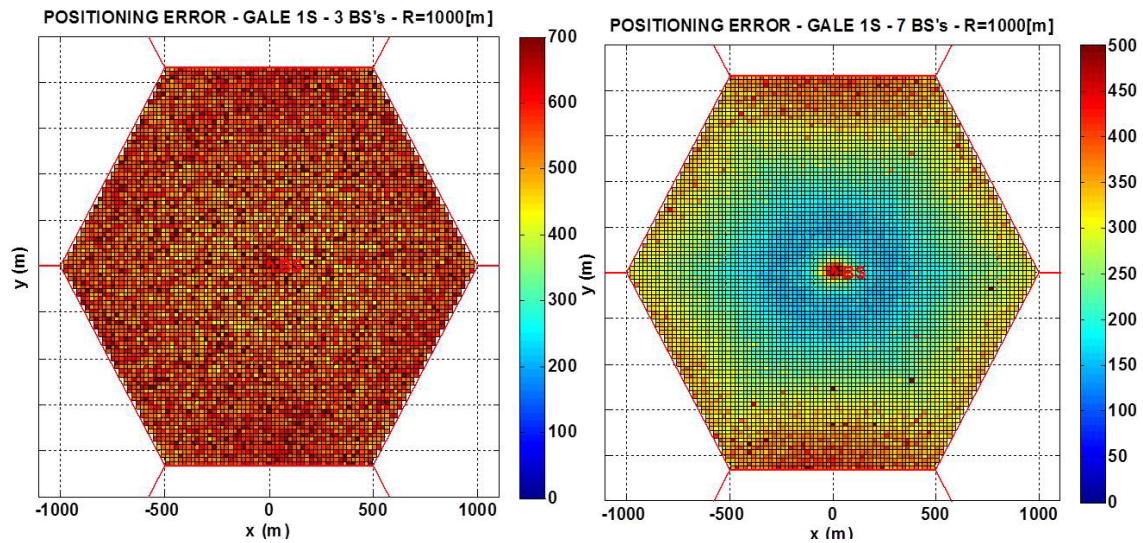


Figure 2.16. Average Subscriber Positioning Error for a NLOS moderate dispersive scenario based on TOA for the One Step GALE algorithm when the cell radius $R= 1000$ m. A) Left: Using the 3 nearest BS's. B) Right: Using the whole set of 7 available BS's.

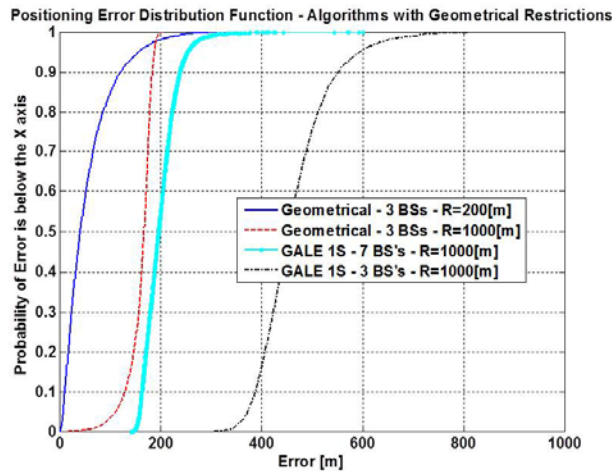


Figure 2.17. CDF for the subscriber positioning error within a NLOS moderate dispersive scenario and a TOA based scheme for GALE and Geometrical positioning algorithms.

Figure 2.17 also shows that errors reduce with the application of the Geometrical estimator when the cell is smaller with $R=200$ m. In this case positioning error is below 67 m for the 70% of the cases and below 158 m for the 95% of the cases.

Experiment 2.5: TOA measures provided from NLOS BSs in a moderate dispersive environment – Mitigating NLOS condition by weighting measures and using geometrical restrictions

This scenario is the same as the three precedent experiments, but in this case the intention is to test a new hybrid algorithm that fuses the NLOS WLLS method and the

Geometrical estimator to obtain the best of each one. NLOS WLLS is scored in the simulations above as our best algorithm, but it exhibits strong accuracy degradation near the cell boundaries, whilst the Geometrical estimator makes much better therein. The intention is to develop a new hybrid algorithm very alike to NLOS WLSS but with a better performance at the boundaries.

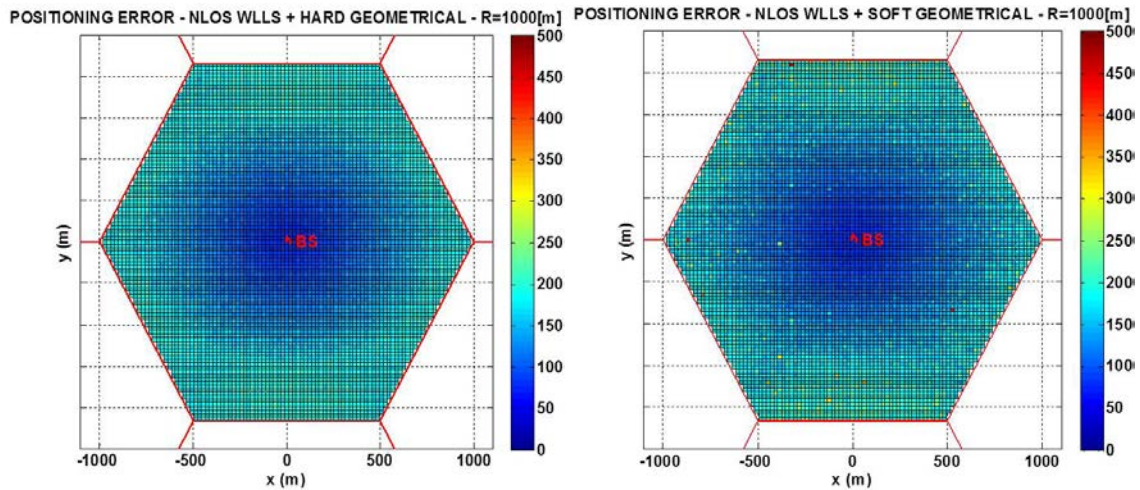


Figure 2.18. Average Subscriber Positioning Error for a NLOS moderate dispersive scenario based on TOA for the NLOS WLLS plus Geometrical restrictions algorithm when the cell radius $R=1000$ m. A) Left: Hard fusion. B) Right: Soft fusion.

Two fusion methods have been proposed to make this job. The first one performs a hard fusion by simply choosing the result from the Geometrical estimator when the NLOS WLLS algorithm estimates the subscriber position within the 30% of the cell radius closer to the boundaries, whilst the second method prefers a soft estimation by averaging the results from NLOS WLLS and the Geometrical estimator in this portion of the cell.

Figure 2.19 shows the CDF's for the positioning error of algorithms involved within this experiment. Soft fusion is clearly the winner alternative to achieve the improved specified algorithm. The hard fusion gets a much better error reduction at the boundaries but at a higher expense of the accuracy of the original NLOS WLLS algorithm. On the other hand, the soft fusion preserves the properties of the original algorithm and it reduces errors at the boundaries. Note for i.e. that error is below 162 m for the 70% of the cases and below 208 m for the 95% of the cases for the original NLOS WLLS algorithm. These values change to 163 m and 191 m respectively when the geometrical restriction is added using the soft fusion.

In addition, Figure 2.19 shows that the hard fusion algorithm improves the Geometrical estimator.

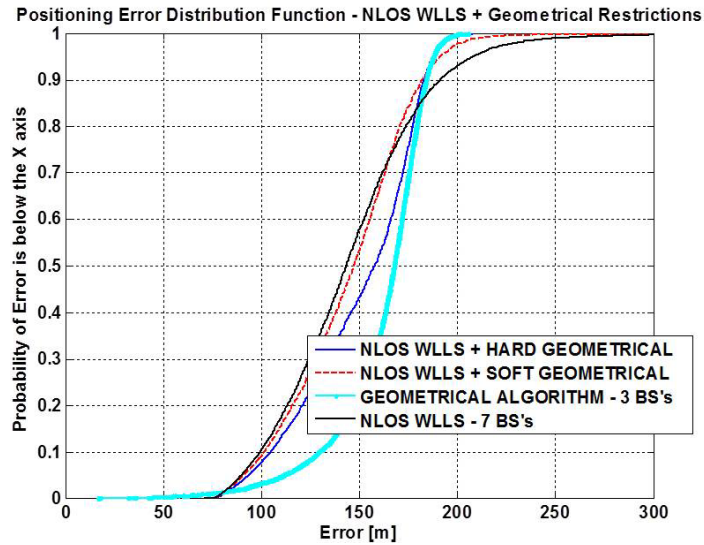


Figure 2.19. CDF for the subscriber positioning error within a NLOS moderate dispersive scenario and a TOA based scheme by weighting measures and using Geometrical restrictions.

Experiment 2.6: TOA measures provided from NLOS BSs in a high dispersive environment – Mitigating NLOS condition by weighting measures

A much more aggressive scenario is considered in this experiment. It assumes that NLOS condition is present in the seven BS's as before, and the required parameters for the Greenstein model take the following values: $T_1=0.7$ [us], $\varepsilon=0.5$, $\sigma_x=8.0$ [dB], $\sigma_\xi=4.0$ [dB], and $\rho=-0.75$. Particularly, T_1 has been almost doubled respect the experiments above to adjust our data to certain measurements reported in [22]. It could be the case of environments with a second cluster or even a third cluster of arrivals. This condition has been experimentally observed in 13% of the cases within Typical Urban scenery [16].

Clearly, from comparison between Figure 2.20 and Figure 2.12, this new scenario offers more difficult for the subscriber positioning, and a stronger degradation near the boundaries. In fact, Figure 2.21 exhibits as the average positioning error is below 293m for the 70% of the cases, and below 407 m for the 95% of the cases when the NLOS WLLS method is performed, and degrades below 308 m and below 407 m respectively when the WLLS algorithm is used instead.

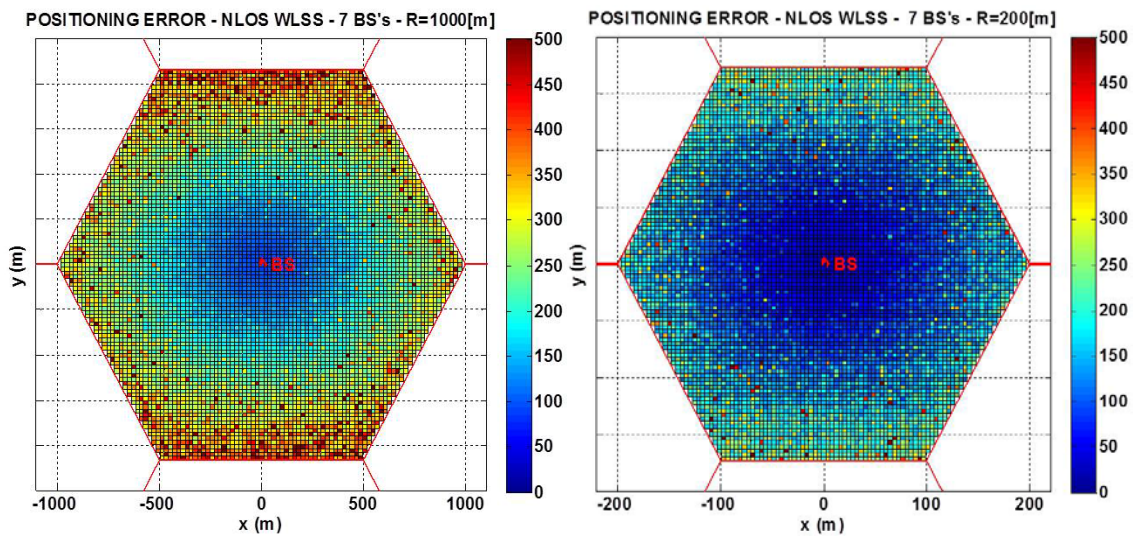


Figure 2.20. Average Subscriber Positioning Error for a NLOS highly dispersive scenario based on TOA for the NLOS WLLS algorithm when measures related to 7 BS's are used. A) Left: the cell radius $R=1000$ m. B) Right: $R=200$ m.

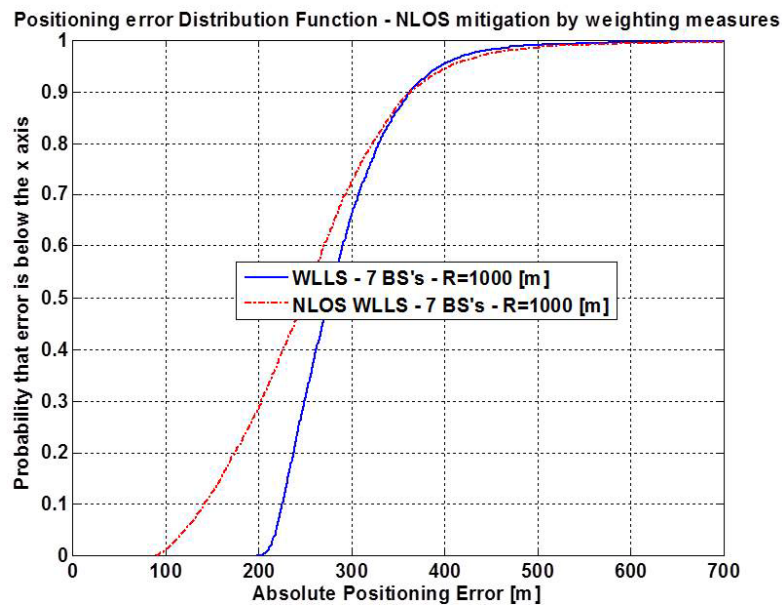


Figure 2.21. CDF for the subscriber positioning error within a NLOS highly dispersive scenario and a TOA based scheme for both WLLS and NLOS WLLS methods and 7 BS's when cell radius $R=1000$ m.

Experiment 2.7: TOA measures provided from NLOS BSs in a mixed dispersive environment – Mitigating NLOS condition by weighting measures and incorporating Geometrical restrictions

Scenario described in the experiment above is clearly too aggressive, and therefore the objective of this new situation is to define a more realistic case where a much higher dispersion ($T_1=0.7$ [us]) appears within the 13% of the cases, whilst the more conservative dispersive environment with $T_1=0.4$ [us] usually domains. This last scenario assumes that NLOS condition is present in the seven BS's as before, and the required parameters for the Greenstein model take the following values: $\varepsilon=0.5$, $\sigma_x=8.0$ [dB], $\sigma_\xi=4.0$ [dB], and $\rho=-0.75$.

Figure 2.22 illustrates the behavior of both the WLLS method and the NLOS WLLS plus Geometrical Restrictions algorithm for this mixed dispersive situation. The latter method clearly mitigates better the NLOS condition.

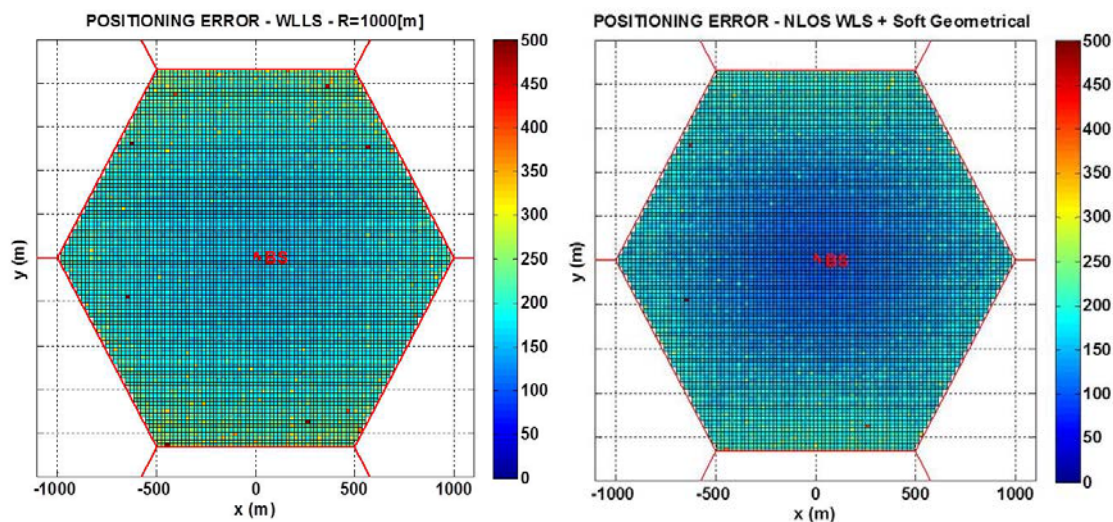


Figure 2.22. Average Subscriber Positioning Error for a NLOS mixed dispersive scenario based on TOA when the cell radius $R=1000$ m and 7 BS's are used to perform positioning. A) Left: WLLS algorithm. B) Right: NLOS WLLS + Soft Geometrical restrictions.

Figure 2.23 compares the CDF's for the positioning error from various mitigation techniques. It includes the Geometric algorithm described within experiment 4, the WLLS algorithm, and the proposed algorithms that fusion NLOS WLLS and Geometrical restrictions as they are described within experiment 5. These results confirms the NLOS WLLS plus soft geometrical restrictions algorithm as the best among the whole set of implemented methods. In fact, this algorithm exhibits average positioning errors below 173 m in 70% of the cases, and below 205 m in 95% of the cases. NLOS WLLS plus hard geometrical restrictions algorithms also makes a good job and registers average positioning errors below 184 m in 70% of the cases and below 200 m in the 95% of the cases. These latter values are very similar to the provided by

the Geometric algorithm which exhibits average positioning errors below 186 m in the 70% of the cases and below 200 m in the 95% of the cases in spite a good portion of its data registers up to 20 m of additional error. In addition, the original NLOS WLLS algorithm achieves an average positioning error below 176 m in the 70% of the cases and below 229 m in the 95% of the cases, whilst WLLS algorithm reaches an average positioning error below 195 m for the 70% of the cases and below 239 m for the 95% of the cases. It means that NLOS WLLS plus soft Geometrical restrictions provides an additional mitigation of around of 30-50 m when it is compared with the WLLS method.

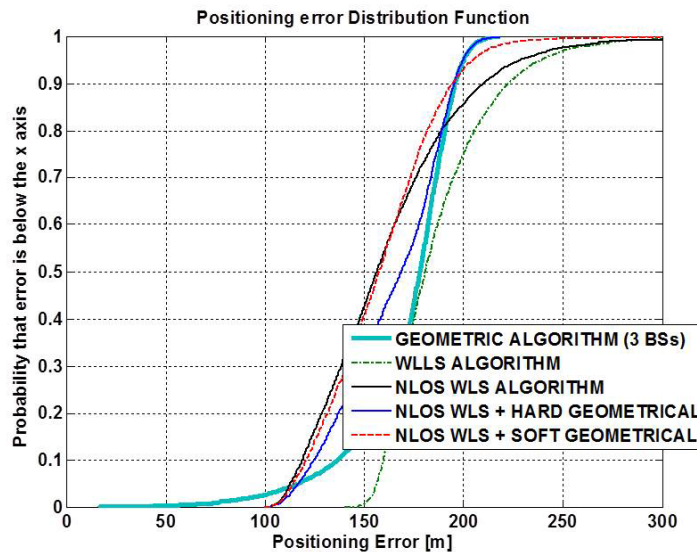


Figure 2.23. CDF for the subscriber positioning error within a NLOS mixed dispersive scenario and a TOA based scheme for both WLLS and NLOS WLLS plus Geometrical restrictions methods when 7 BS's with cell radius $R=1000$ m are used.

2.4 Summary and Discussion

The NLOS condition strongly degrades the performance of subscriber positioning in wireless communication systems. The traditional robust algorithms, originally developed to use the LOS signal, completely fail in current dispersive scenarios due to the measurement error can't be modeled just as a zero mean Gaussian variable. Therefore, newer approaches that better describe the error statistics have been proposed at the literature [59]-[61],[64] and they may be applied to estimate the subscriber position. However the final accuracy will be dependent of the adjustment between the proposed statistics and the true ones. Furthermore, actual error statistics vary with space and time. Hence, an accurate description would require a very complex dynamic formulation, and also to a greater computational burden.

Since a perfect statistical characterization of the NLOS condition is not a practical solution within the subscriber positioning context, several NLOS mitigation techniques

have been proposed. Some of them consider the weighting of the available measures in order to get the better of each one, and from the whole set of them [54][59][62],[65]-[69]. These weighting factors may be extracted from the signal statistics [59][62][65], as well as from lateral information related to the physics of the problem[54],[66]-[69].

Moreover, other methods prefer to make inferences from the problem geometry, and hence incorporate certain geometrical restrictions in order to improve the accuracy [58][60][63].

Whatever is the NLOS mitigation approach finally performed; the NLOS discrimination is an important procedure to achieve the best results. After all, the discrimination stage enables the proper choice of the statistics, the selection of the quality factors to weight the measures, and the right application of the geometrical restrictions used in the positioning algorithms.

From the wide range of algorithms available at the literature for providing subscriber positioning, the linear methods are attractive due to their simplicity, and the fact that they always provide a solution, avoiding convergence issues associated with iterative nonlinear algorithms as it was shown with the simulations in section 2.3. Within the first group, the WLLS approaches are particularly interesting due to their capabilities to apprehend the relevant signal characteristics through the weighting matrices, although they require well defined models to derive the weighting factors. Therefore these methods were chosen for their evaluation at the simulation stage.

In order to test the most relevant approaches for positioning and NLOS mitigation within a realistic environment, a simulation platform based on the Greenstein model was built for small sized cells. This platform includes the main characteristics of the propagating signal with the help of a robust model that is in the core of more complex current ones. Furthermore, this platform is well suited for system level simulations, and it will be enhanced at chapter 4 to include the effects of signal space-time diversity.

Besides the Torrieri's iterative solution, and the simple and traditional LLS method, a new mitigation algorithm that considers both the weighting of the measures and the inclusion of soft geometrical restrictions has been proposed within this chapter for the positioning based on TOA [72]. This new algorithm makes a better work than those provided by the literature [58][70] and used as reference. In fact, this new algorithm achieves a positioning error below 163 m for the 70% of the cases and below 191 m for the 95% of the cases within a moderate dispersive environment ($T_1=0.4$ [us]). These values are at least 10% lower than those provided by the WLLS algorithm used as reference. Therefore average positioning error decreases between 17 m and 50 m for this new method, and between 25 m and 60 m when it is compared with Yi Long NLOS mitigation algorithm [70]. These results confirm the fact that better results are provided from hybrid techniques instead of the use of a single one, and when the right models are employed to characterize the signal. However, 163 m is still too high when it is compared with the 100 m specified by the E911 regulation. Therefore, a scheme for taking advantage of space-time diversity is proposed at chapter 4, to enhance the accuracy provided by these methods.

A harder scenario where a very aggressive dispersion is presented in around 13% of the cases has also been studied. Our better proposal exhibits average positioning errors below 173 m in the 70% of the cases, and below 205 m in the 95% of the cases. It means a positioning error degradation of around 10-15 m respect to the moderate dispersive situation, but also implies a gain of around 30-50 m in accuracy in comparison to the Yi Long algorithm used as a reference. Moreover, since 13% of aggregate dispersion leads to just a 6% of accuracy degradation, these results also show the robustness of our proposed algorithm. However, these results have been provided for TOA based positioning, and new algorithms will be provided for TDOA based positioning in chapter 4.

2.5 Annex A2.1 A Linear Least Squares Received Signal Strength (LLS-RSS) based Positioning Algorithm

The general expression for RSS in a fading channel is a function of distance d , between transmitter and receiver as it is shown in (2.83), where β' refers to the loss path propagation factor and signal strength is measured in decibels [38]. Therefore, factor β appears from logarithm base conversion.

$$P_r \Big|_{dB} = K - 10\beta' \log|d| = K - \beta \ln|d_i| = m_i$$

$$\text{with } d_i = \|\mathbf{x} - \mathbf{r}_i\| = \sqrt{(x - x_i)^2 - (y - y_i)^2}; \quad \forall i = 1, 2, \dots, L \quad (2.83)$$

$$\text{and } \beta = 10\beta' / \ln(10)$$

The RSS measured at BS _{i} is noted as m_i , and it is expressed as in (2.84):

$$m_i = K - \frac{\beta}{2} \ln \left| (x - x_i)^2 - (y - y_i)^2 \right|; \quad \forall i = 1, 2, \dots, L \quad (2.84)$$

If RSS measures for each BS from the serving BS as in (2.85), it becomes (2.86) and (2.87).

$$m_1 - m_i = -\frac{\beta}{2} \ln|x^2 + y^2| + \frac{\beta}{2} \ln \left| (x - x_i)^2 - (y - y_i)^2 \right|; \quad \forall i = 2, 3, \dots, L \quad (2.85)$$

$$m_1 - m_i = \frac{\beta}{2} \ln \left| \frac{(x - x_i)^2 - (y - y_i)^2}{x^2 + y^2} \right|; \quad \forall i = 2, 3, \dots, L \quad (2.86)$$

$$m_1 - m_i = \frac{\beta}{2} \ln \left[\frac{x^2 + y^2 - 2(x_i x + y_i y) + x_i^2 + y_i^2}{x^2 + y^2} \right]; \quad \forall i = 2, 3, \dots, L \quad (2.87)$$

The expression above may be re-written in the form of (2.88) replacing identities in (2.35) and (2.37):

$$m_1 - m_i = \frac{\beta}{2} \ln \left[\frac{r^2 - 2(x_i x + y_i y) + r_i^2}{r^2} \right]; \quad \forall i = 2, 3, \dots, L \quad (2.88)$$

Furthermore, when subscriber is located near the serving BS, it is also possible to transform (2.88) into (2.90) since (2.89) is proven:

$$\text{When } \frac{r}{r_i} < 1 \rightarrow \left(\frac{r}{r_i} \right)^2 \ll 1 \quad (2.89)$$

$$m_1 - m_i = \frac{\beta}{2} \ln \left[\frac{1 - 2(x_i x + y_i y) / r_i^2}{(r/r_i)^2} \right]; \quad \forall i = 2, 3, \dots, L \quad (2.90)$$

Further, (2.90) becomes (2.91), where the first logarithm may be estimated as a linear function around one for $(r/r_i) < 1/5$ with an error inferior to 21%, and the second one around of $(r/r_i) = 1/5$ also with an error lower than 21% for $(r/r_i) > 0,05$ as it is shown

in (2.92), and therefore the general expression for the set of k-1 equations is exhibited within (2.93).

$$m_1 - m_i = \frac{\beta}{2} \left\{ \ln \left[1 - 2(x_i x + y_i y) / r_i^2 \right] - \ln (r / r_i)^2 \right\}; \quad \forall i = 2, 3, \dots, L \quad (2.91)$$

$$m_1 - m_i = \frac{\beta}{2} \left\{ -\frac{2}{r_i^2} (x_i x + y_i y) - 2 \left[\ln \left(\frac{1}{5} \right) + 5 \left(\frac{r}{r_i} - \frac{1}{5} \right) \right] \right\}; \quad \forall i = 2, 3, \dots, L \quad (2.92)$$

$$x_i x + y_i y = r_i^2 \left[\frac{1}{\beta} (m_i - m_1) + 1 - \ln \left(\frac{1}{5} \right) \right] - 5 r r_i; \quad \forall i = 2, 3, \dots, L \quad (2.93)$$

It also should be noted as r_i approximately equates to $2R$, being R the cell radius, and since errors achieved from linearization keep lower than 10% for the range of r/r_i between 0,10 and 0,30; this estimator is adequate for subscriber positions between 20% and 60% of the serving BS radius.

2.6 Annex A2.2 Derivation of the first two moments for the RMS Delay Spread defined as the Greenstein Model

The derivation of these moments is eased by the fact that ξ is lognormal and therefore, it is related to Ξ as it is shown in (2.94), and therefore, it admits to be expressed in relation to a new scaled variable \mathbf{z} with mean m_z and standard deviation σ_z as it is shown in (2.95):

$$\xi = e^{\Xi \cdot \ln 10 / 10} = e^{\mathbf{z}}; \quad \text{with } \mathbf{z} = \frac{\ln 10}{10} \Xi \quad (2.94)$$

$$m_z = E\{\mathbf{z}\} = \frac{\ln 10}{10} m_\xi; \quad \sigma_z = \sqrt{\text{var}\{\mathbf{z}\}} = \frac{\ln 10}{10} \sigma_\xi \quad (2.95)$$

The computation of ξ may be related to the characteristic function $\Phi_z(s) = E\{e^{s\mathbf{z}}\}$ as follows:

$$E\{\xi\} = E\{e^{\mathbf{z}}\} = \Phi_z(s=1) = e^{s \cdot m_z + s^2 \cdot \sigma_z^2 / 2} \Big|_{s=1} = e^{m_z + \sigma_z^2 / 2} \quad (2.96)$$

Similarly, the second moment may be performed as it is shown in (2.97):

$$E\{\xi^2\} = E\{e^{2\mathbf{z}}\} = \Phi_z(s=2) = e^{s \cdot m_z + s^2 \cdot \sigma_z^2 / 2} \Big|_{s=2} = e^{2m_z + 2\sigma_z^2} \quad (2.97)$$

And the variance may be achieved as in (2.98):

$$\text{var}\{\xi\} = E\{\xi^2\} - E^2\{\xi\} = e^{2m_z + 2\sigma_z^2} - e^{2m_z + \sigma_z^2} = e^{2m_z} \left(e^{2\sigma_z^2} - e^{\sigma_z^2} \right) \quad (2.98)$$

Moreover, the statistics for the RMS delay spread are finally derived within (2.99), (2.100) and (2.101):

$$E\{\tau_{rms}\} = E\{T_1 d^\varepsilon e^{\mathbf{z}}\} = T_1 d^\varepsilon e^{m_z + \sigma_z^2 / 2} \quad (2.99)$$

$$E\{\tau_{rms}^2\} = E\{T_1^2 d^{2\varepsilon} e^{2\mathbf{z}}\} = T_1^2 d^{2\varepsilon} e^{2m_z + 2\sigma_z^2} \quad (2.100)$$

$$\sigma_{\tau_{rms}} = \sqrt{\text{var}\{\boldsymbol{\tau}_{rms}\}} = T_1 d^\varepsilon \sqrt{\text{var}\{e^z\}} = T_1 d^\varepsilon \sqrt{e^{2m_z + \sigma_z^2} (e^{\sigma_z^2} - 1)} \quad (2.101)$$

When \mathbf{d} within (2.5) is assumed to be a random variable, uniformly distributed between 0 and D , expressions within (2.99) and (2.101) takes the form in (2.102) and (2.103), and the second moment of the RMS Delay Spread variable is required. This moment is figured out in (2.104):

$$E\{\boldsymbol{\tau}_{rms}\} = E\{T_1 \mathbf{d}^\varepsilon e^z\} = T_1 e^{m_z + \sigma_z^2/2} E\{\mathbf{d}^\varepsilon\} \quad (2.102)$$

$$\sigma_{\tau_{rms}} = \sqrt{E\{\boldsymbol{\tau}_{rms}^2\} - E^2\{\boldsymbol{\tau}_{rms}\}} \quad (2.103)$$

$$E\{\boldsymbol{\tau}_{rms}^2\} = E\{(T_1 \mathbf{d}^\varepsilon \boldsymbol{\xi})^2\} = T_1^2 e^{2m_z + 2\sigma_z^2} E\{\mathbf{d}^{2\varepsilon}\} \quad (2.104)$$

Furthermore, it is easy to understand that the required moments in expressions (2.102) and (2.104) take the form in (2.105) and (2.106):

$$E\{\mathbf{d}^\varepsilon\} = \int_0^D \frac{1}{D} x^\varepsilon dx = \frac{D^\varepsilon}{1 + \varepsilon} \quad (2.105)$$

$$E\{\mathbf{d}^{2\varepsilon}\} = \int_0^D \frac{1}{D} x^{2\varepsilon} dx = \frac{D^{2\varepsilon}}{1 + 2\varepsilon} \quad (2.106)$$

Finally, replacing result in (2.105) within (2.102), the required expression in (2.77) results. On the other hand, replacing expressions (2.77) and the result in (2.106) within (2.103), the expression in (2.78) results.

2.7 Annex A2.3 Derivation of the first two moments for TDOA measures for environments described by the Greenstein model

A TDOA measure refers to the difference of the instants of arrival from signals transmitted between the subscriber and two different BSs. The Time Of Arrivals to a particular receiver are described by an exponential distribution whose RMS delay spread is a random variable related with the distance between transmitter and receiver as it is specified for the Greenstein model in the expression (2.5). TDOA measures are specified as in (2.107), and their statistics may be easily achieved with the use of the characteristic function reminding that TOA measures are uncorrelated exponential distributed random variables whose characteristic functions have the form within (2.108).

$$\boldsymbol{\tau}_{i,l} = \boldsymbol{\tau}_i - \boldsymbol{\tau}_l \quad (2.107)$$

$$\Phi_{\tau_i}(s) = E\{e^{s\tau_i}\} = (1 - s\tau_{irms})^{-1}; \quad \forall \text{Re}\{s\} < 1/\tau_{irms} \quad (2.108)$$

The form of the characteristic function for the algebraic addition of the two independent random variables in (2.107) corresponds to the product within (2.109):

$$\begin{aligned}\Phi_{\tau_{i,l}}(s) &= E\left\{e^{s(\tau_i - \tau_l)}\right\} = \Phi_{\tau_i}(s)\Phi_{\tau_l}(-s) \\ \Phi_{\tau_{i,l}}(s) &= (1 - sT_{irms})^{-1}(1 + sT_{1rms})^{-1}; \quad \forall \operatorname{Re}\{s\} \in \left(-\frac{1}{T_{1rms}}, \frac{1}{T_{irms}}\right)\end{aligned}\quad (2.109)$$

This latter product may be expressed as in (2.110) after partial-fraction decomposition, and the corresponding PDF is eventually derived as in (2.111):

$$\Phi_{\tau_{i,l}}(s) = \frac{\frac{T_{irms}}{1 - sT_{irms}} + \frac{T_{1rms}}{1 + sT_{1rms}}}{\frac{T_{irms}}{1 - sT_{irms}} + \frac{T_{1rms}}{1 + sT_{1rms}}}; \quad \forall \operatorname{Re}\{s\} \in \left(-\frac{1}{T_{1rms}}, \frac{1}{T_{irms}}\right)\quad (2.110)$$

$$f_{\tau_{i,l}}(\tau_{i,l}) = \frac{1}{T_{irms} + T_{1rms}} \left[e^{-\frac{\tau_{i,l}}{T_{irms}}} u(\tau_{i,l}) + e^{\frac{\tau_{i,l}}{T_{1rms}}} u(-\tau_{i,l}) \right]\quad (2.111)$$

However, it must be reminded that RMS Delay spreads in (2.111) are also random; hence, a better approximate expression is achieved by replacing these parameters by more suitable parameters such as their mean values in (2.99). Therefore, it takes the form in (2.112).

$$f_{\tau_{i,l}}(\tau_{i,l}) = \frac{1}{T_1 e^{\sigma_z^2/2} (d_i^\varepsilon + d_1^\varepsilon)} \left[e^{-\frac{\tau_{i,l}}{T_1 d_i^\varepsilon e^{\sigma_z^2/2}}} u(\tau_{i,l}) + e^{\frac{\tau_{i,l}}{T_1 d_1^\varepsilon e^{\sigma_z^2/2}}} u(-\tau_{i,l}) \right]\quad (2.112)$$

From (2.109), it is easy to derive the two first moments for the TDOA measure by evaluating the two first derivatives of the characteristic function at $s=0$, and eventually averaging these results over the log-normal variables. These moments are exhibited in (2.113) and (2.114):

$$E\{\tau_{i,l}\} = \frac{d}{ds} \Phi_{\tau_{i,l}}(s=0) = E\{\tau_{irms}\} - E\{\tau_{1rms}\} = T_1 e^{m_z + \sigma_z^2/2} (d_i^\varepsilon - d_1^\varepsilon)\quad (2.113)$$

$$E\{\tau_{i,l}^2\} = \frac{d^2}{ds^2} \Phi_{\tau_{i,l}}(s=0) = E\{2\tau_{irms}^2 - 3\tau_{irms}\tau_{1rms} + 2\tau_{1rms}^2\}\quad (2.114)$$

$$E\{\tau_{i,l}^2\} = T_1^2 \left[2d_i^{2\varepsilon} e^{2m_z + 2\sigma_z^2} - 3d_i^\varepsilon d_1^\varepsilon e^{2m_z + \sigma_z^2} + 2d_1^{2\varepsilon} e^{2m_z + 2\sigma_z^2} \right]$$

From (2.114) and (2.113) the variance of the TDOA measure results as in (2.115):

$$\operatorname{var}\{\tau_{i,l}\} = T_1^2 e^{2m_z + \sigma_z^2} \left[(2e^{\sigma_z^2} - 1)(d_i^{2\varepsilon} + d_1^{2\varepsilon}) - d_i^\varepsilon d_1^\varepsilon e^{2m_z + \sigma_z^2} \right]\quad (2.115)$$

And consequently, this variance will be lower than the product exhibited in (2.116):

$$\operatorname{var}\{\tau_{i,l}\} < T_1^2 e^{2m_z + \sigma_z^2} (2e^{\sigma_z^2} - 1)(d_i^{2\varepsilon} + d_1^{2\varepsilon})\quad (2.116)$$

Another important parameter required when weighting TDOA measures corresponds to the cross moment of these measures. It may compute as follows:

$$E\{\tau_{i,l}\tau_{j,l}\} = E\{(\tau_i - \tau_l)(\tau_j - \tau_l)\} = E\{\tau_i\tau_j\} - E\{\tau_i\tau_l\} - E\{\tau_l\tau_j\} + E\{\tau_l^2\}\quad (2.117)$$

Due to the propagation timings from the subscriber to each BS are independent, (2.117) turns into (2.118), and after replacing the corresponding expressions from (2.99) and (2.100) within (2.118), it takes the form in (2.119).

$$E\{\tau_{i,l}\tau_{j,l}\} = E\{\tau_i\}E\{\tau_j\} - E\{\tau_i\}E\{\tau_1\} - E\{\tau_1\}E\{\tau_j\} + E\{\tau_1^2\} \quad (2.118)$$

$$E\{\tau_{i,l}\tau_{j,l}\} = T_1^2 e^{2m_z + \sigma_z^2} (d_i^\varepsilon - d_1^\varepsilon)(d_j^\varepsilon - d_1^\varepsilon) \quad (2.119)$$

2.8 Annex A2.4 Signals required for Greenstein Model

Greenstein model requires two correlated log-normal random variables. In the following the procedure to obtain these two variables, \mathbf{X} and $\mathbf{\Xi}$, is presented.

First of all, let's remind that the linear combination of two Gaussian random variables is also Gaussian, and this new variable is correlated to the original ones. Therefore, \mathbf{X} may be related to $\mathbf{\Xi}$ and to a normal variable \mathbf{W} as it is shown in (2.120), where w_1 and w_2 are weighting factors that shall be determined in order to satisfy the requirements of the model.

$$\mathbf{X} = w_1 \mathbf{\Xi} + w_2 \mathbf{W} \quad (2.120)$$

It is easy to probe that since \mathbf{X} and $\mathbf{\Xi}$ are zero mean variables, \mathbf{W} will also be. Moreover, due to \mathbf{W} and $\mathbf{\Xi}$ are uncorrelated Gaussians, the characteristic function of \mathbf{X} corresponds to the product of these characteristic functions as it is shown in (2.121):

$$\Phi_{\mathbf{X}}(s) = E\{e^{s\mathbf{X}}\} = E\{e^{s(w_1\mathbf{\Xi} + w_2\mathbf{W})}\} = E\{e^{sw_1\mathbf{\Xi}}e^{sw_2\mathbf{W}}\} = \Phi_{\mathbf{\Xi}}(w_1s)\Phi_{\mathbf{W}}(w_2s) \quad (2.121)$$

Finally, the characteristic function of \mathbf{X} is exhibited in (2.122), and in fact, it corresponds to a Gaussian distributed random variable whose variance σ_x^2 is shown in (2.123):

$$\Phi_{\mathbf{X}}(s) = \exp\left[\left(w_1^2\sigma_\xi^2 + w_2^2\right)s^2/2\right] \quad (2.122)$$

$$\sigma_x^2 = w_1^2\sigma_\xi^2 + w_2^2 \quad (2.123)$$

On the other hand, the cross-correlation between \mathbf{X} and $\mathbf{\Xi}$ may be computed as it is shown in (2.124):

$$E\{\mathbf{X}\mathbf{\Xi}\} = E\{(w_1\mathbf{\Xi} + w_2\mathbf{W})\mathbf{\Xi}\} = E\{w_1\mathbf{\Xi}^2\} = w_1\sigma_\xi^2 \quad (2.124)$$

Furthermore, since the correlation above is also expressed as $\rho \cdot \sigma_x \cdot \sigma_\xi$, it is easy to figure out w_1 as the exhibited in (2.125), and w_2 as in (2.126).

$$w_1 = \frac{\rho\sigma_x}{\sigma_\xi} \quad (2.125)$$

$$w_2 = \sigma_x \sqrt{1 - \rho^2} \quad (2.126)$$

In summary, weights computed in (2.125) and (2.126) must be set in (2.120) to achieve the required log-normal random variables.

2.9 References

- [1] W.C.Y. Lee, “Mobile Communications Engineering”, McGraw-Hill, New York, 1997.
- [2] W.C. Y. Lee, “Mobile Communications Design Fundamentals”, John Wiley & Sons Inc., 1993.
- [3] Theodore S. Rappaport, “Wireless Communications, Principles & Practice”, Prentice Hall, New Jersey, 1996.
- [4] William C. Jakes, “Microwave Mobile Communications”, IEEE Press, New Jersey, 1994.
- [5] José María Hernando Rábanos, Cayetano Lluch Mesquida, “Comunicaciones Móviles de Tercera Generación - UMTS”, Telefónica Móviles España, S.A., 2001.
- [6] Arogyaswami J. Paulraj and Boon Chong Ng, “Space-Time Modems for Wireless Personal Communications”, IEEE Personal Communications Magazine, pp. 36-48, February, 1998.
- [7] Richard B. Ertel and Paulo Cardieri, Kevin W. Sowerby, Theodore S. Rappaport and Jeffrey H. Reed, “Overview of Spatial Channel Models for Antenna Array Communication Systems”, IEEE Personal Communications Magazine, February, 1998.
- [8] Bernard Sklar, “Rayleigh Fading Channels in Mobile Digital Communication Systems. Part I: Characterization”, IEEE Communications Magazine, Vol. 35, No. 7, July, 1997, DOI: 10.1109/35.601748.
- [9] Kaveh Pahlavan, Prashant Krishnamurthy, “Principles of Wireless Networks”, Prentice Hall Communications Engineering and Emerging Technologies Series, 2002.
- [10] Bernard Sklar, “Rayleigh fading Channels in Mobile Digital Communication Systems. Part II: Mitigation”, IEEE Communications Magazine, Vol. 35, No. 7, July, 1997, DOI: 10.1109/35.601748.
- [11] Richard van Nee and Ramjee Prasad, “OFDM for Wireless Multimedia Communications”, Artech House, 2000. ISBN 0-89006-530-6.
- [12] Camillo Gentile, Sofía Martínez and Alfred Kik, “A Comprehensive Spatial-Temporal Channel Propagation Model for the Ultrawideband Spectrum 2-8 GHz”, IEEE Transactions on Antennas and Propagation, Vol. 58, No. 6, June 2010, DOI: 10.1109/TAP.2010.2046834.
- [13] K.I. Pedersen, P.E. Mogensen, B. Fleury, “A Stochastic Model of the Temporal and Azimuthal Dispersion seen at the Base Station in Outdoor Propagation Environments”, IEEE Transactions on Vehicular Technology, May 2000.
- [14] Salvatore Bellofiore, Constantine A. Balanis, Jeffrey Foutz and Andreas S. Spanias, “Smart-Antenna Systems for Mobile Communication Networks Part 1: Overview and Antenna Design”, IEEE Antenna’s and Propagation Magazine, Vol. 44, No. 3, June 2002, DOI: 10.1109/MAP.2002.1039395.

-
- [15] P. Lusina, F. Kohandani and S.M. Ali, "Antenna parameter effects on spatial channel models", *The Institution of Engineering and Technology Communication*, Vol. 3, No. 9, 2009, DOI: 10.1049/iet-com.2008.0414.
- [16] Henrik Asplund, Andrés Alayón Glazunov, Andreas F. Molisch, Klaus I. Pedersen and Martin Steinbauer, "The COST 259 Directional Channel Model – Part II: Macrocells", *IEEE Transactions on Wireless Communications*, Vol. 5, 12, 2006, DOI: 10.1109/TWC2006.256967.
- [17] Patrice Pajusco, "Experimental Characterization of D.O.A. at the Base Station in Rural and Urban Area", *IEEE Conference on Vehicular Technology (VTC'98)*, pp. 993-997, May, 1998.
- [18] Larry J. Greenstein, Vinko Erceg, Yu Shuan Yeh, and Martin V. Clark, "A New Path-Gain/Delay-Spread Propagation Model for Digital Cellular Channels", *IEEE Transactions on Vehicular Technology*, Vol. 46, No.2, pp. 477-485, May, 1998.
- [19] Philippe Laspougeas, Patrice Pajusco, Jean-Claude Bic, "Radio Propagation in Urban Small Cells Environment at 2GHz: Experimental Spatio-Temporal Characterization and Spatial Wideband Channel Model", *IEEE Conference on Vehicular Technology (VTC 2000)*, pp. 885-892, May, 2000.
- [20] Philippe Laspougeas, Patrice Pajusco, Jean-Claude Bic, "Spatial Radio Channel for UMTS in Urban Small Cells Area", *IEEE Conference on Vehicular Technology (VTC 2000)*, 2000.
- [21] U. Martín, "Spatio-temporal radio channel characteristics in urban macrocells", *IEE Proceedings-Radar, Sonar Navigation*, Vol. 145, No.1, pp. 44-49, February, 1998.
- [22] Henrik Asplund, Kjell Larsson and Peter Okvist, "How typical is the 'Typical Urban' channel model?", *IEEE Vehicular Technology Conference*, 2008, DOI: 10.1109/VETECS.2008.82.
- [23] TIA/EIA/IS-2000-2, "Physical Layer Standard for cdma2000 Spread Spectrum Systems", August 1999.
- [24] Mohamed Ibnkahla, "Signal Processing for Mobile Communications Handbook", chapter 10, pp. 17-20, CRC Press, Taylor and Francis Group, 6000 Broken Sound Parkway NW, Suite 300, Boca Ratón, FL 33487-2742, August 2004.
- [25] Harry Holma, Antti Toskala, "WCDMA FOR UMTS. Radio Access for Third Generation Mobile Communications", John Wiley & Sons, Ltd, West Sussex, PO19 1UD, England, June 2000.
- [26] Shedman Tam, Hunter Lee, "MSF whitepaper on Location Services in LTE Networks – MSF-TR-SERVICES-005-FINAL", *Multiservice Forum*, 2009.
- [27] M. Oğuz Sunay, "Evaluation of Location Determination Technologies Towards Satisfying the FCC E-911 Ruling", *Bell Labs, Lucent Technologies, USA*, 2001.
- [28] Harin A. Karini, "Advanced Location-Based Technologies and Services", *CRC Press*, 2013, ISBN: 9781466518186.
- [29] Jeffrey H. Reed, Kevin J. Krizman, Brian D. Woerner, and Theodore Rappaport, "An Overview of the Challenges and Progress in Meeting the E-911 Requirements for Location Service", *IEEE Communications Magazine*, April 1998.

- [30] Sven Fischer, “Observed Time Difference Of Arrival (OTDOA) Positioning in 3GPP LTE”, Qualcomm Technologies, Inc., June 2014.
- [31] Yehia R. Hamdy, and Sami A. Mawjoud, “Assessment of Uplink Time Difference Of Arrival (U-TDOA) Position Location Method in Urban Area and Highway in Mosul City”, *Al-Rafadain Engineering Journal*, Vol.21, Issue 2, Spetial section pp. 54-65, April 2013.
- [32] James J. Caffery, Jr. and Gordon L. Stüber, “Overview of Radiolocation in CDMA Cellular Systems”, *IEEE Communications Magazine*, pp. 38-45, April 1998.
- [33] James Caffery, Jr. and Gordon L. Stüber, “Subscriber Location in CDMA Cellular Networks”, *IEEE Transactions on Vehicular Technology*, Vol. 47, No.2, pp. 406-416, May 1998.
- [34] Guillaume Decarreau, Sylvie Mayrargue, Montse Nájjar, Josep Vidal, “IST-1999-10322 SATURN D632, Report on impact of proposed location techniques on UTRAN”, France Telecom R&D, Universitat Politècnica de Catalunya, September 2002.
- [35] Don J. Torrieri, “Statistical Theory of Passive Location Systems”, *IEEE Transactions on Aerospace and Electronic Systems*, Vol. AES-20, No. 2, pp. 183-198, March 1984.
- [36] Olga Muñoz, Margarita Cabrera, et al, “SATURN D232: Recommendations for WP6 activities”, Universitat Politècnica de Catalunya, June 2000.
- [37] Seyed A. Zekavat and R. Michael Buehrer, “Handbook of Position Location - Theory, Practice and Advances”, IEEE Press – John Wiley and Sons, 2012.
- [38] Fredrik Gustafsson and Fredrik Gunnarsson, “Mobile Positioning using Wireless Networks – Possibilities and fundamental limitations based on available wireless network measurements”, *IEEE Signal Processing Magazine*, Vol. 22, No.4, July 2005, DOI: 10.1109/MSP.2005.1458284.
- [39] Ali H. Sayed, Alireza Tarighat and Nima Khajehnouri, “Network-Based Wireless Location”, *IEEE Signal Processing Magazine*, Vol. 22 , No. 4, July 2005, DOI: 10.1109/MSP.2005.1458275.
- [40] Y.T. Chan and K.C. Ho, “A Simple and efficient Estimator for Hyperbolic Location”, *IEEE Transactions on Signal Processing*, Vol. 42, 8, 1994, DOI: 10.1109/78.301830.
- [41] F.K.W. Chan, H.C. So, J. Zheng and K.W.K. Lui, “Best Linear Unbiased Estimator Approach for Time-Of-Arrival Based Localisation”, *The Institution of Engineering and Technology Signal Processing*, Vol. 2, 2, 2008, DOI: 10.1049/iet-spr:20070190.
- [42] H.-W. Wei, Q. Wan, Z.-X. Chen and S.-F. Ye, “Multidimensional scaling-based passive emitter localisation from range-difference measurements”, *The Institution of Engineering and Technology Signal Processing*, Vol. 2, 4, pp. 415-423 2008, DOI: 10.1049/iet-spr:20070207.
- [43] Josep Vidal, Marga Cabrera, René Játiva, Montse Nájjar, Alba Pagès, Carine Simon, “IST-1999-10322 SATURN D621 - Location Based Services Performance Evaluation (Location Techniques)”, Universitat Politècnica de Catalunya, June 2001.

-
- [44] George P. Yost and Shankari Panchapakesan, "Automatic Location Identification using a Hybrid Technique", IEEE Vehicular Technology Conference, pp. 264-267, 1998.
- [45] Gezici S., Zhi Tian, Giannakis G.B., Kobayashi Hisashi, Molisch A.F., Poor H.V., Sahinoglu, Z., "Localization via ultra-wideband radios: a look at positioning aspects for future sensor networks", IEEE Signal Processing Magazine, Volume 22, Issue 4, 2005. DOI: 10.1109/MSP.2005.1458289.
- [46] Li Cong and Weihua Zhuang, "Hybrid TDOA/AOA Mobile User Location for Wideband CDMA Cellular Systems", IEEE Transactions on Wireless Communications, Vol. 1, No. 3, 2002, DOI: 10.1109/TWC.2002.800542.
- [47] Josep Vidal et al, "Positioning Limits for UMTS mobiles in Delay and Angular Dispersive Channels", International Symposium on Location Based Services for Cellular Users, LOCELLUS 2001, February 2001.
- [48] Alba Pagès-Zamora, Dana H. Brooks, Josep Vidal Manzano, "Least-Squares Location from DOA Measurements", 2000.
- [49] Alba Pagès-Zamora, Josep Vidal, Dana H. Brooks, "Closed-Form Solution for Positioning based on Angle of Arrival Measurements", IEEE International Symposium on Personal, Indoor and Mobile Radio Communications (PIMRC), Vol. 4, pp. 1522-1526, 2002.
- [50] Martin Hellebrandt, Rudolf Mathar, and Markus Scheibenbogen, "Estimating Position and Velocity of Mobiles in a Cellular Radio Network", IEEE Transactions on Vehicular Technology, Vol. 46, No. 1, February 1997.
- [51] Santiago Silva, René Játiva, "Seguimiento de Dispositivos Móviles en un Sistema de Comunicaciones Móviles Celulares", Revista Avances en Ciencias e Ingenierías, Vol. 1, No. 1, 2009.
- [52] Andreu Urruela, Josep Sala and Jaume Riba, "Average Performance Analysis of Circular and Hyperbolic Geolocation", IEEE Transactions on Vehicular Technology, Vol. 55, No. 1, January 2006, DOI: 10.1109/TVT.2005.861172.
- [53] Chris Drane, Chris Rizos, "Positioning Systems in Intelligent Transportation Systems", Artech House Inc., Norwood, 1998.
- [54] Olga Muñoz et al, "SATURN D231: Overview of UMTS User Location Possibilities and Limitations", Universitat Politècnica de Catalunya, March 2000.
- [55] Paúl Prócel, Luis Prócel, René Játiva, Julio Arauz, "Desarrollo de una Aplicación de Servicios Basados en Localización para Redes de tipo Global System for Mobile (GSM) y Universal Mobile Telecommunications System (UMTS) usando el emulador Mobile Positioning System 6.0.1 provisto por la empresa ERICSSON", Revista Avances en Ciencias e Ingenierías, Vol. 1, No. 1, 2009.
- [56] "Technical Specification Group Radio Access Network; Stage 2 functional specification on User Equipment (UE) positioning in UTRAN (Release 6) – 3GPP TS 25.305 V6.1.0 (2004-06)", 3RD Generation Partnership Project, 2004.
- [57] J. Borkowski and J. Lempäinen, "Practical Network-Based Techniques for Mobile Positioning in UMTS", EURASIP Journal on Applied Signal Processing, 2006. DOI: 10.1155/ASP/2006/12930.

- [58] Kai-Ten Feng, Chao-Lin Chen, and Chien-Hua Chen, "GALE: An Enhanced Geometry-Assisted Location Estimation Algorithm for NLOS Environments", *IEEE Transactions on Mobile Computing*, Vol. 7, 2, 2008, DOI: 10.1109/TMC.2007.70721.
- [59] Li Cong and Weihua Zhuang, "Nonline-of-Sight Error Mitigation in Mobile Location", *IEEE Transactions on Wireless Communications*, Vol. 4, No. 2, 2005, DOI: 10.1109/TWC.2004.843040.
- [60] Saipradeep Venkatraman and James Caffery Jr., "A Statistical Approach to Non-line-of-Sight BS Identification", *International Symposium on Wireless Personal Multimedia Communications*, Vol. 1, 2002, DOI: 10.1109/WPMC.2002.1088180.
- [61] Denis B. and Daniele N., "NLOS Ranging Error Mitigation in a Distributed Positioning Algorithm for Indoor UWB Ad-Hoc Networks", *International Workshop on Wireless Ad-Hoc Networks*, 2004, DOI: 10.1109/IWWAN.2004.1525602.
- [62] Jaume Riba and Andreu Urruela, "A Non-Line-Of-Sight Mitigation Technique based on ML-Detection", *IEEE International Conference on Acoustics, Speech and Signal Processing*, Vol. 2, 2004, DOI: 10.1109/ICASSP.2004.1326217.
- [63] Wang Wei, Xiong Jin-Yu, and Zhu Zhong-Liang, "A New Error Mitigation Algorithm in Location Estimation", *IEEE Transactions on Vehicular Technology*, Vol. 54, 6, 2005, DOI: 10.1109/TVT.2005.858177.
- [64] Al-Jazzar S. and Caffery J., "ML & Bayesian TOA Location Estimators for NLOS Environments", *56th IEEE Vehicular Technology Conference*, Vol. 2, 2002, DOI: 10.1109/VETEFCF.2002.1040790.
- [65] Hemin Li, Zhongliang Deng, Yanpei Yu, "Investigation on a NLOS Error Mitigation algorithm for TDOA Mobile Location", *IET International Conference on Communication Technology and Application (ICCTA2011)*, 2011, DOI: 10.1049/cp.2011.0787.
- [66] Soo-Young Lee and Jong-Tae Park, "NLOS Error Mitigation in a Location Estimation of Object based on RTLS using Kalman Filter", *International Joint Conference SICE-ICASE*, 2006, DOI: 10.1109/SICE.2006.314868.
- [67] Zhongliang Deng, Yanpei Yu, Weiguo Guan, Litao He, "NLOS Error Mitigation Based on Modified Kalman Filter for Mobile Location in Cellular Networks", *IEEE International Conference on Wireless Communications and Signal Processing (WCSP)*, 2010, DOI: 10.1109/WCSP.2010.5633466.
- [68] Weiguo Guan, Zhongliang Deng, Yanpei Yu, Yuetao Ge, "A NLOS Mitigation Method for CDMA2000 Mobile Location", *Second IEEE International Conference on Network Infrastructure and Digital Content*, 2010, DOI: 10.1109/ICNIDC.2010.5657865.
- [69] J.M. Huerta, J. Vidal, A. Giremus, J.Y. Tournet, "Joint particle filter and UKF position tracking in severe non-line-of-sight situations", *IEEE Journal of Selected Topics in Signal Processing*, Vol. 3, 5, pp. 874-888, October 2009, DOI: 10.1109/JSTSP.2009.2027804.
- [70] Yi Long, Jiyan Huang, Yijiang Pan, Jiang Du, "Novel TOA Location Algorithms based on MLE and MMSEE for NLOS Environments", *IEEE*

-
- International Conference on Communications, Circuits and Systems, Vol. 2, 2013, DOI: 10.1109/ICCCAS.2013.6765283.
- [71] James Caffery Jr., “A new approach to the geometry of TOA location”, IEEE Vehicular Technology Conference”, 2000, DOI: 10.1109/VETECONF.2000.886153.
- [72] René Játiva, David Sánchez, Josep Vidal, “NLOS Mitigation Based on TOA for Mobile Subscriber Positioning Systems by Weighting Measures and Geometrical Restrictions”, IEEE Asia-Pacific International Conference on Computer Aided System Engineering”, pp. 325-330, July 2015. DOI: 10.1109/APCASE.2015.64.

Chapter 3

Dispersive Source Models and Cramer-Rao Bounds

In order to evaluate different Location Determination Technologies (LDT) [1]-[3], a well suited link level simulator is required. This simulator should use reliable channel models which reflect accurately the wireless signals behavior and the relative geometry among base stations and mobile stations as it was commented at chapter 2. Moreover, it also should provide very general but reliable results and also be computational efficient. Such kind link level simulator has been provided at chapter 2, and also in the framework of the SATURN project [4]. However, by considering that there is a close relation between the quality of the measures and the positioning estimation, permanent efforts have been made to characterize wireless channel [5]-[8], and practical estimators have been derived. For instance, Bengtsson [9], Besson [10], and Valaee [11] have described several techniques based on signal subspace to estimate the Direction Of Arrival (DOA) and the angular spread for wireless dispersive signal, whereas Raleigh [12] and Wax [13], among others [14] have studied the problem of Joint Space-Time estimation in a multipath environment.

Furthermore, since the final behavior of a specific positioning technique depends on the way the signal parameters are estimated, a general comparison of different techniques is difficult. For this reason, in this chapter the problem of estimating the Time Of Arrival (TOA) of the received signal is studied from the perspective of the Cramer-Rao Bounds (CRB) for both propagation conditions: Rice and Rayleigh. This way, the limiting variances can be used to get an insight about the positioning accuracy based on timing without resorting to any particular estimation method. Furthermore, information provided by the CRBs will be eventually incorporated to our simulation platform to evaluate the benefits of space-time diversity on subscriber positioning.

Although other approaches exist for the computation of the CRB for TOA, to the best of our knowledge, ours is in fact the most complete of its kind in the literature, since it incorporates a way to take into account spatial and temporal correlation among channel estimates, and the impact of the roll-off factor, in addition to the number of sensors and the number of estimates that are typical from other approaches [15]-[19]. Moreover, our model assumes an exponential dispersion for delays, which is characteristic of mobile channels, instead of just a single path [15]-[18], or two or three paths [20][21]. We also take into consideration the speed of subscribers, and provide proper expressions for the cases of both low and high speed subscribers. Furthermore, we provide asymptotic expressions for the general case. The coincidence of these expressions with the exact ones assures its use, especially in case of high levels of SNR and a large number of channel vector estimates.

Finally, it is important to highlight the fact that our model assumes no biased measurements, in other words, we assume that the first arrival, although weak due the shadowing, is in fact related to the LOS component. This consideration should be taken into account when our results are plugged to the positioning problem, especially in NLOS environments. In fact, the NLOS condition that was studied at chapter 2 is an important issue for the location problem; and therefore the identification of the NLOS situation and the mechanisms for its mitigation are still a current research topic [22]-[31]. For example, it is conceptually interesting to consider the use of Bayesian mechanisms which take advantage of system dynamics and add any previous knowledge available, in order to smartly select, among a set of measurements, those with capacity to lead to a more confident estimation. Some of these strategies use variations of the Kalman Filter (KF) to incorporate this intelligence to the Positioning Computing Function [27]-[29], and employ some lateral information such as the signal quality indicator associated to LOS/NLOS [27] or prior knowledge to adjust NLOS data toward the corresponding LOS values [25].

The contents of this chapter are outlined as follows. Firstly, this chapter briefly supports the use of a dispersive model, and makes a quick review of Time Of Arrival (TOA) and Direction Of Arrival (DOA) estimation in section 3.1. At section 3.2, the document introduces the dispersive models, the assumptions performed, and a brief discussion related to signal dispersion and the coherence time for delays, required prior to introducing the channel model and eventually, the procedures to compute the true and asymptotic Cramer-Rao Bounds (CRB) for the timing. The CRB characteristics for LOS and NLOS models are also discussed. At section 3.3, results from simulations are exhibited, the NLOS condition and its impact on positioning is commented at section 3.4, the relevant conclusions from these results are summarized at section 3.5, and some recommendations are outlined at section 3.6.

3.1 Why to use a Dispersive Source Model

In the previous chapter, it was commented that new channel models have been emerged in order to include angular spread, and some of them have been contrasted with results from measurements campaigns [32]-[39]. One of these campaigns has been performed by the Danish Aalborg University, and this study [39] concludes that the probability density function (PDF) for delays may be modeled as having an exponential shaping for a confidence level of 78% and the PDF for azimuths may be modeled as Gaussian shaped for a confidence level of 83%. It also shows that angular spread and delay spread mechanisms are correlated, and that correlation factor for i.e. reaches a value of 0.72 for the measurement sites of Aarhus and Stockholm. However, this research work also concludes that the azimuth-delay joint density probability may be expressed as in (3.1) since the conditional distribution functions for azimuths $f_A(\theta|\tau)$ and delays $f_D(\tau|\theta)$ are essentially independent of de timing (τ) and the azimuth (θ) respectively. The same work also justifies the use of a Laplacian distribution or a Gaussian distribution for the Power Angular Spectrum (PAS), and the use of an exponential distribution for the Power Delay Spectrum (PDS). It also points out the

relations among the delay spread and the angular spread, and the variances for delays and azimuths.

$$f(\theta, \tau) = f_A(\theta) f_D(\tau) \tag{3.1}$$

This last work is especially relevant since it allows characterizing the wireless channel using well known PDFs, reducing the number of parameters required for simulations and so far the computational complexity. Furthermore, a stochastic model of this kind reduces the computational burden and eases the simulation tasks.

3.1.1 Overview of Direction Of Arrival Estimation

Direction Of Arrival (DOA) estimation is a very known problem and it has been studied in lots of contexts and for different signals in the last decades [40][41]. Various algorithms have been proposed to achieve better accuracies and reduce computational complexity. Figure 3.1 summarizes the methods available for estimating this parameter, and classifies them into two groups, the spectral based methods such as beamforming, Capon or MUSIC (Multiple Signal Classification) and the parametric methods such as IQML (Iterative Quadratic Maximum Likelihood), WSF (Weighted Subspace Fitting) or ESPRIT (Estimation of Signal Parameters by Rotational Invariance Techniques) among others.

Spectral based methods are the simplest, DOA is usually associated to the peaks of a function, and hence just one dimensional search is required. Beamforming and Capon methods correspond to this category, but their statistical performance is poor [40]. MUSIC algorithm on the other hand exhibits better characteristics. Parametric methods make assumptions on the signal shape and so they are sensitive to the model used. Maximum Likelihood (ML) methods (MLM) are based on the application of the ML principle to the statistics of the observed data, and the minimization of their associated cost functions usually requires a multi-dimensional grid search, and therefore these are computationally very extensive methods.

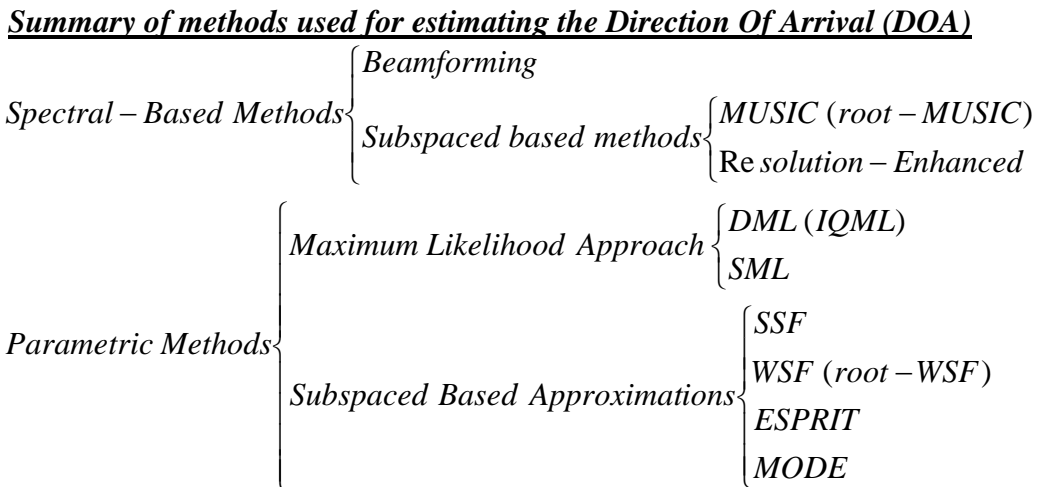


Figure 3.1. Overview of methods available for DOA Estimation.

MODE algorithm results from applying the ML principle on the statistics of certain linear combinations of the sample eigenvectors. It is more accurate than MUSIC and some ML based methods [42], and it is asymptotically efficient. Furthermore, this algorithm is computationally less intensive than MLM; and in case of an arbitrary geometry array, its loss function depends on the unknown DOA in a simpler way than for MLM and therefore its evaluation is easier. It has been shown in [43] as MUSIC under some smooth assumptions and for the case of uncorrelated signals may be seen as a realization of a ML estimator with a large number of samples. It is no longer true when signal is correlated, and hence MUSIC just corresponds to a brute force approximation.

When signal is assumed to be deterministic but unknown and a ML criterion is applied, the Deterministic Maximum Likelihood (DML) algorithm emerges and when signal waveforms are modeled as random processes, it leads to a Stochastic Maximum Likelihood (SML) algorithm. If noise is also Gaussian, it becomes a Stochastic Gaussian Maximum Likelihood (SGML) algorithm [44]. It must be noted that for large samples, the asymptotic accuracy of signal parameter estimates depend only on the second order properties (powers and correlations) of the signal waveform, so it is not further important if noise is really Gaussian. SML outperforms to DML, but difference is meaningful only for small number of sensors. For the case of a Uniform Linear Array (ULA), an iterative procedure for minimizing the DML criterion corresponds to the Iterative Quadratic Maximum Likelihood (IQML) algorithm. A DML type algorithm called CML (Conditional Maximum Likelihood) and its Least Squares approximation LSML are also studied in [44]. It shows as LSML degrades when SNR changes widely over the processed frequency band, but it is also comparable to SGML for high SNR.

Subspaced based approximations claim for providing the best of MLM (Maximum Likelihood Methods) but reducing the computational burden. SSF (Signal Subspace Fitting), WSF (Weighted Subspace Fitting) and NSF (Noise Subspace Fitting) may be counted among them.

Rooting techniques has been adopted for ULA structures, and algorithms such as root-MUSIC, root-WSF or ESPRIT are available, being root-WSF a strong candidate for the “best” method of this kind [40][45]. An interesting work which considers the use of two identical sub-arrays for DOA estimation is presented in [46]. Arrays geometry is irrelevant but the relative position of them is well known. Therefore, both manifolds are dependent, and this condition is exploited to achieve estimators based on signal subspace and ESPRIT.

3.1.2 Overview of Time Of Arrival Estimation

Time Of Arrival (TOA) estimation is another very frequent problem and profuse related literature may be found [12]-[14], [47]-[52]. It is an analog problem to the DOA estimation, and criteria used for the estimation of this parameter and commented in the previous section may be applied to estimate TOA. However, TOA and DOA estimation problems are not identical, and particularities associated to each parameter must be considered. ML solutions to this problem may be found in [48]. This latter work also

proposes the use of IQML in the frequency domain and considers the use of MODE. A family of MUSIC algorithms to solve this problem is proposed in [50], and finally, algorithms intended to work under low SNR are presented in [49] and [51]. These two approaches are quite different but exhibit a common characteristic, the fact of improving the data quality by selecting just a piece of them. This choice is made via a threshold. The Time Difference Of Arrival (TDOA) estimation problem is considered in [52] for a multipath environment and it proposes the use of an Expectation-Maximization (EM) algorithm as a viable estimator.

3.1.3 Overview of Joint Estimation of Time Delays and Direction of Arrival

Although joint estimation of time delays and DOA is a very useful problem, there is less literature about this topic. It is important not just because classical techniques degrades when reflections overlap in time, but also because more accurate estimates are expected to reduce location estimates, and a joint estimation might reduce both errors simultaneously. DML and SML criteria are used to solve this problem [12], and an iterative algorithm in the frequency domain is proposed in [13] to reduce the multidimensional grid search associated to MLM into two sets of simple one-dimensional maximization problem. Furthermore, several MUSIC algorithms have also been proposed to solve this problem [53]-[55]. Particularly [53] proposes the use of a spatiotemporal array manifold model for an asynchronous DS-CDMA system in a fast fading multipath channel instead of the traditional covariance matrix of the received signal to extract the direction information. Moreover, [54] performs a Fourier transformation to the received signal, and uses this data to compute the covariance matrix whose eigenvectors associated with the noise subspace are extracted to achieve the MUSIC spectrum for DOA-delay joint estimation; work in [55] also prefers the work at the Fourier domain, includes the notion of coherent space-time distributed signals, to eventually construct spectrum functions for both space and time delay, and provides expressions to achieve maximum pairing of space-time parameters. On the other side, some calibration problems associated to frequency offset and antenna pattern have been reported in [56], providing mitigation techniques to this issue.

3.1.4 Dispersive Source Models and Direction of Arrival Estimation

It was commented before that MLM are associated in general to a multidimensional grid search, due to the large number of unknown parameters, for i.e. a spatial signature and a delay for each path, and hence they are computationally complex algorithms, and the study of their properties is not an easy task.

Furthermore, from a viewpoint of a mobile location application, most of these parameters are nuisance, since the relevant parameters correspond to the most probable source bearing and the time of arrival of the line of sight (LOS) path. Thus, it is clear that new models have been proposed discarding the nuisance parameters and considering the stochastic signal behavior instead of a set of punctual sources. They are known as dispersive source models since signal is view as emitted from just one source

but received scattered (in time and space). This dispersion is weighted through a function called angular-temporal correlation kernel (ATCK) [57].

Accordingly to the temporal correlation between the estimates of the channel vector, sources may be classified as Incoherent Dispersive (ICD), Fully Coherent Dispersive (FCD) and Partially Coherent Dispersive (PCD). The ICD case corresponds to null temporal correlation, the FCD case to a time invariant channel with unitary correlation coefficient, and the more realistic PCD case to an intermediate situation with a temporal correlation coefficient between zero and one. Particular ML estimators for these three cases are provided in [57].

A more elaborated model for uniform linear arrays (ULA) is presented in [10]. This paper performs an unstructured covariance matrix model, and considers the use of Covariance Matching Estimators (COMET) under a low angular spread assumption, and the use of EXIP principle for reducing the 2-D minimization problem to two successive 1-D searches. The same problem is solved in [58]., assuming a Lorentzian distribution for the arriving rays via a ML approach for both high SNR and low SNR, and a very simple and improved estimator is achieved for the high SNR case.

MUSIC type algorithms for dispersive source models are proposed in [11] for ICD and PCD sources. This paper reports better accuracies and lower bias when performance of these algorithms is compared to MUSIC. Some low complexity estimators for DOA and angular spread based in root-MUSIC, ESPRIT or MODE are formulated in [9] under a low angular spread assumption. However, they exhibit good characteristics even for some large spreads, as it is shown from simulation results [9].

When reflected waves are grouped in wavefronts due to the finite resolution in temporal and spatial domains, and when they are separable in the DOA-delay plane, a LS algorithm [59] may be used, however the extension of this algorithm by using dispersive models is not straightforward since the statistic of each cluster should be known. The use of clusters following a Poisson process for modeling the received signal in ultra wide band (UWB) is reported in [21].

3.2 Dispersive Source Models and Cramer-Rao Bounds

As it can be seen in the previous section a large list of estimators for azimuths and delays is available. Each of them has its own characteristics and their performances differ one from another, and so on their associated error. Hence the evaluation of LDT's through the study of positioning error will be difficult since if a particular estimator is used, results will be affected by the performance of the selected estimator.

In order to provide a more general information relative to the estimation error, not conditioned to a particular estimator, it will be assumed that the involved measures (delays and angles) are estimated in the best possible way, that is, using a ML approach with large data records, thus achieving a variance equal to the Cramer-Rao bound

(CRB). It means that estimators are assumed to be asymptotically efficient. In this way, those limiting variances can be fed to equation (3.2) as in [4] or to our simulation platform in chapter 2 with the goal to obtain limiting variances for the positioning error. Note that, as the measurements are assumed to be generated with ML methods, the estimation errors in \mathbf{C}_w can be considered Gaussian, and the computed variances of location errors in \mathbf{C}_x will be the CRB for the location if the Best Linear Unbiased Estimates from equation (3.2) are used.

$$\mathbf{C}_x^{BLUE} = (\mathbf{G}^H \mathbf{C}_w^{-1} \mathbf{G})^{-1} \quad (3.2)$$

Being \mathbf{G} in this expression a matrix related to the geometry of the problem.

It is important to remark that the own nature of the location problem, as defined in above equation is that the positioning error variance may be computed from the variance of the measurements, and that any improvement in the variance for the measurements error is directly translated as a reduction of the variance in positioning. In this sense, the accuracy in the measurements may be improved if adequate use of temporal and spatial diversity in the estimated propagation channel is done [60]. Therefore, multiple channel measurements may be collected at different time instants and they may be recorded from different sensors.

A key point in the assumptions made hereafter is that the system is an asynchronous DS-CDMA system, and that the estimated parameters (azimuths, delays) are computed on the estimated channel. This approach is at the same time convenient (since typically the channel estimation will be available at the receiver) and nearly optimum, in the sense that, as many power-controlled users are present, the interference can be approximately Gaussian. The channel estimated by correlation systems is thus optimum. In this sense, care should be taken to derive these results to TDMA systems.

LDT's may use the Received Signal Strength (RSS) in addition to azimuths and delays. Available data is transferred to the Position Computing Function (PCF), and various position schemes rise in relation to the type of available measurements. If the same kind of measurements are used for positioning we are talking about a homogeneous system and if we are using two or more different sets of measurements we are referring to a heterogeneous one [4]. A more recent review of network-based wireless location is available in [61]. In particular this paper derives expressions for positioning systems based on TOA, TDOA and AOA under LOS condition, and it suggests the addition of certain geometrical restrictions when AOA measurements and some statistical information about NLOS error are available to solve the equations system within the location estimation process. It also proposes the cost functions required in parameter estimation used for the Positioning Computing Function (PCF) for both single user and multiuser environments. Furthermore, it introduces the use of Bayesian techniques for Amplitude Of Arrival (AMPOA) estimation recognizing the capacity of IEEE 802.11 b,g wireless system to provide RSS and SNR measurements. On the other side [62] generalizes the location estimation problem and exhibits optimization criteria for estimating position. Particularly it briefly introduces Nonlinear Least Squares (NLS), Weighted Nonlinear Least Squares (WNLS), Maximum

Likelihood (ML) and Gaussian Maximum Likelihood (GML), and it suggests the application of steepest descent and Gauss-Newton algorithms on these criteria to perform estimation. It also studies the fundamental limitations on positioning through the use of Fisher Information Matrix (FIM).

3.2.1 Considerations in the Propagation channel model

From the viewpoint of location, the use of dispersive models for the delay power spectrum and angular power spectrum seem to be appropriate to reduce the number of nuisance parameters and to correctly describe the propagation channel in highly dispersive environments as it is the outdoor urban case. Furthermore, due there is an insufficient amount of reported works on field measurements justifying models for the joint angle-delay power spectrum $P(\theta, \tau)$, independence between the angular and delay distribution in analogy to (3.1) will be assumed in this work, following to [39] since this conclusion is supported for a measurement campaign and it is quite convenient to reduce the complexity of the analysis. However, this model may not necessarily fit to single particular propagating conditions since it results from averaging measurements taken over many placements [14].

Hence, the joint angle-delay power spectrum $P(\theta, \tau)$ takes the form shown in Figure 3.2, being the Power Angular Spectrum (PAS) Laplacian or Gaussian shaped, and the Power Delay Spectrum (PDS) defined by an exponential function.

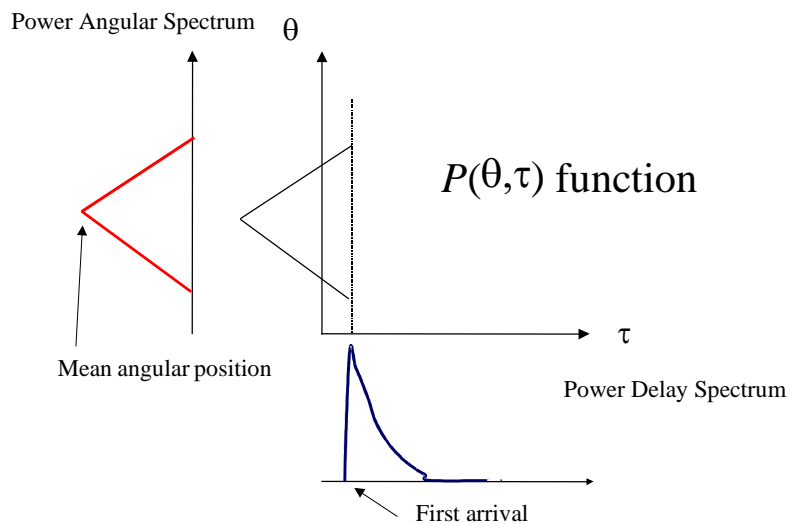


Figure 3.2. Joint angular-delay power spectrum assumed for the propagation channel.

This NLOS model admits further developments, by adding a Line Of Sight (LOS) component at the first arrival coming from the mean angular position. This LOS model is studied at Section 3.2.4.5.

Assumptions made along this work are the following:

- AS 1. Channel introduces multipath propagation; therefore signal is dispersive in space and time from the LOS component. Statistical independence for angular and temporal dispersion processes is assumed. The first TOA is the parameter of interest of the problem, whilst the angular parameters are nuisance parameters required for the characterization of the CRB.
- AS 2. In spite the channel has a coherence time for the taps amplitudes [63][64], delay and angle information may remain within tolerable limits much longer due to the relative high proportion between light speed and mobile speed, and the relative large distances between transmitter and receiver. Therefore, many channel estimates can be collected in time so as to improve the accuracy of the timing and angle estimates.
- AS 3. The first arrival is analysed as the one bearing timing for position information. Measures for TOA are computed from channel estimates available at the receiver through a correlation function. A full ML estimation of all propagation parameters (delays and angles) is considered an approach that is too expensive in a dispersive channel, where the number of parameters could be too large, and might lead to inconsistent estimates if the available number of channels is low.
- AS 4. Noise present in the channel estimates is white and Gaussian, which is a reasonable assumption after matched filter [65]. Our analysis does not consider strictly a multi user environment, but this assumption is reasonable even in this case since all other users have been at least partially cancelled.
- AS 5. The Power Angular Spectrum (PAS) is symmetric, dispersive, and exhibits just a single mode with the mean value associated to the right angular position of the transmitter (the UE if the PAS is computed at the BS). Gaussian and Laplacian [6],[37]-[39],[59] models usually describe the marginal probability $P(\theta)$:

$$P(\theta) = \int P(\theta, \tau) d\tau \quad (3.3)$$

A single modality is a reasonable assumption as long as the channel bandwidth is large, and therefore the channel estimated at chip time includes only rays impinging from a narrow solid angle. Furthermore, some experimental evidence shows that the probability of having more than a cluster in a Typical Urban reaches 13% and it reduces to 8% in Suburban Areas [6].

- AS 6. A continuous power spectrum is used in delay for the marginal function $P(\tau)$:

$$P(\tau) = \int P(\theta, \tau) d\theta \quad (3.4)$$

It is assumed to fit an exponential shaping [38][39][63], estimated at a fraction of chip time. For the extraction of timing information, the same angular distribution for all delays is assumed. This may not be very realistic but allows

reducing the number of parameters in the model and keeps the problem tractable [21][59].

Note that our basic model may be used to study some NLOS scenarios since each tap of the channel impulse response is a zero mean random variable. Certainly, a LOS situation implies a non-zero mean where the first arrival is considered as the one conveying unbiased location of the UE. Therefore, and in order to achieve more general results, this basic model has been enhanced to introduce the LOS condition as a symmetric kernel for the angular distribution with a peak discontinuity at the true angular position of the source, as it is described in section 3.2.4.5.

AS 7. A first order autoregressive (AR) Markov process for the evolution of the channel along the time due to Doppler is assumed [66].

Note that this model is very parsimonious and convenient for the purpose of location, since only a few parameters of interest are going to be computed, rather than all delays and angles which are usually nuisance parameters and yield the problem too complicated. In fact, first arrival is the desired parameter for positioning purposes, since in most cases, positioning accuracy just slightly improves with the use of only their first arriving paths [20][67]. In addition, the computation of the positioning most likely requires the transmission of a certain number of parameters to a Positioning Signal Measurement Function (PSMF) device [68], which is usually placed remotely, and therefore the transmission of the channel estimates, instead of the received signal itself, saves signalling channel bandwidth.

3.2.2 Coherence Time and Delay Dispersion

Channel estimation is limited by mobility. Coherence time corresponds to the interval in which channel is essentially considered time invariant, and it is related to the inverse of the Doppler variation. It is easy to perceive that timing estimation will be affected at least by an error related with the displacement of the MS in the observation interval. Hence, this coherence time for the first arriving signal path may be related with the maximum allowed delay uncertainty (ε) introduced by the movement, and the radial component of the speed vector (v_r) of the mobile, but not on the distance, as it is shown in (3.5).

$$\begin{aligned} \varepsilon &= \Delta d / c = v_r t / c = v_r K T_{slot} / c \\ K &= \frac{\varepsilon \cdot c}{T_{slot} \cdot v_r} = \frac{\varepsilon \cdot c}{T_{slot} \cdot v \cos \phi} \end{aligned} \quad (3.5)$$

Where ϕ corresponds to a particular direction of the subscriber's movement. It can also be measured in number of channel estimates K (assuming one estimate per FDD time slot, of duration T_{slot}). Furthermore, since K is dependent of the direction of movement ϕ , it is assumed to be uniform and bounded by ϕ_{max} , as in (3.6):

$$f_{\Phi}(\phi) = \begin{cases} \frac{1}{\phi_{\max}}; & 0 \leq \phi \leq \phi_{\max} \\ 0; & \text{otherwise} \end{cases} \quad (3.6)$$

And the expressions required to compute the mean number of channel estimates may be derived as in (3.7):

$$E\{K\} = \frac{\varepsilon \cdot c}{T_{\text{slot}} \cdot v} E\{\sec \phi\} = \frac{\varepsilon \cdot c}{T_{\text{slot}} \cdot v \cdot \phi_{\max}} \int_0^{\phi_{\max}} \sec \phi \, d\phi = \frac{\varepsilon \cdot c}{T_{\text{slot}} \cdot v \cdot \phi_{\max}} \log \left[\tan \left(\frac{\phi_{\max}}{2} + \frac{\pi}{4} \right) \right] \quad (3.7)$$

It is easy to see in (3.5) that when the speed vector is orthogonal to the line linking UE and BS ($\phi = \pm\pi/2$), the number of allowed K goes to infinity since there are no delay variations due to the transversal speed vector and therefore it is impossible to meet a specified delay uncertainty by increasing the number of estimates. Furthermore, a practical limit has to be imposed to the observation time T_{acq} (associated with the latency experienced by the user in the availability of the position) in order to deliver the timing to the Position Computing Function (PCF) of channel estimates, resulting in a limited number of channel estimates allowed, and hence a maximum angle ϕ_{\max} different to $\pi/2$ may be determined by using equation (3.8):

$$\phi_{\max} = \arccos \left(\frac{c \cdot \varepsilon}{T_{\text{acq}} \cdot v} \right) \quad (3.8)$$

Figure 3.3 exhibits a set of characteristics relating the number of channel vector estimates, the mobile speed and the expected accuracy in TOA estimation for typical parameters of a WCDMA system, a chip rate of 3.84 Mcps and a timeslot of 666.66 μs . T_{acq} has been set to 1.5 s.

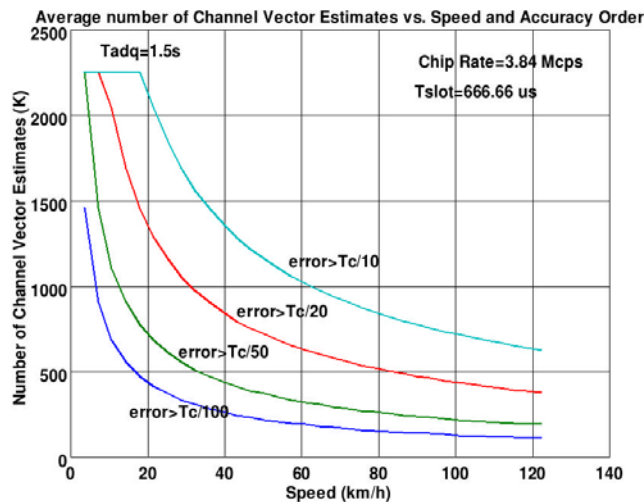


Figure 3.3. Mean number of channel estimates that may be used to determine timing channel parameters, assuming a maximum acquisition time of 1.5 seconds, and for different maximum errors in delay given as fractions of chip time.

Note from Figure 3.3 as the maximum number of observations is limited by the acquisition time and for the mobile speed, therefore a typical value for this parameter is between 250 and 2200 to avoid accuracy degradation. It is clear from the figure than a faster MS will have less time for channel acquisition and a compromise will be required in order to achieve the best possible timing accuracy.

From a systemic viewpoint, mobile location may be improved when system dynamic [69] and previous knowledge from the statistical of measurements are used [27], and also from the use of a heterogeneous set of measurements [29][69][70].

3.2.3 Channel Model

In the following, a dispersive source model for delays is provided and it will be used to compute Cramer-Rao bounds for the first arrival timing.

The observed signal is a set of K channel vector estimates collected over a set of N_s sensors in the antenna array. Each channel vector estimate \mathbf{z} is of length N , and it is assumed to be estimated after correlation of a known sequence with the received signal.

Signal received by j -th sensor is noted as $y^{(j)}(t)$, and may be expressed as the summation of multipath components and noise $n^{(j)}(t)$. Each replica of the transmitted signal $x(t)$ arriving at delay τ_i is affected by a time-varying unit-power steering coefficient $b_{i,j}(t)$, the path attenuation factor $\gamma_i(t)$, and a time invariant (over time intervals of length KT_s) Doppler frequency f_i ; being T_s the time between two consecutive channel estimates, as in (3.9):

$$y^{(j)}(t) = \sum_{i=1}^{N_{paths}} b_{ij}(t) \gamma_i(t) x(t - \tau_i) e^{j2\pi f_i t} + n^{(j)}(t) \quad (3.9)$$

Where the i -th index is related to the multipath component and N_{paths} is the number of impinging paths at the receiver. The transmitted signal $x(t)$ corresponds to the convolution of a pseudo-noise sequence $p(n)$ with the symmetric pulse shape $g_p(t)$ as shown in (3.10):

$$x(t) = \sum_n g_p(t - nT) p(n) \quad (3.10)$$

Where, T is the symbol time. Moreover, a correlator estimates the channel from the received signal $y^{(j)}(t)$ at each sensor j , and temporal lag s , with the help of the pseudo-noise sequence $p(n)$ of N_p symbols, as it is shown in (3.11):

$$z_s^{(j)}(t) = \frac{1}{N_p} \sum_n y^{(j)}(t + \tau_s + nT) p^*(n) \quad (3.11)$$

Where $z_s^{(j)}(t)$ corresponds to the estimated channel coefficient at j -th sensor and s -th lag, as a function of time. By replacing, (3.9) in (3.11), and assuming zero mean noise, it is easy to show that (3.12) results.

$$\begin{aligned}
 z_s^{(j)}(t) &= \frac{1}{N_p} \sum_n \sum_{i=1}^{N_{paths}} b_{ij}(t) \gamma_i(t) e^{j2\pi f_i t} x(t - \tau_i + \tau_s + nT) p^*(n) + w_i^{(j)}(t) = \\
 &= \frac{1}{N_p} \sum_{n,k} \sum_{i=1}^{N_{paths}} b_{ij}(t) \gamma_i(t) e^{j2\pi f_i t} g(t - \tau_i + \tau_s - (k-n)T) p(k) p^*(n) + w_i^{(j)}(t) = \\
 &= \sum_{i=1}^{N_{paths}} b_{ij}(t) \gamma_i(t) e^{j2\pi f_i t} g(t + \tau_s - \tau_i) + w_i^{(j)}(t)
 \end{aligned} \tag{3.12}$$

Where, in the last equality we have used the fact that the sequence $p(n)$ is uncorrelated of unit power, and the assumption that within N_p symbols the steering coefficient and path attenuation factor are constants. This equation shows that the estimated channel is obtained synchronously with the transmission time, therefore we can assume $t = kT_s$ and hence temporal variation of $z_s^{(j)}(t)$ depends on k in (3.13) and also Doppler frequencies are re-scaled:

$$z_s^{(j)}(k) = \sum_{i=1}^{N_{paths}} b_{ij}(k) \gamma_i(k) e^{j2\pi f_i T_s k} g(\tau_s - \tau_i) + w_s^{(j)}(k) \tag{3.13}$$

The residual noise component $w_s^{(j)}(k)$ is given in (3.14), and may be modelled as a zero mean complex white Gaussian random process (AS 4).

$$w_s^{(j)}(k) = \frac{1}{N_p} \sum_{k'} n^{(j)}(kT_s + \tau_s + k'T) p^*(k') \tag{3.14}$$

Furthermore, the channel vector estimation at sensor j and at slot k , $\mathbf{z}^{(j)}(k)$, may be expressed in terms of the shaping pulse and the noise estimation vector $\mathbf{w}^{(j)}(k)$ as in (3.15):

$$\mathbf{z}^{(j)}(k) = \mathbf{G}_s \mathbf{b}^{(j)}(k) + \mathbf{w}^{(j)}(k) \tag{3.15}$$

Where the i -th element of vector $\mathbf{b}^{(j)}(k)$ contains $b_{ij}(k) \gamma_i(k) \exp(j2\pi f_i T_s k)$ and the i -th column of the $N \times N$ square matrix \mathbf{G}_s in (3.16) contains the shaping pulse delayed by τ_i samples.

$$\mathbf{G}_s(\beta) = \frac{1}{\sqrt{T_s}(1-\beta/4)} \begin{bmatrix} \mathbf{g}_{s_1} & \mathbf{g}_{s_2} & \dots & \mathbf{g}_{s_N} \end{bmatrix} \tag{3.16}$$

Moreover, β is the roll-off factor shaping the transmission pulse, and each one of the pulse shape vectors, \mathbf{g}_{s_i} , in (3.16) may be modeled as in (3.17):

$$\mathbf{g}_{s_i}^T = \left[g_{-i+1} \quad \dots \quad \underset{\substack{\uparrow \\ \textit{i th element}}}{1} \quad \dots \quad g_{N-i} \right] \tag{3.17}$$

Where its elements g_k are described by (3.18):

$$g_k = \frac{\text{sinc}\left(\frac{k}{N_{spc}}\right) \cos\left(\frac{\pi\beta k}{N_{spc}}\right)}{1 - \left(2\beta k / N_{spc}\right)^2} \tag{3.18}$$

Being N_{spc} the number of acquired samples per chip time, and the length N of vectors in (3.17) the number of lags in channel estimates.

From (3.15), we can compute correlation matrix for two channel estimates from slots k, m and sensors j, j' , as follows:

$$\begin{aligned} E\left\{\mathbf{z}^{(j)}(k)\mathbf{z}^{(j')}(m)\right\} &= \mathbf{G}_s E\left\{\mathbf{b}^{(j)}(k)\mathbf{b}^{(j')H}(m)\right\} \mathbf{G}_s^T + \sigma_w^2 \mathbf{I}_N = \\ &= \rho_{jj'} \alpha^{k-m} \mathbf{G}_s \mathbf{\Lambda}_\tau \mathbf{G}_s^T + \sigma_w^2 \mathbf{I}_N \end{aligned} \quad (3.19)$$

Where $\mathbf{\Lambda}_\tau$ is a diagonal matrix that models the signal temporal dispersion, and the exponential power contribution. The last factorization is possible under the assumption of statistical independence for angular and temporal dispersion processes (AS 1) and also for multipath propagation and Doppler shift mechanisms. In fact, the i, l element of the signal correlation matrix in (3.20):

$$\begin{aligned} E\left\{\mathbf{b}^{(j)}(k)\mathbf{b}^{(j')H}(m)\right\}_{i,l} &= E\left\{b_{ij}(k)\gamma_i(k)e^{j2\pi f_i k T_s} b_{ij'}^*(m)\gamma_l(m)e^{-j2\pi f_l m T_s}\right\} = \\ &= \rho_{jj'} r_{il} \alpha^{k-m} \delta_{il} \end{aligned} \quad (3.20)$$

adopts the definitions in (3.21):

$$\begin{aligned} E\left\{b_{ij}(k)b_{ij'}^*(m)\right\} &= \rho_{jj'}; \\ E\left\{e^{j2\pi T_s(f_i k - f_l m)}\right\} &= \alpha^{k-m}; \\ E\left\{\gamma_i(k)\gamma_l(m)\right\} &= r_{il} \delta_{il} \\ r_{ii} &= E\left\{\gamma_i(k)\gamma_i(m)\right\} = P_s e^{-\lambda(i-k_0)} u(i-k_0) \end{aligned} \quad (3.21)$$

Where $\rho_{jj'}$ refers to the correlation between signatures at sensors j and j' ; α refers to temporal correlation between channel estimates in two consecutive slots when temporal variation has been modeled as a first order AR Markov process (AS 7); and r_{il} refers to correlation between delays in lags i and l , and k_0 refers to the Time Of Arrival (TOA) of the first path.

Particularly, r_{il} is zero for paths at different lags since they fade independently and are assumed uncorrelated. Furthermore, the form of r_{ii} in (3.21) responds to the assumption of having an exponential power delay profile (AS 6) with parameter λ_n , and it is very suitable for a NLOS condition.

Additionally, if vectors are arranged as in (3.22):

$$\begin{aligned} \mathbf{w} &= \left[\mathbf{w}^{(1)}(1)^T \quad \dots \quad \mathbf{w}^{(1)}(K)^T \quad \dots \quad \mathbf{w}^{(N_s)}(K)^T \right]^T \\ \mathbf{z} &= \left[\mathbf{z}^{(1)}(1)^T \quad \dots \quad \mathbf{z}^{(1)}(K)^T \quad \dots \quad \mathbf{z}^{(N_s)}(K)^T \right]^T \end{aligned} \quad (3.22)$$

both signal and noise components may be described as temporally stationary, complex Gaussian random process with certain means and correlation matrices. Noise is zero mean, temporally uncorrelated and independent of the propagation channel vectors and of variance σ_w^2 .

When estimates in \mathbf{z} are achieved under a NLOS condition, channel angular spread will tend to increase [6][34]. It is the case for instance of a receiver at the mobile station (MS) in an urban environment. In this case, propagation is Rayleigh [71], and \mathbf{z} may also be modelled as zero mean with correlation matrix \mathbf{R}_z . The general case for the model corresponds however to Line Of Sight (LOS) condition and Rice propagation [72]. In this case, the mean vector, $\boldsymbol{\mu}_z$, is not null. It could be the case of a receiver at the base station (BS) in a suburban environment. Therefore, we can model noise and signal as in (3.23):

$$\mathbf{w} \sim CN(\mathbf{0}, \sigma_w^2 \mathbf{I}), \quad \mathbf{z} \sim CN(\boldsymbol{\mu}_z, \mathbf{R}_z) \quad (3.23)$$

Correlation matrix for channel estimates, \mathbf{R}_z , in (3.24):

$$\mathbf{R}_z = E\{\mathbf{z}\mathbf{z}^H\} \quad (3.24)$$

is related to channel estimates at different slots, sensors and lags, and takes the form in (3.25):

$$\mathbf{R}_z = \mathbf{R}_\phi(\boldsymbol{\rho}) \otimes \mathbf{T}(\alpha) \otimes P_s \mathbf{G}_s(\beta) \boldsymbol{\Lambda}_\tau(\lambda_n) \mathbf{G}_s^H(\beta) + \sigma_w^2 \mathbf{I} \quad (3.25)$$

in terms of their temporal and spatial components [72][73]. In this expression, the dispersed signal power factor, P_s , refers to the variance of the received estimated path-power for first arrival from temporally dispersive signal in case of Rayleigh propagation. Additionally, the temporal correlation matrix, $\mathbf{T}(\alpha)$, takes into consideration the temporal variation for the channel, and it is assumed equal for all delays; the spatial correlation matrix, $\mathbf{R}_\phi(\boldsymbol{\rho})$, contains the correlation coefficients for signatures between sensors; and \otimes denotes the Kronecker product [74].

The exponential model used for delays is usually proposed in channel models, and it is given by (3.26):

$$\{\boldsymbol{\Lambda}_\tau\}_{i,i} = \exp[-(i - k_0)\lambda_n] u(i - k_0) \quad (3.26)$$

in terms of both, the first arrival position k_0 , and the dimensionless parameter λ_n . This latter is inversely related to delay spread normalized by the symbol time, and therefore it is tightly related to channel coherence bandwidth. In the following, λ_n will be called the normalized coherence bandwidth [63][64].

The spatial correlation matrix, $\mathbf{R}_\phi(\boldsymbol{\rho})$ is modeled as in (3.27):

$$\mathbf{R}_\phi(\boldsymbol{\rho}) = \begin{bmatrix} 1 & \rho_{12} & \cdots & \rho_{1N_s} \\ \rho_{12}^* & 1 & \cdots & \rho_{2N_s} \\ \vdots & \vdots & \ddots & \vdots \\ \rho_{1N_s}^* & \rho_{2N_s}^* & \cdots & 1 \end{bmatrix} \quad (3.27)$$

Where dependency with the source mean bearing and its angular spread meets through the correlation vector $\boldsymbol{\rho}$, as it will be explained later in (3.34).

$\mathbf{T}(\alpha)$ is modeled as a first order AR Markov process, as it is shown in (3.28):

$$\mathbf{T}(\alpha) = \begin{bmatrix} 1 & \alpha & \alpha^2 & \cdots & \alpha^{K-1} \\ \alpha & 1 & & \ddots & \alpha^{K-2} \\ \alpha^2 & & \ddots & & \\ \vdots & \ddots & & & \\ \alpha^{K-1} & & & & 1 \end{bmatrix} \quad (3.28)$$

Where α is the temporal correlation coefficient between two consecutive vector samples, and ρ_{ij} is the spatial correlation coefficient between sensors i and j . Note also as \mathbf{G}_s corresponds to the identity matrix when sampling at the symbol rate.

Regarding the temporal correlation between consecutive estimates, the channel vector correlation matrix may be modeled as a Fully Coherent Dispersive (FCD) Source, a Partially Coherent Dispersive (PCD) source, or an Incoherent Dispersive (ICD) Source. The general case corresponds to PCD, being FCD a particular case where estimates are completely correlated ($\alpha=1$), and ICD the case where estimates are uncorrelated ($\alpha=0$).

In case of Rice propagation, the first arrival has a non-null mean and disturbs the exponential distribution for delays. Expression (3.13) becomes (3.29), whilst (3.15) turns into (3.30), where f_0 is the Doppler frequency for the LOS component, and $\mathbf{g}^{(k_0)}$ identifies the pulse shape vector for this arrival:

$$z_s^{(j)}(k) = \sum_{i=0}^{N_{paths}} b_{ij}(k) \gamma_i(k) e^{j2\pi f_i T_s k} \mathbf{g}(\tau_s - \tau_i) + w_s^{(j)}(k) \quad (3.29)$$

$$\mathbf{z}^{(j)}(k) = b_{0j}(k) \gamma_0(k) e^{j2\pi f_0 T_s k} \mathbf{g}^{(k_0)} + \mathbf{G}_s \mathbf{b}^{(j)}(k) + \mathbf{w}^{(j)}(k) \quad (3.30)$$

Note that the right part of the summation in (3.30) corresponds to the dispersed NLOS signal and has a null expected value. Moreover, since delay dispersion and Doppler mechanisms are assumed independent, the mean channel gain may be easily computed as follows:

$$E\{\mathbf{z}^{(j)}(k)\} = E\{b_{0j}\gamma_0(k) e^{j2\pi f_0 T_s k} \mathbf{g}^{(k_0)}\} = A_0 E\{b_{0j}\} E\{e^{j2\pi f_0 T_s k}\} \mathbf{g}^{(k_0)} \quad (3.31)$$

Where the time dependency of the steering vector has been discarded since its value is expected to remain unchanged for the LOS path along the position acquisition (AS 5). Moreover, A_0 corresponds to the mean signal level for the LOS component. If $\boldsymbol{\mu}_z$ denotes the mean channel vector arranged as \mathbf{z} and \mathbf{w} , in (3.22), it could be expressed in terms of the spatial signature for the LOS component \mathbf{b}_ϕ , the expected Doppler vector \mathbf{a}_t , and the pulse shape vector for first arrival $\mathbf{g}^{(k_0)}$, as follows:

$$\boldsymbol{\mu}_z = E\{\mathbf{b}\} \otimes E\{e^{j2\pi f_0 T_s k}\} \otimes A_0 \mathbf{g}^{(k_0)} \quad (3.32)$$

The spatial signature described by the LOS component when a Uniform Linear Array (ULA) is used may be computed from problem geometry and signal angular distribution, as it is shown in (3.33):

$$\mathbf{b}_\phi = E\{\mathbf{b}\}$$

$$\text{with } [E\{\mathbf{b}\}]_n = E\{b_n\} = \frac{1}{\sqrt{2\pi}\Delta_\phi} \int_{-\pi}^{\pi} e^{-\frac{(\phi-\phi_0)^2}{2\Delta_\phi^2}} e^{-jn\pi\sin(\phi)} d\phi \quad (3.33)$$

In this case, spatial distribution is modelled as Gaussian (AS 5), centred around ϕ_0 , with angular spread Δ_ϕ , and subscript n corresponds to the sensor position for $n \in [0, N_s - 1]$. Some works report that Laplacian distribution can provide a good match to this angular distribution [6][39][40], and suggest this effect may be produced for the integration of local and distance scatters; but when a Laplacian kernel is used in (3.34) instead of a Gaussian one, meaningless variations are achieved for results in this model.

Reminding that the correlation matrix \mathbf{R}_ϕ was computed in a similar way, as described in (3.34), the expected spatial signature is finally described as in (3.35).

$$\mathbf{R}_\phi = E\{(b_{n_1})(b_{n_2}^*)\} = \frac{1}{\sqrt{2\pi}\Delta_\phi} \int_{-\pi}^{\pi} e^{-\frac{(\phi-\phi_0)^2}{2\Delta_\phi^2}} e^{-j(n_1-n_2)\pi\sin(\phi)} d\phi \quad (3.34)$$

$$\mathbf{b}_\phi(\boldsymbol{\rho}) = [1 \quad \rho_{12} \quad \rho_{13} \quad \dots \quad \rho_{1N_s}]^H \quad (3.35)$$

Note from (3.32) and from the fact that temporal variation due to Doppler may again be modelled as a first order AR Markov process (AS 7), as the temporal vector, $\mathbf{a}_t(\alpha)$, is a function of α , and it takes the form in (3.36).

$$\mathbf{a}_t(\alpha) = [1 \quad \alpha \quad \alpha^2 \quad \dots \quad \alpha^{K-1}]^T \quad (3.36)$$

Therefore (3.32) becomes (3.37):

$$\boldsymbol{\mu}_z = \mathbf{b}_\phi(\boldsymbol{\rho}) \otimes \mathbf{a}_t(\alpha) \otimes A_0 \mathbf{g}^{(k_0)}(\boldsymbol{\beta}) \quad (3.37)$$

3.2.4 Computing the Cramer Rao Bounds for Delay Estimates

As it was mentioned before, working with the lower bound of an unbiased estimator let us determinate the best possible behaviour in the estimation of a particular parameter of interest. It is true that other bounds besides CRB exist, such as the Barakin Bound (BB) [75] or the Ziv-Zakai Bound (ZZB) [76]; however the use of the CRB is adequate for modelling Gaussian Processes [76][77]. CRB is also useful to identify if a particular estimator is the Minimum Variance Unbiased (MVU) estimator and if a MVU estimator really exists. Furthermore, in the case such MVU estimator does not exist, it can still predict the performance of maximum likelihood estimates in an approximate sense for certain conditions of high Signal to Noise Ratio (SNR) or when a large number of observations is available [77].

BB claims to be the greatest lower bound on MSE (BB) for uniformly unbiased estimator, but it is generally incomputable analytically [75]. However, it is interesting to note that CRB and BB could be considered as key representatives of two general kinds of bounds, respectively the Small-Error bounds and Large-Error bounds [75]. Precisely, some research in [75] has shown that in non-linear estimation problems three

distinct regions of operation can be observed. In the asymptotic region, the MSE is small and, in many cases, close to the Small-Error bounds (CRB). In the a priori performance region where SNR and/or the number of independent observations are very small, observations provide little information and the MSE is close to that obtained from the prior knowledge about the problem. Between these two extremes, there is a transition region which exhibits a threshold behavior corresponding to a “performance breakdown”. It is important to have in mind this behavior of CRB for the analysis of the results to avoid making incorrect conclusions when the CRB is not useful anymore.

In addition to the deterministic CRB which models some parameters as unknown deterministic variables, the Bayesian CRB (BCRB) models some unknown parameters as random. However, it has been reported that in certain cases, application of Bayes Theorem and expectation operator artificially decouple some parameters such as the channel and the unknown symbols for instance, even though they are really coupled [78]. It originates that results predicted by CRBs or BCRBs are too optimistic. To solve this issue, some modifications to the classical CRBs have been proposed lately. It means to postpone the application of expectation operator required for FIM computation, in a way that matrix inversion is performed first and then as a second step, expectation operator is applied to compute the modified CRB (MCRB). Reported results show as the corresponding estimators attains the MCRBs for moderate and high SNR regimens, and also as MCRBs coincides with original CRBs for a low SNR regimen [78]. In some environments such as GNSS, where SNR is very low and the pulse shape is not enough smooth as for CRB may be used, ZZB and modified ZZB (MZZB) are proposed [76].

After this brief discussion that highlights the importance of Cramer Rao Bounds, not only as means to quantify errors from a set of parameters to be estimated, but also as a modeling tool since it allows for the evaluation of the impact of various parameters in the estimation error; let us continue with derivation of this bound for our model, introduced mainly in (3.23), (3.25) and (3.32). Consequently, the following parameter vector is defined in (3.38):

$$\mathbf{\Psi} = [k_0, \lambda_n, \beta, P_s, \sigma_w^2, \alpha, \mathbf{p}^T, A_o]^T \quad \mathbf{p} = [\rho_{1,\text{Re}}, \rho_{2,\text{Re}}, \dots, \rho_{N,\text{Re}}, \rho_{1,\text{Im}}, \rho_{2,\text{Im}}, \dots, \rho_{N,\text{Im}}]^T \quad (3.38)$$

Where k_0 is the time of arrival normalized for the chip time, λ_n is the normalized coherence bandwidth, \mathbf{p} is a vector containing the real and imaginary parts of the complex correlation coefficients among sensors, and the remaining parameters have been defined before. All of them but k_0 are nuisance parameters.

Moreover, in case of a Rayleigh fading channel, there is no a dominant LOS path and therefore A_o is zero and it is discarded, reducing the parameter vector to (3.39):

$$\mathbf{\Psi} = [k_0, \lambda_n, \beta, P_s, \sigma_w^2, \alpha, \mathbf{p}^T]^T \quad \mathbf{p} = [\rho_{1,\text{Re}}, \rho_{2,\text{Re}}, \dots, \rho_{N,\text{Re}}, \rho_{1,\text{Im}}, \rho_{2,\text{Im}}, \dots, \rho_{N,\text{Im}}]^T \quad (3.39)$$

Since channel vector estimates being stacked in \mathbf{z} are assumed complex Gaussian distributed as described in (3.23), the probability density function for \mathbf{z} is expressed as in (3.40):

$$p(\mathbf{z}) = \frac{1}{\pi^{K.N_s.N} \det(\mathbf{R}_z)} \exp\left[-(\mathbf{z} - \boldsymbol{\mu}_z)^H \mathbf{R}_z^{-1} (\mathbf{z} - \boldsymbol{\mu}_z)\right] \quad (3.40)$$

And the Cramer-Rao Bounds for the parameters specified in (3.38) correspond to the diagonal elements within the inverse of the Fisher Information Matrix (FIM). Furthermore, FIM elements for the Rice LOS model may be expressed as it is seen in (3.41) and in case of Rayleigh fading as in (3.42) [77].

$$[\mathbf{F}_\Psi^{LOS}]_{pq} = -E \left[\frac{\partial^2 \ln \{p(\mathbf{z}; \Psi)\}}{\partial \Psi_p \partial \Psi_q} \right] = \text{tr} \left(\mathbf{R}_z^{-1} \frac{\partial \mathbf{R}_z}{\partial \Psi_p} \mathbf{R}_z^{-1} \frac{\partial \mathbf{R}_z}{\partial \Psi_q} \right) + 2 \text{Re} \left(\frac{\partial \boldsymbol{\mu}_z^H}{\partial \Psi_p} \mathbf{R}_z^{-1} \frac{\partial \boldsymbol{\mu}_z}{\partial \Psi_q} \right) \quad (3.41)$$

$$[\mathbf{F}_\Psi]_{pq} = -E \left[\frac{\partial^2 \ln \{p(\mathbf{z}; \Psi)\}}{\partial \Psi_p \partial \Psi_q} \right] = \text{tr} \left(\mathbf{R}_z^{-1} \frac{\partial \mathbf{R}_z}{\partial \Psi_p} \mathbf{R}_z^{-1} \frac{\partial \mathbf{R}_z}{\partial \Psi_q} \right) \quad (3.42)$$

Also note that \mathbf{R}_z corresponds to the covariance matrix for the general Rice case in (3.41) and it is equal to the correlation matrix for the Rayleigh case in (3.42) since the mean is null for this latter case.

3.2.4.1 Cramer-Rao Bounds for the NLOS Rayleigh Fading Model

It will be shown below as (3.42) becomes (3.43) when \mathbf{R}_z^{-1} and their partial derivatives are computed and replaced in the above expression.

$$\mathbf{F}_\Psi = \sum_{k=1}^{N_s} \sum_{k_1=1}^K \mathbf{G}_{k,k_1} \mathbf{J}_{\bar{\Psi}} \mathbf{G}_{k,k_1}^T + C_1 \mathbf{e}_{N_p}^{(6)} \mathbf{e}_{N_p}^{(6)T} + \sum_{q_1=1}^{2N} \sum_{q_2=1}^{2N} C_2^{(q_1, q_2)} \mathbf{e}_{N_p}^{(6+q_1)} \mathbf{e}_{N_p}^{(6+q_2)T} \quad (3.43)$$

Terms in (3.43) are defined as it is seen in expressions (3.44)-(3.50). Particularly note that a singular value decomposition has been performed over the Temporal Correlation Matrix \mathbf{T} , and over the Spatial Correlation Matrix \mathbf{R}_ϕ , as it is shown in (3.44):

$$\begin{aligned} \mathbf{T} &= \mathbf{U}_t \boldsymbol{\Lambda}_t \mathbf{U}_t^H, \quad \mathbf{U}_t = [\mathbf{u}_t^{(1)}, \mathbf{u}_t^{(2)}, \dots, \mathbf{u}_t^{(K)}] \\ \boldsymbol{\Lambda}_t &= \text{diag} [\lambda_t^{(1)}, \lambda_t^{(2)}, \dots, \lambda_t^{(K)}] \\ \mathbf{R}_\phi &= \mathbf{U}_\phi \boldsymbol{\Lambda}_\phi \mathbf{U}_\phi^H, \quad \mathbf{U}_\phi = [\mathbf{u}_\phi^{(1)}, \mathbf{u}_\phi^{(2)}, \dots, \mathbf{u}_\phi^{(N_s)}] \\ \boldsymbol{\Lambda}_\phi &= \text{diag} [\lambda_\phi^{(1)}, \lambda_\phi^{(2)}, \dots, \lambda_\phi^{(N_s)}] \end{aligned} \quad (3.44)$$

$$\mathbf{e}_v^{(q)} = [0, \dots, 0, \underset{\uparrow}{1}, 0, \dots, 0]^T$$

\uparrow
qth element

$$N_p = 6 + 2N_c; \quad N_c = N_s (N_s - 1) / 2$$

Being $\lambda_t^{(k)}$ and $\lambda_\phi^{(k)}$ the eigenvalues of \mathbf{T} and \mathbf{R}_ϕ respectively. Similarly, $\mathbf{u}_t^{(k)}$ and $\mathbf{u}_\phi^{(k)}$ corresponds to the eigenvectors of these correlation matrices. N_c in (3.44) is the number of parameters associated with the spatial correlation matrix and therefore it

depends on the array size N_s , being N_p the total number of parameters in our model and K the number of channel vector estimates.

$$\bar{\Psi} = [k_0, \lambda_n, \beta, \gamma_{k,k_1}, \sigma_w^2]^T \quad \mathbf{G}_{k,k_1} = \begin{bmatrix} 1 & 0 & 0 & 0 & 0 \\ 0 & 1 & 0 & 0 & 0 \\ 0 & 0 & 1 & 0 & 0 \\ 0 & 0 & 0 & \lambda_\phi^{(k)} \lambda_t^{(k_1)} & 0 \\ 0 & 0 & 0 & 0 & 1 \\ 0 & 0 & 0 & P_s \lambda_\phi^{(k)} \frac{\partial \lambda_t^{(k_1)}}{\partial \alpha} & 0 \\ \mathbf{0} & \mathbf{0} & \mathbf{0} & P_s \frac{\partial \lambda_\phi^{(k)}}{\partial \mathbf{p}} \lambda_t^{(k_1)} & \mathbf{0} \end{bmatrix}_{(6+2N_c) \times 5} \quad (3.45)$$

$$\frac{\partial \lambda_\phi^{(k)}}{\partial \mathbf{p}} = \left[\frac{\partial \lambda_\phi^{(k)}}{\partial \rho_{1,\text{Re}}}, \frac{\partial \lambda_\phi^{(k)}}{\partial \rho_{2,\text{Re}}}, \dots, \frac{\partial \lambda_\phi^{(k)}}{\partial \rho_{N,\text{Re}}}, \frac{\partial \lambda_\phi^{(k)}}{\partial \rho_{1,\text{Im}}}, \frac{\partial \lambda_\phi^{(k)}}{\partial \rho_{2,\text{Im}}}, \dots, \frac{\partial \lambda_\phi^{(k)}}{\partial \rho_{N,\text{Im}}} \right]^T \quad (3.46)$$

$$\begin{aligned} \gamma_{k,k_1} &= \lambda_\phi^{(k)} \lambda_t^{(k_1)} P_s \\ \dot{\lambda}_t^{(k_1)} &= \frac{d\lambda_t^{(k_1)}}{d\alpha_t} \quad \dot{\mathbf{u}}_t^{(k_1)} = \frac{d\mathbf{u}_t^{(k_1)}}{d\alpha_t} \end{aligned} \quad (3.47)$$

$$\left\{ \mathbf{J}_{\bar{\Psi}} \right\}_{pq} = \text{tr} \left(\mathbf{R}_{k,k_1}^{-1} \frac{\partial \mathbf{R}_{k,k_1}}{\partial \bar{\Psi}_p} \mathbf{R}_{k,k_1}^{-1} \frac{\partial \mathbf{R}_{k,k_1}}{\partial \bar{\Psi}_q} \right) \quad (3.48)$$

$$\mathbf{R}_{k,k_1} = \lambda_\phi^{(k)} \lambda_t^{(k_1)} P_s \mathbf{G}_s \mathbf{\Lambda}_\tau \mathbf{G}_s^T + \sigma_w^2 \mathbf{I}_N \quad (3.49)$$

Note that the required FIM in (3.43) is built with the weighted contribution of the information provided by each new spatial and temporal estimation through the partial FIMs in (3.48) taking advantage of the structure of the power delay profile in (3.49).

$$\begin{aligned} C_1 &= -P_s^2 \sum_{k=1}^{N_s} \sum_{k_1=1}^K \sum_{l_1=1}^K \lambda_\phi^{(k)^2} \left(\lambda_t^{(k_1)} - \lambda_t^{(l_1)} \right)^2 \mathbf{u}_t^{(k_1)H} \dot{\mathbf{u}}_t^{(l_1)} \mathbf{u}_t^{(l_1)} \dot{\mathbf{u}}_t^{(k_1)} \text{tr} \left\{ \mathbf{R}_{k,k_1}^{-1} \mathbf{G}_s \mathbf{\Lambda}_\tau \mathbf{G}_s^T \mathbf{R}_{k,l_1}^{-1} \mathbf{G}_s \mathbf{\Lambda}_\tau \mathbf{G}_s^T \right\} \\ C_2^{(q_1, q_2)} &= -P_s^2 \sum_{k=1}^{N_s} \sum_{l=1}^{N_s} \sum_{k_1=1}^K \lambda_t^{(k_1)^2} \left(\lambda_\phi^{(k)} - \lambda_\phi^{(l)} \right)^2 \left(\mathbf{u}_\phi^{(k)T} \frac{\partial \mathbf{u}_\phi^{(l)}}{\partial \rho_{q_1}} \right) \left(\mathbf{u}_\phi^{(l)T} \frac{\partial \mathbf{u}_\phi^{(k)}}{\partial \rho_{q_2}} \right) \text{tr} \left\{ \mathbf{R}_{k,k_1}^{-1} \mathbf{G}_s \mathbf{\Lambda}_\tau \mathbf{G}_s^T \mathbf{R}_{l,k_1}^{-1} \mathbf{G}_s \mathbf{\Lambda}_\tau \mathbf{G}_s^T \right\} \end{aligned} \quad (3.50)$$

Derivations are certainly quite algebraic extensive, and their main steps will be commented on briefly.

First of all \mathbf{R}_z^{-1} is expressed as in (3.51) by using the Kronecker product properties [74], with \mathbf{R}_{k,k_1} defined as in (3.49):

$$\mathbf{R}_z^{-1} = \sum_{k=1}^{N_s} \mathbf{u}_\phi^{(k)} \mathbf{u}_\phi^{(k)H} \otimes \sum_{k_1=1}^K \mathbf{u}_t^{(k_1)} \mathbf{u}_t^{(k_1)H} \otimes \sum_{k_2=1}^N \mathbf{e}_{k_2}^{(N)} \mathbf{e}_{k_2}^{(N)H} \mathbf{R}_{k,k_1}^{-1} \quad (3.51)$$

Derivatives required in (3.42) must also be computed, and it is easy to show they take the form described in equation (3.52), being \mathbf{A}, \mathbf{B} and \mathbf{C} the matrices contained in Table 3.1.

$$\frac{\partial \mathbf{R}_z}{\partial \Psi_p} = \mathbf{A} \otimes \mathbf{B} \otimes \mathbf{C} \quad (3.52)$$

For instance, when derivative relative to k_0 is required, the corresponding value of p within the table is one, and the corresponding result is assembled as $\partial \mathbf{R}_z / \partial \Psi_{p=1} = \partial \mathbf{R}_z / \partial k_0 = \mathbf{R}_\phi \otimes \mathbf{T}_K \otimes P_s \partial \Lambda_\tau / \partial k_0$.

Table 3.1. Elements required in (3.53) to assemble the FIM in (3.43) for a Rayleigh Fading Channel.

p	Ψ_p	\mathbf{A}	\mathbf{B}	\mathbf{C}
1	k_0	\mathbf{R}_ϕ	\mathbf{T}_K	$P_s \partial \Lambda_\tau / \partial k_0$
2	λ_n	\mathbf{R}_ϕ	\mathbf{T}_K	$P_s \partial \Lambda_\tau / \partial \lambda_n$
3	β	\mathbf{R}_ϕ	\mathbf{T}_K	$P_s \partial (\mathbf{G}_s \Lambda_\tau \mathbf{G}_s^T) / \partial \beta$
4	P_s	\mathbf{R}_ϕ	\mathbf{T}_K	$\mathbf{G}_s \Lambda_\tau \mathbf{G}_s^T$
5	σ_w^2	\mathbf{I}_{N_s}	\mathbf{I}_K	\mathbf{I}_N
6	α	\mathbf{R}_ϕ	$\partial \mathbf{T} / \partial \alpha$	$P_s \mathbf{G}_s \Lambda_\tau \mathbf{G}_s^T$
$7:Np$	ρ_{p-6}	$\partial \mathbf{R}_\phi / \partial \rho_{p-6}$	\mathbf{T}_K	$P_s \mathbf{G}_s \Lambda_\tau \mathbf{G}_s^T$

From inserting equations (3.51) and (3.52) in (3.42), and after some simplifications (3.53) originates. Finally, by replacing the values from Table 3.1, as in the above example, expression (3.43) is reached.

$$\left[\mathbf{F}_\Psi \right]_{pq} = \sum_{k=1}^{N_s} \sum_{l=1}^{N_s} \mathbf{u}_\phi^{(k)H} \mathbf{A}_p \mathbf{u}_\phi^{(l)} \mathbf{u}_\phi^{(l)H} \mathbf{A}_q \mathbf{u}_\phi^{(k)} \sum_{k_1=1}^K \sum_{l_1=1}^K \mathbf{u}_t^{(k_1)H} \mathbf{B}_p \mathbf{u}_t^{(l_1)} \mathbf{u}_t^{(l_1)H} \mathbf{B}_q \mathbf{u}_t^{(k_1)} \text{tr} \left(\mathbf{R}_{k,k_1}^{-1} \mathbf{C}_p \mathbf{R}_{l,l_1}^{-1} \mathbf{C}_q \right) \quad (3.53)$$

3.2.4.2 CRBs for timing when sampling is performed at the chip rate and a NLOS Rayleigh Fading Model

Expression in (3.43) admits further simplifications when the sampling is performed at the chip rate. If it is the case, \mathbf{G} becomes the identity matrix \mathbf{I} , and the roll-off factor may be discarded, reducing the number of parameter required to compute

the Fisher matrix, as it is shown in Table 3.2. Hence (3.43) becomes (3.54), and (3.45) becomes (3.55):

$$\mathbf{F}_\Psi = \sum_{k=1}^{N_s} \sum_{k_1=1}^K \mathbf{G}_{k,k_1} \mathbf{J}_{\bar{\Psi}} \mathbf{G}_{k,k_1}^T + \mathbf{C}_1 \mathbf{e}_{N_p}^{(5)} \mathbf{e}_{N_p}^{(5)T} + \sum_{q_1=1}^{2N} \sum_{q_2=1}^{2N} \mathbf{C}_2^{(q_1, q_2)} \mathbf{e}_{N_p}^{(5+q_1)} \mathbf{e}_{N_p}^{(5+q_2)T} \quad (3.54)$$

$$\bar{\Psi} = [k_0, \lambda_n, \gamma_{k,k_1}, \sigma_w^2]^T \quad \mathbf{G}_{k,k_1} = \begin{bmatrix} 1 & 0 & 0 & 0 & 0 \\ 0 & 1 & 0 & 0 & 0 \\ 0 & 0 & 0 & \lambda_\phi^{(k)} \lambda_t^{(k_1)} & 0 \\ 0 & 0 & 0 & 0 & 1 \\ 0 & 0 & 0 & P_s \lambda_\phi^{(k)} \frac{\partial \lambda_t^{(k_1)}}{\partial \alpha} & 0 \\ \mathbf{0} & \mathbf{0} & \mathbf{0} & P_s \frac{\partial \lambda_\phi^{(k)}}{\partial \rho} \lambda_t^{(k_1)} & \mathbf{0} \end{bmatrix}_{(5+2N_c) \times 5} \quad (3.55)$$

Table 3.2. Elements required in (3.53) to assemble the FIM in (3.54) for a Rayleigh Fading Channel when sampling is performed at the chip time.

p	Ψ_p	\mathbf{A}	\mathbf{B}	\mathbf{C}
1	k_0	\mathbf{R}_ϕ	\mathbf{T}_K	$P_s \partial \Lambda_\tau / \partial k_0$
2	λ_n	\mathbf{R}_ϕ	\mathbf{T}_K	$P_s \partial \Lambda_\tau / \partial \lambda_n$
3	P_s	\mathbf{R}_ϕ	\mathbf{T}_K	Λ_τ
4	σ_w^2	\mathbf{I}_{N_s}	\mathbf{I}_K	\mathbf{I}_N
5	α	\mathbf{R}_ϕ	$\partial \mathbf{T} / \partial \alpha$	$P_s \Lambda_\tau$
6: N_p	ρ_{p-5}	$\partial \mathbf{R}_\phi / \partial \rho_{p-5}$	\mathbf{T}_K	$P_s \Lambda_\tau$

3.2.4.3 Asymptotic expressions for the CRBs of delay estimates in case of a PCD source

Computing the CRB's from the previous equations may be computationally expensive, especially when the number of available channel vector estimates K is high. Therefore, it is necessary to work within reasonable approximates to reduce this burden. A closed expression for the asymptotic eigenvalues from matrix \mathbf{T} for PCD sources is provided in [57], and it is reproduced below:

$$\lambda_K^{(k)} \approx \frac{1 - \alpha^2}{1 + \alpha^2 - 2\alpha \cos\left(\frac{k\pi}{K+1}\right)} \quad (3.56)$$

Equation (3.56) allows the computation of analytic derivatives with respect to α . For the asymptotic case, \mathbf{C}_1 in equation (3.54) is negligible and FIM may be expressed as:

$$\mathbf{F}_\Psi \approx \sum_{k=1}^{N_s} \sum_{k_1=1}^K \mathbf{G}_{k,k_1} \mathbf{J}_{\bar{\Psi}} \mathbf{G}_{k,k_1}^T + \sum_{q_1=1}^{2N_c} \sum_{q_2=1}^{2N_c} C_2^{(q_1, q_2)} \mathbf{e}_{N_p}^{(5+q_1)} \mathbf{e}_{N_p}^{(5+q_2)} \quad (3.57)$$

3.2.4.4 CRBs for delay estimates in case of Fully Coherent Dispersive Sources

Expressions above are useful for PCD sources, but in case of FCD sources they cannot be used since \mathbf{T} under this assumption just have one eigenvector different to zero and equal to \mathbf{K} , and another more suitable factorization must be done. Hence, in order to achieve adequate expressions for this special case, definitions of the terms described in (3.44) and (3.51) from the last section are modified respectively as in (3.58) and (3.59):

$$\mathbf{T} = \mathbf{1}_K \mathbf{1}_K^T \quad (3.58)$$

$$\mathbf{R}_z^{-1} = \sum_{k=1}^{N_s} \mathbf{u}_\phi^{(k)} \mathbf{u}_\phi^{(k)H} \otimes \left[\frac{1}{\sigma_w^2} \mathbf{P} \otimes \mathbf{I}_M + \frac{1}{K} \mathbf{1}_K \mathbf{1}_K^T \otimes \mathbf{R}_k^{-1} \right] \quad (3.59)$$

Where \mathbf{P} and \mathbf{R}_k are given by equations (3.60) and (3.61), being $\mathbf{1}_K$ a vector of length K with all its components equal to one.

$$\mathbf{P} = \mathbf{I}_K - \frac{1}{K} \mathbf{1}_K \mathbf{1}_K^T \quad (3.60)$$

$$\mathbf{R}_k = K P_s \lambda_\phi^{(k)} \mathbf{\Lambda}_\tau + \sigma_w^2 \mathbf{I}_M \quad (3.61)$$

The number of parameters for this case reduces as it can be seen in (3.62). The matrices \mathbf{A} , \mathbf{B} and \mathbf{C} used for derivatives are expressed in Table 3.3, and FIM elements for FCD sources may be computed as in expression (3.63), being their components defined as it is shown in (3.64)-(3.67).

$$\Psi = [k_o, \lambda_n, r, \sigma_w^2, \mathbf{p}^T] \quad (3.62)$$

$$\mathbf{F}_\Psi = \sum_{k=1}^{N_s} \mathbf{G}_k \mathbf{J}_{\bar{\Psi}_1} \mathbf{G}_k^T + \sum_{q_1=1}^{2N_c} \sum_{q_2=1}^{2N_c} C_3^{(q_1, q_2)} \mathbf{e}_{N_p}^{(q_1)} \mathbf{e}_{N_p}^{(q_2)T} + \frac{N_s (K-1) N}{\sigma_w^4} \mathbf{e}_{N_p}^{(4)} \mathbf{e}_{N_p}^{(4)T} \quad (3.63)$$

$$\bar{\Psi}_1 = [k_o, \lambda_n, \gamma_k, \sigma_w^2]^T \quad \mathbf{G}_k = \begin{bmatrix} 1 & 0 & 0 & 0 \\ 0 & 1 & 0 & 0 \\ 0 & 0 & K \lambda_\phi^{(k)} & 0 \\ 0 & 0 & 0 & 1 \\ 0 & 0 & P_s K \frac{\partial \lambda_\phi^{(k)}}{\partial \mathbf{p}} & 0 \end{bmatrix} \quad (3.64)$$

$$\gamma_k = K \lambda_\phi^{(k)} P_s \quad (3.65)$$

$$\left\{ \mathbf{J}_{\bar{\Psi}_1} \right\}_{pq} = tr \left(\mathbf{R}_k^{-1} \frac{\partial \mathbf{R}_k}{\partial \bar{\Psi}_{1p}} \mathbf{R}_k^{-1} \frac{\partial \mathbf{R}_k}{\partial \bar{\Psi}_{1q}} \right) \quad (3.66)$$

$$C_3^{(q1,q2)} = \sum_{k=1}^{N_s} \sum_{l=1}^{N_s} -(\lambda_\phi^{(k)} - \lambda_\phi^{(l)})^2 \left(\mathbf{u}_\phi^{(l)T} \frac{\partial \mathbf{u}_\phi^{(k)}}{\partial \rho_{q1}} \right) \cdot \left(\mathbf{u}_\phi^{(k)T} \frac{\partial \mathbf{u}_\phi^{(l)}}{\partial \rho_{q2}} \right) \text{tr} \left\{ \mathbf{R}_k^{-1} \frac{\partial \mathbf{R}_k}{\partial \gamma_k} \mathbf{R}_l^{-1} \frac{\partial \mathbf{R}_l}{\partial \gamma_l} \right\} \quad (3.67)$$

Table 3.3. Elements required in (3.53) to assemble the FIM in (3.63) for a Rayleigh Fading Channel in case of a FCD source.

p	Ψ_p	\mathbf{A}	\mathbf{B}	\mathbf{C}
1	k_0	\mathbf{R}_ϕ	$\mathbf{1}_K \mathbf{1}_K^T / K$	$K P_s (\partial \Lambda_\tau / \partial k_0)$
2	λ_n	\mathbf{R}_ϕ	$\mathbf{1}_K \mathbf{1}_K^T / K$	$K P_s (\partial \Lambda_\tau / \partial \lambda_n)$
3	P_s	\mathbf{R}_ϕ	$\mathbf{1}_K \mathbf{1}_K^T$	Λ_τ
4	σ_w^2	\mathbf{I}_{N_s}	\mathbf{I}_K	\mathbf{I}_N
5: N_p	ρ_{p-4}	$\partial \mathbf{R}_\phi / \partial \rho_{p-4}$	$\mathbf{1}_K \mathbf{1}_K^T / K$	$R \Lambda_\tau$

3.2.4.5 LOS Model for Delay Dispersion

In case of a LOS condition, the fading is Rice distributed and therefore the mean channel vector estimate $\boldsymbol{\mu}_z$ is not null, and it is described in (3.37) in terms of the expected spatial signature \mathbf{b}_ϕ , the Doppler vector $\boldsymbol{\alpha}_t$, the pulse shaping vector for the first arrival $\mathbf{g}^{(k_0)}$, and the mean signal level for the LOS component A_0 . All these components were defined in expressions (3.27)-(3.36).

Since the mean channel vector is different to zero for the LOS case, the parameter vector is described in (3.38) and the computation of the FIM in (3.41) adds some derivatives that must also be computed. It is easy to show these take the form in (3.68):

$$\frac{\partial \boldsymbol{\mu}_z}{\partial \Psi_p} = \mathbf{D} \otimes \mathbf{E} \otimes \mathbf{F} \quad (3.68)$$

Being \mathbf{D}, \mathbf{E} and \mathbf{F} the vectors contained in Table 3.3. For instance, when derivative relative to k_0 is required, the corresponding value of p within the table is one, and $\partial \boldsymbol{\mu}_z / \partial \Psi_{p=1} = \partial \boldsymbol{\mu}_z / \partial k_0 = \mathbf{b}_\phi \otimes \boldsymbol{\alpha}_t \otimes A_0 \partial \mathbf{g}^{(k_0)} / \partial k_0$.

Table 3.4. Elements required in (3.69) to assemble FIM for a Rice Fading Channel.

p	Ψ_p	\mathbf{D}	\mathbf{E}	\mathbf{F}
1	k_0	\mathbf{b}_ϕ	$\boldsymbol{\alpha}_t$	$A_0 \partial \mathbf{g}^{(k_0)} / \partial k_0$
2	λ_n	-	-	-
3	β	\mathbf{b}_ϕ	$\boldsymbol{\alpha}_t$	$A_0 \partial \mathbf{g}^{(k_0)} / \partial \beta$
4	P_s	-	-	-
5	σ_w^2	-	-	-
6	α	\mathbf{b}_ϕ	$\boldsymbol{\alpha}_t$	$A_0 \mathbf{g}^{(k_0)}$
7: N_{p-1}	ρ_{p-6}	$\partial \mathbf{b}_\phi / \partial \rho_{p-6}$	$\boldsymbol{\alpha}_t$	$A_0 \mathbf{g}^{(k_0)}$
N_p	A_0	\mathbf{b}_ϕ	$\boldsymbol{\alpha}_t$	$\mathbf{g}^{(k_0)}$

It may be shown that (3.41) becomes (3.69) when \mathbf{R}_z^{-1} in (3.51) and the partial derivatives in (3.68) are replaced within(3.41):

$$\mathbf{F}_\Psi^{LOS} = \mathbf{F}_\Psi + 2\text{Re} \left\{ \mathbf{1}_{N_s}^T \sum_{k=1}^{N_s} \mathbf{u}_\phi^{(k)} \mathbf{u}_\phi^{(k)H} \odot \mathbf{D}_p \mathbf{D}_q^H \mathbf{1}_{N_s} \mathbf{1}_K^T \sum_{k_1=1}^K \mathbf{u}_t^{(k_1)} \mathbf{u}_t^{(k_1)H} \odot \mathbf{E}_p \mathbf{E}_q^H \mathbf{1}_K \mathbf{F}_p^T \mathbf{R}_{k,k_1}^{-1} \mathbf{F}_q \right\} \quad (3.69)$$

In above expression, \mathbf{F}_Ψ corresponds to the Fisher Information Matrix for the NLOS model in(3.43), but since the parameter A_0 was added for the LOS model, \mathbf{G}_{k,k_1} in (3.55) must be replaced for \mathbf{G}_{k,k_1}^{LOS} in(3.70). Furthermore, $\bullet \odot \bullet$ notes the Hadamard Product.

$$\mathbf{G}_{k,k_1}^{LOS} = \begin{bmatrix} \mathbf{G}_{k,k_1} \\ \mathbf{0} \end{bmatrix}_{(7+2N_c) \times 5} \quad (3.70)$$

3.2.5 Model for angular dispersion

Since signal bearing may be used to enhance positioning accuracy, this section performs a briefly review of the accuracy limits in Direction of Arrival (DOA). Note that multipath could be modeled as punctual sources coming from particular unknown bearings, and the work in [79] derives CRB for this situation. However, our interest refers to the accuracy limits for angular dispersive channels. This problem was studied in [57] for flat fading multipath channels. In this latter case, the received signal vector $\mathbf{y}(t)$ contains the signal received at the N_s sensors and may be described as it is shown in equation (3.71):

$$\mathbf{y}(t) = \sum_{n=1}^{N_{rays}} \mathbf{a}_n s(t - \tau_n) + \mathbf{n}(t) \quad (3.71)$$

Where \mathbf{a}_n represents the array response vector for ray n , N_{rays} is the number of rays because of local scattering and multipath propagation, and τ_n is the propagation time of the considered path.

Equation (3.71) becomes (3.72) when rays are grouped in clusters. In this case channel is frequency selective:

$$\mathbf{y}(t) = \sum_{m=0}^{N-1} \sum_{n=1}^{N_{r,m}} \mathbf{a}_{n,m} s((k-m)T_c) + \mathbf{n}(t) = \sum_{m=0}^{N-1} \mathbf{b}_m(t) s((k-m)T_c) + \mathbf{n}(k) \quad (3.72)$$

In a DS-SS system, channel estimation may be done by demodulating the pilot; therefore the channel vector estimates are given by equation(3.73):

$$\mathbf{z}_m(k) = \sum_{l=kG_c}^{(k+1)G_c-1} \mathbf{y}(lT_c) s^*((l-m)T_c) \quad (3.73)$$

Where, m subscript refers to the lag of the arriving path. In above expression, T_c corresponds to the chip time, G_c is called the processing gain and it is defined as the rate between the time interval for channel estimation and the chip period, and m is an offset used to identify the relative position of different paths arriving to the receiver or channel impulse response component. Including all the arrivals implies to incorporate two parameters for each multipath clusters [59]. Therefore, in the following only the first arrival cluster will be retained, and index m will be discarded; hence, vector estimates can be grouped into a single vector as it is shown below:

$$\mathbf{z} = [\mathbf{z}^T(0), \mathbf{z}^T(1), \dots, \mathbf{z}^T(K-1)]^T \quad \mathbf{z}(k) = [z_0(k), \dots, z_{N_s}(k)]^T \quad (3.74)$$

Assuming this vector as complex Gaussian distributed with zero mean, corresponding to a Rayleigh channel, its correlation matrix \mathbf{R}_z in (3.75) may be expressed as it is shown in (3.76):

$$\mathbf{z} \rightarrow CN(\mathbf{0}_{KM \times 1}, \mathbf{R}_z) \quad (3.75)$$

$$\mathbf{R}_z = \sigma_s^2 \mathbf{T}(\alpha) \otimes \mathbf{R}_\phi(\theta_o, \Delta) + \sigma_n^2 \mathbf{I} \quad (3.76)$$

$\mathbf{T}(\alpha)$ and $\mathbf{R}_\phi(\theta_o, \Delta)$ were defined previously and correspond to the temporal and spatial components of the channel vector correlation matrix \mathbf{R}_z respectively, and $\bullet \otimes \bullet$ is the Kronecker product operator. Some works suggest that the correlation matrix $\mathbf{R}_\phi(\theta_o, \Delta)$ follows a Laplacian kernel [38][39], whilst others prefer the Gaussian [37][57]. Minor differences between the two assumptions have been found along this work.

For this case, parameter vector Ψ takes the form in (3.77), and the FIM in order to compute Cramer Rao lower bounds (CRB) for DOA is given by (3.78):

$$\Psi = [\theta_o, \Delta, \sigma_n^2, \sigma_s^2, \alpha] \quad (3.77)$$

$$\mathbf{F}_\Psi = \sum_{k=1}^K \mathbf{G}_k \mathbf{J}_\Psi \mathbf{G}_k^T + C \mathbf{e}_5^{(5)} \mathbf{e}_5^{(5)T} \quad (3.78)$$

Vector Ψ contains the parameters involved in derivation. Bearing (θ_o) and angular spread (Δ) are the parameters of interest, and the remaining ones: signal power, noise power and temporal correlation between two consecutive channel estimates are nuisance. Vectors and matrices used in equation (3.78) are defined in [57] and will not be reproduced here for the sake of brevity. Cramer-Rao bounds derived by using this dispersive angular model are also provided in [57], and they can be used for studying the impact of bearing based or hybrid positioning techniques. This model may be enhanced easily if multipath cluster statistics are known, for instance assuming an exponential distribution for delays as it was done before for timing estimation model. If

it were the case, parameter vector should also include normalized coherence bandwidth λ_n .

Work in [57] exhibits results that show as estimation error improves as channel passes from FCD to ICD. Furthermore bearing estimation error tends to a floor limit of around 3.5° for FCD and 0.5° for ICD. In the latter case, this floor is achieved for a SNR near to 25 dB. Some degradation is performed for lower SNRs, for i.e. this value reduces to 0.70° for a SNR of 15 dB. These results may be easily translated to arc range errors within the 1% and 6% of the relative distance from the subscriber to the BS. This predicts for i.e. arc errors within 10m and 60m when distance between MS and BS is around 1km, and arc errors within 1m and 6m when MS is ten times closer to the BS. All these results are performed for an angular spread of 10° and a bearing of 45° when 50 channel estimates and four sensors are available. In case of “local scatterers in the vicinity of the mobile or due to wavefronts that propagate through random inhomogeneous media” signal becomes corrupted with multiplicative noise [58] and a different model has been performed in this condition for the case of spatially distributed sources in [58]. Furthermore [58] proposes some estimators for bearing estimation that explodes the fact that “self-coherence of interferences is higher at shorter distances between receivers” and therefore the use of minimal subapertures helps to cancel them. CRBs exhibited in [58] show as bearing estimation errors reduce for i.e. from around 0.50° to 0.15° when passing from 20 snapshots to 200 snapshots for a SNR of 10 dB and 8 sensors in the Uniform Linear Array (ULA). Estimators achieve CRB for moderate to high SNRs. When SNR=0 dB, results show as estimation error is approximately two times higher as the predicted for the CRBs.

Rayleigh model in [57] has been modified in [5] introducing a LOS path, therefore it becomes a Rice model. Results from this paper show as bearing estimation error diminishes when a LOS component is present, and this improvement has no floor in relation with a higher SNR when Rice factor tends to infinity. This condition corresponds to a LOS punctual source. In this case, and for a SNR of 10 dB, the bearing estimation error is around 0.17° when the number of snapshots is $K=50$ and six sensors are used. Simulation scenario exhibits a uniform angular spread of 13° and a signal bearing of 30° . These results also show as a higher angular spread degrades bearing estimation, especially for a Rayleigh channel and low SNR. For i.e., when SNR=0 dB and angular spread is 30° , bearing error estimation pass from around 0.5° in case of a LOS punctual source to 2° in case of a Rayleigh channel. Of course error estimation improves when a large number of sensors, is available.

3.3 Simulations and Results

3.3.1 Performance of Asymptotic Expressions

Figure 3.4 and Figure 3.5 respectively show the CRBs behavior for the estimated timing k_0 and the normalized coherence bandwidth λ_n as a function of the temporal correlation for various values of the number of the observed channel estimates, K , for the NLOS Rayleigh fading model in (3.42). Results were provided by using both the

exact expressions in (3.43) and expressions achieved with the use of asymptotic eigenvalues from matrix \mathbf{T} in (3.56).

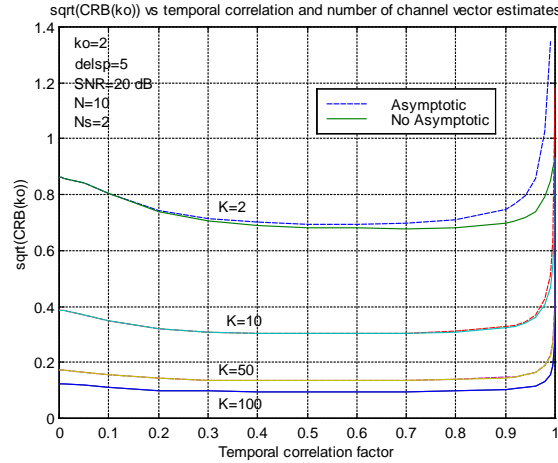


Figure 3.4. CRB of the first arriving path k_0 as a function of the temporal correlation coefficient α , and for different number of available measured channels, for the asymptotic (dashed) and no asymptotic (solid) expressions. SNR set to 20 dB and delay spread to $5T_c$.

Asymptotic expressions for the first arrival timing k_0 fit very closely to exact ones for as few as 10 observations for this high SNR of 20 dB as it is shown in Figure 3.4. However, higher values of K were required when SNR were poor. For instance, when SNR was set to 0 dB, 50 observations instead of 10 were required to have a similar performance along the whole range of the temporal correlation.

From results in Figure 3.5 for the CRB of the normalized coherence bandwidth λ_n , is evident as asymptotic expressions for this parameter are more sensitive to the temporal correlation coefficient than their analog expressions for timing. In fact, higher discrepancies were achieved for this parameter, and 50 observations were required to achieve a good fitting. For both parameters, the largest differences were achieved for a high temporal correlation coefficient very close to one where expected accuracies rapidly degrade.

Due to that the timing is the parameter of interest for location purposes, and since from analysis exhibited in Figure 1, it is expected that the average value of K will be larger than 100, very accurate results may be provided from the use of these asymptotic expressions.

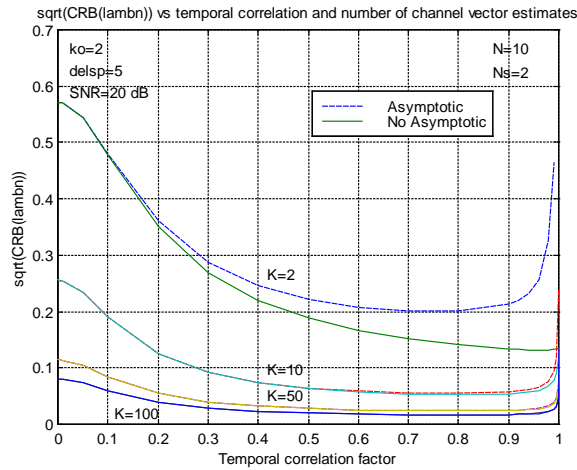


Figure 3.5. CRB of the inverse of the normalized delay spread λ_n for different values of the temporal correlation coefficient, and for different number of available measured channels, for the asymptotic (dashed) and no asymptotic (solid) expressions. SNR set to 20 dB and delay spread to $5 T_c$.

Figure 3.6 shows how exact expressions for the CRBs for timing in (3.43) almost fit perfectly with results provided for reduced expressions for FCD channels when temporal correlation α was set to one. Certainly, the use of FCD expressions is desirable since they reduce computational burden considerably. Similar results were also found for the normalized coherence bandwidth.

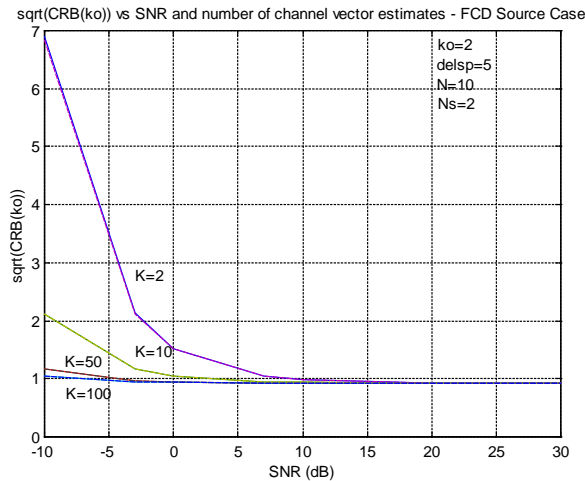


Figure 3.6. CRB of the first arriving path k_0 for different values of the SNR, for the FCD equations (solid) and PCD, setting $\alpha = 1$ (dashed). Delay spread set to $5 T_c$.

3.3.2 Performance of CRBs for timing and normalized coherence bandwidth for the NLOS Rayleigh fading model

In order to put CRB results exhibited in this document in relation with potential errors introduced in terms of distance range, (3.79) will be used:

$$e = c \cdot \sqrt{CRB(k_0)} T_c \quad (3.79)$$

Where, e , correspond to the range error estimation, c , to light speed and T_c to the system chip time. Consequently, an estimation error of around the chip time results in a range error in the order of 240 m for IS-95 and around of 80 m for WCDMA since chip period is a little more than three times higher for IS-95 in relation to WCDMA. In the sequel, a WCDMA system will be referred by default when range errors will be presented.

Otherwise, as it was mentioned before, channel coherence bandwidth, B_c , is proportional to parameter λ_n , and to the chip rate, R_c . The exact proportionality factor depends on application but is lower to $1/2\pi$ [63][64], therefore it will be set to $1/10$ as it is shown in(3.80), and the estimation error of this bandwidth may be related to the CRB for λ_n as in(3.81).

$$B_c \approx \frac{1}{10} \lambda_n R_c \quad (3.80)$$

$$e_{B_c} \approx \frac{1}{10} R_c \sqrt{CRB(\lambda_n)} \quad (3.81)$$

With the use of(3.81), it is easy to understand that error estimation for the coherence bandwidth is close to 1% of the chip rate when the square root of the CRB is close to $1/10$. It would correspond for i.e. to an uncertainty of around 38 KHz for a WCDMA system and around of 12 KHz for IS-95.

3.3.2.1 Changes in CRBs with channel temporal correlation factor and SNR

Figure 3.7 and Figure 3.8 provide information about the behaviour of the CRBs for the first arriving path k_0 and the normalized coherence bandwidth λ_n within Λ_τ in (3.26), in terms of the temporal correlation factor α , and Signal to Noise Ratio (SNR).

As shown in Figure 3.7, the timing accuracy increased when the temporal correlation between channel estimates reduced. In fact, for a SNR near 15dB, just one sensor available and 32 channel observations, the range error reduced from around 85 m for a FCD channel to 17 m when an ICD channel.

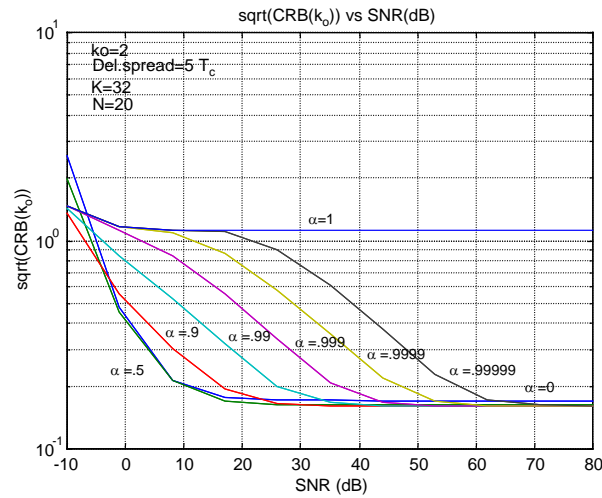


Figure 3.7. CRB of the first arriving path k_0 for different values of the SNR, and different values of the temporal correlation α . Number of channel vector estimates set to 32 and delay spread set to $5 T_c$.

On the other side, note in Figure 3.8 as error bound for normalized coherence bandwidth estimation also reduced for lower temporal correlations coefficients; in fact, an improvement is registered when correlation goes from 1 to 0. Recall this situation corresponds to mobile subscribers changing from low to high speed respectively, or when channel estimates were achieved from more separated slots. CRB always diminishes for higher SNR's, with some limiting floor value, which is significantly higher for the high temporal correlation case. Note for i.e. as the value of this error bound degraded from a value slightly better than 3% for the PCD source case ($\alpha=0.9$) to around 9% for the FCD case when the SNR corresponded to 10dB, two sensors were being used and the source angular spread corresponded to 5° . Similarly, it degraded from 2.2% for the PCD source case ($\alpha=0.9$) to around 8% for the FCD case when four sensors were being used. Therefore, an estimation improvement less than 25% was achieved when passing from two sensors to four. In addition, some reduction in the error bound was shown when angular spread increases from 5° to 18° .

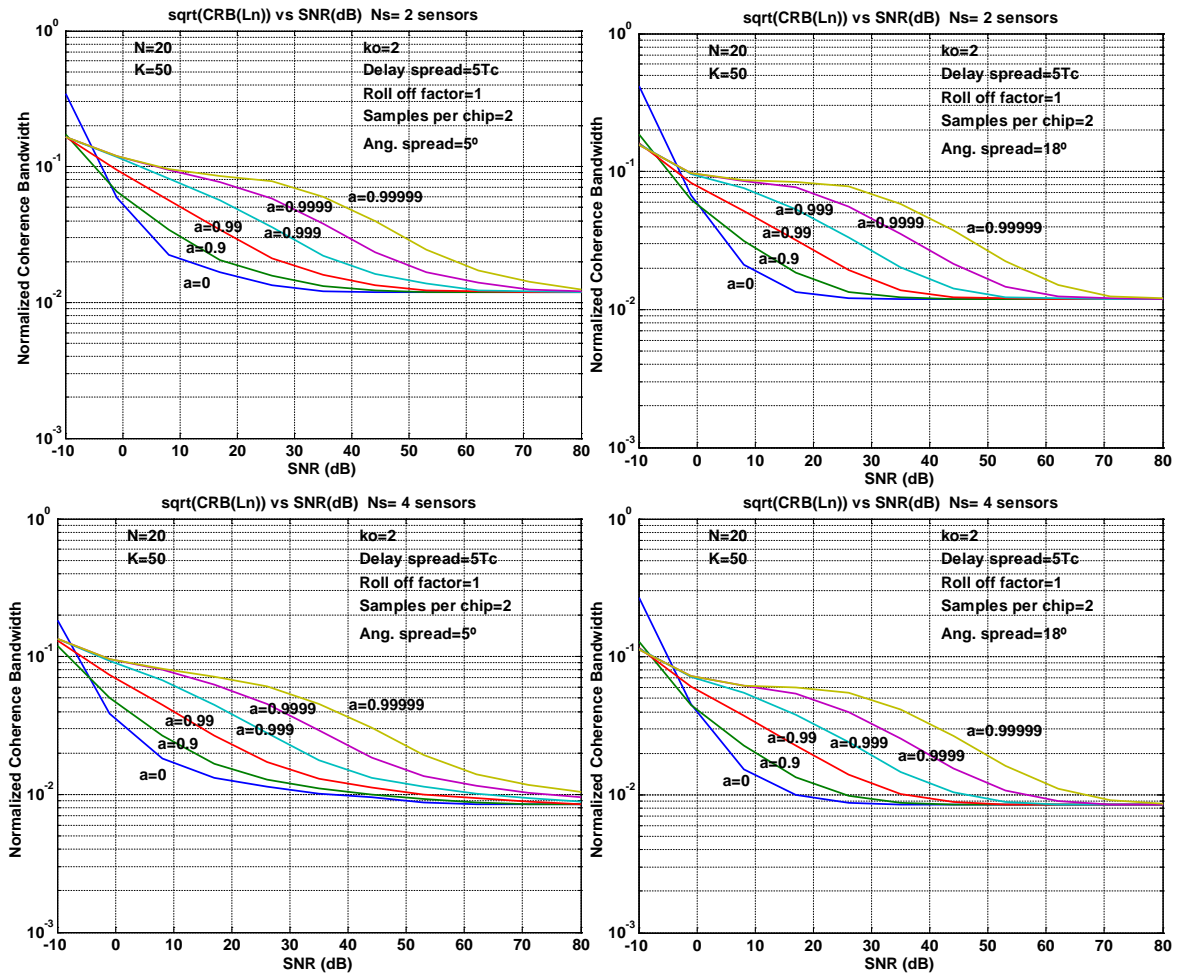


Figure 3.8. CRB of the inverse of the normalized delay spread λ_n for different values of the SNR, different values of the temporal correlation α_t , different values for angular delay spread, and different values for the number of sensors. Number of channel vector estimates set to 50, delay spread set to $5 T_c$, and roll-off factor set to one. a) Top left: Angular spread set to 5° and two sensors; b) Top right: Angular spread set to 18° and two sensors; c) Bottom left: Angular spread set to 5° and four sensors; d) Bottom right: Angular spread set to 18° and four sensors.

3.3.2.2 Improvement in CRBs for timing with the use of sensors in space diversity

Figure 3.9 and Figure 3.10 show the behaviour of the CRB for the first arrival when signals from various sensors are available. Figure 3.9 shows bounds when uncorrelated signals were recorded at different sensors. It could well be a case of timing estimation at the UE for the downlink (DL), or in spatial diversity antennas at the BS, for uplink (UL) measurements.

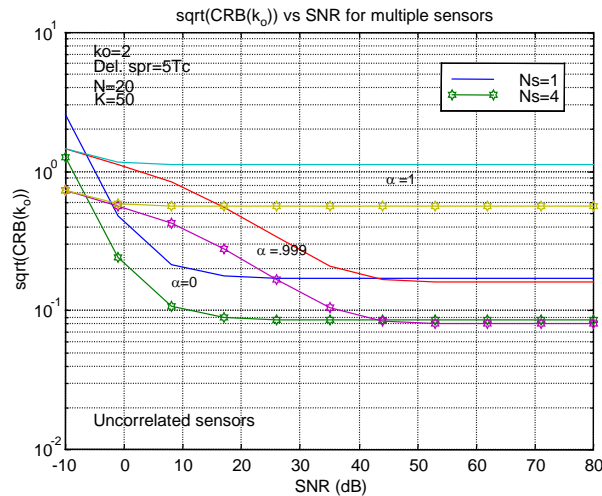


Figure 3.9. CRB of the first arriving path k_0 for different values of the SNR, and different values of the temporal correlation α . One and four sensors are used assuming uncorrelated received signals in each. The number of sensors is 1 (solid) and 4 (solid-bullet). Delay spread set to $5T_c$ and for 50 channel vector observations.

On the other hand, Figure 3.10 shows the case where 4 sensors in $\lambda/2$ were used in two environments with angular spreads of 5 and 10 degrees, which could be the case of UL measurements. These results showed that adding multiple antennas improved the accuracy of estimates significantly, but that angular spread did not significantly influence delay estimation.

In fact, comparing these figures, the best situation corresponded precisely to having completely uncorrelated sensors, and CRB degraded gracefully as angular spread decreased. Differences were not really dramatic in relative terms, since computed errors were between 0,095 and 0,125 of the chip time, but they were more visible in range terms. For instance, range errors for a SNR of 15 dB were between 7.5 m and 10 m for WCDMA and between 23 m and 30 m for IS-95.

The inclusion of multiple sensors provided similar gains in timing accuracy, from moderate to high SNR, regardless of the value of the temporal coefficient. Note for i.e. as timing bound improves from around 20% of the chip time or sampling interval with just one sensor to around 10% of the chip time with four sensors for ICD sources and it improves from 60% of the chip time to 30% of the chip time for a coefficient α of .999 and a SNR near to 15 dB. It means that a gain factor of around two is achieved. In range terms, error decreases from 50 m to 25 m for ICD sources when a four sensor array is used instead a lonely sensor.

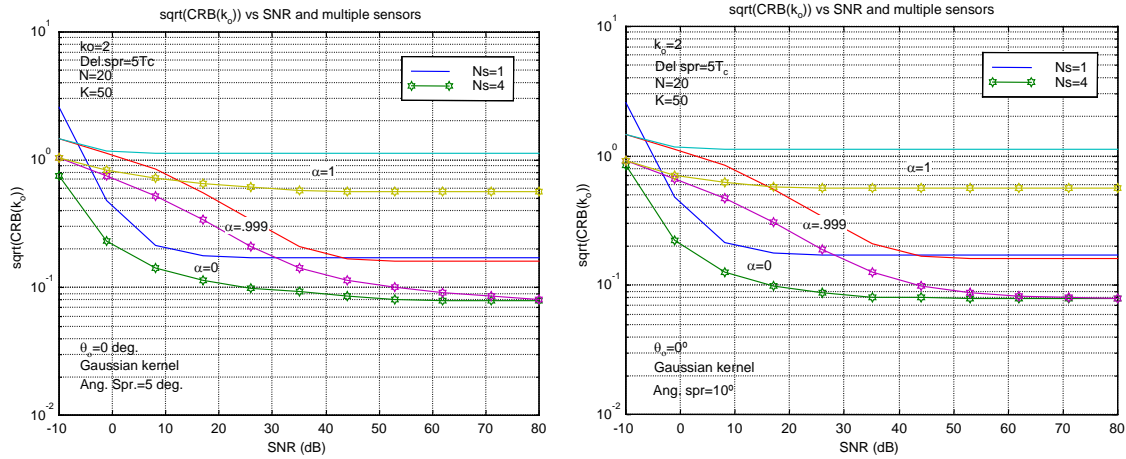


Figure 3.10. CRB of the first arriving path k_0 for different values of the SNR, and different values of the temporal correlation α . One and four sensors are used assuming different angular spread in the received signals in each. The number of sensors is 1 (solid) and 4 (solid-bullet). Delay spread set to $5 T_c$ and the number of channel vector estimates set to 50. a) Left: angular spread set to 5° , b) Right: angular spread set to 10° .

3.3.2.3 Changes in CRBs for timing with roll-off factor when sampling is faster than the chip rate

Figure 3.11 and Figure 3.12 show that a marginal improvement in the timing error bound was performed when roll-off factor β was modified from 0.5 to 1.0. For i.e. there was an improvement of just around 10% for a SNR of 15dB for ICD sources. It accounts for less than a meter in range terms.

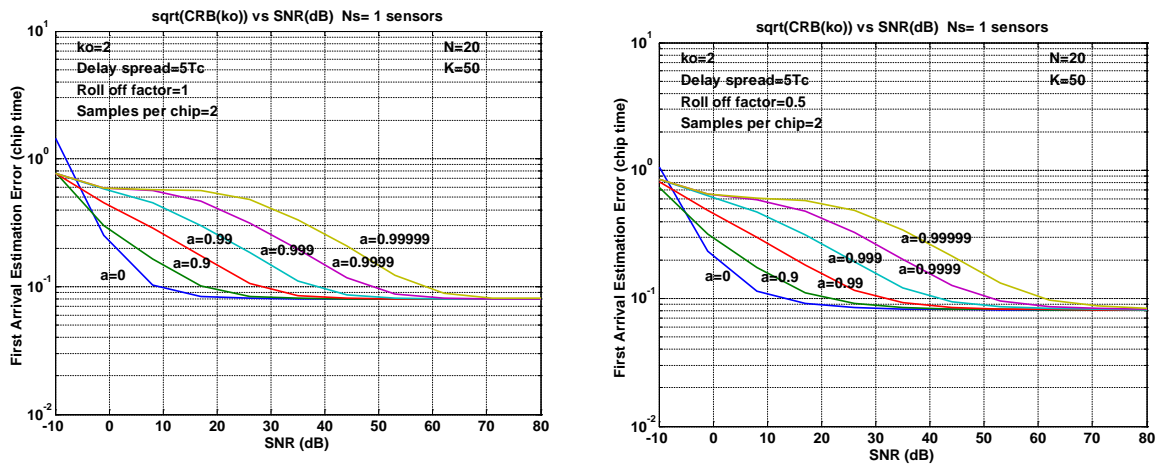


Figure 3.11. CRB of the first arriving path k_0 for different values of the SNR, and different values of the temporal correlation α . Delay spread set to $5 T_c$. Just one sensor and two different roll-off factors are used. Number of channel vector estimates set to 50. a) Left: β set to 0,5; b) Right: β set to 1.0.

On the other hand, curves in both figures look very similar, since just a very slight degradation lower than 15% appeared when the temporal spread reduced from $5T_c$ to $2T_c$. Differences in this latter case count for less than 4 meters.

Otherwise, if we compare these results, especially those in Figure 3.11 with those exhibited in Figure 3.9, some improvement were reached. For instance, it can be seen that for a temporal correlation factor α of 0,999 the timing error variance was around $0,2T_c$ for a SNR of 40dB, when sampling was performed to the chip rate, and it reduced around the half ($0,1T_c$) when sampling rate was twice faster. These improvements were mainly achieved from the fact we doubled the number of estimates with respect to the the prior case.

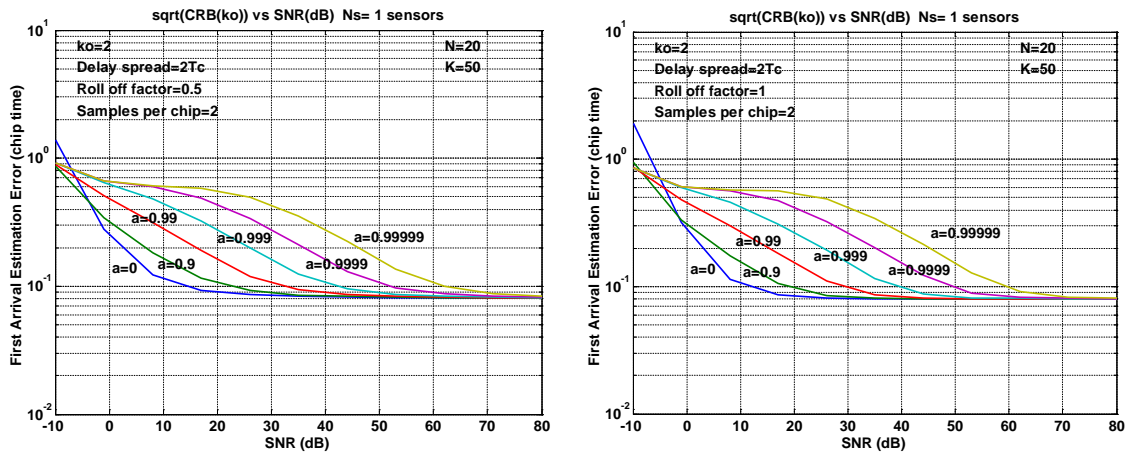


Figure 3.12. CRB of the first arriving path k_0 for different values of the SNR, and different values of the temporal correlation α . Delay spread set to $2T_c$. Just one sensor and two different roll-off factors are used. Number of channel vector estimates set to 50. a) Left: β set to 0,5; b) Right: β set to 1,0.

Figure 3.13 shows similar results in timing error with independence of the angular and delay spread of the source. Again, major improvements were associated with a lower degree of correlation for the measures, whilst improvements related to angular and delay spreads were decreased to a few meters in range terms. These improvements were performed for wider angular spreads, especially when SNR was low. For instance, timing error estimation when SNR was around 5dB improved from around $10^{-1}T_c$ (8 meters) to $8 \times 10^{-2}T_c$ (6.4 meters) when angular spread increased from 5° to 18° , for a delay spread of $5T_c$ and having temporally uncorrelated estimates; and it improved from $4 \times 10^{-1}T_c$ (3.2 meters) to around $3 \times 10^{-1}T_c$ (2.4 meters) for highly temporally correlated estimates ($\alpha=0,99999$). Similarly, timing error estimation when SNR was around 50dB improved again from $10^{-1}T_c$ to $8 \times 10^{-2}T_c$ for highly temporally correlated estimates ($\alpha=0,99999$). In summary, timing error kept practically invariant with respect to the source delay spread, and most of the improvement was due to the increase in the angular spread. This gain reduced for higher SNRs where errors tended to be asymptotic to a minimum of $4 \times 10^{-2}T_c$ (3.2 m in range terms) for the case of using 4 sensors.

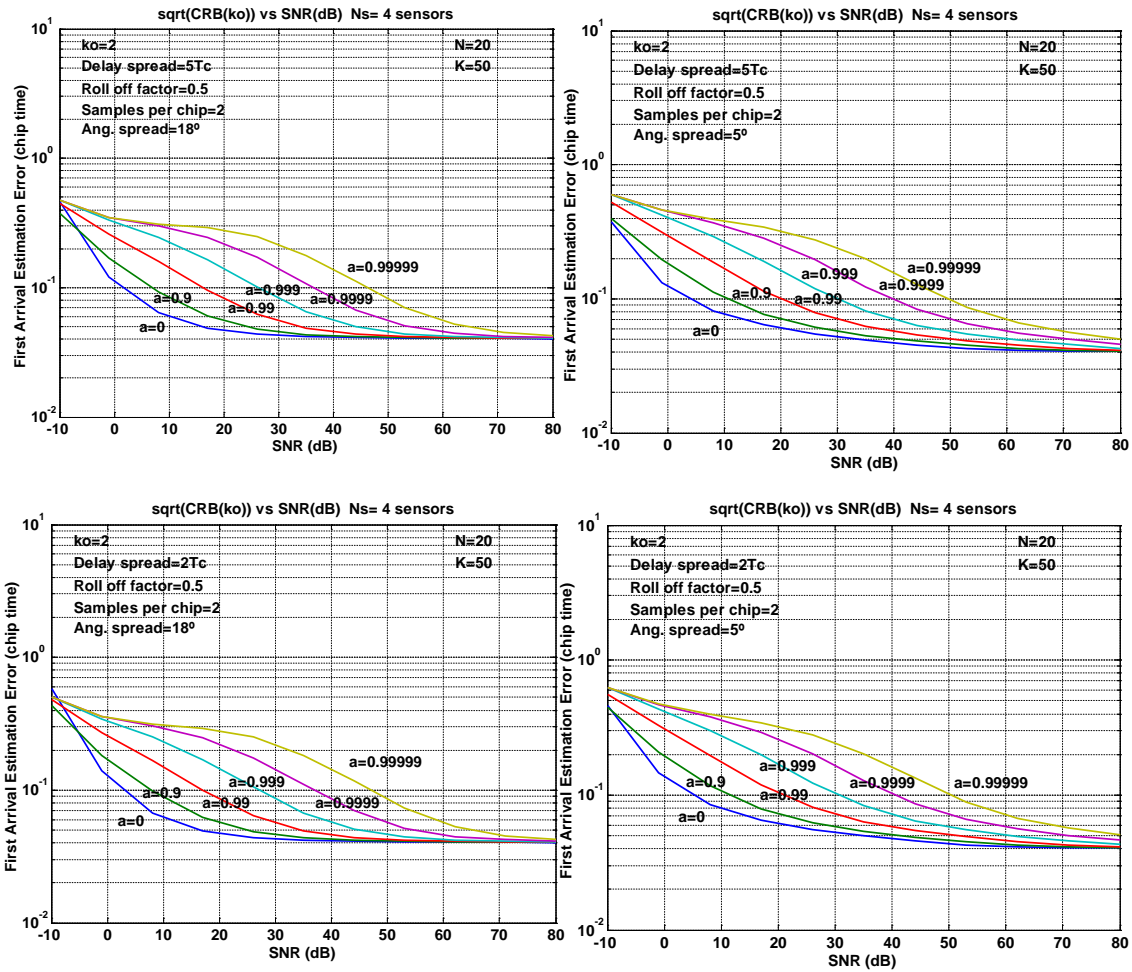


Figure 3.13. CRB of the first arriving path k_0 for different values of the SNR, different values of the temporal correlation α , different values of delay spread, and different values of angular spread. Four sensors, the number of channel vector estimates set to 50, the sampling rate set twice the chip rate, and a roll-off factor of 0,5 are used. a) Top Left: delay spread set to $5T_c$, angular spread set to 18° ; b) Top Right: delay spread set to $5T_c$, angular spread set to 5° ; c) Bottom Left: delay spread set to $2T_c$, angular set to 18° ; d) Bottom Right: delay spread set to $2T_c$, angular spread set to 5° .

3.3.2.4 Dependence of timing CRB with respect to angular model

Figure 3.14 shows the Cramer-Rao bound behaviour for the timing k_0 when different angular kernels are considered. It is apparent that the Gaussian kernel provided slightly higher errors than the Laplacian but these differences are negligible. Therefore, the use of a Gaussian kernel in our model is adequate for describing the signal angular dispersion.

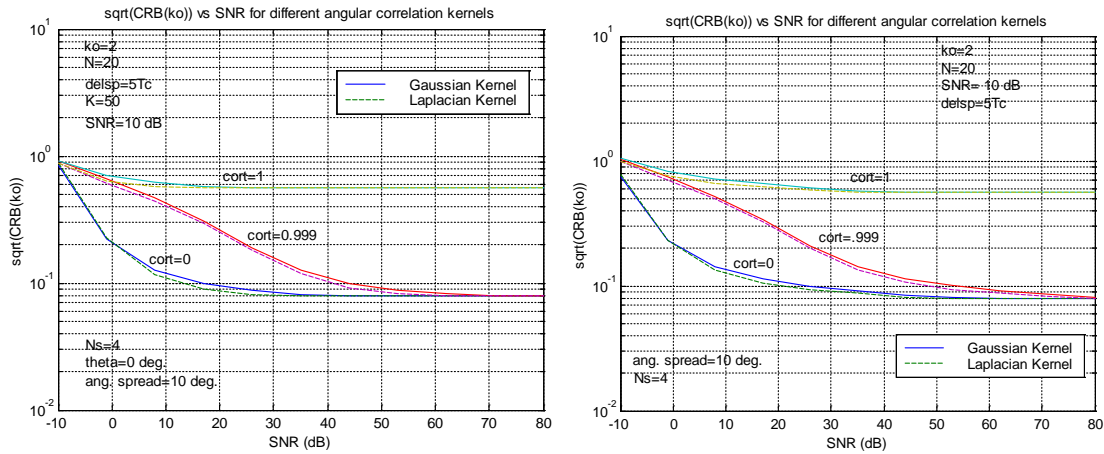


Figure 3.14. CRB of the first arriving path k_0 as a function of SNR for different values of the temporal correlation coefficient α . Four sensors are used and two different kernels are provided for the angular dispersion function: Gaussian and Laplacian. 50 channel vector estimates and a delay spread of $5 T_c$ a) Left: angular spread set to 5° , b) Right: angular spread set to 10° .

3.3.2.5 Improvement in CRBs for timing and coherence bandwidth with the number of observations

Figure 3.15 shows as first arrival timing estimation error bound improves as the number of channel vector estimates K increases, for different number of sensors and temporal correlation factors among the observed estimates. In case of highly temporally correlated channels, it is shown as it is very difficult to reduce the error bounds, even for a large number of observations (high values of K) or when multiple antennas are used. In all other cases, the use of multiple antennas reduces the CRB sensibly. As an example note from Figure 13 a) that error reduced to the third from 4.8 m to 1.2m in range terms, in case of $\alpha=0.9$; and just to half from 9.6 m to 4.8 m when $\alpha=0.999$ and K passed from 10 to 100. The influence of the angular spread is another factor to be considered: spatial uncorrelated sensors allowed a better estimation of the timing, but improvement considered in range terms was more important in case of having highly temporally correlated estimates since in this case, for example, it accounted for around 8m for $K=100$ and just around of 1.5m when channel estimates were temporally uncorrelated.

Interpretation of results should be made very carefully when the number of observations is related to the time correlation factor α . Channel estimates achieved from two consecutive slots will exhibit a high temporal correlation factor, while ICD estimates would be performed using much more separated slots.

On the other hand, and from the perspective of the computation of CRBs, the use of uncorrelated sensors implies a reduction in complexity since the spatial correlation disappears as a nuisance parameter and computation becomes simpler and faster.

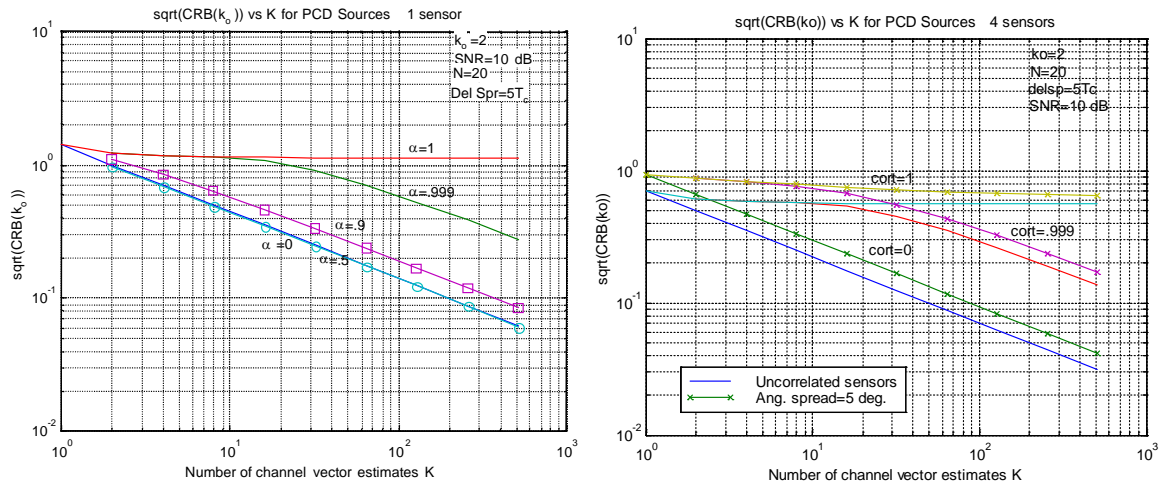


Figure 3.15. CRB of the first arriving path k_0 as a function of the number of recorded channel estimates K , for different values of the temporal correlation coefficient α . SNR=10 dB, and a delay spread of $5T_c$. a) Left: one sensor, b) Right: four sensors and two possible scenarios: uncorrelated sensors case and low angular spread case (angular spread of 5°).

3.3.2.6 CRBs for timing versus the normalized coherence bandwidth

Figure 3.16 shows the relation between timing accuracy and delay spread. Results showed as delay spread hardly influenced the variance of the timing estimation when delay spread was larger than three times the chip time. This was the case as long as the analysis window was large enough (20 samples in this case), otherwise some degradation was found. When delay spread was lower than this value, timing estimation degraded, especially in case of spreads below the chip time. However, it should be remembered that a lower delay spread is characteristic of a LOS condition, and results in Figure 3.16 refer to the NLOS Rayleigh model in (3.53).

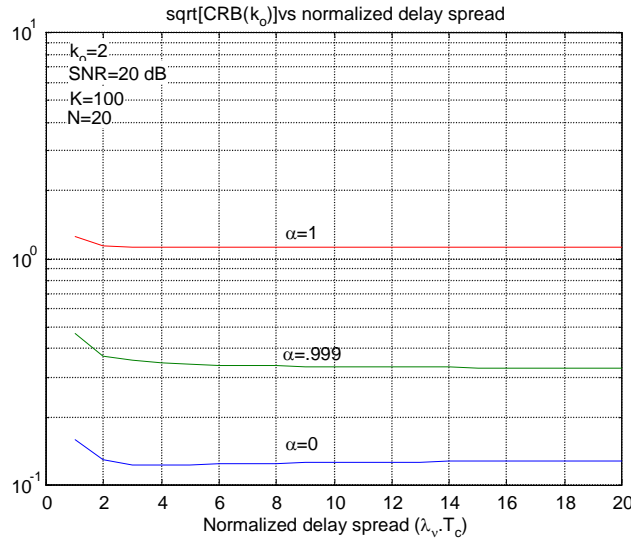


Figure 3.16. CRB of the first arriving path k_0 for different values of the delay spread λ_n and temporal correlation α . Almost no influence is found provided that a large observation window ($N = 20$ in this case) is chosen.

3.3.3 Performance of CRBs for timing and normalized coherence bandwidth for the LOS Rice fading model

3.3.3.1 Changes in CRBs with the dispersed Signal to Noise Ratio (SNR), the power level of the Line of Sight (LOS) component and the temporal correlation among channel vectors estimates

Figure 3.17 and Figure 3.18 exhibits the error bound for the timing and the normalized Coherence Bandwidth λ_n for a LOS Rice model in (3.69) as a function of the dispersed signal to noise ratio (SNR) for two different values of the average LOS power. First of all, note that the timing error reduced for highly temporally correlated environments when a LOS component was present. This behaviour was precisely the opposite of what was expected for a NLOS condition. Furthermore, timing bounds computed for this LOS model were lower than the expected for the NLOS condition, and they reduced as LOS power increased. Improvement achieved for higher temporal correlation is almost negligible for temporal correlation factors higher than 0.99. For i.e., note that the timing error for a SNR of 15 dB and an ICD source ($\alpha=0$) with a LOS power 3dB below the dispersed signal power when two sensors were used corresponded to $5.5 \times 10^{-2} T_c$. This bound reduced to $4.8 \times 10^{-2} T_c$ for a PCD source ($\alpha=0.9$), and to $3.0 \times 10^{-2} T_c$ for a FCD source ($\alpha=0.99999$). When the LOS power increased to 3dB higher than the dispersed signal power, the bound reduced from $3.2 \times 10^{-2} T_c$ to $2.5 \times 10^{-2} T_c$ and finally to $1.5 \times 10^{-2} T_c$ for ICD ($\alpha=0$), PCD ($\alpha=0.9$) and FCD ($\alpha=0.99999$) cases respectively. In range terms, it means that positioning error went from around 4.4 m (ICD) to 2.4 m (FCD) for the first case and from 2.6 m to 1.2m for the latter. Another interesting observation is the fact that timing error reduced without bound when SNR

increased for this LOS model. It means that timing accuracy would be theoretically limited just for SNR in case of LOS condition.

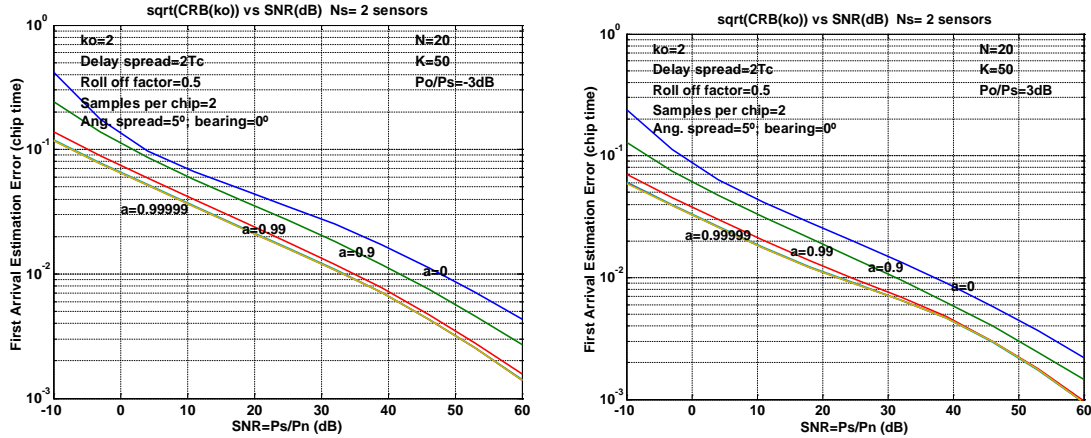


Figure 3.17. CRB of the first arriving path k_0 as a function of dispersed signal to noise ratio (SNR) and temporal correlation α for different values of the LOS component power. Two sensors, the number of channel vector estimates set to 50, the sampling rate set twice the chip rate, and a roll-off factor of 0,5 are used. Delay spread set to $2T_c$ and angular spread set to 5° . Bearing direction is the broadside. a) Left: LOS Power set 3dB lower than the Dispersed signal Power; b) Right: LOS Power set 3dB higher than the Dispersed signal Power.

These results perhaps seem to be too optimistic, but they are consistent with the model structure that supposes the LOS signal is perfectly characterized. In fact, if the signal we are looking for is practically deterministic, which it is especially true in high SNR conditions; it is possible to estimate the timing with a very high accuracy.

On the other hand, the bounds for the normalized Coherence Bandwidth λ_n , seemed not to be disturbed for a change in the LOS power level, and the tendency respect to the temporal correlation coefficient remained as in the NLOS model. For i.e., note that from Figure 3.18, as the error bound for a SNR of 10 dB and a PCD source ($\alpha=0.9$) with a LOS power ± 3 dB higher than the dispersed signal power when two sensors were used corresponded to 4% and it degraded to 11% for a FCD source ($\alpha=0.99999$). These values were higher than those expected from the NLOS model, but they were also bound limited when SNR increased. In this case, the minimum error bound achievable was around 1.2%. This slight degradation exhibited in CRB for the LOS model came from the fact that the vector of unknown parameters included a new one to estimate [77], and due this new LOS parameter did not disturb temporal dispersion statistics in the model. However, it is important to remark, that a LOS condition is associated with a less dispersed signal both temporally and spatially [6][8][27], and this fact has to be considered in the analysis to extract pondered conclusions from these results. Furthermore, from a positioning viewpoint, timing is the most relevant parameter, and the coherence bandwidth can be considered a nuisance parameter; nevertheless from a systemic perspective this parameter could provide some side information about the quality of the measure [27].

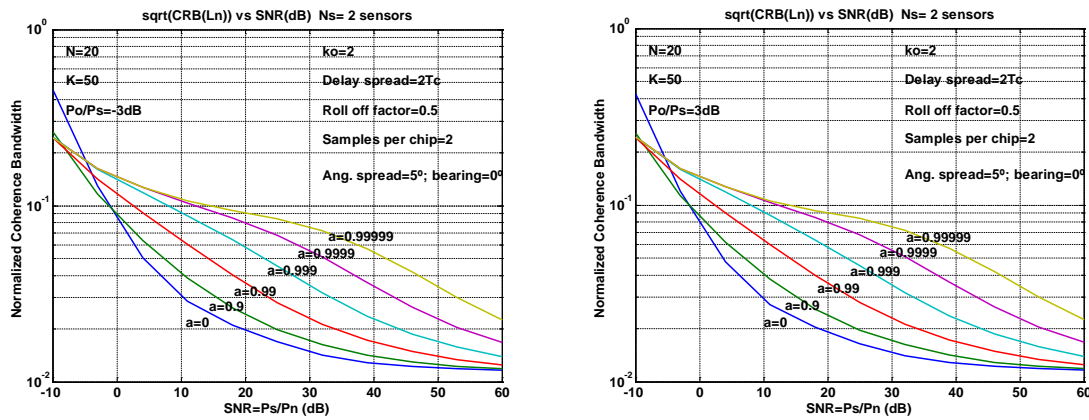


Figure 3.18. CRB of the inverse of the normalized delay spread λ_n as a function of dispersed signal to noise ratio (SNR) and temporal correlation α for different values of the LOS component power. Two sensors, the number of channel vector estimates set to 50, the sampling rate set twice the chip rate, and a roll-off factor of 0,5 are used. Delay spread set to $2T_c$ and angular spread set to 5° . Bearing direction is the broadside. a) Left: LOS Power set 3dB lower than the Dispersed signal Power; b) Right: LOS Power set 3dB higher than the Dispersed signal Power.

3.3.3.2 Performance of the Timing CRB's with the mean Direction of Arrival of the Emission, the Power Level of the Line of Sight (LOS) Component, the temporal correlation among channel vector estimates and the number of sensors

Figure 3.19 shows the behaviour of the timing bound with the mean direction of arrival of the received signal for different power values of the LOS component when dispersed signal to noise ratio equals to 10 dB. It is interesting to note that the timing error reached a minimum for values close to 30° , and how this improvement was more important in relative terms for higher levels of the LOS component and for more temporally correlated signals, since in these cases signal became almost deterministic and therefore it was easier to discriminate from noise.

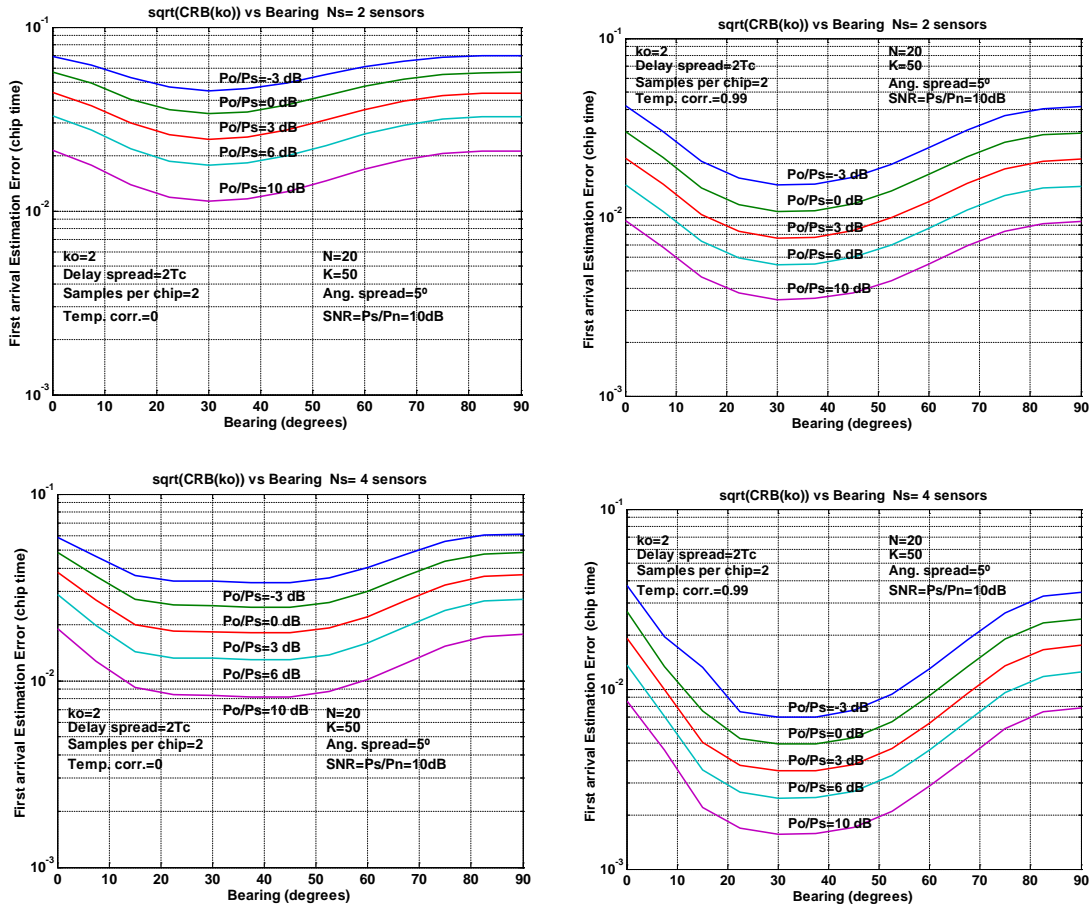


Figure 3.19. CRB of the first arriving path k_0 as a function of the signal bearing and the power level of the LOS component for different values of the temporal correlation factor among channel vector estimates. Number of channel vector estimates set to 50, sampling rate set to twice the chip rate, roll-off factor set to 0.5, Delay spread set to $2T_c$, angular spread set to 5° and dispersed signal SNR to noise ratio (SNR) set to 10 dB. a) Top Left: Two sensors - ICD source ($\alpha=0$); b) Top Right: Two sensors - Highly Temporal Correlated Source ($\alpha=0,99$); c) Bottom Left: four sensors - ICD source ($\alpha=0$); d) Bottom Right: Four sensors - Highly Temporal Correlated Source ($\alpha=0,99$).

For i.e. timing error bound improved from around $5.7 \times 10^{-2} T_c$ to $3.4 \times 10^{-2} T_c$ (from 4.6 m to 2.7 m in range terms) when LOS power was 0 dB higher than the dispersed signal power and bearing changed from 0° to 30° , while error reduced from around $2.2 \times 10^{-2} T_c$ to $1.2 \times 10^{-2} T_c$ (from 1.8 m to 1 m) when LOS power was 10dB higher than the dispersed signal power and bearing changed again from 0° to 30° . Both of these examples exhibited an improvement better than 40%. On the other hand, figure 17 shows that an important improvement was possible when four sensors were used instead of two, especially for a highly correlated source ($\alpha=0,99$). Note for i.e. the improvement achieved from passing from two sensors to four sensors when the power LOS level was 0 dB higher than the dispersed signal for the FCD source. In this case,

error bound went from around $1.1 \times 10^{-2} T_c$ to around $5.0 \times 10^{-3} T_c$. In other words, the range error diminished from 90 cm to around half that distance.

For the LOS model, a better gain was performed from the introduction of new sensors for high PCD sources. For i.e., a gain factor of around 1.35 was achieved when passing from two sensors to four for ICD sources and around two for highly PCD sources. Bearing also impacted the timing error performance. A higher gain was found when the mean signal bearing was around 35° , and the range of the improvement region widened around this bearing when more sensors were added and a higher LOS power was available. This gain decayed when the LOS path weakened and the Rice propagation turned into Rayleigh. Gains associated with bearing shrank the timing error below half for high power LOS signals, and these errors were reduced around 45% when the LOS power changed from -3dB to 3 dB over the disperse component when 4 sensors were used.

3.3.3.3 CRBs for timing with the roll-off factor of the shaping pulse, the dispersed Signal to Noise Ratio (SNR), the number of sensors and the signal Direction of Arrival

Figure 3.20 and Figure 3.21 relate CRB for the first arriving path with roll-off factor of the shaping pulse and with signal bearing.

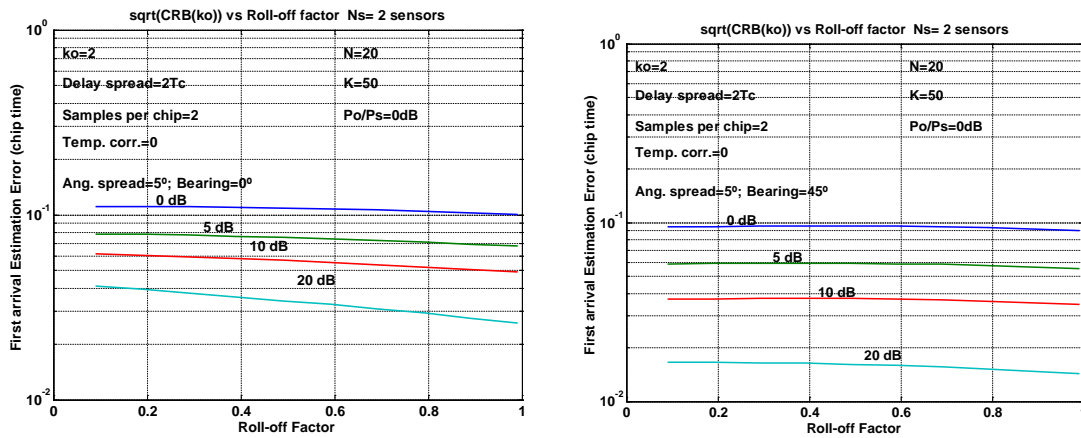


Figure 3.20. CRB of the first arriving path k_0 as a function of the roll-off factor of the shaping pulse and the dispersed signal to noise ratio (SNR) for a LOS power level 0dB higher than the dispersed signal and an ICD source ($\alpha=0$). Number of channel vector estimates set to 50, sampling rate set to twice the chip rate, Delay spread set to $2T_c$, and angular spread set to 5° . a) Left: Two sensors – Bearing= 0° ; b) Right: Two sensors – Bearing= 45° .

Results in these figures demonstrated the timing error bound improved for a higher roll-off factor when signal arrived directly from the broadside, especially for high signal to noise ratios. This enhancement is possibly related with the sharper form of the first arrival related to the increase in the bandwidth. However, the gain with roll-

off factor was negligible when bearing changed to 45° due the better array performance for this bearing.

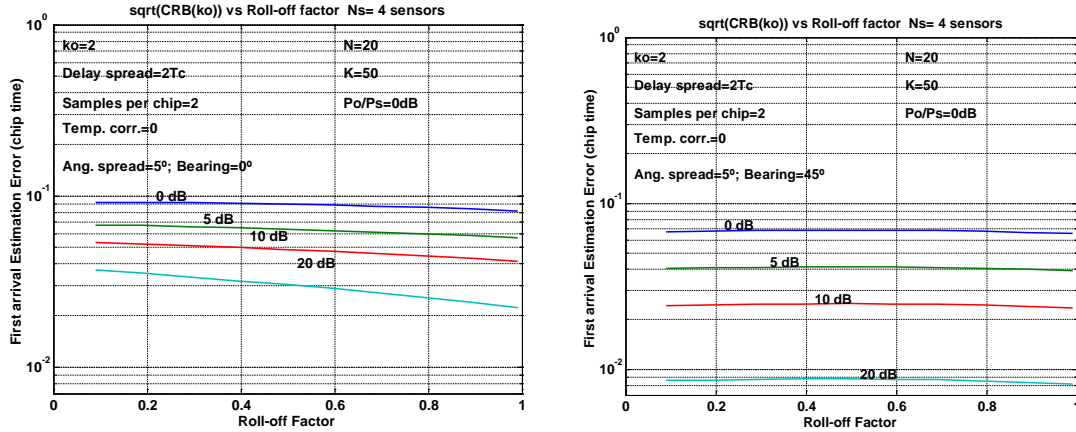


Figure 3.21. CRB of the first arriving path k_0 as a function of the roll-off factor of the shaping pulse and the dispersed signal to noise ratio (SNR) for a LOS power level 0dB higher than the dispersed signal and an ICD source ($\alpha=0$). Number of channel vector estimates set to 50, sampling rate set to twice the chip rate, Delay spread set to $2T_c$, and angular spread set to 5° . a) Left: Four sensors – Bearing= 0° ; b) Right: Four sensors – Bearing= 45° .

For example, note from the graphics that as the timing error reduced from the value of $3 \times 10^{-2} T_c$ for a roll-off factor of 0.5 to around $2 \times 10^{-2} T_c$ for a roll-off factor of 1.0 when four sensors were used, the dispersed signal to noise ratio was set to 20dB, and signal arrived directly from the broadside. On the other hand, when direction of arrival changed to 45° , timing error kept very close to $0.85 \times 10^{-2} T_c$ for the same signal conditions. Of course, lower errors were achieved when a larger number of sensors were used. The behavior described by these results is very reasonable since modifying the pulse shape to a higher roll-off implies the availability of a higher bandwidth, and hence a more defined spectral line and also the reduction of the side-lobes. It helps to reduce the probability of misestimating the first arrival. Furthermore, array geometry responds to bearing, and it can help to discriminate the LOS component from the dispersed one.

3.3.4 Positioning Accuracy for Location Determination Technologies

In the following, positioning accuracy for LDT based on timing and signal bearing estimates using estimation error bounds as methodology is studied for uplink (UL) and downlink (DL) measurements in realistic propagation conditions. Results from experiences 1-6 commented below have been performed using the simulation tool provided by the SATURN project and they are part of [4].

Experience 1. Figure 3.22 shows the variance in the positioning for two different configurations: 2 and 4 antennas at the BS, and a UE equipped with 1 and 2 antennas respectively when measurements are performed by the BS for a LDT based on TOA. A significant improvement is observed for a higher number of sensors, but regions closed to BS still exhibit very poor positioning accuracy due to hearability. In order to surpass this problem a high bit rate (HBR) channel should be used since it is associated to a higher SNR.

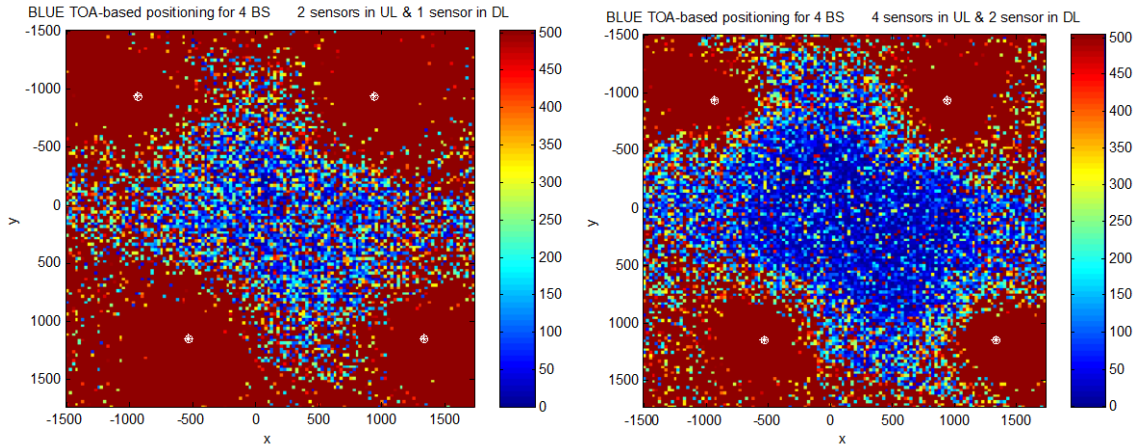


Figure 3.22. Positioning error for LDT based on TOA measurements performed in the uplink. a) Left: two sensors in UL and four in DL, b) Right: four sensors in UL and two in DL. (Courtesy of [4])

Experience 2. Since timing errors depends on the SNR, different requirements in SNR will affect the estimation and the positioning accuracy. It may be seen for i.e. in Figure 3.23 results for a TOA positioning method based on the round trip time (RTT) for two traffic channels.

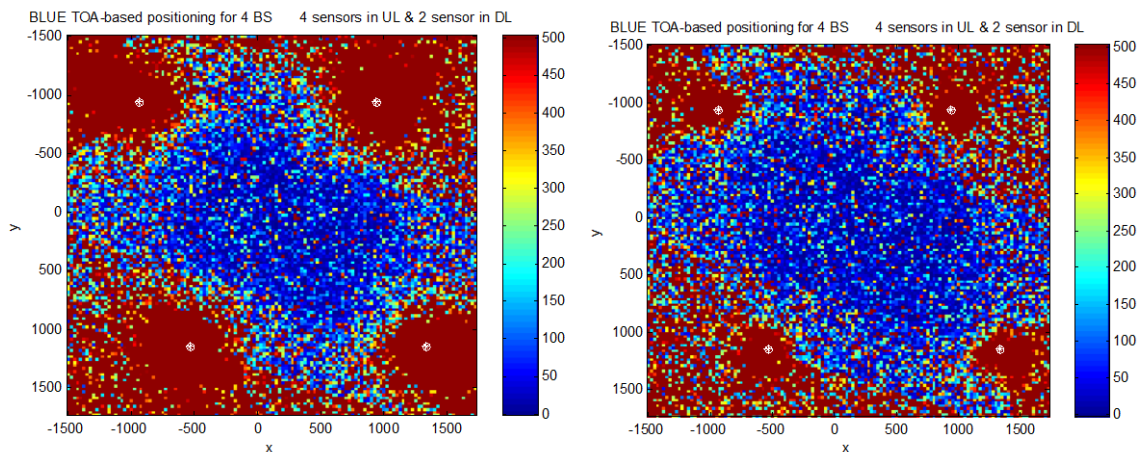


Figure 3.23. TOA positioning using RTT with traffic channels of 12.2 Kbps (left) and 384 Kbps (right). The required E_b/N_0 is 5 dB and 1 dB respectively. The higher bit rate service is more demanding in terms of SINR, and hence better timing estimation is obtained. (Courtesy of [4])

This figure reveals the convenience of using a higher bit rate (HBR) of 284 kbps instead of the lower bit rate (LBR) of 12.2 kbps because the HBR channel is associated to a higher SINR. Four antennas in UL and two sensors in DL has been use within this experience.

Experience 3. Figure 3.24 evaluates a positioning method based exclusively on signal bearings (DOA). However, this is not a very realistic situation, since it assumes that every UE is listened by all BS, and it is only possible if forced soft handovers to multiple BS are set up. Accuracy is quite poor for LBR traffic channels, even if 4 sensors are used, while the more demanding requirements in terms of SINR of HBR services allow more accurate positioning. The near-far situation in the region closer to the BS is visible.

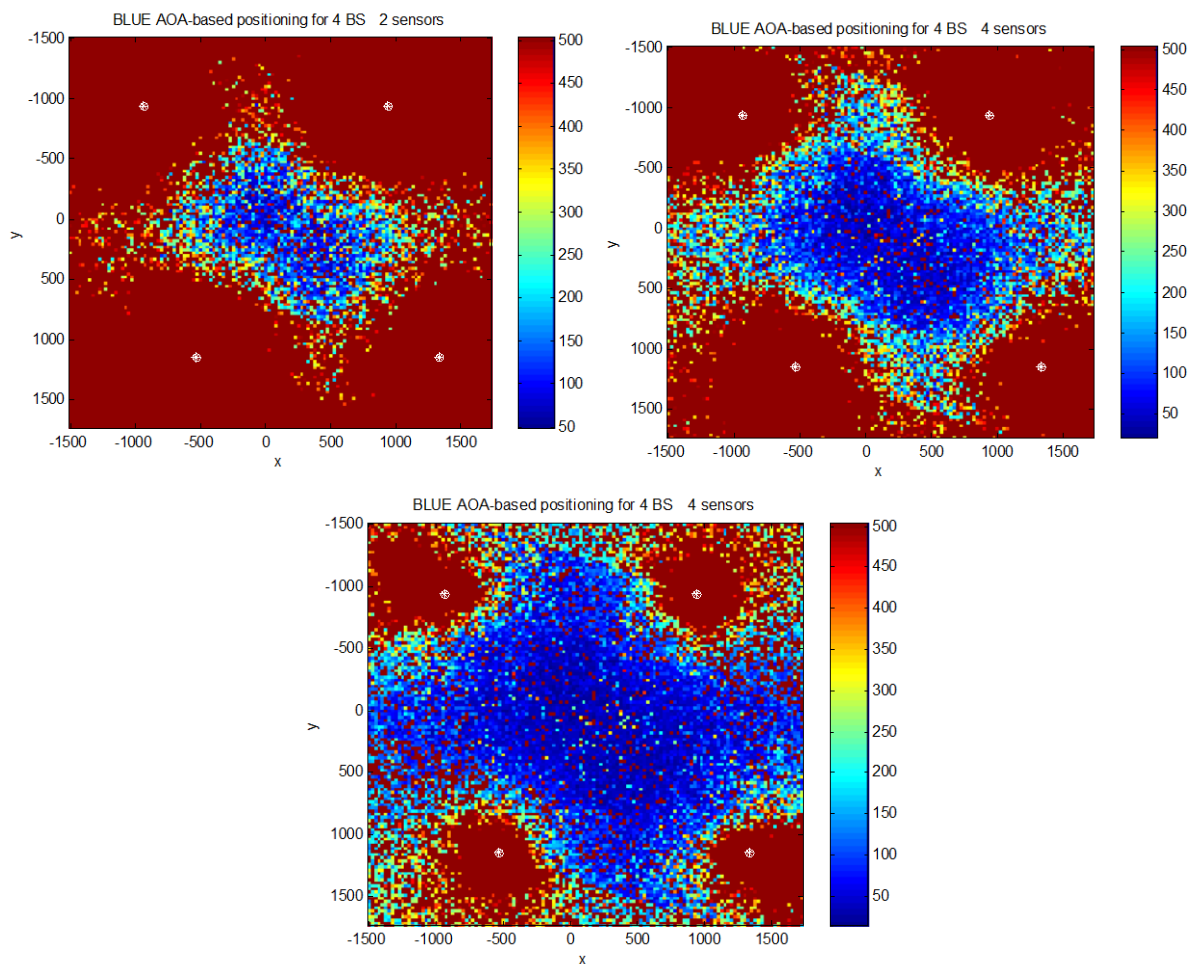


Figure 3.24. Bounds in positioning error for pure AOA measurements based method for the uplink. a) Top left: two sensors and LBR (12.2 kbps) service, b) Top right: four sensors and LBR service, c) Bottom: HBR service (384 Kbps). (Courtesy of [4])

Experience 4. A more realistic scenario corresponds to the joint use of AOA and TOA information by considering that the UE is not in soft handover with all the BS, but only those in the “active set” (those BS being received within 5 dB of the serving station). It may be seen as accuracy improves especially in regions close to the BS due to the presence of two reliable measurements: angle and RTT. Note however that red spots appear in this region due to the fact that AOA is not used in NLOS placements. This problem may be overcome with the use of an additional DL-TDOA measurement. As previously, HBR channels are preferred for better accuracy.

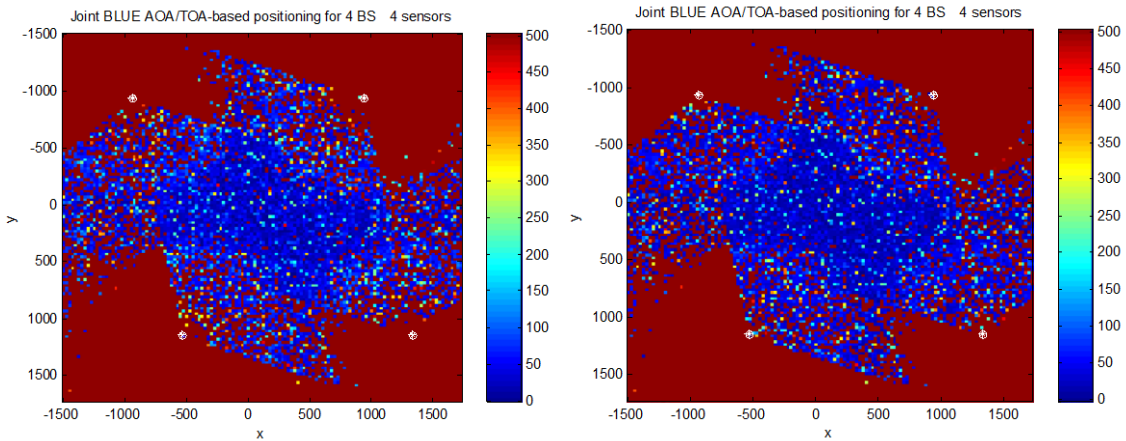


Figure 3.25. Positioning accuracy when both RTT and AOA measurements are jointly used and four sensors are available in the UL. a) Left: LBR (12kbps), b) Right: HBR (384 kbps). Accuracy improves significantly especially in the regions close to the BS. (Courtesy of [4])

Experience 5. Cumulative functions of the error standard deviation are plotted in Figure 3.26, for different positioning methods when the Best Linear and Unbiased Estimator (BLUE) is used for solving positioning equations.

These results correspond to four antennas at the BS and a single antenna at the UE for both LBR and HBR channels and Idle Period Down Link (IPDL) active. This figure reveals as the additional use of AOA information improves positioning accuracy respect to TOA and TDOA+TOA based methods. Note as the slopes of curves adding AOA information are steeper for larger abscise values, due to the improvement registered in regions close to BS. The best situation arrives for the joint use of TDOA, TOA and AOA. It exhibits errors lower than 15 m for the 80% of the cases. On the other hand methods based on homogeneous measurements are far from the maximum accuracy, being perhaps TDOA the best alternative among them since for i.e. errors lower than 50 m for the 80% of the cases are achieved compared to around 110 m for the TOA based method for HBR channels. These last results show as positioning accuracy improves when all available data is used. It is a known premise that measurements of different kind are translated to diverse positioning errors, therefore their use may lead to better overall position results [17][29][61][81].

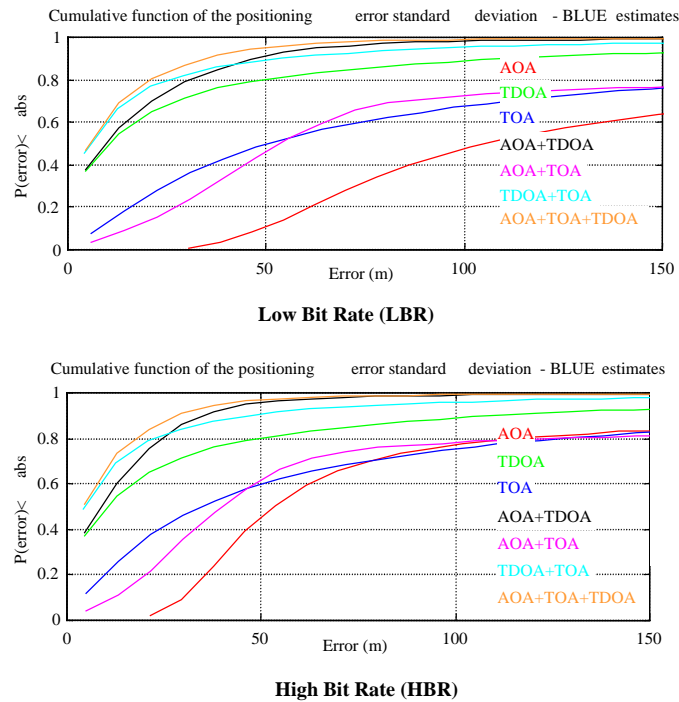


Figure 3.26 Cumulative function of the positioning error when the Best Linear and Unbiased Estimator (BLUE) is used to solve equations and four antennas at the BS and a single antenna at the UE are used. a) Top: LBR channel, b) Bottom: HBR channel. Idle Period Down Link (IPDL) is used. (Courtesy of [4])

3.4 NLOS Condition and Positioning

An important problem in mobile positioning is the surging of NLOS condition. Due to it, the whole set of measures of TOA, TDOA, AOA and SS could be strongly biased and therefore also the position estimates. In last years, some research about this topic has enhanced our comprehension about its identification, relevance and mitigation mechanisms [25][27]. This topic has been treated more widely at chapter 2 of this document.

In the current literature, these NLOS mitigation algorithms may be classified within two categories: In the first one, NLOS induced errors are modeled as additive biases to the LOS data in relation to a known or unknown distribution. It is also possible to identify LOS/NLOS conditions and ponder the measurements, using a quality weight matrix, or exploiting previous knowledge to adjust NLOS data toward the corresponding LOS values [25]. In the second category, multipath delay profile is considered as a whole in place of a set of independent TOA, AOA and SS measurements. It is possible in this case to perform geo-location from signature recognition of previous stored data [25][82][83]. Although these works report good results, for i.e. Database Correlation Method (DCM) in [83] provide a location error of

25 m for 68% of the calls in comparison to only 215 m obtained for OTDOA; an important problem associated to this solution is the large quantity of storing required by databases and also the high computational burden involved on pattern recognition and matching. These issues limit its application to small and moderate environments.

In this sense, it is more conceptually interesting the use of Bayesian mechanisms which take advantage of system dynamic and add any previous knowledge available, in order to smartly select, among a set of measurements, those with capacity to lead to a more confident estimation. Some of these strategies use variations of Kalman Filter (KM) to incorporate this intelligence to PCF. It is the case of [27], where the jointly use of a Particle Filter (PF) and an Unscented Kalman Filter (UKF) to reduce the computational burden and improve the accuracy is studied, in comparison with the use of a more traditional KF [29]. This work uses a signal quality indicator associated to LOS/NLOS obtained from a real measurements campaign.

In general, these algorithms look for taking the best of a higher number of pieces of available data, and of an overestimated number of reference stations, since it is a fact very well known in research literature that location estimation schemes based in heterogeneous measurements tend to achieve better results than those based on homogeneous measurements [17][18][20][34][61][81][82].

3.5 Summary and Conclusions

This chapter introduces the models for dispersive sources and supports their use for the study of the error behaviour in the timing estimation. It also summarizes the main schemes for TOA and DOA estimation. Furthermore, an important piece of this research describes the use of the Cramer-Rao Bounds to study the impact of various factors involved in the signal timing estimation for a mobile scenario modeled by a space-time dispersive channel.

Our CRB-based model for TOA considers the sampling rate, the roll-off factor of the shaping pulse, the spatial and temporal correlation among channel estimates, and the availability of multiple channel vector estimates and multiple sensors in the antenna array at the receiver. Moreover, it studies both Rayleigh and Rice fading propagation situations; and therefore, it explores the difficulties and opportunities associated with timing estimation in LOS and NLOS environments.

Particularly, our model makes a contribution by taking into account the spatial and temporal correlation among channel estimates, and the impact of the roll-off factor of the shaping pulse, in addition to the number of sensors and the number of estimates that are typical from other approaches. It also includes an exponential dispersion for delays which is characteristic of mobile channels instead of just a few paths as in prior approaches. Furthermore, this paper also includes some asymptotic expressions for certain interesting cases related with high speed and low speed subscribers.

Since, it is expected that any reduction in signal estimation errors will contribute to a better positioning performance and due to the most accurate positioning techniques use timing measures, our model does contribute to get an insight to the TOA estimation and to its impact on positioning.

From above results, the following conclusions can be derived:

1. Results in section 3.3.1 show as asymptotic expressions in 3.2.4.3 may be used instead of exact ones to compute Cramer-Rao bounds when a number of observations larger than ten are available. Due to a sufficient number of observations will be supply during the acquisition time, even when the mobile speed is high, the use of these expressions lead to reliable results.
2. Reduced expressions in 3.2.4.4 for the FCD sources in a NLOS environment provide a good match if they are compared to exact ones, and provide a worst case for the error bounds, so their use is also safe enough.
3. A minor difference is achieved when Gaussian or Laplacian kernels are used for modelling the angular dispersion, so it is irrelevant for the model the use of any of them, as it is show from results in 3.3.2.4. To keep coherence in the analysis the Gaussian Kernel was used (AS 5) along this work.
4. Estimation errors for the timing and the normalized coherence bandwidth decrease when the SNR increases; but this improvement is highly conditioned depending on the propagation scenario and the kind of source. In case of NLOS Rayleigh propagation, as it is show in 3.3.2.1, these estimation errors degrade rapidly when passing from PCD sources with temporal correlation higher than 0.9 to FCD sources, reaching a limit floor at high SNRs, so a higher SNR does not force to a lower timing error. On the other hand, in the case of LOS Rice propagation, the larger improvement in timing estimation is achieved when passing from an ICD source to a PCD source (temporal correlation factors between zero and 0.99). Moreover, the timing accuracy improves practically without bound for higher SNRs, as it is shown from results in 3.3.3.1. For i.e. if four sensors are available, with $K=50$, and the SNR in a NLOS ICD channel passes from 15 dB to 60 dB, the timing error bound reduces from 19% of the chip time (15 m range) to 4% (3.2 m range). However, in a LOS condition, where LOS signal is 3dB higher than the dispersed one, a variation of SNR from 10 dB to 55 dB reduces this error from 4% of the chip time to 0.3%.
5. Bounds for the normalized Coherence Bandwidth λ_n , seems not to be disturbed for a change in the LOS power level, as it is shown from results in 3.3.3.1, and the tendency respect to the temporal correlation coefficient remains as in the NLOS model. However, these values are some higher than those expected from the NLOS model, as it is expected from the fact that the vector of unknown parameters includes a new one to estimate, and due this LOS parameter does not disturb temporal dispersion statistics in the model. However, it is important to remark, that

a LOS condition is associated to a less dispersive signal both temporally and spatially, and this fact has to be considered in the analysis to extract pondered conclusions from these results.

6. Estimation errors for the timing and the normalized coherence bandwidth also decrease as the number of observations increases, but this reduction is very conditioned on the propagation scenario and the kind of source: ICD, PCD or FCD. In the case of NLOS, a larger record of observations is required to keep the accuracy, for higher temporal correlations among channel estimates, as shown from results in 3.3.2.5; however in the case of a LOS scenario an uncorrelated dispersed signal component implies a random perturbation that degrades the accuracy on the signal of our interest, as shown from results in 3.3.3.1. Therefore, the positioning accuracy is very sensitive to the mobility of UE in a NLOS environment, being the higher errors associated to static equipment, since this latter case corresponds to a value of α near to one.
7. The use of multiple antennas introduces not just new observations but also diversity, and therefore it helps to improve accuracy. In this sense, better results are achieved when a higher number of sensors are available in the antenna array. However, the impact of these improvements is associated with temporal and spatial coherence of the scattered signal, as it is shown from results in 3.3.2.2, 3.3.3.2, and 3.3.3.3. For NLOS condition, inclusion of multiple sensors provides similar gains in timing accuracy, from moderate to high SNR, regardless of the value of the temporal coefficient. A gain factor of around two is achieved when passing from one sensor to four confirming observations in [17]. In the LOS case however, this gain almost doubles in the case of highly PCD sources and the bearing also impacts the timing error performance. This gain decays when the LOS path weakens and the Rice propagation turns into Rayleigh. Improvements are always obtained when an antenna array is used instead of a single sensor, and certain progresses of around 20% are also achieved when passing from a narrow spread source to a spatially well-scattered signal. Furthermore, results for positioning accuracy from section 3.3.4 confirm that a better performance is obtained when multiple sensors are available for both cases DL and UL measurements, and also that the use of larger data records reduces dramatically the positioning error.
8. Bearing also impacts timing error performance when more than one sensor is used. A higher gain is found when mean signal bearing is around 35° and, the range of improvement region widens around this bearing when more sensors are used and a higher SNR is available, as it is show in 3.3.3.2.
9. Under Non Line Of Sight (NLOS) condition, the roll off factor has negligible effect in error bounds, and improvement essentially comes from the fact of getting more estimates as sampling is performed faster than the chip rate. On the other hand, under LOS condition, a higher roll-off factor helps to improve the bound for the timing error bound, as it is show in 3.3.3.3, possibly due to the sharper form of the first arrival in this case, related to the increase in the bandwidth. In any case, some

reports note that the positioning accuracy may improve for higher bandwidths [20][21].

10. To get a quantitative idea of the achievable accuracy, first of all let us suppose a NLOS environment, when one sensor is used, the sampling rate is equal to the chip rate, $K=50$ and the ICD source case. If these conditions are kept, the first path time of arrival estimation error is around of 19% of the chip time (around 15 m in range terms), for a SNR = 15 dB. This error reduces below the 10% of the chip time (8 meters) when 4 sensors are used, and reduces near the 4% (4 meters) when $K = 320$ and 4 sensors. Otherwise, for a highly correlated source case, where temporal correlation is 0.999, the error is 70% of the chip time (56 m), it reduces to 35% (28 m) for 4 sensors and near to 18% (14.4 m) for $K=320$ and 4 sensors. On the other hand, for a LOS condition, when the sampling rate is twice the chip rate, $K=50$ and the LOS power level is the same as the dispersive signal, with a SNR = 10 dB, 4 sensors available and a FCD channel considered, the timing error reduces below 5% of the chip time (4 m). These improvements are expected to be kept in the positioning accuracy.
11. The joint use of multiple heterogeneous measurements yields better global performance, as shown in section 3.3.4. Positioning based on timing is much better than approaches based on AOA. However, gains from the use of multiple antennas is high and although AOA-based positioning methods yield poor estimates, their combined use with other measurements such as TOA and TDOA is important. The use of heterogeneous measures for improving positioning has also been studied in the context of ultra wide band (UWB) radios [20][21][80]. For example, a hybrid method based on TOA/Signal Strength is studied in [20]. It proposes the use of NLOS determination techniques and the estimation of just the first path arrived to LOS nodes to reduce algorithm complexity. On the other side, [21] studies hybrid TOA/AOA positioning under non overlapping assumption (NLOA), and models multipath as grouped in clusters that follow Poisson distribution, and within each cluster TOA following a mix of two Poisson processes. Under NOLA assumption achieved accuracy does not depend of the rest of delays and it would be the same of do not have multipath.

3.6 Recommendations

1. In spite that our CRB model provides valuable information about the timing estimation error, special careful should be taken to extrapolate these results to the mobile subscriber positioning issue, due to the different nature of Rayleigh and Rice propagation models. For i.e. in obstructed environments, the shadowing may lead to important delay spreads, while in LOS condition, low delays are usual. In addition, some obstructed scenarios may lead to signal clustering, and if that is the case, even with the first arrival being accurately estimated, the positioning could be biased. Fortunately, there are some methods to identify these scenarios [29,34,63] and to reduce the harmful effects of this NLOS condition. Moreover, since positioning is a

complex problem that involves the acquisition from signals transmitted and received from different parts of the network, it is also dependent on the problem geometry.

2. The use of larger data records reduces dramatically the positioning error. Therefore, the coherence time of delays and angles should be studied carefully to take advantage of this circumstance. In fact, positioning accuracy is very sensitive to the subscriber mobility, being the highest errors associated with static equipment in NLOS condition, due to the impossibility taking advantage of temporal diversity. The use of adaptive algorithms that takes account of system dynamics is recommended to improve the quality of the positioning [27]-[29].
3. Since that the final positioning accuracy is a result of the holistic system operation, a function that controls and coordinates the use of the different kind of measures in relation to their quality should be performed to get the best of them. For example, in UMTS FDD mode, the UE is expected to be in soft handover for the 20-30% of situations with at least 2 BS [4]. It should be taken account to combine efficiently TOA/TDOA equations to obtain higher accuracies, besides of the potential benefits achieved from the use of IPDL and multiple antennas. Moreover, due to the higher SINR required in the UL channel in HBR DPCH channels, these are better suited for location services based on or aided by TOA/AOA using DPCH. However, no significant improvement is obtained when used in combination with DL-TDOA [4]. IPDL strategies increase the SINR when measuring time delays at the MS and avoid the hearability problem, and hence a better positioning accuracy is achieved, but to the cost of some loss in system capacity. All these trade-offs require further attention due to their impact on the overall behavior of the communications system.

3.7 References

- [1] Alba Pagès-Zamora, Dana H. Brooks, Josep Vidal Manzano, “Least-Squares Location from DOA Measurements”, 2000.
- [2] Alba Pagès-Zamora, Josep Vidal, Dana H. Brooks, “Closed-Form Solution for Positioning based on Angle of Arrival Measurements”, IEEE International Symposium on Personal, Indoor and Mobile Radio Communications (PIMRC 2002), Vol. 4, pp. 1522-1526, September 2002.
- [3] Josep Vidal et al, “Positioning Limits for UMTS mobiles in Delay and Angular Dispersive Channels”, International Symposium on Location Based Services for Cellular Users, LOCELLUS 2001, February 2001.
- [4] Josep Vidal, Marga Cabrera, René Játiva, Montse Nájjar, Alba Pagès, Carine Simon, “IST-1999-10322 SATURN D621, *Location Based Services Performance Evaluation (Location techniques)*”, Universitat Politècnica de Catalunya, June, 2001. <http://www.ist-saturn.org>
- [5] Garold Fuks, Jason Goldberg, and Hagit Messer, “Bearing Estimation in a Ricean Channel – Part I: Inherent Accuracy Limitations”, IEEE Transactions on Signal Processing, Vol. 49, No. 5, 2001.
- [6] H. Asplund, A.A. Glazunov, A.F. Molisch, K.I. Pedersen, M. Steinbauer, “The COST 259 Directional Channel Model – Part II: Macrocells”, IEEE Transactions on Wireless Communications, Vol. 5, No. 12, pp. 3434-3450, 2006. DOI:10.1109/TWC2006.256967.
- [7] P. Lusina, F. Kohandani, S.M. Ali, “Antenna parameter effects on spatial channel models“, The Institution of Engineering and Technology Communications, **3**, 9, 1463-1472, 2009. DOI:10.1049/iet-com.2008.0414.
- [8] C. Gentile, S. Martínez, A. Kik, “A Comprehensive Spatial-Temporal Channel Propagation Model for the Ultrawideband Spectrum 2-8 GHz”, IEEE Trans. Antennas Propag. **58**, 6, 2069-2077 (2010). doi:10.1109/TAP.2010.2046834.
- [9] Mats Bengtsson and Björn Ottersten, “Low-complexity estimators for Distributed sources”, IEEE Transactions on Signal Processing, Vol. 48, No. 8, August 2000. DOI:10.1109/78.851999.
- [10] Olivier Besson and Petre Stoica, “Decoupled Estimation of DOA and Angular Spread for a spatially Distributed Source”, IEEE Transactions on Signal Processing, Vol. 48, No. 7, pp. 1872-1882, July 2000. DOI:10.1109/78.847774.
- [11] Shahrokh Valaee, Benoit Champagne, and Peter Kabal, “Parametric Localization of Distributed Sources”, IEEE Transactions on Signal Processing, Vol. 43, No. 9, pp. 2144-2153, September 1995. DOI:10.1109/78.414777.
- [12] Gregory G. Raleigh and Tibor Boros, “Joint Space-Time Parameter Estimation for Wireless Communication Channels”, IEEE Transactions on Signal Processing, Vol. 46, No. 5, pp. 1333-1343, May 1998. DOI:10.1109/78.668795.
- [13] Mati Wax, and Amir Leshem, “Joint Estimation of Time Delays and Directions of Arrival of Multiple Reflections of a known Signal”, IEEE Transactions on Signal Processing, Vol. 45, No. 10, pp. 2477-2484, October 1997. DOI:10.1109/78.640713.

- [14] J. Lee, C. Lee, J. Chun, J. Lee, "Joint Estimation of Space-Time Distributed Signal Parameters", IEEE Conference on Vehicular Technology, Vol. 2, pp. 822-828, October 2000. DOI:10.1109/VETECS.2000.887118.
- [15] G.N. Tavares, L.M. Tavares, "The True Cramer-Rao Lower Bound for Data-Aided Carrier-Phase-Independent Time-Delay Estimation from Linearly Modulated Waveforms", IEEE Transactions on Communications, Vol. 54, 1, pp. 128-140, 2006. DOI:10.1109/TCOMM.2005.861655.
- [16] S. Buzzi, H.V. Poor, "On parameter estimation in long-code DS/CDMA systems: Cramer-Rao bounds and least-squares algorithms", IEEE Transactions on Signal Processing, Vol. 51, 2, pp. 545-559, 2002. DOI:10.1109/TSP.2002.806987.
- [17] C. Botteron, A. Host-Madsen, M. Fattouche, "Cramer-Rao bound for location estimation of a mobile in asynchronous DS-CDMA systems", IEEE International Conference on Acoustics, Speech, and Signal Processing, Volume 4, 2001. DOI: 10.1109/ICASSP.2001.940439.
- [18] C. Botteron, A. Host-Madsen, M. Fattouche, "Effects of system and environment parameters on the performance of network-based mobile station position estimators", IEEE Transactions on Vehicular Technology, Volume 53, Issue 1, 2004. DOI: 10.1109/TVT.2003.822029.
- [19] K. Schmeink, R. Adam, P.A. Hoeher, "Performance limits of channel parameter estimation for joint communication and positioning", EURASIP Journal on Advances in Signal Processing, 2012. DOI:10.1186/1687-6180-2012-178.
- [20] S. Gezici, Zhi Tian, G.B. Giannakis, Kobayashi Hisashi, A.F. Molisch, H.V. Poor, Z. Sahinoglu, "Localization via ultra-wideband radios: a look at positioning aspects for future sensor networks", IEEE Signal Processing Magazine, Volume 22, Issue 4, 2005. DOI: 10.1109/MSP.2005.1458289.
- [21] A. Mallat, J. Louveaux, L. Vandendorpe, "UWB Based Positioning in Multipath Channels: CRBs for AOA and for Hybrid TOA-AOA Based Methods", IEEE International Conference on Communications, 2007. DOI: 10.1109/ICC.2007.957.
- [22] B. Denis, N. Daniele, "NLOS Ranging Error Mitigation in a Distributed Positioning Algorithm for Indoor UWB Ad-Hoc Networks", International Workshop on Wireless Ad-Hoc Networks, pp. 356-360, 2004. DOI:10.1109/IWWAN. 2004.1525602.
- [23] J. Riba, A. Urruela, "A Non-Line-Of-Sight Mitigation Technique based on ML-Detection", IEEE International Conference on Acoustics, Speech, and Signal Processing, Vol. 2, pp. 153-156, 2004. DOI:10.1109/ICASSP.2004.1326217.
- [24] Li Cong, Weihua Zhuang, "Nonline-of-Sight Error Mitigation in Mobile Location", IEEE Transaction on Wireless Communications, Vol. 4, 2, pp. 560-573, 2005. DOI:10.1109/TWC.2004.843040.
- [25] Yihong Qi, Hisashi Kobayashi, H. Suda, "Analysis of wireless geolocation in a non-line-of-sight environment", IEEE Transactions on Wireless Communications, Volume 5, Issue 3, 2006. DOI: 10.1109/TWC.2006.1611097.
- [26] Kegen Yu, Y.J. Guo, "NLOS Error Mitigation for Mobile Location Estimation in Wireless Networks", IEEE Vehicular Technology Conference, pp. 1071-1075, 2007. DOI:10.1109/VETECS.2007.228.

-
- [27] J.M. Huerta, J. Vidal, A. Giremus, J. Y. Tournet, "Joint Particle Filter and UKF Position Tracking in Severe Non-Line-of-Sight Situations", *IEEE Journal of Selected Topics in Signal Processing*, Volume 3, Issue 5, 2009. DOI: 10.1109/JSTSP.2009.2027804.
- [28] L. Chen, R. Piché, H. Kuusniemi, R. Chen, "Adaptive mobile tracking in unknown non-line-of-sight conditions with application to digital TV networks", *EURASIP Journal on Advances in Signal Processing*, 2014. DOI:10.1186/1687-6180-2014-22.
- [29] Cheng-Tse Chiang, Po-Hsuan Tseng, Kai-Ten Feng, "Hybrid TOA/TDOA based unified Kalman tracking algorithm for wireless networks", *IEEE International Symposium on Personal Indoor and Mobile Radio Communications (PIMRC)*, pp. 1707-1712, 2010. DOI: 10.1109/PIMRC.2010.5671921.
- [30] Hemin Li, Zhongliang Deng, Yanpei Yu, "Investigation on a NLOS Error Mitigation algorithm for TDOA Mobile Location", *IET International Conference on Communication Technology and Application*, pp. 839-843, 2011. DOI:10.1049/cp.2011.0787.
- [31] Yi Long, Jiyang Huang, Yijiang Pan, Jiang Du, "Novel TOA Location Algorithms based on MLE and MMSEE for NLOS Environments", *IEEE International Conference on Communications, Circuits and Systems*, Vol. 2, pp. 46-49, 2013. DOI:10.1109/ICCCAS.2013.6765283.
- [32] U. Martín, "Spatio-temporal radio channel characteristics in urban macrocells", *IEE Proceedings-Radar, Sonar Navigation*, Vol. 145, No.1, pp. 44-49, February, 1998.
- [33] Patrice Pajusco, "Experimental Characterization of D.O.A. at the Base Station in Rural and Urban Area", *IEEE Conference on Vehicular Technology (VTC'98)*, pp. 993-997, May, 1998.
- [34] Larry J. Greenstein, Vinko Erceg, Yu Shuan Yeh, and Martin V. Clark, "A New Path-Gain/Delay-Spread Propagation Model for Digital Cellular Channels", *IEEE Transactions on Vehicular Technology*, Vol. 46, No.2, pp. 477-485, May, 1998.
- [35] Richard B. Ertel and Paulo Cardieri, Kevin W. Sowerby, Theodore S. Rappaport and Jeffrey H. Reed, "Overview of Spatial Channel Models for Antenna Array Communication Systems", *IEEE Personal Communications Magazine*, February, 1998.
- [36] Philippe Laspougeas, Patrice Pajusco, Jean-Claude Bic, "Radio Propagation in Urban Small Cells Environment at 2GHz: Experimental Spatio-Temporal Characterization and Spatial Wideband Channel Model", *IEEE Conference on Vehicular Technology (VTC 2000)*, pp. 885-892, May, 2000.
- [37] Philippe Laspougeas, Patrice Pajusco, Jean-Claude Bic, "Spatial Radio Channel for UMTS in Urban Small Cells Area", *IEEE Conference on Vehicular Technology (VTC 2000)*
- [38] K.I. Pedersen, P.E. Mogensen, B. Fleury, "A Stochastic Model of the Temporal and Azimuthal Dispersion seen at the Base Station in Outdoor Propagation Environments", *IEEE Transactions on Vehicular Technology*, May 2000.

- [39] Klaus Ingemann Pedersen, "Antenna Arrays in Mobile Communications. Channel Modeling and Receiver Design for DS-CDMA Systems", Ph. D. Thesis, Aalborg University, January 2000.
- [40] Chia-Chin Chong, Chor-Min Tan, David I. Laurenson, Stephen McLaughlin, Mark A. Beach, and Andrew R. Nix, "A New statistical Wideband Spatio-Temporal Channel Model for 5-GHz Band WLAN Systems", *IEEE Journal on Selected Areas in Communications*, Vol. 21, No. 2, February 2003.
- [41] Hamid Krim and Mats Viberg, "Two Decades of Array Signal Processing Research", *IEEE Signal Processing Magazine*, pp. 67-94, July 1996.
- [42] Petre Stoica, and Kenneth C. Sharman, "Maximum Likelihood Methods for Direction of Arrival Estimation", *IEEE Transactions on Acoustics, Speech and Signal Processing*, Vol. 38, No.7, July 1990.
- [43] Petre Stoica and Arye Nehorai, "MUSIC, Maximum Likelihood, and Cramer-Rao Bound", *IEEE Transactions on Acoustics, Speech, and Signal Processing*, Vol. 37, No. 5, May 1989.
- [44] Peter M. Schultheiss and Hagit Messer, "Optimal and Suboptimal Broad-Band Source Location Estimation", *IEEE Transactions on Signal Processing*, Vol. 41, No. 9, September 1993.
- [45] Mats Bengtsson, Björn Ottersten, "Rooting techniques for Estimation of Angular Spread with an Antenna Array", *IEEE 47th Conference on Vehicular Technology (VTC 1997)*, Vol. 2, pp. 1158-1162, May 1997.
- [46] Björn Ottersten, and Thomas Kailath, "Direction of Arrival Estimation for Wide Band Signals using the ESPRIT Algorithm", *IEEE Transactions on Acoustics, Speech and Signal Processing*, Vol. 38, No. 2, February 1990.
- [47] Titus Lo, John Litva, and Henry Leung, "A New Approach for Estimating Indoor Radio Propagation Characteristics", *IEEE Transactions on Antennas and Propagation*, Vol. 42, No. 10, pp. 1369-1376, October 1994.
- [48] A. Lee Swindlehurst, "Time Delay and Spatial Signature Estimation using known Asynchronous Signals", *IEEE Transactions on Signal Processing*, Vol. 46, No. 2, February 1998.
- [49] Sven Fischer, Hans Grubeck, Ari Kangas, Havish Koorapaty, Erik Larsson, Patrik Lundqvist, "Time of Arrival Estimation of Narrowband TDMA Signals for Mobile Positioning", *Personal Indoor Mobile Radio Communications (PIMRC'98)*, 1998.
- [50] Thomas Östman, Stefan Parkvall, "An improved MUSIC algorithm for Estimation of Time Delays in Asynchronous DS-CDMA Systems", *IEEE Transactions on Communications*, Vol. 47, No. 11, November 1999.
- [51] T.G. Manickam, R. J. Vaccaro, and D. W. Tufts, "A Least Squares Algorithm for Multipath Time Delay Estimation", *IEEE Transactions on Signal Processing*, Vol. 42, No. 11, November 1994.
- [52] Scott P. Belanger, "An EM algorithm for multisensor TDOA/DD estimation in a multipath propagation environment", *IEEE International Conference on Acoustics, Speech and Signal Processing (ICASSP)*, Vol. 6, pp. 3117-312, 1996. DOI: 101109/ICASSP.1996.550536.

-
- [53] Z. Gu and E. Gunawan, "Joint space-time estimation for DS-CDMA system in fast fading multipath channel", *Electronic Letters*, Vol. 37, No. 23, pp. 1407-1408, November 2001. DOI: 10.1049/el:20010928.
- [54] Laghmardi Nouredine, Harabi Ferid and Gharsallah Ali, "A Joint space-time estimation algorithm for wideband signals with high resolution capabilities", *IEEE International Multi-Conference on Systems, Signals and Devices (SSD)*, 2009. DOI: 10.1109/SSD.2009.4956659.
- [55] Jiang Yang, Hao Li, and Wei Zhang, "An effective method of joint DOA-delay estimation for coherent space-time distributed signals", *IEEE International Symposium on Computational Intelligence and Design*, Vol. 2, pp. 191-194, 2014. DOI: 10.1109/ISCID.2014.255.
- [56] Anja Klein, Werner Mohr, Ralf Thomas, Peter Weber, and Bernhard Wirth, "Direction of Arrival of Partial Waves in Wideband Mobile Radio Channels for Intelligent Antenna Concepts", *IEEE*, 1996.
- [57] Raviv Raich, Jason Goldberg, and Hagit Messer, "Bearing Estimation for a Distributed Source: Modelling, Inherent Accuracy Limitations and Algorithms", *IEEE Transactions on Signal Processing*, Vol. 48, No. 2, pp. 429-441, February 2000. DOI: 10.1109/78.823970.
- [58] Olivier Besson, Petre Stoica and Alex B. Gershman, "Approximate Maximum Likelihood Estimators for Array Processing in Multiplicative Noise Environments", *IEEE Transactions on Signal Processing*, Vol. 48, No. 9, pp. 2506-2518, September 2000. DOI: 10.1109/78.863054.
- [59] Martin Nilsson, Björn Völcker and Björn Ottersten, "A cluster approach to spatio-temporal channel estimation", *IEEE International Conference on Acoustics, Speech and Signal Processing*, Vol.5, pp. 2757-2760, 2000. DOI: ICASSP.2000.861069.
- [60] Richard J. Kozick and Brian M. Sadler, "Distributed Source Localization with multiple Sensor Arrays and Frequency-selective Spatial Coherence", *IEEE Statistical Signal and Array Processing (SSAP 2000)*, pp. 419-423, 2000. DOI: 10.1109/SSAP/2000.870158.
- [61] Sayed A.H., Tarighat A., Khajehnouri N., "Network-Based Wireless Location: challenges faced in developing techniques for accurate wireless location information", *IEEE Signal Processing Magazine*, Volume 22, Issue 4, 2005. DOI: 10.1109/MSP.2005.1458275.
- [62] Gustafsson F., Gunnarsson F., "Mobile positioning using wireless networks: possibilities and fundamental limitations bases on available wireless network measurements", *IEEE Signal Processing Magazine*, Volume 22, Issue 4, 2005. DOI: 10.1109/MSP.2005.1458284.
- [63] William C. Jakes, *Microwave Mobile Communications*, 10th Edition, IEEE Press, New York, 1994.
- [64] Theodore S. Rappaport, *Wireless Communications – Principles and Practice*, 10th Edition, Prentice Hall, New Jersey, 1996.
- [65] A. Artés, F. Pérez, J. Cid, R. López, C. Mosquera, F. Pérez, *Comunicaciones Digitales*, 1st Edition, Pearson Educación S.A., pp. 470-473, Madrid, 2007.
- [66] C.D. Lai, "First order autoregressive Markov processes", *Stochastic Processes and their applications*, Vol. 7, 1, pp. 65-72, 1978.

- [67] Y. Qi, H. Suda, H. Kobayashi, "On time-of-arrival positioning in a multipath environment", IEEE Vehicular Technology Conference, Vol 5, pp. 3540-3544, 2004. DOI: 10.1109/VETECONF.2004.1404723.
- [68] H.A. Karimi, "Advanced Location-Based Technologies and Services", 1st Edition, CRC Press, Boca Raton, 2013.
- [69] Josep Vidal, Montse Nájjar et al., "Positioning Accuracy when Tracking UMTS mobiles in delay and angular dispersive channels", IEEE Conference on Vehicular Technology (VTC 2001), 2001.
- [70] Y. Wang, "Linear least squares localization in sensor networks", EURASIP Journal on Wireless Communications and Networking, 51, 2015. DOI: 10.1186/s13638-015-0298-1.
- [71] René Játiva E., Josep Vidal, "Estimación del Tiempo de Llegada en un canal Rayleigh desde una perspectiva de la Cota Inferior de Cramer-Rao", Revista Avances en Ciencias e Ingenierías, pp. 5-10, Abril 2009.
- [72] René Játiva E., Josep Vidal, "Cota Inferior de Crámer-Rao en la Estimación del Tiempo de Llegada", Revista Avances en Ciencias e Ingenierías, pp. C14-C21, Julio 2012. ISSN 1390-5384.
- [73] René Játiva E., Josep Vidal and Margarita Cabrera, "Cramer Rao Bounds in Time Of Arrival Estimation for a Distributed Source", Mobile Communications Summit, IST2001, pp. 236-244, September 2001.
- [74] Jan R. Magnus and Heinz Neudecker, Matrix Differential Calculus with Applications in Statistics and Econometrics, John Wiley & Sons, New York, 1999.
- [75] Menni T., Chaumette E., Larzabal P., "Reparameterization and constraints for CRB: duality and a major inequality for system analysis and design in the asymptotic region", IEEE International Conference on Acoustics, Speech and Signal Processing (ICASSP), 2012. DOI: 10.1109/ICASSP.2012.6288682.
- [76] Emmanuele Andrea, Luise Marco, "Fundamental limits in signal time-of-arrival estimation in AWGN and multipath scenarios with application to next-generation GNSS", 5th ESA Workshop on Satellite Navigation Technologies and European Workshop on GNSS Signals and Signal Processing (NAVITEC), 2010. DOA: 10.1109/NAVITEC.2010.5708049.
- [77] Steven M. Kay, Fundamentals of Statistical Signal Processing – Estimation Theory, Prentice Hall, New Jersey, 1993.
- [78] Omar, S.M., Slock D., Bazzi O., "Recent insights in the Bayesian and deterministic CRB for blind SIMO channel estimation", IEEE International Conference on Acoustics, Speech and Signal Processing (ICASSP), 2012. DOI: 10.1109/ICASSP.2012.6288683.
- [79] Stoica Petre, Larsson E.G., Gershman A.B., "The stochastic CRB for array processing: a textbook derivation", IEEE Signal Processing Letters, Volume 8, Issue 5, 2001. DOI: 10.1109/97.917699.
- [80] Amigo A.G., Mallat A., Vandendorpe L., "Multiuser and multipath interference mitigation in UWB TOA estimation", IEEE International Conference on Ultra-Wideband (ICUWB), 2011. DOI: 10.1109/ICUWB.2011.6058887.

-
- [81] Catovic A., Sahinoglu Z., “The Cramer-Rao bounds of hybrid TOA/RSS and TDOA/RSS location estimation schemes”, *IEEE Communications Letters* Volume 8, Issue 10, 2004. DOI: 10.1109/LCOMM.2004.835319.
 - [82] Pahlavan K, Xinrong Li, Makela J.P., “Indoor geolocation science and technology”, *IEEE Communications Magazine*, Volume 40, Issue 2, 2002. DOI: 10.1109/35.983917.
 - [83] Suvi Ahonen and Pekka Eskelinen, “Mobile Terminal Location for UMTS”, *IEEE AESS Systems Magazine*, 2003.

Chapter 4

Timing and Direction of Arrival Estimation

Chapter 3 provided worth information about the possibility of improving timing estimation with the use of multiple sensors. In fact, the best results were achieved when a high SNR was available and also when the number of channel vector estimates increased. However, Signal to Noise Ratio (SNR) is affected by propagating conditions for paths between the subscriber and the Base Stations (BS). Infrastructure communications networks dispose of power control schemes between the mobile unit (MU) and the BS that provides the access to the network services, to assure the signal quality (SNR) and therefore the robustness of the communication link. This BS is called the central site or the control BS. However, when a signal transmitted for the MU is received by the non-control BSs, it could be strongly attenuated, especially at distant BSs when the MU is near to the central site. Similarly, signals received at the MU from distant BSs could be not properly received. This is the so called near-far hearability problem that impacts the quality of the acquired measures and consequently the results of positioning as shown in [1][2]. Low SNRs and longer distances are associated with shadowing and also with the NLOS condition as predicted by the Greenstein model [3] commented at chapter 2. This signal behavior makes difficult to achieve a set of unbiased timing measures, and although some techniques for NLOS mitigation were tested at chapter 2, our interest at this stage is to achieve a robust set of timing measures with a reduced bias and a lower variance.

In order to take the best of these estimates to improve the positioning, this chapter studies the problems associated with the detection of a weak first arrival and also with the timing estimation in a multipath environment. An incorrect decision taken at the detector of the first arrival may result on a bias, when the first arrival is taken as noise, or worse in an early detection when noise is taken as an arrival. Moreover, a signal compound originates at the receiver due to multipath propagation, degrading the timing resolution at the detection stage by introducing an additional bias, due to that the too close impinging arrivals may be mistaken as a just one.

Particularly, in section 4.1, the scheme for the timing detection and high resolution timing estimation suitable for positioning applications is introduced. We also identify at this section the difficulties associated to the constraints introduced from communication systems based on Direct Sequence Spread Spectrum (DS-SS) which provide the context to this research. Section 4.2 explores the possibility of using antenna arrays as a mean to mitigate the Non Line Of Sight (NLOS) condition. To do so, the Cramer-Rao Bounds (CRBs) computed in chapter 3 are integrated into the positioning simulation platform described in chapter 2 for different antenna configurations; and the benefits of using space-time diversity are revealed. On the other hand, a GLRT detector used for the coarse timing estimation as part of the scheme introduced at section 4.1, is

studied and evaluated at section 4.3. A simple model that relates the false alarm probability and the timing error for different configurations of the proposed GLRT is part of the study performed at this section. Moreover, some high resolution techniques for timing and direction of arrival estimation are studied and evaluated in section 4.4. From these tests, the issues associated to the estimation of these parameters are pointed out, and criteria for achieving high accurate results are provided.

4.1 Timing detection and estimation scheme

The timing information provided from a single channel estimate is not significant enough for positioning purposes since each arrived path fades independently due to Doppler [4][5], and the receiver is usually synchronized to the channel tap with the largest absolute value, which may not be the one bearing the position information as was illustrated in Figure 2.2 in chapter 2.

The time over which the delay of incoming rays suffers an insignificant variation is called “delay coherence time”, and it can be effectively used to combine impulse responses, so that the detection of the first arrival is improved. On the other hand, in case of a Wideband Code Division Multiple Access (WCDMA) system for example [6]-[8], a pilot channel in downlink (DL) and training sequences in uplink (UL) and DL dedicated channels are provided, allowing channel estimation under different situations of SNR. These estimates are used to demodulate data channels and are provided to rake receivers [9] to capture the received signal power. Therefore, these channel estimates are usually processed in such a way that the most representative channel fingers in terms of power are retained. Unfortunately these do not necessarily include the non-reflected signal arrival, especially in NLOS situations.

The estimation-detection proposed scheme [10][11] for the determination of the first arrival is shown in Figure 4.1 and departs from the channel vector estimates obtained out of the received array signal $\mathbf{x}(n)$.

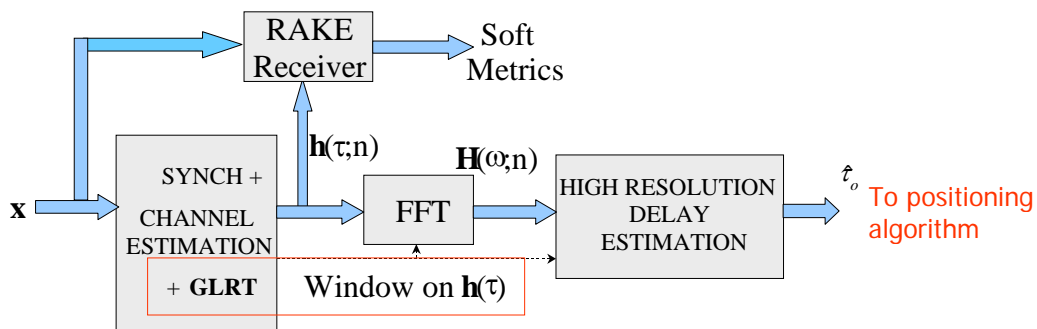


Figure 4.1: Scheme for Timing Detection used for the wireless subscriber positioning application.

Note that in order to achieve an accurate timing, a lag window prior to the component at the first finger of the rake receiver is observed to determine the presence

of earlier arrivals. It corresponds to a coarse detection of a possible low-power first arrival. The selected lag window along with the set of computed channel estimates are then passed to the high-resolution timing estimation, which determines the first arrival using parametric methods over the Fourier transformed channel estimates. Section 4.4 is devoted to this utility. Finally, the computed parameters are reported to the Position Computation Function (PCF), which provides the subscriber location.

The quality of the timing estimates is very much dependent on the SNR as well as on the propagation channel conditions as was shown in the chapter 3 using the CRBs. UTRAN specifications provide the means to transfer a parameter related to the quality of these measurements to the PCF, however there is no a preferred indicator. Research in [12] for example suggests the use of SINR, delay spread or geographical mapping among others to identify the LOS/NLOS situation as part of the methodology to estimate the mobile positioning and perform its tracking. In case of using geographical mapping, simple expressions for approximate computation of CRBs are provide in [13], and these may be used to improve the positioning accuracy as shown in [1].

4.2 Assessing positioning performance bounds using CRB with antenna arrays

In order to evaluate the effect of introducing antenna arrays in our system model, it must be recognized that the estimation of the first arrival improves when a higher SNR, and a larger number of sensors are available as it was studied in chapter 3. Therefore, the SNR must be taken in consideration for each station where a measure is performed. Furthermore, a minimum received power is required to assure the communication link and performing the measures. A signal with a level below this threshold would not be detected and the measure wouldn't be achieved. The SNR goals for BSs in Universal Mobile Telecommunication System (UMTS) and Long Term Evolution (LTE) wireless systems are exhibited at Table 4.1 as reference and as part of several physical characteristics that may be of interest.

Table 4.1 Important Operating Characteristics for LTE and UMTS systems.

System	Channel Bandwidth (BW)	f_{offset}	P_{out} Dynamic Range	Transmission Operating band unwanted emission levels	Reference Received Power P_{ref} @ BW (dBm @ MHz)	SNR BS goals (dB)
LTE	Mean of the 2 LTE carrier's bandwidth	BW/2	>20 dB	-48.3 dBm	-106.8@ 1.4	4.7-19.7
UMTS	5 MHz	2.5 MHz	>18 dB	-10.8 dBm	-121@ 12.2 kbps	21.1-25.1

All these values with the exception of the transmission operating band unwanted emission levels have been provided by 3GPP standards [14]. However, these emission

levels have been computed from the mask provided by [14] for an offset frequency f_{offset} , of 2.5 MHz. The Transmission Operating band unwanted emission level defines the maximum emission level in the operating band, and it corresponds to -10.8 [dBm] for UMTS. On the other hand, the Reference Received Power P_{ref} , corresponds to the receiver sensitivity, and it reaches -121 [dBm] for a low rate channel in UMTS. In general, sensitivity worsens with the channel bandwidth and imposes a practical limit that compromises the transmission rate with the link distance and therefore with the SNR goal. For example UMTS performs well with a SNR of 21.1 [dB] for a low rate QPSK modulated transmission, but it requires a higher SNR of 25.1 for a faster 64QAMcode. SNR in Table 4.1 corresponds to the rate between the total signal energy in the subframe on a single antenna port and the noise energy in a bandwidth corresponding to the transmission bandwidth over the duration of a subframe [15]. Furthermore, signal fading introduces random propagation losses to the links that are partially compensated by the power dynamic range of the transmission antenna P_{out} . This range is higher than 18 dB in UMTS as it is shown in Table 4.1. In addition, and in order to assure the information integrity, communication wireless communication systems provide certain ways of data redundancy.

In spite that above values refer to data channels, and that the location process in UMTS uses the measurements extracted from the Common Pilot Channel (CPICH) jointly with IPDL (Idle Period in the Down Link), this information certainly provides an insight about the signal behavior and the operation signal levels. Particularly, it is important the total power dynamic range because this can help to perform better estimates.

4.2.1 Antenna Arrays and Quality of the First Arrival Estimation

A simulation platform was introduced at chapter 2 to evaluate the behavior of positioning algorithms and their capabilities to mitigate the NLOS condition. The Greenstein gain-delay propagation model [3] is in the core of this simulator due to its aptitude to catch the characteristics of realistic wireless channels [16]. Otherwise, CRBs [17] for the first arrival estimation, studied at chapter 3, relates the timing estimation error with the space-time diversity. This section is devoted to the incorporation of the information for the timing error, provided by the CRBs for a NLOS Rayleigh fading model, into the subscriber position estimation system model as a mean of evaluating the impact of using antenna arrays and time diversity over subscriber positioning in realistic conditions.

In order to perform a successful integration of these two models, certain difficulties associated with discrepancies appearing at the bases of the formulation of these models will be commented below:

1. Timing as described by the Greenstein's propagation model is exponential distributed, and therefore timing estimation will be biased. This characteristic is very suitable for modeling NLOS wireless environments in realistic

conditions as was commented at chapter 2. However, the CRBs provide a mean to compute the variance of any unbiased estimator, the timing in our case; and although no such estimator would exist, it is still probable to achieve estimators that attain the bounds in an approximate sense [17], asymptotically at large SNRs and for a large number of estimates. After all, the Greenstein's model predicts lower delay spreads, and therefore lower biases, at higher SNRs; being the incorporation of the information provided by the CRBs reasonably sure in these cases [1],[18]-[21].

2. Since that CRBs are low error bounds, they fail in predicting the minimum variance at low SNR, as was commented at chapter 3. Furthermore, the attainable mean square error from the use of complex practical estimators may be even lower than the predicted by the CRBs [20][21], and a much better predictor of the minimum square error at low SNRs, may be achieved from the use of previous knowledge about signal behavior. For instance, [20] shows that when a coarse timing within a symbol interval is available, a better prediction of the normalized minimum variance for a fading channel correspond precisely to the variance for a timing uncertainty uniformly distributed within the symbol time. Moreover, results in [21] shows that a bias appears in the timing estimation at low SNRs.

Therefore, the following assumption will be considered for the integration of our CRB model for timing, commented at chapter 3, to the simulation platform based on the Greenstein's propagation model commented at chapter 2:

ASM1. The simulation platform will offer a mean to evaluate the impact of space-time diversity on mobile subscriber positioning based on timing under realistic conditions. Therefore, signal is assumed to be properly described by the Greenstein's propagation model.

ASM2. The SNR at the receivers that belong to the communications link between the control site and the subscriber is assumed to be kept under control due to power control schemes provided by the network. Therefore the signal level is high enough in this case to be modeled for a single multipath cluster as described by the CRBs model in chapter 3. The SNR for the other links are computed from the objective SNR at this link using the Greenstein's model as commented in chapter 2. Furthermore, for all those cases where signal is received with a moderate/high SNR, it is assumed to be also properly modeled by using a single multipath cluster. This assumption is suitable for 87% of the cases in a typical urban environment, rising to 94% at rural areas [16].

ASM3. A two-state approach is assumed to describe the signal behavior. In those cases where signal clearly degrades, and therefore SNR is too weak to keep a low estimation error as predicted by the CRBs, the signal statistics of the Greenstein model will be preferred instead of the Gaussian error. These

too low SNR cases are not properly described by CRBs due to the introduced bias at the estimation and hence an exponential distribution better describes the signal. A threshold has been defined to discriminate between cases of low and high errors, corresponding to high/moderate SNR and weak SNR respectively. The use of this two-state approach is more realistic than that provided in [1] where estimates are supposed always attaining the CRBs. Furthermore, this approach is convenient in the sense that all available measures will be used to perform the subscriber positioning no matter the quality of each one.

An additional difficulty does appear to define the threshold required to discriminate between the two states as defined by ASM3. The use of Bayesian CRBs (BCRBs) or Weighted CRBs (WCRBs) instead of CRBs could be possible alternatives [20][21], but their use is not exempt of problems. For example, the WCRBs require the definition of proper weighting indexes and in both cases new models should be derived. Finally, a threshold of 0.5 times the chip time (T_c) has been selected considering that in most of the cases (98%), for the simulator geometry, the signal delay spread is lower than $2 T_c$ [18] and therefore the deviation errors as predicted by the square root of the CRBs are lower than the timing deviation as predicted by the Greenstein model for this threshold (a relation higher than 1/4). Hence, error is not quite small to assure that CRBs are working properly. Furthermore the relation between the deviation error predicted by the CRB respect to the quantization error for a signal within a chip time for this threshold reaches a value of 1.73 confirming that the CRB is not providing a good estimation possibly due to the scarce SNR level. A brief study related with the proportion of cases where our two-state approach model rejects the use of the CRBs in relation with the selected threshold is found in Annex 4.1. From these results we can infer that around 5% of the cases will be out of the low error state when 8 sensors are used. This proportion will increase for a lower number of sensors in the antenna array.

Once the threshold has been selected, it is easy to understand that the positioning simulator works initially as described in chapter 2 (ASM1, ASM2), by computing the values of SNR and delay spread (DS) for the signal received in each one of the seven communications links provided by the geometry. Since that the threshold for the timing error has been set as $(CRB\{k_0|DS\})^{0.5}=0.5T_c$ for each given delay spread, the corresponding SNR that verifies this condition may be computed for any particular configuration as described by the CRB model, defining the operational region where the use of CRBs succeeds in predicting the minimum mean square error (ASM3). When the SNR at the receiver is below this minimum, timing error estimation is provided by the Greenstein model due to assumption ASM3. On the contrary, when SNR is higher than this value, a Gaussian error is preferred (ASM3), and the use of space-time diversity helps to acquire the first arrival as predicted by computing the CRBs. Figure 4.2 clearly describes the defined low error region for the CRB model for several configurations of the antenna array. These curves have been computed using a bi-exponential interpolation [18][22] from the original data provided by the CRB model commented in chapter 3.

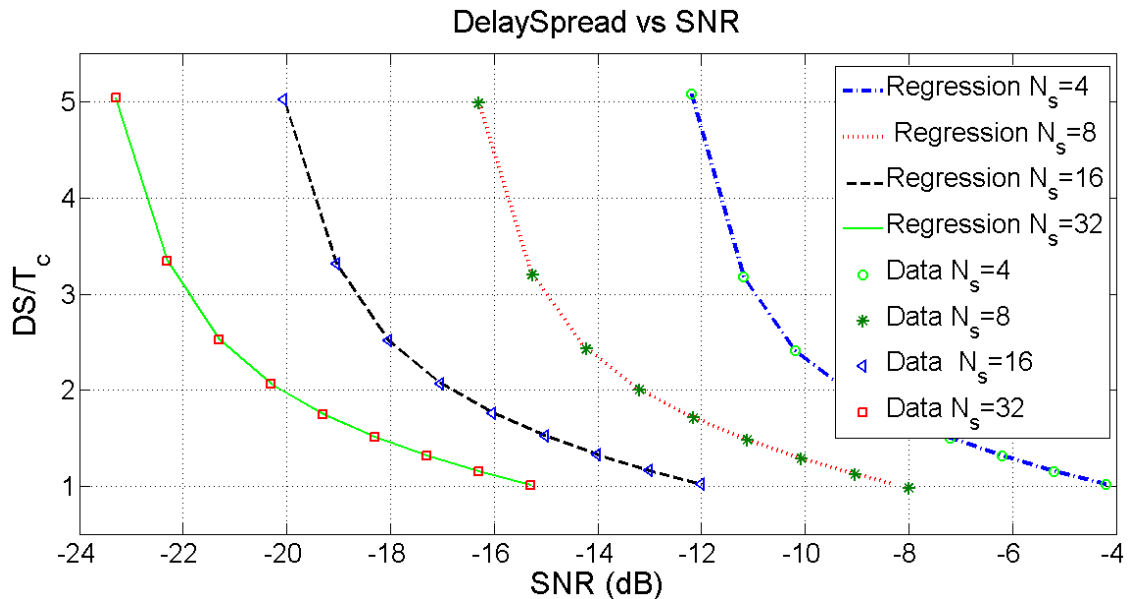


Figure 4.2: Normalized Delay Spread vs. SNR when $(\text{CRB}\{k_0|DS\})^{0.5}=0.5T_c$ and $K=250$ estimates.

This region matches the upper-right portion of the $DS - SNR$ plane over the corresponding curve. Observe as this region enhances for wider delay spreads and larger arrays. For example when $DS=T_c$ and $N_s=4$, the safe region corresponds to SNRs higher than -4 (dB). This region improves to SNRs higher than -11 [dB] when $DS=3T_c$ for the same configuration; and a gain of around 11 [dB] is achieved when passing from $N_s=4$ to $N_s=32$ sensors. All these values were computed for $K=250$ channel estimates.

4.2.2 Simulations for Subscriber Positioning based on TDOA

In order to explore the benefits of using antenna arrays in the subscriber positioning problem, a set of simulations will be performed for a Time Differences Of Arrival (TDOA) based system.

The system simulator [23][24] was introduced in chapter 2, and it consists of seven hexagonal cells of radius $R=1$ km. The control site is located at the coordinate system origin, and a rectangular grid has been constructed within the control cell to evaluate subscriber positioning algorithms' behavior for each point within the cell. 1000 realizations for each position at the grid have been used to get the results. A realistic scenario where NLOS is present in the seven BS's, has been considered. The required parameters for the Greenstein model take the following values suitable for the urban case [3]: $T_1=0.4 \mu\text{s}$, $\varepsilon=0.5$, $\beta=3.7$, $\sigma_x=8.0$ dB, $\sigma_\xi=4.0$ (dB), and $\rho=-0.75$. Particularly, T_1 has been set in agreement to the GTU COST 259 model [16] and it may be considered a moderate dispersive environment. All the TDOA measures are referred to the central

site BS₁, and therefore the equations' system to be solved corresponds to the described by expressions (4.1) and (4.2) as it was described in section 2.3.1 of chapter 2.

$$\mathbf{Ax} = \mathbf{b} \quad (4.1)$$

$$A = \begin{bmatrix} x_2 & y_2 \\ x_3 & y_3 \\ \vdots & \vdots \\ x_L & y_L \end{bmatrix}; \quad \mathbf{b} = -r \begin{bmatrix} m_2 \\ m_3 \\ \vdots \\ m_L \end{bmatrix} + \frac{1}{2} \begin{bmatrix} r_2^2 - m_2^2 \\ r_3^2 - m_3^2 \\ \vdots \\ r_L^2 - m_L^2 \end{bmatrix}$$

$$\text{with } m_i = c\tau_{i,1}; \quad \forall i = 2, 3, \dots, L \quad (4.2)$$

$$r_i^2 = x_i^2 + y_i^2; \quad \forall i = 2, 3, \dots, L; \quad \text{and } r^2 = x^2 + y^2$$

Solution for (4.1) is described in (4.3):

$$\hat{\mathbf{x}} = (\mathbf{A}^T \mathbf{W} \mathbf{A})^{-1} \mathbf{A}^T \mathbf{W} \mathbf{b} \quad (4.3)$$

Where, it is well known that the weighting matrix \mathbf{W} takes the form in (4.4) in terms of the error covariance matrix \mathbf{C}_n , as it is shown in [25][26]. However, the weighting matrix depends of the distances between the subscriber and the Base Stations, and also the solution depends of the range between the subscriber and the control site, r .

$$\mathbf{W}_{TDOA} = [4 \text{diag}(d_2, d_3, \dots, d_L) \mathbf{C}_{n,TDOA} \text{diag}(d_2, d_3, \dots, d_L)]^{-1}; \quad (4.4)$$

$$\text{with } d_i = \|\mathbf{x} - \vec{\mathbf{r}}_i\|; \quad \forall i = 2, 3, \dots, L$$

To incorporate this data, it is pertinent to have a way to estimate this range information, and various perspectives are possible. One of them involves achieving a LLS solution for the subscriber position and using this information to estimate the ranges required in (4.2)-(4.4). However, the approach used in this document prefers the application of WLLS even for the initial estimation. In this case, the weighting matrix \mathbf{W} is simply the inverse of the matrix in (4.5), and due the system is linear, the range r is discarded ($r=0$) from (4.1) prior to the computation of the positioning provided by (4.3). Certainly this procedure provides a poor estimation as it will be discussed below, but it will be good enough for the refinement of the weighting matrix in a second step.

$$\mathbf{C}_n^1 = \begin{bmatrix} 2 & 1 & \dots & 1 \\ 1 & 2 & \dots & 1 \\ & & \ddots & \\ 1 & 1 & \dots & 2 \end{bmatrix} \quad (4.5)$$

The error covariance matrix used for initialization \mathbf{C}_n^1 in (4.5) is obtained assuming that our TDOA errors \mathbf{n}_i may be expressed in terms of the errors introduced by the propagating signal between the subscriber and the BS's involved in positioning as in (4.6) and (4.7), and also assuming these random variables as independent due the communication links corresponds to different propagation paths. Furthermore, if these

variables are identically distributed, the scale factor between the elements in the main diagonal respect to the off-diagonal ones is 2.

$$\text{var}\{\mathbf{n}_i\} = \text{var}\{\mathbf{e}_i - \mathbf{e}_1\} = \text{var}\{\mathbf{e}_i\} + \text{var}\{\mathbf{e}_1\} = \sigma_i^2 + \sigma_1^2 \quad \forall i = 2, 3, \dots, L \quad (4.6)$$

$$\text{cov}\{\mathbf{n}_i, \mathbf{n}_j\} = E\{(\mathbf{e}_i - \mathbf{e}_1)(\mathbf{e}_j - \mathbf{e}_1)\} = \text{var}\{\mathbf{e}_1\} = \sigma_1^2 \quad \forall i \neq j \quad (4.7)$$

Of course, these assumptions ignore the dependence of the signal statistics with the distances between the subscriber and each one of the BSs, but they are suitable for the initialization stage where these ranges are unknown. Therefore, the superscript 1 at the notation in \mathbf{C}_n^1 denotes its provisional character as a first approximation.

For the second step, information provided by the Greenstein model may be incorporated to the noise correlation coefficients originating new error correlation matrices described in (4.8) and (4.9).

$$\mathbf{C}_n^2 = T_1^2 \begin{bmatrix} \hat{d}_2^{2\varepsilon} + \hat{d}_1^{2\varepsilon} & \hat{d}_1^{2\varepsilon} & \cdots & \hat{d}_1^{2\varepsilon} \\ \hat{d}_1^{2\varepsilon} & \hat{d}_3^{2\varepsilon} + \hat{d}_1^{2\varepsilon} & & \hat{d}_1^{2\varepsilon} \\ & & \ddots & \\ \hat{d}_1^{2\varepsilon} & \hat{d}_1^{2\varepsilon} & \cdots & \hat{d}_L^{2\varepsilon} + \hat{d}_1^{2\varepsilon} \end{bmatrix} \quad (4.8)$$

Matrix \mathbf{C}_n^2 in (4.8) simply emerges by replacing the error variances in (4.6) and (4.7) with the square of the mean value of the RMS Delay Spread derived from Greenstein's model in expression (2.75) in chapter 2, and discarding the scale factor. These values are now distance dependent as required. Again, the superscript 2 at the notation in \mathbf{C}_n^2 denotes its use at the second step. Of course the distances required to formulate (4.8) are replaced by their coarse estimations achieved at the completion of the initialization step.

$$\mathbf{C}_n^3 = T_1^2 \begin{bmatrix} K_1(d_1^{2\varepsilon} + d_2^{2\varepsilon}) - (d_1 d_2)^\varepsilon & \cdots & K_2(d_{L-1}^\varepsilon - d_1^\varepsilon)(d_L^\varepsilon - d_1^\varepsilon) \\ \vdots & \ddots & \vdots \\ K_2(d_{L-1}^\varepsilon - d_1^\varepsilon)(d_L^\varepsilon - d_1^\varepsilon) & \cdots & K_1(d_1^{2\varepsilon} + d_L^{2\varepsilon}) - (d_1 d_L)^\varepsilon \end{bmatrix} \quad (4.9)$$

$$\text{with } K_1 = 2e^{\sigma_z^2} - 1; \quad K_2 = e^{\sigma_z^2} - 1;$$

Matrix \mathbf{C}_n^3 results from the more cumbersome work over the Greenstein model as it is shown in the Annex A2.3 of chapter 2. However, this modeling requires the knowledge of the additional parameter σ_z , related with signal dispersion; and it is clearly computationally heavier. Furthermore, the use of (4.9) results in larger errors when coarse estimates for distances d_i from step one, are used to compute this weighting matrix at the second step. Therefore, equation (4.8) will be preferred to perform the required positioning.

Experiment 4.1: Application of WLLS algorithm to TDOA-based positioning when six surrounding BSs are available, and the central site is used as reference. $N_s=1$ and SNR1=10 [dB] for a moderate dispersive environment.

Figure 4.3 exhibits the average positioning errors for subscribers within a cell of radius $R=1000$ (m) when WLLS algorithm in (4.3) is performed over UL-TDOA measures. Results from the application of the algorithm for the initialization step are exhibited at the top-left. In this case parameter r is set to zero and matrix \mathbf{C}_n^1 in (4.5) is used to achieve the weighting matrix. Clearly, the position estimation is quite coarse at this stage; however it provides the range information d_i , required to formulate the matrix \mathbf{C}_n^2 in (4.8). When this matrix is used to perform positioning, and again $r=0$, results are shown at the top-right. An improvement in accuracy of at least 150 [m] is evident when these two graphics are compared.

At the bottom-left, results from the completion of the WLLS algorithm are exhibited. At this stage, the parameter r has been estimated from the positioning achieved at the latter step. In spite of some improvement is evident, especially at the borders; several spots with degraded accuracy appear within the whole cell. This degraded spots due to estimation errors in r , make difficult the improvement quantification from a visual inspection. Finally, at the bottom-right, results from the application of a geometrical restriction to our WLLS algorithm are shown. This constraint comes from the observation that the positioning accuracy improves near the central site and degrades near the cell boundaries. In fact, parameter r is overestimated at the boundaries, reaching values higher than the cell radius. When this happens, the constraint sets $r=R$ and compels the solution to be within the central site. The benefit from the application of this restriction is evident when graphics at this figure are compared. Particularly, degraded spots have disappeared, and clearly a good portion of errors are below between 100 [m] and 250 [m].

Figure 4.4 exhibits the distribution functions for wireless subscriber positioning error achieved from the application of different stages of WLLS algorithm when TDOA estimates are achieved from uplink and also from downlink. Figure 4.4 shows as refinement provided by added constraint improves the positioning in at least 40 [m] for 70% of the cases and much more for the remainder, when measures are taken at the uplink (UL). For measures taken at the downlink (DL), improvement associated to the geometrical constraint is something lower, around 30 [m] for 70% of the cases.

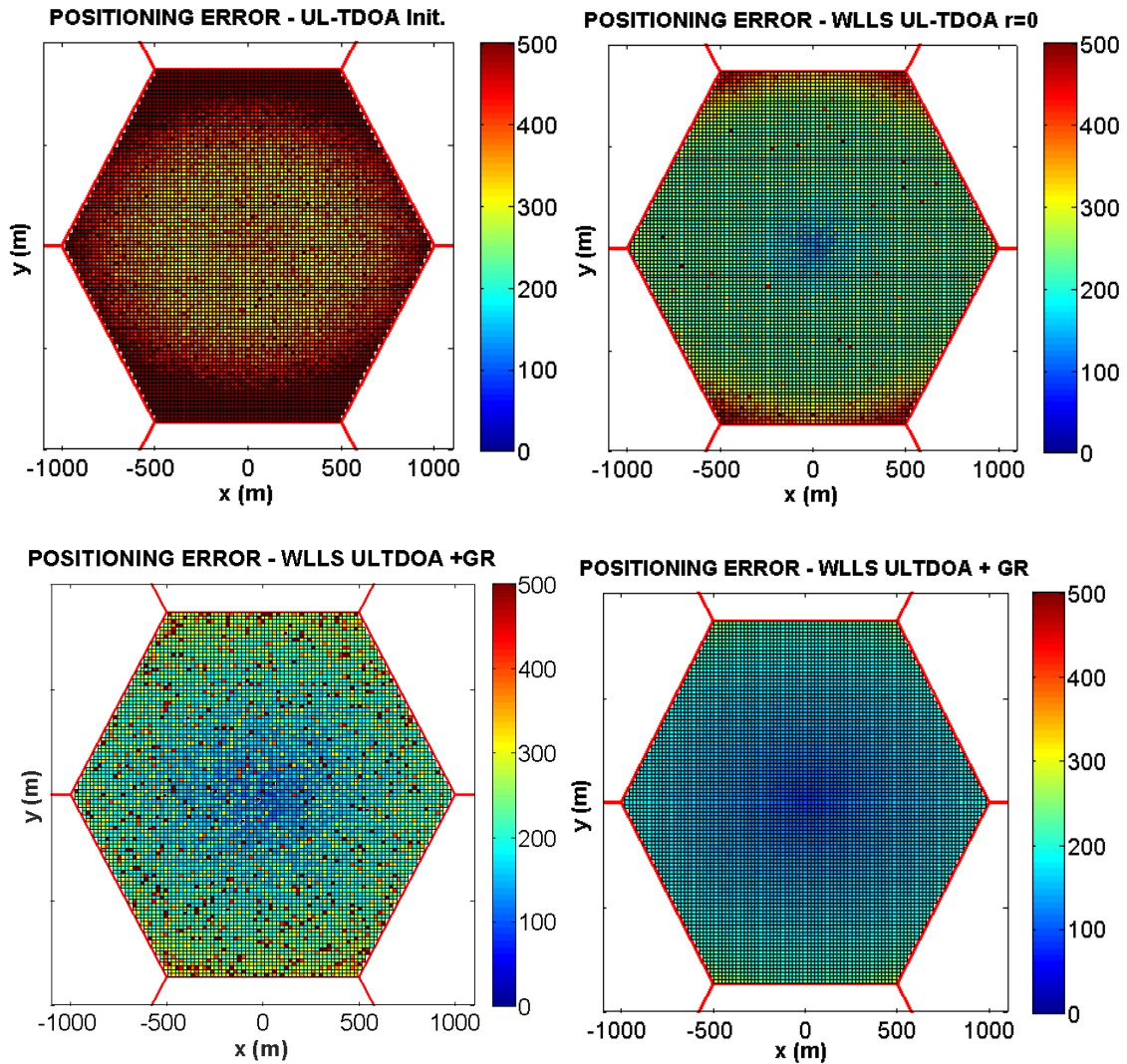


Figure 4.3: Average positioning error for a wireless subscriber within a cell of radius $R=1$ km when the reference SNR at the central site is $SNR_1=10$ [dB]; $N_s=1$, and TDOA measures are performed at the uplink. A) Top Left: Initial Positioning; B) Top Right: WLLS when $r=0$; C) Bottom Left: WLLS; D) Bottom Right: WLLS plus Geometrical Restrictions.

Furthermore, Figure 4.4 also shows that positioning is systematically better for measures taken at the uplink (UL) due to in this case the whole set of TDOA measures uses the same timing reference for the central site. It does not occur at the DL, since Idle Period in Down Link (IPDL) is used in this case to perform the measure at the subscriber. The average positioning error is reduced from 241 [m] with DL-TDOA, to 211 [m] with UL-TDOA for the 70% of the cases, when the constraint is added to the original WLLS algorithm. However, it is important to keep in mind that SNR at downlink is better than the corresponding at the uplink due to power limitations at the mobile, previously to judge about the goodness of these methods.

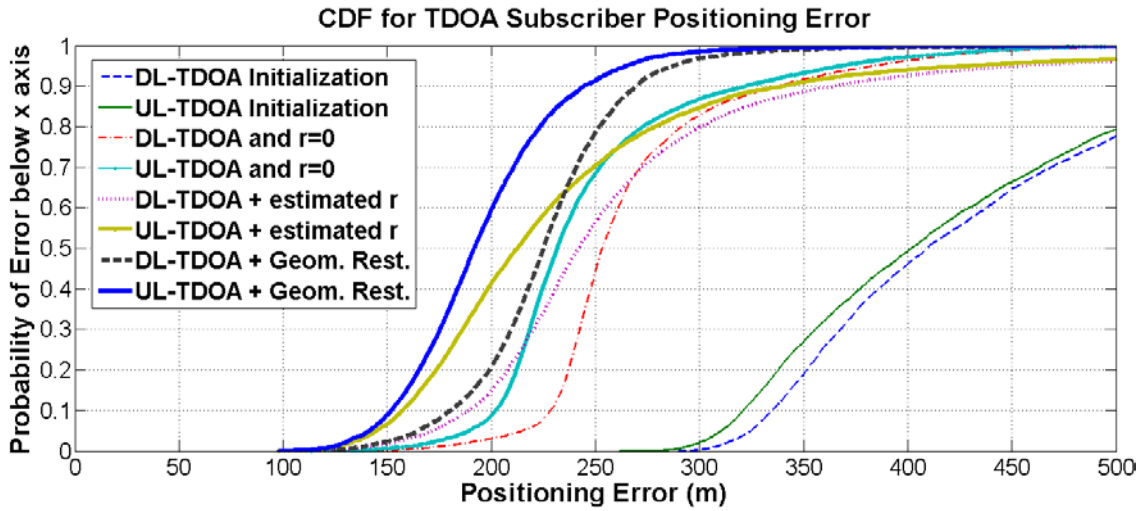


Figure 4.4: Distribution Function for the Average Positioning Error for a subscriber within a cell of radius $R=1$ km when the reference SNR at the central site is $SNR_1=10$ [dB]; $N_s=1$, and WLLS algorithm performs TDOA measures at downlink and uplink.

Experiment 4.2: Impact of space-time diversity over subscriber positioning accuracy when WLLS algorithm is applied. TDOA measures are provided from/to the six surrounding BSs, and the central site is used as reference. Multiple sensors and channel estimates are available within a moderate dispersive environment.

Results from this experiment are provided in Figure 4.5, Figure 4.6 and Figure 4.7. These outcomes correspond to the integration of Greenstein propagation model and Cramer-Rao Bound model for timing into the positioning simulation platform. Propagation conditions in these simulations correspond as before to a moderate dispersive environment. However, due to the incorporation of CRBs for timing, new parameters associated to the procedures to explode space-time diversity to achieve an improved timing estimation, have been added. They are the number of channel estimates K , and the number of sensors N_s , at the antenna array, among others explained at chapter 3. Particularly, these simulations correspond to a Partially Coherent Dispersive (PDS) channel, where the temporal correlation between two consecutive estimates is $\alpha=0.99$, the roll-off factor has been set to one, the angular spread $\Delta=5^\circ$, and signal arrives from the broadside.

At top-left, Figure 4.5 exhibits the positioning accuracy when TDOA measures are performed at the subscriber, for $N_s=4$ sensors at the antenna array, $K=50$ estimates available for timing, and the reference SNR at the mobile station for signal coming from control site has been set to 10 [dB]. The first observation from this figure it is the appearing from certain accuracy degradation near the central site. It is not really surprising, reminding that our positioning algorithm was tuned for statistics suitable for the Greenstein model, and now we have two concurrent models within the cell. Furthermore, SNR at the receiver for the available signal at the link between subscriber and the central site doesn't change due to power control, however the SNR does

degrade for those links between subscriber and any of the rest of BSs when the MS approximates to the central site and goes away from these stations.

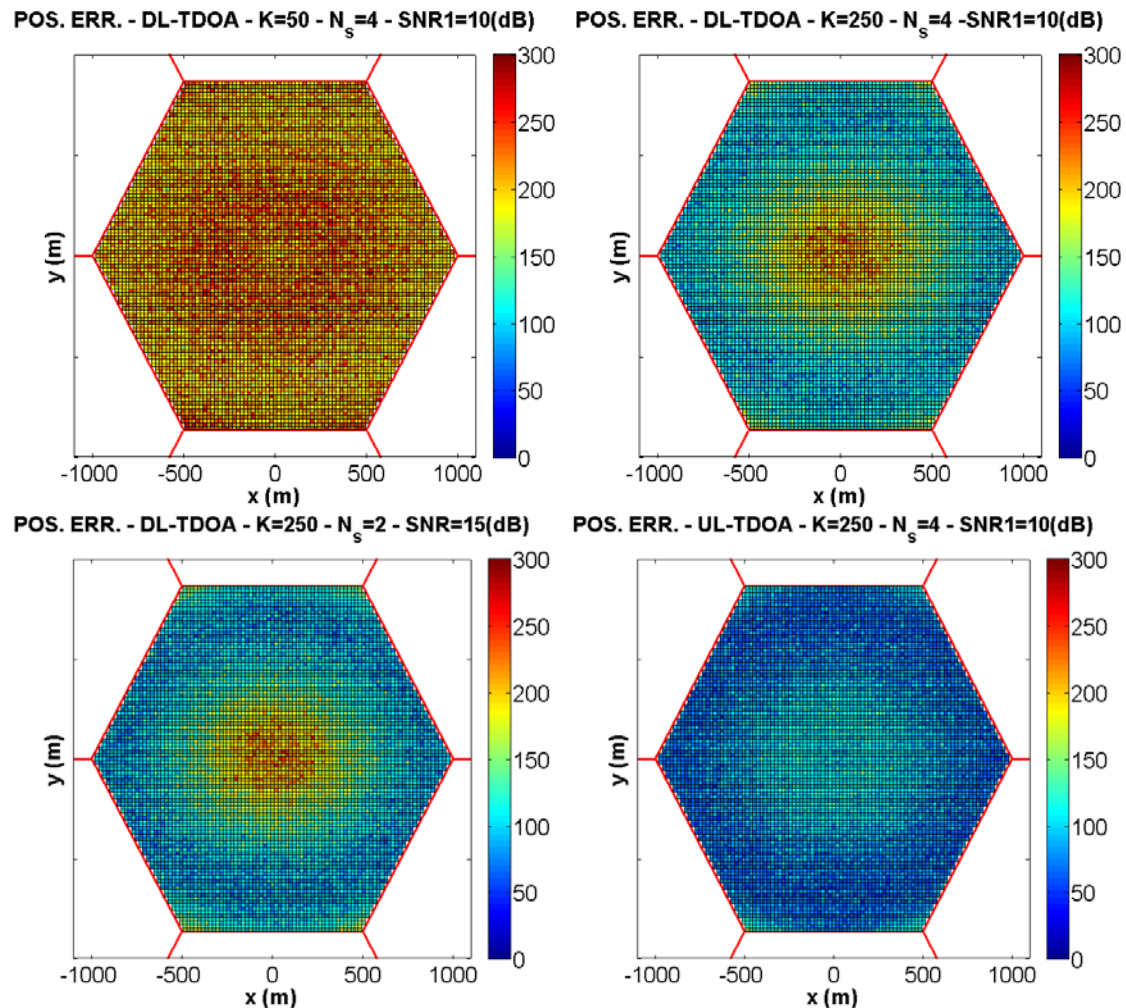


Figure 4.5: Impact of space-time diversity over average TDOA-based positioning error for a wireless subscriber within a cell of radius $R=1$ km. A) Top Left: $SNR1=10$ [dB], $N_s=4$, $K=50$ estimates performed at the downlink (DL); B) Top Right: $SNR1=10$ [dB], $N_s=4$, $K=250$ estimates performed at DL; C) $SNR1=15$ [dB], $N_s=2$, $K=250$ estimates performed at DL; D) Bottom Right: $SNR1=10$ [dB], $N_s=4$, $K=250$ estimates performed at the uplink (UL).

The result from a poor SNR in one of the two signals required to perform the TDOA measure is a poor measure. For subscribers located near to the boundaries, signal provided for both links have a good quality and therefore also the corresponding TDOA measure.

At top-right, Figure 4.5 shows results from the use of a higher number of estimates to achieve timing measures. $K=250$ for this case, and although the near-far effect commented above is still present, CRBs predict a more accuracy estimation from the use of time diversity, and therefore positioning exhibits a clear improvement of around 90 [m]. At bottom-right, this figure shows the results for measures performed at

the network and a new improvement is registered. Furthermore, at bottom-left, the result for a new configuration with $K=250$ and $N_s=2$ sensors is exhibited, when the reference SNR has increased to 15 [dB]. Accuracy for this configuration degrades in relation with the latter, but is very similar to DL-TDOA based positioning when $N_s=4$ and the reference SNR= 10 [dB] since the higher SNR compensates the reduction in the size of the antenna array.

Figure 4.6 shows the subscriber's average positioning error resulting from TDOA measures when 16 sensors are available at the uniform linear array (ULA) in the receiver, and 50 channel vector estimates are used to improve the timing estimation for measures performed both at uplink and at downlink. To the left, results from measures achieved at the network are exhibited; whilst to the right, results for positioning when the timing reference to the central site differs at each measure, are shown.

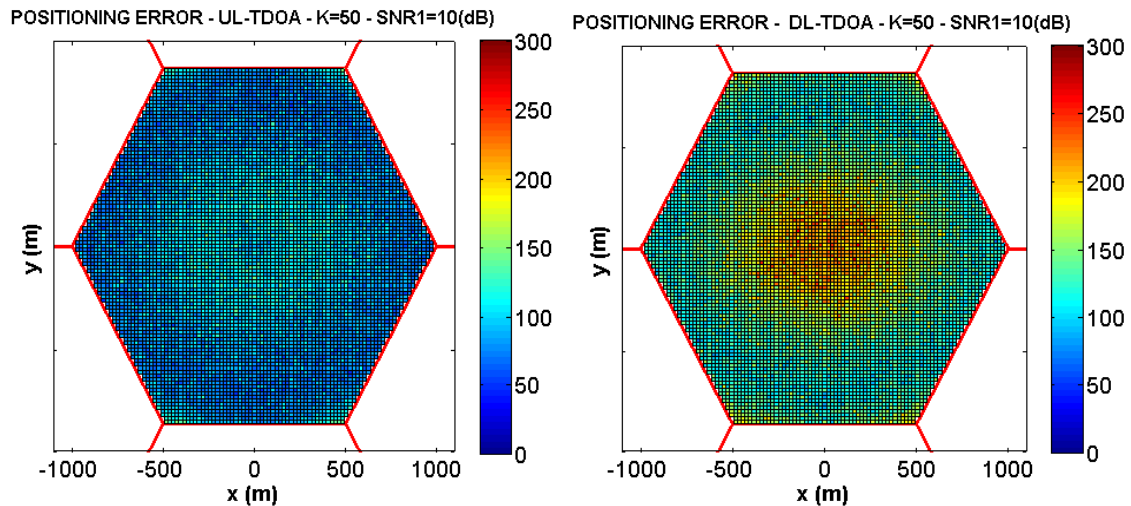


Figure 4.6: Impact of space-time diversity over average TDOA-based positioning error for a wireless subscriber within a cell of radius $R=1$ km when the reference SNR at the central site is $SNR1=10$ [dB], $N_s=16$, and $K=50$ estimates. A) Left: estimates are performed at uplink (UL); B) Top Right: estimates are performed at downlink (DL).

This latter case could correspond well to positioning based on DL-TDOA. However, it is not probable to have so large array at the downlink. Nevertheless, this result is useful to confirm how positioning degrades near the central site, whilst remains uniformly well at the boundaries even for large antenna configurations due the near-far effect commented previously. This effect is less important for positioning based on UL-TDOA since the use of a common reference for the whole set of measures leads to achieve a better solution.

Figure 4.7 confirms the benefit of using space and temporal diversity.

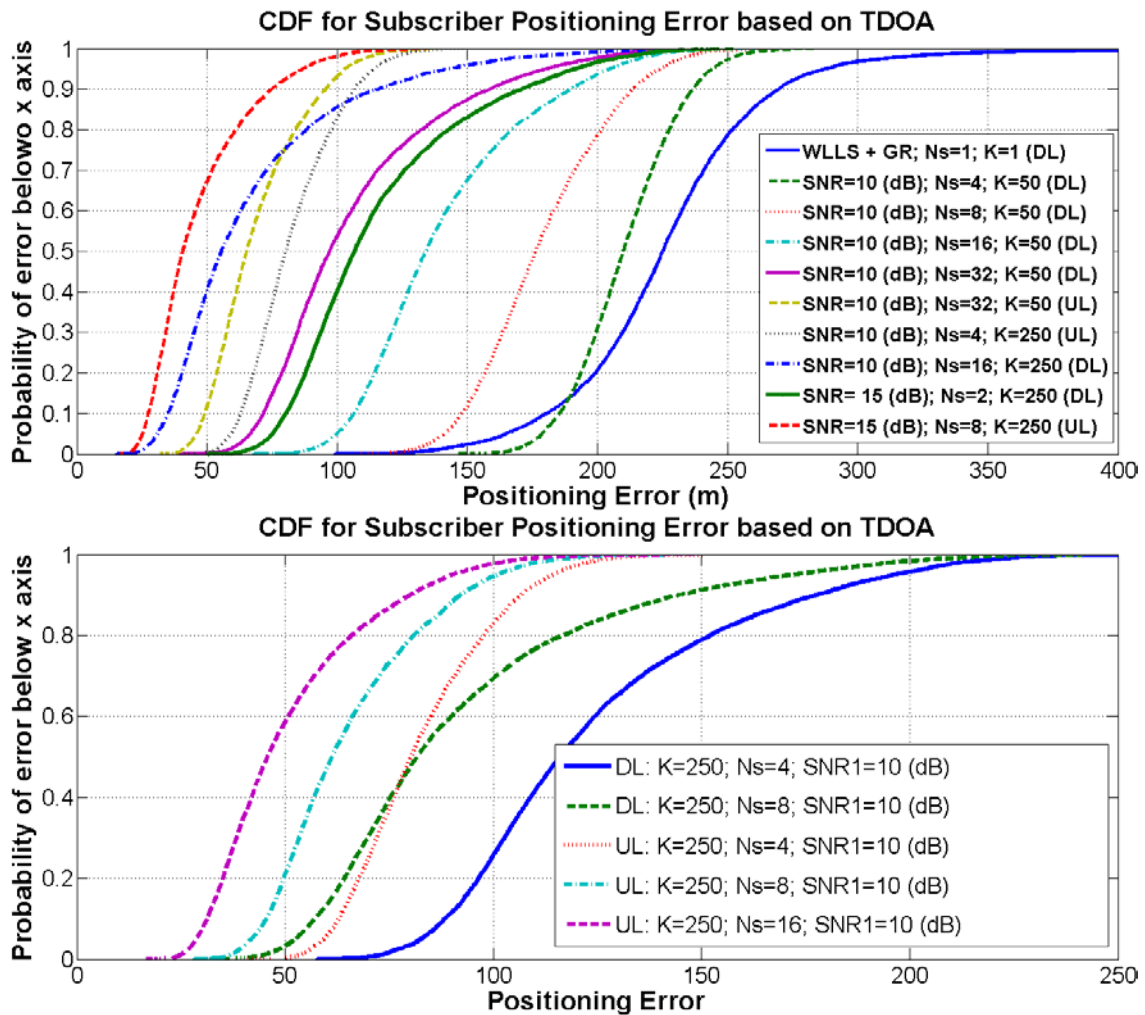


Figure 4.7: Distribution Function for the Average Positioning Error for a subscriber within a cell of radius $R=1$ km for several configurations when the positioning algorithm performs TDOA measures either at downlink or uplink, and space-time diversity is used to achieve better timing estimates. Top: miscellaneous results for $K=1$, 50 and 50 estimates; $N_s=2$, 4, 8, 16 and 32 sensors, and the reference SNR at the central site $SNR_1=10$ [dB] and 15 [dB]. Bottom: miscellaneous results for $SNR_1=10$ [dB]; $K=250$; and $N_s=4$, 8, and 16 sensors.

Compare for example the original configuration with $N_s=1$, $K=1$, to above scenario with $N_s=16$, $K=50$. In this case, positioning error improves from 241 [m] to 153 [m] for the 70% of the cases, and from 287 [m] to 205 [m] for 95% of the cases.

Furthermore, when $K=50$ channel vector estimates, and four sensors are used, average positioning improves in 20 [m] respect to the initial case for 70% of the cases, and improves another 30[m] when the number of sensors doubles. When the number of sensors reaches sixteen a new improvement of 38 [m] is achieved. Therefore an average positioning error below 116 [m] is achieved with 32 sensors for 70% of the cases, and below 181 [m] for the 95% of the cases. For positioning based on UL-TDOA, these errors reduce even more for the same configuration with $N_s=32$ and $K=50$:

to 76 [m] and 103[m] respectively. When a larger number of channel vector estimates are available, great improvements can also be achieved. For example, with four sensors and $K=250$, positioning error reduces to 114 [m] for 95% of the cases for UL-TDOA. When just two sensors at the subscriber, for a higher SNR of 15 [dB], and $K=250$, the positioning error is below to 126 [m] for 70% of the cases.

In summary, NLOS condition strongly degrades the performance of subscriber positioning in wireless communication systems, and even robust algorithms, originally developed for LOS signal, fail. However, a better use of signal statistics to properly weigh the measures and imposing certain geometrical restrictions help to mitigate this problematic condition and therefore to improve positioning. Furthermore, our simulation platform integrates the simple but reliable link level Greenstein propagation model to a Rayleigh-fading model based on the CRB to take account of spatial and temporal diversity, and study the possibility of improving timing estimation to achieve a much better positioning. Our results show that important improvement is always possible for architectures that take advantage of temporal and spatial diversity, especially for positioning based on UL-TDOA.

4.3 Discriminating Signal from Noise: The Detection Problem

Strictly speaking, determining the exact sampling time is a high resolution estimation problem. It is described by the right block of Figure 4.1 and treated in section 4.4. However, the goal of this section is discuss the problem of discriminating signal from noise as described by the left block of Figure 4.1. It corresponds to a detection problem very close related to the synchronization procedure in any wireless communication system. For example, the synchronization process in a DS-CDMA system such as W-CDMA includes slot and frame synchronization, scrambling code group and code identification, frequency acquisition and cell identification [7]. Scrambling codes are used to differentiate transmitters, whilst spreading codes are used to differentiate physical channels from the same transmitter. A matched filter to the Primary- Synchronization Channel (P-SCH) is required to perform slot synchronization in the downlink, and due to a low operating SNR, the matched filter outputs have to be noncoherently accumulated over many slots to prevent phase rotations from propagating across different short sequences matched filters, getting reliable decision statistics. The secondary Synchronization Channel (S-SCH) is used to achieve frame synchronization and identify the scrambling code group identity, by correlating against the 16 available S-SCH sequences. Moreover, the scrambling code detection is based on the Common Pilot Channel (CPICH), correlating against all the scrambling codes within the identified group. These sequences are known by the receiver. Eventually, a cell is identified with the help of CPICH, after frequency acquisition required for reducing the frequency error so that the MS can decode the broadcast information [7]. From a practical viewpoint, the hypothesis that a particular chip is the first in the sequence is made by sampling the output of matched filter to the sequence. This sampling is performed once, or at most a few times per chip, since better results are achieved when

the sampling testing point is nearer to the exact synchronization, and then performing non coherent integration to effectively measure the energy within a certain interval. The testing device then compares this measurement to a reference threshold level prior to take a decision. The two possible choices are stopping and finishing synchronization or advancing time and performing a new test.

Theoretically, the whole sequence should be tested. In case of cdma2000 [27], the scrambling sequence may reach tens of milliseconds, whilst that in W-CDMA, it lasts just 10 milliseconds [7], but generally the receiver has a reasonable estimate of the correct time, and the initial time of user sequences are also known [1][5][20]. Therefore the test for looking for the first arrival is reduced to a small number of possible chip intervals rather than to the sequence length. Moreover, a reduced number of chip intervals to be tested is preferred to reduce the mean acquisition time [28]. The coarse sequence alignment stage is called acquisition, where timing is achieved within a fraction of the chip time, and the posterior fine alignment is usually called tracking [29]. Furthermore, with the goal to surpass some negative effects such as clock instability and Doppler [1][5][7][30], corrections should be made continuously to keep an accurate timing through time tracking and it is usually performed by an early-late gate. The conventional acquisition is performed by using a serial search algorithm [31] due to its low complexity, where the uncertainty timing region is divided in small periods frequently called cells [28][29][32]. Generally these cells correspond to a chip interval, but in case of oversampling they will be shorter. The conventional serial search algorithm tests consecutive cells until acquisition is achieved. However, in the last years new approaches have appeared, such as the fixed step serial search or the bit reversal algorithm where the test is performed in specific non-consecutive order. These approaches claim to get a lower mean acquisition time at the cost of a higher complexity [29]. The studies performed in this document suppose the use of a serial search algorithm since our goal is to get a better understanding of the issues associated to timing estimation due to the quality of these measures affect the positioning problem as was studied in chapter 3.

4.3.1 Statistical Fundamentals

As was explained above, synchronization and signal detection in general imply to properly discriminate the presence of the desired signal from the received background noise, being the latter not just from thermal origin, but mainly provided by the interference from other users and other channels associated to the same user, since separation afforded by codes is not perfect. Therefore, this problem is studied in a general way and from a statistical viewpoint in this section, and some notions from the decision theory are introduced.

In general, signal and noise exhibit different probability density functions (PDFs), and therefore devices (detectors) used to discriminate among them employ some associated statistics to provide a quantitative measure on the certainty of each possible

choices. Each of them is called hypothesis and the selection procedure is known as a “statistical test” or simply as the test.

When a test is performed, it is important to quantify the statistical errors appearing from incorrect choices: the hypothesis selected is in effect false. Two errors are possible: null hypothesis is true and the test decides for the alternative (type I error) or alternative is true but the test decides for the null (type II error). In general, null hypothesis corresponds to the possibility of having just noise, and therefore type I error is associated to a false alarm probability while type II error is associated to the probability of missing the presence of a signal. Performing a test requires setting a threshold and it is selected to achieve some specified false alarm probability called the test size.

It is evident that ideally, null false alarm and no signal missing are desirable; but it is clear that when false alarm probability reduces, signal missing probability increases and vice versa, and therefore a compromise among them is required. Neyman-Pearson theorem provides a criterion to get test statistics taking account this tradeoff.

Neyman-Pearson Theorem: To maximize the detection probability P_D for a given false alarm probability $P_{fa} = \alpha$, this theorem decides for the alternative hypothesis \mathcal{H}_1 if the likelihood ratio $L(\mathbf{x})$ in (4.10) is higher than the threshold γ , where the threshold is found as it is shown in (4.11). The proof of this theorem may be found in [33].

$$L(\mathbf{x}) = \frac{p(\mathbf{x}; \mathcal{H}_1)}{p(\mathbf{x}; \mathcal{H}_0)} > \gamma \quad (4.10)$$

$$P_{fa} = \int_{\{\mathbf{x}: L(\mathbf{x}) > \gamma\}} p(\mathbf{x}; \mathcal{H}_0) d\mathbf{x} = \alpha \quad (4.11)$$

Minimum Bayes Risk Detector: Another interesting criterion is the so called minimum probability of error or its generalization to multiple hypotheses testing known as Bayes Risk. The main idea behind these criteria is assigning probabilities to the various hypotheses to express a prior belief in the likelihood of them. If the M possible hypothesis $\{\mathcal{H}_0, \mathcal{H}_1, \dots, \mathcal{H}_{M-1}\}$ are available, and the cost assigned to the decision to choose \mathcal{H}_i when \mathcal{H}_j is true is denoted by C_{ij} , the expected cost or Bayes risk, \mathcal{R} is expressed as in (4.12).

$$\mathcal{R} = \sum_{i=0}^{M-1} \sum_{j=0}^{M-1} C_{ij} P(\mathcal{H}_i | \mathcal{H}_j) P(\mathcal{H}_j) \quad (4.12)$$

When the restriction in (4.13) is set, the probability of error P_e is equal to the Bayes Risk \mathcal{R} , and the minimum P_e decision rule corresponds to decide \mathcal{H}_k if condition in (4.14) verifies. The interested reader may see [33] for a demonstration.

$$C_{ij} = \begin{cases} 0 & i = j \\ 1 & i \neq j \end{cases} \quad (4.13)$$

$$P(\mathcal{H}_k | \mathbf{x}) > P(\mathcal{H}_i | \mathbf{x}) \quad i \neq k \quad (4.14)$$

The conditional probability $P(\mathcal{H}_i | \mathbf{x})$ expresses the hypothesis probability after the data is observed, and therefore, the above rule states that the minimum P_e is reached maximizing the a posteriori probability and it is known as the maximum a posteriori probability (MAP) criterion. When all the prior probabilities are equal, MAP criterion becomes the maximum likelihood decision rule in (4.15).

$$p(\mathbf{x} | \mathcal{H}_k) > p(\mathbf{x} | \mathcal{H}_i) \quad i \neq k \quad (4.15)$$

4.3.2 Composite Hypothesis Testing

Both the Neyman-Pearson theorem and likelihood decision rule trust in the complete knowledge of PDFs under the considered hypothesis. However, when realistic problems are considered, just a partial knowledge of PDFs is possible due to several unknown parameters and the direct application of these criteria is not possible. Therefore, practical detectors must consider the estimation of these parameters as part of the engineering problem, prior to their implementation. Statistical fundamentals for parameter estimation may be found in [34][35] and an extensive study of Decision Theory in [33].

The Neyman-Pearson test generalizes to the Generalized Likelihood Ratio Test (GLRT) described in the next section when some parameters required to properly define the PDFs under different hypothesis are unknown. On the other hand, the Bayesian approach test takes the form shown in (4.16), and decides hypothesis \mathcal{H}_1 as true when this expression is verified. The conditional PDF is noted as $p(\mathbf{x} | \boldsymbol{\theta}_i; \mathcal{H}_i)$ and the prior PDF as $p(\boldsymbol{\theta}_i)$.

$$\frac{p(\mathbf{x}; \mathcal{H}_1)}{p(\mathbf{x}; \mathcal{H}_o)} = \frac{\int p(x | \boldsymbol{\theta}_1; \mathcal{H}_1) p(\boldsymbol{\theta}_1) d\boldsymbol{\theta}_1}{\int p(x | \boldsymbol{\theta}_o; \mathcal{H}_o) p(\boldsymbol{\theta}_o) d\boldsymbol{\theta}_o} > \gamma \quad (4.16)$$

Besides these two general tests, some tests have been developed for the case of hypothesis having the same PDF but with different values for the unknown parameter. They are the Wald Test and the Rao Test. Both of them are claimed to achieve the same asymptotic performance as the GLRT, but their formulation is quite more complex since they require the Fisher information matrix of the estimation of the parameter vector under \mathcal{H}_1 ($\boldsymbol{\theta}_1$). Furthermore, for the case of an unknown parameter, such it is the case of a very low signal in noise, the locally most powerful (LMP) test may be a good alternative, however its derivation is even more complex, so the use of the GLRT has been preferred for our study. Some of these tests have been explored in the context of

radar in [36]-[41], and LMP has been studied in the context of cognitive radios [42], but general concepts may be extrapolated to another problems. Some adaptive versions of these detectors are compared in [40][43] and the invariance principle to achieve new more tractable detectors is applied in [38][39],[41]-[44].

4.3.3 The Generalized Likelihood Ratio Test (GLRT)

The Generalized Likelihood Ratio Test (GLRT) may be expressed as the ratio among the probabilities under the two possible hypotheses when the unknown parameters have been previously estimated using the maximum likelihood (ML) criterion such it is shown in (4.17), being the parameters vector $\hat{\boldsymbol{\theta}}_i$ the maximum likelihood estimation (MLE) of $\boldsymbol{\theta}_i$. This vector may be different under each hypothesis.

$$L_G(\mathbf{x}) = \frac{p(\mathbf{x}; \hat{\boldsymbol{\theta}}_1, \mathcal{H}_1)}{p(\mathbf{x}; \hat{\boldsymbol{\theta}}_o, \mathcal{H}_o)} > \gamma \quad (4.17)$$

In the following, a detector based on a GLRT is derived and its performance is evaluated [11][45][46].

4.3.3.1 Channel model

A pilot channel is available in DS-SS systems to perform channel estimation. In WCDMA for example, besides of CPICH, the use of the time-multiplexed pilot symbols within the dedicated traffic channel is also possible at the downlink. The use of CPICH has the advantage that this channel is transmitted with a higher power, and that all the symbols in a frame may be used instead of a few ones as in the case of the dedicated traffic channel. Of course, the received signal has been previously descramble/dispersing in order to use the pilot symbols for channel estimation. The estimated channel $\hat{\mathbf{h}}$ is dependent of the time and selected lag, and is modeled as an N_s -sized vector, containing one component per receiving antenna as it is seen in (4.18), being the noise, \mathbf{n} modeling mainly the thermal noise plus the interferences, which are dominant at the receiver in a well calibrated communication system.

$$\begin{aligned} \hat{\mathbf{h}}(\tau_i; t) &= \mathbf{w}_{\tau_i}(t) + \mathbf{n}(t) \\ \hat{\mathbf{h}}(\tau_i; t) &= [h_o(\tau_i; t), h_1(\tau_i; t), \dots, h_{N_s}(\tau_i; t)]^T \end{aligned} \quad (4.18)$$

For each delay lag τ_i , the noise \mathbf{n} is assumed to be a temporally stationary, zero mean complex Gaussian random process, temporally and spatially uncorrelated with variance equal to σ_n^2 . On the other hand, the term $\mathbf{w}_{\tau_i}(t)$ corresponds to the effective signal component, and it is modeled as a complex vector Gaussian process temporally correlated due to Doppler and that also exhibits some spatial correlation due to dispersion. As it was studied in chapter 3, the general case corresponds to a Rice propagation where the mean is not null and is related to the LOS component. However a zero mean is adequate for the NLOS model.

Let us stack the channel vector estimates in (4.18) collected along successive time intervals (slots) within the acquisition time ($T_{acq}=KT_s$) for each lag τ_i , and call this new vector \mathbf{h} , where temporal indices have been discarded:

$$\begin{aligned}\mathbf{h} &= \mathbf{h}_{\tau_i}(t) = \left[\hat{\mathbf{h}}(\tau_i; t)^T \quad \hat{\mathbf{h}}(\tau_i; t + T_s)^T \quad \dots \quad \hat{\mathbf{h}}(\tau_i; t + (K-1)T_s)^T \right]^T \\ \mathbf{h} &\rightarrow CN(\boldsymbol{\mu}, \mathbf{R}_h) \\ \mathbf{n} &\rightarrow CN(\mathbf{0}, \sigma_n^2 \mathbf{I})\end{aligned}\tag{4.19}$$

Where, T_s corresponds to the time interval between two consecutive estimations and K is the number of available estimates. The channel vector correlation matrix from estimates \mathbf{R}_h may be expressed as in (4.20) and the mean value vector $\boldsymbol{\mu}$ as described in (4.21):

$$\mathbf{R}_h = E\{\mathbf{h}\mathbf{h}^H\} = \mathbf{R}_\phi \otimes \mathbf{T}_k + \sigma_n^2 \mathbf{I}_{KN_s}\tag{4.20}$$

\mathbf{R}_h includes the temporal and spatial effects due to Doppler and dispersion, being \mathbf{T}_k the temporal correlation matrix for each component of $\mathbf{w}_{\tau_i}(t)$, and \mathbf{R}_ϕ the matrix containing the correlation factors among sensors, as it was explained at chapter 3 [47][48]. Moreover, \otimes refers to the Kronecker product operator. Note that this model implicitly includes a possible LOS component in the estimated channel as a rank-one term in the correlation matrix. The mean vector $\boldsymbol{\mu}$ is described as:

$$\boldsymbol{\mu} = \mathbf{b}_\phi(\rho) \otimes \boldsymbol{\alpha}_t(\alpha)\tag{4.21}$$

Being the spatial signature for the LOS component \mathbf{b}_ϕ , and the expected Doppler vector $\boldsymbol{\alpha}_t$, described respectively by expressions (3.35) and (3.36) of the chapter 3.

4.3.3.2 Deriving a GLRT Detector

Due to multipath, several signals arrive to the receiver, and in order to get the best of them from the viewpoint of the positioning application, they must be properly detected. With the goal of estimating the first arrived path, the channel estimates filter along the observation time are computed and arranged onto the matrix $\mathbf{X}(\tau_i)$. From the observed data for the considered lag, two conjectures are possible: just noise is present (hypothesis \mathcal{H}_0) or signal plus noise is present (alternative \mathcal{H}_1).

$$\begin{aligned}\mathcal{H}_0: \quad \mathbf{X}(\tau_i) &= \mathbf{N} \\ \mathcal{H}_1: \quad \mathbf{X}(\tau_i) &= \mathbf{H}(\tau_i)\end{aligned}\tag{4.22}$$

\mathbf{X} , \mathbf{N} and \mathbf{H} matrices have $m = K/p$ columns and pN_s rows (corresponding to p consecutive estimates over N_s sensors), and they result from rearranging observed data and channel estimates as in (4.23) and (4.24) respectively.

$$\mathbf{X}^T(\tau_i) = \begin{bmatrix} \mathbf{x}_{\tau_i}^T(n) & \mathbf{x}_{\tau_i}^T(n-1) & \cdots & \mathbf{x}_{\tau_i}^T(n-p+1) \\ \mathbf{x}_{\tau_i}^T(n+p) & \mathbf{x}_{\tau_i}^T(n+p-1) & \cdots & \mathbf{x}_{\tau_i}^T(n+1) \\ \vdots & \vdots & \ddots & \vdots \\ \mathbf{x}_{\tau_i}^T(n+K-p) & \mathbf{x}_{\tau_i}^T(n+K-p-1) & \cdots & \mathbf{x}_{\tau_i}^T(n+K-2p+1) \end{bmatrix} \quad (4.23)$$

$$\mathbf{H}^T(\tau_i) = \begin{bmatrix} \hat{\mathbf{h}}_{\tau_i}^T(n) & \hat{\mathbf{h}}_{\tau_i}^T(n-1) & \cdots & \hat{\mathbf{h}}_{\tau_i}^T(n-p+1) \\ \hat{\mathbf{h}}_{\tau_i}^T(n+p) & \hat{\mathbf{h}}_{\tau_i}^T(n+p-1) & \cdots & \hat{\mathbf{h}}_{\tau_i}^T(n+1) \\ \vdots & \vdots & \ddots & \vdots \\ \hat{\mathbf{h}}_{\tau_i}^T(n+K-p) & \hat{\mathbf{h}}_{\tau_i}^T(n+K-p-1) & \cdots & \hat{\mathbf{h}}_{\tau_i}^T(n+K-2p+1) \end{bmatrix} \quad (4.24)$$

Using the above definitions, it may be easily verified that the channel vector correlation matrix is expressed as in (4.25), and it may be estimated as in (4.26):

$$\mathbf{R}_h = E\{\mathbf{h}\mathbf{h}^H\} \quad (4.25)$$

$$\hat{\mathbf{R}}_h = \frac{p}{K} \mathbf{H}\mathbf{H}^H \quad (4.26)$$

Parameter p determines the size of the temporal correlation matrix \mathbf{T}_k and effectively defines the duration of the temporal correlation function. Therefore, the averaging is performed over the number of rows K/p , whose value has to be chosen to verify that it is higher than pN_s , to obtain a statistically significant matrix estimate. Note that when a LOS signal with a Doppler term is present, channel evolution is slow due to the high correlation among consecutive estimates, and the necessary limitation in the value of p may impair the detector.

Since the PDFs for the observed data under both hypotheses are well defined in (4.19), and assuming that secondary data is available for noise variance estimation, the Generalized Likelihood Ratio Test (GLRT) in (4.17) becomes (4.27), and it decides the alternative hypothesis \mathcal{H}_1 when the likelihood ratio $L(\mathbf{X})$ exceeds a threshold γ , maximizing in this way the detection probability for a given false alarm probability. Once the threshold has been selected, the GLRT detector provides a constant false alarm rate (CFAR). The threshold is chosen to provide the specified CFAR. This topic is discussed with more details in the next section.

$$L(\mathbf{X}(\tau_i)) = \frac{p(\mathbf{X}(\tau_i); \hat{\mathbf{R}}_h, \mathcal{H}_1)}{p(\mathbf{X}(\tau_i); \hat{\sigma}_n^2 \mathbf{I}, \mathcal{H}_0)} > \gamma \quad (4.27)$$

The PDFs required in (4.27) take the form in (4.28):

$$\begin{aligned}
p(\mathbf{X}(\tau_i); \hat{\mathbf{R}}_h, \mathcal{H}_1) &= \frac{\exp[-tr(\mathbf{X}^H \mathbf{R}_h^{-1} \mathbf{X})]}{\pi^{KN_s} \det(\mathbf{R}_h)} = \frac{\exp[-tr(\mathbf{R}_h^{-1} \mathbf{X} \mathbf{X}^H)]}{\pi^{KN_s} \det(\mathbf{R}_h)} \\
p(\mathbf{X}(\tau_i); \hat{\sigma}_n^2 \mathbf{I}, \mathcal{H}_0) &= \frac{\exp\left[-\frac{1}{m\hat{\sigma}_n^2} tr(\mathbf{X} \mathbf{X}^H)\right]}{\pi^{KN_s} (m\hat{\sigma}_n^2)^{pN_s}}
\end{aligned} \tag{4.28}$$

Where $m=K/p$ corresponds to the number of columns in \mathbf{X} matrix. Furthermore, it may be found that the ML estimates for channel vector correlation matrix and the noise variance correspond to the expressions shown in (4.29):

$$\begin{aligned}
\hat{\mathbf{R}}_h &= \frac{1}{m} \mathbf{X} \mathbf{X}^H \\
\hat{\sigma}_n^2 &= \frac{1}{N_{sd}} \mathbf{x}^H \mathbf{x}
\end{aligned} \tag{4.29}$$

N_{sd} in the expression (4.29) corresponds to the length of the secondary data vector \mathbf{x} , used for noise variance estimation; and they may be taken from the output of the matched filter for a lag beyond the timing window where data is extracted to perform the test. For example, in the simulated case at section 2 of this chapter, delay spread takes values mainly between two and three times the chip time, but it extends up to 5-6 chips in certain cases. Therefore a proper lag could well be found 7 chip times after the most powerful arrival has been detected. N_{sd} should be chosen large enough to avoid that detector performance degrades, and therefore it may be set equal to the number of observed slots within the acquisition time due to this value is generally adequate.

Inserting PDF's expressions from (4.28) into (4.27), being the unknown parameters replaced by their estimates, and after some simplifications the log-likelihood ratio takes the form shown in (4.30), and finally inserting the expression for the vector correlation matrix estimation from (4.29), discarding the constants, and rearranging some terms, the likelihood function becomes (4.31).

$$\begin{aligned}
\ln[L(\mathbf{X}(\tau_i))] &= -KN_s + pN_s \ln(m\hat{\sigma}_n^2) + \frac{1}{m\hat{\sigma}_n^2} tr[\mathbf{X}(\tau_i) \mathbf{X}(\tau_i)^H] \\
&\quad - \ln[\det(\hat{\mathbf{R}}_h)] > \ln(\gamma)
\end{aligned} \tag{4.30}$$

$$L(\mathbf{X}(\tau_i)) = \frac{1}{\hat{\sigma}_n^2} tr(\mathbf{X}(\tau_i) \mathbf{X}(\tau_i)^H) - m \ln[\det(\mathbf{X}(\tau_i) \mathbf{X}(\tau_i)^H)] > \gamma' \tag{4.31}$$

Above expression corresponds to the GLRT detector, which is an incoherent squared combining of all the time-space estimates of the channel, and hence depends on the process power, and it is affected by a term which depends on the spatio-temporal power distribution, since $\mathbf{X}(\tau_i) \mathbf{X}(\tau_i)^H$ is a scaled estimation of the channel vector correlation matrix as defined in equation (4.29), when alternative H_1 is true. This test should be applied over each τ_i within a certain timing window so as to assess the instant

of the first arrival. In the sequel, and for simplicity of notation, the term τ_i will be removed from equations.

The value of the threshold is related to the probability of false alarm due to this detector is CFAR. It will be shown in the following how the threshold is chosen and how much critical it is with respect to the RMS error on the estimated time of arrival.

4.3.3.3 False alarm and detection probabilities

In the following, some foundations for false alarm and detection probabilities for the GLRT detector in (4.31) are derived. Firstly, let the correlation matrix for the observed data be expressed in terms of its eigenvalues $\hat{\lambda}_i$ as in (4.32):

$$\begin{aligned} \text{tr}(\mathbf{X}^H \mathbf{X}) &= \text{tr}(m \hat{\mathbf{R}}_x) = \sum_{i=1}^{pN_s} m \hat{\lambda}_i \\ \det(\mathbf{X}^H \mathbf{X}) &= \det(m \hat{\mathbf{R}}_x) = m^{pN_s} \prod_{i=1}^{pN_s} \hat{\lambda}_i \end{aligned} \quad (4.32)$$

Therefore, the likelihood function $L(\mathbf{X})$ in (4.31) becomes $L(\mathbf{\Lambda})$, in terms of the eigenvalues as in (4.33).

$$L(\mathbf{\Lambda}) = m \sum_{i=1}^{pN_s} \left[\frac{\hat{\lambda}_i}{\hat{\sigma}_n^2} - \ln(m \hat{\lambda}_i) \right] \quad (4.33)$$

In order to compute false alarm and detection probabilities, and reminding that eigenvalues from random matrices are also random, it is convenient to take an insight into their statistical properties.

First of all, note that the estimated correlation matrix for the observed data follows a complex Wishart distribution noted as $\tilde{W}(pN_s, m)$, since it is computed as the product of a complex Gaussian matrix $\mathbf{X}(pN_s, m)$ (with elements distributed as in (4.19)) by its hermitian. Random matrices have relevant properties proved in [49]:

Property 1: The joint density $f_{\mathbf{\Lambda}}$ of the eigenvalues $\lambda_1 \geq \dots \geq \lambda_r$ of a Wishart hermitian random matrix $\tilde{W}(r, s)$ takes the form :

$$f_{\mathbf{\Lambda}}(\mathbf{\Lambda}) = \frac{2^{-rs} \pi^{r(r-1)}}{\tilde{\Gamma}_r(s) \tilde{\Gamma}_r(r)} \exp\left(-\frac{1}{2} \sum_{i=1}^r \lambda_i\right) \prod_{i=1}^r \lambda_i^{s-r} \prod_{i < j}^r (\lambda_i - \lambda_j)^2 \quad (4.34)$$

where the complex multivariate gamma function above is defined as:

$$\begin{aligned} \tilde{\Gamma}_r(a) &= \pi^{r(r-1)/2} \prod_{i=1}^r \Gamma(a - i + 1) \\ \text{with } \Gamma(n) &= (n-1)! \end{aligned} \quad (4.35)$$

Property 2: The pdf of the smallest eigenvalue of a matrix from $\tilde{W}(r, s)$ is $c_{r,s} \lambda^{s-r} e^{-\lambda r/2} P_{r,s}(\lambda)$, where $c_{r,s}$ is a constant, and $P_{r,s}(\lambda)$ is a polynomial of degree is $(s-r)(r-1)$.

Property 3: If m and n tend to infinity in such a way that r/s tends to a limit: $y \in [0, 1]$, then λ_{\max} for $\tilde{W}(r, s)$ satisfies (4.36):

$$\frac{1}{s} \lambda_{\max} \rightarrow \sigma_n^2 (1 + \sqrt{y})^2 \quad (4.36)$$

Property 4: If m and n tend to infinity in such a way that r/s tends to a limit: $y \in [0, 1]$, then λ_{\min} for $\tilde{W}(r, s)$ satisfies (4.37):

$$\frac{1}{s} \lambda_{\min} \rightarrow \sigma_n^2 (1 - \sqrt{y})^2 \quad (4.37)$$

Property 5: For a matrix from $\tilde{W}(r, s)$ the determinant has the distribution of a product of chi-squared random variables : $\chi_{2s}^2 \chi_{2(s-1)}^2 \cdots \chi_{2(s-r+1)}^2$, and therefore the expected value for the determinant is $2^s \frac{r!}{(s-r)!}$.

Therefore, eigenvalues from the noise correlation matrix required to evaluate (4.33), are also random variables. The histogram of these eigenvalues using 10000 realizations to describe their PDFs when the null hypothesis is true, have been plotted on Figure 4.9 and Figure 4.10 for different sizes of the observed matrix. These two figures exhibit the probability functions computed from previously ordered eigenvalues, and compare them with the non-ordered distributions. It is clear from these results that each eigenvalue has its own distribution, which changes when the observation matrix modifies its size as predicted by property 2. Furthermore, they also differ from the non-ordered eigenvalues distributions. However the dynamic range of the eigenvalues dispersion may be estimated from properties 3 and 4. For example, in the case illustrated on Figure 4.9b, eigenvalues should belong to the interval (0.59; 1.52) as predicted from these properties, whilst for the case on Figure 4.10a, the interval would change to (0.40; 1.86). These values are quite close to those exhibited by the distributions achieved with the whole set of the matrix eigenvalues.

Moreover, (4.34) provides a closed but very complex expression for the joint eigenvalue density of a Wishart matrix, and although it is theoretically possible studying the problems of false alarm and detection for our GLRT detector with the help of this expression, as shown in (4.38) and (4.39) respectively, it is a task that goes beyond the scope of this research due the complexity of the statistics in (4.34), and the nonlinear form within (4.33).

$$P_{fa} = \int_{R \subset \Lambda / L(\Lambda) > \gamma | \mathcal{Z}_0} f_{\Lambda}(\Lambda) d\Lambda \quad (4.38)$$

$$P_D = \int_{R \subset \Lambda / L(\Lambda) > \gamma | \mathcal{Z}_1} f_{\Lambda}(\Lambda) d\Lambda \quad (4.39)$$

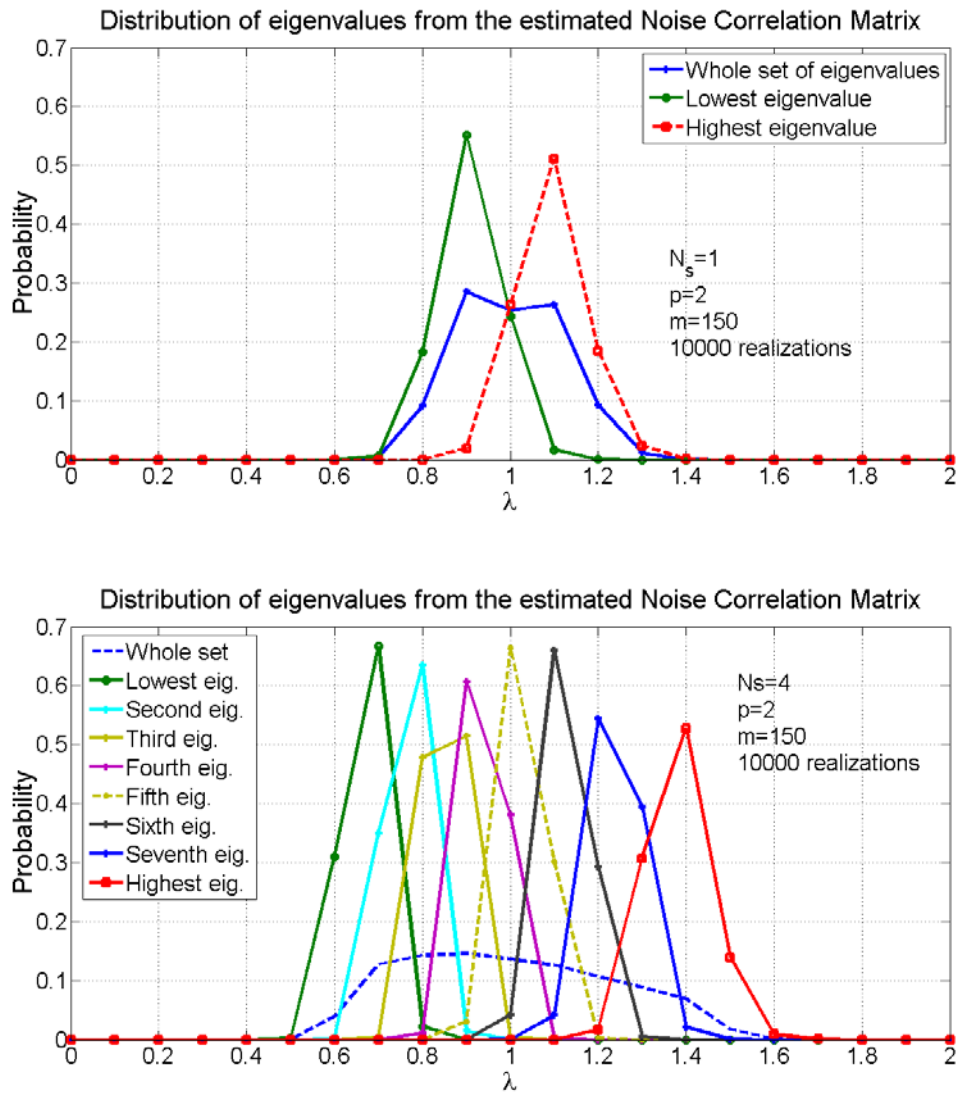


Figure 4.8: Probability Density Functions for the eigenvalues from the estimated data correlation matrix, in case of the null hypothesis is true, for different sizes of the observation matrix X. Top: $p=2$ slots, $N_s=1$ sensor, $m=150$; Bottom: $p=2$ slots, $N_s=4$ sensors, $m=150$.

However, under some assumptions and with the help of above properties, it is still possible to extract some conclusions. For example, when the average eigenvalues in Table 4.1 are replaced within (4.33), it is possible to infer a value near to whom the threshold should be set. Furthermore, with independence of the kind of source: noise or

a highly correlated source due to LOS propagation, it is easy to recognize that the matrix trace in the first term of (4.31) tends to the same value of $KN_s \sigma_n^2$ in both cases, whilst the matrix determinant certainty regulates when $L(\mathbf{X})$ is higher or above the threshold. When signal is present, the determinant is lower than one, and this second term increases rapidly. On the contrary, when we just have noise, this term could be positive or negative in relation with the specific eigenvalues of the realization. Therefore, by discarding all eigenvalues but the minimum from this latter term, we achieve a bound near to whom the threshold should be set, as it is shown in (4.40).

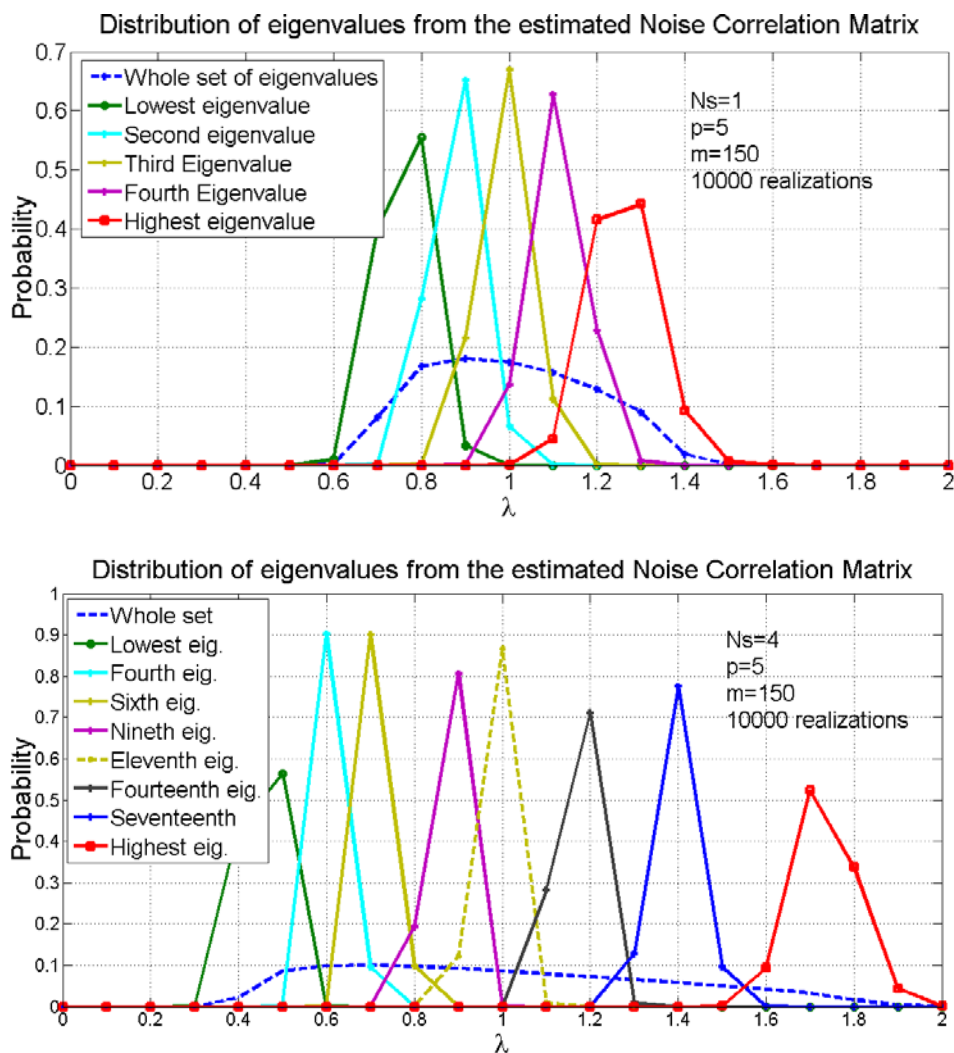


Figure 4.9: Probability density functions for the eigenvalues from the estimated data correlation matrix, in case of the null hypothesis is true, for different sizes of the observation matrix \mathbf{X} : a) Top: $p=5$ slots, $N_s=1$ sensor, $m=150$; Bottom: $p=5$ slots, $N_s=4$ sensors, $m=150$.

$$KN_s < \gamma < KN_s - \frac{m \ln(\hat{\lambda}_{\min})}{\hat{\sigma}_n^2} \quad (4.40)$$

For example, if we have $K=750$ estimates, just one sensor so $N_s=1$; and we set $p=15$; therefore $m=K/p=50$ and the estimated correlation matrix is $\tilde{W}(15,50)$. Moreover $y=15/50=0.3$, and minimum eigenvalue as provided by property 4 takes a value of $0.409\sigma_n^2$. Therefore, the threshold should be located between 750 and 794.7 when σ_n^2 is one. On the other side, when detector configuration changes to $N_s=4$, $p=5$, and $m=150$, the threshold should be located between 3000 and 3136.3 as predicted by (4.40).

Table 4.2: Parameters associated to the eigenvalues' distributions of the estimated Correlation Matrix from observations, when null hypothesis is true for different configurations. 10^4 simulations have been performed to compute these moments.

pN_s	K	$E\{\lambda_i\}$	σ_i	σ_Σ	σ_T
2	150	0.908, 1.09	0.0656, 0.0734	0.0576	0.0577
8	150	0.669, 0.765, 0.852, 0.939, 1.03, 1.13, 1.24, 1.38	0.0408, 0.0382, 0.0382, 0.0339, 0.0425, 0.0462, 0.0528, 0.0663	0.0290	0.0289
5	150	0.761, 0.878, 0.989, 1.10, 1.26	0.0484, 0.0468, 0.0494, 0.0555, 0.0683	0.0369	0.0365
20	150	0.454, 0.515, 0.568, 0.619, 0.669, 0.719, 0.769, 0.820, 0.873, 0.928, 0.984, 1.04, 1.11, 1.17, 1.24, 1.31, 1.40, 1.49, 1.59, 1.73	0.0267, 0.0244, 0.0239, 0.0237, 0.0239, 0.0243, 0.0253, 0.0257, 0.0269, 0.0281, 0.0290, 0.0303, 0.0313, 0.0335, 0.0353, 0.0382, 0.0408, 0.0449, 0.0516, 0.06502	0.0183	0.0183

It is easy to show as the trace of the estimated correlation matrix is chi-squared distributed with $2N_s K$ grades of freedom since the trace may be expressed as the sum of the square norm of the $N_s K$ elements in the observation matrix. On the other hand, the determinant of this matrix may be considered as the product of $N_s p$ chi-squared random variables as it is described by property 5 commented above. Therefore the likelihood ratio in (4.31) admits the form in (4.41):

$$L = \frac{1}{\hat{\sigma}_n^2} \chi_{2N_s K}^2 - \ln \left[\chi_{2m}^2 \chi_{2(m-1)}^2 \cdots \chi_{2(m-pN_s+1)}^2 \right] > \gamma \quad (4.41)$$

The difficult to derive theoretical expressions for false alarm probability from (4.41) comes from that natural logarithm is a non-linear function. An attempt to achieve approximate expressions after the linearization of the logarithm may be bound at Annex 4.2 [45]. However, results are poor when they are compared to Monte Carlo simulations

in Figure 4.11 and Figure 4.12. These simulations have been performed by using $K=750$ estimates for each realization, and 10^6 realizations for each different configuration of the detector.

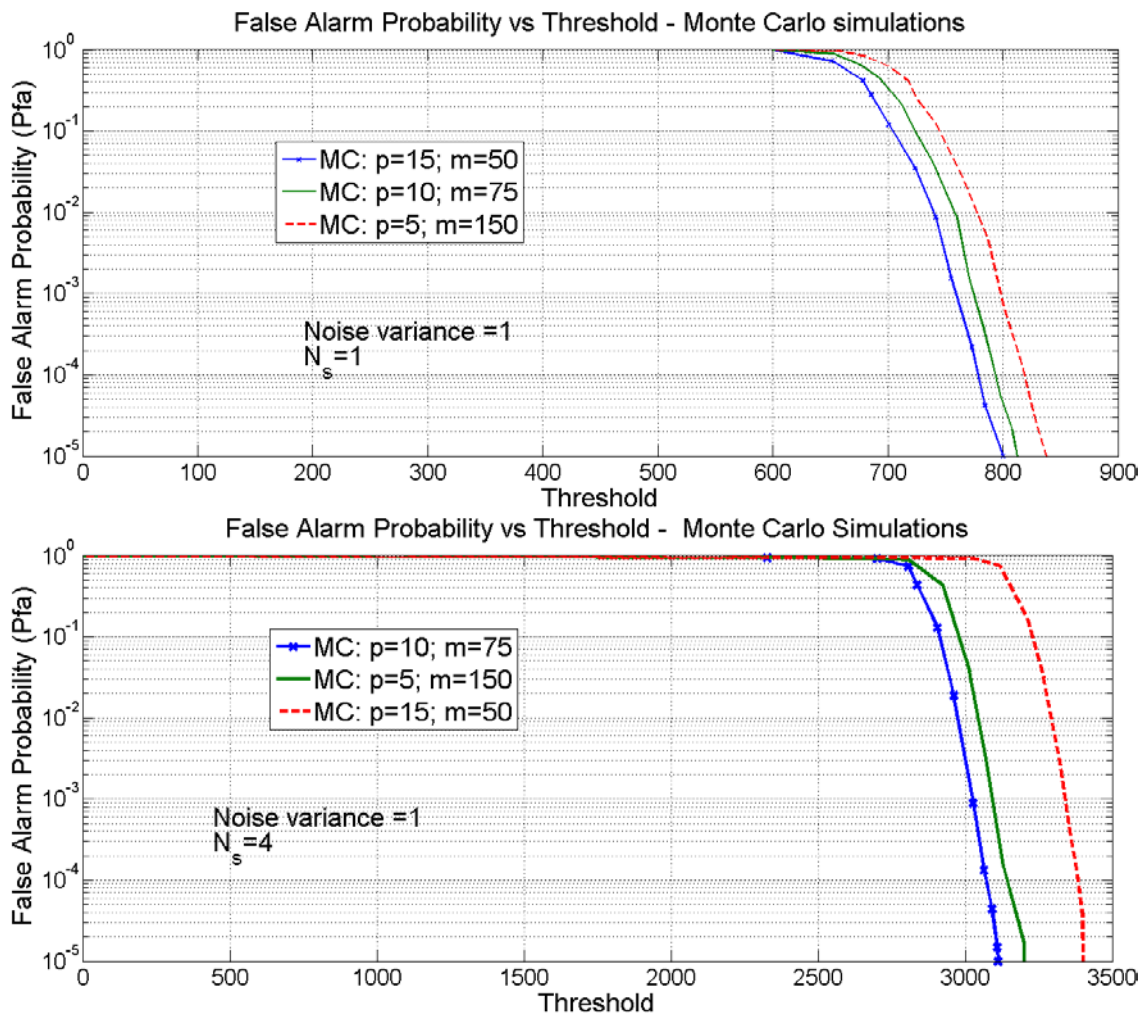


Figure 4.10: False alarm characteristics for different configurations of the unstructured GLRT detector. Monte Carlo simulations are compared for one (top) and four sensors (bottom).

These results show as false alarm changes in relation to the configuration of the detector. In general, a higher threshold is required to keep false alarm constant when the size of the estimated correlation matrix (p) decreases, although in this case m increases since $K=mp$ remains constant. When the number of sensors increases, the size of the detector is scaled by N_s as predicted by (4.40), and the threshold displaces approximately in the same relation, but since the curve slope is steeper, some gain is achieved. Note for example that a false alarm probability of 10^{-5} is achieved when

threshold is set to 810 for a detector with $N_s=1$, $p=10$, $m=75$; whilst the same false alarm is achieved for a threshold of 3200 when the number of sensors increases to $N_s=4$. It means that a much more reduced false alarm probability would be achieved if we set this detector to the scaled threshold of 3240.

Furthermore, a non-typical behavior is shown for the detector when $N_s=4$, $p=15$, $m=50$. It is due that in this case the relation $y=pN_s/m$ is higher than one, and property 3 is not kept anymore. Therefore, this latter relation should be maintained below to one during the signal detection procedure to minimize the false alarm.

Figure 4.12 shows the effect of using a small number of slots to perform the noise variance estimation. It can be seen that false alarm characteristic degrades rapidly in terms of the record length used to estimate this variance. For example, when $N_s=1$, $p=15$, $m=50$, and the threshold is set to 800, false alarm passes from 10^{-5} in case of a perfect knowledge of the noise variance to 10^{-1} if 100 slots have been used to estimate its value. It means that a much larger record of noise is required to keep the good properties of our GLRT detector in terms of the false alarm probability. However, it is still possible by using a larger observation window, and extracting samples from multiple lags beyond 7 chip times of the most powerful arrival; let's say, for example lags from 7 to 10.

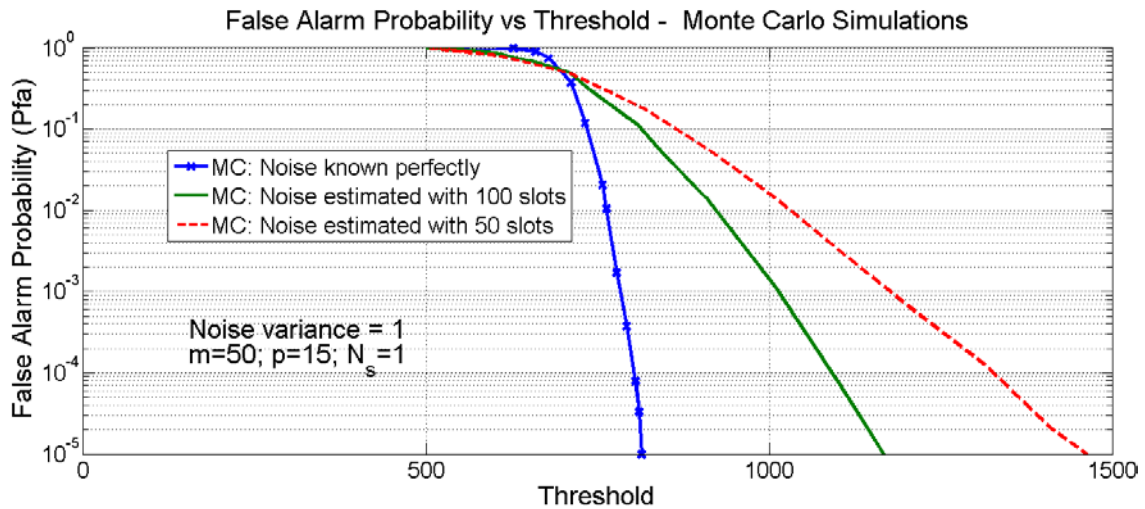


Figure 4.11: False Alarm Characteristics for different values of the secondary record length (N_{sd}) used for the noise variance estimation required in (4.31). $p=15$ slots, $m=50$, and one available sensor. $N_{sd} \rightarrow \infty$, and then it degrades to 100 slots and to 50 slots.

4.3.3.4 A simplified model for detectability in a coarse timing estimator

In order to determine the threshold for low false alarm probabilities, we have to bear in mind that the objective is to have accurate positioning and therefore, false alarm and detection probabilities have to be related to error in position. In other words signal

detectability should be studied. Furthermore, it will be assumed that the first arrived path is confined within a temporal window of S samples before the RAKE receiver synchronization time, and sampling being at chip time T_c . The first path (in the sequel it will be called the LOS path) is assumed to be located randomly within this window. Path searching process as defined by (4.31) is repeated along the window until hypothesis H_1 is verified. When a new path is detected, this arrival is chosen as the first. On the other hand, if the whole window is tested and H_1 is not verified, the first arrival is missed. The size of the observation window S may be chosen taking advantage of the property that paths arrive in clusters [29]. Therefore a length of two times the delay spread may be suitable to set its length.

Mean square error of the timing estimates is a good indicator of their quality as was studied in chapter 3, and for this coarse estimation stage is related with probabilities of false alarm and detection through the probability of detecting an arrival $\hat{\tau}_o$ at lag n when the true arrival τ_o is located at lag m , noted as $\Pr(n/m)$. Moreover, ε_q is an error term which accounts for the temporal quantization of the delay axis as one sample per chip, and it is well known that for uniform quantization the error is uniformly distributed and its variance is $T_c^2/12$.

The timing error may be produced by a false detection when searching the direct path in a wrong time lag, or by missing the LOS due to an insufficient signal level. When a false detection happens, the error will be called e_f ; and when the LOS path (before the most powerful arrival to which the RAKE receiver is synchronized), is missed, it will be called e_m . Expressions for these errors are:

$$e_f = \frac{\tau_o - \tau_{RAKE} - \hat{\tau}_o}{T_c} = \frac{(mT_c + \varepsilon_q T_c) - nT_c}{T_c} = (m - n) + \varepsilon_q \quad (4.42)$$

$$e_m = \frac{\tau_o - \tau_{RAKE}}{T_c} = m + \varepsilon_q$$

From a Bayesian perspective, the mean squared error is the weighed sum of these two possible disjoint cases, along the whole searching window, as it is shown in (4.43):

$$E\{e^2\} = \sum_{m=1}^S \Pr(m) \left[p_{miss} E\{e_m^2\} + \sum_{\substack{n=1 \\ n \neq m}}^S \Pr(n|m) E\{e_f^2\} \right] \quad (4.43)$$

Where, $\Pr(m)$ denotes the probability that the first arrival is found within the m -cell; and p_{miss} refers to the probability of missing the first arrival during the detection procedure. Since the missing also implies that all the S cells have been tested and no false alarm has been produced, (4.43) becomes (4.44):

$$E\{e^2\} = \sum_{m=1}^S \frac{1}{S} \left[(1-P_D)(1-P_{fa})^{S-1} E\{e_m^2\} + \sum_{\substack{n=1 \\ n \neq m}}^S \Pr(n|m) E\{e_f^2\} \right] \quad (4.44)$$

Where, P_{fa} and P_D refers to the false alarm and detection probabilities as defined respectively in (4.38) and (4.39). Both false alarm and detection probabilities have been computed from simulations by evaluating (4.31) and have been extracted from Figure 4.11 and Figure 4.12. Inserting (4.42) in (4.44), and discarding null terms (4.45) results:

$$E\{e^2\} = \sum_{m=1}^S \frac{1}{S} \left\{ (1-P_D)(1-P_{fa})^{S-1} (m^2 + E\{e_q^2\}) + \sum_{\substack{n=1 \\ n \neq m}}^S p(n|m) ((m-n)^2 + E\{e_q^2\}) \right\} \quad (4.45)$$

Rearranging terms and after some simplifications, variances for timing estimates may be computed as in (4.46):

$$E\{e^2\} = \frac{1}{S} \sum_{m=1}^S \sum_{\substack{n=1 \\ n \neq m}}^S p(n|m) (m-n)^2 + (1-P_{fa})^{S-1} (1-P_D) \sum_{n=1}^S n^2 + E\{e_q^2\} \quad (4.46)$$

where $p(n|m)$ is computed as in (4.47):

$$p(n|m) = p(\hat{\tau}_o = nT_c | \tau_o = mT_c + \varepsilon_q T_c) = \begin{cases} P_{fa} (1-P_{fa})^{n-1} & n < m \\ P_D (1-P_{fa})^{n-1} & n = m \\ P_{fa} (1-P_{fa})^{n-2} (1-P_D) & n > m \end{cases} \quad (4.47)$$

with $\varepsilon_q \in [-1/2, 1/2]$

On the other hand, and following an analogue procedure, an expression for bias results in (4.48):

$$E\{e\} = \frac{1}{S} \sum_{m=1}^S \sum_{n=1}^S p(n|m) (m-n) + (1-P_{fa})^{S-1} (1-P_D) S \frac{(S+1)}{2} \quad (4.48)$$

However, this expression does not provide any relevant additional information, and just (4.46) will be used for the simulations.

Results from coarse timing estimation

In order to determine the performance of the detection scheme, a signal with spatial correlation between sensors has been generated using the angular distributed source model proposed in [48] as it was explained in chapter 3. The case of correlated sensors corresponds to an angular spread of 5 degrees and a mean direction of arrival of zero. A direct LOS path has been included, corresponding to a mean term in the

estimated impulse response. Its Doppler frequency assumes a mobile speed of 50 [km/h] arriving from broadside, where sensors are linearly and uniformly spaced.

Temporal correlation due to Doppler has been simulated using a first order AR process with correlation coefficients of 0.1 and 0.999. Channel estimates for the lag (cell) under test are provided to detector and arranged in matrix \mathbf{X} as described in section 4.3.3.2, with 100 or 50 columns by $p=15$ rows, as specified within Figure 4.13 to Figure 4.15. 10^5 Monte Carlo realizations were provided to evaluate detection probability and 10^6 to evaluate false alarm. Furthermore, S has been set to 5 chip times (cells) for simulations in this section. This value is suitable for signal with delay spreads between 1.5 and 3 chip times.

Figure 4.13 infers the behavior of GLRT detector using the proposed model when one sensor is available at the receiver for two different configurations: the first one uses $K=750$ slots arranged in $p=15$ rows and $m=50$ columns; whilst the second one doubles the number of slots and arranges the matrix in $p=10$ rows and $m=150$ columns. These configurations are tested for different scenarios in terms of the dispersed-signal to noise ratio, and for different power relations between the first arrival and the dispersed signal used by the RAKE receiver. These results show that even with just one sensor and a poor SNR of 0 dB, the best possible accuracy is achieved when the threshold is set to get a false alarm of around 10^{-3} when the first arrival is at the same level that the scattered signal used by the RAKE receiver. Of course, a strong degradation is suffered when this SNR reduces below the noise level, and a much better behavior is registered when SNR is higher. In fact, our results show that when the scattered SNR reaches the 3 [dB], first arrival is always detected if it holds to the scattered signal level, therefore the estimation error for these cases is just due to the quantization. It is interesting to note as the second configuration is more robust than the first, providing lower errors for the same false alarm due to a larger available data record. The graph at the bottom of Figure 4.13 also includes the case when the LOS component is removed, and just the null mean NLOS component remains. The minimum of the curve displaces to a point related to a lower threshold relating to a higher false alarm of around 10^{-2} for this case. Furthermore, due to the fact that the error characteristic exhibits a minimum, some prior signal knowledge is worth to select threshold. In practice, however, there is little chance that this knowledge is available, and once the threshold is set from the characteristics described in (4.39), paths arriving with a lower SNR will not be detected.

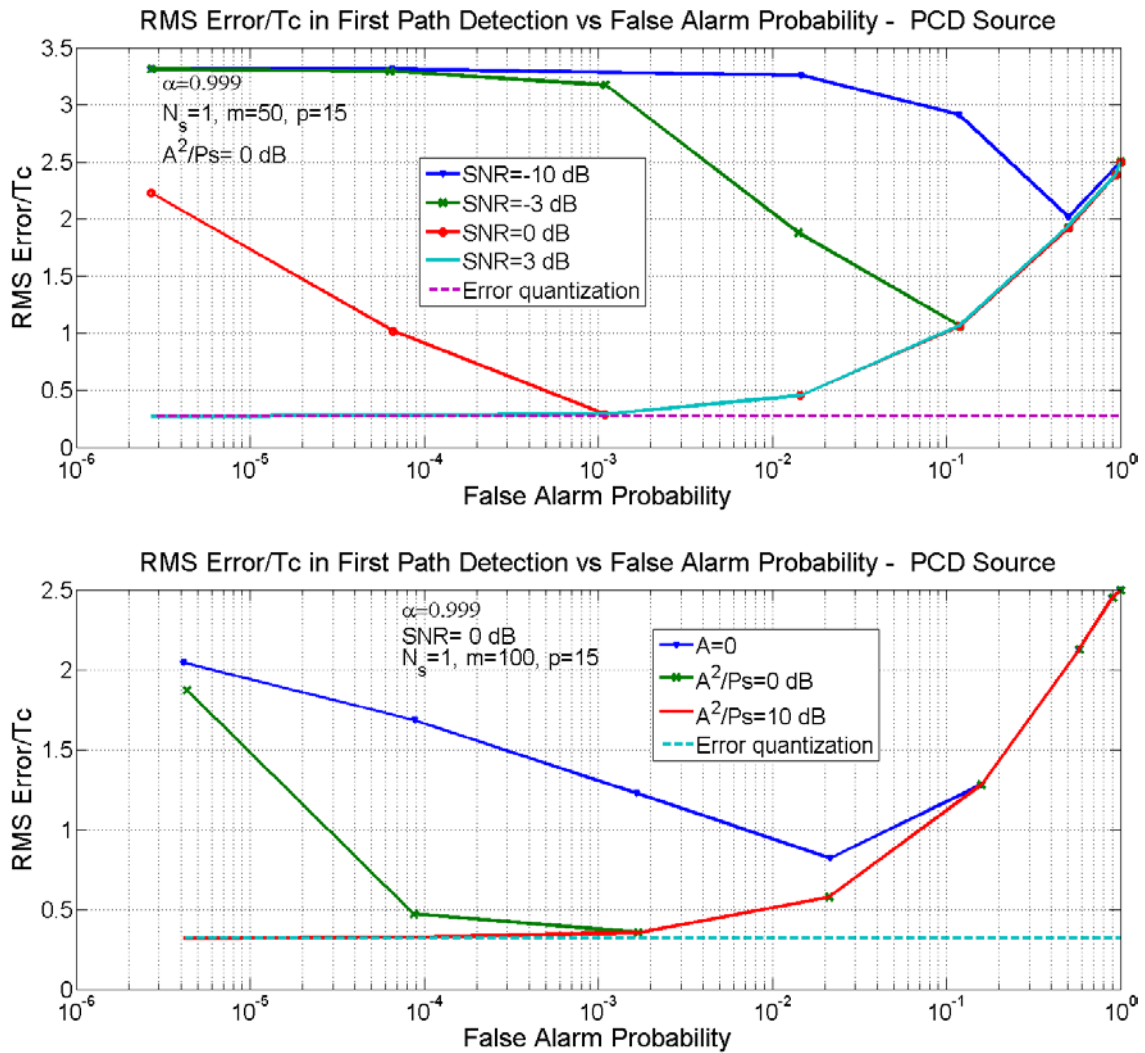


Figure 4.12: First arrival detection error as a function of P_{fa} when one sensor is available and for a highly correlated source case. a) Top: SNR changes, $p=15$ and $m=50$ columns. b) Bottom: SNR holds but ratio between the direct path and the scattered power within the considered lag changes, $p=15$ slots and $K=100$.

Figure 4.14 reveals the positive effects of adding more sensors to the detector, and shows that the presence of more sensors allows an even wider range of optimum thresholds values, and that weaker arrivals can be detected. Note from the graph at the top as the minimum is achieved for a false alarm threshold of 10^{-3} , and how it reduces near to 10^{-4} when two spatially uncorrelated sensors or instead four correlated sensors are available. Furthermore, when these sensors are spatially correlated just a slight degradation appears due to the perturbation of the statistics. On the other hand if SNR reduces to -3 dB such it is the case at the bottom of the figure, the minimum error improves and reduces almost to the half when four sensors are used instead of one. However, to take advantage of this behavior, a prior knowledge of signal statistics is required, since a lower threshold will force the false alarm to grow; and this risk is just justifiable with an overall improvement in the positioning application.

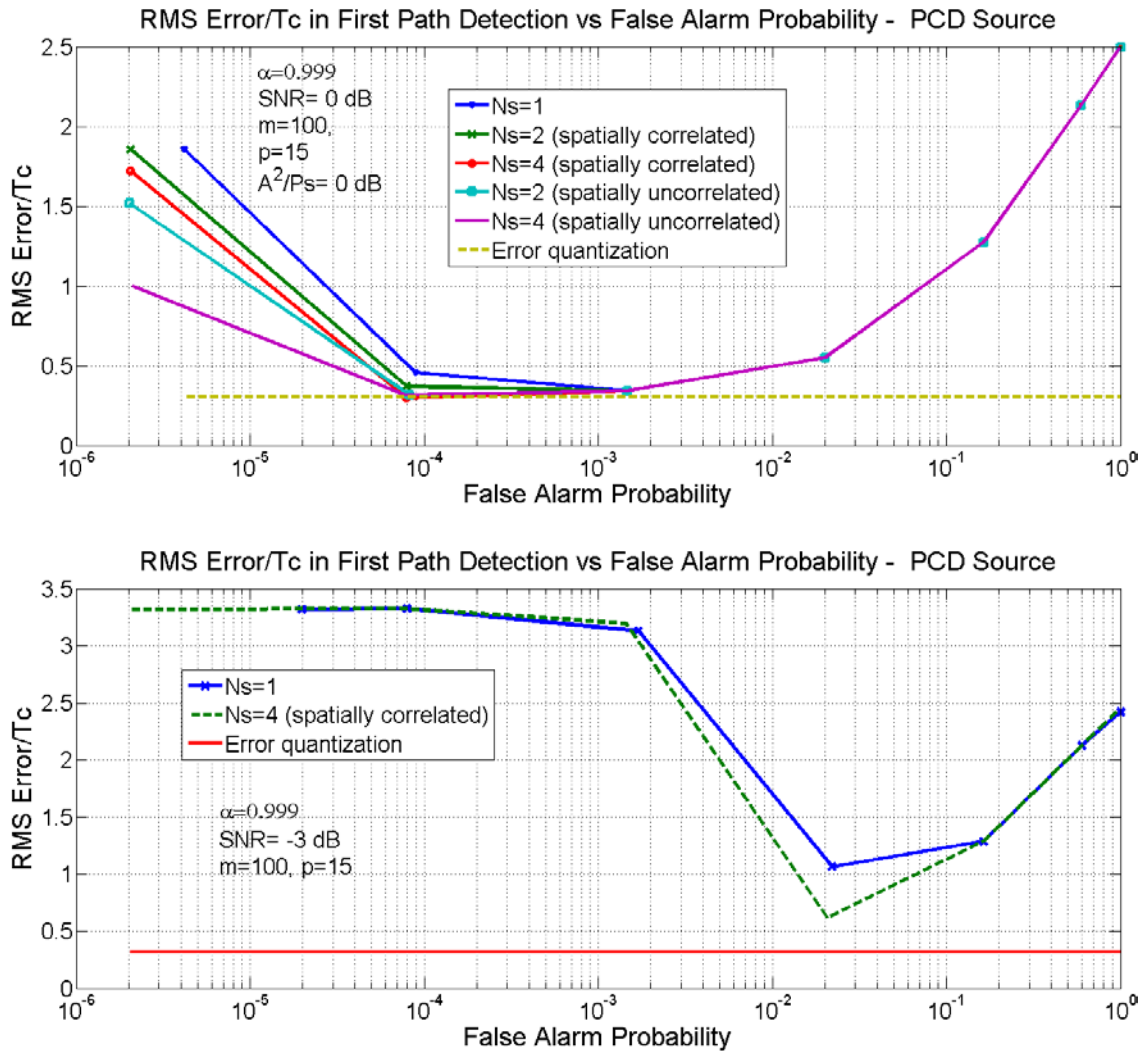


Figure 4.13: First arrival detection error as a function of P_{fa} and the number of sensors for a highly correlated source case. a) Top: SNR=0 dB, $p=15$ and $m=100$; b) Bottom: SNR= -3 dB, $p=15$ and $m=100$.

Finally, Figure 4.15 shows that increasing the data record length leads to important detection gains. It is important to remark however that the number of available estimates is limited, especially by Doppler as it was studied at the section 3.2.2 of the chapter 3, and also for system requirements according to the related positioning application.

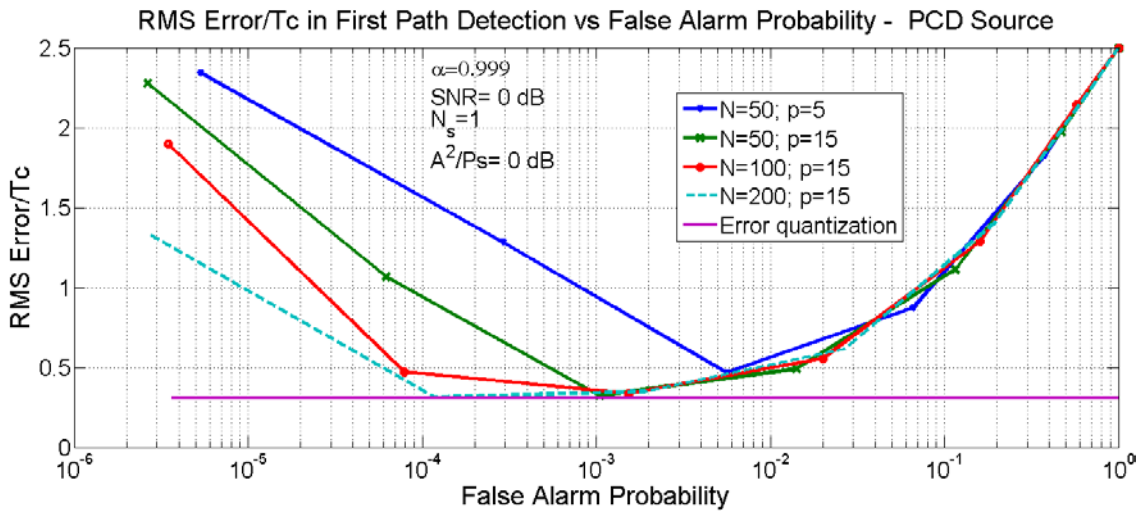


Figure 4.14: First arrival detection error as a function of P_{fa} and different detector configurations (m, p): SNR=0 dB and a direct-to-scattered power ratio of 0 dB.

4.3.3.5 Summary and Conclusions

The main observations related to coarse timing detection and GLRT detector are below:

- Chip level synchronization corresponds to a problem of signal detection, and statistical fundamentals for discriminating signal from noise has been studied in this section within the context of the proposed GLRT detector.
- Particularly, the statistical behaviour for the provided GLRT detector has been evaluated from Monte Carlo simulations for different configurations. Simulations show that similar results are achieved when arrangement dimensions change but the number of channel estimates is kept constant. On the other hand, when the number of sensors or in general when the number of available channel estimates increase, the detector performance improves.
- A simple model to relate false alarm probability and timing error has been provided to verify the impact of scattered signal no noise ratio, direct path to scattered power ratio, and the use of antenna arrays in the performance of the proposed GLRT detector. Results reveal that this detector is very sensible to SNR, and that important improvements in terms of detection probability may be achieved when adding more sensors for the case of very weak signals. Some improvement is achieved for uncorrelated sensors, but the gain in relation to correlation sensors is negligible.
- Results also show that detection improves when a direct path is present, even in the case of the total signal power is kept constant.

- The proposed GLRT detector requires the use of a threshold, and weaker arrivals will be missed. Therefore this detector should be applied after synchronization when some prior information about signal is available in order to properly set this threshold to reduce the probability to get biased timing estimations.
- Simulations show that when our GLRT detector is set to provide a false alarm probability of 10^{-3} , and a Rice component is present with the same level of the scattered signal for SNRs higher than 0 dB, the detection of the arrival is always possible. Detection error in these cases is the minimum, and corresponds to the quantization. The MSE for a quantization cell of the chip time reaches a value of $0.29T_c$. This result is important since it provides the optimum operation point for this detector and reveals that weaker signals will be missed.

4.4 High Resolution Timing and Direction of Arrival Estimation

Given the limited performance of the coarse timing estimation, this section is devoted to study the problem of high resolution estimation for both timing and Direction Of Arrival (DOA), when multiple sensors are available. High resolution timing is studied at section 4.4.1 whilst DOA estimation is briefly studied at section 4.4.2. Direction of arrival may be used as complementary information for mobile positioning, as it was discussed at chapter 2, or as a nuisance parameter to improve the estimation of timing

4.4.1 Performing High Resolution Timing Estimation

Following with the scheme on Figure 4.1 introduced at section 4.1, we will study in this section the behavior of a pair of high resolution timing estimators to achieve the best possible estimates provided to the Position Computing Function (PCF) as described in chapter 2. Therefore, our data will be a collection of N impulse response vectors infected with noise when there is a signal arrival, or simply noise when no signal is present at a certain lag. The signal model assumed for the estimated channels recorded in a time interval of duration KT_s is as follows:

$$y(\tau; n) = \sum_{i=1}^L a_i(n)g(\tau - \tau_i) + v(\tau; n); \quad n = 1, \dots, K \quad (4.49)$$

The parameters in the above expression are the delays τ_i , and the time-varying amplitudes $a_i(t)$ of the L propagation paths. $g(\tau)$ is the pulse shape of the modulation. The noise $v(\tau;n)$ that perturbs the estimated channel is assumed temporally not correlated among successive slots (n), and correlated in the lag (τ) domain due to the matched filter performed at the receiver. The K multiple channel estimates have to be obtained within the time coherence of the channel delays which is much longer than the coherence of the channel amplitudes.

If Discrete Fourier Transform (DFT) is computed from channel vector estimates, a more convenient expression shown in (4.50) is possible:

$$y(w;n) = \sum_{i=1}^L a_i(n) g(w) \exp(-jw\tau_i) + v(w;n) \quad (4.50)$$

From above expression, it is apparent that the delays' estimation problem is equivalent to the estimation of the position of spectral lines. Stacking the samples of the transformed domain in a single vector, (4.50) may be rewritten as (4.51):

$$\mathbf{y}(n) = \begin{bmatrix} y(\omega_0;n) \\ y(\omega_1;n) \\ \vdots \\ y(\omega_{M-1};n) \end{bmatrix} = \sum_{i=1}^L a_i(n) \mathbf{G} \mathbf{e}_{\tau_i} + \mathbf{v}(n) = \mathbf{G} \mathbf{E}_{\tau} \mathbf{a}(n) + \mathbf{v}(n) \quad (4.51)$$

\mathbf{G} in (4.51) is a diagonal matrix containing the DFT of the raised cosine pulse shaping filter and \mathbf{E}_{τ} is defined below.

$$\mathbf{E}_{\tau} = \begin{bmatrix} \mathbf{e}_{\tau_1} & \cdots & \mathbf{e}_{\tau_L} \end{bmatrix} \quad \mathbf{e}_{\tau_i} = \begin{bmatrix} e^{-jw_0\tau_i} & e^{-jw_1\tau_i} & \cdots & e^{-jw_p\tau_i} \end{bmatrix}^T \quad (4.52)$$

As the ML solution of the problem leads to a multidimensional search [41], a plethora of algorithms have appeared in the last thirty years to reduce the complexity to a one-dimensional problem [50]-[52], and yet achieving an asymptotic optimum behaviour. Minimum variance (MV) type algorithms [10][53][54] will be applied here in order to derive simple techniques with low implementation requirements. At the same time, they will enable the development of simple adaptive versions.

4.4.1.1 Minimum variance timing estimation

In the minimum variance solution, the reduction of the complexity is achieved by considering signals separation through filtering. In the following lines, the main operations performed over the signal with the applications of this method are summarized. Let us rewrite equation (4.51) as composed of a single path of interest plus an additional noise term $\tilde{\mathbf{v}}(n)$ accounting for the noise present in the channel estimates plus the non-interesting paths:

$$\mathbf{y}(n) = a_j(n)\mathbf{G}\mathbf{e}_{\tau_j} + \tilde{\mathbf{v}}(n) \quad (4.53)$$

The MV filter is a matched decorrelating filter \mathbf{w} which separates the different paths of the desired signals, whose output is given by (4.54):

$$z(n) = \mathbf{w}^H \mathbf{y}(n) = a_j(n)\mathbf{w}^H \mathbf{G}\mathbf{e}_{\tau_j} + \mathbf{w}^H \tilde{\mathbf{v}}(n) \quad (4.54)$$

The filter should satisfy that $\mathbf{w}^H \mathbf{G}\mathbf{e}_{\tau_j} = 1$, and an improved performance is achieved when \mathbf{w} is chosen so as to maximise the output SNR. Let the filter output power be written as in (4.55) and therefore SNR may be defined as in (4.56).

$$E\{|z(n)|^2\} = \mathbf{w}^H E\{\mathbf{y}(n)\mathbf{y}(n)^H\} \mathbf{w} = E\{|a_j(n)|^2\} + \mathbf{w}^H E\{\tilde{\mathbf{v}}(n)\tilde{\mathbf{v}}(n)^H\} \mathbf{w} \quad (4.55)$$

$$SNR = \frac{E\{|a_j(n)|^2\}}{\mathbf{w}^H E\{\tilde{\mathbf{v}}(n)\tilde{\mathbf{v}}(n)^H\} \mathbf{w}} \quad (4.56)$$

Since the numerator does not depend on \mathbf{w} , the maximization of this expression is equivalent to minimize the noise output power, or equivalently:

$$\mathbf{w} = \arg \min_{\mathbf{w}^*} \mathbf{w}^H E\{\mathbf{y}(n)\mathbf{y}(n)^H\} \mathbf{w} \quad \text{subject to } \mathbf{w}^H \mathbf{G}\mathbf{e}_{\tau_j} = 1 \quad (4.57)$$

Using Lagrange multipliers, the cost function, J to minimize takes the following form:

$$J = \mathbf{w}^H \mathbf{R}_y \mathbf{w} + \lambda (\mathbf{w}^H \mathbf{G}\mathbf{e}_{\tau_j} - 1) \quad (4.58)$$

It is simple to derive the MV solution for both the filter \mathbf{w} and the spectral representations for delays [53][54]:

$$\mathbf{w}(\tau) = \frac{\mathbf{R}_y^{-1} \mathbf{G}\mathbf{e}_{\tau}}{\mathbf{e}_{\tau}^H \mathbf{G}^H \mathbf{R}_y^{-1} \mathbf{G}\mathbf{e}_{\tau}} \quad P(\tau) = \frac{1}{\mathbf{e}_{\tau}^H \mathbf{G}^H \mathbf{R}_y^{-1} \mathbf{G}\mathbf{e}_{\tau}} \quad (4.59)$$

Note that one filter is found per each delay, but the final power delay spectrum does not include the explicit expression of the filter. Full rank estimates of the correlation matrix may be obtained by ergodic averaging over n ($n=1, \dots, K$), provided that $K \geq M$. In practice, for reasonable results and to obtain meaningful statistics values of K must range beyond $2.5M$. Note that the window length for ergodic averaging goes beyond the coherence time of the amplitudes of the channel taps (it may be seen in equation (4.53) as the amplitudes are time varying), but it has to be shorter than the coherence time of the delay values τ_i .

4.4.1.2 Normalized minimum variance estimation (NMV)

In practice the presence of the shaping filter \mathbf{G} causes the appearance of significant side lobes in the MV solution that may be misinterpreted as arrivals (as it is exhibited in Figure 4.36 and Figure 4.37). On the other hand, as equation (4.55) is giving a measurement of the signal power plus the interfering power, it is a magnitude strongly dependent on the bandwidth of \mathbf{w} , which, on its turn, depends on the

distribution of the delays τ in our received signal. It can be easily seen that, if $\tilde{\mathbf{v}}(n)$ were merely noise, the output power would be given by:

$$P(\tau) = E\left\{\left|a_j(n)\right|^2\right\} + \sigma_v^2 \mathbf{w}(\tau)^H \mathbf{w}(\tau) \quad (4.60)$$

Therefore, a more meaningful measurement allowing equal noise level throughout all values of τ is given by (4.61) [52][53][54]:

$$S(\tau) = \frac{P(\tau)}{\mathbf{w}(\tau)^H \mathbf{w}(\tau)} \quad (4.61)$$

It can be further written as:

$$S(\tau) = \frac{\mathbf{e}_\tau^H \mathbf{G}^H \mathbf{R}_y^{-1} \mathbf{G} \mathbf{e}_\tau}{\mathbf{e}_\tau^H \mathbf{G}^H \mathbf{R}_y^{-2} \mathbf{G} \mathbf{e}_\tau} \quad (4.62)$$

Figure 4.16 shows the timing that is obtained in a severe multipath situation by using the NMV approach compared to using a simple maximum-of-the-impulse-response strategy. Signal has been sampled at two samples per symbol and closed signal arrivals may be resolved for realistic values of SNR.

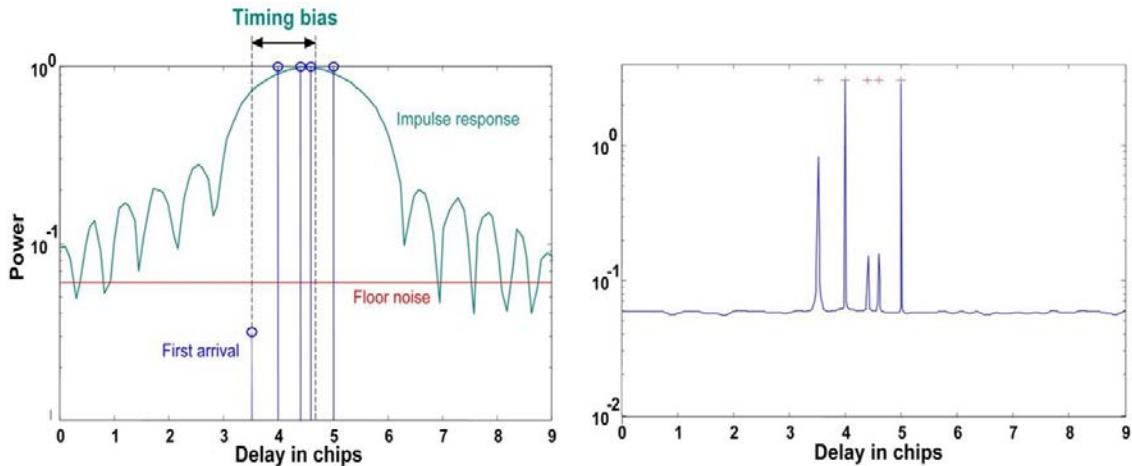


Figure 4.15: Left: If the first arrival is computed as the maximum of the impulse response, a significant bias is observed in the case of multipath. The true arrivals are denoted with circles. Right: The estimation of all the incoming rays using the NMV technique allows the right determination of the first arrival (true arrivals are denoted by crosses).

From an spectral estimation point of view, $P(\tau)$ represents the MV power spectrum estimation of a set of cisoids in noise, while $S(\tau)$ is the MV power spectrum density estimation (also called Normalized MV), the later achieving better resolution properties [52]. In addition, the side lobes of the NMV solution are significantly attenuated with respect to the MV solution as it will be shown in a later section.

4.4.1.3 Use of antenna arrays for enhanced timing estimation

When the receiver incorporates multiple antennas, the diversity provided may be efficiently used to determine better estimates of the delays. It will be reasonably assumed that the separation of the antenna elements is small compared to the distance where the signal reflections have happened, and that the difference in sampling instants at different sensors is much lower than the delay estimation resolution. This allows making the assumption that the delays values are the same all through the sensors, although their instantaneous powers might differ.

In the conventional literature for antenna arrays receivers, its application is mainly focused to signal separation (interference cancelling) or range extension. These applications are dealt in section 4.4.1.5, where spatial filtering helps in determining the first low-power arrivals provided that all other arrivals bear a different spatial signature.

In addition to that, the accuracy in timing estimation may be improved in coherent scenarios when multiple antennas are available, as described in the next section.

4.4.1.4 Reduction of source coherence

In static environment where Doppler variation is negligible, the observed propagation channel changes very slowly in time. The multiple K replicas exhibit a temporal correlation very close to 1 and the temporal coherence of the different rays that form the multipath structure of the propagation channel eventually leads to rank deficiency in matrix \mathbf{R}_y . This provokes a disappearance of the rays in the delays spectrum which is common to MUSIC, MV, NMV, MEM and other spectral estimation methods that use the correlation matrix as estimation tool [55]-[57], unless some spectrum averaging is done. Since ESPRIT is inherently performing averaging it is robust to this problem.

On the other hand, if multiple sensors are available, they offer a potential to reduce this coherence if the channel does not exhibit complete spatial correlation. Channel estimations obtained from multiple sensors can be used to generate additional updates in \mathbf{R}_y as follows: assume that the channel estimations obtained at the N_s sensors are given by

$$\mathbf{y}^i(n) = a_j^i(n)\mathbf{G}\mathbf{e}_{\tau_j} + \tilde{\mathbf{v}}^i(n) \quad i = 1, \dots, N_s \quad (4.63)$$

Updating of the correlation matrix may be done as:

$$\hat{\mathbf{R}}_y(n+1) = (1-\alpha)\hat{\mathbf{R}}_y(n) + \alpha \left(\sum_{i=1}^{N_s} \mathbf{y}^i(n+1)\mathbf{y}^i(n+1)^H \right) \quad (4.64)$$

Note that all the adaptive formulations defined above are still valid if the recursion is run once for every rank-one update of the matrix, be it originated from the temporal collection of estimated channels (n index) or spatial collection (i index).

Even when the multipath structure is not coherent, the use of multiple antennas brings SNR gain that translates in better resolution of weak multipath components.

4.4.1.5 Spatial Filtering

An alternate use of multiple sensors for timing estimation is to use prior spatial cancelling so that resolution is improved provided that close-in-delay arrivals have different spatial signatures. To define a scheme under these premises, let us define matrix \mathbf{Y} as follows:

$$\mathbf{Y}(n) = \begin{bmatrix} \mathbf{y}^1(n) & \mathbf{y}^2(n) & \cdots & \mathbf{y}^{N_s}(n) \end{bmatrix} \quad n = 1, \dots, N_{coh} \quad (4.65)$$

where the definition of the temporal window N_{coh} is well below the coherence time of the channel amplitudes. It will be assumed that a linear combination of signals from different sensors $\mathbf{Y}(n)\mathbf{b}$ is able to reduce the mutual leakage from close arrivals, provided that they are far apart in angle. To this end, we will define the following criterion:

$$J(\mathbf{b}, \alpha, \lambda) = \sum_{n=1}^{N_{coh}} \|\mathbf{Y}(n)\mathbf{b} - \alpha \mathbf{g}_\tau\|_2^2 - \lambda (\mathbf{b}^H \mathbf{b} - 1) \quad (4.66)$$

Note that the beamformer \mathbf{b} is computed every N_{coh} channel samples (the path amplitude is approximately constant within the coherence window) and depends on the delay value under study τ . The restriction of unit norm for \mathbf{b} allows preserving the noise power for all delays and over time. The term α depends on time and will preserve the fast fading variation of the channel arrival over time. The solution of equation (4.66) leads to the following expressions (after estimation of α and its inclusion in (4.66)):

$$\begin{aligned} \left(\hat{\mathbf{R}}_y - \mathbf{M}_y \mathbf{P}_{\mathbf{g}_\tau} \mathbf{M}_y \right) \mathbf{b} &= \lambda \mathbf{b} & \mathbf{P}_{\mathbf{g}_\tau} &= \frac{\mathbf{g}_\tau \mathbf{g}_\tau^H}{\mathbf{g}_\tau^H \mathbf{g}_\tau} \\ \mathbf{M}_y &= \sum_{n=1}^{N_{coh}} \mathbf{Y}(n) & \hat{\mathbf{R}}_y &= \sum_{n=1}^{N_{coh}} \mathbf{Y}(n) \mathbf{Y}^H(n) \end{aligned} \quad (4.67)$$

The beamformer \mathbf{b} is the eigenvector associated to the least eigenvalue, as λ represents the power of signal components not associated to the desired signal \mathbf{g}_τ :

$$\lambda = \mathbf{b}^H \left(\mathbf{R}_y - \mathbf{M}_y \mathbf{P}_{\mathbf{g}_\tau} \mathbf{M}_y \right) \mathbf{b} \quad (4.68)$$

Therefore, one beamformer has to be computed every N_{coh} channel samples for each τ under exploration using equation (4.67). The spatially filtered signal takes the form in (4.69):

$$\bar{\mathbf{y}}_{\tau}(n) = \mathbf{Y}(n)\mathbf{b} \quad (4.69)$$

The transformed signal in (4.69) is to be used as commented before to determine the delays spectrum. Note the dependence of vector \mathbf{b} on τ , and therefore as many vectors $\bar{\mathbf{y}}_{\tau}(n)$ as delays under test must be build. While the beamformers can be computed adaptively, the main complexity of this technique consists of the computation of one inverse matrix per lag τ under exploration.

Though this approach provides in principle much higher timing resolution due to spatial signal separation, in practice, close arrivals come often from the same angular position and gains obtained from spatial filtering do not justify the added complexity.

4.4.1.6 Timing estimation results using MV approaches

In this section, a group of simulations will be deployed to study the behavior of the MV and NMV approaches for both the Line Of Side (LOS) and the Non Line Of Side (NLOS) conditions, for typical configurations of angular and delay spread, for one and four sensors and for different mobile speeds of 3, 10, 50 and 100 km/h. The maximum integration time corresponding to the time of collection of channel vector estimates is chosen as the minimum between one second and the coherence time of the delays which depends on the mobile speed, as it was studied in chapter 3. This value corresponds approximately to 0.14 s for the higher mobile speed of 100 km/h, and holds equal to 1.0 s for the lower speeds of 3 and 10 km/h. Plots show the cumulative function of the timing estimates in different conditions. The first arrival is always placed at the zero value of the horizontal axis.

The detection of the first arrivals has been done by thresholding the delay spectrum, according to the guidelines of Annex 4.2 [53]. Different thresholds are used for MV and NMV, but both were chosen using the same criteria. Values of 2.7 dB and 7.5 dB above the expected floor noise level are used for NMV and MV respectively.

The legends in the figures contain some acronyms for identification purposes, namely: ‘avr’ and ‘std’. The first corresponds to the average of the errors made in the detection of the first arrival for the whole set of realizations and therefore to the bias in the estimation; whilst the latter corresponds to the error standard deviation for the data set. In general, bias is small and practically negligible (below $0.1T_c$) for high SNR’s and four sensors for a LOS condition. On the other hand, error standard deviation is around $0.25 T_c$ for four sensors, and around $0.5T_c$ for one sensor, but depends greatly on the propagation scenario.

Experiment 4.3: Effect of multiple antennas and angular spread. Figure 4.17 and Figure 4.18 show the behavior of the NMV algorithm for different angular spreads, for a LOS condition and a SNR of 8 [dB]. Graphics show some improvement for the higher signal angular spread and the low speed subscriber. For the higher speed, there is no an important change associated to the angular spread. It can be seen on Figure 4.17 a) that the error standard deviation reduces from $0.63 T_c$ to $0.36 T_c$ for a mobile speed of 10 [km/h], and from $0.45 T_c$ to $0.13 T_c$ for 3 [km/h], and remains near to $0.29 T_c$ for 100 [km/h].

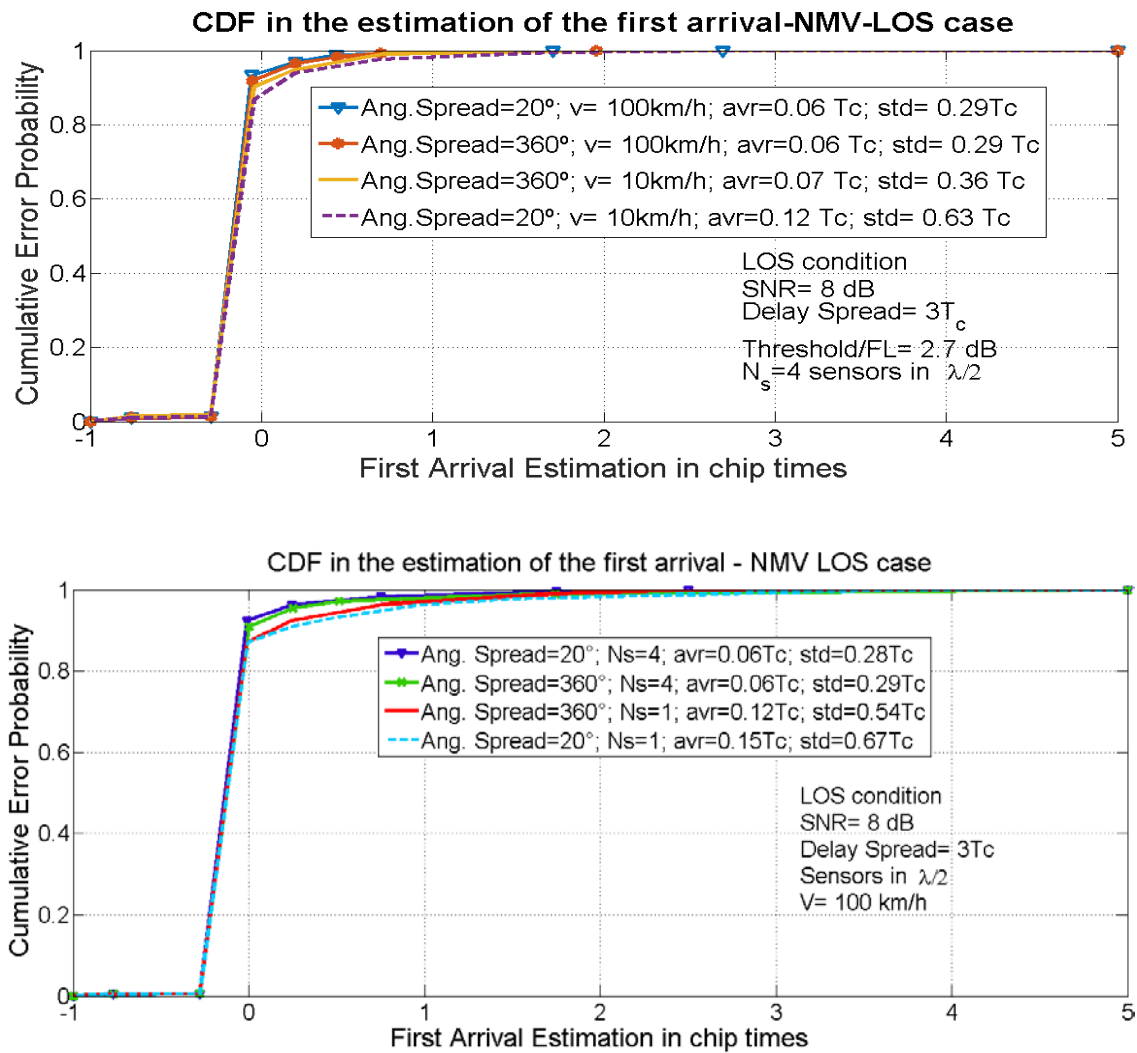


Figure 4.16: Cumulative Error Probability in the Estimation of the First Arrival - LOS condition and SNR=8 dB. a) Top: Four sensors array, different signal angular spreads of 20° and 360°, a delay spread of $3T_c$, and mobile speeds of 10 [km/h] and 100 [km/h]. b) Bottom: different signal angular spreads of 20° and 360°, a delay spread of $3T_c$, a mobile speed of 100 [km/h], and two configurations of one and four sensors.

Error also reduces, by adding more sensors. It decays for i.e. from $0.54 T_c$ to $0.29 T_c$, when the number of available sensors increases from one to four, for a signal delay spread of $3 T_c$, as it is shown on Figure 4.17 b); and it passes from $0.48 T_c$ to $0.23 T_c$ for a signal delay spread of $1.5 T_c$, as it is shown on Figure 4.18 b).

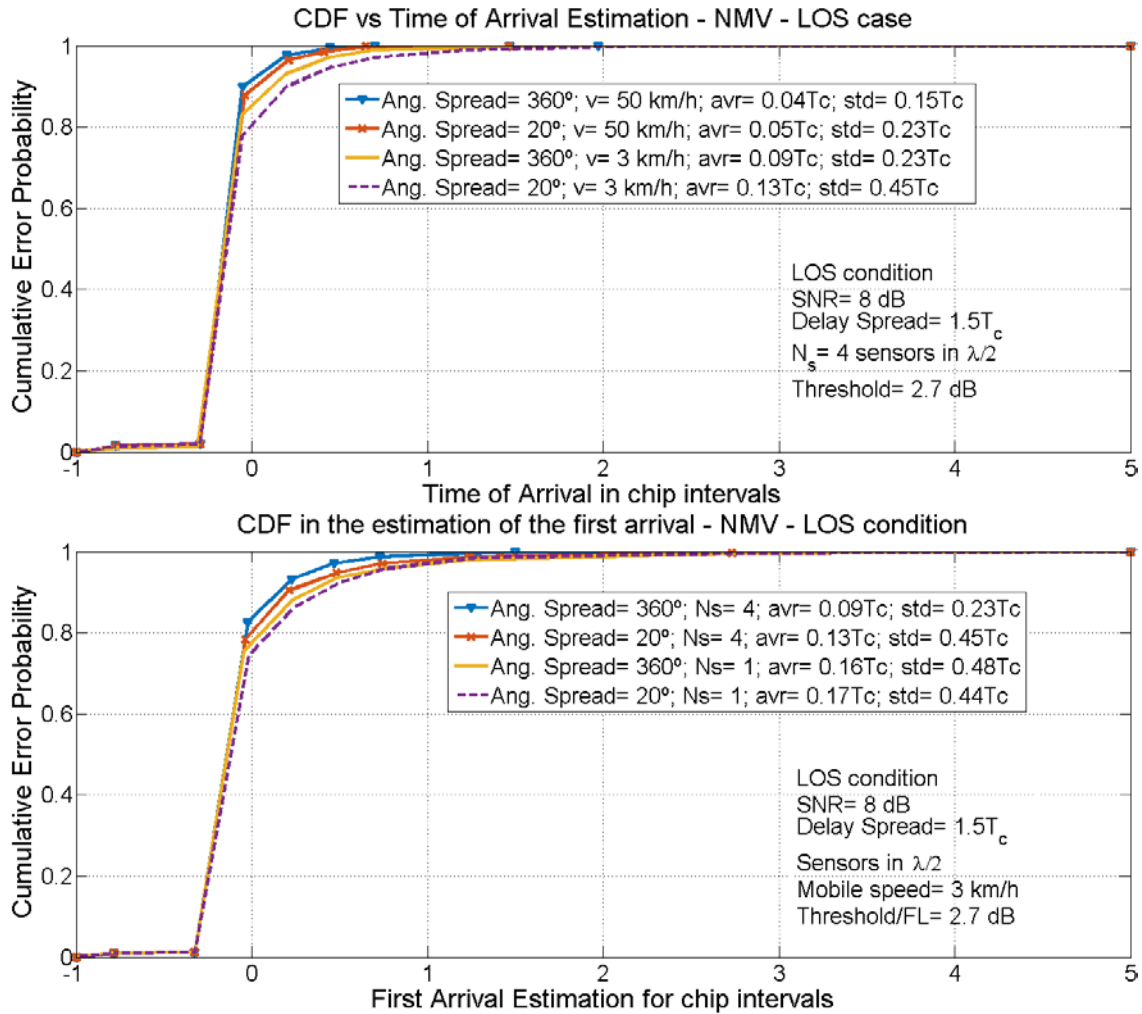


Figure 4.17: Cumulative Error Probability in the Estimation of the First Arrival - LOS condition for a delay spread of $1.5T_c$ when SNR=8 [dB]. a) Top: Four sensors array, different signal angular spreads of 20° and 360° , and mobile speeds of 3 [km/h] and 50 [km/h]. b) Bottom: different angular spreads of 20° and 360° , and two configurations of one and four sensors for a mobile speed of 3 [km/h].

The worst error within the results from this experiment corresponds to the case when there is just one sensor available and the mobile speed is high (100 [km/h]). For this case, the bias reaches a value of $0.15 T_c$, and error standard deviation a value of $0.67 T_c$. This latter value is even higher than $0.45 T_c$, achieved for the similar case with

the lowest speed of 3 [km/h]. This case reveals the required trade-offs between the mobile speed, and the estimation rate in order to achieve the best of time-space diversity in the application of the algorithms.

Experiment 4.4: Effect of SNR for different configurations. Figure 4.19 compares the behavior of the NMV approach for two different SNR's of 8 dB and 15 dB. Qualitatively, these results are similar to the precedent experiment, but better errors are achieved for a higher SNR. The signal angular spread is also of 360° , and the delay spread is of $1.5 T_c$. The error reduces from $0.23 T_c$ to $0.21 T_c$ when four sensors are available and from $0.48 T_c$ to $0.45 T_c$, when just one sensor is used. Bias is negligible (for i.e. $0.05 T_c$ for a SNR of 15 dB) when four sensors are available and small (for i.e. $0.14 T_c$ for a SNR of 15 dB) for just one sensor.

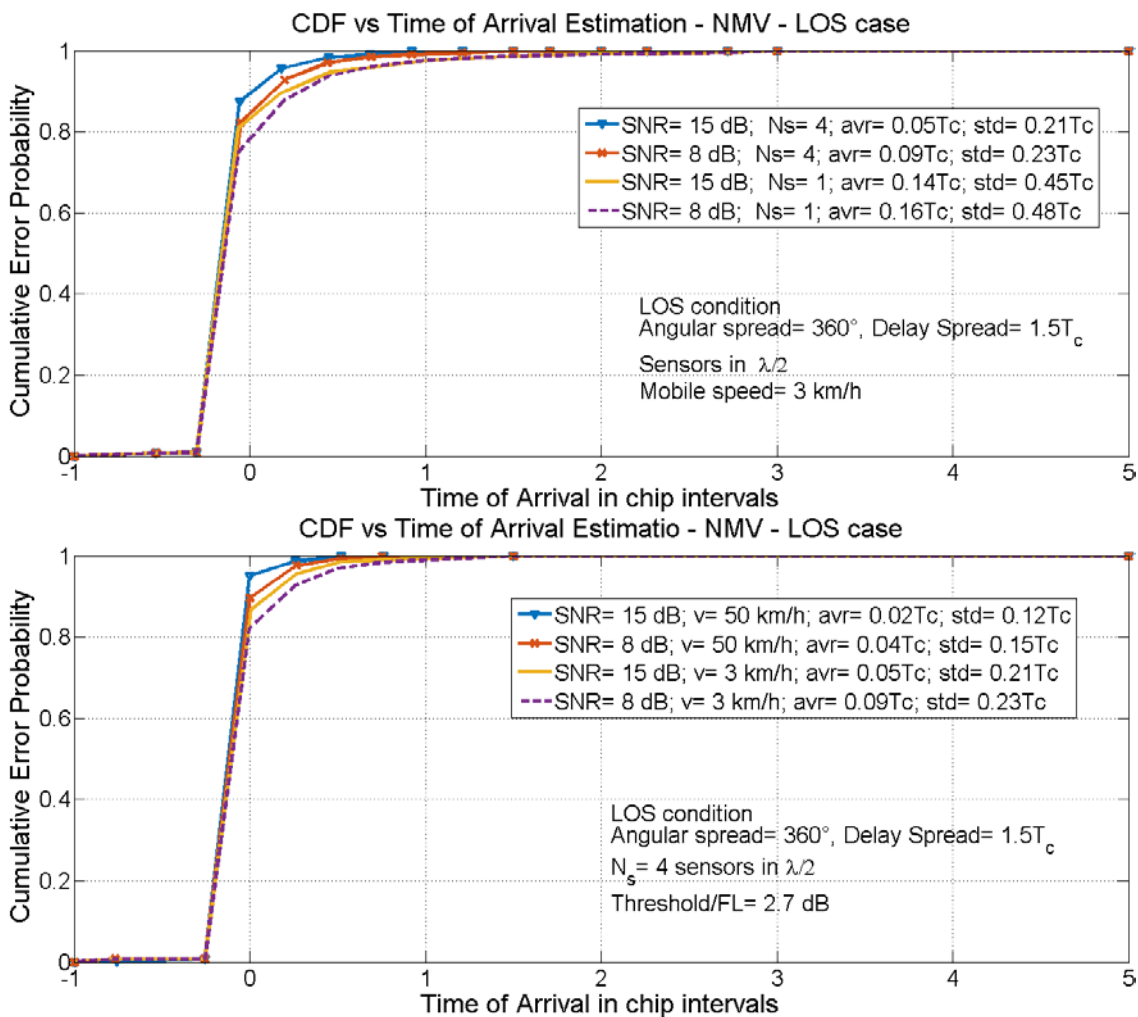


Figure 4.18: Cumulative Error Probability in the Estimation of the First Arrival - LOS condition for a signal angular spread of 360° , a delay spread of $1.5 T_c$, and SNR's of 8 [dB] and 15 [dB]. a) Top: two different configurations of one and four sensors, and b) Bottom: two mobile speeds of 3 [km/h] and 50 [km/h]. Threshold is set to 2.7 [dB] over the floor noise level.

Bias and also error standard deviation also improve with the mobile speed, as it is shown from Figure 4.19 b) when passing from a 3 [km/h] to 50 [km/h].

Experiment 4.5: Influence of the delay spread. Figure 4.20 and Figure 4.21 show the performance of the NMV approach as a function of the signal delay spread, for different scenarios of SNR, signal delay spread and the number of available sensors.

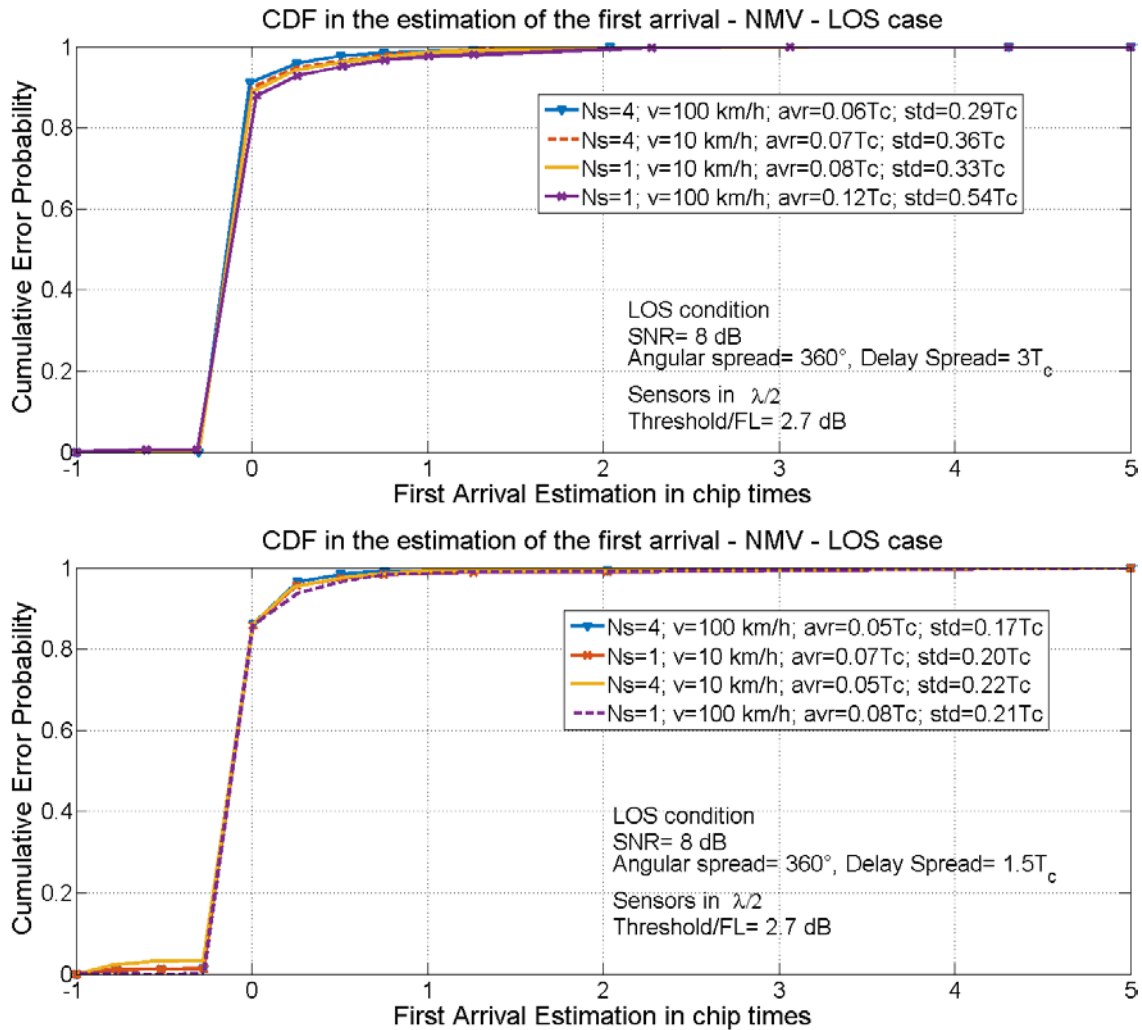


Figure 4.19: Cumulative Error Probability in the estimation of the First Arrival. LOS condition, and a signal angular spread of 360°, for different scenarios and configurations. a) Top: SNR of 8 dB, a delay spread of $3T_c$, two different mobile speeds of 10 [km/h] and 100 [km/h], and configurations of one and four sensors. b) Bottom: SNR of 8 [dB], a delay spread of $1.5T_c$, two different mobile speeds of 10 [km/h] and 100 [km/h], and configurations of one and four sensors.

Some improvement in terms of bias and error variance correspond to lower signal delay spreads, higher number of sensors, higher mobile speeds and higher SNR. It may be seen for i.e. as error decays from $0.36 T_c$ to $0.22 T_c$ when the delay spread improves

from $3 T_c$ to $1.5 T_c$, if four sensors are available and the mobile speed is of 10 km/h. Furthermore, it improves from $0.51 T_c$ to $0.21 T_c$ for a mobile speed of 3 km/h and four sensors and from $0.54 T_c$ to $0.21 T_c$ for a mobile speed of 100 km/h and just one sensor. Note also, as error reduces when the mobile speed goes up, for i.e. it reduces from $0.74 T_c$ to $0.18 T_c$ when mobile goes from 3 km/h to 50 km/h, and one sensor is used, for a signal delay spread of $1.5 T_c$. It may be seen as error reduces from $0.54 T_c$ with one sensor to $0.29 T_c$ with four sensors for a mobile speed of 100 km/h and a SNR of 8 dB; and from $0.74 T_c$ with one sensor to $0.51 T_c$ with four sensors for a mobile speed of 3 km/h and a SNR of 15 dB.

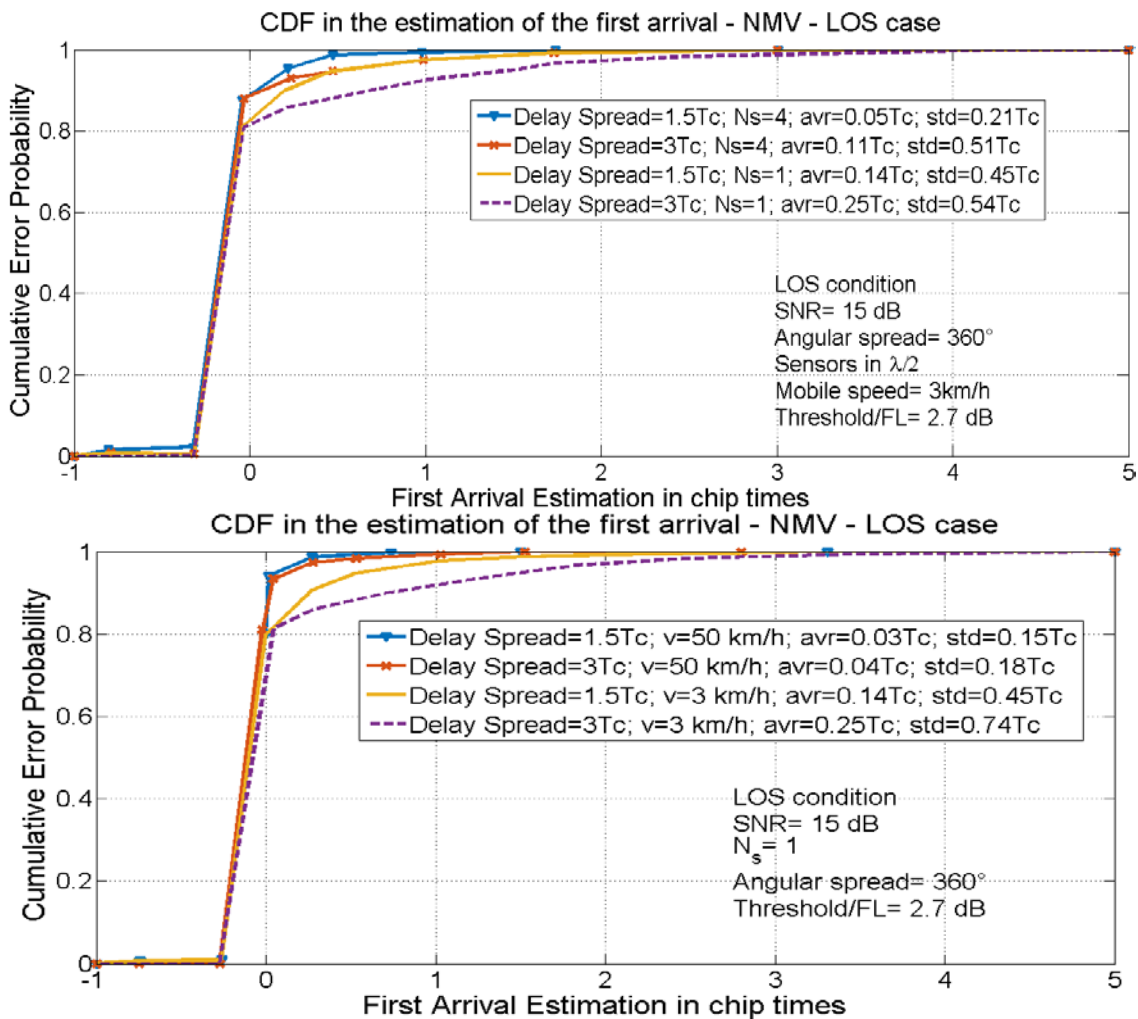


Figure 4.20: Cumulative Error Probability in the estimation of the First Arrival. LOS condition, and a signal angular spread of 360° , for different scenarios and configurations. a) Top: SNR of 15 [dB], signal delay spreads of $1.5T_c$ and $3T_c$ for configurations of one and four sensors, and a mobile speed of 3 [km/h]. d) Bottom: SNR of 15 [dB], signal delay spread of $1.5T_c$ and $3T_c$ for mobile speeds of 3 [km/h] and 50 [km/h]. Threshold is set to 2.7 [dB] above the expected noise floor level.

Experiment 4.6: Performance in situations of NLOS (low power of the first arrival). Figure 4.22 and Figure 4.23 show the performance of NMV in case of a Non Line Of Sight (NLOS) condition, where the power of the first arrival is 10 [dB] (Figure 4.22) or instead 15 [dB] (Figure 4.23) below the later ones. Error degrades if it is compared to the LOS case, but estimates almost remain unbiased (bias around $0.08T_c$) when four sensors are available and the power ratio between the first and the later arrivals is of 10 [dB]. The worst case corresponds to one sensor and a high mobile speed. In this case, bias and error variance are too high, especially for higher delay spreads; for i.e. for a mobile speed of 100 [km/h] and a delay spread of $5T_c$, bias is of $1.05T_c$, and error standard deviation is of $3.11T_c$, as it can be seen in the figure.

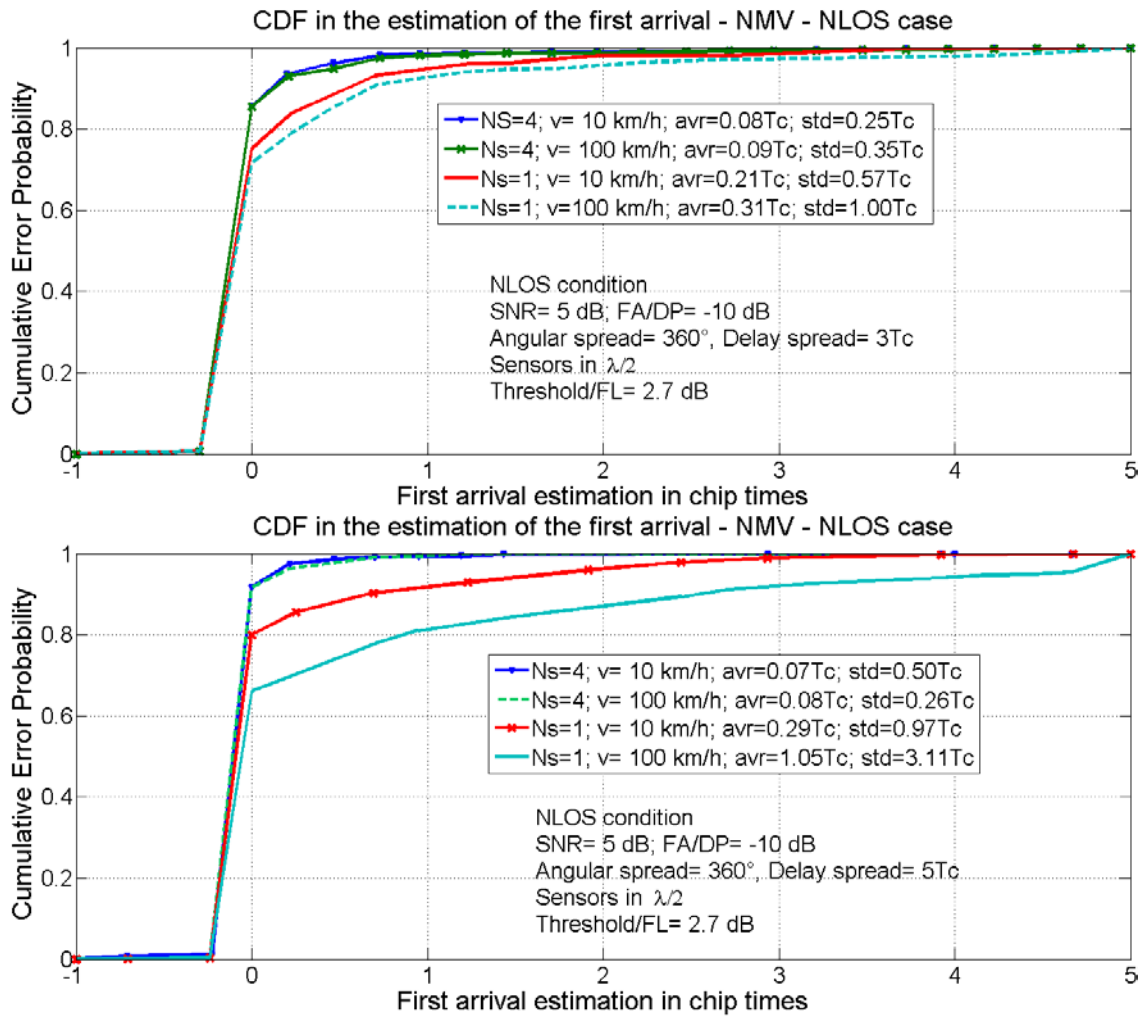


Figure 4.21: Cumulative Error Probability in first arrival estimation using a NMV approach for the NLOS condition, a SNR of 5 dB, an angular spread of 360°, four sensors and mobile speeds of 10 and 100 km/h. a) Top: One and four sensors, two mobile speeds and a delay spread of 3 times the chip interval. b) Bottom: One and four sensors, two mobile speeds and a delay spread of 5 times the chip interval.

On the other hand, Figure 4.23 shows an increased bias and error standard deviation when first arrival is weaker (-15 dB) respect to the later arrivals. However, when four sensors are used, this degradation is greatly reduced.

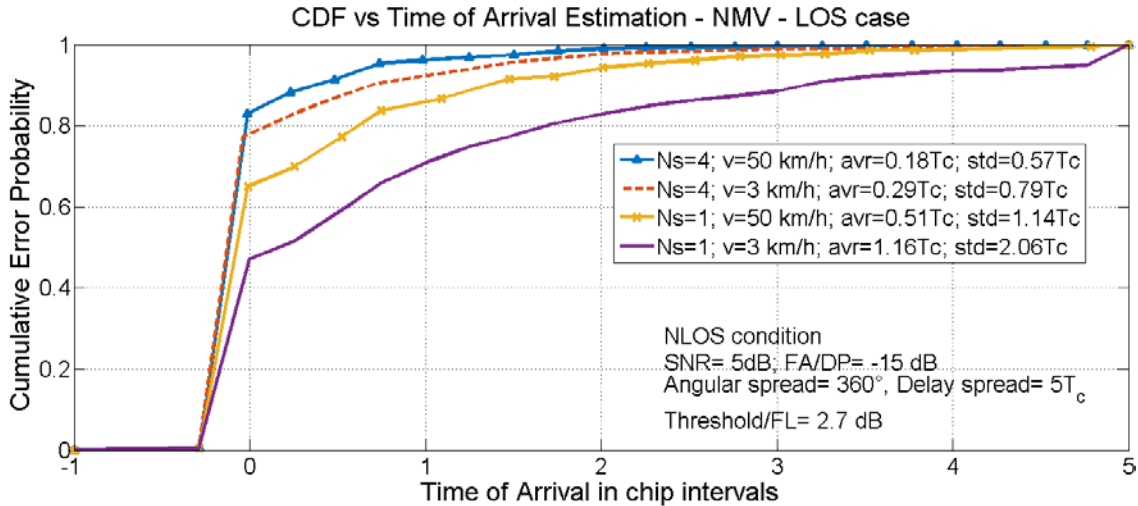


Figure 4.22: Cumulative Error Probability in first arrival estimation using a NMV approach for the NLOS condition, a SNR of 5 dB, a signal angular spread of 360° , a delay spread of $5T_c$, and configurations of one and four sensors for mobile speeds of 3 km/h and 50 km/h.

Experiment 4.7: Performance of the MV approach. Figure 4.24 exhibits some characteristics for the MV approach. It may be seen that behavior is very similar for the whole range of mobile speed and available sensors (one or four). However, error standard deviation degrades if it is compared to the NMV approach, and an important early detection due to side-lobes appears. These results confirm that the NMV works much better with the purpose of positioning, and its use is adequate to achieve accurate delay time of arrival estimation. Early detections may be surpassed by choosing a higher threshold as shown in Annex 4.3, however the capacity of the MV method to detect a weak first arrival completely reduces.

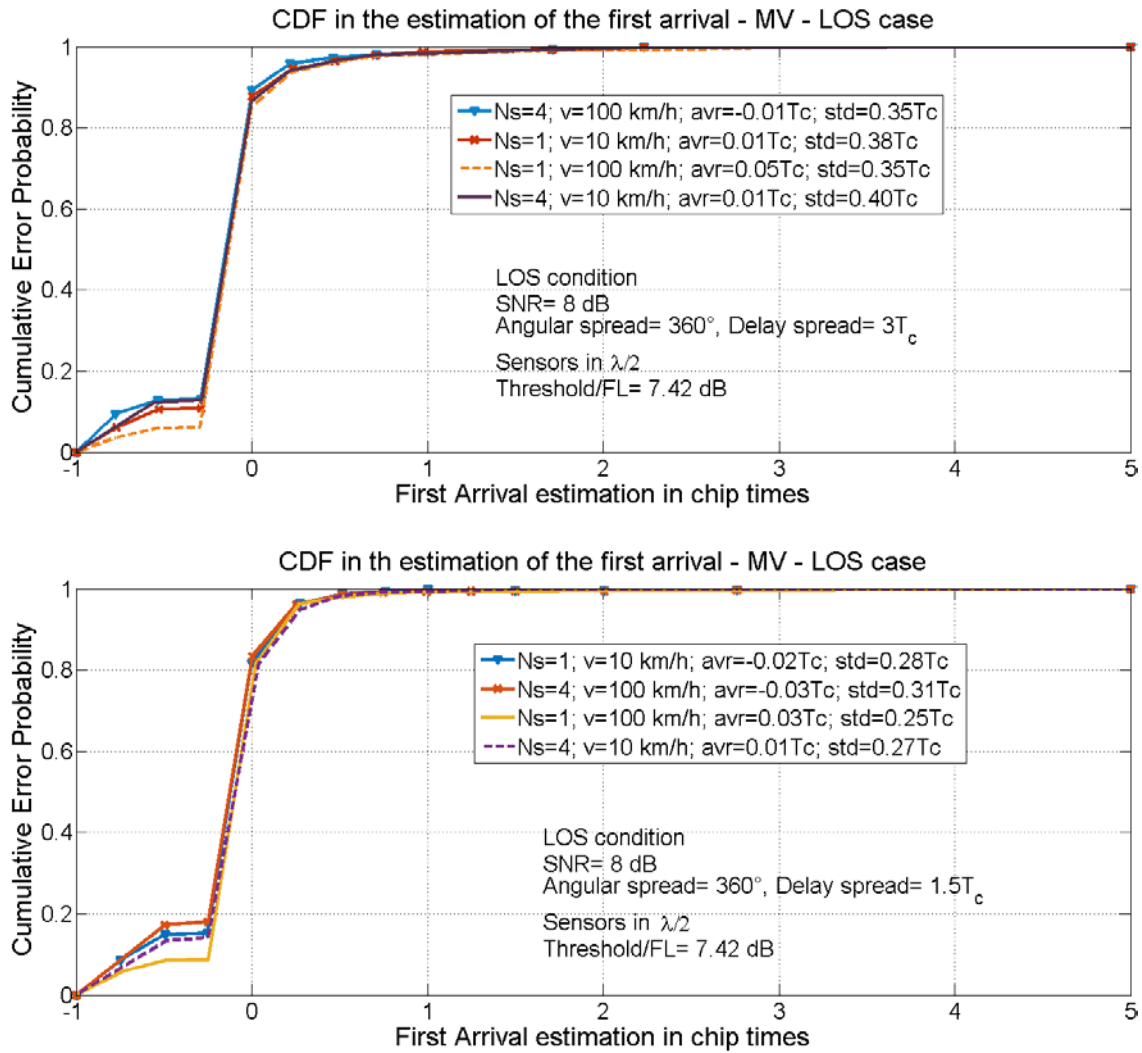


Figure 4.23: Cumulative Error Probability in the estimation of the First Arrival. LOS condition, angular spread of 360° , one and four sensors and a mobile speed of 10 km/h. a) Top: Delay Spreads of $3T_c$ and a SNR of 8 dB. b) Bottom: Delay Spread of $1.5T_c$ and a SNR of 8 dB. Threshold is set to 7.42 dB above the noise floor level.

4.4.2 Performing High Resolution AOA Estimation

4.4.2.1 Normalized Minimum Variance AOA Estimation

Since delays have been accurately estimated from power delay spectrum in (4.59) or in (4.62), their associated direction of arrivals may be estimated in an analog way to the timing problem of the previous section, by exploiting the array structure, as it is seen in the following lines.

First of all, the filter output in (4.54) may be expressed as in (4.70), when very close N_j paths within the lag “j” arrive from different directions, and a_m in (4.71) models the bearing sensor response.

$$z(n) = a_j(n) + \mathbf{w}^H \tilde{\mathbf{v}}(n) = \sum_{k=1}^{N_j} \alpha_{j,k}(n) a_m(n) + \tilde{\mathbf{v}}(n) \quad (4.70)$$

$$a_m = \exp\left(-j2\pi \frac{d_m}{\lambda} \sin(\theta)\right) \quad (4.71)$$

Rearranging terms and noting explicitly as data depends of sensor position within the array (m) and isolating the path “ k ”, (4.70) becomes (4.72), being N_s the number of array elements.

$$z_m(n) = \alpha_{j,k}(n) a_{m,k}(n) + \check{v}_m(n) \quad \forall m \in [0, N_s - 1] \quad (4.72)$$

If data is disposed as the vector shown in (4.73), expression (4.74) straight forwards easily.

$$\mathbf{z}_a(n) = [z_0(n) z_1(n) \cdots z_{N_s-1}(n)]^T \quad (4.73)$$

$$\mathbf{z}_a(n) = \alpha_{j,k}(n) \mathbf{a}_k(n) + \check{\mathbf{v}}_m(n) \quad (4.74)$$

Following an analog procedure to the previous section, and remaining that we are trying to minimize the interference coming from arrivals with different bearings, providing a spatial filter \mathbf{w}_a , and exhibiting the dependence of steering vector with bearing, the cost function to minimize corresponds to (4.75), being λ the Lagrange operator and $\mathbf{w}_a^H \mathbf{a}(\theta) = 1$ the required constraint. \mathbf{R}_θ is the spatial correlation matrix defined as $E\{\mathbf{z}_a \mathbf{z}_a^H\}$.

$$J(\theta) = \mathbf{w}_a^H \mathbf{R}_\theta \mathbf{w}_a + \lambda (\mathbf{w}_a^H \mathbf{a}(\theta) - 1) \quad (4.75)$$

Finally, it may be shown that the angular spectrum is given by (4.76), and the estimated DOA’s correspond to the angular argument which maximize the spectrum.

$$S(\theta) = \frac{\mathbf{a}^H(\theta) \hat{\mathbf{R}}_\theta^{-1} \mathbf{a}(\theta)}{\mathbf{a}^H(\theta) \hat{\mathbf{R}}_\theta^{-2} \mathbf{a}(\theta)} \quad (4.76)$$

The channel estimates recorded on multiple antennas can be used to jointly determine delays and angles of arrival using the MV or NMV formulation. To that end, let us adopt the model in equation (4.53) for the antenna k :

$$\mathbf{y}^{(k)}(n) = a_i(n) \mathbf{G} \mathbf{e}_{\tau_i} e^{j\phi_i^k} + \tilde{\mathbf{v}}(n) \quad (4.77)$$

Where ϕ_i denotes the electrical angle corresponding to the i arrival $\phi_i=(2\pi d/\lambda) \sin\theta_i$. Let us stack the signal from all the antennas in (4.54) in a single vector. The filter should satisfy $\mathbf{w}^H \mathbf{G} \mathbf{e}_i=1$, where $\mathbf{e}_i = \text{vec}(\mathbf{e}_{\phi_i} \otimes \mathbf{e}_{\tau_i})$ and $\mathbf{e}_{\phi_i} = [1 \ e^{j\phi_i} \ e^{j2\phi_i} \ \dots \ e^{j(N_s-1)\phi_i}]^T$.

4.4.2.2 Simulations and Results for AOA Estimation using the NMV Approach

Figure 4.25 shows typical angular spectra computed using the NMV approach in (4.76) for the different estimated delays from the delay spectrum in (4.62) for two different array configurations: two sensors and 8 sensors.

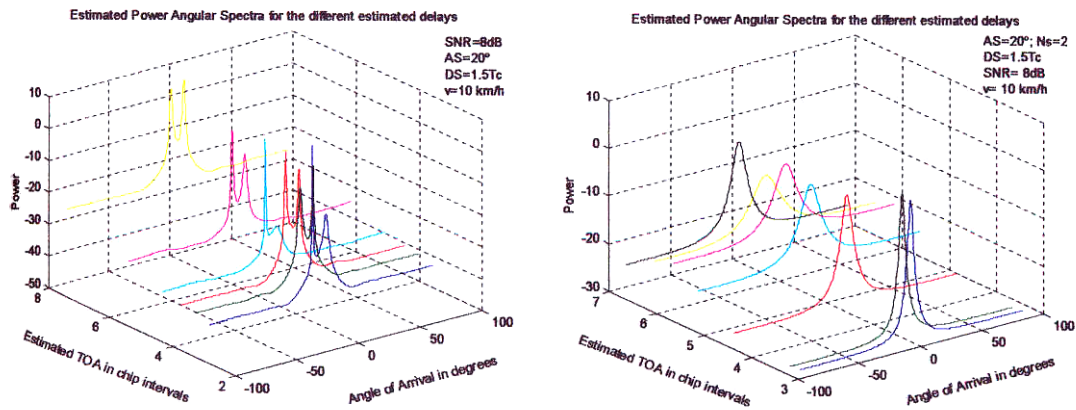


Figure 4.24: Estimated NMV Angular Spectrum for the different estimated delays using a NMV scheme. Delay spread corresponds to 1.5 times the chip period, the angular spread corresponds to 20°, and SNR=8 dB. a) Left: 8 sensors used; and b) Right: 2 sensors used.

It is clear from this example as more defined peaks are achieved for a higher number of sensors, improving spatial resolution.

Figure 4.26 shows polar diagrams for signal angular-temporal estimation for two different environments and two array configurations. First environment correspond to a more realistic case where angular spread is small and around 20°, and second environment correspond to the case where signal arrives from anywhere (angular spread of 360°), being the latter possible in case of NLOS condition. Delays are expressed as radials in terms of the chip period, and bearings respect to the array broadside as the angular extensions. True arrivals are visualized as ‘o’ and estimates as ‘x’, being the most powerful bearings in the angular spectrum contained within squares.

In the following, some experimental results from Monte Carlo simulations are exhibit to evaluate the performance of the NMV approach for bearing estimation. Each Error Cumulative Probability characteristic displayed from Figure 4.27 to Figure 4.31 result from 1000 Monte Carlo realizations, and for an acquisition time of one second for the low mobile speed of 3 km/h, and for the delays coherence time of around 180 ms for

the higher mobile speed of 100 km/h. Graphics for the case of temporally filtered data and also for the case of non-temporally filtering are presented for their comparison.

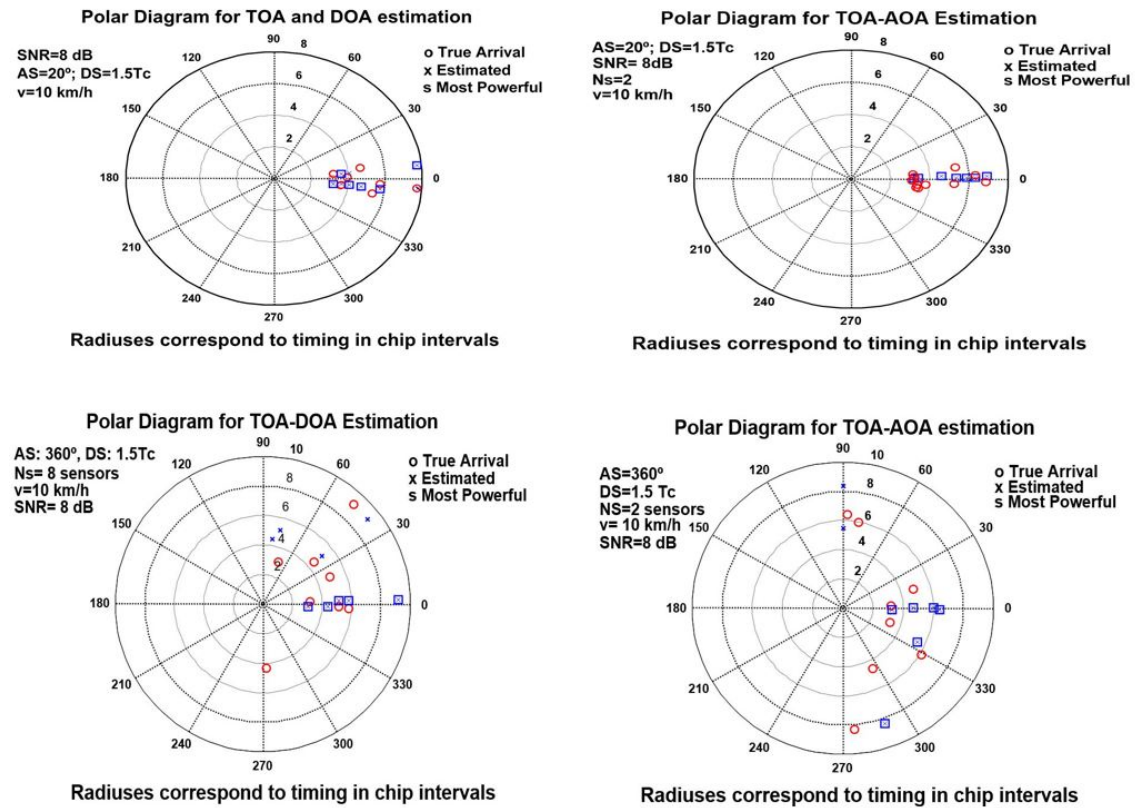


Figure 4.25: Polar Diagrams from TOA and DOA estimates when the NMV approach is used to estimate both parameters. Radius corresponds to the delay time expressed in terms of the chip interval. Estimates are represented as ‘x’ being the square pointing out the most powerful peaks within the angular spectra. Delay spread is set to 1.5 times the chip period, and SNR=8 dB. Sensors are linearly spaced. a) Top left: angular spread of 20° and 8 available sensors. b) Top right: angular spread of 20° and 2 sensors. c) Bottom left: angular spread of 360° and 8 available sensors. d) Bottom right: angular spread of 360° and 2 sensors.

Experiment 4.8: Effect of angular spread and the number of sensors in AOA estimation.

Along this experiment, two error measurements are computed: first of all, the error performed in the estimated direction of the first arrived path as it is shown in Figure 4.27 a) and b); and a measure of the overall error computed as the difference between the averaged AOA from all the incoming paths and the average AOA from all the estimated directions of arrival in the angular spectra, as it is shown in Figure 4.28 a) and b).

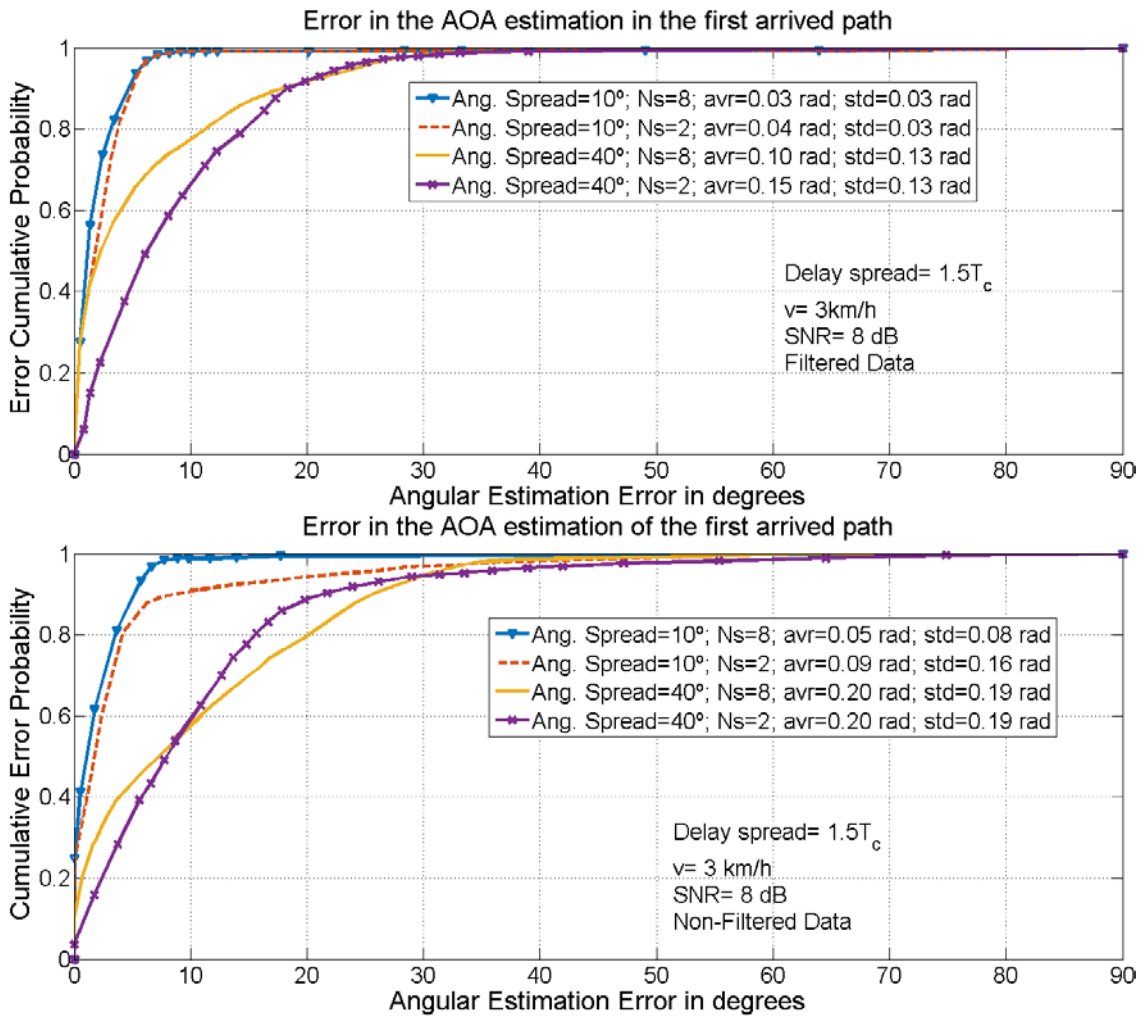


Figure 4.26: Cumulative Error Probability for the estimated Direction Of Arrival computed from angular NMV spectra for delays acquired from a NMV algorithm. Delay spread is set to 1.5 times the chip interval, and characteristics for both 8 sensors and two sensors are shown, for angular spreads of 10° and 40°. SNR=8 dB. a) Top: error computed just for the first detected arrival and when data is temporally filtered prior to compute the angular spectrum. b) Bottom: error computed just for the first arrival and when data is not filtered to compute the angular spectrum.

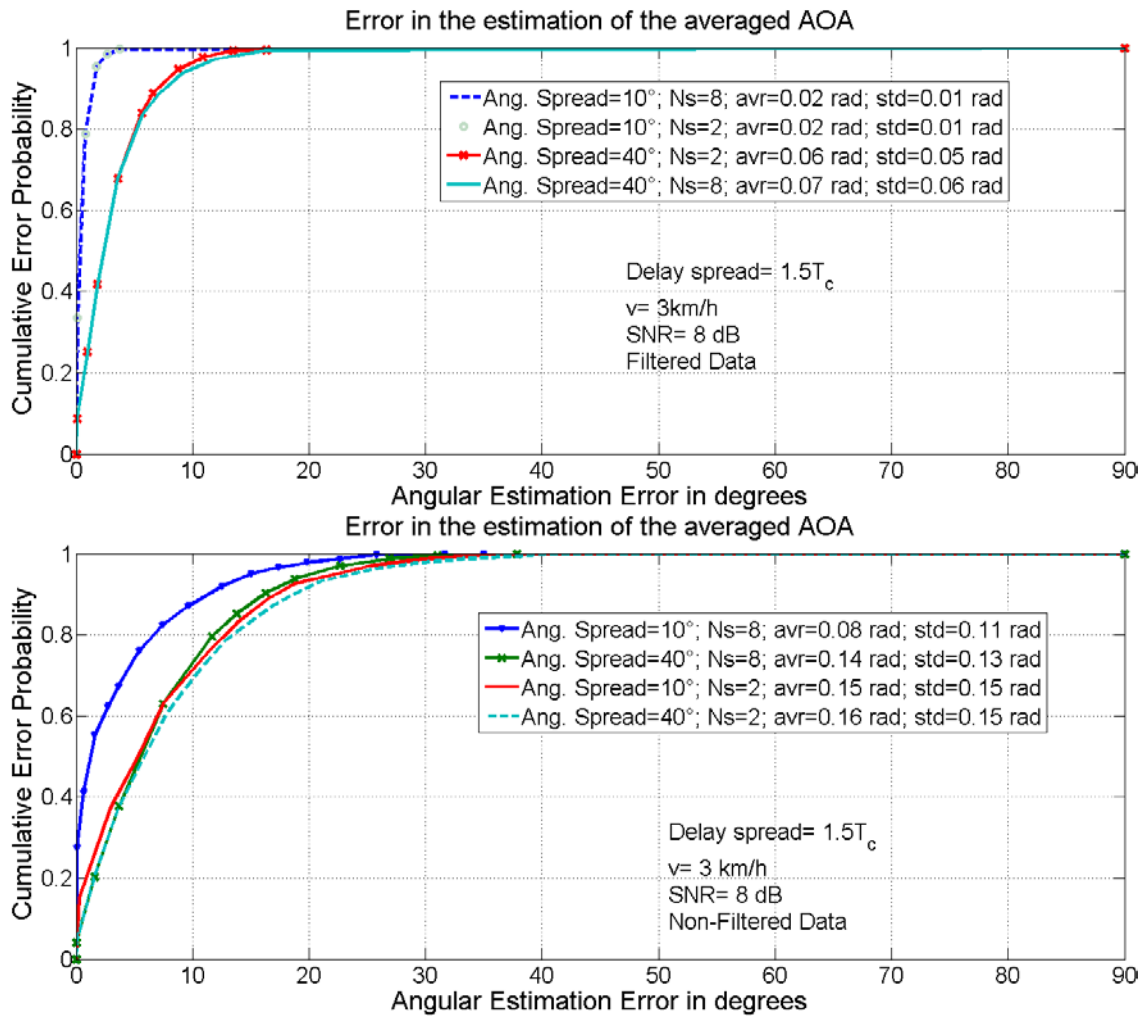


Figure 4.27: Cumulative Error Probability for the estimated Direction Of Arrival computed from angular NMV spectra for delays acquired from a NMV algorithm. Delay spread is set to 1.5 times the chip interval, and characteristics for both 8 sensors and two sensors are shown, for angular spreads of 10° and 40° . SNR=8 dB. a) Top: error computed for the averaged DOA from all the detected paths when data is temporally filtered before to compute the angular spectrum. b) Bottom: error computed for the averaged DOA when data is not filtered to compute the angular spectrum.

This set of graphic matches to a low delay spread of $1.5 T_c$, a low-medium angular spread and a SNR of 8 dB. It may be noted as lower errors are achieved when the temporally filtered data is used instead of the original data, both in terms of mean and variance for all the observed cases. As a reference, mean error associated to the first arrival reduces almost to the half (from 0.09 rad to 0.04 rad) and its standard deviation to a fifth (from 0.19 rad to 0.03 rad) for an angular spread of 10° and when just two sensors are available. Furthermore, the mean overall error reduces from 0.15 rad to 0.02 rad and its standard deviation from 0.15 rad to 0.01 rad for the same case as it is shown in Figure 4.28 a) and b). More accurate estimates are performed when more sensors are available, and for i.e. mean error associated to the first arrival reduces from 0.15 rad to

0.10 rad when the number of sensors increases from 2 to 8 and for an angular spread of 40° . A very low improvement is achieved for the narrower angular spread of 10° , due to resolution (around $1/N_s$) and angular spread are comparable. Remain that T_c designs the chip period.

Experiment 4.9: Effect of mobile speed. This experience studies the error behavior as a function of mobile speed for different array configurations (two and eight sensors). A very wide angular spread of 360° is currently used but results are valid for narrower spreads.

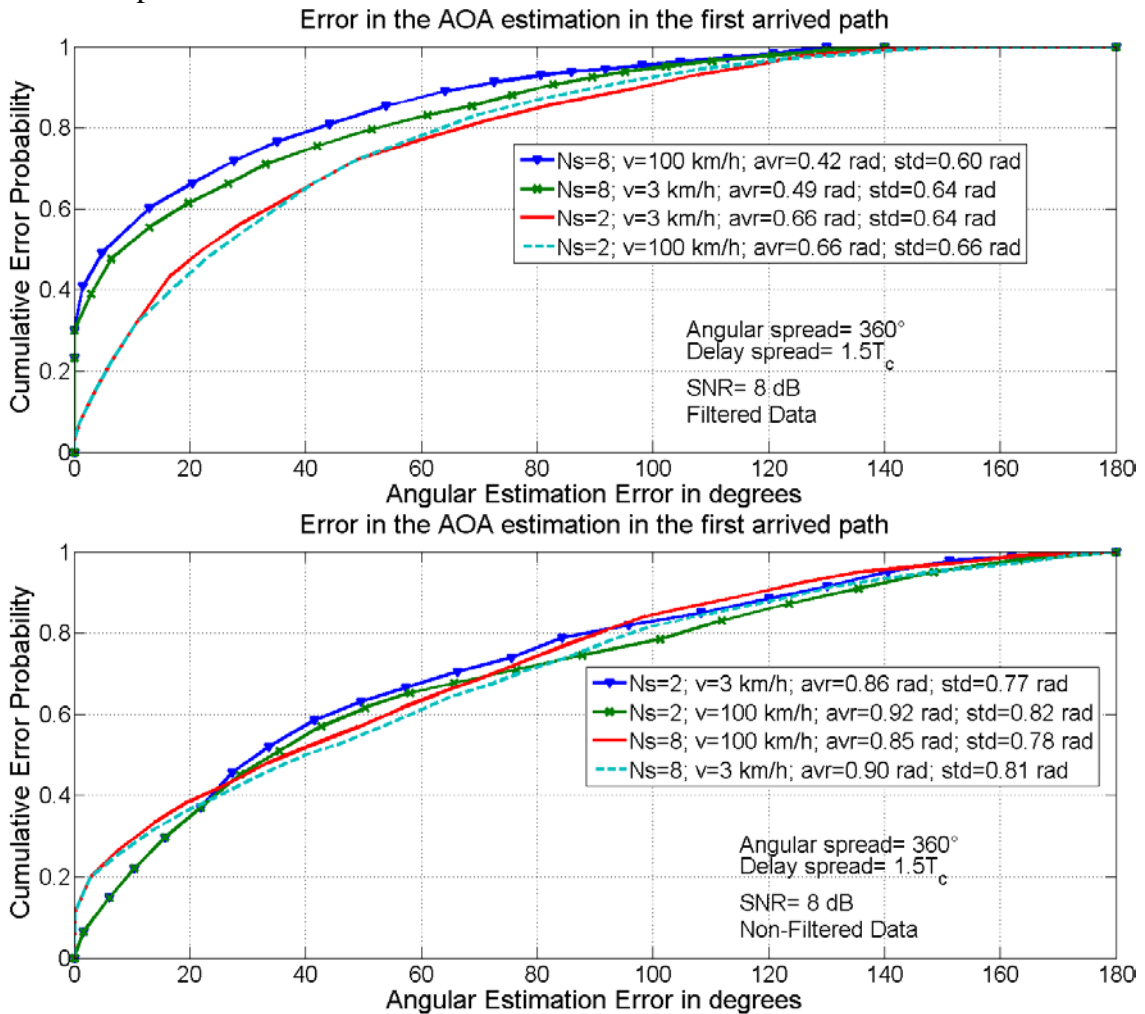


Figure 4.28: Cumulative Error Probability for the estimated Direction Of Arrival of the first path computed from Monte Carlo simulations and NMV spectra. First delay is estimated using also a NMV algorithm. Delay spread is set to 1.5 times the chip period and angular spread corresponds to 360° . Characteristics are exhibit for both 8 sensors and 2 sensors and for mobile speeds of 3 km/h and 100 km/h. SNR= 8 dB. a) Top: Data is temporally filtered before to compute the angular spectrum, and b) Bottom: Data is not filtered to compute the angular spectrum.

As it may be seen in Figure 4.29 a very slight gain is achieved for the higher speed of 100 km/h and for i.e. mean error reduces from 0.49 rad to 0.42 rad when

mobile speed increases from 3 km/h to 100 km/h for temporally filtered data and 8 available sensors. Improvements associated to the mobile speed are not important and results are very similar for the whole considered range (3-100 km/h). These results are very poor if they are compared to environments with lower angular spreads such as the above experiment.

Experiment 4.10: Effect of delay spread. Figure 4.30 compares error for environments with different delay spreads and for two array configurations (two sensors and eight sensors).

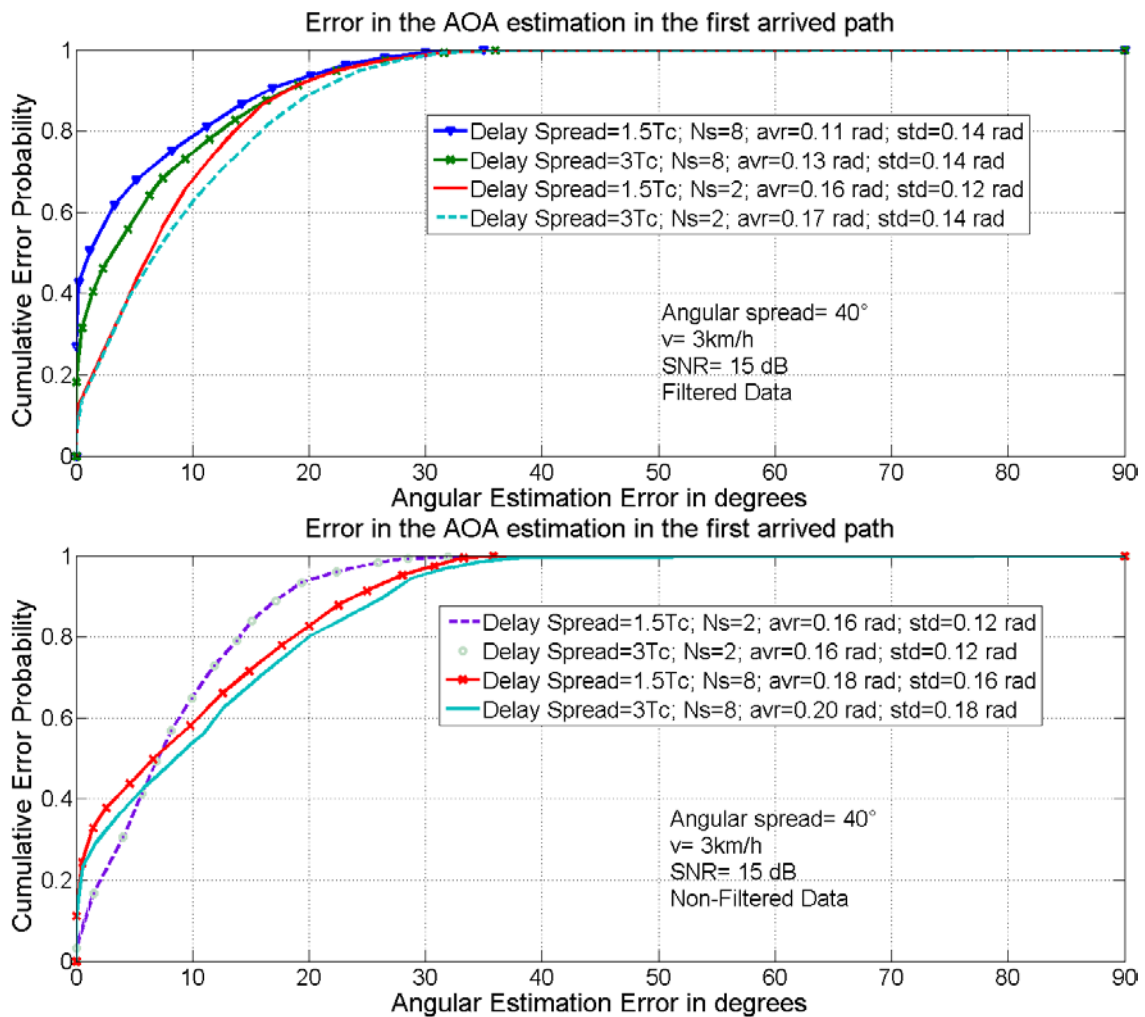


Figure 4.29: Cumulative Error Probability in the estimated direction of the first arrived path computed from Monte Carlo simulations and NMV spectra. First delay is estimated using also a NMV algorithm. Angular spread corresponds to 40°. Characteristics are exhibit for both 8 sensors and 2 sensors and for delay spreads of 1.5 and 3 times the chip time. SNR=15 dB and a mobile speed of 3 km/h. a) Top: Data is filtered before to compute angular spectrum. b) Bottom: Data is not filtered to compute angular spectrum.

This simulation shows better results for lower delay spreads; however improvement is small, even for a large number of elements. As a reference, mean error associated to the first arrival reduces from 0.13 rad to 0.11 rad when delay spread decays from $3T_c$ to $1.5T_c$ for an 8 sensors array and when data is temporally filtered, and mean error reduces from 0.20 rad to 0.18 rad when original data is used instead.

Experiment 4.11: Comparing error measures. Figure 4.31 compares the two considered error measures for two different array configurations (two sensors and eight sensors) for a higher delay spread of $5T_c$.

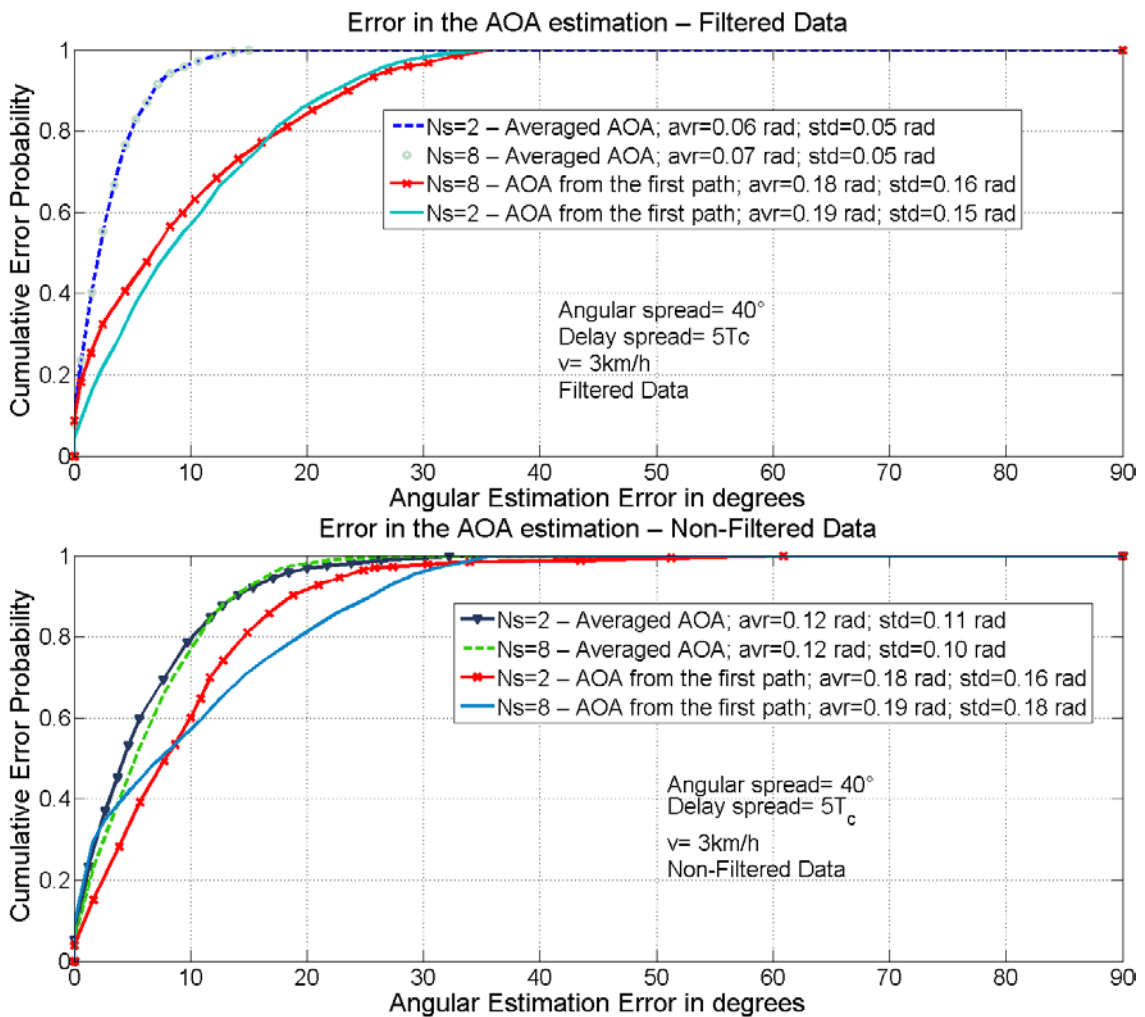


Figure 4.30: Cumulative Error Probability for the estimated Direction Of Arrival computed from Monte Carlo simulations and NMV spectra for both bearing and delay parameters. Delay spread is set to 5 times the chip period and angular spread corresponds to 40°. Characteristics are exhibit for the cases of having 8 available sensors or instead just 2 and error is evaluated for the DOA of the first arrived path and for the averaged DOA from the estimated paths. SNR=8 dB and mobile speed is 3 km/h. a) Left: Data is filtered before to compute angular spectrum. b) Right: Data is not filtered to compute angular spectrum.

It may be noted as the overall measure outperforms the error associated to the first arrived path for this case. In this example, mean error reduces from 0.18 rad to 0.07 rad and standard deviation from 0.16 rad to 0.05 rad when the overall measure is used instead of the error associated to the first arrival. It is important to note that an averaged DOA may be a better choice for positioning application, in cases where signal arrives with a very narrow delay and angular spread.

4.4.3 Summary and Conclusions

Main observations related with high resolution timing and DOA estimation are commented below:

- Since among all positioning technologies, timing-based systems provide the better accuracy, the high resolution timing estimation issue has been studied in this chapter. To extract the delay associated to the first arrival, channel information originally estimated at the lag-time domain is taken to the frequency domain. Furthermore, taking advantage of the large coherence time for delays and the bulky set of channel estimates available, the best inference about the timing for the first arrival is performed. Particularly, results relative to the behaviour of two important methods for spectral estimation have been exhibited: the Minimum Variance (MV) method and the Normalized Minimum Variance (NMV) algorithm.
- Results from the application of these methods to simulated signal in realistic conditions have revealed their limits and possibilities as a mean of improving the timing estimates required by the Positioning Computation Function (PCF), and therefore improving the quality of mobile subscriber positioning. Particularly, from the application of the MV algorithm, side-lobes appear at the spectrum that might lead to a false early detection of the first arrival. These side-lobes are considerably more reduced for the NMV method, enabling the use of a much lower threshold, therefore, the use of this latter algorithm is recommended to perform an enhanced timing estimation.
- The timing estimation improves with the use of larger records of channel estimates, a higher mobile speed, a higher SNR and a lower delay spread. However a trade-off between the number of estimates and the mobile speed must be performed, in order to get the best of these methods. The use of antenna arrays certainly improves detection, especially when first arrival is weak, SNR decays, and sensors are spatially uncorrelated. Whatever the case, the timing error deviation has been reduced to a fraction of the signal delay spread, with the use of these high resolution methods; and therefore their efficiency to enhance timing estimation has been probed.
- The NMV method has also been applied to estimate the DOA of the multiple paths, and analogue results have been achieved. Therefore, more reduced errors have been performed for lower signal angular spreads, a larger number

of sensors at the antenna array, a larger number of channel estimates; and some improvement have also been achieved for higher mobile speeds and lower signal delay spreads. However, the gain associated to delay spread is small and in certain cases negligible.

- The DOA estimated from the first arrival has been shown to be considerably worse than the estimated from the whole set of arrivals, especially for large angular spreads. Therefore, the more probable DOA should be related to the average of DOAs achieved for the whole set of arrivals.

4.5 Positioning Accuracy when using a two stage detection and estimation approach

In this section, the results from the whole chapter are summarized, and they are related to the positioning problem. Table 4.3 shows two types of results. The first group refers to the expected root mean square error (RMSE) from the application of the GLRT detector derived in section 4.3, during the coarse detection stage of the first arrival, and it is specified for a SNR= 0 dB, since that the optimum threshold corresponding to a false alarm of 10^{-3} was found for this level with the use of 750 - 1500 slots (50-100 frames in WCDMA), four sensors, and an observation window length $S=5$ (an adequate value for a delay spread of $1.5T_c$). The reduction in the number of sensors and the increase of delay spread degrade this minimum error dispersing it away from the quantization level. These errors have been assigned proportionally for the remaining configurations following the tendency of the data.

Table 4.3 Summary of timing errors achieved in the detection and estimation stages.

N_s	DS (T_c)	SNR (dB)	Bias (T_c)	RMSE (T_c)	Comment
1	1.5	0	-	0,50	Coarse Detection
1	1.5	8	0,12	0,34	NMV High Resolution Detection
1	1.5	15	0,03	0,15	NMV High Resolution Detection
1	3.0	0	-	0,75	Coarse Detection
1	3.0	8	0,10	0,46	NMV High Resolution Detection
1	3.0	15	0,04	0,18	NMV High Resolution Detection
4	1.5	0	-	0,29	Coarse Detection
4	1.5	8	0,07	0,22	NMV High Resolution Detection
4	1.5	15	0,02	0,12	NMV High Resolution Detection
4	3.0	0	-	0,50	Coarse Detection
4	3.0	8	0,07	0,37	NMV High Resolution Detection
4	3.0	15	0,03	0,17	NMV High Resolution Detection

The second group of data in Table 4.3 has been derived from results in section 4.4 (experiments 4.3 – 4.5) related to the application of the NMV high resolution timing estimation, as part of the second stage of our proposal. For each one of these experiments, the bias and the error standard deviation in the estimation of the first arrival were computed for a mobile subscriber by using 1000 experimental realizations. Furthermore, from a weighted average of these data in relation to the mobile speed, their average results are achieved for a mobile subscriber with an average speed between 50 and 55 km/h for two different configurations of the antenna: one sensor and four sensors.

Above data clearly shows the performance of the two stage estimation-detection scheme proposed in section 4.1, and exhibited in Figure 4.1 for the determination of the timing of the first arrival. These results show that effectively a lower error is achieved for higher SNRs, lower signal delay spreads and a larger number of elements at the antenna array. However, these results also reveal that the improvement of timing accuracies are restrained by the ability of the high resolution algorithm to resolve too closer paths for one side, and by the bias introduced due to the missing of the weaker signals once the optimum threshold is set. Results from Table 4.3 for the high SNR regimen are comparable to timing errors described by the CRBs for 50 frames (750 slots in WCDMA) as it is easily seen in Figure 3.13 for a PCD channel with $\alpha=0.99$ and a delay spread of $2T_c$. Furthermore, timing accuracy at the low SNR regimen is not just limited by the optimum threshold selected at the detection stage but also for the threshold imposed to avoid early detections due to the side lobe that appears at the NMV spectrum. This latter threshold will mask weaker arrivals, introducing bias especially to those measures taken at receivers from links related to distant BSs. However, the methods described in chapter 2 for TOA measures and in section 4.2.2 for TDOA can palliate this problem.

To illustrate this behaviour, an exponential interpolation has been performed in Matlab ® for each one of the four SNR/RMSE characteristics contained at Table 4.3, to derive the operational curves of our two-stage approach, and this information has been feed to the positioning simulation platform analogously to the methodology used to integrate the CRBs in section 4.2. However, in this case the error distribution of the error is assumed exponential as described by the Greenstein model for SNRs lower than a specified edge (0 dB or 3 dB) introduced for modelling the overall composite effect of thresholds used at both detection and estimation stages. On the other hand, when SNR is higher than this threshold, a Gaussian distribution for the error is preferred with standard deviation as predicted by the operational curves.

Figure 4.31 exhibits the distribution functions for the positioning error of a mobile subscriber with an average speed of 50 km/h, when the two-stage approach in Figure 4.1 has applied using the operational curves derived from data contained in Table 4.3.

This figure shows an important improvement in the positioning accuracy from the application of the detection-estimation methodology, when it is compared with the

application of the raw data provided by the Greenstein model, and TDOA measures are used to perform the positioning. In fact, positioning errors lower than 180 m for the 70% of the cases and lower than 214 m for the 95% of the cases were registered with the original information. These errors reduced almost to the half: to lower than 100 m for the 70% of the cases, and lower than 114 m for the 95% of the cases when the two-stage approach was applied, and for a high SNR of 21.1 dB available at the link between the subscriber and the central site used as reference. For a moderate SNR of 15 dB, the positioning errors reduced below to 121 m for the 70% of the cases and below to 128 m for the 95 % of the cases with the application of the proposed signal processing, an improvement of around 35% - 40%. These results were achieved using a composite threshold of 3 dB, and therefore are appropriate for describing the operation of the detection-estimation scheme as commented in sections 4.3.3.4 and 4.4.1.6. Meaningless differences with the use of 4 sensors in relation to just one were registered. These observations agree with the results in experiments 4.3 – 4.5, where just small improvements were appreciated with the use of 4 sensors, being the most important improvement related with the availability of higher SNRs.

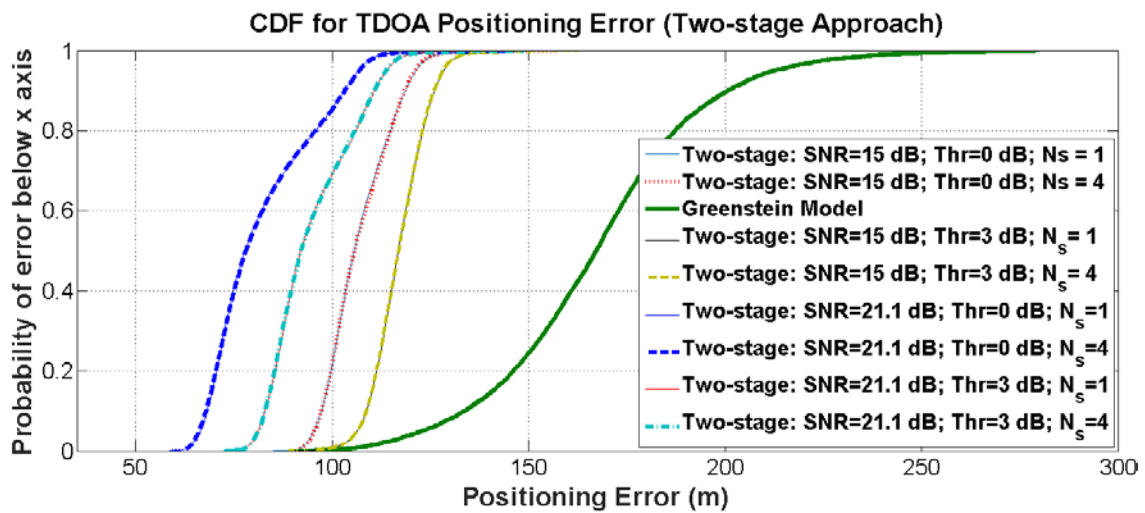


Figure 4.31: Distribution Function for the Average Positioning Error for a subscriber within a cell of radius $R=1$ km. A two-stage detection-estimation approach has been performed for $N_s=1$ and 4 sensors, and for a reference SNR at the central site $SNR=15$ [dB] and 21.1 [dB], for two different operational thresholds of 0 dB and 3 dB.

Figure 4.31 also shows curves for a lower operational threshold of 0 dB. These curves could well correspond to the use of the two-stage approach with both re-engineered detection and high resolution estimation stages so that a better threshold of 0 dB could be appropriate. If a composite operational threshold of 0 dB were appropriate, improvements between 6% and 12% could be achieved.

4.5.1 General Conclusions

Main observations related with the contents of this chapter are commented below:

- Timing estimation errors provided by the Cramer Rao Bounds have been integrated on the positioning simulation platform developed at chapter 2 for the cases of high and middle SNR regimen, providing an insight of the limits of techniques for timing based positioning when space-time diversity is used to enhance the quality of these estimates. Results provided from these simulations reveal that the near-far effect degrades TDOA-based positioning of subscribers located near the control BS due to the low level of SNR at the distant link. Therefore, a more accurate positioning is expected near the boundaries with the use of this technique. This observation was also confirmed with the incorporation of the operational curves of the two-state approach to the positioning simulator.
- The issue of timing estimates degradation at the low SNR regimen is better understood reminding that the chip level synchronization corresponds to a problem of discriminating signal from noise. This problem was boarded with the study and implementation of the GLRT detector proposed in section 4.3, where false alarm and detection probabilities were computed and integrated to a simple model provided to verify the impact of scattered signal no noise ratio, direct path to scattered power ratio, and the use of antenna arrays in the performance of the proposed GLRT detector for different configuration of this detector. Results from this study reveal that this detector is very sensible to SNR, and that important improvements in terms of detection probability may be achieved for the case of very weak signals when adding a higher number of observations to the detector. These newer estimates can be provided with the use of a larger number of sensors at the antenna array or by using a larger number of slots.
- These results also show that detection improves when a direct path is present, even in the case of the total signal power is kept constant; and that once the optimum threshold has been selected at the detection stage, it defines the SNR operation level below which a weaker signal will be missed and therefore the achieved measure will be biased. Hence, this detector should be applied after synchronization when some prior information about signal is available in order to properly set this threshold to reduce the probability to get biased timing estimations.
- Since range errors are very sensible to the timing errors, and the uncertainty within a chip time for WCDMA reaches almost 80 m, the second stage uses a high resolution estimation algorithm to reduce this error to a fraction of this bound (8-15 m). To extract the delay associated to the first arrival, channel information originally estimated at the lag-time domain is taken to the frequency domain. Furthermore, taking advantage of the large coherence time for delays and the bulky set of channel estimates available, the best inference about the

timing for the first arrival is performed. Two important methods for spectral estimation have been studied to perform this task: the Minimum Variance (MV) method and the Normalized Minimum Variance (NMV) algorithm.

- Results from the application of these methods to simulated signal in realistic conditions have revealed some limitations of these techniques due to the appearing of side-lobes at the spectrum that might lead to a false early detection of the first arrival. This issue mainly affects to the MV algorithm since side-lobes are considerably more reduced for the NMV method, enabling the use of a much lower threshold, therefore, the use of this latter algorithm is recommended to perform an enhanced timing estimation. Moreover, simulations reveal that errors below 114 m are possible, with the application of the proposed two-stage scheme, when using the NMV timing estimation in high SNR regimens.
- The timing estimation improves with the use of larger records of channel estimates, a higher mobile speed, a higher SNR and a lower delay spread. However a trade-off between the number of estimates and the mobile speed must be performed, in order to get the best of these methods. The use of antenna arrays certainly improves detection, especially when first arrival is weak, SNR decays, and sensors are spatially uncorrelated. Whatever the case, the timing error deviation has been reduced to a fraction of the signal delay spread, with the use of these high resolution methods; and therefore their efficiency to enhance timing estimation has been probed.
- The NMV method has also been applied to estimate the DOA of the multiple paths since this information may help to enhance positioning algorithms, and similar results have been achieved. Therefore, more reduced errors have been performed for lower signal angular spreads, a larger number of sensors at the antenna array, and a larger number of channel estimates. Some improvement has also been achieved for higher mobile speeds and lower signal delay spreads. However, the gain associated to delay spread is small and in certain cases negligible. Furthermore, the DOA estimated from the first arrival has been shown to be considerably worse than the estimated from the whole set of arrivals, especially for large angular spreads. Therefore, the more probable DOA should be related to the average of DOAs achieved for the whole set of arrivals.
- At last but not the least, the overall timing accuracy from the proposed two stage detection-estimation procedure not just depends on the properties of the high resolution estimation algorithm at the high SNR regimen, but also of the combined operation of the detector and the estimation algorithm at the low SNR regimen. A better test implemented at the detection stage can certainly enhance the probability of detecting the first arrival, but this path will be masked by the estimation algorithm if its level is weaker than the threshold used to overcome the early detection due to the side lobe of the high resolution spectrum. Therefore, a better solution using this two stage approach must consider the improvement of these two components.

4.6 Annex 4.1 Proportion of cases where the error variance as predicted by CRB is higher than a predefined threshold

The integration of the CRB model to the simulation platform based on the Greenstein's propagation model enables the evaluation of the benefits of space-time diversity over positioning. The CRB is an optimistic measure, in this case, of the expected error variance of the first arrival timing estimation, and depends of the model parameters such as the number of vector channel estimates K used in timing estimation, the length of the observation window, the number of antennas N_s , the signal delay spread, but particularly of the SNR. When the SNR is too low, first arrival estimation degrades and therefore the value for the CRB increases. Reasonably, the estimation variance for the first arrival should be well down the signal delay spread to decide that the timing has been successfully achieved (ASM2, ASM3). On the contrary, when this error is in the order of the quantization, the use of the bounds is not safe, and the statistics of the Greenstein's model is preferred (ASM1). Therefore, the first arrival is possibly missed and timing estimation is biased.

In the following, a measure of the impact of the selected threshold required to discriminate the low-error region in the CRB model as defined in ASM3 is proposed in (4.78). It corresponds to the proportion of cases p_f , where the CRB is higher than the specified threshold and therefore it is not a low-error bound anymore.

$$p_f = \text{prob} \left\{ \sqrt{\text{CRB} \{k_0 | \text{SNR0}\}} > \text{threshold} \right\} \quad (4.78)$$

Where $\text{CRB} \{k_0 | \text{SNR0}\}$ denotes the Cramer-Rao Bound in the estimation of the first arrived path for a particular scenario where the referential Signal to Noise Ratio SNR0 , at a distance of one kilometer from the transmitter is known, and where the **SNR** at the receiver is a random variable that may be computed from SNR0 as in (4.79):

$$\mathbf{SNR} = \text{SNR0} - 10\beta \log(\mathbf{d}) + \mathbf{X} \quad (4.79)$$

Being \mathbf{d} , a uniformly distributed random variable with values between R and $3R$ in order to catch the performance of the most distant subscriber positions of the whole group of BSs within the system, and R is the cell radius. Furthermore, \mathbf{X} corresponds to the Gaussian random dispersion from the path gain as described by the Greenstein model in chapter 2.

Assuming the noise power is constant, the SNR0 is essentially limited by the transmitter power dynamic range, and therefore the proportion of cases where the use of the CRB is not safe according to assumption ASM3, are exhibited in Figure 4.32 for a SNR0 range between 0 and 25 [dB], and two selected thresholds of $0.25T_c$ and $0.50T_c$; where T_c is the chip time. Furthermore, T_c has been set to 0.26 μsec since it is a suitable value for WCDMA [58]. These thresholds were selected reminding that in case of NLOS biased estimates, the values for the RMS delay spread tend to increase, and they reach an expected value of $3.5T_c$, becoming as high as $5T_c$, as it was predicted by the

Greenstein model at chapter 2 when $\beta=3.7$ for this case. Therefore, our thresholds have been selected to discriminate values much lower than these limits (ASM3).

With the purpose of extracting pondered conclusions from these results, when the uncertainty in the estimation of the first arrival predicted by the Cramer-Rao Bound is lower than $0.25T_c$, it will be assumed that it has been performed successfully; when this uncertainty takes values between the two thresholds, that this estimation has suffered some degradation; and when uncertainty is greater than $0.50T_c$, that the first arrival is possibly missed.

Additionally, for computing the CRB for the first arrival required in (4.78), the length of the observation window has been set to $20T_c$, the signal angular spread has been set to 5° , the number of channel vector estimates to 250, the temporal correlation factor between consecutive channel vector estimates to 0.99, and the number of sensors in the antenna array to 8 and 32 respectively.

The Greenstein model has been set to the standard parameters as it was discussed in chapter 2. Therefore, $T_1=0.4$ [μsec], $\sigma_\xi=2$ [dB], $\sigma_x=8$ [dB], $\varepsilon=0.5$, and $\rho=-0.75$. In addition, the cell radius has been set to $R=1$ km.

Figure 4.32 shows the proportion of cases where the CRB possibly fails in predicting the minimum variance and the first arrival is missed, for two configurations of the antenna array, respectively with 8 and 32 sensors.

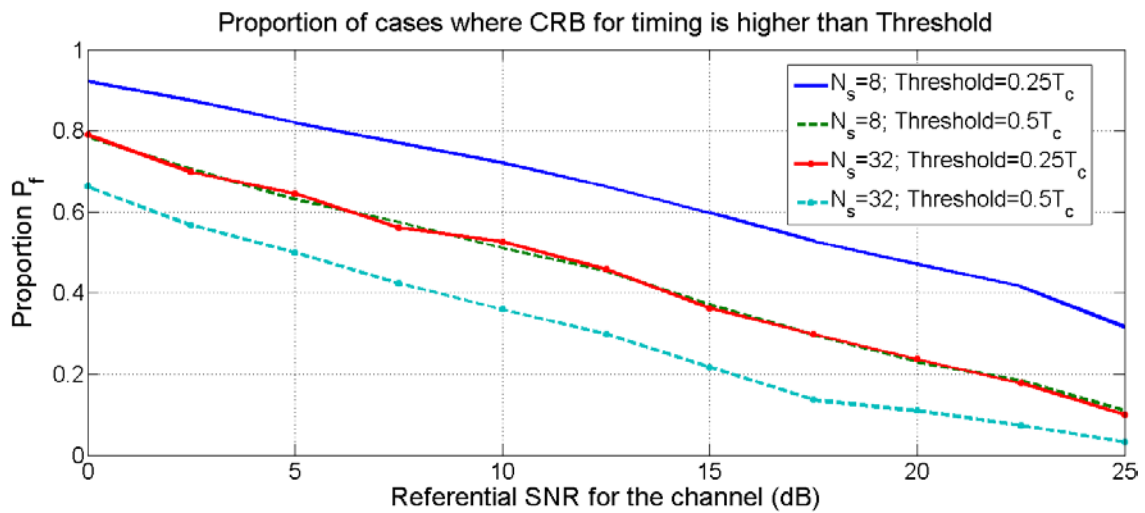


Figure 4.32: Proportion of cases where CRB for timing possibly fails in predicting the minimum variance, in terms of the reference value for Signal to Noise Ratio, SNR0. Subscribers have been placed at random between R and $3R$ from the transmitter, with $R=1$ km and two specified thresholds.

This graph put in evidence that when 8 sensors are available, and for a high power transmission, at least the 68% of the positions between 1 km and 3 km are able to perform first arrival estimation successfully. Moreover, an additional group of 21% of the cases might achieve a mild degradation, and just 11% of the cases could miss the first arrival. However, as the reference transmission power decays, the probability of missing the first arrival increases almost linearly at a rate of 2.5%/dB. Hence, for a middle power transmission where $SNR_0=12.5$ [dB], the probability of missing the first arrival reaches 45%, and a good portion of 34% of the total would perform a successful estimation. Furthermore, increasing the number of sensors helps to improve the portion on cases where mitigation is effective. Note as when $N_s=32$, this proportion increases up to 90%, whilst the portion of fail reduces to 3% for the high power reference channel with $SNR_0=25$ [dB]. When SNR_0 reduces to the half, the number of cases where the NLOS mitigation procedure fails would be 30%. These results show as the probability of NLOS mitigation is very sensitive to SNR, and how a large number of sensors could be used to enhance the mitigation range. However, the overall effect depends of the problem geometry, and final performance will be appreciated from results exhibited in the system simulator in section 4.2.2.

Since the estimation of the first arrival trusts on the fact of this arrival belong to a well conformed signal cluster, the probability of achieving a poor estimate of the Delay Spread p_{f_1} , has also been computed from the CRB model, analogously to timing in (4.78), as it is shown in (4.80):

$$p_{f_1} = \text{prob} \left\{ \sqrt{CRB \{DS | SNR_0\}} > \text{threshold} \right\} \quad (4.80)$$

Figure 4.33 exhibits this probability for the case of 16 sensors at the antenna.

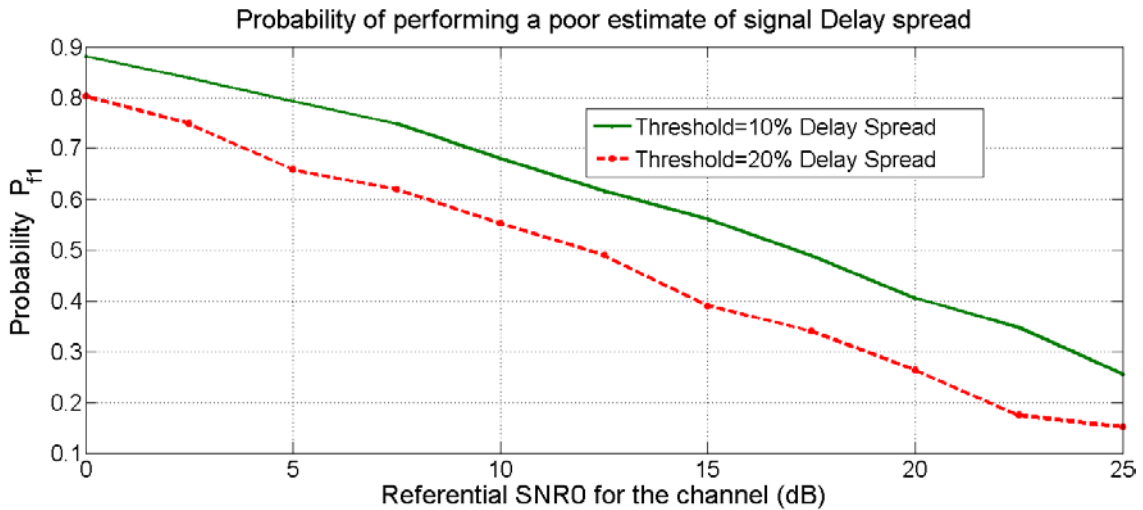


Figure 4.33: Probability of performing a poor estimate of the signal delay spread for subscribers placed at random, between R and $3R$ from the transmitter, in terms of the reference Signal to Noise Ratio, SNR_0 , with $R=1$ km, and for two specified thresholds, when $N_s=16$ sensors.

Further, it includes two thresholds corresponding respectively to 10% and 20% of the Delay Spread. Therefore, this probability reaches a value within 50%-60% when the threshold is set between 10% - 20% of the delay spread, and $SNR_0 = 12.5$ [dB]. These values fit well with the probability of missing the first arrival for the same case. Therefore, both values are comparable and suggest the same phenomenon: an important improving in the timing estimation accuracy with the use of larger number of sensors at the antenna array.

It is important to remark that this proportions have been achieved using a linear distribution with the distance and therefore is just referential. The proportion of cases within our simulation platform belongs to a surface so it is approximately related to the square of the proportions provided by these characteristics.

4.7 Annex 4.2 A basic approach to false alarm and detection probability at the GLRT detector

From section 4.3.3.3, let us define two auxiliary variables y_i and g_i as:

$$y_i = \frac{\hat{\lambda}_i}{(\lambda_i/2)} \sim \chi_2^2 \quad g_i = \frac{\lambda_i}{\sigma_n^2} = \frac{(\lambda_s)_i}{\sigma_n^2} + 1 \quad (4.81)$$

Making some arrangements in (4.33), this expression transforms as follows:

$$\begin{aligned} L(\Lambda) &= \frac{1}{\hat{\sigma}_n} \sum_{i=1}^{N_s P} \left[m(\lambda_i/2) \frac{\hat{\lambda}_i}{(\lambda_i/2)} - \ln \left(\frac{\hat{\lambda}_i}{(\lambda_i/2)} \right) - \ln \left(\frac{m\lambda_i}{2} \right) \right] = \\ &= \sum_{i=1}^{N_s P} \left[\frac{m}{2} g_i y_i - \ln(y_i) - \ln \left(\frac{mg_i \sigma_n^2}{2} \right) \right] = \sum_{i=1}^{N_s P} z_i \end{aligned} \quad (4.82)$$

In above expression, z_i is the Taylor series expansion around 2 of the terms within the summation (which amounts to an approximation of the random variable around its mean value):

$$z_i = \frac{mg_i}{2}(2 + \varepsilon) - \ln(2 + \varepsilon) - \ln \left(\frac{mg_i \sigma_n^2}{2} \right) = f(0) + \left. \frac{\partial f}{\partial \varepsilon} \right|_{\varepsilon=0} \varepsilon + \mathcal{O}(\varepsilon^2) \quad (4.83)$$

The first order approximation may be expressed as in (4.84):

$$z_i \approx mg_i - \ln(mg_i \sigma_n^2) + \frac{mg_i - 1}{2}(y_i - 2) \quad (4.84)$$

Since the probability density function (pdf) for y_i noted as $f_y(y)$ tends to be chi-squared when non ordered eigenvalues are considered, and in order to compute the pdf for z_i , noted as $f_z(z)$, the following expression may be used:

$$f_{z_i}(z_i) = \left. \frac{f_{y_i}(y_i)}{\left| \frac{dz_i}{dy_i} \right|} \right|_{y_i=f^{-1}(z_i)} = \left. \frac{f_{y_i}(y_i)}{\left| \frac{mg_i - 1}{2} \right|} \right|_{y_i = \frac{z_i + \ln(mg_i \sigma_n^2) - 1}{(mg_i - 1)/2}} = \left. \frac{f_{y_i}(y_i)}{\left| \frac{mg_i - 1}{2} \right|} \right|_{y_i=a_i(z_i+b_i)} \quad (4.85)$$

From (4.85) and recalling that the characteristic function and the pdf are a Fourier transform pair, and also that the characteristic function for a chi-squared distribution is given by:

$$\phi_{y_i} = \frac{1}{2j\omega + 1} \quad (4.86)$$

The characteristic function for z_i and $L(\mathbf{X})$ are expressed respectively by (4.87) and (4.88):

$$\phi_{z_i}(z_i) = F\left\{a_i f_{y_i}(y_i)\Big|_{y_i=a_i(z_i+b_i)}\right\} = a_i F\left\{f_{y_i}[a_i(z_i+b_i)]\right\} = \phi_{y_i}\left(\frac{\omega}{a_i}\right) \exp(j\omega b_i) \quad (4.87)$$

$$\phi_{L(\mathbf{X})} = \prod_{i=1}^{N_s p} \phi_{z_i} = \prod_{i=1}^{N_s p} \frac{1}{2j\frac{\omega}{a_i} + 1} \exp(j\omega b_i) \quad (4.88)$$

As we want to compute the probability of false alarm, we are interested in the case when just noise is present (hypothesis H_o is true). g_i defined in (4.81) is 1, and (4.88) reduces to:

$$\phi_{L(\mathbf{X}=\mathbf{N})} = \frac{1}{\left(2\frac{\omega}{a}j + 1\right)^{N_s p}} \exp(j\omega b p N_s) \quad (4.89)$$

$$a = \frac{2}{m-1}; \quad b = \ln(m\sigma^2) - 1 \quad (4.90)$$

The pdf for $L(\mathbf{X} = \mathbf{N})$ is shown in (4.91), where $u(\cdot)$ is the unit step function, and false alarm probability is expressed finally as in (4.93):

$$f_L(L) = F^{-1}(\phi_L) = \frac{(a/2)^{pN_s}}{(pN_s - 1)!} (L + bpN_s)^{pN_s - 1} \exp\left[-\frac{a}{2}(L + bpN_s)\right] u(L + bpN_s) \quad (4.91)$$

$$P_{fa} = \int_{\gamma'}^{\infty} f_L(L) dL = \int_{\gamma_x = a(\gamma' + bpN_s)}^{\infty} \frac{x^{\frac{2pN_s}{2} - 1}}{2^{\frac{2pN_s}{2}} \Gamma\left(\frac{2pN_s}{2}\right)} \exp\left(-\frac{x}{2}\right) dx = Q_{\chi^2_{2pN_s}}(\gamma_x) \quad (4.92)$$

Following an analogous procedure for detection probability, it may be shown that its final expression is given by (4.94) for the case of Partially Coherent Distributed (PCD) signal. Temporal correlation coefficients for this case correspond to values between 0 and 1.

And after some algebraic procedures shown in (4.92), false alarm and detection probabilities may be express as in equations (4.93) and (4.94):

$$P_{fa} = Q_{\chi^2_{2pN_s}} \left\{ \frac{2}{m-1} \left[\gamma' + pN_s \left\{ \ln(m\hat{\sigma}_n^2) - 1 \right\} \right] \right\} \quad (4.93)$$

$Q_{\chi}(\cdot)$ defines the right tail cumulative function for a chi-squared distributed variable with $2pN_s$ degrees of freedom, when K channel vectors (mp) and N_s sensors are used, and provided that secondary data for the estimation of the noise level is large

enough. Probability of detection given by (4.94) has been derived by using a linear approximation in an analogue way to false alarm.

$$P_D = \sum_{n=0}^{pN_s-1} C_n \exp\left(-\frac{\gamma' - pN_s + pN_s \ln(m) + G}{\beta_n}\right) \quad (4.94)$$

The variables used in above expression are defined as follows, being λ_ϕ and λ_τ the eigenvalues of \mathbf{R}_ϕ and \mathbf{T}_k respectively.

$$\begin{aligned} C_n &= \prod_{i=0; i \neq n}^{m-1} \frac{1}{1 - \beta_i / \beta_n} \\ G &= \sum_{i=0}^{pN_s-1} \log(\lambda_i) \\ \beta_n &= m\lambda_n / \sigma_n^2 - 1 \\ \lambda_n &= \lambda_{\phi_i} \lambda_{\tau_j} \quad \forall i = 1, \dots, N_s; \quad j = 1, \dots, p \end{aligned} \quad (4.95)$$

When an adequate probability of false alarm has been defined by selecting a threshold from (4.93), probability of detection will be given by channel characteristics. Note that P_D is a function of SNR , $K=mp$, N_s , as well as of the temporal and spatial correlation.

These expressions resulting from a first order approximation in the Taylor's expansion and under the assumption of all the eigenvalues has the same mean distribution seem to be not very accurate, but it may be noted that the 50% probability point in general coincides, and simulations reveal that characteristics decay very fast beyond this point.

4.8 Annex 4.3: Characterization of the MV and NMV timing estimates

It is important to get some insight in the performance of the MV and NMV for a proper design in a practical implementation. In particular, the parameters of interest are a) the resolution of the timing estimate, b) the sidelobes and its influence, c) the step size in the one-dimensional search and c) the threshold for detection of the first arrivals. As the problem is intractable when multiple arrivals are considered, the single arrival plus noise case will be studied.

Under this premise, the signal model is defined as in equation (4.53), where the noise is white and \mathbf{G} is the square root raised cosine filter in transmission. The correlation matrix (and its inverse computed using the inversion lemma) of the signal is therefore given by the expression:

$$\mathbf{R}_y = \alpha^2 \mathbf{f} \mathbf{f}^H + \sigma_v^2 \mathbf{I} \quad \mathbf{R}_y^{-1} = \sigma_v^{-2} \mathbf{I} - \sigma_v^{-2} \frac{\alpha^2 \mathbf{f} \mathbf{f}^H}{\sigma_v^2 + \alpha^2 \mathbf{f} \mathbf{f}^H} \quad (4.96)$$

The constant α^2 accounts for the power of the single arrival and \mathbf{f} is the delay signature of this channel path arriving at delay τ_0 :

$$\mathbf{f} = \mathbf{G} \mathbf{e}_{\tau_0} \quad (4.97)$$

By replacing equation (4.96) in the MV and NMV expressions ((4.59) and (4.62) respectively) it is easy to derive the following expressions (where $SNR = \alpha^2 / \sigma_v^2$):

$$P(\tau) = \frac{\sigma_v^2 (\alpha^2 + \sigma_v^2)}{\sigma_v^2 + \alpha^2 (1 - |\varepsilon_\tau|^2)} = \sigma_v^2 \frac{1 + SNR}{1 + SNR (1 - |\varepsilon_\tau|^2)} \quad (4.98)$$

$$S(\tau) = \sigma_v^2 \frac{(1 + SNR) (1 + SNR (1 - |\varepsilon_\tau|^2))}{1 + (2SNR + SNR^2) (1 - |\varepsilon_\tau|^2)}$$

that depend on the inner product between the delay manifold vector and the delay signature of the incoming channel path:

$$\varepsilon_\tau = \mathbf{f}^H \mathbf{g}_\tau = \mathbf{e}_{\tau_0}^H \mathbf{G}^H \mathbf{G} \mathbf{e}_\tau \quad (4.99)$$

Note that both $P(\tau)$ and $S(\tau)$ present a maximum at the position of the incoming delay ($|\varepsilon_\tau|^2 = 1$), with an amplitude equal to the power of the arrival plus noise level:

$$P(\tau) = S(\tau) = \alpha^2 + \sigma_v^2 \quad (4.100)$$

Equation (4.99) depends strongly on the shape of \mathbf{G} . Figure 4.34 plots the absolute value in terms of τ for a square root raised cosine window and for a constant window (which would be the one usually used in a spectrum estimation problem). Clearly, the latter case exhibits much higher side lobes attenuation and a slightly wider main lobe.

The resolution in the peaks is better for the NMV solution as can be derived from equations in (4.98). Figure 4.35 plots these expressions for different values of the argument and clearly shows a narrower behavior for the NMV close to $|\varepsilon_\tau|^2=1$, that is, close to the position of the peaks of the delay spectrum. In practice, equal power peaks with a separation below 1/5 of a chip can be resolved with the NMV solution.

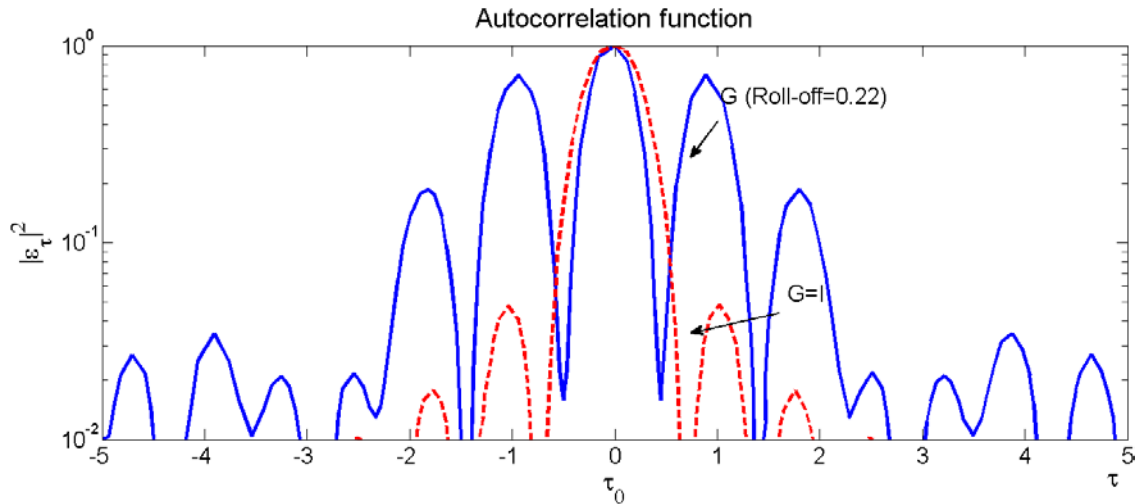


Figure 4.34: Autocorrelation function of the sinc and the square root raised cosine windows (with roll-off factor 0.22, as for the air interface of UMTS).

As the estimation of the arrivals will be decided on the basis of the detection of the maximal of the MV or NMV spectra, it is important to determine if these estimates present side lobes which could be misinterpreted as arrivals.

The level of the side lobes can be determined from the maximal of the expressions in equation (4.98). As these expressions are strictly increasing as a function of $|\varepsilon_\tau|^2$, the side lobes have to be positioned at the side lobes of $|\varepsilon_\tau|^2$. The values of $|\varepsilon_\tau|^2$ at the side lobes for \mathbf{G} with a roll-off factor 0.22 are given by $|\varepsilon_\tau|^2=0,675$ and $|\varepsilon_\tau|^2=0,182$.

The level of the first and second side lobes over the floor noise, both for $P(\tau)$ and $S(\tau)$ are shown in the following figure as a function of the SNR.

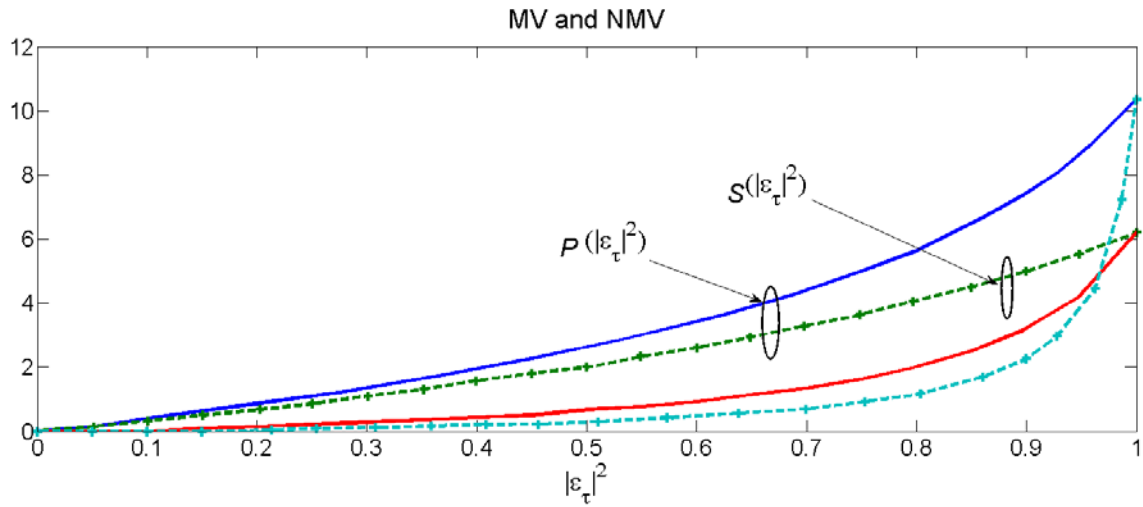


Figure 4.35. MV and NMV as a function of the argument, for different values of the SNR: 10 dB (solid line) and 5 dB (cross-solid line).

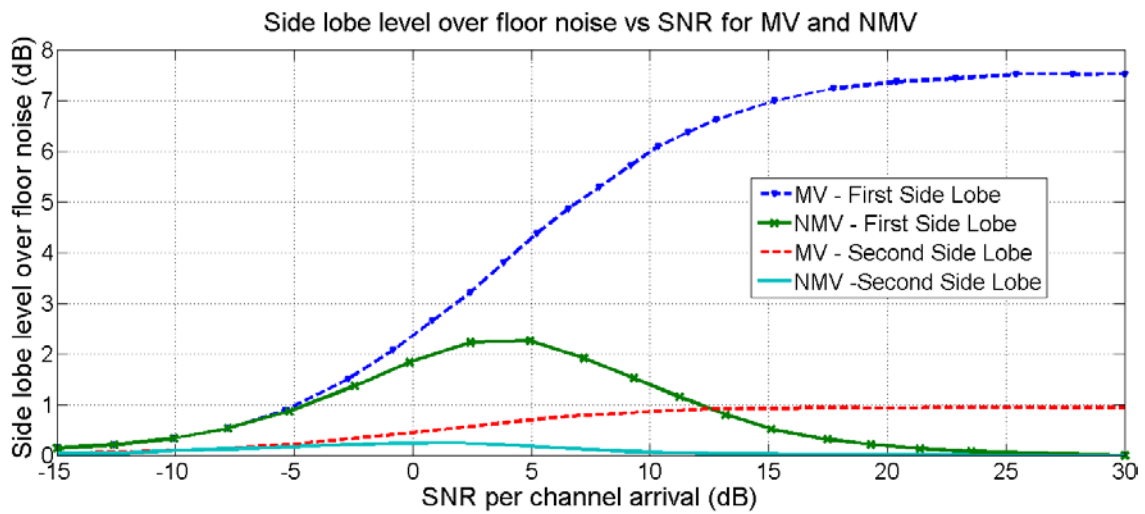


Figure 4.36: Side lobe level below the maximum of the spectrum (signal+noise power) for the first side lobe (solid line) and for the second side lobe (dashed line), both for MV and NMV delay spectra.

It is important to note that:

1. The harmful effect of the side lobe level decreases with higher SNRs. Moreover, due to the lower level of this side lobe for the NMV solution, the use of this methodology is preferred since it reduces the effect of masking of early arrivals by more powerful late arrivals.

2. The side lobe level of NMV has an absolute maximum of 2.2 dB ($=1.8621\sigma^2$) over the noise level, while the MV solution has a maximum at 7.5 dB. Clearly, the threshold has to be set over these values to avoid an early detection. However, once the threshold is set, weaker arrivals will be lost.
3. The value of second side lobe at 0.251 dB over the noise floor (see Figure 4.36) allows determining a threshold which can be used to update the floor noise level estimation.
4. These conclusions can be derived in a multipath non-coherent scenario. Otherwise, the MV and NMV methods fail to determine the maximum. We assume here that the presence of multiple sensors (or spectrum averaging techniques) avoid rank deficiency of the signal matrix (as long as the spatial signatures have enough diversity and the number of significant arrivals do not exceed the number of sensors), as mentioned in section 4.4.1.5.

These observations allow us to decide in favor of NMV as a high resolution detector of arrivals. Figure 4.37 shows a typical delay spectrum both for the MV and NMV solutions. Clearly, the NMV offers improved performance in terms of side lobes even in the multipath case.

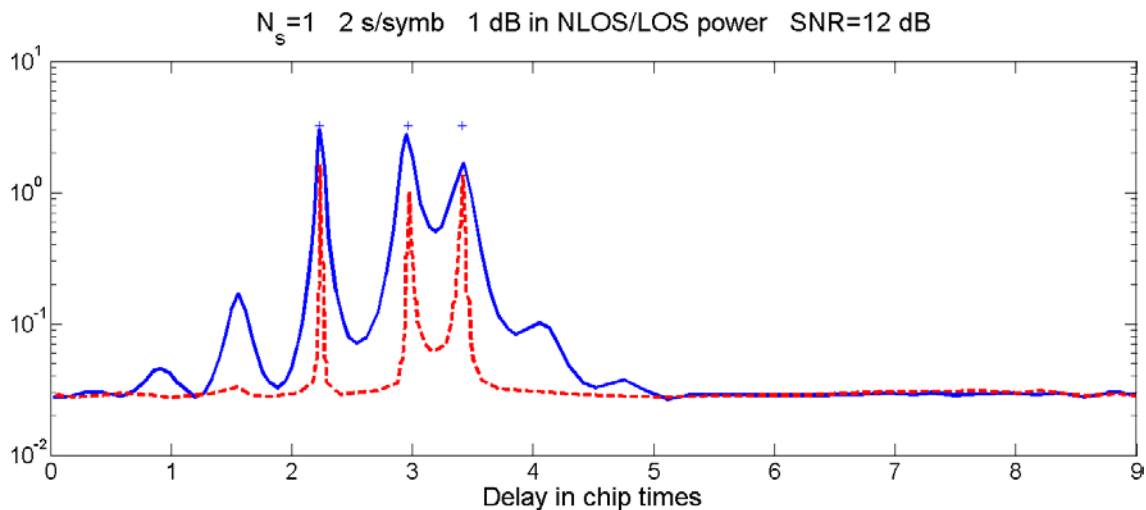


Figure 4.37. Typical MV (solid) and NMV (dashed) delay spectra computed for a single sensor and an overall SNR of 12 dB. The level of the side lobes is very much attenuated in the NMV solution. The true positions of the channel paths are 2.23; 2.96 and 3.40 chips (denoted by crosses).

4.9 References

- [1] J. Vidal, M. Cabrera, R. Játiva, M. Nájjar, A. Pagès, C. Simon, “IST-1999-10322 SATURN – D621 Location Based Services Performance Evaluation (Location Techniques)”, Universitat Politècnica de Catalunya, June 2001. <http://www.ist-saturn.org>.
- [2] Mohamed Adnan Landolsi, Ali H. Muqaibel, Abdullah S. Al-Ahmari, “Near-Far Problem Impact on Mobile Radiolocation Accuracy in CDMA Wireless Cellular Networks”, IEEE International Conference on Telecommunications and Malaysia International Conference on Communications, May 2007. DOI: 10.1109/ICTMICC.2007.4448594.
- [3] L. J. Greenstein, V. Erceg, Yu Shuan Yeh, and M. V. Clark, “A New Path-Gain/Delay-Spread Propagation Model for Digital Cellular Channels”, IEEE Transactions on Vehicular Technology, Vol. 46, No.2, pp. 477-485, May 1998. DOI: 10.1109/25.580786.
- [4] G.N. Tavares, L.M. Tavares, “The True Cramer-Rao Lower Bound for Data-Aided Carrier-Phase-Independent Time-Delay Estimation from Linearly Modulated Waveforms”, IEEE Transactions on Communications, Vol. 58, No. 1, 2006. DOI: 10.1109/TCOMM.2005.861655.
- [5] G.N. Tavares, L.M. Tavares, A. Petrolino, “On the True Cramér-Rao Lower Bound for Data-Aided Carrier –Phase-Independent Frequency Offset and Symbol Timing Estimation”, IEEE Transactions on Communications, Vol. 58, No. 2. DOI: 10.1109/TCOMM.2010.02.090023.
- [6] H. Holma and A. Toskala, “WCDMA for UMTS – Radio Access for Third Generation Mobile Communications”, John Wiley and Sons, Ltd, England 2000.
- [7] Yi-Pin Eric Wang, and Tony Ottosson, “Cell Search in W-CDMA”, IEEE Journal on Selected Areas in Communications, Vol. 18, No. 8, pp. 1470-1482, August 2000. DOI: 10.1109/49.864011.
- [8] José María Hernando Rábanos, Cayetano Lluch Mesquida, “Comunicaciones Móviles de Tercera Generación - UMTS”, Telefónica Móviles España, S.A., 2001.
- [9] John G. Proakis, “Digital Communications”, McGraw-Hill, New York, 1995.
- [10] R. Játiva, J. Vidal, “First Arrival Detection for Positioning in Mobile Channels”, IEEE International Symposium on Personal, Indoor and Mobile Radio Communications, PIMRC 2002, Vol. 4, pp. 1540-1544, September 2002. DOI: 10.1109/PIMRC.2002.1045437.
- [11] R. Játiva, J. Vidal, “GLRT detector for NLOS error reduction in wireless positioning systems”, IST Mobile and Wireless Telecommunications Summit, June 2002.
- [12] J.M. Huerta, J. Vidal, A. Giremus, J. Y. Tournet, “Joint Particle Filter and UKF Position Tracking in Severe Non-Line-of-Sight Situations”, IEEE Journal of Selected Topics in Signal Processing, Volume 3, Issue 5, 2009. DOI: 10.1109/JSTSP.2009.2027804.
- [13] Yehia R. Hamdy, and Sami A. Mawjoud, “Assessment of Uplink Time Difference Of Arrival (U-TDOA) Position Location Method in Urban Area and

- Highway in Mosul City”, *Al-Rafadain Engineering Journal*, Vol.21, Issue 2, Special section pp. 54-65, April 2013.
- [14] Sebastian-Ioan Ene, “A base station systems study for LTE, UMTS and GSM/Edge”, Delft University of Technology, June 2011.
- [15] 3GPP TS 136.104 version 9.4.0 release 9; “LTE; Evolved Universal Terrestrial Radio Access (E-UTRA); Base Station (BS) radio transmission and Reception”, July 2010.
- [16] H. Asplund, A. Alayón Glazunov, A. F. Molisch, K. I. Pedersen and M. Steinbauer, “The COST 259 Directional Channel Model – Part II: Macrocells”, *IEEE Transactions on Wireless Communications*, Vol. 5, No. 12, 2006. DOI: 10.1109/TWC.2006.256967.
- [17] S. M. Kay, *Fundamentals of Statistical Signal Processing – Estimation Theory*, Prentice Hall, New Jersey, 1993.
- [18] E. Garzón, S. Valdiviezo, R. Játiva and J. Vidal, “Fast Computation of Cramer-Rao Bounds for TOA”, *IEEE Latin America Conference on Computational Intelligence*, November 2016.
- [19] T. Menni, E. Chaumette, P. Larzabal, Reparameterization and constraints for CRB: duality and a major inequality for system analysis and design in the asymptotic region. *IEEE International Conference on Acoustics, Speech and Signal Processing*, pp. 3545-3548, 2012. Doi:10.1109/ICASSP.2012.6288682.
- [20] Xiao Li, Yik-Chung Wu and Erchin Serpedin, “On Performance Bounds for Timing Estimation under Fading Channels”, *IEEE Wireless Communications and Networking Conference*, 2009. WCNC 2009. DOI: 10.1109/WCNC.2009.4917845.
- [21] S.M. Omar, D. Slock, O. Bazzi, Recent insights in the Bayesian and deterministic CRB for blind SIMO channel estimation. *IEEE International Conference on Acoustics, Speech and Signal Processing*, pp. 3549-3552, 2012. DOI: 10.1109/ICASSP.2012.6288683.
- [22] J. Bukac, “Positive bi-exponential Interpolation”, *Journal of Interpolation and Approximation in Scientific Computing*, 2013. DOI: 10.5899/2013/jiasc-00010.
- [23] R. Játiva, D. Sánchez and J. Vidal, “NLOS Mitigation Based On TOA for Mobile Subscriber Positioning Systems by Weighting Measures and Geometrical Restrictions”, *IEEE Asia-Pacific Conference on Computer Aided Systems Engineering*, pp. 325-330, July 2015. DOI: 10.1109/APCASE.2015.64.
- [24] R. Játiva, E. Garzón and J. Vidal, “Space-Time Diversity for NLOS Mitigation in TDOA-Based Positioning Systems”, *IEEE International Engineering Summit, II Cumbre Internacional de las Ingenierías*, March 2016. DOI: 10.1109/IESummit.2016.7459771.
- [25] S. A. Zekavat and R. M. Buehrer, “*Handbook of Position Location - Theory, Practice and Advances*”, IEEE Press – John Wiley and Sons, 2012.
- [26] Chan Y.T. and Ho K.C., “A Simple and efficient Estimator for Hyperbolic Location”, *IEEE Transactions on Signal Processing*, Vol. 42, 8, 1994, DOI: 10.1109/78.301830.
- [27] TIA/EIA/IS-2000-2, “Physical Layer Standard for cdma2000 Spread Spectrum Systems”, August 1999.

-
- [28] Jihad Ibrahim and R. Michael Buehrer, “Two-Stage Acquisition for UWB in Dense Multipath”, *IEEE Journal on Selected Areas in Communications*, Vol. 24, No. 4, April 2006. DOI: 10.1109/JSAC.2005.863832.
- [29] Sinan Gezici, “Mean Acquisition Time Analysis of Foxed-Step Serial Search Algorithms”, *IEEE Transactions on Wireless Communications*, Vol. 8, No. 3, March 2009. DOI: 10.1109/TWC.2009.080147.
- [30] U. Mengali and A. N. D’Andrea, “Synchronization Techniques for Digital Receivers”, Plenum Press, New York, 1997.
- [31] A. J. Viterbi, “CDMA – Principles of Spread Spectrum Communication”, Addison-Wesley Wireless Communications Series, Massachusetts, 1997.
- [32] F. Benedetto, G. Giunta, E. Guzzon, “Reducing Mean Acquisition Time in Code Synchronization for Wireless Communications”, *IEEE International Symposium on Personal, Indoor and Mobile Radio Communications*, 2013. DOI: 10.1109/PIMRC.2013.6666220.
- [33] S. M. Kay, “Fundamentals of Statistical Signal Processing – Detection Theory”, Prentice Hall, New Jersey, 1998.
- [34] L. L. Scharf, “Statistical Signal Processing – Detection, Estimation, and Time Series Analysis”, Addison – Wesley Publishing Company, Massachusetts, 1990.
- [35] C. W. Helstrom, “Elements of Signal Detection and Estimation”, Prentice Hall, New Jersey, 1995.
- [36] E. Conte, A. De Maio, and G. Ricci, “GLRT-Based Adaptive Detection Algorithms for Range-Spread Targets”, *IEEE Transactions on Signal Processing*, Vol. 49, No. 7, July 2001.
- [37] E. J. Kelly, “Performance of an Adaptive Detection Algorithm; Rejection of Unwanted Signals”, *IEEE Transactions on Aerospace and Electronic Systems*, Vol. AES-25, No. 2, March 1989.
- [38] S. Bose, A. O. Steinhardt, “Optimum Array Detector for a Weak Signal in Unknown Noise”, *IEEE Transactions on Aerospace and Electronic Systems*, Vol. 32, No. 3, July 1996.
- [39] S. Bose and A. O. Steinhardt, “A Maximal Invariant Framework for Adaptive Detection with Structured and Unstructured Covariance Matrices”, *IEEE Transactions on Signal Processing*, Vol. 43, No. 9, September 1995.
- [40] K. A. Burgess and B. D. Van Veen, “Subspace-Based Adaptive Generalized Likelihood Ratio Detection”, *IEEE Transactions on Signal Processing*, Vol. 44, No. 4, April 1996.
- [41] A. Lee Swindlehurst and P. Stoica, “Maximum Likelihood Methods in Radar Array Signal Processing”, *Proceedings of the IEEE*, Vol. 86, No. 2, February 1998.
- [42] David Ramírez, Javier Vía and Ignacio Santamaría, “The Locally Most Powerful Test for Multiantenna Spectrum Sensing with uncalibrated receivers”, *IEEE International Conference on Acoustics, Speech and Signal Processing*, March 2012. DOI: 10.1109/ICASSP.2012.6288655.
- [43] S. Kraut, L. L. Scharf, and T. McWhorter, “Adaptive Subspace Detectors”, *IEEE Transactions on Signal Processing*, Vol. 49, No. 1, January 2001.

-
- [44] S. M. Kay and J. R. Gabriel, "Optimal Invariant Detection of a Sinusoid with Unknown Parameters", *IEEE Transactions on Signal Processing*, Vol. 50, No.1, January 2002.
- [45] J. Vidal, R. Játiva, "First Arriving Path Detection for Subscriber Location in Mobile Communication Systems", *IEEE International Conference on Acoustics, and Statistical Signal Processing*, Vol. 3, pp. III-2733 – III-2736, May 2002. DOI: 10.1109/ICASSP.2002.5745213.
- [46] R. Játiva, J. Vidal, "Coarse First Arriving Path Detection for Subscriber Location in Mobile Communication Systems", *XI European Signal Processing Conference (EUSIPCO 2002)*, September 2002.
- [47] R. Játiva, J. Vidal, "Estimación del Tiempo de Llegada en un canal Rayleigh desde una perspectiva de la Cota Inferior de Cramer-Rao", *Revista Avances en Ciencias e Ingenierías*, pp. 5-10, Abril 2009.
- [48] R. Raich, J. Goldberg, and H. Messer, "Bearing Estimation for a Distributed Source: Modelling, Inherent Accuracy Limitations and Algorithms", *IEEE Transactions on Signal Processing*, Vol. 48, No. 2, February 2000.
- [49] Alan Edelman, "Eigenvalues and Condition Numbers of Random Matrices", PhD Thesis, Massachusetts Institute of Technology, May 1989.
- [50] S. L. Marple, "A tutorial overview of modern spectral estimation", *International conference on Acoustics, Speech and Signal Processing*, Vol. 4, pp. 2152-2157, May 1989. DOI: 10.1109/ICASSP.1989.266889.
- [51] P. Stoica and R. Moses, "Introduction to Spectral Analysis", Prentice Hall, New Jersey, 1997.
- [52] M. A. Lagunas, A. Gasull, "An Improved Maximum Likelihood Method for Power Spectral Density Estimation", *IEEE Transactions on Acoustics, Speech and Signal Processing*, Vol. 32, pp. 170-172, February 2000.
- [53] J. Vidal, R. Játiva, M. Nájara, A. Castro, "IST-1999-10322 SATURN – D631 Experimental preparation and verification", *Universitat Politècnica de Catalunya*, February 2003.
- [54] J. Vidal, M. Nájara, R. Játiva, "High resolution time-of-arrival detection for wireless positioning systems", *IEEE Vehicular Technology Conference, VTC-2002-Fall*, Vol. 4, pp. 2283-2287, 2002. DOI: 10.1109/VETEFCF.2002.1040627.
- [55] Yung-Yi Wang, Jiunn-Tsair Chen and Wen-Hsien Fang, "TST-MUSIC for Joint DOA-Delay Estimation", *IEEE Transactions on Signal Processing*, Vol. 49, No.4, April 2001.
- [56] D. Linebarger, R. DeGroat, E. Dowling, G. Fudge and P. Stoica, "Analysing the effects of Constraints and Inter-Signal Coherence on the MUSIC algorithm", *International Conference on Acoustics, Speech, and Signal Processing, ICASSP-95*, Vol. 3, pp. 1657 -1660, May 1995.
- [57] M. Wax and I. Ziskind, "Detection of the Number of Coherent Signals by the MDL Principle", *IEEE Transactions on Acoustics, Speech, and Signal Processing*, Vol. 37, No. 8, August 1989.
- [58] 3GPP TS 25.104 version 9.2.0 release 9; "Technical Specification Group Radio Access Network; Base Station (BS) radio transmission and Reception (FDD)", December 2009.

Conclusions, Recommendations and Future Research Topics

In the following lines, the most relevant results reached along this thesis are summarized, and some recommendations in order to perform future research are pointed out.

Conclusions

This thesis boards an antique problem in the framework of an accelerated and ever changing technological environment. Looking for the position of an emitter is not new, however the technological developments and the growing of wireless communications in the last decade not just offer new possibilities in terms of value added services, but exhibit new problems that promote the study of these new constraints and the research of emergent methods for fighting their associated issues. Positioning technologies refer to the ways in which the measured signals from network and/or a mobile subscriber are treated to compute the position of this latter. This document provides enough information concerning to the solution of the positioning problem with the use of a group of measurements extracted from signals exchanged in a wireless communications system.

This document provides a general view to the subscriber location problem within the third generation of mobile communications systems, but emphasizes the concerns related to the statistical signal processing, because this area has taken a special relevance not just as a tool for the study of telecommunications signals and systems, but also in the whole electronics world as a mean for providing high quality solutions to usual problems related with signal detection and its estimation.

In terms of system normalization, the location service within the Universal Mobile Terrestrial System was concluded, but some work related to procedures to keep subscriber anonymity and the mechanisms for protecting positioning information during its transference along the network was left, restraining perhaps the growth of new location based services with the exception of those related to navigation aids.

Two main positioning architectures are possible, and the mobile-based approach has gained relevance in the last years with the rising of smart phones incorporating GPS devices. However, the research within this document pays more attention to network based subscriber location not just because this approach is more compatible with the signal processing field, but also because these techniques keep their relevance in a world moving to an internet of thing network that will require of sensors positioning for the construction of new relational services.

From the whole range of enabling positioning technologies, the best performance for homogeneous positioning techniques is reached out for timing-based positioning systems. The AOA based positioning technique exhibits the worse performance among the considered techniques within this research, and its use is recommendable just in association to applications with loose requirements in terms of positioning accuracy, or as a mean to enhance the behavior of the main procedure. Therefore, timing techniques have been the object of this research. They include to TDOA-, OTDOA- and TOA-based positioning. However, as the location accuracy may be enhanced by adding space-time diversity, using a set of heterogeneous measures, and/or the application of complementary approaches; this research boards these topics with the construction of a space-time signal model for Rayleigh and Rice fading propagation. From this model, Cramer-Rao Bounds have been computed as a way to estimate the accuracy of timing measures required to perform the positioning.

Moreover, the Non Line Of Sight condition strongly degrades the positioning accuracy in wireless communication systems, and even the traditional robust algorithms, such as the Torrieri's solution originally developed for LOS environments, completely fail in current dispersive scenarios due to the measurement error can't be modeled just as a zero mean Gaussian variable, when actual error statistics vary with space and time. Hence, an accurate signal description would require a very complex dynamic formulation, and also to a greater computational burden, being the positioning results dependent of the adjustment between the proposed statistics and the reality. This document discusses possible solutions to mitigate the NLOS issue; and as part of this research, several positioning technologies and methods have been evaluated in realistic conditions, using a link level simulation platform that incorporates the main channel effects concerning to signals propagating between the transmitter and the receiver. Results from these simulations provide interesting guidelines to be considered in the mitigation of the NLOS condition in the outline of mobile subscriber positioning.

The simulation platform is based on the Greenstein model, which is in the core of more complex current models. This platform was built in order to test the most relevant approaches for positioning and NLOS mitigation within small sized cells. This propagation model is quite robust and is part of the core of more complex current models. Therefore, this platform is well suited for system level simulations, and also includes the effects of signal space-time diversity with the help of CRB models.

Since a perfect statistical characterization of the NLOS condition is not a practical solution within the subscriber positioning context, several NLOS mitigation techniques have been proposed. Some of them consider the weighting of the available measures, by using factors that may be extracted from the signal statistics, as well as from lateral information related to the physics of the problem. Others prefer to make inferences from the problem geometry, and hence incorporate certain geometrical restrictions in order to improve the accuracy. Whatever is the NLOS mitigation approach finally performed; the NLOS discrimination is an important procedure to achieve the best results. After all, the discrimination stage enables the proper choice of the statistics, the selection of the

quality factors to weight the measures, and the right application of the geometrical restrictions used in the positioning algorithms. Therefore, our NLOS mitigation proposal includes a NLOS discrimination stage, and explores taking advantage of space-time diversity.

From the wide range of algorithms available at the literature for providing subscriber positioning, the linear methods are attractive due to their simplicity, and the fact that they always provide a solution, avoiding convergence issues associated to iterative nonlinear algorithms as it was shown along this research. WLLS approaches are particularly interesting due to their capabilities to apprehend the relevant signal characteristics with the use of weighting matrices, although they require well defined models to derive the weighting factors. Therefore, these methods were chosen as part of our solution and they were evaluated at the simulation stage. Particularly, a new mitigation algorithm that considers both the weighting of the measures and the inclusion of soft geometrical restrictions was derived for TOA- and TDOA-based positioning. This new algorithm makes a better work than those provided by the literature and used as reference within a moderate dispersive environment. For example, the average positioning error decreases between 25 m and 60 m with the use of our algorithm when it is compared with Yi Long TOA-based NLOS mitigation approach. Furthermore, for a scenario with a very aggressive dispersion presented in around 13% of the cases, our positioning algorithm exhibits average positioning errors below 173 m within the 70% of the cases. It suggests a positioning error degradation of around 10-15 m respect to the moderate dispersive situation, but also implies a gain of around 30-50 m in accuracy in comparison to the Yi Long algorithm used as reference. Furthermore, since 13% of aggregate dispersion leads to just a 6% of accuracy degradation, these results also show the robustness of our proposed algorithm. These results confirm the fact that a better accuracy is provided from hybrid techniques instead of the use of a single one, and when the right models are employed to characterize the signal. These figures are further improved with the use of space-time diversity.

This research uses the Cramer-Rao Bounds to study the impact of various factors involved in signal timing estimation for a mobile scenario characterized by a space-time dispersive channel. Our TOA model considers the sampling rate, the roll-off factor of the shaping pulse, the spatial and temporal correlation among channel estimates, and the availability of multiple channel vector estimates and multiple sensors in the antenna array at the receiver. Furthermore, it studies both Rayleigh and Rice fading propagation situations; and therefore, it explores the difficulties and opportunities associated with timing estimation in LOS and NLOS environments. Particularly, our model makes a contribution by taking into account the spatial and temporal correlation among channel estimates, and the impact of the roll-off factor of the shaping pulse, in addition to the number of sensors and the number of estimates that are typical from other approaches. It describes the spatial scattering by using a Gaussian distribution, and also includes an exponential dispersion for delays which is characteristic of mobile channels instead of just a few paths as in prior approaches. Furthermore, this document also includes asymptotic expressions for interesting cases related both to high speed subscribers as well as to low speed ones. Moreover, due to that any reduction in the signal estimation

errors will lead to a better positioning; this model does contribute to get an insight not just of timing estimation but also to its impact on positioning.

Results derived from CRBs along this research show as the estimation errors for the timing and the normalized coherence bandwidth decrease when the SNR increases but also as this improvement is highly conditional depending on the propagation scenario and the kind of source. In case of NLOS Rayleigh propagation, these estimation errors degrade rapidly when passing from PCD sources to FCD sources, reaching a limit floor at high SNRs, so a higher SNR does not force a lower error. On the other hand, in the case of LOS Rice propagation, the larger improvement is achieved when passing from an ICD source to a PCD one, and timing accuracy improves practically without bound for higher SNRs. The bounds for the normalized Coherence Bandwidth seem not to be disturbed for a change in the LOS power level; and the tendency with respect to the temporal correlation coefficient, remains as in the NLOS model. Estimation errors, for the timing and the normalized coherence bandwidth, also decrease when the number of observations increases, but again this reduction is very conditioned on the propagation scenario and the kind of source: ICD, PCD or FCD. In the case of NLOS, a larger record of observations is required to keep the accuracy for higher temporal correlations among channel estimates, however in the case of a LOS scenario an uncorrelated dispersed signal component implies a random perturbation that degrades the accuracy on the signal of interest.

Furthermore, the use of multiple antennas introduces not just new observations but also diversity, and therefore it helps to improve accuracy. In this sense, better results are achieved when a higher number of sensors are available in the antenna array. However, the impact of these improvements is associated with temporal and spatial coherence of the scattered signal. For the NLOS condition, inclusion of multiple sensors provides similar gains in timing accuracy, from moderate to high SNR, regardless of the value of the temporal coefficient. A gain factor of around two is achieved when passing from one sensor to four. In LOS condition however, this gain almost doubles in the case of highly PCD sources and the bearing also impacts the timing error performance. This gain decays when the LOS path weakens and the Rice propagation turns into Rayleigh. Improvements are always obtained when an antenna array is used instead of a single sensor, and certain progresses of around 20% are also achieved when passing from a narrow spread source to a spatially well-scattered signal.

Moreover, under a NLOS condition, the roll off factor has negligible effect in error bounds, whilst under LOS condition, a higher roll-off factor helps to improve the bound for the timing error, possibly due to the sharper form of the first arrival in this case, related to the increase in the bandwidth.

Errors from the measures translate directly into range errors for positioning based on TOA, and these certainly degrade the subscriber's positioning. However, it would be inappropriate to think about the range errors as the final positioning error. Positioning is a more complex procedure that involves the acquisition from signals transmitted and

received from different parts of the network, and therefore it is also dependent on the problem geometry.

Furthermore, positioning uncertainty is also reduced by using a larger number of base stations or anchor nodes than strictly necessary for the solution of the equations system. However, this is not an easy task, especially within infrastructure networks where the availability of BSs is limited by design; and where the provision of new stations has impacts, not just in the network procedures but also over to the network performance in terms of capacity and SINR. However, the larger number of nodes potentially available in ad hoc networks and communication emergent systems justifies the additional complexity with the goal to achieve a better accuracy.

Accuracy may improve if some information about the uncertainty of the parameters employed by the location technique is provided to the position computing function as it was shown with the application of the WLLS approach. This information may be acquired from an experimental measurement campaign or from the use of statistical models. This research prefers the latter approach and this document shows how this information may be derived from our simple but very suited propagation model.

Since the discrimination of the NLOS condition is an important part of any mitigation procedure, this research considers this topic at the very beginning of the problem: the signal detection. There are some methods available to discriminate a strongly attenuated signal from noise. One of them is the so called Generalized Likelihood Ratio Test. This document provides a GLRT detector as the NLOS/LOS discrimination stage, and studies its behavior using Monte Carlo simulations. A very simplified mathematical analysis is performed to verify the impact of the SNR, the scattered signal to direct path ratio and the number of sensors for a highly correlated source case. Better results are observed for temporally uncorrelated sources and uncorrelated sensors. Furthermore, the GLRT detector is very sensible to the SNR and important improvements in terms of detection probability may be achieved for the case of very weak signals when adding a higher number of observations to the detector. These newer estimates can be provided with the use of a larger number of sensors at the antenna array or by using a larger number of slots. These results also show that detection improves when a direct path is present, even in the case of the total signal power is kept constant, and that once the optimum threshold is selected at the detection stage, it defines the SNR operation level below which a weaker signal will be missed and therefore the achieved measure will be biased.

On the other hand and strictly speaking, determining the exact timing at which a signal arrives is an estimation problem. Results from simulations show that high resolution techniques such as the NMV estimation of delays and directions of arrival are adequate for their use within positioning applications. Lower errors for delay and direction estimates are achieved from channels characterized by narrower angular and delay spreads. These errors also diminish when more sensors are available, and when the correlation factor between consecutive slots is lower. Therefore, higher speed

mobile subscribers are in general better detected, and they exhibit better positioning figures. However, a compromise should be achieved between the mobile speed and the number of consecutive slots used by the estimator, since that a larger register involves not just a higher latency but also accuracy degradation due to movement. In case of tracking applications, the system dynamics may be used to keep and improve the positioning accuracy. Results from the application of these methods to simulated signal in realistic conditions have revealed some limitations of these techniques due to the appearing of side-lobes at the spectrum that might lead to a false early detection of the first arrival. Fortunately, this problem is considerably more reduced for the NMV method, enabling the use of a much lower threshold; therefore, the use of this latter algorithm is recommended to perform an enhanced timing estimation.

Moreover, whilst timing information provided by the first arrival is relevant for positioning, simulations reveal that even for propagation environments which exhibit low delay spreads and hence high delays concentrations, it is pertinent to use the angular information corresponding to all the arriving paths and not just the direction of arrival associated to the first of them, as a better estimate of the subscriber direction.

It is important to note that the overall timing accuracy from the proposed two stage detection-estimation procedure not just depends on the properties of the high resolution estimation algorithm at the high SNR regimen, but also of the combined operation of the detector and the estimation algorithm at the low SNR regimen. A better test implemented at the detection stage can certainly enhance the probability of detecting the first arrival, but this path will be masked by the estimation algorithm if its level is weaker than the threshold used to overcome the early detection due to the side lobe of the high resolution spectrum. Therefore, a better solution using this two stage approach must consider the improvement of these two components. Furthermore, all the research supported by simulations reveals that the best results are performed from the application of multiple concurrent techniques. In this case, very good results are provided not just by improving the quality of the timing estimates with the use of the proposed two-stage NLOS mitigation scheme and by taking advantage of the space-time diversity with the help of antenna arrays at the receivers, but also by recognizing the presence of the NLOS condition and eventually by performing the proper weighting over the measures.

Recommendations and Future Research Topics

In spite that our CRB model provides valuable information about the timing estimation error, special careful should be put to extrapolate these results to the mobile subscriber positioning issue, due to the different nature of Rayleigh and Rice propagation models. For i.e. in obstructed environments, the shadowing may lead to important delay spreads, while in LOS condition, lower delays are usual. In addition, some obstructed scenarios may lead to signal clustering, and if that is the case, even with the first arrival being accurately estimated, the positioning could be biased.

Fortunately, there are some methods to identify these scenarios and to reduce the harmful effects of this NLOS condition.

New enhanced CRB models that better describe signal behavior have emerged in the last years and they should be studied more carefully in order to extend the functionalities of the simulation platform.

Since new emergent technologies are available at the telecommunications environment, new propagation models should be studied to study the positioning problem in these new contexts.

Since the statistics of the mobile channel changes with space and time, new approaches that take advantage of the system dynamics should be studied in order to get the best of the measures and improve the accuracy. It also could be a good step to explore the navigational applications.

Since the location accuracy improves with the use of heterogeneous measures, the rational use of these measures is an interesting open research area.

In order to take advantage of time diversity, a large number of channel vector estimates are recorded within the coherence time for delays and directions of arrival. This coherence time is related to the subscriber speed and both of them must be estimated within a certain margin of accuracy in order to obtain the best performance from the estimation algorithms. When the system choice for the acquisition time is too small respect to the coherence time, the resulting accuracy degrades due to a lack of available data. Furthermore, time diversity is being wasted. On the other hand, when the acquisition time is excessive compared to the coherence time, the assumption of wide sense stationarity fails, and the parameters estimation degrades. Mechanisms used to determine this coherence time should be studied, and some adaptive algorithms might be developed for reaching the optimal working point.

René Játiva, David Sánchez, Josep Vidal, “NLOS Mitigation Based on TOA for Mobile Subscriber Positioning Systems by Weighting Measures and Geometrical Restrictions”, IEEE Asia-Pacific International Conference on Computer Aided System Engineering”, pp. 325-330, July 2015. DOI: 10.1109/APCASE.2015.64.

ATTENTION !

Pages 248 to 254 of the thesis are available at the editor’s web
<http://ieeexplore.ieee.org/document/7287040/>

René Játiva E., Josep Vidal and Margarita Cabrera, “Cramer Rao Bounds in Time Of Arrival Estimation for a Distributed Source”, Mobile Communications Summit, IST2001, pp. 236-244, September 2001.

Cramer Rao Bounds in Time of Arrival Estimation for a Distributed Source

René Játiva E., Josep Vidal, Marga Cabrera

Dept. of Signal Theory and Communications, Universitat Politècnica de Catalunya
Campus Nord, Modul D5, Jordi Girona, 1-3, 08034 Barcelona, SPAIN

Abstract: This paper presents a model used for studying accuracy in Time of Arrival Estimation in the frame of subscriber location. Cramer Rao Bounds are derived and some results are presented for both the general and the asymptotic case. The most general case of Partially Coherent Distributed Sources is studied and also the particular cases of Incoherently Distributed Sources and Full Coherent Distributed Sources.

I. Introduction

Some recent works have shown that using both direction of arrival and time of arrival may be useful to improve accuracy in location of mobile subscribers (i.e. see [Vid01]). Furthermore, from the viewpoint of location, where the first path time of arrival and its most probable bearing are the major parameters to estimate, the use of distributed models seems to be appropriate to reduce the number of nuisance parameters to describe the propagation channel in highly dispersive environments as in the outdoor urban case, and hence the computational burden required for algorithms to estimate them.

Accuracy in positioning when measurements are uncorrelated is given by Ec. 1. See [Vid01], where \mathbf{x} is the mobile position vector, \mathbf{A} is the matrix which maps the observation vector \mathbf{m} to the mobile position in the real world, and σ_w^2 is the error variance of the measurements in \mathbf{m} .

$$\mathbf{C}_x^{BLUE} = \sigma_w^2 (\mathbf{A}^H \mathbf{A})^{-1} \quad \text{Ec. 1}$$

Note from above expression that an improvement in the error variance of the measurements leads to a better positioning accuracy. The accuracy in the measurements may be improved if adequate use of temporal and spatial diversity of the estimated propagation channel is done. In the former case, multiple channels are collected at different time instants. In the latter case, the channels are recorded from different sensors. Both cases will be studied in this contribution.

There are some literature related to parameter estimation using distributed source models, for i.e. [Bes00], [Ben00], and [Rai00]. A different approach to the estimation problem is provided for i.e. by [Ral98], [Val95] and [Wax97]. The interested reader is referred therein.

In the following a distributed source model for delays is shown, Cramer Rao Bounds for this model are derived and some results are presented.

Some assumptions used along this paper follows:

- AS 1. The channel is assumed to have a time coherence for the taps amplitudes which follows the usual Jake's expression. However, the time coherence of the delay and angle information is much longer. Therefore, many channel estimates can be collected in time so as to improve the accuracy of the timing and angle estimates.
- AS 2. Noise present in the channel estimates is white and Gaussian, which is a reasonable assumption after despreading, since all other users have been (at least) partially cancelled, provided that the number of users be high and power control be active.

- AS 3. The channel is angularly incoherent, which corresponds to a situation in which the user equipment (UE) is moving and different reflected rays experience uncorrelated fast fading.
- AS 4. A first order linear Markov model for the time variation of the channel is assumed.
- AS 5. A continuous power spectrum is used in delay for the marginal function $P(\tau) = \int P(\theta, \tau) d\theta$ and it will assume to fit an exponential shape, according to [Ped00], estimated at chip time. For the extraction of timing information, we will assume the same angular distribution for all the delays. This may not be very realistic but allows reducing the number of parameters.

Note that this model is very parsimonious and convenient for the purpose of location, since only a few parameters of interest are to be computed, rather than all time delays which are usually nuisance parameters and yield the problem too complicated to solve in highly dispersive scenarios.

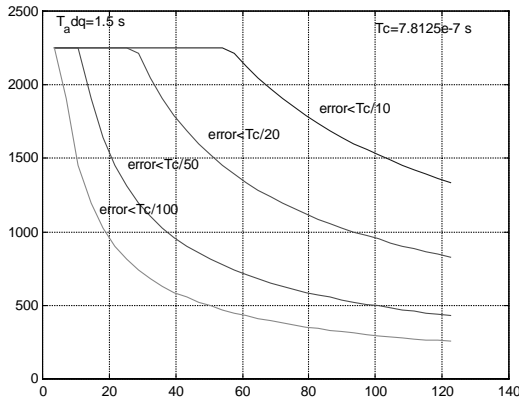


Figure 1 Mean number of allowed channel estimates in timing detection.

The coherence time for the first arriving signal path depends on the maximum allowed delay variation, the radial component of the speed vector (v_{radial}), but not on the distance Figure 1 shows the average number of channel vector estimates that can be used for estimation as a function of mobile speed and for a specified accuracy order. Subscriber is supposed to move in any direction with equal probability.

In the following, the expressions used for compute values required for Figure 1 will be derived.

$$\text{error} = \Delta d / c = v_{\text{radial}} t / c = v_{\text{radial}} K T / c = v \cos \phi \cdot K T / c$$

$$E\{K\} = \frac{\text{error} \cdot c}{T \cdot v} E\{\sec \phi\} = \frac{\text{error} \cdot c}{T \cdot v \cdot \phi_{\max}} \int_0^{\phi_{\max}} \sec \phi \cdot d\phi = \frac{\text{error} \cdot c}{T \cdot v \cdot \phi_{\max}} \log \left[\tan \left(\frac{\phi_{\max}}{2} + \frac{\pi}{4} \right) \right]$$

Ec. 2

The maximum allowed angle ϕ_{\max} required in Ec. 2 must be determined using Ec. 3.

$$\phi_{\max} = \arccos \left(\frac{c \cdot \text{error}}{T_{\text{adq}} \cdot v} \right) \tag{Ec. 3}$$

Note from Figure 1 that the maximum number of observations is limited by the acquisition time and for the mobile speed, so a typical value for this parameter is between 250 and 2200 to avoid accuracy degradation.

II. A Distributed Model for Delays

The observed signal is a set of K channel vector estimates collected over a set of N_s sensors. Each channel vector estimate is of length N ($N-1$ delays), \mathbf{z} , and are assumed to be Gaussian distributed, with certain space and time correlation matrices..

This signal is infected with noise, \mathbf{w} , which is assumed to be a zero mean, temporally stationary, complex Gaussian random process, which accounts for the noise in the estimated channel. The Gaussianity of the noise comes from the fact that, in the uplink of the FDD mode of UTRAN, the

interference includes many users of controlled power. It is assumed to be temporally uncorrelated and independent of the propagation channel vectors.

Therefore, we have:

$$\mathbf{w} \sim CN(\mathbf{0}, \sigma_w^2 \mathbf{I}_{N_f}), \quad \mathbf{z} \sim CN(\mathbf{0}_{KN_s M \times 1}, \mathbf{R}_s) \quad \text{Ec. 4}$$

where the channel vector correlation matrix is modeled as a Partially Coherent Distributed (PCD) Source described by Ec. 5.

$$\mathbf{R}_z = \mathbf{R}_\phi(\rho) \otimes \mathbf{T}(\alpha_t) \otimes r \cdot \Lambda_\tau(\lambda_n) + \sigma_w^2 \mathbf{I} \quad \text{Ec. 5}$$

In the above expression $\mathbf{T}(\alpha_t)$ is the temporal component, $\mathbf{R}_\phi(\rho)$ contains the correlation coefficients between sensors and Λ_τ is a diagonal matrix that models delays contributions. $\{\Lambda_\tau\}_{k,k} = \exp(-(k-k_0)\lambda_n)u(k-k_0)$, and $\cdot \otimes \cdot$ is the Kronecker product operator.

$\mathbf{T}(\alpha_t)$ and $\mathbf{R}_\phi(\rho)$ are modeled as: 1

$$\mathbf{T}(\alpha_t) = \begin{bmatrix} 1 & \alpha_t & \alpha_t^2 & \dots & \alpha_t^{K-1} \\ \alpha_t & \ddots & & & \\ \alpha_t^2 & \ddots & & & \vdots \\ \vdots & & & & \alpha_t \\ \alpha_t^{K-1} & \dots & \alpha_t^2 & \alpha_t & 1 \end{bmatrix} \quad \mathbf{R}_\phi(\rho) = \begin{bmatrix} 1 & \rho_{12} & \dots & \rho_{1N_s} \\ * & 1 & & \rho_{2N_s} \\ \rho_{12} & & & 1 \\ \vdots & & & \vdots \\ * & * & & * \\ \rho_{1N_s} & \rho_{2N_s} & \dots & 1 \end{bmatrix}$$

where α_t is the temporal correlation coefficient between two consecutive vector samples, and ρ_{ij} is the spatial correlation coefficient between sensors i and j .

III. Cramer Rao Bounds

Cramer Rao Bound is useful as a mean to quantify errors from estimate these parameters. For the model in Ec. 5 the following parameter vector is defined:

$$\Psi = [k_0, \lambda_n, r, \sigma_w^2, \alpha_t, \rho^T]^T, \quad \rho = [\rho_{R1}, \rho_{R2}, \dots, \rho_{RN-coef}, \rho_{I1}, \rho_{I2}, \dots, \rho_{IN-coef}]^T \quad \text{Ec. 6}$$

where k_0 is the time of arrival normalized for the chip time, λ_n is the inverse of delay spread normalized for the chip time, and the remaining parameters are nuisance parameters.

The FIM elements for this model may be expressed as follows [Kay-I]:

$$[\mathbf{F}_\Psi]_{pq} = tr \left(\mathbf{R}_z^{-1} \frac{\partial \mathbf{R}_z}{\partial \Psi_p} \mathbf{R}_z^{-1} \frac{\partial \mathbf{R}_z}{\partial \Psi_q} \right) \quad \text{Ec. 7}$$

And it can be shown that the FIM may be expressed as:

$$\mathbf{F}_\Psi = \sum_{k=1}^{N_s} \sum_{l=1}^K \mathbf{G}_{k,k,l} \mathbf{J}_{\Psi} \mathbf{G}_{k,k,l}^T + C_l \mathbf{e}_{N_p}^{(5)} \mathbf{e}_{N_p}^{(5)T} + \sum_{q1=1}^{2N_{coef}} \sum_{q2=1}^{2N_{coef}} C_2^{(q1,q2)} \mathbf{e}_{N_p}^{(q1)} \mathbf{e}_{N_p}^{(q2)T} \quad \text{Ec. 8}$$

Where,

$$\bar{\Psi} = [k_0, \lambda_n, \gamma_{k,k1}, \sigma_w^2]^T \quad \mathbf{G}_{k,k1} = \begin{bmatrix} 1 & 0 & 0 & 0 \\ 0 & 1 & 0 & 0 \\ 0 & 0 & \lambda_\phi^{(k)} \lambda_t^{(k1)} & 0 \\ 0 & 0 & 0 & 1 \\ 0 & 0 & r \lambda_\phi^{(k)} \dot{\lambda}_t^{(k1)} & 0 \\ 0 & 0 & r \frac{\partial \lambda_\phi^{(k)}}{\partial \rho} & 0 \end{bmatrix}$$

$$\left\{ \mathbf{J}_{\bar{\Psi}} \right\}_{pq} = \text{tr} \left(\mathbf{R}_{k,k1}^{-1} \frac{\partial \mathbf{R}_{k,k1}}{\partial \bar{\Psi}_p} \mathbf{R}_{k,k1}^{-1} \frac{\partial \mathbf{R}_{k,k1}}{\partial \bar{\Psi}_q} \right)$$

Ec. 9

and the rest of involved elements are described as follows:

$$\frac{\partial \lambda_\phi^{(k)}}{\partial \boldsymbol{\rho}} = \left[\frac{\partial \lambda_\phi^{(k)}}{\partial \rho_{R1}}, \frac{\partial \lambda_\phi^{(k)}}{\partial \rho_{R2}}, \dots, \frac{\partial \lambda_\phi^{(k)}}{\partial \rho_{RN_coef}}, \frac{\partial \lambda_\phi^{(k)}}{\partial \rho_{I1}}, \frac{\partial \lambda_\phi^{(k)}}{\partial \rho_{I2}}, \dots, \frac{\partial \lambda_\phi^{(k)}}{\partial \rho_{IN_coef}} \right]^T$$

$$\gamma_{k,k1} = \lambda_\phi^{(k)} \lambda_t^{(k1)} r; \quad \mathbf{R}_{k,k1} = \lambda_\phi^{(k)} \lambda_t^{(k1)} r \boldsymbol{\Lambda}_t + \sigma_w^2 \mathbf{I}; \quad \dot{\lambda}_t^{(k1)} = \frac{d\lambda_t^{(k1)}}{d\alpha_t}, \quad \dot{\mathbf{u}}_t^{(k1)} = \frac{d\mathbf{u}_t^{(k1)}}{d\alpha_t}$$

$$C_1 = r^2 \sum_{k=1}^{Ns} \sum_{l=1}^K \sum_{ll=1}^K (\lambda_t^{(k1)} - \lambda_t^{(ll)})^2 \left(\mathbf{u}_t^{(ll)H} \dot{\mathbf{u}}_t^{(k1)} \right)^2 \text{tr} \left\{ \mathbf{R}_{k,k1}^{-1} \frac{\partial \mathbf{R}_{k,k1}}{\partial \gamma_{k,k1}} \mathbf{R}_{k,1l}^{-1} \frac{\partial \mathbf{R}_{k,1l}}{\partial \gamma_{k,1l}} \right\}$$

$$C_2^{(q1,q2)} = \sum_{k=1}^{Ns} \sum_{l=1}^{Ns} \sum_{kl=1}^K - (\lambda_\phi^{(k)} - \lambda_\phi^{(l)})^2 \left(\mathbf{u}_\phi^{(l)T} \frac{\partial \mathbf{u}_\phi^{(k)}}{\partial \rho_{q1}} \right) \cdot \left(\mathbf{u}_\phi^{(k)T} \frac{\partial \mathbf{u}_\phi^{(l)}}{\partial \rho_{q2}} \right) \lambda_t^{(k1)2} \text{tr} \left\{ \mathbf{R}_{k,k1}^{-1} \frac{\partial \mathbf{R}_{k,k1}}{\partial \gamma_{k,k1}} \mathbf{R}_{l,k1}^{-1} \frac{\partial \mathbf{R}_{l,k1}}{\partial \gamma_{l,k1}} \right\}$$

$$\mathbf{T} = \mathbf{U}_t \boldsymbol{\Lambda}_t \mathbf{U}_t^H, \quad \mathbf{U}_t = [\mathbf{u}_t^{(1)}, \mathbf{u}_t^{(2)}, \dots, \mathbf{u}_t^{(K)}] \quad \boldsymbol{\Lambda}_t = \text{diag}[\lambda_t^{(1)}, \lambda_t^{(2)}, \dots, \lambda_t^{(K)}]$$

$$\mathbf{R}_\phi = \mathbf{U}_\phi \boldsymbol{\Lambda}_\phi \mathbf{U}_\phi^H, \quad \mathbf{U}_\phi = [\mathbf{u}_\phi^{(1)}, \mathbf{u}_\phi^{(2)}, \dots, \mathbf{u}_\phi^{(Ns)}] \quad \boldsymbol{\Lambda}_\phi = \text{diag}[\lambda_\phi^{(1)}, \lambda_\phi^{(2)}, \dots, \lambda_\phi^{(Ns)}]$$

$$\mathbf{e}_q^{(v)} = [0, \dots, 0, \underset{\substack{\uparrow \\ q^{\text{th}} \text{ element}}}{1}, 0, \dots, 0]^T$$

$q^{\text{th}} \text{ element}$

$$Np = 5 + 2N_coef; \quad N_coef = Ns(Ns - 1) / 2$$

where,

$K = \text{number of snapshots}$

$Ns = \text{number of sensors}$

IV. Asymptotic Expressions for the PCD Case

Computing CRB's from may be computationally expensive, specially when the number of channel vector estimates K is high. Therefore, it is necessary to work with reasonable approximates to reduce this burden. [Rai00] provides a closed expression for asymptotic eigenvalues from matrix \mathbf{T} for PCD sources. This expression has been used to compute CRB's when K is large.

Note that, for the asymptotic case, C_1 in Ec. 8 is negligible and FIM may be expressed as:

$$\mathbf{F}_{\Psi} \approx \sum_{k=1}^{N_s} \sum_{l=1}^K \mathbf{G}_{k,l} \mathbf{J}_{\bar{\Psi}} \mathbf{G}_{k,l}^T + \sum_{q1=1}^{2N} \sum_{q2=1}^{2N} C_2^{(q1,q2)} \mathbf{e}_{N_p}^{(q1)} \mathbf{e}_{N_p}^{(q2)} \quad \text{Ec. 10}$$

V. CRB's for Full Coherent Distributed Sources

The above expressions are useful for PCD sources, but in case of FCD sources they can not be used. Hence, it is convenient to get adequate expressions for this special case where $\mathbf{T} = \mathbf{1}_K \mathbf{1}_K^T$. The parameter vector reduces to:

$$\Psi = [k_0, \lambda_n, r, \sigma_w^2, \mathbf{p}^T]$$

and the FIM elements for FCD sources may be shown to be computed as:

$$\mathbf{F}_{\Psi} = \sum_{k=1}^{N_s} \mathbf{G}_k \mathbf{J}_{\bar{\Psi}_1} \mathbf{G}_k^T + \sum_{q1=1}^{2N} \sum_{q2=1}^{2N} C_3^{(q1,q2)} \mathbf{e}_{N_p}^{(q1)} \mathbf{e}_{N_p}^{(q2)T} + \frac{N_s(K-1)N}{\sigma_w^4} \mathbf{e}_{N_p}^{(4)} \mathbf{e}_{N_p}^{(4)T} \quad \text{Ec. 11}$$

where

$$\bar{\Psi}_l = [k_0, \lambda_n, \gamma_k, \sigma_w^2]^T \quad \mathbf{G}_k = \begin{bmatrix} 1 & 0 & 0 & 0 \\ 0 & 1 & 0 & 0 \\ 0 & 0 & K\lambda_\phi^{(k)} & 0 \\ 0 & 0 & 0 & 1 \\ 0 & 0 & r \frac{\partial \lambda_\phi^{(k)}}{\partial \mathbf{p}} & 0 \end{bmatrix} \quad \gamma_k = K\lambda_\phi^{(k)} r$$

$$\left\{ \mathbf{J}_{\bar{\Psi}_1} \right\}_{pq} = \text{tr} \left(\mathbf{R}_k^{-1} \frac{\partial \mathbf{R}_k}{\partial \bar{\Psi}_{1p}} \mathbf{R}_k^{-1} \frac{\partial \mathbf{R}_k}{\partial \bar{\Psi}_{1q}} \right)$$

$$C_3^{(q1,q2)} = \sum_{k=1}^{N_s} \sum_{l=1}^{N_s} -(\lambda_\phi^{(k)} - \lambda_\phi^{(l)})^2 \left(\mathbf{u}_\phi^{(l)T} \frac{\partial \mathbf{u}_\phi^{(k)}}{\partial \rho_{q1}} \right) \left(\mathbf{u}_\phi^{(k)T} \frac{\partial \mathbf{u}_\phi^{(l)}}{\partial \rho_{q2}} \right) \text{tr} \left\{ \mathbf{R}_k^{-1} \frac{\partial \mathbf{R}_k}{\partial \gamma_k} \mathbf{R}_l^{-1} \frac{\partial \mathbf{R}_l}{\partial \gamma_l} \right\}$$

and

$$\mathbf{R}_k = Kr\lambda_f^{(k)} \Lambda_\tau + \sigma_w^2 \mathbf{I}_M \quad \text{Ec. 12}$$

VI. Performance of Asymptotic Expressions

Figure 2 shows a high SNR case for various values of K. It can be seen as asymptotic expressions fit very closely to exact expressions when K is higher to 10. When SNR is poor higher values of K are required. For instead, when SNR=0 dB, 50 observations instead of 10 are required to have a similar performance.

Note how asymptotic expressions are more sensitive for lambn and hence errors are greater for this parameter, when they are produced. However, since the average expected K is higher than 200 very accurate results may be provided from asymptotic expressions.

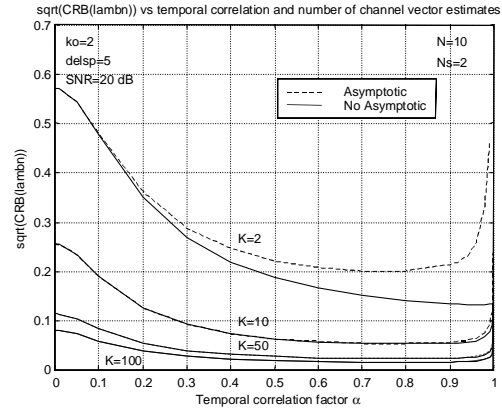
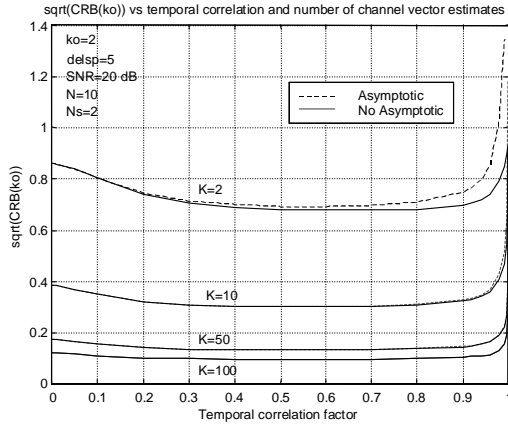


Figure 2 CRB of the first arriving path k_0 and CRB of the normalised delay spread λ_n for different values of the temporal correlation coefficient, and different number of available measured channels, for the asymptotic (dashed) and no asymptotic (solid) expressions. SNR=20dB.

VII. Performance of FCD Expressions

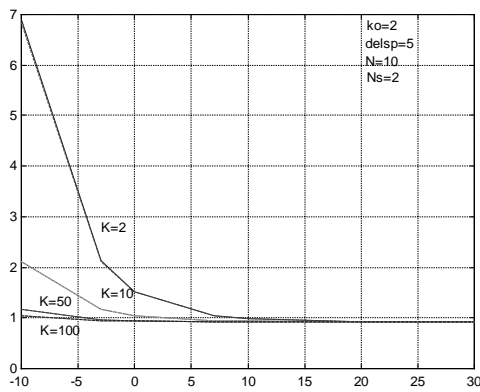


Figure 3 shows how PCD expressions almost fit perfectly with results provided for reduced FCD expressions when temporal correlation is set to one. Certainly, it must be noted that FCD expressions reduce computational burden considerably, hence their use is desirable. Similar results are found for the delay spread and are not included.

Figure 3 CRB of the first arriving path for different values of the SNR, for the FCD equations (solid) and PCD, setting $\alpha=1$.

VIII. Performance of TOA and Delay Spread with channel temporal coherence

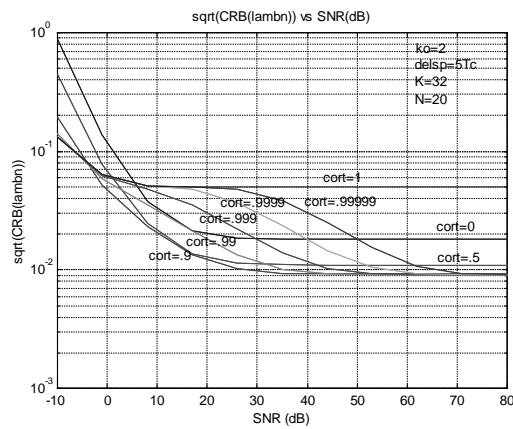
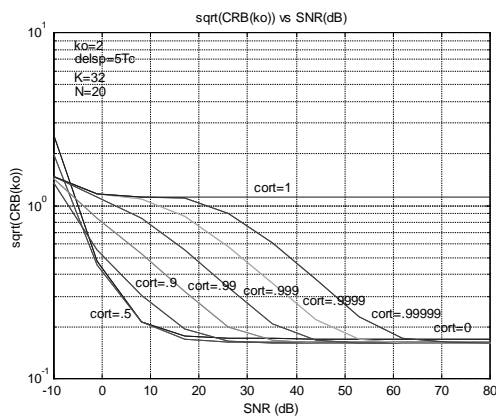


Figure 4 CRB of the first arriving path k_0 and CRB of λ_n for different values of SNR, and different values of the temporal correlation α .

Figure 4 provides information about the behavior of parameter estimation for the first arriving path k_0 and the inverse of the normalized delay spread λ_n in Λ_t . It can be seen how error estimation reduces for low temporal correlations between 0 and .5, and increases as the FCD case is reached. Recall that these situations correspond respectively to UE moving at high and low speed respectively. CRB always diminishes for higher SNR's, with some limiting floor value, which is significantly higher for the high temporal correlation case.

IX. Performance of TOA and Delay Spread with multiple sensors in diversity

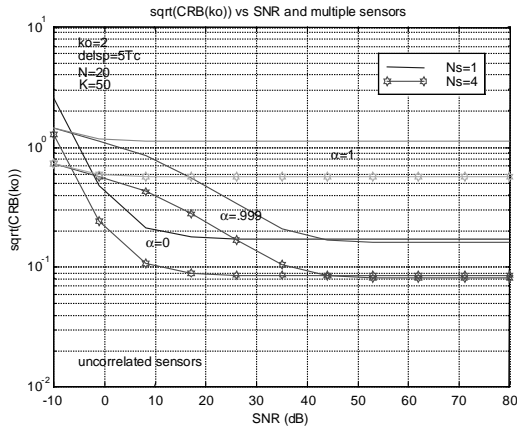


Figure 5 and Figure 6 show the behavior of estimation error when signals from various sensors are provided. Figure 5 shows bounds when signals recorded in different sensors are uncorrelated, which could well be the case of timing estimation at the UE for down link (DL), or in spatial diversity antennas at the BS, for uplink (UL) measurements. On the other hand Figure 6 shows a case where 4 sensors in $\lambda/2$ are used and angular spread is 5 and 10 degrees, which could be the case in the BS for UL measurements.

Figure 5 CRB of the first arriving path k_0 for different values of the SNR, and different values of the temporal correlation. One and four sensors and uncorrelated received signals in each.

It seems clear that adding multiple antennas improves estimates significantly, but angular spread does not influence significantly the delay estimation. In fact the best situation is the completely uncorrelated sensors, and CRB degrades gracefully as angular spread decreases. Note below that CRB are slightly better for Laplacian angular correlation kernel, but in general this variations are negligible compared to Gaussian angular correlation kernel.

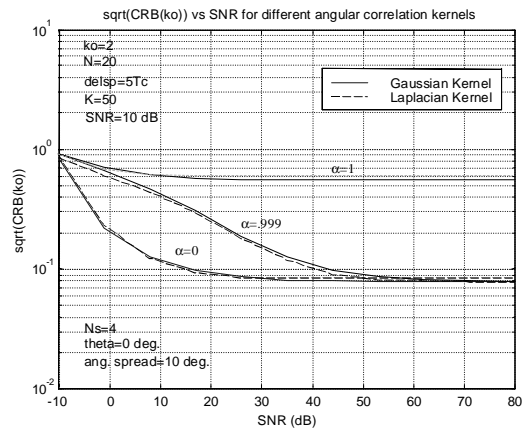
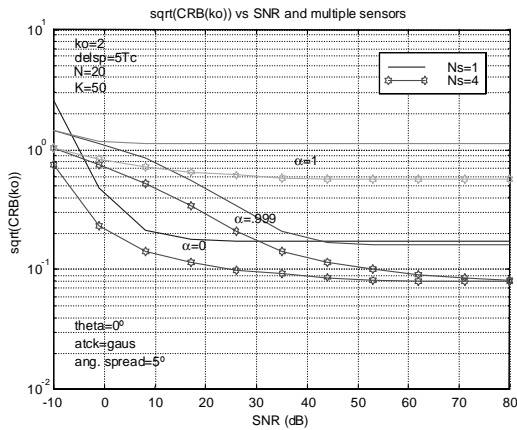


Figure 6 CRB of the first arriving path k_0 for different values of the SNR, and different values of the temporal correlation. One and four sensors and different angular spread for received signals.

X. Improvement of TOA and Delay Spread Estimates with the number of observations

Figure 7 shows how estimation improves as K increases. For highly temporal correlated channels, it is difficult to reduce the CRB, even for high values of K . The use of arrays seems not to improve the situation significantly.

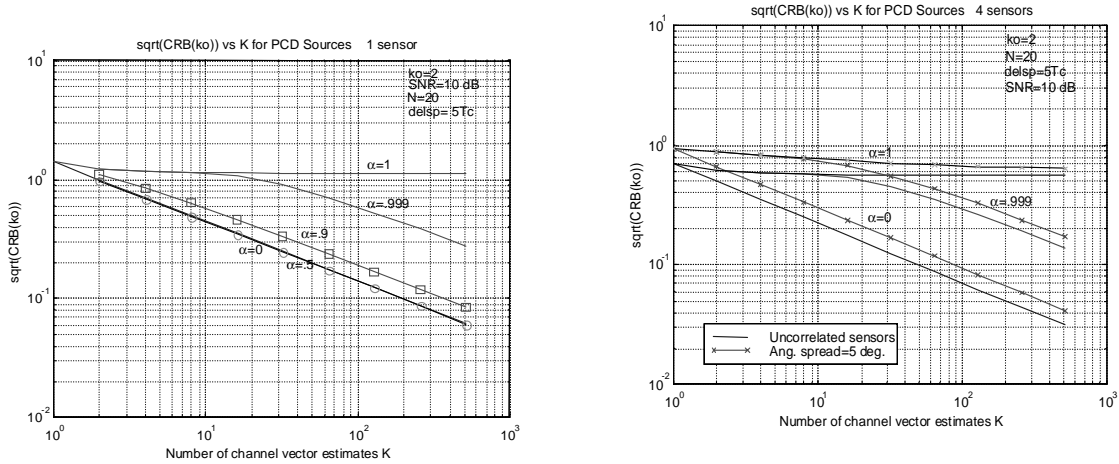


Figure 7 CRB of the first arriving path k_0 for different values of the number of recorded channels K , and different values of the temporal correlation α , for one and four sensors.

XI. Performance of TOA and Delay Spread with Delay Spread

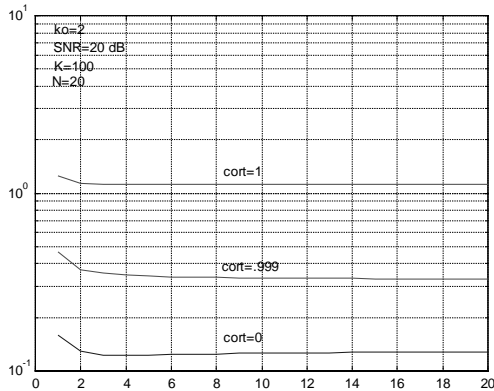


Figure 8 shows the importance of choosing the observation window large enough to avoid a signal with very large delay spread degrades estimation performance. It must be noted however that delay spread is expected to be lower than 15 times the chip time.

Figure 8 CRB of the first arriving path k_0 for different values of the delay spread and temporal correlation α .

XII. Conclusions

1. Asymptotic expressions may be used instead of exact ones to compute Cramer Rao Bounds, because there is a large number of observations available during the acquisition time, even though the mobile speed is high.
2. Reduced expressions for the FCD provide a good match (or a worst case bound), so their use is safe enough.
3. Delay Spread estimation error is more sensitive to channel temporal correlation than first time of arrival estimation error. However, this can be considered a nuisance parameter.
4. Improvements are always obtained when an antenna array is used instead of a single sensor, both when there is high correlation between sensors ($\lambda/2$ array) and when there is low correlation.
5. Estimation errors decrease as the number of observations increases, but this reduction is very conditioned by the time correlation coefficient.

6. Better results are obtained when angular spread is low. Bounds provided for uncorrelated sensors could be considered the worst case bounds.
7. For i.e, when one sensor is used, $K=50$ and for the ICD source case the first path time of arrival estimation error is around of 17% of the chip time, for $SNR=20$ dB. This error reduces below the 10% of the chip time when 4 sensors are used, and reduces near the 2% when $K=500$. Otherwise, for a highly correlated source case, where temporal correlation is .999, the error is below 50% of the chip time, it reduces to 30% for 4 sensors and near to 10% for $K=500$. These improvements are expected to hold in the positioning accuracy.
8. It must be noted that as the temporal correlation ranges between 0 and .9 there is a very little variation (see Figure 7), and it degrades rapidly above this value.

XIII. Acknowledgements

This work has been carried out in the framework of the EC-funded project SATURN as part of a PHD thesis research. Authors thank SATURN people for the information provided. This work has been partially supported by EC-IST-199-10322, TIC99-0849, TIC2000-1025, FIT-070000-2000-649, BIDE 874/OC-EC and AECL.

References

- [Ben00]** Mats Bengtsson and Björn Ottersten, "Low-Complexity Estimators for Distributed Sources", IEEE Transactions on Signal Processing, Vol. 48, No. 8, August 2000.
- [Bes00]** Olivier Besson, and Petre Stoica, "Decoupled Estimation of DOA and Angular Spread for a Spatially Distributed Source", IEEE Transactions on Signal Processing, Vol. 48, No. 7, July 2000.
- [Kay-1]** Steven M. Kay, Fundamentals of Statistical Signal Processing – Estimation Theory. New Jersey: Prentice Hall, 1993.
- [Ped00]** Klaus Ingemann Pedersen, Ph.D. Thesis, "Antenna Arrays in Mobile Communications – Channel Modeling and Receiver Design for DS-CDMA Systems", Aalborg University, January 2000.
- [Rai00]** Raviv Raich, Jason Goldberg, and Hagit Messer, "Bearing Estimation for a Distributed Source: Modeling, Inherent Accuracy Limitations and Algorithms", IEEE Transactions on Signal Processing, Vol.48, No.2, February 2000.
- [Ral98]** Gregory G. Raleigh and Tibor Boros, "Joint Space-Time Parameter Estimation for Wireless Communication Channels", IEEE Transactions on Signal Processing, Vol. 46, No.5, May 1998.
- [Val95]** Shahrokh Valaee, Benoit Champagne, and Peter Kabal, "Parametric Localization of Distributed Sources", IEEE Transactions on Signal Processing, Vol. 43, No.9, September 1995.
- [Vid01]** Josep Vidal et al, "Positioning limits for UMTS Mobiles in Delay and Angular Dispersive Channels", International Symposium on Location Based Services for Cellular Users (LOCCELLUS 2001), February 2001.
- [Wax97]** Mati Wax, and Amir Leshem, "Joint Estimation of Time-Delays and Direction of Arrival of Multiple Reflections of a Known Signal", IEEE Transactions on Signal Processing, Vol. 45, No. 10, October 1997.

Josep Vidal, Montse Nájjar, Margarita Cabrera, René Játiva, “Positioning accuracy when tracking UMTS mobile in delay and angular dispersive channels”, IEEE Vehicular Technology Conference, VTC 2001 Spring, Vol. 4, pp. 2575-2579, May 2001. DOI: 10.1109/VETECS.2001.944066.

ATTENTION!

Pages 267 to 271 of the thesis are available at the editor’s web i
<http://ieeexplore.ieee.org/document/944066/>

René Játiva E., Josep Vidal, “Estimación del Tiempo de Llegada en un canal Rayleigh desde una perspectiva de la Cota Inferior de Cramer-Rao”, Revista Avances en Ciencias e Ingenierías, pp. 5-10, Abril 2009.

ESTIMACIÓN DEL TIEMPO DE LLEGADA EN UN CANAL RAYLEIGH DESDE UNA PERSPECTIVA DE LA COTA INFERIOR DE CRAMER-RAO

René P. Játiva E.^{*1} Josep Vidal M.²

1 Colegio de Ciencias e Ingeniería, USFQ.

2 Departamento de Teoría de la Señal y Comunicaciones, Universidad Politécnica de Cataluña.

Resumen

Este documento presenta un modelo utilizado para el estudio de los parámetros de interés que modifican la precisión en la estimación del instante de Tiempo de Arribo (TOA) de la señal emitida por un suscriptor móvil que opera en un sistema en acceso múltiple por división en código (CDMA) que hace uso de un receptor RAKE como parte de su operación. Este modelo se ajusta a sistemas tales como IS-95, CDMA 2000 o WCDMA, para señales que se propagan en condición Rayleigh. Este trabajo muestra el desempeño del receptor en función del número de estimaciones de canal disponibles, el número de sensores que conforman el arreglo de antenas y el tipo de fuente de señal cuando la tasa de muestreo es superior a la tasa de chip. La señal recibida se modela a partir de distribuciones estocásticas, y se consideran tanto los casos de fuentes distribuidas parcialmente coherentes, como los casos de fuentes completamente coherentes y completamente incoherentes.

Palabras Clave. Cramer-Rao Bounds (CRB), CDMA, Rayleigh Channel, RAKE receiver.

Introducción

Los sistemas de posicionamiento de suscriptor móvil han adquirido gran relevancia en la última década debido al gran potencial que presentan para la provisión de una nueva gama de servicios basados en localización (LBS), sobretodo en sociedades donde la penetración de usuarios móviles es superior al 60%, tales como las encontramos en América del Norte y Europa por ejemplo, donde según varios reportes el gasto que realizan los usuarios en LBS totalizaron sumas de alrededor de doscientos millones de dólares a finales de 2006.

Si bien es cierto que los esquemas de posicionamiento de unidades móviles en general pueden clasificarse como basados en red y basados en GPS, son muy variadas las técnicas que pueden aplicarse dentro del primer grupo, siendo las más importantes las técnicas basadas en la estimación de la Diferencia de los instantes de Tiempo de Arribo Observados (OTDOA), de forma que incluso se ha estandarizado el uso de esta técnica para sistemas móviles de Tercera Generación.

Un componente fundamental en sistemas móviles que operan con Acceso Múltiple por División de Código (CDMA) es el receptor RAKE que permite identificar las componentes de señal originadas en propagación multitrayecto, y posibilita su aprovechamiento en términos de diversidad.

Los resultados mostrados en este artículo asumen que el proceso de estimación del primer retardo se hace para un sistema CDMA que utiliza un receptor RAKE, y que el proceso de estimación del primer retardo es el mejor posible. En efecto se estudia el impacto que se tiene sobre la precisión en la estimación del TOA para el primer retardo en función de parámetros tales como: el

número de estimaciones de canal disponibles, el número de sensores que constituyen el arreglo de la antena, el grado de coherencia temporal en las estimaciones de canal que se utilizan para el proceso de estimación de TOA y el período de muestreo cuando éste se realiza a una velocidad mayor que la tasa de chips del sistema.

Materiales y métodos

Este trabajo está muy relacionado con otro anterior, en el que se estudió el impacto de varios de estos parámetros pero bajo el supuesto de que la tasa de muestreo de la señal se realizaba a la tasa de chip [1].

Para este estudio se considera una señal dispersa caracterizada estocásticamente, y el error en la estimación del instante de llegada (TOA) se calcula utilizando la Cota Inferior de Cramer-Rao (CRB) a partir del modelo de señal que describe el escenario móvil.

El modelo toma en cuenta las siguientes consideraciones:

1. Se asume que el canal tiene un tiempo de coherencia para las amplitudes que siguen las expresiones de Jake usuales, sin embargo el tiempo de coherencia de retardos y ángulos de llegada es mucho mayor, siendo posible obtener muchas estimaciones de canal a objeto de mejorar la precisión de las estimaciones de TOA.
2. El ruido presente en las estimaciones de canal es blanco y gaussiano.
3. El ruido es incoherente en retardo y ángulo, lo cual corresponde a una situación en la cual el suscriptor móvil se mueve y los diferentes rayos reflejados experimentan desvanecimiento rápido incorrelado.

4. Se asumen un modelo lineal de Markov de primer orden para la variación temporal en el canal.
5. Un espectro de potencia continua se utiliza para modelar la función de densidad marginal de retardo, y se asume que esta se ajusta a una exponencial según se propone en Pedersen [2], y se la estima a una fracción del tiempo de chip. Se asume también la misma distribución angular para todos los retardos.

Este modelo es muy conveniente para propósitos de localización puesto que interesa calcular tan solo algunos parámetros de interés en lugar de todos los retardos, lo que complicaría el modelo innecesariamente y tornaría su solución demasiado complicada en escenarios altamente dispersivos.

Modelo De Canal

El vector de canal, $\mathbf{z}^{(i)}(k)$, para un sensor particular “j” y un lag “k” puede modelarse en términos del coeficiente correspondiente con el cual la señal firma sobre el arreglo de sensores en la antena, b_j , la potencia estimada para el trayecto recibido, P_i , su frecuencia Doppler normalizada f_i , y el vector correspondiente al pulso conformador $\mathbf{g}^{(i)}$; además de una componente de ruido $\mathbf{w}^{(i)}(k)$, donde k_0 corresponde al instante de muestreo para el primer retardo.

$$\mathbf{z}^{(j)}(k) = \sum_{i=k_0}^N b_j P_i e^{j2\pi f_i k} \mathbf{g}^{(i)} + \mathbf{w}^{(j)}(k) \quad (1.1)$$

El vector $\mathbf{g}^{(i)}$ contiene las muestras del pulso conformador, siendo “i” la posición de su máximo, $g_p(0)$, y se muestra en (1.2).

$$\mathbf{g}^{(i)} = [g_p \quad -i+1 \quad \cdots \quad g_p \quad 0 \quad \cdots \quad g_p \quad N-i]^T \quad (1.2)$$

Si el vector de canal, $\mathbf{z}^{(i)}(k)$, y su correspondiente vector de ruido se arreglan como se muestra en (1.3), tanto la señal como el ruido pueden describirse como procesos aleatorios Gaussianos de media cero y con ciertas matrices de correlación como se indica en (1.4). Se asume que el ruido es temporalmente incorrelado, independiente de la señal y de varianza σ_w^2 . La matriz de correlación para las estimaciones del vector de canal, \mathbf{R}_z , puede expresarse en términos de sus componentes temporal y espacial, como se muestra en (1.5). En esta expresión, el factor de potencia de la señal P_s , se refiere a la varianza de la potencia recibida estimada para el primer retardo de la señal temporalmente dispersa en el caso de propagación Rayleigh; la matriz de conformación de pulso, $\mathbf{G}_s(\beta)$, modela la contribución del pulso conformador, mientras que $\mathbf{\Lambda}_\tau$ es una matriz diagonal que modela la dispersión temporal de la señal y su distribución de potencia exponencial. Por otro lado, la matriz de correlación temporal, $\mathbf{T}(\alpha)$, toma en consideración la variación temporal del canal, y se asume idéntica para todos los retardos; la matriz de

correlación espacial, $\mathbf{R}_\phi(\rho)$, contiene los coeficientes de correlación para las firmas entre sensores, y \otimes denota el producto de Kronecker.

$$\mathbf{w} = \begin{bmatrix} w_1^1 & 1 & \cdots & w_N^1 & 1 & \cdots \\ \cdots & w_1^1 & k & \cdots & w_N^1 & k \\ \cdots & w_1^1 & K & \cdots & w_N^{N_s} & K \end{bmatrix}^T \quad (1.3)$$

$$\mathbf{w} \sim CN \mathbf{0}, \sigma_w^2 \mathbf{I}, \quad \mathbf{z} \sim CN \mathbf{0}, \mathbf{R}_z \quad (1.4)$$

$$\mathbf{R}_z = \mathbf{R}_\phi(\rho) \otimes \mathbf{T}(\alpha) \otimes P_s \mathbf{G}_s \beta \mathbf{\Lambda}_\tau(\lambda_n) \mathbf{G}_s^H \beta + \sigma_w^2 \mathbf{I} \quad (1.5)$$

La ecuación (1.6) muestra el modelo exponencial usado para los retardos, en términos de la posición del primer arribo, k_0 , y del inverso de la dispersión de retardos normalizado para el tiempo de chip, λ_n .

$$\mathbf{\Lambda}_\tau_{k,k} = \exp[-k - k_0 \lambda_n] u_{k-k_0} \quad (1.6)$$

La matriz de correlación espacial, $\mathbf{R}_\phi(\rho)$ se modela como en (1.7), $\mathbf{T}(\alpha)$ como un proceso auto-regresivo (AR) de primer orden, como se muestra en (1.8); y la forma general para \mathbf{G}_s se exhibe en (1.9). α es el coeficiente de correlación temporal entre dos vectores de canal consecutivos, y ρ_{ij} es el coeficiente de correlación entre los sensores “i” y “j”. Note también que \mathbf{G}_s corresponde a la matriz identidad cuando el muestreo se realiza a la tasa de chips.

$$\mathbf{R}_\phi(\rho) = \begin{bmatrix} 1 & \rho_{12} & \cdots & \rho_{1N_s} \\ \rho_{12}^* & 1 & \cdots & \rho_{2N_s} \\ \vdots & \vdots & \ddots & \vdots \\ \rho_{1N_s}^* & \rho_{2N_s}^* & \cdots & 1 \end{bmatrix} \quad (1.7)$$

$$\mathbf{T}(\alpha) = \begin{bmatrix} 1 & \alpha & \cdots & \alpha^{K-1} \\ \alpha & 1 & \cdots & \alpha^{K-2} \\ \vdots & \vdots & \ddots & \vdots \\ \alpha^{K-1} & \alpha^{K-2} & \cdots & 1 \end{bmatrix} \quad (1.8)$$

$$\mathbf{G}_s \beta = \frac{1}{\sqrt{T_c} \sqrt{1-\beta/4}} [\mathbf{g}_{s_1} \quad \mathbf{g}_{s_2} \quad \cdots \quad \mathbf{g}_{s_{N_s}}] \quad (1.9)$$

Observe que cada uno de los vectores de conformación de pulso, \mathbf{g}_{s_i} , en (1.9) puede modelarse como en (1.10), donde sus elementos g_k se describen por (1.11). Más aún, β es el factor de roll-off, y N_{spc} corresponde al número de muestras adquiridas por periodo de chip:

$$\mathbf{g}_{s_i}^T = \left[g_{-i+1} \quad \cdots \quad \underset{\substack{\uparrow \\ \text{ith element}}}{1} \quad \cdots \quad g_{N-i} \right] \quad (1.10)$$

$$g_k = \frac{\text{sinc}\left(\frac{k}{N_{\text{spc}}}\right) \cos\left(\frac{\pi\beta k}{N_{\text{spc}}}\right)}{1 - 2\beta k/N_{\text{spc}}} \quad (1.11)$$

Los elementos de la matriz de correlación espacial, \mathbf{R}_ϕ , se calculan como se muestra en (1.12):

$$\begin{aligned} \mathbf{R}_\phi_{n_1, n_2} &= E \quad b_{n_1} \quad b_{n_2}^* \\ &= \frac{1}{\sqrt{2\pi\Delta_\phi}} \int_{-\pi}^{\pi} e^{-\frac{\phi - \phi_0}{2\Delta_\phi^2}} e^{-j n_1 - n_2 \pi \sin \phi} d\phi \end{aligned} \quad (1.12)$$

Derivación de las Cotas de Cramer-Rao

Las cotas de Cramer-Rao (CRB) son muy útiles en la cuantificación de los errores que resultan de la estimación de parámetros de un modelo estocástico. Para el modelo en (1.4), (1.5) se define el vector de parámetros, Ψ , en (1.13), donde \mathbf{p} es un vector que contiene las partes reales e imaginarias de los coeficientes de correlación entre sensores, tal como se muestra en (1.14).

$$\Psi = \left[k_0, \lambda_n, \beta, P_s, \sigma_w^2, \alpha, \mathbf{p}^T \right]^T \quad (1.13)$$

$$\mathbf{p} = \left[\rho_{1, \text{Re}}, \dots, \rho_{N_c, \text{Re}}, \rho_{1, \text{Im}}, \dots, \rho_{N_c, \text{Im}} \right]^T \quad (1.14)$$

En este vector de parámetros, k_0 se refiere al instante de la primera llegada normalizado para el tiempo de chip, T_c ; λ_n es el inverso de la dispersión de retardos normalizado para el intervalo de chip, y los demás parámetros ya han sido definidos antes. El parámetro de interés es precisamente k_0 .

Adicionalmente, note que N_c cuenta el número de coeficientes de correlación espacial y se relaciona con el número de sensores como se muestra en (1.15).

$$N_c = \frac{N_s}{2} N_s - 1 \quad (1.15)$$

Las CRB para este modelo se calculan a partir de la Matriz de Información de Fisher (FIM), cuyos elementos se calculan como se muestra en (1.16) [3]:

$$\left[\mathbf{F}_\Psi^{LOS} \right]_{pq} = \text{tr} \left(\mathbf{R}_z^{-1} \frac{\partial \mathbf{R}_z}{\partial \Psi_p} \mathbf{R}_z^{-1} \frac{\partial \mathbf{R}_z}{\partial \Psi_q} \right) \quad (1.16)$$

Si la matriz de correlación espacial, $\mathbf{R}_\phi(\mathbf{p})$, se descompone en términos de sus autovalores, λ_ϕ , y de sus autovectores, \mathbf{u}_ϕ ; y se define \mathbf{U}_ϕ como la matriz que contiene los autovectores, y Λ_ϕ , como la matriz diagonal que contiene los autovalores, como se exhibe en (1.17); y un procedimiento análogo se utiliza para la matriz de Correlación Temporal, $\mathbf{T}(\alpha)$, como se muestra en (1.18), y se reemplazan estas expresiones en (1.5), es posible encontrar una expresión simplificada para \mathbf{R}_z^{-1} , que se muestra en (1.19).

$$\begin{aligned} \mathbf{R}_\phi &= \mathbf{U}_\phi \Lambda_\phi \mathbf{U}_\phi^H \\ \mathbf{U}_\phi &= \left[\mathbf{u}_\phi^{(1)}, \mathbf{u}_\phi^{(2)}, \dots, \mathbf{u}_\phi^{(N_s)} \right] \\ \Lambda_\phi &= \text{diag} \left[\lambda_\phi^{(1)}, \lambda_\phi^{(2)}, \dots, \lambda_\phi^{(N_s)} \right] \end{aligned} \quad (1.17)$$

$$\begin{aligned} \mathbf{T} &= \mathbf{U}_t \Lambda_t \mathbf{U}_t^H \\ \mathbf{U}_t &= \left[\mathbf{u}_t^{(1)}, \mathbf{u}_t^{(2)}, \dots, \mathbf{u}_t^{(K)} \right] \\ \Lambda_t &= \text{diag} \left[\lambda_t^{(1)}, \lambda_t^{(2)}, \dots, \lambda_t^{(K)} \right] \end{aligned} \quad (1.18)$$

$$\begin{aligned} \mathbf{R}_z^{-1} &= \sum_{k=1}^{N_s} \mathbf{u}_\phi^k \mathbf{u}_\phi^{kH} \otimes \sum_{k_1=1}^K \mathbf{u}_t^{k_1} \mathbf{u}_t^{k_1H} \\ &\quad \otimes \lambda_\phi^k \lambda_t^{k_1} P_s \mathbf{G}_s \Lambda_\tau \mathbf{G}_s^H + \sigma_w^2 \mathbf{I}^{-1} \end{aligned} \quad (1.19)$$

Las derivadas de \mathbf{R}_z , respecto a los parámetros en (1.13) toman la forma en (1.20), siendo \mathbf{A}_i , \mathbf{B}_i y \mathbf{C}_i las matrices que se contienen en la Tabla 1.

$$\frac{\partial \mathbf{R}_z}{\partial \Psi_i} = \mathbf{A}_i \otimes \mathbf{B}_i \otimes \mathbf{C}_i \quad i = p, q \quad (1.20)$$

Si se reemplazan la expresión para \mathbf{R}_z^{-1} en (1.19), y las derivadas en (1.20) en (1.16), puede demostrarse que la FIM puede calcularse por la expresión (1.21).

$i=p,q$	Ψ_i	\mathbf{A}_i	\mathbf{B}_i	\mathbf{C}_i
1	k_0	\mathbf{R}_ϕ	\mathbf{T}	$P_s \mathbf{G}_s \frac{\partial \Lambda_\tau}{\partial k_0} \mathbf{G}_s^T$
2	λ_n	\mathbf{R}_ϕ	\mathbf{T}	$P_s \frac{\partial \Lambda_\tau}{\partial \lambda_n}$
3	β	\mathbf{R}_ϕ	\mathbf{T}	$P_s \frac{\partial (\mathbf{G}_s \Lambda_\tau \mathbf{G}_s^T)}{\partial \beta}$
4	P_s	\mathbf{R}_ϕ	\mathbf{T}	$\mathbf{G}_s \Lambda_\tau \mathbf{G}_s^T$
5	σ_w^2	\mathbf{I}_{N_s}	\mathbf{I}_K	\mathbf{I}_N

6	α	\mathbf{R}_ϕ	$\frac{\partial \mathbf{T}}{\partial \alpha}$	$P_s \mathbf{G}_s \mathbf{\Lambda}_\tau \mathbf{G}_s^T$
7+6+N _c	$\rho_{i-6,Re}$	$\frac{\partial \mathbf{R}_\phi}{\partial \rho_{i-6,Re}}$	\mathbf{T}	$P_s \mathbf{G}_s \mathbf{\Lambda}_\tau \mathbf{G}_s^T$
7+N _c : 6+2N _c	$\rho_{i-6,Im}$	$\frac{\partial \mathbf{R}_\phi}{\partial \rho_{i-6,Im}}$	\mathbf{T}	$P_s \mathbf{G}_s \mathbf{\Lambda}_\tau \mathbf{G}_s^T$

Tabla 1. Resultados de las derivadas de la Matriz de Correlación de Estimaciones de Canal \mathbf{R}_z requeridas en (1.20).

$$\mathbf{F}_\Psi = \sum_{k=1}^{N_s} \sum_{k_1=1}^K \mathbf{H}_{k,k_1} \mathbf{J}_{\bar{\Psi}} \mathbf{H}_{k,k_1}^T + C_1 \mathbf{e}_{N_p}^{(6)} \mathbf{e}_{N_p}^{(6)T} + \sum_{q_1=1}^{2N_c} \sum_{q_2=1}^{2N_c} C_2^{(q_1, q_2)} \mathbf{e}_{N_p}^{(6+q_1)} \mathbf{e}_{N_p}^{(6+q_2)T} \quad (1.21)$$

Donde la FIM para este modelo se relaciona con la FIM calculada para un vector reducido de parámetros que se muestra en (1.22) conforme se indica en (1.23) y (1.24), a través de la matriz \mathbf{H}_{k,k_1} que se muestra en (1.25).

$$\bar{\Psi} = [k_0, \lambda_n, \beta, \gamma_{k,k_1}, \sigma_w^2]^T \quad (1.22)$$

$$\gamma_{k,k_1} = P_s \lambda_\phi^k \lambda_{\phi}^{k_1} \quad (1.23)$$

$$\mathbf{J}_{\bar{\Psi}} = tr \left(\mathbf{R}_{k,k_1}^{-1} \frac{\partial \mathbf{R}_{k,k_1}}{\partial \bar{\Psi}_p} \mathbf{R}_{k,k_1}^{-1} \frac{\partial \mathbf{R}_{k,k_1}}{\partial \bar{\Psi}_q} \right) \quad (1.24)$$

Las derivadas respecto al vector de coeficientes de correlación entre sensores requeridas en (1.25) se calculan como se muestra en (1.26)-(1.28).

$$\mathbf{H}_{k,k_1} = \begin{bmatrix} 1 & 0 & 0 & 0 & 0 \\ 0 & 1 & 0 & 0 & 0 \\ 0 & 0 & 1 & 0 & 0 \\ 0 & 0 & 0 & \lambda_\phi^{(k)} \lambda_{\phi}^{(k_1)} & 0 \\ 0 & 0 & 0 & 0 & 1 \\ 0 & 0 & 0 & P_s \lambda_\phi^{(k)} \frac{\partial \lambda_{\phi}^{(k_1)}}{\partial \alpha} & 0 \\ \mathbf{0} & \mathbf{0} & \mathbf{0} & P_s \frac{\partial \lambda_\phi^{(k)}}{\partial \rho} \lambda_{\phi}^{k_1} & \mathbf{0} \end{bmatrix} \quad (1.25)$$

$$\frac{\partial \lambda_\phi^{(k)}}{\partial \rho} = \left[\frac{\partial \lambda_\phi^{(k)}}{\partial \rho_{Re}}, \frac{\partial \lambda_\phi^{(k)}}{\partial \rho_{Im}} \right]^T \quad (1.26)$$

$$\frac{\partial \lambda_\phi^{(k)}}{\partial \rho_{Re}} = \left[\frac{\partial \lambda_\phi^{(k)}}{\partial \rho_{1,Re}}, \dots, \frac{\partial \lambda_\phi^{(k)}}{\partial \rho_{N_c,Re}} \right]^T \quad (1.27)$$

$$\frac{\partial \lambda_\phi^{(k)}}{\partial \rho_{Im}} = \left[\frac{\partial \lambda_\phi^{(k)}}{\partial \rho_{1,Im}}, \dots, \frac{\partial \lambda_\phi^{(k)}}{\partial \rho_{N_c,Im}} \right]^T \quad (1.28)$$

El término C_1 requerido en (1.21) modela el efecto del coeficiente de correlación temporal, α , sobre la FIM, como una contribución de la diversidad espacial y temporal, mientras que los términos $C_2^{(q_1, q_2)}$ corresponden a la contribución de los coeficientes de correlación espacial a la FIM. El vector $\mathbf{e}_v^{(i)}$ se introduce por conveniencia de notación y se muestra en (1.29).

$$\mathbf{e}_v^{(i)} = \left[0, \dots, 0, \underset{\substack{\uparrow \\ i \text{th element}}}{1}, 0, \dots, 0 \right]^T \quad (1.29)$$

Note en (1.30) - (1.33) como F_1 corresponde a la contribución de las estimaciones temporales y F_2 modela la diversidad temporal y el efecto del pulso conformador.

$$C_1 = -P_s^2 \sum_{k=1}^{N_s} \lambda_\phi^{k^2} \sum_{k_1=1}^K \sum_{l_1=1}^K F_1^{k_1, l_1} F_2^{k, k_1, l_1} \quad (1.30)$$

$$F_1^{k_1, l_1} = \lambda_\tau^{(k_1)} - \lambda_\tau^{(l_1)^2} \mathbf{u}_t^{(k_1)H} \dot{\mathbf{u}}_t^{(l_1)} \mathbf{u}_t^{(l_1)H} \dot{\mathbf{u}}_t^{(k_1)} \quad (1.31)$$

$$F_2^{k, k_1, l_1} = tr \mathbf{R}_{k, k_1}^{-1} \mathbf{G}_s \mathbf{\Lambda}_\tau \mathbf{G}_s^T \mathbf{R}_{k, l_1}^{-1} \mathbf{G}_s \mathbf{\Lambda}_\tau \mathbf{G}_s^T \quad (1.32)$$

$$\dot{\mathbf{u}}_t^{(k_1)} = \frac{d\mathbf{u}_t^{(k_1)}}{d\alpha} \quad (1.33)$$

Los términos $C_2^{(q_1, q_2)}$ se definen en (1.34)-(1.36) y se calculan como resultado de la diversidad temporal y espacial. Los términos E_1 corresponden precisamente a la contribución espacial, mientras que los términos E_2 se relacionan con la diversidad temporal debida al receptor RAKE y al efecto del pulso conformador.

$$C_2^{(q_1, q_2)} = -P_s^2 \sum_{k_1=1}^K \lambda_\tau^{k_1^2} \sum_{k=1}^{N_s} \sum_{l=1}^{N_s} E_1^{k, l} E_2^{k_1, k, l} \quad (1.34)$$

$$E_1^{k, l} = \lambda_\phi^{(k)} - \lambda_\phi^{(l)^2} \left(\mathbf{u}_\phi^{(k)T} \frac{\partial \mathbf{u}_\phi^{(l)}}{\partial \rho_{q_1}} \right) \cdot \left(\mathbf{u}_\phi^{(l)T} \frac{\partial \mathbf{u}_\phi^{(k)}}{\partial \rho_{q_2}} \right) \quad (1.35)$$

$$E_2^{k,l,k_1} = \text{tr} \mathbf{R}_{k,k_1}^{-1} \mathbf{G}_s \mathbf{\Lambda}_\tau \mathbf{G}_s^T \mathbf{R}_{l,k_1}^{-1} \mathbf{G}_s \mathbf{\Lambda}_\tau \mathbf{G}_s^T \quad (1.36)$$

Las derivadas de los auto-vectores de la matriz de correlación temporal respecto al coeficiente de correlación temporal, α , requeridas en (1.31) se calcularon numéricamente para obtener las cotas de Cramer-Rao en este artículo.

Resultados y discusión

A continuación se presentan algunos resultados de interés que relacionan el error en la determinación del primer retardo con algunos parámetros relevantes del modelo.

Comportamiento del Error en la estimación del Instante de Llegada de la señal (TOA) cuando se utilizan múltiples sensores en diversidad y el vector de canal se muestrea a la tasa de chip.

La figura 1 muestra el comportamiento del error de estimación cuando se utilizan señales de varios sensores. El ejemplo propuesto corresponde a las cotas para un entorno con una dispersión angular de 10° y una dispersión temporal de $2T_c$, cuando se utilizan 4 sensores espaciados $\lambda/2$; el cual bien podría corresponder al caso del enlace ascendente en el que las mediciones se realizan en la estación base (BS). La gráfica revela que la adición de múltiples sensores en el arreglo de la antena mejora la estimación del primer retardo significativamente. Así se tiene que para una relación señal a ruido de 10 dB, la cota del error en la estimación del primer retardo se reduce desde alrededor de $0,85T_c$ cuando se usa un único sensor hasta aproximadamente la mitad ($0,44T_c$) cuando se emplean cuatro sensores y la fuente de señal se modela como parcialmente coherente

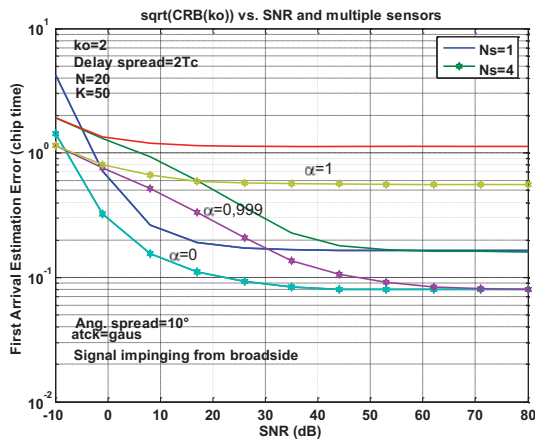


Figura 1. Cotas de Cramer-Rao para el trayecto correspondiente a la primera llegada k_0 en función de la SNR para varios valores del factor de correlación temporal, α . Un sensor (línea sólida) y cuatro sensores (línea sólida-estrella) se usan para una fuente con una dispersión angular de 10° , una dispersión de retardos de $2T_c$ y 50 observaciones del vector de canal.

con un factor de correlación temporal, $\alpha=0,999$. La situación es algo mejor para fuentes de señal incoherentes ($\alpha=0$). En este caso el error se reduce desde aproximadamente $0,23T_c$ cuando se emplea un sensor hasta cerca de la mitad cuando se emplea un arreglo con cuatro sensores. El peor caso corresponde a fuentes de señal completamente coherentes. El error en este caso es de alrededor de $1,2T_c$ para un sensor y se reduce hasta algo más de la mitad cuando se utilizan cuatro sensores.

La dispersión angular no es un aspecto especialmente relevante, a pesar de que el mejor caso corresponde a sensores completamente incorrelados, y que el error de estimación presenta una pequeña reducción conforme la dispersión angular reduce.

Comportamiento del Error en la estimación del Instante de llegada de la señal (TOA) cuando la estimación del vector de canal se realiza a dos veces la tasa de chip.

La figura 2 muestra el comportamiento de la cota del error en la estimación del primer retardo el vector de canal se muestrea a dos veces la tasa de chip, para diferentes valores del factor de roll-off, β , y muestra como una mejoría marginal apenas se alcanza cuando se modifica el factor de roll-off de 0,5 a 1. Por otro lado si estos resultados se comparan con los que se muestran en la figura 1, el error en la estimación de TOA se reduce ligeramente. Así por ejemplo, se observa que para un factor de correlación temporal, α , de 0,999 y cuando se emplea únicamente un sensor, el error en la estimación del primer retardo es de alrededor de $0,85T_c$ para una SNR de 10dB y de alrededor de $0,2T_c$ para una SNR de 40dB, cuando el muestreo se realiza a la tasa de chip, y que este valor reduce a alrededor de la mitad cuando la tasa de muestreo es dos veces más rápida.

La figura 2 muestra que resultados similares se esperan con independencia de la dispersión angular de la fuente de señal. Sin embargo, ligeras ganancias se consiguen cuando la dispersión angular es mayor, especialmente cuando la relación señal a ruido, SNR, es baja. Por ejemplo, el error en la estimación del primer retardo cuando la SNR es de alrededor de 5dB y se emplea una antena con 4 sensores se reduce desde alrededor de $10^{-1}T_c$ hasta $8 \times 10^{-2}T_c$ cuando la dispersión angular crece desde 5° hasta 18° y se utilizan estimaciones del vector de canal temporalmente incorreladas; y se reduce desde $4 \times 10^{-1}T_c$ hasta alrededor de $3 \times 10^{-1}T_c$ cuando las estimaciones del vector de canal están altamente correladas ($\alpha=0,99999$). En forma similar, el error en la estimación del primer retardo cuando la SNR es de alrededor de 50dB mejora de $10^{-1}T_c$ a $8 \times 10^{-2}T_c$ para el caso en que la fuente de señal está temporalmente muy correlada ($\alpha=0,99999$).

Finalmente, es importante destacar que el error de estimación del primer retardo se mantiene prácticamente

invariante con respecto a la dispersión temporal de la fuente y que la precisión mejora cuando el número de estimaciones de vector de canal disponibles aumenta,

sobretudo cuando la fuente de señal es temporalmente incoherente, es decir para valores bajos de α .

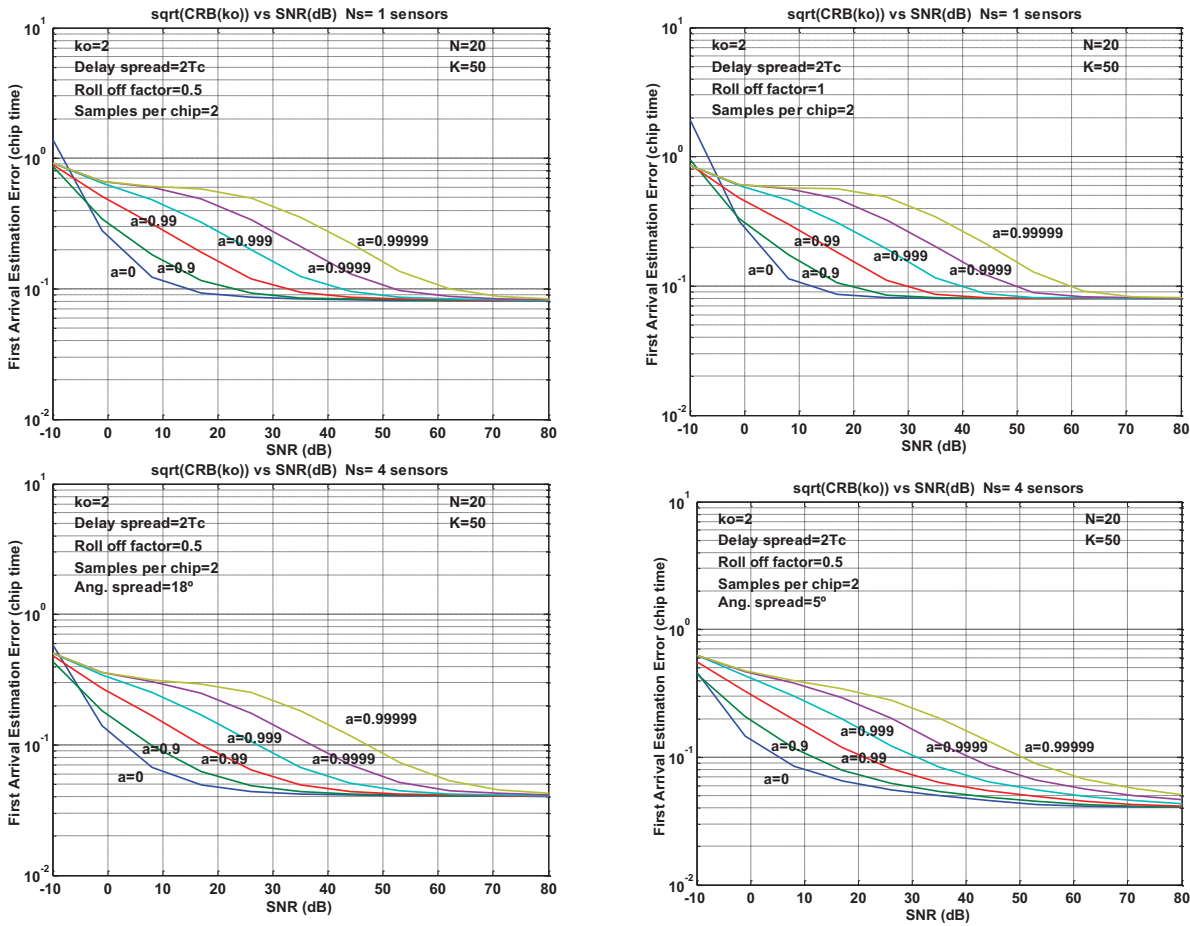


Figura 2: Cotas de Cramer-Rao para el trayecto correspondiente a la primera llegada k_0 en función de la SNR para diversos valores del factor de correlación temporal, α . Dos factores de roll-off se utilizan y se presentan resultados para un sensor y para un arreglo de cuatro elementos dispuestos con una separación de $\lambda/2$. La dispersión temporal es de $2T_c$. A) Superior Izquierda: Un sensor, β de 0.5. B) Superior Derecha: Un sensor, β de 1.0. C) Inferior Izquierda: Cuatro sensores, β de 0.5, y dispersión angular de 18° . C) Inferior Derecha: Cuatro sensores, β de 0.5, y dispersión angular de 5° .

Referencias bibliográficas

1. Játiva, R.; Vidal, J. 2003. “La Cota Inferior de Cramer-Rao en la Estimación del Instante de Llegada al usar Modelos de Fuente Distribuida”. Revista CIENCIA Vol.6, N.2, 185-196.
2. Pedersen, K. 2000. “Antenna Arrays in Mobile Communications – Channel Modeling and Receiver Design for DS-CDMA Systems”, Tesis Doctoral de la Universidad de Aalborg.
3. Kay, S. 1993. *Fundamentals of Statistical Signal Processing – Estimation Theory*. New Jersey: Prentice Hall.

René Játiva E., Josep Vidal, “Cota Inferior de Crámer-Rao en la Estimación del Tiempo de Llegada en un Canal Rice”, Revista Avances en Ciencias e Ingenierías, pp. C14-C21, Julio 2012. ISSN 1390-5384.

Cota Inferior de Crámer-Rao en la Estimación del Tiempo de Llegada en un Canal Rice

René P. Játiva E.^{1*} Josep Vidal M.²

¹Colegio de Ciencias e Ingeniería –El Politécnico–, Universidad San Francisco de Quito
Diego de Robles s/n y Vía Interoceánica, Quito, Ecuador

²Departamento de Teoría de la Señal y Comunicaciones Universidad Politécnica de Cataluña
E-mail: rjativa@usfq.edu.ec

Editado por/Edited by: D. Cárdenas, M.Sc.

Recibido/Received: 06/02/2012. Aceptado/Accepted: 06/20/2012.

Publicado en línea/Published on Web: 06/30/2012. Impreso/Printed: 06/30/2012.

Abstract

This document introduces a Rice mobile channel model suitable for the study of parameters of interest that modifies the accuracy in the estimation of the Time Of Arrival (TOA) for the signal emitted from a mobile station, operating in a DS-SS. This work shows the receiver performance in terms of the available number of channel estimates, the number of sensors in the antenna array and the type of signal source when sampling rate is higher than the chip rate. Received signal is modeled from time-space stochastic distributions and the cases of partially coherent distributed sources as well as fully coherent distributed sources and fully incoherent distributed sources are considered.

Keywords. Cramer-Rao Bounds (CRB), Direct Sequence Spread Spectrum (DS-SS), Rice Channel, Temporal and Spatial Diversity.

Resumen

Este documento introduce un modelo para el estudio de un canal móvil de tipo Rice, utilizado para el estudio de los parámetros de interés que modifican la precisión en la estimación del instante de Tiempo de Arribo (TOA) de la señal emitida por un suscriptor móvil que opera en un sistema en acceso múltiple por división en código (CDMA) que hace uso de un correlador como parte de su operación. Este trabajo muestra el desempeño del receptor en función del número de estimaciones de canal disponibles, el número de sensores que conforman el arreglo de antenas y el tipo de fuente de señal cuando la tasa de muestreo es superior a la tasa de chip. La señal recibida se modela a partir de distribuciones estocásticas, y se consideran tanto los casos de fuentes distribuidas parcialmente coherentes, como los casos de fuentes completamente coherentes y completamente incoherentes.

Palabras Clave. Cramer-Rao Bounds (CRB), CDMA, Rice Channel, Diversidad Temporal y Espacial.

Introducción

Los servicios basados en localización (LBS) continúan creciendo a un ritmo vertiginoso. Nadie discute sus beneficios sino más bien el abuso del que podemos ser objeto si su uso es indiscriminado. En efecto, casi todos encontraremos útil en ciertas circunstancias, el poder pagar una lata de gaseosa sencillamente presionando una tecla de nuestro teléfono celular, si encontramos una máquina dispensadora a nuestro alcance, pero muchos objetaremos la molestia de cierta publicidad al entrar en el área de un centro comercial. En todo caso, sea cual sea la aplicación que puede darse a la información de posición, lo cierto es que la investigación en esta área continúa en la búsqueda de nuevos y mejores esquemas que permitan el estimar la posición con un mayor grado

de certidumbre. Así por ejemplo, atendiendo a la degradación de la posición inherente al uso de dispositivos móviles equipados con GPS en interiores, se ha procurado precisamente caracterizar mejor esta señal [1], además como buscar nuevas alternativas que complementen o faciliten este trabajo tales como sistemas basados en plataformas inerciales [2], Wi-Fi, RFID, Bluetooth, Infrarojos [3], ultrasonido [4], sensores dópler [5], etc.

El interés de este artículo es contribuir a entender mejor desde una perspectiva conceptual los beneficios y limitaciones que involucra el uso de sistemas de espectro disperso de secuencia directa (DS-SS del inglés Direct Sequence Spread Spectrum) en la estimación del instante de llegada (TOA del inglés Time Of Arrival) de la señal. Recordemos que el uso de DS-SS permite al

ISSN 1390-5384



receptor identificar las componentes de señal originadas en propagación multitrayecto, y posibilita su aprovechamiento en términos de diversidad. Esta información puede utilizarse como variable de mediación para el estudio del comportamiento de esquemas de posicionamiento basados en red, el cual ha sido objeto de interesantes investigaciones a lo largo del tiempo [6, 7].

Los resultados mostrados en este artículo complementan los presentados en [8, 9] y asumen que el proceso de estimación del primer retardo es el mejor posible. En este sentido es un modelo simplificado pues asume la presencia de un único clúster de señal originado por la propagación multitrayecto. Sin embargo esta asunción es muy razonable en entornos con línea de vista (LOS del inglés Line Of Sight), es decir que el canal de propagación es de tipo Rice. Los lectores interesados en el modelamiento estadístico de canal basado en geometría (GBSC), sus propiedades y su aplicación a comunicaciones móviles de tercera y cuarta generación pueden referirse a [10, 11, 12].

A partir de la determinación de la Cota Inferior de Crámer-Rao (CRLB de sus siglas en inglés), se estudia el impacto sobre la precisión en la estimación del TOA para el primer retardo en función de parámetros tales como: el número de estimaciones de canal disponibles, el número de sensores que constituyen el arreglo de la antena, el grado de coherencia temporal en las estimaciones de canal que se utilizan para el proceso de estimación de TOA y el período de muestreo cuando éste se realiza a una velocidad mayor que la tasa de chips del sistema.

Consideraciones del Modelo

Este trabajo está estrechamente relacionado con otro en el que se estudió el impacto de varios de estos parámetros pero bajo el supuesto de que la señal LOS se encontraba muy atenuada por lo cual el canal de propagación podía modelarse como Rayleigh [10]. En el caso actual se asume que la componente LOS está presente y por ende el canal es Rice. Sin embargo, la señal dispersa está presente y se caracteriza estocásticamente como antes. El error en la estimación del instante de llegada (TOA) se calcula utilizando la Cota Inferior de Cramer-Rao (CRB) a partir del modelo de señal que describe el escenario móvil [8, 9].

El modelo toma en cuenta las siguientes consideraciones:

1. Se asume que el canal tiene un tiempo de coherencia para las amplitudes que siguen las expresiones de Jakes usuales, sin embargo el tiempo de coherencia de retardos y ángulos de llegada es mucho mayor, siendo posible obtener muchas estimaciones de canal a objeto de mejorar la precisión de las estimaciones de TOA.
2. El ruido presente en las estimaciones de canal es blanco y gaussiano.

3. El ruido es incoherente en retardo y ángulo, lo cual corresponde a una situación en la cual el suscriptor móvil se mueve y los diferentes rayos reflejados experimentan desvanecimiento rápido incorrelado.
4. Se asumen un modelo lineal de Markov de primer orden para la variación temporal en el canal.
5. Un espectro de potencia continua se utiliza para modelar la función de densidad marginal de retardo, y se asume que esta se ajusta a una exponencial según se propone en Pedersen [14], y se la estima a una fracción del tiempo de chip. Se asume también la misma distribución angular para todos los retardos. En este sentido se asume que la señal se agrupa en un único clúster lo cual tiene bastante sentido en condiciones LOS, como es en este caso.

Modelo De Canal

La señal observada en un conjunto de K estimaciones del vector de canal sobre N_s sensores. Cada estimación del vector de canal \mathbf{z} es de longitud $N(N-1 \text{ retardos})$, y se asume que se ha conseguido de la correlación de la señal recibida con una secuencia conocida.

La señal que se recibe en el sensor j se nota por $y^{(j)}(t)$, y se conforma de la superposición de las componentes multi-trayecto y del ruido $n^j(t)$. cada componente se ve afectada por el coeficiente de apuntamiento de la antena de potencia unitaria $b_{i,j}(t)$, del factor de atenuación $\gamma_i(t)$, de la frecuencia dópler f_i sobre intervalos de extensión KTs , y del retardo de llegada τ_i , donde “i” identifica a cada componente de entre las N_{paths} que alcanzan el receptor.

$$y^{(j)}(t) = \sum_{i=1}^{N_{paths}} b_{i,j}(t) \gamma_i(t) x(t - \tau_i) e^{j2\pi f_i t} + n^{(j)}(t) \quad (1)$$

La señal transmitida $x(t)$ corresponde a la convolución de la secuencia de pseudo-ruido $p(n)$ con el pulso de conformación $g_p(t)$ como se muestra en (2), donde T es el tiempo de símbolo.

$$x(t) = \sum_n g_p(t - nT) p(n) \quad (2)$$

Un correlador estima el canal a partir de la señal recibida en el sensor j y en el instante s , con la ayuda de la secuencia de pseudo-ruido $p(n)$ de longitud N_p .

$$z_s^{(j)}(t) = \frac{1}{N_p} \sum_n y^{(j)}(t + \tau_s + nT) p^*(n) \quad (3)$$

Si se incorporan las expresiones (1) y (2) en (3), es fácil darse cuenta que el coeficiente de canal, $z_s^{(j)}(k)$, para un sensor particular j y un lag s puede modelarse en términos del coeficiente de apuntamiento de cada sensor, del factor de atenuación del multi-trayecto y su dópler, de la amplitud del pulso conformador, además de una

porción de ruido residual como se muestra en (4). De esta manera, en forma compacta el vector de canal se modela a partir de la firma espacial sobre el arreglo de sensores en la antena, \mathbf{b}_j , la potencia estimada para el trayecto recibido, P_i , su frecuencia Doppler normalizada f_i , y el vector correspondiente al pulso conformador $\mathbf{g}^{(i)}$; además de una componente de ruido $\mathbf{w}^{(j)}$, donde k_0 corresponde al instante de muestreo para el primer retardo, como se muestra en (5).

$$z_s^{(j)}(k) = \sum_{i=1}^{N_{paths}} b_{ij}(k) \gamma_i(k) e^{j2\pi f_i t} g(\tau_s - \tau_i) + w_i^{(j)}(k) \quad (4)$$

$$\mathbf{z}^{(j)}(k) = \sum_{i=k_0}^N b_j P_i e^{j2\pi f_i t} \mathbf{g}(\tau_s - \tau_i) + \mathbf{w}_i^{(j)}(k) \quad (5)$$

El vector $\mathbf{g}^{(i)}$ contiene las muestras del pulso conformador, siendo "i" la posición de su máximo, $g_p(0)$ y se muestra en (6).

$$\mathbf{g}^{(i)} = [g_p(-i+1) \dots g_p(0) \dots g_p(N-i)]^T \quad (6)$$

Tanto la porción correspondiente a la señal del vector de canal, $\mathbf{z}^{(j)}(k)$, como su correspondiente vector de ruido pueden describirse como procesos aleatorios Gaussianos caracterizados por sus correspondientes matrices de correlación. Adicionalmente, en el caso de disponer de una componente de visión directa (LOS), la media del vector de canal no será cero. Si se asume que el ruido es temporalmente incorrelado, independiente de la señal y de varianza σ_w^2 , y notando que la porción correspondiente a la componente NLOS dispersa en la sumatoria en (5) tiene media cero, y que además los mecanismos de dispersión y d\́oppler son independientes, el valor esperado del vector de canal estimado, $\boldsymbol{\mu}_z$ puede calcularse como en (7), donde P_0 es la potencia estimada de la componente LOS, y f_0 su frecuencia d\́oppler:

$$\begin{aligned} E\{\mathbf{z}^{(j)}(k)\} &= E\{b_j P_0 e^{j2\pi f_0 k} \mathbf{g}^{(k_0)}\} \\ &= P_0 E\{b_j\} E\{e^{j2\pi f_0 k}\} \mathbf{g}^{(k_0)} \end{aligned} \quad (7)$$

La expresión (5) puede describirse como en (8), donde el elemento i del vector $\mathbf{b}^{(j)}(k)$ contiene $b_{ij}(k) P_i e^{j2\pi f_i k T_s}$, y la matrix \mathbf{G} modela los retardos del pulso conformador. La longitud de estos vectores N , es el número de estimaciones en la ventana de observación.

$$\mathbf{z}^{(j)}(k) = \mathbf{G} \mathbf{b}^{(j)}(k) + \mathbf{w}^{(j)}(k) \quad (8)$$

Adicionalmente, si los vectores se arreglan linealmente como se muestra en (9), tanto las señales como el ruido pueden describirse como procesos aleatorios Gaussianos con ciertas medias y matrices de covarianza, como se muestra en (10).

$$\mathbf{w}^{(j)} = [\mathbf{w}^{(j)}(1)^T \dots \mathbf{w}^{(j)}(k)^T \dots \mathbf{w}^{(j)}(K)^T]^T \quad (9)$$

$$\mathbf{w} \sim CN(\mathbf{0}, \sigma_w^2 \mathbf{I}), \quad \mathbf{z} \sim CN(\boldsymbol{\mu}_z, \mathbf{R}_z) \quad (10)$$

En este caso el vector de estimaciones de canal toma la forma en (11) y el valor esperado del vector de canal estimado $\boldsymbol{\mu}_z$, se expresa en términos de la firma espacial de la componente LOS \mathbf{b}_ϕ , del vector d\́oppler esperado y del vector de conformación de pulsos correspondiente a la primera llegada, asociada con la componente LOS \mathbf{g}_ϕ^k , como se muestra en (12):

$$\mathbf{z}^{(j)} = (\mathbf{G} \otimes \mathbf{I}_K) \mathbf{b}^{(j)} + \mathbf{w}^{(j)} \quad (11)$$

$$\boldsymbol{\mu}_z = E\{\mathbf{b}\} \otimes E\{e^{j2\pi f_0 k}\} \otimes P_0 \mathbf{g}^{(k_0)} \quad (12)$$

Así mismo, es fácil darse cuenta que la matriz de covarianza para las estimaciones del vector de canal, \mathbf{R}_z , se corresponde con la matriz de Correlación para el caso NLOS y canal Rayleigh [8], y puede expresarse en términos de sus componentes temporal y espacial, como se muestra en (13). En esta expresión, el factor de potencia de la señal P_s , se refiere a la varianza de la potencia recibida estimada para el primer retardo de la señal temporalmente dispersa en el caso de propagación Rayleigh; la matriz de conformación de pulso $\mathbf{G}_s(\beta)$, depende del factor de roll-off β , y modela la contribución del pulso conformador, mientras que Λ_τ es una matriz diagonal que modela la dispersión temporal de la señal y su distribución de potencia exponencial. Por otro lado, la matriz de correlación temporal, $\mathbf{T}(\alpha)$, toma en consideración la variación temporal del canal asociada al efecto d\́oppler, y se asume idéntica para todos los retardos; la matriz de correlación espacial, $\mathbf{R}_\phi(bf\rho)$, contiene los coeficientes de correlación para las firmas entre sensores, y \otimes denota el producto de Kronecker.

$$\mathbf{R}_z = \mathbf{R}_\phi(\rho) \otimes \mathbf{T}(\alpha) \otimes P_s \mathbf{G}_s(\beta) \Lambda_\tau(\lambda_n) \mathbf{G}_s^H(\beta) + \sigma_w^2 \mathbf{I} \quad (13)$$

Basta recordar que la variación temporal se modela como un proceso auto-regresivo de orden 1, que la correlación temporal entre dos slots consecutivos se nota por el coeficiente α , y que la matriz de correlación espacial contiene la correlación de las firmas espaciales entre los sensores del arreglo ρ_{ij} . En efecto, la matriz de correlación espacial $\mathbf{R}_\phi(\rho)$, es Toeplitz y para su caracterización basta conocer la primera columna ρ . Estas matrices toman la forma que se muestra en (14)-(16).

$$\mathbf{R}_\phi(\rho) = \begin{bmatrix} 1 & \rho_{12} & \dots & \rho_{1N_s} \\ \rho_{12}^* & 1 & \dots & \rho_{2N_s} \\ \vdots & \vdots & \ddots & \vdots \\ \rho_{1N_s}^* & \rho_{2N_s}^* & \dots & 1 \end{bmatrix} \quad (14)$$

$$\mathbf{T}(\alpha) = \begin{bmatrix} 1 & \alpha & \dots & \alpha^{K-1} \\ \alpha & 1 & \dots & \alpha^{K-2} \\ \vdots & \vdots & \ddots & \vdots \\ \alpha^{K-1} & \alpha^{K-2} & \dots & 1 \end{bmatrix} \quad (15)$$

$$\mathbf{G}_s(\beta) = \frac{1}{\sqrt{T_c(1-\beta/4)}} [\mathbf{g}_{s1} \quad \mathbf{g}_{s2} \quad \dots \quad \mathbf{g}_{sN}] \quad (16)$$

Más detalles respecto de estas matrices pueden encontrarse en [8, 9].

Si definimos el vector de variación temporal $\alpha_t(\alpha)$ como en (17), la expresión (12) llega a ser la (18), donde $\mathbf{b}_\phi(\rho)$ corresponde precisamente al vector esperado de firmas espaciales.

$$\alpha_t(\alpha) = [1 \quad \alpha \quad \alpha^2 \quad \dots \quad \alpha^{K-1}]^T \quad (17)$$

$$\boldsymbol{\mu}_z = \mathbf{b}_\phi(\rho) \otimes \alpha_t(\alpha) \otimes P_0 \mathbf{g}^{(k_0)}(\beta) \quad (18)$$

Derivación de la Cota Inferior de Crámer-Rao para el canal Rice.

Para derivar las cotas de Crámer-Rao (CRB) para la condición LOS basta con ampliar el vector de parámetros $\boldsymbol{\psi}$, de forma de incluir la variable P_0 , tal como se muestra en (19).

$$\boldsymbol{\Psi} = [k_0, \lambda_n, \beta, P_s, \sigma_w^2, \alpha, \boldsymbol{\rho}^T, P_0]^T \quad (19)$$

En este vector de parámetros, k_0 se refiere al instante de llegada de la componente LOS normalizado para el tiempo de chip, T_c ; λ_n es el inverso de la dispersión de retardos normalizado para el intervalo de chip, y los demás parámetros ya han sido definidos antes. El parámetro de interés es precisamente k_0 .

N_c cuenta el número de coeficientes de correlación espacial y se relaciona con el número de sensores [8].

Las CRB se calculan a partir de la Matriz de Información de Fisher (FIM) a partir de la expresión (20) [8, 13]:

$$[\mathbf{F}_{\boldsymbol{\Psi}}^{LOS}] = \text{Tr} \left(\mathbf{R}_z^{-1} \frac{\partial \mathbf{R}_z}{\partial \boldsymbol{\Psi}_p} \mathbf{R}_z^{-1} \frac{\partial \mathbf{R}_z}{\partial \boldsymbol{\Psi}_q} \right) + 2\text{Re} \left(\frac{\partial \boldsymbol{\mu}_z^H}{\partial \boldsymbol{\Psi}_p} \mathbf{R}_z^{-1} \frac{\partial \boldsymbol{\mu}_z}{\partial \boldsymbol{\Psi}_q} \right) \quad (20)$$

Esta matriz fue calculada para la componente dispersa NLOS [8] a partir de las derivadas de su matriz de correlación respecto de los parámetros en el modelo, y debe actualizarse para el caso de disponer una componente LOS como se muestra en (21) y (22), donde $\mathbf{J}_{\boldsymbol{\psi}}$ se corresponde precisamente con la FIM para el caso de canal Rayleigh y el vector de parámetros algo más reducido. La matriz $\mathbf{B}_{\boldsymbol{\psi}}$ se encarga de introducir los términos faltantes, mientras que la matriz \mathbf{H}^{LOS} de ampliar la dimensión de la FIM anterior para actualizarla al caso actual.

$$\mathbf{F}_{\boldsymbol{\Psi}}^{LOS} = \mathbf{F}_{\boldsymbol{\psi}} + \mathbf{B}_{\boldsymbol{\psi}} \quad (21)$$

$$\mathbf{F}_{\boldsymbol{\psi}} = \sum_{k=1}^{N_s} \sum_{k_1=1}^K H_{k,k_1}^{LOS} \mathbf{J}_{\boldsymbol{\psi}} H_{k,k_1}^{LOS T} + C_1 \mathbf{e}_{N_p}^{(6)} \mathbf{e}_{N_p}^{(6)T} + \sum_{q_1=1}^{2N_c} \sum_{q_2=1}^{2N_c} C_2^{(q_1, q_2)} \mathbf{e}_{N_p}^{(6+q_1)} \mathbf{e}_{N_p}^{(6+q_2)T} \quad (22)$$

$$H_{k,k_1}^{LOS} = \begin{bmatrix} H_{k,k_1} \\ \mathbf{0} \end{bmatrix}_{(7+2N_c) \times 5} \quad (23)$$

Recordemos que el cálculo de las derivadas de la matriz de correlación de estimaciones del canal y su inversa se facilita de la descomposición en valores singulares de

las matrices de correlación espacial (24) y temporal (25) y que pueden calcularse como el producto de Kronecker de tres matrices conforme a la expresión (27) y a los valores mostrados en la Tabla 1 [8].

$$\mathbf{R}_\phi = \mathbf{U}_\phi \boldsymbol{\Lambda}_\phi \mathbf{U}_\phi^H$$

$$\mathbf{U}_\phi = [\mathbf{u}_\phi^{(1)}, \mathbf{u}_\phi^{(1)}, \dots, \mathbf{u}_\phi^{(N_s)}] \quad (24)$$

$$\boldsymbol{\Lambda}_\phi = \text{diag} [\lambda_\phi^{(1)}, \lambda_\phi^{(2)}, \dots, \lambda_\phi^{(N_s)}]$$

$$\mathbf{T} = \mathbf{U}_t \boldsymbol{\Lambda}_t \mathbf{U}_t^H$$

$$\mathbf{U}_t = [\mathbf{u}_t^{(1)}, \mathbf{u}_t^{(1)}, \dots, \mathbf{u}_t^{(K)}] \quad (25)$$

$$\boldsymbol{\Lambda}_t = \text{diag} [\lambda_t^{(1)}, \lambda_t^{(2)}, \dots, \lambda_t^{(K)}]$$

$$\mathbf{R}_z^{-1} = \sum_{k=1}^{N_s} \mathbf{u}_\phi^{(k)} \mathbf{u}_\phi^{(k)H} \otimes \sum_{k_1=1}^{N_s} \mathbf{u}_t^{(k_1)} \mathbf{u}_t^{(k_1)H} \otimes \left(\lambda_\phi^{(k)} \lambda_t^{(k_1)} P_s \mathbf{G}_s \boldsymbol{\Lambda}_\tau \mathbf{G}_s^H + \sigma_w^2 \mathbf{I} \right)^{-1} \quad (26)$$

$$\frac{\partial \mathbf{R}_z}{\partial \boldsymbol{\Psi}_i} = \mathbf{A}_i \otimes \mathbf{B}_i \otimes \mathbf{C}_i \quad i = p, q \quad (27)$$

i=p,q	$\boldsymbol{\Psi}_i$	\mathbf{A}_i	\mathbf{B}_i	\mathbf{C}_i
1	k_0	\mathbf{R}_ϕ	\mathbf{T}	$P_s \mathbf{G}_s \frac{\partial \boldsymbol{\Lambda}_\tau}{\partial k_0} \mathbf{G}_s^T$
2	λ_n	\mathbf{R}_ϕ	\mathbf{T}	$P_s \frac{\partial \boldsymbol{\Lambda}_\tau}{\partial \lambda_n}$
3	β	\mathbf{R}_ϕ	\mathbf{T}	$P_s \frac{\partial (\mathbf{G}_s \boldsymbol{\Lambda}_\tau \mathbf{G}_s^T)}{\partial \beta}$
4	P_s	\mathbf{R}_ϕ	\mathbf{T}	$\mathbf{G}_s \boldsymbol{\Lambda}_\tau \mathbf{G}_s^T$
5	σ_w^2	\mathbf{I}_{N_s}	\mathbf{I}_K	\mathbf{I}_K
6	α	\mathbf{R}_ϕ	$\frac{\partial \mathbf{T}}{\partial \alpha}$	$P_s \mathbf{G}_x \boldsymbol{\Lambda}_\tau \mathbf{G}_s^T$
7:6+N _c	$\rho_{i-6, Re}$	$\frac{\partial \mathbf{R}_\phi}{\partial \rho_{i-6, Re}}$	\mathbf{T}	$P_s \mathbf{G}_x \boldsymbol{\Lambda}_\tau \mathbf{G}_s^T$
7+N _c	$\rho_{i-6, Im}$	$\frac{\partial \mathbf{R}_\phi}{\partial \rho_{i-6, Im}}$	\mathbf{T}	$P_s \mathbf{G}_x \boldsymbol{\Lambda}_\tau \mathbf{G}_s^T$
:6+2N _c				

Tabla 1: Resultados de las derivadas de la Matriz de Correlación de Estimaciones de Canal \mathbf{R}_z en el caso NLOS requeridas en (26).

Las derivadas de los auto-vectores de la matriz de correlación temporal respecto al coeficiente de correlación temporal α , requeridas se calcularon numéricamente para obtener las CRB en este artículo. $\mathbf{B}_{\boldsymbol{\psi}}$ en (21) se calcula como en (28), donde los parámetros requeridos para evaluar esta matriz se muestran en las expresiones (29)-(31) y \odot denota el producto de Hadamard.

$$[\mathbf{B}_{\boldsymbol{\psi}}]_{pq} = 2\text{Re} \left\{ \sum_{k=1}^{N_s} D_{1,p,q}^{(k)} \sum_{k_1=1}^K D_{2,p,q}^{(k_1)} D_{3,p,q}^{(k,k_1)} \right\} \quad (28)$$

En particular $D_{1,p,q}$ en (29) corresponde claramente a la contribución de los diferentes sensores en el arreglo, $D_{2,p,q}$ en (30) revela la contribución de cada estimación temporal, y finalmente $D_{3,p,q}$ en (31) exhibe el impacto de la diversidad multi-trayecto y el pulso conformador sobre la FIM.

$$D_{1,p,q}^{(k)} = \mathbf{1}_{N_s}^T \left(\mathbf{u}_\phi^{(k)} \mathbf{u}_\phi^{(k)H} \odot A_p^{(1)} A_q^{(1)} \right) \mathbf{1}_{N_s} \quad (29)$$

$i=p,q$	Ψ_i	$\mathbf{A}_i^{(1)}$	$\mathbf{A}_i^{(2)}$	$\mathbf{A}_i^{(3)}$
1	k_0	$\mathbf{b}_\phi(\rho)$	$A_0 \alpha$	$\frac{\partial \mathbf{g}(k_0)}{\partial k_0}$
2	λ_n	0	0	0
3	β	$\mathbf{b}_\phi(\rho)$	$A_0 \alpha$	$\frac{\partial \mathbf{g}(k_0)}{\partial k_0}$
4	P_s	0	0	0
5	σ_w^2	0	0	0
6	α_t	$\mathbf{b}_\phi(\rho)$	$A_0 \frac{\partial \alpha}{\partial \alpha_t}$	$\mathbf{g}(k_0)$
$7:6+N_c$	$\rho_{i-6,Re}$	$\frac{\partial \mathbf{b}_\phi}{\partial \rho_{i-6,Re}}$	$A_0 \alpha$	$\mathbf{g}(k_0)$
$7+N_c:6+2N_c$	$\rho_{i-6,Im}$	$\frac{\partial \mathbf{b}_\phi}{\partial \rho_{i-6,Im}}$	$A_0 \alpha$	$\mathbf{g}(k_0)$
$7+2N_c$	A_0	$\mathbf{b}_\phi(\rho)$	α	$\mathbf{g}(k_0)$

Tabla 2: Resultados de la derivación del vector esperado de estimaciones de canal μ_z a insertarse en (29)-(31).

$$D_{2,p,q}^{(k_1)} = \mathbf{1}_K^T \left(\mathbf{u}_T^{(k_1)} \mathbf{u}_T^{(k_1)H} \odot A_p^{(2)} A_q^{(2)} \right) \mathbf{1}_K \quad (30)$$

$$D_{3,p,q}^{(k,k_1)} = A_p^{(3)} R_{k,k_1}^{-1} A_q^{(3)} \quad (31)$$

Los términos $A_p^{(i)}$ y $A_q^{(j)}$ requeridos para el cálculo de los factores anteriores se relacionan con los resultados de las derivadas parciales de μ_z en (20) y deben extraerse de la Tabla 2.

Resultados y discusión

A continuación se presentan algunos resultados de interés que relacionan el error en la determinación del retardo de la componente LOS con algunos parámetros relevantes del modelo:

Resultado 1: Comportamiento de la Cota de Error en la estimación del instante de llegada de la señal (TOA) con la Relación Señal a Ruido de la Señal Dispersa, el nivel de potencia de la componente de visión directa (LOS) y la correlación entre los vectores de canal bajo propagación Rice.

La Figura 1 muestra la cota de error en la estimación del instante de llegada para el caso de propagación Rice como una función de la relación señal a ruido de la componente dispersa para dos valores diferentes de la potencia media de la componente LOS. Para la generación de los resultados el número de estimaciones del vector de canal se ha colocado en 50, la tasa de muestreo en dos veces la tasa de chip, el factor de roll-off en 0.5 y el número de sensores en el arreglo en 2. La dispersión temporal se ha colocado en $2T_c$ y la dispersión angular en 5° . La señal llega frontalmente. La gráfica en la parte superior corresponde al caso en que la componente LOS se encuentra 3 dB por debajo de la potencia de la señal dispersa y la gráfica en la parte inferior al caso en que la componente LOS se encuentra 3dB por encima de la potencia de la señal dispersa.

La primera observación de interés es que el error de estimación se reduce para entornos correlados temporalmente cuando una componente LOS está presente. Este

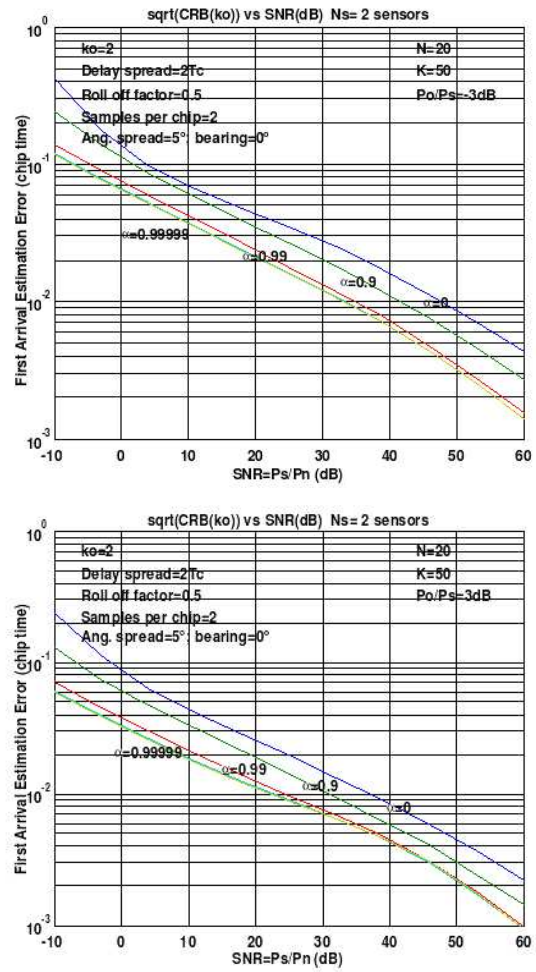


Figura 1: CRB del error en la estimación de la componente LOS en función de la relación señal a ruido de la componente dispersa y del factor de correlación temporal α .

comportamiento es precisamente el opuesto al esperado en el caso de propagación Rayleigh. En efecto, las cotas calculadas para el caso de propagación Rice son más bajas que las esperadas bajo la condición NLOS y decaen todavía más conforme la potencia de la componente LOS se incrementa. La mejoría es notoria al pasar de fuentes completamente incoherentes (ICD) hasta fuentes parcialmente coherentes (PCD) con factores de correlación menores a 0,99. Después de este valor la mejoría es despreciable. Por ejemplo observe en la Figura 1 como el error conseguido para una fuente ICD con $\text{SNR}=20\text{dB}$ para la componente dispersa y potencia de componente LOS 3dB por debajo de la componente NLOS corresponde aproximadamente a $4,5 \times 10^{-2} T_c$ y decae a $2,5 \times 10^{-2} T_c$ en el caso de una fuente PCD con $\alpha = 0,9$, y a $2,0 \times 10^{-2} T_c$ en el caso de una fuente completamente coherente (FCD) con $\alpha = 0,99999$. Si comparamos estos valores con los resultados esperados para el caso de propagación Rice en el cual tenemos una cota de error de aproximadamente $0,7 T_c$ para el caso FCD y de $0,15 T_c$ para el caso ICD, tenemos una mejoría sustancial para el caso FCD de alrededor de 35 y de algo más de 3 para el caso ICD. Si asumimos op-

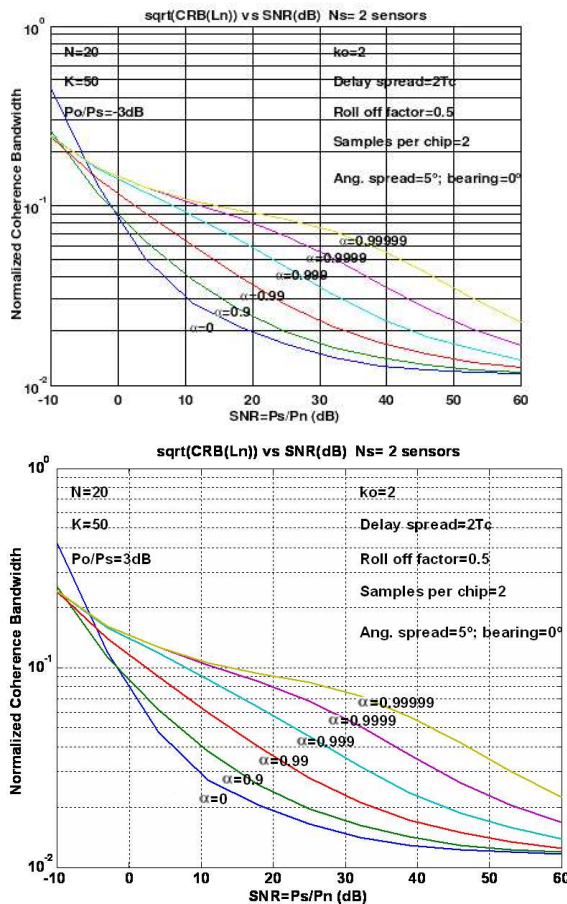


Figura 2: CRB del factor inverso normalizado de la dispersión angular λ_n en función de la relación señal a ruido de la componente dispersa (SNR) y del factor de correlación temporal, α . Número de estimaciones del vector de canal colocado en 50, tasa de muestreo igual a dos veces la tasa de chip, roll-off factor de 0,5 y dos sensores. Factor de dispersión temporal igual a $2T_c$, dispersión angular de 5° . La señal llega frontalmente hacia el arreglo. A) Superior: Potencia de la componente LOS 3dB por debajo de la Potencia de la señal dispersa. B) Inferior: Potencia de la componente LOS 3dB por encima de la señal dispersa.

timistamente una relación lineal entre la incertidumbre en la estimación de TOA y el posicionamiento del suscriptor móvil estamos hablando de alrededor de 55m en el caso FCD NLOS respecto de 1,7m en el caso FCD LOS. Cuando la potencia de la componente LOS crece en 6B respecto del valor anterior, la cota del error en la estimación del TOA reduce a la mitad para el caso FCD. Este resultado muestra la importancia que tiene el disponer de una componente LOS en la estimación de TOA y por ende en la determinación de la posición a partir de la observación de los instantes de llegada de la señal y la degradación que implica la pérdida de la LOS en entornos obstruidos y el esfuerzo que debe ponerse en la mitigación de los efectos adversos de la condición NLOS.

La segunda observación interesante es el hecho de que la incertidumbre en la estimación del error reduce sin cota conforme la SNR mejora en condiciones de LOS, lo cual significa que idealmente en este caso la incer-

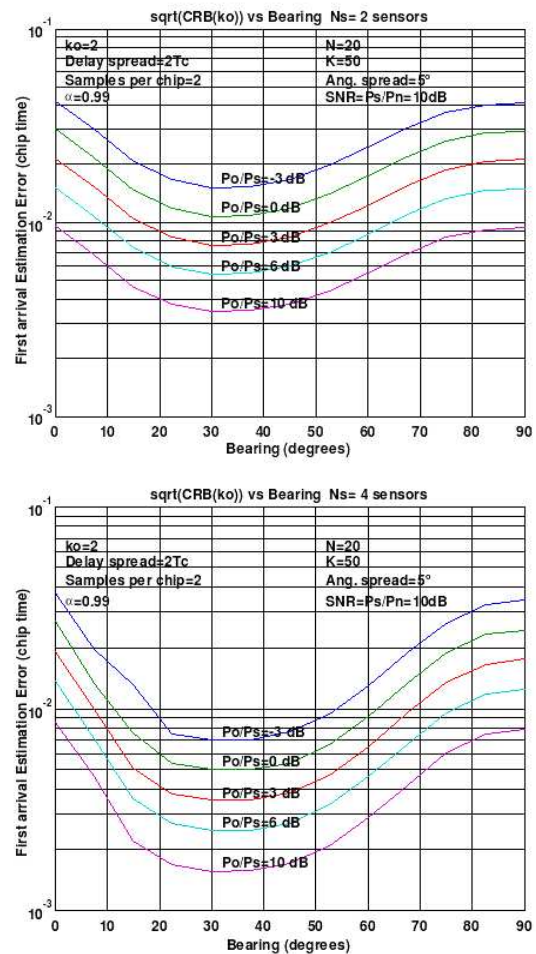


Figura 3: CRB del error en la estimación del TOA de la componente LOS en función de la dirección de llegada de la señal (DOA) y del nivel de potencia de la componente LOS. Número de estimaciones del vector de canal colocado en 50, tasa de muestreo igual a dos veces la tasa de chip y roll-off factor de 0,5. Factor de dispersión temporal igual a $2T_c$, dispersión angular de 5° y relación señal a ruido de la componente dispersa $SNR=10$ dB. Fuente altamente correlada temporalmente ($\alpha=0,99$). A) Superior: Dos sensores. B) Inferior: Cuatro sensores.

tidumbre estaría limitada únicamente por la relación SNR. Por ejemplo, cuando la $SNR=5$ dB para la componente dispersa y $\alpha = 0,99$, la cota de error pasa de $6 \times 10^{-2} T_c$ a $3 \times 10^{-2} T_c$ cuando la potencia de la componente LOS se incrementa en 6 dB. Esto significaría que se reduce la incertidumbre en el posicionamiento desde aproximadamente 5 m a aproximadamente la mitad.

Por otra parte, como se observa en la Figura 2, las cotas correspondiente al factor inverso normalizado de dispersión temporal λ_n , parecen no ser molestadas por el cambio en el nivel de la potencia de la componente LOS, y la tendencia respecto del coeficiente de correlación temporal se mantiene en forma muy aproximada a lo observado en el modelo NLOS. Por ejemplo, mire en la figura como la cota del error para una $SNR=20$ dB y una fuente PCD con $\alpha = 0,9$ y potencia de la componente LOS ± 3 dB respecto de la potencia de la señal dispersa cuando se usan dos sensores corresponde a 2.0×10^{-2} y crece

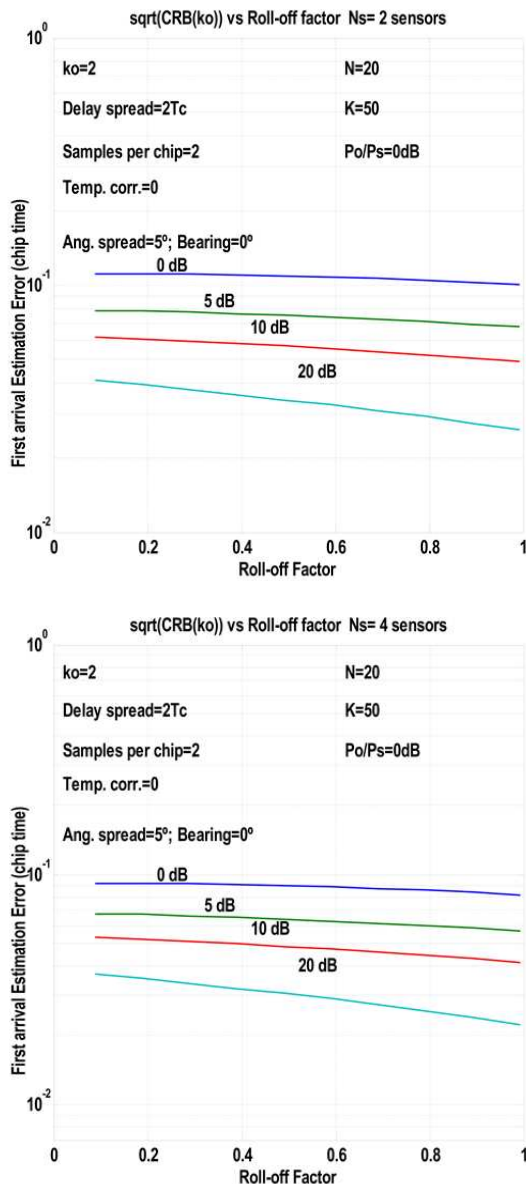


Figura 4: CRB del TOA en función del factor de roll-off y la relación señal a ruido de la componente dispersa (SNR) para el caso en que el nivel de potencia de la componente LOS es igual al nivel de potencia de la señal dispersa y una fuente ICD ($\alpha=0$). Número de estimaciones del vector de canal colocado en 50, tasa de muestreo igual a dos veces la tasa de chip, coeficiente de dispersión temporal igual a $2 T_c$, dispersión angular de 5° y señal llegando frontalmente. a) Superior: Dos sensores; b) Inferior: Cuatro sensores.

a 9.0×10^{-2} para una fuente FCD ($\alpha = 0,99999$). Estos valores son algo mayores que los esperados para el caso NLOS, pero están bien acotados cuando se incrementa la SNR. En este caso el mínimo error está acotado por 1.2×10^{-2} .

Resultado 2: Comportamiento de la Cota de Error en la estimación del instante de llegada con la dirección de llegada de la emisión, los niveles de potencia de la componente LOS, el factor de correlación temporal entre las estimaciones del vector de canal y el número de sensores.

La Figura 3 muestra el comportamiento de las cotas de error en el instante de llegada de la componente LOS en relación con la dirección media de llegada de la señal recibida para diferentes valores de la potencia de la componente LOS cuando la relación señal a ruido de la componente dispersa es igual a 10 dB. Es interesante notar que el error en la estimación del TOA alcanza un mínimo para un valor cercano a 30° , y que esta mejora es más importante para niveles mayores de la componente LOS. Por ejemplo, la cotas de error pasan de alrededor de $3.0 \times 10^{-2} T_c$ a $1.1 \times 10^{-2} T_c$ cuando la potencia de la componente LOS es igual a la potencia de la señal dispersa y la dirección de llegada cambia de 0° a 30° , mientras que el error se reduce de alrededor de $x10^{-2} T_c$ a $3.5 \times 10^{-3} T_c$ cuando la potencia de la componente LOS es 10dB mayor que la potencia de la componente dispersa, y la dirección de llegada cambia de 0° a 30° y se utilizan dos sensores. Por otro lado se observa que una mejora importante es posible cuando se utilizan cuatro sensores en lugar de cuatro especialmente para una fuente altamente correlada temporalmente ($\alpha = 0,99$). En efecto, para el caso de cuatro sensores y potencia LOS de 10dB sobre la dispersa, y DOA de 30° , la cota se reduce a aproximadamente $1.5 \times 10^{-3} T_c$, es decir aproximadamente la mitad de su análogo con dos sensores. Todos estos valores conducirán idealmente a incertidumbres en la estimación de la posición de un suscriptor móvil menores a 1 metro.

Resultado 3: Comportamiento de la Cota de Error en la estimación del instante de llegada con el factor de roll-off, la relación señal a ruido de la componente dispersa (SNR), y el número de sensores en el caso de Propagación Rice.

La Figura 4 muestra el comportamiento del error en la estimación del instante de llegada de la componente LOS como una función del factor de roll-off del pulso conformador cuando se utiliza un arreglo conformado por múltiples sensores.

La Figura 4 muestra como la cota de error en la estimación del instante de llegada de la componente LOS decrece para valores altos del factor de roll-off cuando la señal llega frontalmente al arreglo, especialmente para altos valores de la relación SNR. Por ejemplo, la cota de error reduce desde $3 \times 10^{-2} T_c$ para $\beta=0,5$ hasta alrededor de $2 \times 10^{-2} T_c$ para $\beta=1$, cuando se usan cuatro sensores y para una SNR de 20dB para la componente dispersa. Nuevamente puede observarse también que mejores resultados se obtienen cuando se utiliza un número mayor de sensores.

Conclusiones

Se ha desarrollado un análisis comparativo de los efectos sobre la incertidumbre en la estimación de la componente LOS de un sistema DS-SS para una señal afectada por propagación multitrayecto y dispersa temporalmente y espacialmente. Los resultados se han calculado asumiendo dos muestras por chip y varios factores de

roll-off. Se trata de un modelo de canal Rice que complementa la información obtenida en condición NLOS y propagación Rayleigh [8].

El modelo muestra un potencial incremento en la certidumbre en la estimación del instante de llegada de la componente LOS conforme se incrementa la relación señal a ruido de la componente LOS respecto de la componente dispersa y de la potencia de la señal respecto del ruido. Es particularmente interesante notar que la certidumbre se incrementa en este caso cuando se trata de una fuente con una alta correlación temporal, lo cual es lo opuesto a lo que acontece en el caso de propagación Rayleigh. El modelo muestra también cierta ganancia en función de la dirección de apuntamiento de la antena, posiblemente asociado al manejo de la diversidad espacial en el arreglo. Finalmente, se verifica una ligera ganancia en relación al roll-off utilizado; sin embargo su efecto es más notorio para relaciones de señal a ruido más elevadas y definitivamente no tiene un efecto deficiente en el grado de incertidumbre de la señal.

Referencias

- [1] El Natour Al Bitar H. et al. 2006. "Analysis of the GPS acquisition environments: indoors and outdoors". *Information and Communication Technologies, ICTTA*.
- [2] Chao-Min Su et al. 2010. "Sensor-Aided Personal Navigation Systems for Handheld Devices". *39th International Conference on Parallel Processing Workshops*.
- [3] Baniukevic, A. et al. 2011. "Improving Wi-Fi Based Indoor Positioning Using Bluetooth Add-Ons". *39th International Conference on Parallel Processing Workshops*.
- [4] Filonenko, V., Cullen, C., and Carswell, J. 2010. "Investigating Ultrasonic Positioning on Mobile Phones". *International Conference on Indoor Positioning and Indoor Navigation (IPIN)*.
- [5] Schelkshorn, S. and Detlefsen, J. 2008. "Position Finding based on Multiple Doppler Sensors". *Proceedings of the 5th European Radar Conference*.
- [6] Urruela, A. and Sala, J. 2006 "Average Performance Analysis of Circular and Hyperbolic Geolocation". *IEEE Transactions on Aerospace and Electronic Systems*. AES-20.
- [7] Torrieri, D. 1984 "Statistical theory of passive location systems". *IEEE Transactions on Vehicular Technology*. 55, 1, 52–66.
- [8] Játiva, R. and Vidal, J. 2009. "Estimación del Tiempo de Llegada en un Canal Rayleigh desde una perspectiva de la Cota Inferior de Cramer-Rao". *Revista AVANCES EN CIENCIAS E INGENIERÍAS*. 1, 5–10
- [9] Játiva, R. and Vidal, J. 2003. "La cota Inferior de Cramer-Rao en la Estimación del Instante de Llegada al usar Modelos de Fuente Distribuida". *Revista CIENCIA*. 6, 185–196.
- [10] Arias, M., and Mandersson, B. 2007. "Time Domain Cluster PDF and its application in Geometry Based Statistical Channel Models". *The 18th Annual IEEE International Symposium on Personal, Indoor and Mobile Radio Communications (PIMRC'07)*.
- [11] Oestges, C. et al 2005. "Impact of Fading Correlations on MIMO Communication Systems in Geometry-Based Statistical Channel Models". *IEEE Transactions on Wireless Communications*. 4, 3, 1112–1120.
- [12] Qi Yao, Yi Yuan, et al 2012. "Comparison of the Statistical Properties of the LTE-A and IMT-A Channel Models". *IEEE Wireless Communications and Networking Conference: PHY and Fundamentals*.
- [13] Raich, R., Goldberg, J. and Messer, H. 2000. "Bearing Estimation for a Distributed Source: Modeling, Inherent Accuracy Limitations and Algorithms". *IEEE Transactions on Signal Processing*. 48, 2, 429–441 .
- [14] Pedersen, K. 2000. "Antenna Arrays in Mobile Communications – Channel Modeling and Receiver Design for DS-CDMA Systems". *Tesis Doctoral de la Universidad de Aalborg*.

René Játiva, Josep Vidal, “GLRT detector for NLOS error reduction in wireless positioning systems”, IST Mobile and Wireless Telecommunications Summit, June 2002.

GLRT Detector for NLOS Error Reduction in Wireless Positioning Systems

René Játiva E., Josep Vidal

Universitat Politècnica de Catalunya, Dept. of Signal Theory & Communications
Campus Nord, Modul D5, Jordi Girona, 1-3, 08034 Barcelona, Spain
Tel: +34 93 4011066, emails: {rjativa,pepe}@gps.tsc.upc.es

ABSTRACT

The objective of this paper is to determine the potentialities of a detection scheme within the framework of subscriber location. Usually, it is the first arrival that bears the necessary information for user location. In NLOS situations, this first arrival is very much attenuated with respect to the RAKE synchronisation time instant, and it is placed well before this point. The determination of a window comprising this point is a must for a later use of a high resolution technique. Using a Generalized Likelihood Ratio Test (GLRT), an improved coarse first arriving path detector from propagation channel estimates is derived. Furthermore, an expression for false alarm probability is provided and detector performance is evaluated for different receiver configurations and signal propagation conditions.

I. INTRODUCTION

From the viewpoint of subscriber location, accurate estimates of Time of Arrival (TOA) from received signal are required, and in order to use angular information, a proper first path detection acquires special relevance. See [1], [2] for details. However, first path arrived to the receiver may not necessarily be the one bearing the highest power. In the NLOS case, for i.e. the first arrival may suffer attenuation higher than other later arrivals, receiver is usually synchronized to the highest power path and therefore will provide a wrong TOA information. For the case of Code Division Multiple Access (CDMA) Spread Spectrum Systems such as W-CDMA a pilot channel or training sequences are provided, allowing channel estimation. These estimates are used to demodulate data channels and feed RAKE receivers. However RAKE receivers rely most powerful signal arrivals. As mentioned, these do not necessarily include first arrival path, in particular for NLOS situations.

The scheme proposed in this paper consists in searching the first arriving path from a set of vector channel estimates obtained from multiple receiving antennas, and computed from correlation measurements over CPICH downlink channel (suitable for OTDOA positioning) or DPCH in uplink or downlink (for RTT measurements) [4]. For this purpose, a lag window before the first RAKE finger component is studied, and

an statistical test is performed to discriminate properly between noise and signal. See [6] for an approach similar to this contribution but based on the maximum power arrival. The finding of a first path allows the determination of a window over which high resolution techniques could be used to obtain better accuracies [] (see figure 1). It will be assumed that the receiver has previously obtained slot, frame and frequency synchronisation.

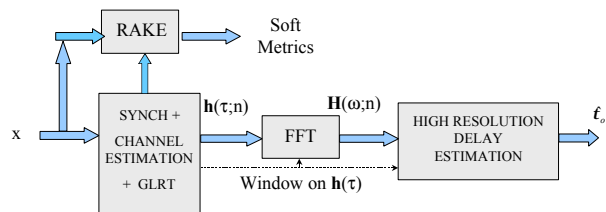


Figure 1: First arrival path detection block diagram.

II. ESTIMATED CHANNEL MODEL

With these premises, the vector of observations will be a collection of channel impulse response vectors infected with noise (when there is a signal arrival) or simply noise (when no signal is present at a certain lag).

After matched filter, the estimated channel sampled at chip rate may be modeled as:

$$\begin{aligned} \hat{\mathbf{h}}(\tau_o; t) &= \mathbf{h}(\tau_o; t) + \mathbf{n}(t) \\ \mathbf{h}(\tau_o; t) &= \alpha \exp(j\omega_d t) \mathbf{a} + \mathbf{w}(t) \end{aligned} \quad (1)$$

where the first term in the summation accounts for possible LOS component, ω_d is the Doppler frequency, \mathbf{a} is the array steering vector and the k th element is expressed as follows:

$$a_k = \exp\left[-j \frac{2pd_k}{I} \sin(\mathbf{q}_o)\right] \quad (2)$$

and \mathbf{w} models the scattered signal component. The term \mathbf{n} accounts for the estimation noise and is assumed to be a temporally stationary, complex Gaussian random process, temporally uncorrelated and independent of the channel vectors.

Stacking the vector impulse response in time for each lag τ_o :

$$\begin{aligned}
\mathbf{h}(\tau_o; n) &= \\
&= \left[\hat{\mathbf{h}}(\tau_o; nT_s)^T \quad \hat{\mathbf{h}}(\tau_o; (n-1)T_s)^T \quad \cdots \quad \hat{\mathbf{h}}(\tau_o; (n-p+1)T_s)^T \right]^T \\
\mathbf{n} &\rightarrow CN(\mathbf{0}, \sigma_n^2 \mathbf{I}) \\
\mathbf{h} &\rightarrow CN(\mathbf{0}, \mathbf{R}_n + \sigma_n^2 \mathbf{I}) \quad (3)
\end{aligned}$$

where T_s corresponds to the time interval between two consecutive estimations, (if using the CPICH in UMTS, it is the slot time) and K is the number of estimates (or a given number of slots). p is the duration in number of slots of the temporal correlation. of impulse responses.

\mathbf{R}_n is the channel vector correlation matrix from estimates, expressed in more general form by (4), and σ_n^2 is the noise variance:

$$\mathbf{R}_n = \mathbf{R}_f \otimes \mathbf{T}_k + \sigma_n^2 \mathbf{I} \quad (4)$$

\mathbf{T}_k is the temporal correlation matrix among the channels estimated in different slots, \mathbf{R}_f contains the correlation coefficients between sensors, and \otimes is the Kronecker product operator. Note that we are implicitly including the LOS component as a rank-one term in the correlation matrix.

Note that we are implicitly assuming that the TOA values have long coherence window times, much longer than the channel amplitudes coherence time.

III. GENERALIZED LIKELIHOOD RATIO TEST

With the goal of determining the first signal arrival, we compute and arrange all estimated channels within a temporal window of size KT_s , on $\mathbf{X}(\tau_o)$ matrix. The two possible conjectures are that observed data is just noise (hypothesis H_0) or that signal plus noise is present (alternative H_1). See [3]:

$$\begin{aligned}
H_0 : \mathbf{X}(\tau_o) &= \mathbf{N} \\
H_1 : \mathbf{X}(\tau_o) &= \mathbf{H}(\tau_o)
\end{aligned}$$

where \mathbf{X} , \mathbf{N} and \mathbf{H} matrices have K rows and pN_s columns, and results of rearranging data, noise and impulse response estimates vectors respectively as follows:

$$\mathbf{X}(\tau_o) = \begin{bmatrix} \mathbf{h}^T(\tau_o; n) \\ \mathbf{h}^T(\tau_o; n+p) \\ \vdots \\ \mathbf{h}^T(\tau_o; n+K-p) \end{bmatrix}$$

A Generalized Likelihood Ratio Test (GLRT) Detector decides H_1 if the likelihood ratio $L(\mathbf{X}(\tau_o))$ exceeds a threshold γ . It maximizes detection probability for a given false alarm probability, and may be expressed as shown in (5):

$$L(\mathbf{X}(\tau_o)) = \frac{pdf(\mathbf{X}(\tau_o) / \hat{\mathbf{R}}_n; H_1)}{pdf(\mathbf{X}(\tau_o) / \hat{\sigma}_n^2; H_0)} > \gamma \quad (5)$$

This test is performed by first estimating ML signal parameters, as if signal were present, and then comparing likelihood of H_1 with the true parameters replaced for their estimates to that of H_0 .

If temporal correlation between consecutive estimates is different to zero and below to one, we are treating the most general case of a Partially Coherent Distributed (PCD) source, and above expression leads to (6):

$$L(\mathbf{X}) = \frac{1}{\hat{\mathbf{S}}_n} tr(\mathbf{X}(\tau_o)^H \mathbf{X}(\tau_o)) - \log[\det(\mathbf{X}(\tau_o)^H \mathbf{X}(\tau_o))] > \mathbf{g}' \quad (6)$$

Note that $\mathbf{X}(\tau_o)^H \mathbf{X}(\tau_o) / N$ is an estimation of the vector channel correlation matrix and, combined with the trace operator, becomes an incoherent accumulation. This test has to be applied over different τ_o values within a certain window so as to assess a coarse instant of the first arrival. In the sequel the term τ_o will be removed from the equations.

IV. FALSE ALARM PROBABILITY

When the noise level is available (as it is usually the case at the receiver), and it is used for noise variance (σ_n^2) estimation, Constant False Alarm Rate (CFAR) detectors may be built [5]. Operating with expression (6) in the null hypothesis, it may be shown that false alarm probability P_{fa} is described approximately by:

$$P_{fa} = \mathbf{Q}_{\chi^2_{2pN_s}} \left\{ \frac{2}{N-1} \left[\gamma' + pN_s \left\{ \log(N\sigma_n^2) - 1 \right\} \right] \right\} \quad (7)$$

where $\mathbf{Q}_c(\cdot)$ defines the right tail cumulative function for a chi squared distributed variable with $2pN_s$ degrees of freedom, when K channel vectors and N_s sensors are used, and provided that the number of secondary data is high enough. The proof is omitted due to lack of space but may be provided under request. Expression (7) is of utmost importance since it allows the definition of a threshold in equation (6) for the verification of the hypothesis.

On the other hand, the probability of detection is given by:

$$P_D = \sum_{n=0}^{pN_s-1} C_n \exp\left(-\frac{\mathbf{g}' - pN_s + pN_s \log(N) + G}{\mathbf{b}_n}\right) \quad (8)$$

where,

$$C_n = \prod_{i=0; i \neq n}^{N-1} \frac{1}{1 - \mathbf{b}_i / \mathbf{b}_n}$$

$$G = \sum_{i=0}^{pN_s-1} \log(\mathbf{I}_i)$$

$$\mathbf{b}_n = N \mathbf{I}_n / \mathbf{S}_n^2 - 1$$

$$\mathbf{I}_n = \mathbf{I}_{f_i} \mathbf{I}_{t_j} \quad \forall i = 1 : N_s; j = 1 : p$$

with λ_ϕ and λ_τ being the eigenvalues of \mathbf{R}_f and \mathbf{T}_k respectively. When an adequate probability of false alarm has been defined by selecting a threshold from (7), probability of detection will be given by channel characteristics. Note that P_D in (8) is a function of SNR, K , N_s , and temporal and spatial correlation.

V. EVALUATING FIRST ARRIVAL DETECTABILITY

In order to evaluate the performance of this detector, the first arrived path is supposed to be confined within a temporal window of length L samples before the first significant path available at RAKE receiver. Sampling is supposed to be at chip time. A first arrival component is generated and placed randomly within this window.

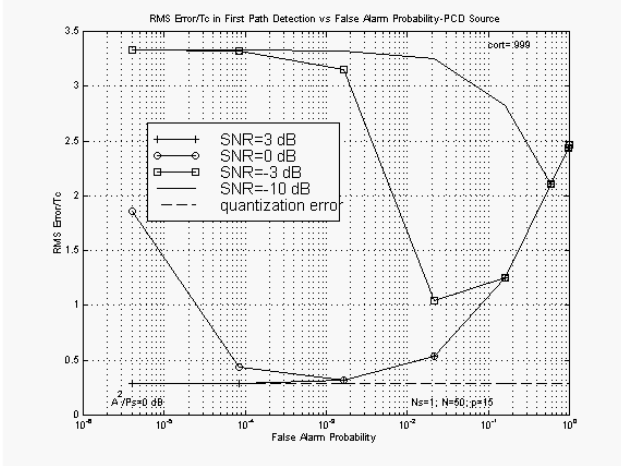


Figure 2: First arrival RMS detection error as a function of P_{fa} and for different SNR. One sensor, and a high temporal correlation.

Path searching process defined by (6) is repeated along the window until alternative H_1 is verified. If a new path is not detected, finger path is chosen as the earliest. L has been set to $5T_c$ for figures shown in this paper. Under the defined channel setup, mean square error is related to false alarm and detection probabilities through equation (9); where $p(n/m)$ corresponds to the probability of detecting an arrival at lag n when arrival is located at lag m , and e_q is an error term included due to the temporal quantization of the delay axis, as 1 sample per chip:

$$E\{e^2\} = \frac{1}{L} \sum_{m=1}^L \sum_{n=1}^L p(n/m) \cdot (m-n)^2 + (1-P_{fa})^{L-1} (1-P_D) \sum_{n=1}^L n^2 + E\{e_q^2\} \quad (9)$$

$$p(n/m) = \begin{cases} P_{fa} (1-P_{fa})^{n-1} & n < m \\ P_D (1-P_{fa})^{n-1} & n = m \\ P_{fa} (1-P_{fa})^{n-2} (1-P_D) & n > m \end{cases}$$

$$p(n/m) = p(\mathbf{t}_o = nT_c / \mathbf{t}_o = mT_c + e_q)$$

$$e_q \in [-1/2T_c, 1/2T_c]$$

\mathbf{R}_f has been built using the distributed source model proposed in [7], and for Monte Carlo Simulations 10^5 realization were used to evaluate Detection Probability and 10^6 to evaluate false alarm. For a highly correlated spatial distribution (as it would be the case in the

uplink), the case of correlated sensors an angular spread of 5 degrees and a mean direction of arrival of zero degrees is supposed. Temporal correlation of the scattering was simulated using a first order AR process. Correlation factors of 0.1 and 0.999 are used, accounting for moving and static terminals respectively. Direct path arrives from broadside and sensors are linearly and uniformly spaced. Doppler frequency for direct path corresponds to a mobile speed of 50 km/h, $N=100$ and $p=15$ for figures 2-3 and 7.

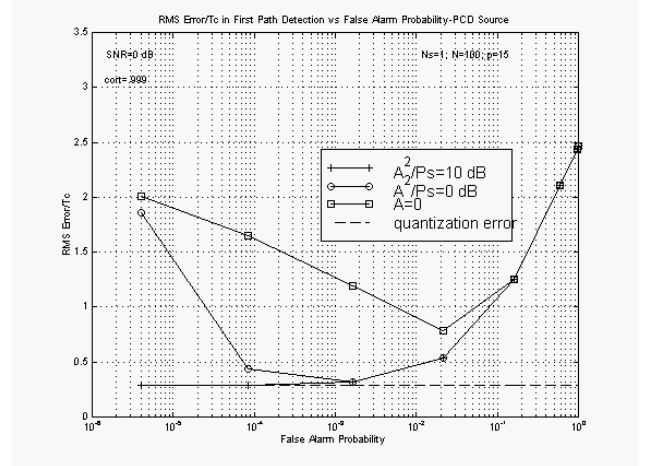


Figure 3: First arrival RMS detection error as a function of P_{fa} and for different powers of the direct path. One sensor, and high temporal correlation.

Figure 2 shows the RMS error in determination of the first arrival for different values of the false alarm probability. Even with just one sensor and a poor SNR of 0 dB (after correlation by the pilot sequence) for the first arrival a good accuracy is achieved when a false alarm around 10^{-3} is chosen. At higher values of SNR the error is not very sensitive to the value of the threshold. Figure 3 shows how detection improves in a highly correlated scenario when a direct path is present, compared to raw scattering.

Figure 6 shows that temporal uncorrelation of the scattering term is a beneficial factor in all cases.

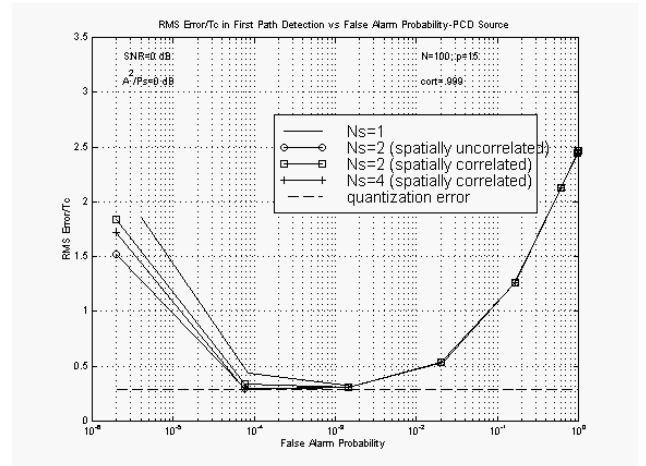


Figure 4: First arrival RMS detection error as a function of P_{fa} and the number of sensors, for spatially correlated and uncorrelated sources.

Increasing the number of sensors or the data record length leads in some cases to important detection gains as it can be seen in figures 4-5, and weaker signals may be detected.

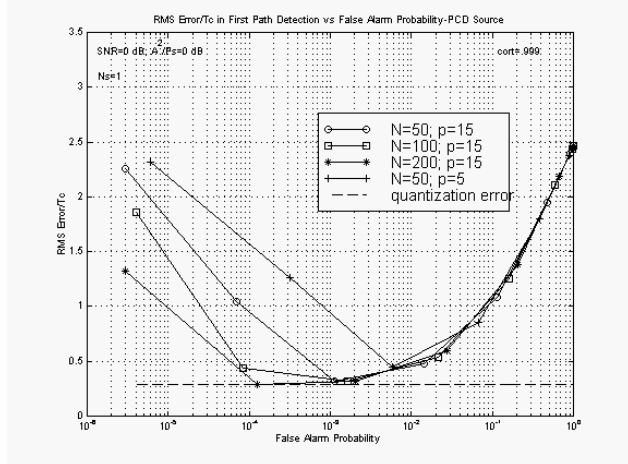


Figure 5: First arrival RMS detection error as a function of P_{fa} and data record length. Different values of the assumed duration of the temporal correlation are used.

VI. SUMMARY AND CONCLUSIONS

A method for improving subscriber location accuracy has been described. A CFAR detector for PCD sources has been derived in (6), and some results have been shown for different environments and detector configurations. It has been shown that given a low SNR and a false alarm probability, by enhancing data records or increasing the number of sensors, better results are observed for temporally uncorrelated sources and uncorrelated sensors.

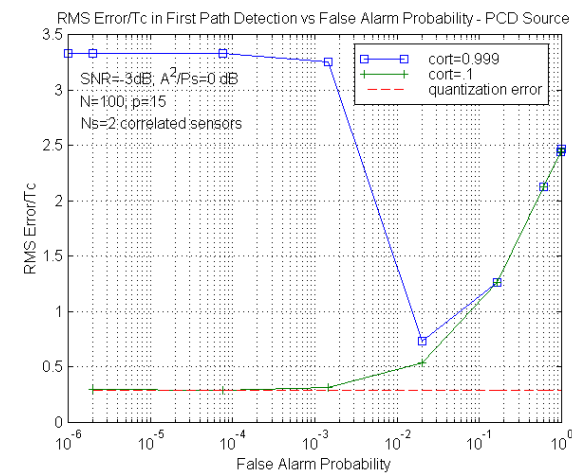


Figure 6: First arrival RMS detection error as a function of P_{FA} and for different temporal correlation values.

VII. ACKNOWLEDGEMENTS

This work has been carried out in the framework of the EC-funded project SATURN (www.ist-saturn.org) and supported by Spanish Government Grants: TIC99-0849,

TIC2000-1025, FIT-070000-2000-649, Generalitat of Catalunya grant CIRIT 2000SGR 00083 and FUNDACYT- BIDE 874/OC-EC.

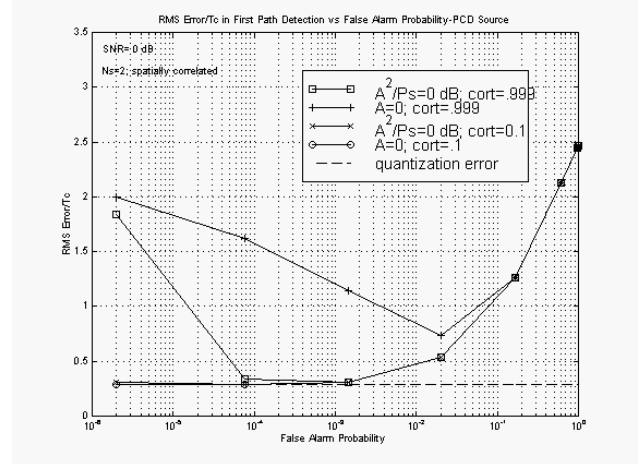


Figure 7: First arrival RMS detection error as a function of P_{FA} and for different temporal correlation values and direct path powers.

REFERENCES

- [1] Josep Vidal, René Játiva and Marga Cabrera, "Positioning Limits for UMTS Mobiles in Delay and Angular Dispersive Channels", International Symposium on Location Based Services for Cellular Users, February 2001.
- [2] René Játiva E, Josep Vidal, and Marga Cabrera, "Cramer Rao Bounds in Time of Arrival Estimation for a Distributed Source", IST Mobile Communication Summit, September 2001.
- [3] Steven M. Kay, "Fundamentals of Statistical Signal Processing - Detection Theory", Prentice-Hall, 1998.
- [4] Yi-Pin Eric Wang, and Tony Ottosson, "Cell Search in W-CDMA", IEEE Journal on Selected Areas in Communications, vol. 18, no 8, August 2000.
- [5] Ernesto Conte, Antonio De Maio, and Giuseppe Ricci, "GLRT-Based Adaptive Algorithms for Range-Spread Targets", IEEE Transactions on Signal Processing, Vol. 49, No. 7, July 2001.
- [6] Sven Fischer, Hans Grubeck, et al, "Time of Arrival Estimation of Narrowband TDMA Signals for Mobile Positioning", PIMRC'98, Sept. 1998, pp. 451-465.
- [7] Raviv Raich, Jason Goldberg, and Hagit Messer, "Bearing Estimation for a Distributed Source: Modeling, Inherent Accuracy Limitations and Algorithms", IEEE Transactions on Signal Processing, Vol. 48, No. 2, February 2000.
- [8] A. Zoch, G. Fettweis, "Cell Search Performance Analysis for W-CDMA", IEEE International Conference on Communications, vol. 2, 2002.
- [9] J. Winter, C. Wengerter, "High Resolution Estimation of the Time of Arrival for GSM Location", VTC2000-Spring Tokyo. 2000, Volume: 2, 2000.

René Játiva, Josep Vidal, “First Arrival Detection for Positioning in Mobile Channels”, IEEE International Symposium on Personal, Indoor and Mobile Radio Communications, PIMRC 2002, Vol. 4, pp. 1540-1544, September 2002. DOI: 10.1109/PIMRC.2002.1045437.

FIRST ARRIVAL DETECTION FOR POSITIONING IN MOBILE CHANNELS

René Játiva E., Josep Vidal

Dept. of Signal Theory and Communications, Universitat Politècnica de Catalunya (UPC)
 rjativa@gps.tsc.upc.es, pepe@gps.tsc.upc.es

Abstract. - The objective of this paper is to determine the potentialities of an optimal detection scheme within the framework of subscriber location.

The use of a Generalized Likelihood Ratio Test (GLRT) for detecting the first arriving path from the estimated channel observations in a multipath environment in severe NLOS conditions is described, and a high-resolution estimation algorithm for the time of arrival (TOA) is presented. Finally, the scheme performance is evaluated for different configurations.

Keywords. - GLRT Detector, TOA Estimation, NLOS error reduction in positioning systems.

I. INTRODUCTION

From the viewpoint of subscriber location, accurate estimates of Time of Arrival (TOA) from received signal are required, and proper first path detection acquires special relevance. See [1], [2] for details. However, first path arrived to the receiver may not necessarily be the one bearing the highest power.

Particularly, in the NLOS case, first arrival may suffer attenuation higher than other later arrivals and due of receiver is usually synchronized to the highest power path; it will provide a wrong TOA information.

For the case of Code Division Multiple Access (CDMA) Spread Spectrum Systems such as IS-95, and WCDMA a pilot channel is provided, allowing channel estimation. These estimates are used to demodulate data channels and are used for RAKE receivers. However these receivers are based on the capture of the received signal power and thresholds used for path detection are set high enough to match the most powerful ones. As mentioned, unfortunately these do not necessarily include first arrival path in NLOS situations.

The scheme proposed in this paper consists in searching the first arriving path from the channel vector estimates. It could well be the case of WCDMA after target cell search [4], and channel estimates provided from Common Pilot Channel (CPICH) in the uplink or Dedicated Physical Channel (DPICH) in the downlink. For this purpose, a lag window before the first RAKE finger component is studied, and a test is performed to discriminate properly between noise and signal (Figure 1).

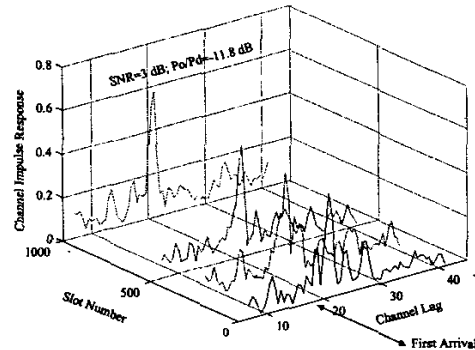


Figure 1. Channel Impulse Response evolution for a mobile unit speed of 75 km/h. First arrival is 12 dB below the dispersed power and SNR=3 dB. This path is usually discarded at these poor conditions.

II. ESTIMATED CHANNEL MODEL

After matched filter, the estimated channel may be modeled as in (1):

$$\hat{\mathbf{h}}(\tau_o, t) = \mathbf{b}(\tau_o, t) + \mathbf{w}(\tau_o, t) \quad (1)$$

where the first term in the summation accounts for possible LOS component, and

$$\mathbf{w}(\tau_o, t) = \mathbf{w}_s(\tau_o, t) + \mathbf{n}(\tau_o, t) \quad (2)$$

Noise \mathbf{n} is assumed to be a temporally stationary, complex Gaussian random process, and temporally uncorrelated and independent of the channel vectors. Stacking the vector impulse response in time for each lag τ_o :

$$\mathbf{h} = \mathbf{h}(\tau_o) = \begin{bmatrix} \hat{\mathbf{h}}(\tau_o; 0)^T & \hat{\mathbf{h}}(\tau_o; T_s)^T & \dots & \hat{\mathbf{h}}(\tau_o; (K-1)T_s)^T \end{bmatrix}^T$$

$$\mathbf{n} \rightarrow CN(\mathbf{0}, \sigma_n^2 \mathbf{I})$$

$$\mathbf{h} \rightarrow CN(\mathbf{0}, \mathbf{R}_h)$$

where T_s corresponds to the time interval between two consecutive estimations, and K is the number of estimates.

\mathbf{R}_h is the channel vector correlation matrix from estimates, expressed in more general form by (4), and σ_n^2 is the noise variance:

$$\mathbf{R}_h = \mathbf{R}_\phi \otimes \mathbf{T}_k + \sigma_n^2 \mathbf{I} \quad (3)$$

\mathbf{T}_k and \mathbf{R}_ϕ correspond to the temporal and spatial correlation matrices respectively, and \otimes is the Kronecker product operator.

Note that we are implicitly including the LOS component as a rank-one term in the correlation matrix.

III. HYPOTHESIS TESTING AND GLRT DETECTOR

Since we are looking for a very attenuated arrival, we compute all estimated channels within a temporal window of size KT_s , and arrange them on $\mathbf{X}(\tau_0)$ matrix. We pretend to discriminate between the two possible conjectures: observed data corresponds to noise (hypothesis H_0) or signal plus noise is present (alternative H_1). See [3],[4]:

$$H_0 : \mathbf{X}(\tau_0) = \mathbf{N}$$

$$H_1 : \mathbf{X}(\tau_0) = \mathbf{H}(\tau_0)$$

where \mathbf{X} , \mathbf{N} and \mathbf{H} matrices have N rows and pN_s columns, and results of rearranging data, noise and impulse response estimates vectors respectively as follows:

$$\mathbf{X} = \begin{bmatrix} \mathbf{x}^T(n) & \mathbf{x}^T(n-1) & \cdots & \mathbf{x}^T(n-p+1) \\ \mathbf{x}^T(n+p) & \mathbf{x}^T(n+p-1) & \cdots & \mathbf{x}^T(n+1) \\ \vdots & \vdots & \ddots & \vdots \\ \mathbf{x}^T(n+K-p) & \mathbf{x}^T(n+K-p-1) & \cdots & \mathbf{x}^T(n+K-2p+1) \end{bmatrix}$$

A Generalized Likelihood Ratio Test (GLRT) is performed by first estimating ML signal parameters, as if signal were present, and then comparing likelihood of H_1 with the true parameters replaced for their estimates to that of H_0 .

A GLRT Detector decides H_1 if the likelihood ratio $L(\mathbf{X})$ exceeds a threshold γ , as follows:

$$L(\mathbf{X}) = \frac{\text{pdf}(\mathbf{X} / \hat{\mathbf{R}}_h; H_1)}{\text{pdf}(\mathbf{X} / \hat{\sigma}_n^2; H_0)} > \gamma \quad (4)$$

It may be shown that the above likelihood ratio may be expressed as in (5) for our model.

$$L(\mathbf{X}) = \frac{1}{\hat{\sigma}_n} \text{tr}(\mathbf{X}^H \mathbf{X}) - \log[\det(\mathbf{X}^H \mathbf{X})] \quad (5)$$

Note that $\mathbf{X}(\tau_0)^H \mathbf{X}(\tau_0) / N$ is an estimation of the channel vector correlation matrix, when alternative H_1 is true. This test has to be applied over all τ_0 within a certain window so as to assess the instant of the first arrival.

Noise variance may be estimated from secondary data, when it is available (as for instance, channel estimates in lags where no signal is present), and GLRT detector such as in (5) may be developed. See for i.e. [4] and [5]. For this detector, false alarm probability P_{fa} is described approximately by:

$$P_{fa} = \mathbf{Q} \left\{ \frac{2}{\chi_{2pN_s}^2} \left[\gamma + pN_s \left\{ \log(N\sigma_n^2) - 1 \right\} \right] \right\} \quad (6)$$

where $\mathbf{Q}_x(\cdot)$ defines the right tail cumulative function for a chi squared distributed variable with $2pN_s$ degrees of freedom, when $K (=pN)$ channel vectors and N_s sensors are used, and provided that the number of secondary data is high enough.

When an adequate probability of false alarm has been defined by selecting a threshold from (6), probability of detection will be given by channel characteristics. Note that P_D will be a function of SNR, K , N_s , and temporal and spatial correlation.

It is interesting to note that false alarm probability corresponds to a scaled chi-squared distribution and that nonlinear transformation introduced by log function in (5) is partially corrected by the displacement in (6).

IV. HIGH RESOLUTION DELAY ESTIMATION

Once a possible window on the lags has been found, a high-resolution delay estimator is required in order to reject the negative effects from the closest paths.

Channel impulse response estimates in (1) for all the lags within the window may be rewrite as in (7), where n corresponds to the temporal evolution, and τ_i and a_i are delays and their time-varying amplitudes for a single sensor respectively.

$$\hat{h}(\tau; n) = \sum_{i=1}^{N_{paths}} a_i(n) g(\tau - \tau_i) + v(\tau; n) \quad (7)$$

The noise perturbing the estimated channel $w(\tau; t)$ is assumed temporally uncorrelated in n , and correlated in lag (τ) domain due to the matched filter performed at the receiver.

A more convenient representation of (7) is obtained after computing the DFT:

$$\hat{h}(w; n) = \sum_{i=1}^{N_{paths}} a_i(n) g(w) \exp(jw\tau_i) + v(w; n) \quad (8)$$

Stacking the samples of the transformed domain in a single vector \mathbf{h}_w for each considered slot n , and defining the diagonal matrix \mathbf{G} as that containing the frequency response of the shaping filter (8) becomes (9), where N_{lags} corresponds to the number of points used for the DFT calculation.

$$\mathbf{h}_w(n) = \sum_{i=1}^{N_{paths}} a_i(n) \mathbf{G} \mathbf{e}_{\tau_i} + v(n) = a_i(n) \mathbf{G} \mathbf{e}_{\tau_i} + \tilde{v}(n) \quad (9)$$

$$\mathbf{e}_{\tau_i} = \left[\exp(jw_1\tau_i) \exp(jw_2\tau_i) \cdots \exp(jw_{N_{lags}}\tau_i) \right]^T$$

$$w_k = \frac{2\pi(k-1)}{N_{lags}}; \quad k = [1 \ 2 \ \cdots \ N_{lags}]$$

Note that above expression distinguishes between a single path of interest and a noise term accounting for the channel estimation noise plus the non-considered paths.

From (9) and (10), it is easy to see that a matched decorrelating filter \mathbf{w} is adequate to properly separate the different paths of the desired signals.

$$\mathbf{z}(n) = \mathbf{w}^H \mathbf{h}_w(n) = a_j(n) \mathbf{w}^H \mathbf{G} \mathbf{e}_\tau + \mathbf{w}^H \tilde{\mathbf{v}}(n) \quad (10)$$

The filter should satisfy $\mathbf{w}^H \mathbf{G} \mathbf{e}_\tau = 1$ and must reduce the noise term, maximizing the SNR defined by (11):

$$SNR = \frac{E \left\{ |a_j(n)|^2 \right\}}{\mathbf{w}^H E \left\{ \tilde{\mathbf{v}}(n) \tilde{\mathbf{v}}(n)^H \right\} \mathbf{w}} \quad (11)$$

The solution of this maximization problem with restrictions leads to the minimum variance (MV) filter and the spectral representation of delays, as it is shown in (12):

$$\mathbf{w}(\tau) = \frac{\mathbf{R}_{h_w}^{-1} \mathbf{G} \mathbf{e}_\tau}{\mathbf{e}_\tau^H \mathbf{G}^H \mathbf{R}_{h_w}^{-1} \mathbf{G} \mathbf{e}_\tau} \quad P(\tau) = \frac{1}{\mathbf{e}_\tau^H \mathbf{G}^H \mathbf{R}_{h_w}^{-1} \mathbf{G} \mathbf{e}_\tau} \quad (12)$$

An alternative solution to this problem that achieves better resolution properties [6], is the called Normalized Minimum Variance (NMV) approach from (13):

$$S(\tau) = \frac{\mathbf{e}_\tau^H \mathbf{G}^H \mathbf{R}_{h_w}^{-1} \mathbf{G} \mathbf{e}_\tau}{\mathbf{e}_\tau^H \mathbf{G}^H \mathbf{R}_{h_w}^{-1} \mathbf{G} \mathbf{G}^H \mathbf{R}_{h_w}^{-1} \mathbf{G} \mathbf{e}_\tau} \quad (13)$$

For simulations in this paper, solutions provided for (13) are very accurate, as it can be seen in figures 2 and 3.

A one-dimensional grid search must be done to determine the first arrival, without any prior knowledge of the powers of the different arrivals. This implies a comparison of the maxima of the peaks of functions $P(\tau)$ or $S(\tau)$ to a threshold level which should be related to the representation of the floor noise in the spectra. This value can be computed approximately provided that knowledge of the base band noise power is known, a value usually known at the receiver. This includes not only the interference and thermal noise level, but also the power of the propagation channel taps not being considered in the RAKE receiver. We will neglect this difference in the sequel.

It may be shown that approximately the mean values taken by the MV and NMV estimates when just noise is present are:

$$P(\tau) = \frac{\sigma_v^2}{\mathbf{e}_\tau^H \mathbf{e}_\tau} \quad S(\tau) = \sigma_v^2 \quad (14)$$

And that their distribution corresponds to a scaled chi-squared, so a threshold γ can be chosen for a certain probability of false alarm which is given by the expression:

$$P_{fa} = Q_{\chi^2_{2N_{slots}}} \left\{ \frac{2N_{slots} \gamma}{\sigma_v^2} \right\} \quad (15)$$

where $Q_{\chi^2}(\cdot)$ defines the right tail cumulative function for a chi-squared distributed variable with $2N_{slots}$ degrees of freedom, and when secondary data record used for the determination of σ_v^2 is large enough.

The potentialities of the MV/NMV solution are shown in the following experiment. A scenario is built in which the positions of the arrivals are [0 0.5 0.8 1 1.5] symbols and the relative powers [-15 0 0 0 0] dB. A SNR of 18 dB is assumed. A mobile speed of 30 Km/h is taken. Figure 2

shows the cumulative function of the error in estimating the first arrival, by using the MV and NMV solutions. The higher resolution of the NMV solution with respect to MV yields a much better results both in bias and variance. The additional cost of NMV is insignificant compared to MV.

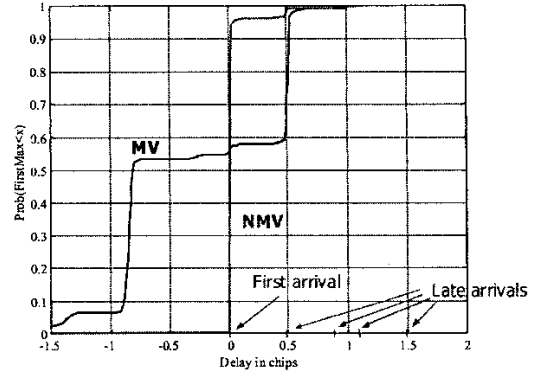


Figure 2: Cumulative function of the estimation error for the first arrival using the MV and NMV solutions. Mobile speed of 30 Km/h, 2 samples per symbol, and a single sensor has been used to record channel estimates.

Figure 3 shows the behavior of high-resolution estimation algorithm for realistic signal conditions when just one sensor is used. Channel estimates were generating using the model provided by [8] for a mobile unit speed of 75 km/h. SNR is just of 3 dB, and the first arrival path to the dispersed power ratio is around -12 dB. Threshold was set to 0.54, and noise variance (σ_v^2) for this realization was of 0.48. There are various paths closed to the first arrival, and some paths disappear along the acquisition time of 1000 slots. The dashed line represents the true first arrival.

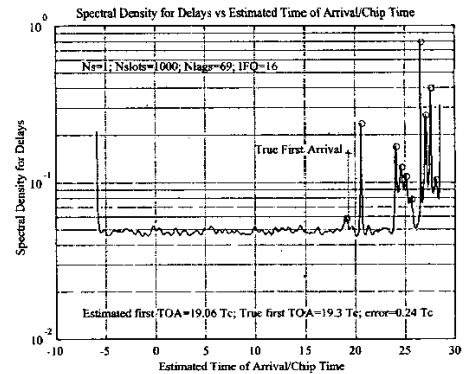


Figure 3: Spectral Density for Delays as a function of Estimated Time of Arrivals in a NLOS condition. 1000 slots, N_lags=69, and an interpolation frequency of 16.

First arrival has been detected and accurately estimated, and a timing error of $0.24T_c$ was registered.

V. EVALUATING FIRST ARRIVED PATH DETECTABILITY

In order to evaluate the performance of our detection scheme, the first arrived path is supposed to be confined within a temporal window of length L samples before the first path available at RAKE receiver. Sampling is supposed to be at chip time and LOS path is placed randomly within this window.

Path searching process defined by (5) is repeated along the window until alternative H_1 is verified. If a new path is not detected, finger path is chosen as the earliest. L has been set to $5T_c$ for figures 4-8. Mean square error is related to false alarm and detection probabilities by (14); where $p(n/m)$ corresponds to the probability of detecting an arrival at lag n when arrival is located at lag m , and ϵ_q is an error term included due to the temporal quantization of the delay axis, as 1 sample per chip. For uniform quantization, as it is the case, its power is $1/12$.

R_ϕ has been computed using the distributed source model proposed in [6], and for Monte Carlo Simulations 10^5 realization were used to evaluate Detection Probability and 10^6 to evaluate false alarm. Scattering was simulated using a first order AR process, and temporal correlation factors of 0.1 and 0.999.

$$E\{\epsilon^2\} = \frac{1}{L} \sum_{m=1}^L \sum_{n=1}^L p(n/m) \cdot (m-n)^2 + (1-P_{fa})^{L-1} (1-P_D) \sum_{n=1}^L n^2 + E\{\epsilon_q^2\} \quad (14)$$

$$p(n/m) = \begin{cases} P_{fa} (1-P_{fa})^{n-1} & n < m \\ P_D (1-P_{fa})^{n-1} & n = m \\ P_{fa} (1-P_{fa})^{n-2} (1-P_D) & n > m \end{cases}$$

$$p(n/m) = p(\hat{\tau}_o = nT_c / \tau_o = mT_c + \epsilon_q)$$

$$\epsilon_q \in [-1/2T_c, 1/2T_c]$$

For the case of correlated sensors an angular spread of 5 degrees and a mean direction of arrival of zero was supposed to compute. Direct path arrives from broadside and sensors are linearly and uniformly spaced. Doppler frequency for direct path corresponds to a mobile speed of 50 km/h, $N=100$ and $p=15$ for figures 5-6 and 8.

Figure 4 shows that even with just one sensor and a poor SNR of 0 dB a good accuracy is achieved when a false alarm around 10^{-3} is chosen.

Note that due to the fact that error characteristics exhibit a minimum, some prior signal knowledge is worth to select threshold. In practice, however, there is little chance that

this knowledge is available and, once the threshold is set, paths arriving with lower SNR will not be detected.

Figure 5 shows how detection improves when scattering is highly correlated and a direct path is present compared to just scattering, while Figure 8 shows that important gain is achieved for temporally uncorrelated signal, even for very poor SNR conditions (-3 dB).

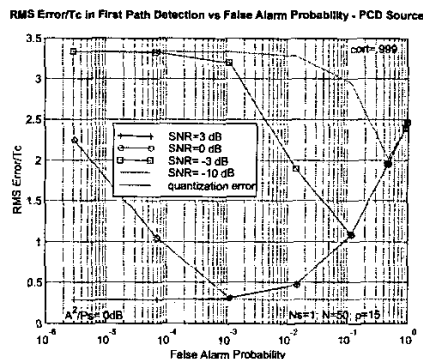


Figure 4: First Arrived Path Detection Error as a function of False Alarm Probability and SNR. One sensor, and a highly PCD Source.

Increasing the number of sensors or the data record length leads in some cases to important detection gains as it can be seen in figures 6-7, and weaker signals may be detected.

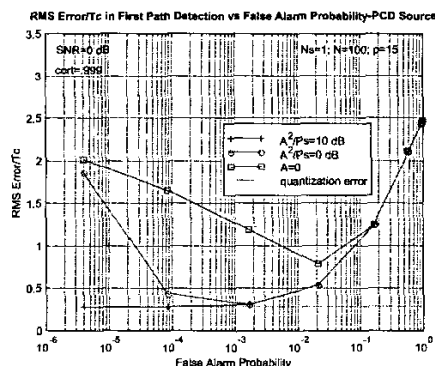


Figure 5: First Arrived Path Detection error as a function of False Alarm Probability and the Direct Path Power. One sensor and a highly PCD Source.

VI. SUMMARY AND CONCLUSIONS

Within the framework of subscriber location, NLOS condition is critical and a method for improving accuracy has been described. A GLRT detector for PCD sources has been derived in (5), a MV/NMV high-resolution estimation scheme has been explained, and some results have been

shown for different environments, detector configurations and realistic critical conditions.

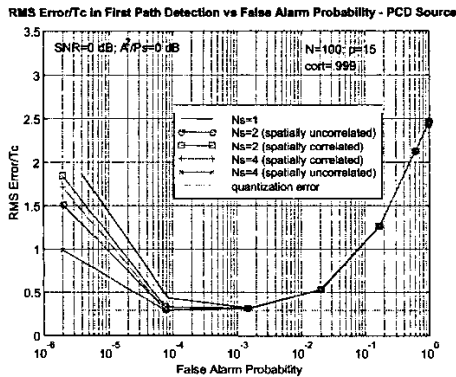


Figure 6: First Arrived Path Detection error as a function of False Alarm Probability and the Number of Sensors. PCD Source.

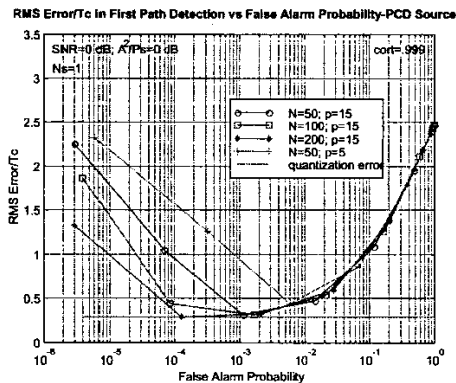


Figure 7: First Arrived Path Detection Error as a function of False Alarm Probability and Data Record Length. PCD Source and different Configurations.

It has been shown that detector is very sensitive to signal power and data record length, and the best results are observed for temporally uncorrelated sources and uncorrelated sensors. Adding more sensors benefits detection problem, especially for temporally uncorrelated signal.

VII. ACKNOWLEDGEMENTS

This work has been carried out in the framework of the EC-funded project SATURN and supported by Spanish Government Grants: TIC99-0849, TIC2000-1025, FIT-070000-2000-649, Generalitat of Catalunya grant CIRIT 2000SGR 00083 and FUNDACYT- BIDE 874/OC-EC.

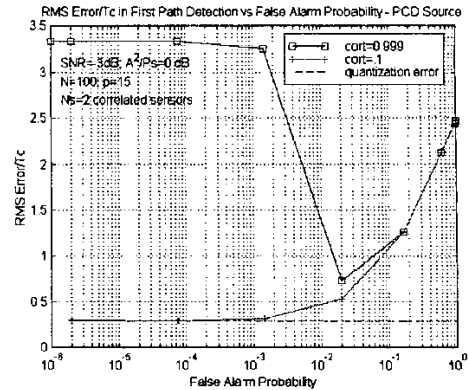


Figure 8: First Arrived Path Detection Error as a function of False Alarm Probability, temporal correlation and Direct Path Power. PCD Source.

VIII. REFERENCES

- [1] Josep Vidal, René Játiva and Marga Cabrera, "Positioning Limits for UMTS Mobiles in Delay and Angular Dispersive Channels", International Symposium on Location Based Services for Cellular Users, February 2001.
- [2] René Játiva E, Josep Vidal, and Marga Cabrera, "Cramer Rao Bounds in Time of Arrival Estimation for a Distributed Source", IST Mobile Communication Summit 2001 – Location Technologies and Services, September 2001.
- [3] Steven M. Kay, "Fundamentals of Statistical Signal Processing - Detection Theory", Prentice-Hall, 1998.
- [4] Louis L. Scharf, "Statistical Signal Processing. Detection, Estimation, and Time Series Analysis", Addison-Wesley Publishing Company, Inc, 1991.
- [5] Ernesto Conte, Antonio De Maio, and Giuseppe Ricci, "GLRT-Based Adaptive Algorithms for Range-Spread Targets", IEEE Transactions on Signal Processing, Vol. 49, No. 7, July 2001.
- [6] Raviv Raich, Jason Goldberg, and Hagit Messer, "Bearing Estimation for a Distributed Source: Modeling, Inherent Accuracy Limitations and Algorithms", IEEE Transactions on Signal Processing, Vol. 48, No. 2, February 2000.
- [7] M. A. Lagunas, A. Gasull, "An Improved Maximum Likelihood Method for Power Spectral Density Estimation", IEEE Transactions on Acoustics, Speech and Signal Processing, vol. 32, pp. 170-172, February 1984.
- [8] Margarita Cabrera, Josep Vidal and Olga Muñoz, "Time Evolutionary Wideband Propagation Channel Model for user positioning in UMTS", IST Mobile Communications Summit 2001, September 2001.

Josep Vidal, René Játiva, “First Arriving Path Detection for Subscriber Location in Mobile Communication Systems”, IEEE International Conference on Acoustics, and Statistical Signal Processing, Vol. 3, pp. III-2733 – III-2736, May 2002. DOI: 10.1109/ICASSP.2002.5745213.

FIRST ARRIVING PATH DETECTION FOR SUBSCRIBER LOCATION IN MOBILE COMMUNICATION SYSTEMS

Josep Vidal, René Játiva E.

Dept. of Signal Theory and Communications
Universitat Politècnica de Catalunya (UPC)

pepe@gps.tsc.upc.es

rjativa@gps.tsc.upc.es

ABSTRACT

The objective of this paper is to determine the potentialities of an optimal detection scheme within the framework of mobile location. A method for detecting the first arriving path from a multipath environment as a mean of enhancing subscriber location is described. A binary hypothesis test is performed, some expressions for Constant False Alarm Rate (CFAR) detectors are derived and their performances are evaluated for different configurations. The use of Generalized Likelihood Ratio Test (GLRT) is also commented and some preliminary results are shown.

1. INTRODUCTION

With the purpose of computing subscriber location, accurate estimates of Time of Arrival (TOA) from received signal is required. Furthermore Line of Sight (LOS) signal is associated to the first path arrived to the receiver, and in order to take advantage of angular information it is important to properly detect this path. Interested reader is referred to [1], and [2].

Code Division Multiple Access (CDMA) Spread Spectrum Systems such as IS-95, and WCDMA provide a pilot channel or training sequences to perform channel estimation. These estimates are used to demodulate data channels and feed RAKE receivers. However RAKE receivers rely on Power control and thresholds used for paths' detection are set high enough to match the most powerful ones. Unfortunately these do not necessarily include LOS path.

Scheme proposed in this paper consists on searching the LOS or at least the first path arrived from the channel vector estimates. For this purpose, a temporal window before the first RAKE component is studied, and a test is performed to discriminate properly between noise and signal.

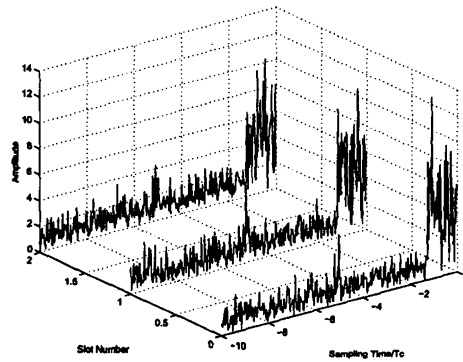


Figure 1: Observed Signal along the searching window over different slots

With this premise, our data vector will be a collection of channel impulse response vectors infected with noise or simply noise.

In Figure 1 for i.e., earlier path used for RAKE is placed at instant $\tau=T_c$, and first arrived path to be detected is the attenuated signal located at $\tau=-5T_c$.

2. ESTIMATED CHANNEL MODEL

After matched filter, the estimated channel may be modeled as in (1):

$$\hat{h}(\tau_o; t) = \alpha \exp(jw_d t) \mathbf{a} + \mathbf{w}(t) \quad (1)$$

where the first term accounts for possible LOS signal amplitude, w_d is the Doppler frequency, \mathbf{a} is the array steering vector in (2), and \mathbf{w} models scattered power and estimation noise, as shown in (3)

$$\mathbf{a}_k = \exp\left[-j \frac{2\pi d_k}{\lambda} \sin(\theta_o)\right] \quad (2)$$

$$\mathbf{w}(t) = \mathbf{w}_s(t) + \mathbf{n}(t) \quad (3)$$

Noise \mathbf{n} is assumed to be a temporally stationary, complex Gaussian random process, and temporally uncorrelated and independent of the channel vectors. Hence:

$$\begin{aligned} \mathbf{h} &= \mathbf{h}(\tau_o) = [\hat{\mathbf{h}}(\tau_o; 0) \hat{\mathbf{h}}(\tau_o; T_s) \dots \hat{\mathbf{h}}(\tau_o; KT_s)] \\ \mathbf{n} &\rightarrow CN(0, \sigma_n^2 \mathbf{I}) \\ \mathbf{h} &\rightarrow CN(0, \mathbf{R}_h) \end{aligned} \quad (4)$$

\mathbf{h} contains temporal evolution of estimates taken at the same relative instant within the searching window, T_s corresponds to the time interval between two consecutive estimations, and K is the number of estimates.

\mathbf{R}_h is the channel vector correlation matrix from estimates, expressed in more general form by (4), and σ_n^2 is the noise variance.

$$\mathbf{R}_h = \mathbf{R}_\phi \otimes \mathbf{T}_k + \sigma_n^2 \mathbf{I} \quad (4)$$

\mathbf{T}_k is the temporal correlation matrix among different slots, \mathbf{R}_ϕ contains the correlation coefficients between sensors, and \otimes is the Kronecker product operator.

3. COMPOSITE HYPOTHESIS TESTING

Since we do not know when signal is arriving, we observe and collect data over \mathbf{x} vector. The two possible conjectures are that observed data is just noise (hypothesis H_0) or that signal plus noise is present (alternative H_1). See [3], [4]:

$$\begin{aligned} H_0 : \mathbf{x}[n] &= \mathbf{n}[n] & n = 0, 1, \dots, K-1 \\ H_1 : \mathbf{x}[n] &= \mathbf{h}[n] & n = 0, 1, \dots, K-1 \end{aligned}$$

Neyman Pearson (NP) Detector decides H_1 if the likelihood ratio $L(\mathbf{x})$ exceeds a threshold γ . It may be expressed as shown in (5).

$$L(\mathbf{x}) = \frac{pdf(\mathbf{x}; H_1)}{pdf(\mathbf{x}; H_0)} > \gamma \quad (5)$$

If temporal correlation between consecutive estimates is different to zero and below to one, we are treating the most general case of a Partially Coherent Distributed (PCD) source, and above expression leads to (6):

$$L(\mathbf{x}) = \mathbf{x}^H (\mathbf{T}_k \otimes \mathbf{R}_\phi) (\mathbf{T}_k \otimes \mathbf{R}_\phi + \sigma_w^2 \mathbf{I})^{-1} \mathbf{x} > \gamma' \quad (6)$$

Note that when \mathbf{T}_k and \mathbf{R}_ϕ are eigen-decomposed, metric in (6) transforms in (7):

$$L(\mathbf{y}) = \sum_{i=1}^N \sum_{j=1}^K \frac{\lambda_{\phi_i} \lambda_{\tau_j}}{\lambda_{\phi_i} \lambda_{\tau_j} + \sigma_w^2} |y_{i,j}|^2 \quad (7)$$

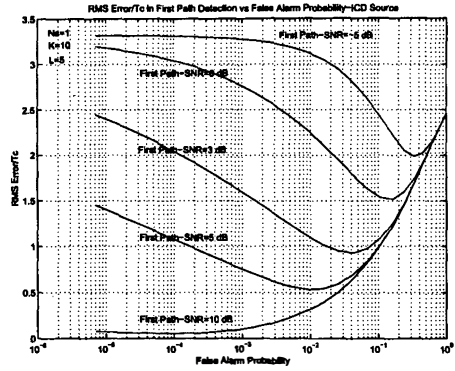


Figure 2: First Arrived Path Detection Error as a function of False Alarm Probability and Path SNR. One sensor and an ICD Source.

$$y_{i,j} = (\mathbf{v}_j^H \otimes \mathbf{u}_i^H) \tilde{\mathbf{x}}$$

$$\tilde{\mathbf{x}} = [\mathbf{x}[0]^H \mathbf{x}[1]^H \dots \mathbf{x}[K-1]^H]^H$$

$$\mathbf{T}_k = \mathbf{V} \Lambda_\tau \mathbf{V}^H; \quad \mathbf{V}^H \mathbf{V} = \mathbf{I}$$

$$\mathbf{R}_\phi = \mathbf{U} \Lambda_\phi \mathbf{U}^H; \quad \mathbf{U}^H \mathbf{U} = \mathbf{I}$$

where \mathbf{V} , \mathbf{U} and Λ_τ , Λ_ϕ collects respectively the eigenvectors and eigen-values of temporal and spatial correlation matrices, and N corresponds to the number of sensors. Note that matrices in (7) are supposed to be known, and therefore an upper bound for the behavior of the scheme may be found.

4. FALSE ALARM AND DETECTION PROBABILITIES

When secondary data is available, such as estimates at instants where no signal is present, and it is used for noise variance (σ_n^2) estimation, Constant False Alarm Rate (CFAR) Detectors may be built. See for i.e. [4] and [5]. Furthermore, it may be shown that false alarm probability P_{fa} is described by (8) and probability of detection P_D by (9):

$$P_{fa} = Q_{\chi^2_{2KN}}(4\gamma / \sigma_n^2) \quad (8)$$

where $Q_\chi(\cdot)$ defines the right tail cumulative function for a chi squared distributed variable with $2KN$ freedom grades, when K channel vectors and N sensors are used.

$$P_D = \sum_{n=0}^{KN-1} \left(\prod_{i=0; i \neq n}^{KN-1} \frac{1}{1 - \lambda_i / \lambda_n} \right) \exp(-\gamma / \lambda_n) \quad (9)$$

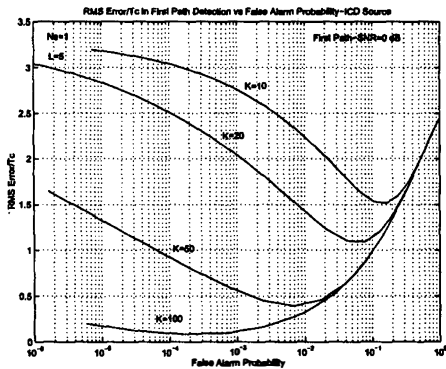


Figure 3: First Arrived Path Detection error as a function of False Alarm Probability and the number of data realizations K. One sensor and an ICD Source.

and,

$$\lambda_n = \lambda_{\phi_i} \lambda_{\tau_j} \quad \forall i=1:N; j=1:K$$

with λ_{ϕ} and λ_{τ} being the eigen-values of R_{ϕ} and T_k respectively, as in (7).

When an adequate probability of false alarm has been defined by selecting a threshold from (8), probability of false alarm will be given by channel characteristics. Note that P_D in (9) is a function of SNR, K, N, and temporal and spatial correlation.

Some refinements for choosing the samples used for detection are possible. See for i.e. [6].

5. GENERALIZED LIKELIHOOD RATIO TEST

This test is performed by firstly estimating signal parameters, as if signal were present, and then comparing likelihood of H_1 with the true parameters replaced for their estimates to that of H_0 .

When GRLT is applied, expressions in (5) changes to (10):

$$L(\mathbf{x}) = \frac{pdf(\mathbf{x} / \hat{\mathbf{T}}_k, \hat{\mathbf{R}}_{\phi}, \hat{\sigma}_x^2; H_1)}{pdf(\mathbf{x} / \hat{\sigma}_n^2; H_0)} > \gamma \quad (10)$$

Expression in (7) holds, but eigen-vectors and eigen-values of correlation matrix are replaced by of their estimates.

A MLE for R and T_k are provided by [7] for a more restrictive model, and some other estimators are proposed in [8].

Probabilities of detection and false alarm will adjust better to expressions in (8) and (9) when good estimates from involved parameters are made.

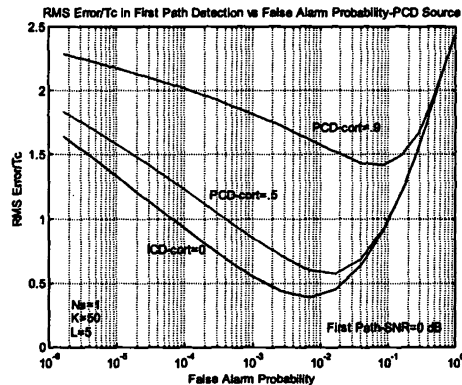


Figure 4: First Arrived Path Detection error as a function of False Alarm Probability and Temporal Correlation. One sensor and a PCD Source.

6. EVALUATING LOS PATH DETECTABILITY

In order to evaluate signal detectability, first arrived path is supposed to be confined within a temporal window of length L samples before the first path available at RAKE receiver. Sampling is supposed to be realized at the chip time and there is no a preferred placement for this path. Path searching process defined by (7) is repeated along the window until alternative H_1 is verified. If a new path is not detected, finger path is chosen as the earliest. L has been set to $5T_c$ for figures shown in this paper. R_{ϕ} has been computed using the distributed source model proposed in [7], and some work research is being made to include the LOS as it was defined in (1). A Laplacian kernel instead of a Gaussian has been used. See [8].

Figures 2 to 6 show the behavior of CFAR Detectors for different channel and signal characteristics. Figure 2 shows as error reduces when SNR increases and false alarm probability is kept constant. It also may be seen that minimum error depends on configuration (SNR, K, N, and temporal and spatial correlation) and requires of a good balance between probability of false alarm and probability of detection. Note for i.e. that with $K=10$ and $SNR=0$ dB, a minimum error of around $1.5 T_c$ may be achieved, and it reduces below $0.5 T_c$ when SNR is above 5 dB. Figure 3 compares detector behavior when LOS path power is low but larger data records are available. We note again that much better results are possible. Observe that minimum is again lower than $.5 T_c$ when K is increased above 50. Figure 4 shows how detection degrades when temporal correlation between channel vector estimates increases. Fortunately, larger data records are available in these cases and some compensation is possible.

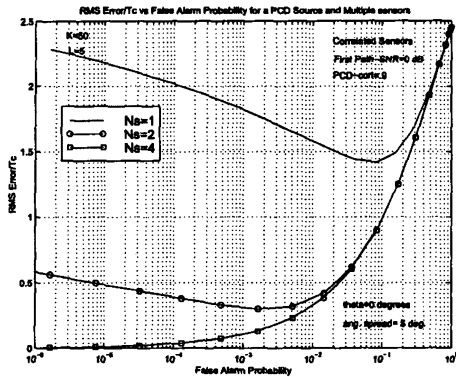


Figure 5: First Arrived Path Detection Error as a function of False Alarm Probability and Number of sensors. PCD Source and Correlated Sensors (ang. Spread=5 degrees).

Figures 5 and 6 show how improvements are made when more sensors are used, specially when channel vectors are temporally correlated, however the final result is better for the ICD Source case.

7. SUMMARY AND CONCLUSIONS

A method for improving accuracy in subscriber location for DS-CDMA communication systems has been described. A CFAR detector for PCD sources has been derived in (7), and some preliminary results have been shown for different environments and detector configurations.

In particular it has been shown that given a low SNR and a false alarm probability, a better performance is always achieved for higher SNR's, larger data records or increasing the number of sensors. Better results are expected for Incoherent Distributed (ICD) sources and uncorrelated sensors.

8. ACKNOWLEDGEMENTS

This work has been carried out in the framework of the EC-funded project SATURN and supported by Spanish Government Grants: TIC98-0412, TIC98-0703, TIC99-0849, TIC2000-1025, FIT-070000-2000-649, Generalitat of Catalunya grant CIRIT 2000SGR 00083, and BIDE 874/OC-EC.

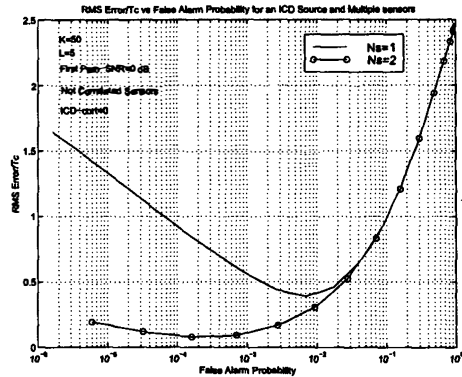


Figure 6: First Arrived Path Detection Error as a function of False Alarm Probability and various uncorrelated sensors. ICD Source.

9. REFERENCES

- [1] Josep Vidal, René Játiva and Marga Cabrera, "Positioning Limits for UMTS Mobiles in Delay and Angular Dispersive Channels", International Symposium on Location Based Services for Cellular Users (LOCCELLUS 2001), February 2001.
- [2] René Játiva E, Josep Vidal, and Marga Cabrera, "Cramer Rao Bounds in Time of Arrival Estimation for a Distributed Source", Submitted to IST Mobile Communication Summit 2001 - Location Technologies and Services, September 2001.
- [3] Steven M. Kay, "Fundamentals of Statistical Signal Processing - Detection Theory", New Jersey: Prentice-Hall, 1998.
- [4] Louis L. Scharf, "Statistical Signal Processing. Detection, Estimation, and Time Series Analysis", Addison-Wesley Publishing Company, Inc, 1991.
- [5] Ernesto Conte, Antonio De Maio, and Giuseppe Ricci, "GLRT-Based Adaptive Algorithms for Range-Spread Targets", IEEE Transactions on Signal Processing, Vol. 49, No. 7, July 2001.
- [6] Sven Fischer, Hans Grubeck, Ari Kangas, Havish Koorapaty, Erik Larsson, Patrik Lundqvist, "Time of Arrival Estimation of Narrowband TDMA Signals for Mobile Positioning", PIMRC 1998.
- [7] Raviv Raich, Jason Goldberg, and Hagit Messer, "Bearing Estimation for a Distributed Source: Modeling, Inherent Accuracy Limitations and Algorithms", IEEE Transactions on Signal Processing, Vol. 48, No. 2, February 2000.
- [8] Olivier Besson, and Petre Stoica, "Decoupled Estimation of DOA and Angular Spread for a Spatially Distributed Source", IEEE Transactions on Signal Processing, Vol. 48, No.7, July 2000.
- [9] K.I. Pedersen, P.E. Mogensen, B.H. Fleury, "Spatial Channel Characteristics in Outdoor Environments and their Impact on BS Antenna System Performance", IEEE Proceedings on Vehicular Technology Conference (VTC'98), Ottawa, Canada, May 1998.

René Játiva, Josep. Vidal, “Coarse First Arriving Path Detection for Subscriber Location in Mobile Communication Systems”, XI European Signal Processing Conference (EUSIPCO 2002), September 2002.

Coarse First Arriving Path Detection for Subscriber Location in Mobile Communication Systems

René Játiva E., Josep Vidal

Universitat Politècnica de Catalunya, Dept. of Signal Theory & Communications
Campus Nord, Modul D5, Jordi Girona, 1-3, 08034 Barcelona, Spain
Tel: +34 93 4011066, emails: {rjativa,pepe}@gps.tsc.upc.es

ABSTRACT

The objective of this paper is to determine the potentialities of a detection scheme within the framework of subscriber location. Usually, it is the first arrival that bears the necessary information for user location. In NLOS situations, this first arrival is very much attenuated with respect to the RAKE synchronisation time instant, and it is placed well before this point. The determination of a window comprising this point is a must for a later use of a high resolution technique. Using a Generalized Likelihood Ratio Test (GLRT), an improved coarse first arriving path detector from propagation channel estimates is derived. Furthermore, an expression for false alarm probability is provided and detector performance is evaluated for different receiver configurations and signal propagation conditions.

I. INTRODUCTION

From the viewpoint of subscriber location, accurate estimates of Time of Arrival (TOA) from received signal are required, and in order to use angular information, a proper first path detection acquires special relevance. See [1], [2] for details. However, first path arrived to the receiver may not necessarily be the one bearing the highest power. In the NLOS case, for i.e. the first arrival may suffer attenuation higher than other later arrivals, receiver is usually synchronized to the highest power path and therefore will provide a wrong TOA information. For the case of Code Division Multiple Access (CDMA) Spread Spectrum Systems such as W-CDMA a pilot channel or training sequences are provided, allowing channel estimation. These estimates are used to demodulate data channels and feed RAKE receivers. However RAKE receivers rely most powerful signal arrivals. As mentioned, these do not necessarily include first arrival path, in particular for NLOS situations.

The scheme proposed in this paper consists in searching the first arriving path from a set of vector channel estimates obtained from multiple receiving antennas, and computed from correlation measurements over CPICH downlink channel (suitable for OTDOA positioning) or DPCH in uplink or downlink (for RTT measurements) [4]. For this purpose, a lag window before the first RAKE finger component is studied, and

an statistical test is performed to discriminate properly between noise and signal. See [6] for an approach similar to this contribution but based on the maximum power arrival. The finding of a first path allows the determination of a window over which high resolution techniques could be used to obtain better accuracies [] (see figure 1). It will be assumed that the receiver has previously obtained slot, frame and frequency synchronisation.

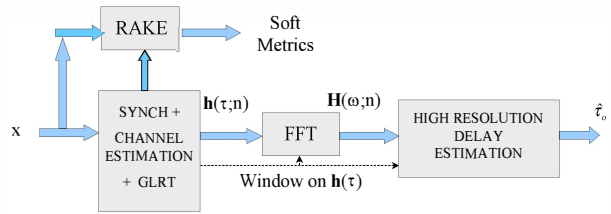


Figure 1: First arrival path detection block diagram.

II. ESTIMATED CHANNEL MODEL

With these premises, the vector of observations will be a collection of channel impulse response vectors infected with noise (when there is a signal arrival) or simply noise (when no signal is present at a certain lag).

After matched filter, the estimated channel sampled at chip rate may be modeled as:

$$\hat{\mathbf{h}}(\tau_o; t) = \mathbf{h}(\tau_o; t) + \mathbf{n}(t) \quad (1)$$

$$\mathbf{h}(\tau_o; t) = \alpha \exp(j\omega_d t) \mathbf{a} + \mathbf{w}(t)$$

where the first term in the summation accounts for possible LOS component, ω_d is the Doppler frequency, \mathbf{a} is the array steering vector and the k th element is expressed as follows:

$$a_k = \exp\left[-j \frac{2\pi d_k}{\lambda} \sin(\theta_o)\right] \quad (2)$$

and \mathbf{w} models the scattered signal component. The term \mathbf{n} accounts for the estimation noise and is assumed to be a temporally stationary, complex Gaussian random process, temporally uncorrelated and independent of the channel vectors.

Stacking the vector impulse response in time for each lag τ_o :

$$\begin{aligned}
\mathbf{h}(\tau_o; n) &= \\
&= \left[\hat{\mathbf{h}}(\tau_o; nT_s)^T \quad \hat{\mathbf{h}}(\tau_o; (n-1)T_s)^T \quad \cdots \quad \hat{\mathbf{h}}(\tau_o; (n-p+1)T_s)^T \right]^T \\
\mathbf{n} &\rightarrow CN(\mathbf{0}, \sigma_n^2 \mathbf{I}) \\
\mathbf{h} &\rightarrow CN(\mathbf{0}, \mathbf{R}_n + \sigma_n^2 \mathbf{I}) \quad (3)
\end{aligned}$$

where T_s corresponds to the time interval between two consecutive estimations, (if using the CPICH in UMTS, it is the slot time) and K is the number of estimates (or a given number of slots). p is the duration in number of slots of the temporal correlation. of impulse responses.

\mathbf{R}_n is the channel vector correlation matrix from estimates, expressed in more general form by (4), and σ_n^2 is the noise variance:

$$\mathbf{R}_n = \mathbf{R}_\phi \otimes \mathbf{T}_k + \sigma_n^2 \mathbf{I} \quad (4)$$

\mathbf{T}_k is the temporal correlation matrix among the channels estimated in different slots, \mathbf{R}_ϕ contains the correlation coefficients between sensors, and \otimes is the Kronecker product operator. Note that we are implicitly including the LOS component as a rank-one term in the correlation matrix.

Note that we are implicitly assuming that the TOA values have long coherence window times, much longer than the channel amplitudes coherence time.

III. GENERALIZED LIKELIHOOD RATIO TEST

With the goal of determining the first signal arrival, we compute and arrange all estimated channels within a temporal window of size KT_s , on $\mathbf{X}(\tau_o)$ matrix. The two possible conjectures are that observed data is just noise (hypothesis H_o) or that signal plus noise is present (alternative H_1). See [3]:

$$\begin{aligned}
H_o : \mathbf{X}(\tau_o) &= \mathbf{N} \\
H_1 : \mathbf{X}(\tau_o) &= \mathbf{H}(\tau_o)
\end{aligned}$$

where \mathbf{X} , \mathbf{N} and \mathbf{H} matrices have K rows and pN_s columns, and results of rearranging data, noise and impulse response estimates vectors respectively as follows:

$$\mathbf{X}(\tau_o) = \begin{bmatrix} \mathbf{h}^T(\tau_o; n) \\ \mathbf{h}^T(\tau_o; n+p) \\ \vdots \\ \mathbf{h}^T(\tau_o; n+K-p) \end{bmatrix}$$

A Generalized Likelihood Ratio Test (GLRT) Detector decides H_1 if the likelihood ratio $L(\mathbf{X}(\tau_o))$ exceeds a threshold γ . It maximizes detection probability for a given false alarm probability, and may be expressed as shown in (5):

$$L(\mathbf{X}(\tau_o)) = \frac{pdf(\mathbf{X}(\tau_o) / \hat{\mathbf{R}}_n; H_1)}{pdf(\mathbf{X}(\tau_o) / \hat{\sigma}_n^2; H_o)} > \gamma \quad (5)$$

This test is performed by first estimating ML signal parameters, as if signal were present, and then comparing likelihood of H_1 with the true parameters replaced for their estimates to that of H_o .

If temporal correlation between consecutive estimates is different to zero and below to one, we are treating the most general case of a Partially Coherent Distributed (PCD) source, and above expression leads to (6):

$$L(\mathbf{X}) = \frac{1}{\hat{\sigma}_n^2} tr(\mathbf{X}(\tau_o)^H \mathbf{X}(\tau_o)) - \log[\det(\mathbf{X}(\tau_o)^H \mathbf{X}(\tau_o))] > \gamma' \quad (6)$$

Note that $\mathbf{X}(\tau_o)^H \mathbf{X}(\tau_o) / N$ is an estimation of the vector channel correlation matrix and, combined with the trace operator, becomes an incoherent accumulation. This test has to be applied over different τ_o values within a certain window so as to assess a coarse instant of the first arrival. In the sequel the term τ_o will be removed from the equations.

IV. FALSE ALARM PROBABILITY

When the noise level is available (as it is usually the case at the receiver), and it is used for noise variance (σ_n^2) estimation, Constant False Alarm Rate (CFAR) detectors may be built [5]. Operating with expression (6) in the null hypothesis, it may be shown that false alarm probability P_{fa} is described approximately by:

$$P_{fa} = \mathbf{Q}_{\chi_{2pN_s}^2} \left\{ \frac{2}{N-1} \left[\gamma' + pN_s \left\{ \log(N\sigma_n^2) - 1 \right\} \right] \right\} \quad (7)$$

where $\mathbf{Q}_\chi(\cdot)$ defines the right tail cumulative function for a chi squared distributed variable with $2pN_s$ degrees of freedom, when K channel vectors and N_s sensors are used, and provided that the number of secondary data is high enough. The proof is omitted due to lack of space but may be provided under request. Expression (7) is of utmost importance since it allows the definition of a threshold in equation (6) for the verification of the hypothesis.

On the other hand, the probability of detection is given by:

$$P_D = \sum_{n=0}^{pN_s-1} C_n \exp\left(-\frac{\gamma' - pN_s + pN_s \log(N) + G}{\beta_n}\right) \quad (8)$$

where,

$$C_n = \prod_{i=0; i \neq n}^{N-1} \frac{1}{1 - \beta_i / \beta_n}$$

$$G = \sum_{i=0}^{pN_s-1} \log(\lambda_i)$$

$$\beta_n = N\lambda_n / \sigma_n^2 - 1$$

$$\lambda_n = \lambda_{\phi_i} \lambda_{\tau_j} \quad \forall i = 1 : N_s; j = 1 : p$$

with λ_ϕ and λ_τ being the eigenvalues of \mathbf{R}_ϕ and \mathbf{T}_k respectively. When an adequate probability of false alarm has been defined by selecting a threshold from (7), probability of detection will be given by channel characteristics. Note that P_D in (8) is a function of SNR, K , N_s , and temporal and spatial correlation.

V. EVALUATING FIRST ARRIVAL DETECTABILITY

In order to evaluate the performance of this detector, the first arrived path is supposed to be confined within a temporal window of length L samples before the first significant path available at RAKE receiver. Sampling is supposed to be at chip time. A first arrival component is generated and placed randomly within this window.

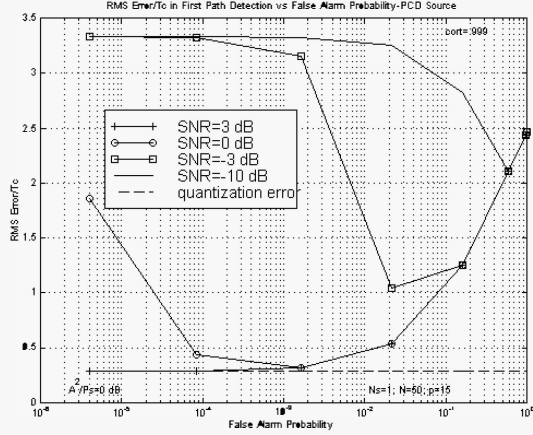


Figure 2: First arrival RMS detection error as a function of P_{FA} and for different SNR. One sensor, and a high temporal correlation.

Path searching process defined by (6) is repeated along the window until alternative H_1 is verified. If a new path is not detected, finger path is chosen as the earliest. L has been set to $5T_c$ for figures shown in this paper. Under the defined channel setup, mean square error is related to false alarm and detection probabilities through equation (9); where $p(n/m)$ corresponds to the probability of detecting an arrival at lag n when arrival is located at lag m , and ε_q is an error term included due to the temporal quantization of the delay axis, as 1 sample per chip:

$$E\{\varepsilon^2\} = \frac{1}{L} \sum_{m=1}^L \sum_{n=1}^L p(n/m) \cdot (m-n)^2 + (1-P_{fa})^{L-1} (1-P_D) \sum_{n=1}^L n^2 + E\{\varepsilon_q^2\} \quad (9)$$

$$p(n/m) = \begin{cases} P_{fa}(1-P_{fa})^{n-1} & n < m \\ P_D(1-P_{fa})^{n-1} & n = m \\ P_{fa}(1-P_{fa})^{n-2}(1-P_D) & n > m \end{cases}$$

$$p(n/m) = p(\hat{\tau}_o = nT_c / \tau_o = mT_c + e_q)$$

$$\varepsilon_q \in [-1/2T_c, 1/2T_c]$$

\mathbf{R}_ϕ has been built using the distributed source model proposed in [7], and for Monte Carlo Simulations 10^5 realization were used to evaluate Detection Probability and 10^6 to evaluate false alarm. For a highly correlated spatial distribution (as it would be the case in the

uplink), the case of correlated sensors an angular spread of 5 degrees and a mean direction of arrival of zero degrees is supposed. Temporal correlation of the scattering was simulated using a first order AR process. Correlation factors of 0.1 and 0.999 are used, accounting for moving and static terminals respectively. Direct path arrives from broadside and sensors are linearly and uniformly spaced. Doppler frequency for direct path corresponds to a mobile speed of 50 km/h, $N=100$ and $p=15$ for figures 2-3 and 6.

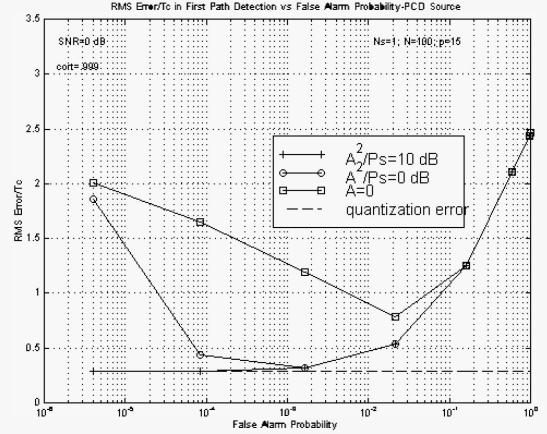


Figure 3: First arrival RMS detection error as a function of P_{FA} and for different powers of the direct path. One sensor, and high temporal correlation.

Figure 2 shows the RMS error in determination of the first arrival for different values of the false alarm probability. Even with just one sensor and a poor SNR of 0 dB (after correlation by the pilot sequence) for the first arrival a good accuracy is achieved when a false alarm around 10^{-3} is chosen. At higher values of SNR the error is not very sensitive to the value of the threshold. Figure 3 shows how detection improves in a highly correlated scenario when a direct path is present, compared to raw scattering.

Figure 6 shows that temporal uncorrelation of the scattering term is a beneficial factor in all cases.

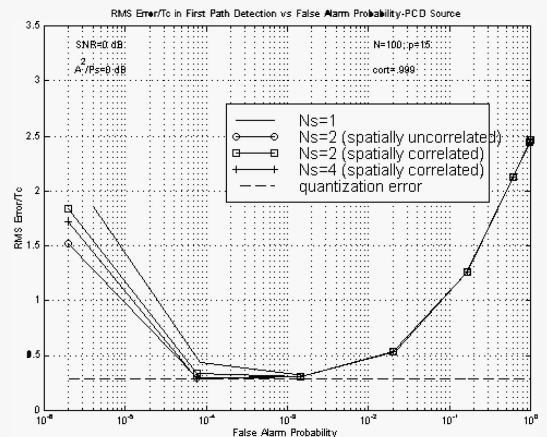


Figure 4: First arrival RMS detection error as a function of P_{FA} and the number of sensors, for spatially correlated and uncorrelated sources.

Increasing the number of sensors or the data record length leads in some cases to important detection gains as it can be seen in figures 4-5, and weaker signals may be detected.

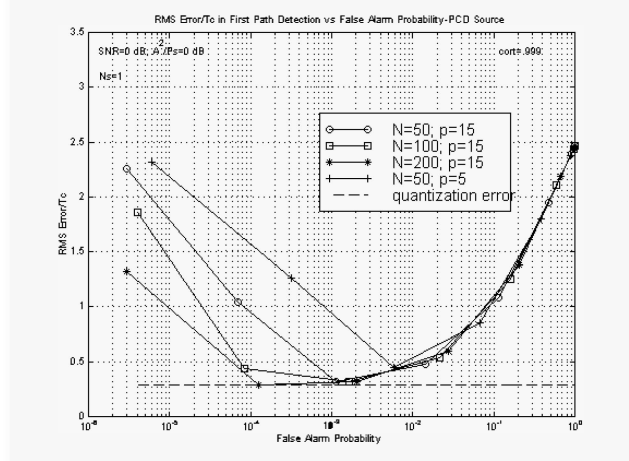


Figure 5: First arrival RMS detection error as a function of P_{FA} and data record length. Different values of the assumed duration of the temporal correlation are used.

VI. SUMMARY AND CONCLUSIONS

A method for improving subscriber location accuracy has been described. A CFAR detector for PCD sources has been derived in (6), and some results have been shown for different environments and detector configurations. It has been shown that given a low SNR and a false alarm probability, by enhancing data records or increasing the number of sensors, better results are observed for temporally uncorrelated sources and uncorrelated sensors.

VII. ACKNOWLEDGEMENTS

This work has been carried out in the framework of the EC-funded project SATURN (www.ist-saturn.org) and supported by Spanish Government Grants: TIC99-0849, TIC2000-1025, FIT-070000-2000-649, Generalitat of Catalunya grant CIRIT 2000SGR 00083 and FUNDACYT- BIDE 874/OC-EC.

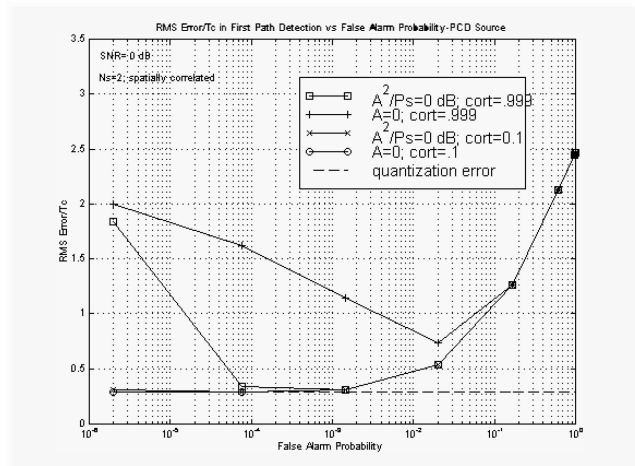


Figure 6: First arrival RMS detection error as a function of P_{FA} and for different temporal correlation values and direct path powers.

REFERENCES

- [1] Josep Vidal, René Játiva and Marga Cabrera, "Positioning Limits for UMTS Mobiles in Delay and Angular Dispersive Channels", International Symposium on Location Based Services for Cellular Users, February 2001.
- [2] René Játiva E, Josep Vidal, and Marga Cabrera, "Cramer Rao Bounds in Time of Arrival Estimation for a Distributed Source", IST Mobile Communication Summit, September 2001.
- [3] Steven M. Kay, "Fundamentals of Statistical Signal Processing - Detection Theory", Prentice-Hall, 1998.
- [4] Yi-Pin Eric Wang, and Tony Ottosson, "Cell Search in W-CDMA", IEEE Journal on Selected Areas in Communications, vol. 18, no 8, August 2000.
- [5] Ernesto Conte, Antonio De Maio, and Giuseppe Ricci, "GLRT-Based Adaptive Algorithms for Range-Spread Targets", IEEE Transactions on Signal Processing, Vol. 49, No. 7, July 2001.
- [6] Sven Fischer, Hans Grubeck, et al, "Time of Arrival Estimation of Narrowband TDMA Signals for Mobile Positioning", PIMRC'98, Sept. 1998, pp. 451-465.
- [7] Raviv Raich, Jason Goldberg, and Hagit Messer, "Bearing Estimation for a Distributed Source: Modeling, Inherent Accuracy Limitations and Algorithms", IEEE Transactions on Signal Processing, Vol. 48, No. 2, February 2000.
- [8] A. Zoch, G. Fettweis, "Cell Search Performance Analysis for W-CDMA", IEEE International Conference on Communications, vol. 2, 2002.
- [9] J. Winter, C. Wengerter, "High Resolution Estimation of the Time of Arrival for GSM Location", VTC2000-Spring Tokyo. 2000, Volume: 2, 2000.

Josep Vidal, Montse Nájjar, René Játiva, “High resolution time-of-arrival detection for wireless positioning systems”, IEEE Vehicular Technology Conference, VTC-2002-Fall, Vol. 4, pp. 2283-2287, 2002. DOI: 10.1109/VETECONF.2002.1040627.

High resolution time-of-arrival detection for wireless positioning systems

Josep Vidal, Montse Najar, René Játiva
Dept. of Signal Theory & Communications
Universitat Politècnica de Catalunya (UPC)
Barcelona, Spain
{pepe,najar,rjativa}@gps.tsc.upc.es

Abstract—It is well known that non-line-of-sight (NLOS) and multipath propagation biases time of arrival (TOA) and Time Difference of Arrival (TDOA) estimates thus reducing accuracy of positioning algorithms. In order to achieve timing error reduction, a high-resolution first arriving path detector from propagation channel estimates is derived based on the minimum variance (MV) estimates and normalized minimum variance (NMV) of the power delay profile. The objective of this paper is to determine the potentialities of this optimal detection scheme within the framework of a realistic wireless positioning system. To this end, the timing measurements obtained are fed to a Kalman tracker which finally determines the position with a high degree of accuracy.

Keywords—Wireless positioning systems, Kalman tracking, OTDOA, High resolution timing estimation, Non line of sight.

I. INTRODUCTION

Accurate estimates of Time of Arrival (TOA) from received wireless communications signals are required for positioning purposes. Two main difficulties appear due to the complicated propagation conditions imposed by the wireless channel: multipath, or delay spread of the channel impulse response, and non-line-of-sight (NLOS) situations, due to transmitted signal blocking. Both situations provoke that the estimation of the first arrival, which bears information related to the position of the mobile terminal, be biased. In particular, due to NLOS, the first arrival suffers stronger attenuation than later arrivals and therefore wrong TOA information is obtained. In the multipath situation (be it LOS or NLOS) the late signal arrivals induce a displacement of the maximum of the impulse response, thus biasing timing estimates, if algorithms which assume a simple frequency-flat channel are used [6]. The resulting positioning systems dealing with those estimates can only provide biased position estimation.

The approach followed in this paper assumes that an estimate of the channel impulse response is available. For the case of Code Division Multiple Access (CDMA) Spread Spectrum Systems such as IS-95 and WCDMA a common pilot channel or dedicated training sequences allow channel estimation [3]. These estimates are used in the RAKE receivers for coherent reception. However, RAKE receivers are based on the capture of the received signal power and thresholds used for path detection are set high enough to match the most powerful ones, which do not necessarily include first arrival path in NLOS situations (see [4] for an

approach based on the maximum power arrival). For this purpose, a lag window before the first RAKE finger component is considered for determining the first arrival.

An important additional assumption is the time persistence of the arrivals. This is taken as much longer than the time coherence of the channel amplitude [12]. In this way, a number of channel estimates can be used to more accurately compute the estimations (see figure 1).

The scheme proposed consists in deriving unbiased estimation of the delay profile of the channel using the MV [7] and NMV [8] approaches. In this way the first, low power estimated arrivals are very robust to multipath. Once an estimate of the first arrival has been determined, a Kalman tracker computes the position and deals with the bias of these estimates caused by the NLOS situation. A reliability parameter computed internally by the Kalman algorithm provides proper weighting among the different timing measurements.

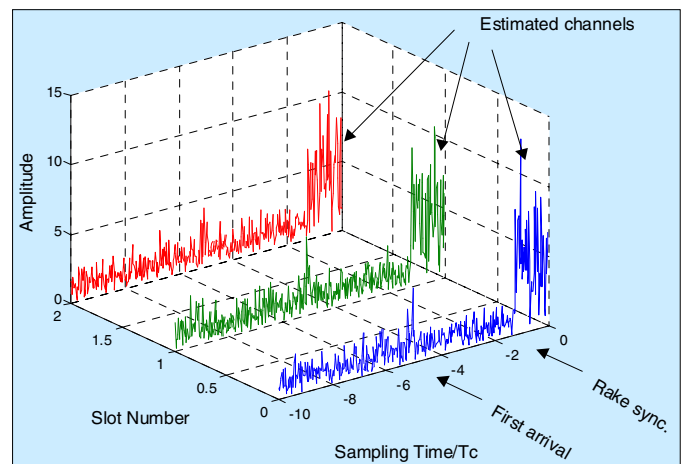


Figure 1. Estimated channel along a lag window over time (different time slots). In a NLOS situation, the first arrival has a power significantly lower than the first RAKE finger, but the position of the arrivals is assumed to have large coherence time.

II. A MODEL FOR THE PROPAGATION CHANNEL

The signal model assumed for the estimated channel, collected over N time instants is as follows:

$$y(\tau; n) = \sum_{i=1}^L a_i(n)g(\tau - \tau_i) + v(\tau; n) \quad n = 1, \dots, N \quad (1)$$

This work has been carried out in the framework of the EC-funded project SATURN (www.ist-saturn.org) and supported by Spanish Government Grants: TIC2000-1025, FIT-070000-2000-649, and Fundacyt- BIDE 874/OC-EC.

in which we are assuming that the parameters are the delays τ_i and time-varying amplitudes $a_i(t)$ of the L propagation paths. $g(\tau)$ is the pulse shape of the modulation. The noise perturbing the estimated channel $v(\tau; n)$ is assumed temporally uncorrelated (in n), and correlated in the lag (τ) domain due to the matched filter performed at the receiver. It is also assumed the availability of N samples of the estimated channel. These multiple copies may be obtained from channel estimates computed at different slots of the common pilot channel signal in the forward link, or the dedicated channel pilot signal in the forward/reverse links, within the time coherence of the channel delays.

A more convenient representation of expression (1) is obtained after computing the DFT on a proper window over the estimated channel [14]:

$$y(\omega; n) = \sum_{i=1}^L a_i(n) g(\omega) e^{j\omega\tau_i} + v(\omega; n) \quad (2)$$

Stacking the samples of the transformed domain in a single vector, (2) may be rewritten as:

$$\begin{aligned} \mathbf{y}(n) &= [y(\omega_0; n) \quad y(\omega_1; n) \quad \cdots \quad y(\omega_{M-1}; n)]^T \\ &= \sum_{i=1}^L a_i(n) \mathbf{G} \mathbf{e}_{\tau_i} + \mathbf{v}(n) = \mathbf{G} \mathbf{E}_{\tau_i} \mathbf{a}(n) + \mathbf{v}(n) \end{aligned} \quad (3)$$

where \mathbf{G} is a diagonal matrix containing the DFT of the pulse shaping filter. As the ML solution of the problem leads to a multidimensional search [9], a plethora of algorithms have appeared in the last 30 years to reduce the complexity to a one-dimensional problem, and yet achieving an asymptotic optimum behavior. Some requirements of these methods are:

1. Previous knowledge of the number of signals (L) to be estimated (e.g. MUSIC [10], ESPRIT [11])
2. SVD decomposition (e.g. MUSIC, ESPRIT)
3. Incoherence of the incoming rays (e.g. MV [7], MUSIC)
4. One-dimensional grid search (e.g. MUSIC, MV)

It should be noticed that although requirement 3 is important, since the number of static UE requiring positioning information will most likely not be negligible, all methods allow the so-called ‘‘spatial smoothing’’ to reduce the problem (except ESPRIT which inherently incorporates it) at the expenses of some reduction in resolution.

With the goal of deriving a simple technique with low implementation requirements, the MV (and its modified version NMV) is selected. It allows also a simple adaptive implementation and options for the use of signals captured at multiple sensors.

III. MINIMUM VARIANCE TIMING ESTIMATION

In the minimum variance solution, the reduction of the complexity is achieved by considering signals separation through filtering. Let us rewrite equation (3) as composed of a single path of interest plus an additional noise term $\mathbf{v}(n)$ accounting for the noise present in the channel estimates plus the non-considered paths:

$$\mathbf{y}(n) = a_j(n) \mathbf{G} \mathbf{e}_{\tau_j} + \mathbf{v}(n) \quad (4)$$

A. Minimum Variance solution

The MV filter is a matched decorrelating filter \mathbf{w} to separate the different paths of the desired signals, whose output is given by:

$$\mathbf{z}(n) = \mathbf{w}^H \mathbf{y}(n) = a_j(n) \mathbf{w}^H \mathbf{G} \mathbf{e}_{\tau_j} + \mathbf{w}^H \mathbf{v}(n) \quad (5)$$

The filter should satisfy $\mathbf{w}^H \mathbf{G} \mathbf{e}_{\tau_j} = 1$. Improved performance is achieved when \mathbf{w} is chosen so as to maximise the output SNR defined as:

$$SNR = \frac{E\{|a_j(n)|^2\}}{\mathbf{w}^H E\{\mathbf{v}(n)\mathbf{v}(n)^H\} \mathbf{w}} \quad (6)$$

Since the numerator does not depend on \mathbf{w} , the maximisation of this expression is equivalent to minimise the output power subject to the constraint. The MV solution for both the filter \mathbf{w} and the spectral representations of the delays is:

$$\mathbf{w}(\tau) = \frac{\mathbf{R}_y^{-1} \mathbf{G} \mathbf{e}_{\tau}}{\mathbf{e}_{\tau}^H \mathbf{G}^H \mathbf{R}_y^{-1} \mathbf{G} \mathbf{e}_{\tau}} \quad P(\tau) = \frac{1}{\mathbf{e}_{\tau}^H \mathbf{G}^H \mathbf{R}_y^{-1} \mathbf{G} \mathbf{e}_{\tau}} \quad (7)$$

Note that one filter is found per delay, though the final power delay spectrum does not include the filter, and therefore it does not have to be computed. Full rank estimates of the correlation matrix may be obtained by ergodic averaging over n , provided that $N \geq L$.

B. Normalised Minimum Variance solution

As equation (5) is giving a measurement of the signal power plus the interfering power, it is a magnitude strongly dependent on the bandwidth of \mathbf{w} , which, on its turn, depends on τ . It can be easily seen that, if $\mathbf{v}(n)$ were merely noise, the output power would be given by:

$$P(\tau) = E\{|a_j(n)|^2\} + \sigma_v^2 \mathbf{w}(\tau)^H \mathbf{G}^H \mathbf{G} \mathbf{w}(\tau) \quad (8)$$

Therefore, a more meaningful measurement allowing equal noise level throughout all values of τ is given by:

$$S(\tau) = \frac{P(\tau)}{\mathbf{w}(\tau)^H \mathbf{G}^H \mathbf{G} \mathbf{w}(\tau)} = \frac{\mathbf{e}_{\tau}^H \mathbf{G}^H \mathbf{R}_y^{-1} \mathbf{G} \mathbf{e}_{\tau}}{\mathbf{e}_{\tau}^H \mathbf{G}^H \mathbf{R}_y^{-1} \mathbf{G}^H \mathbf{G} \mathbf{R}_y^{-1} \mathbf{G} \mathbf{e}_{\tau}} \quad (9)$$

From an spectral estimation point of view, $P(\tau)$ represents the MV power spectrum estimation of a set of cisoids in noise, while $S(\tau)$ is the MV power spectrum density estimation, the later achieving quite better resolution properties [8].

IV. DETECTION OF THE FIRST ARRIVAL ON THE MV/NMV ESTIMATED DELAY SPECTRUM

As it has been stated, a one-dimensional grid search must be done to determine the first arrival, without any prior knowledge of the powers of the different arrivals. This implies a comparison of the maxima of the peaks of functions $P(t)$ or $S(t)$ to a threshold level which should be related to the representation of the floor noise in the spectra. This value can

be computed approximately provided that knowledge of the base band noise power be known, a value usually known at the receiver. This includes not only the interference and thermal noise level, but also the power of the propagation channel taps not being considered in the RAKE receiver. We will neglect this difference in the sequel.

The response of the filter to the noise is given by

$$\mathbf{w}^H E \{ \mathbf{v}(n) \mathbf{v}(n)^H \} \mathbf{w}$$

a term which depends on the multipath structure, on the noise power and on the number of samples per chip considered (implicitly included in matrix \mathbf{G}). An approximate value of this level is given by the response of the estimator to the case when only noise is present

$$\mathbf{R}_y = \sigma_v^2 \mathbf{G} \mathbf{G}^H$$

In turn, the values taken by the MV and NMV estimates are:

$$P(\tau) = \frac{\sigma_v^2}{\mathbf{e}_\tau^H \mathbf{e}_\tau} \quad S(\tau) = \sigma_v^2 \quad (10)$$

Assuming that the size of filter \mathbf{w} is larger than the number of incoming rays, the statistics of both $P(\tau)$ and $S(\tau)$ are asymptotically (large N) chi-squared, so a threshold γ can be chosen for a certain probability of false alarm which is given by the expression:

$$P_{fa} = Q_{\chi^2_{2N}} \left\{ \frac{2N\gamma}{\sigma_v^2} \right\} \quad (11)$$

where $Q_\chi(\cdot)$ defines the right tail cumulative function for a chi-squared distributed variable with $2N$ degrees of freedom, provided that secondary data record used for the determination of σ_v^2 be large enough.

V. COHERENT SCENARIOS

The MV/NMV solutions are not free of the coherence problem of the impinging rays. If all arriving signals exhibit the same Doppler signature, the rank of matrix \mathbf{R}_y is reduced by an amount equal to the number of paths exhibiting the same Doppler minus one. When the subscriber is static, the rank of matrix is reduced to one, regardless of the number of incoming significant delays.

Conventionally, this problem has to be solved by searching another domain which could provide the sufficient diversity, either by using additional sensors (assuming that the rays have linearly independent spatial signatures) or subdividing the frequency manifold (also known as spatial smoothing techniques [13]) at the expense of reducing the resolution.

In the first case the correlation matrix used by the MV/NMV may be computed by averaging the correlation matrices computed at each sensor. In the later case, multiple submanifolds can be built, but in practice a high loss of resolution is observed with respect to the uncoherent case. In the whole, the use of multiple sensors is preferred.

The performance of the MV/NMV solutions is shown in the following experiment.

A realistic scenario has been build according to [15], where 4 base stations give coverage to an area of about 4 Km². Real trajectories recorded with a GPS have been used and overlaid on the area covered by the 4 base stations (figure 2).

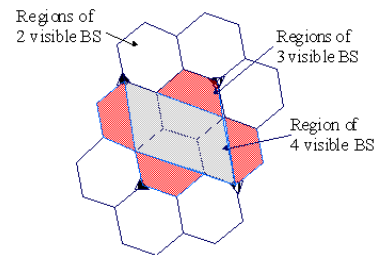


Figure 2. Area covered by 120° sectored base stations.

At every point of the trajectory, realistic values of the SNR, delay spread (exponential shape is assumed for the power delay spectrum), path loss and slow fading [16] are simulated. The values of SNR for the estimated channel in the forward link range from -5 dB (far from the BS) to 25 dB (in the vicinity of a BS). A threshold has been set on the values of the slow fading to determine the points on which NLOS is observed. It is assumed that the slow fading is nearly uncorrelated after 40λ . In this situation, For those points, a bias equal to the delay spread multiplied by a random uniform value has been added to the TOA measure generated through the MV/NMV. Values for different parameters corresponding to the common pilot channel are displayed in table 1.

TABLE I. PILOT CHANNEL PARAMETERS IN THE FORWARD LINK

SC _{PICH}	Total tx. power	Propagation constant	N ₀	Pilot length
33 dBm	41.6 dBm	3.5	-103 dBm	2 slots

In Figure 3, the car trajectory considered for the simulations in the coverage area of the 4 Base Stations is represented. The lower plot shows the two components of the speed vector at each trajectory point.

Figure 4 shows the estimated values of the TOA when the reception is done with two sensors, for the MV and NMV detected first arrivals corresponding to two base stations. Note that all the estimates have positive (or zero) errors with respect to the true delay values (the baseline of each curve). From the results it is apparent that MV solution gives in general better performance. In those trajectory points where the speed is low, MV seems to be more robust to channel temporal coherence, while NMV gives lower variance estimates in high speed zones. In the whole, results seem to be more favourable to MV method. Compared to figure 5, where the same delay values have been computed using a single sensor, significant gains are observed in estimation accuracy.

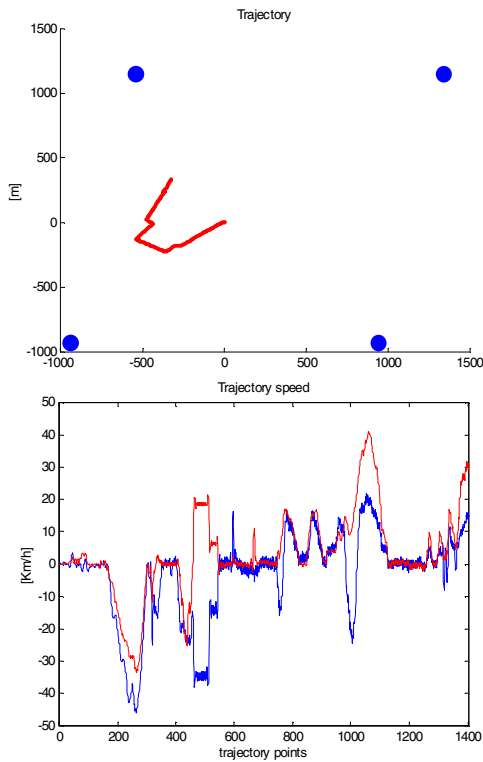


Figure 3. Real trajectory and two dimensional speed.

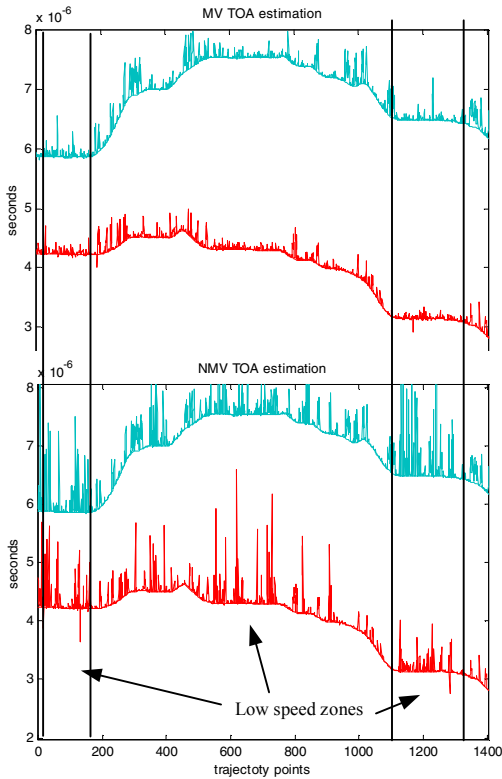


Figure 4. Timing estimation of the first arrival for the MV and NMV methods, in the forward link for pilot channels coming from two different base stations. Two uncorrelated sensors are used at the mobile terminal. MV performs better in the whole. Larger errors are observed when the subscriber is static due to the coherence problem. MV seems to be more robust to this situation.

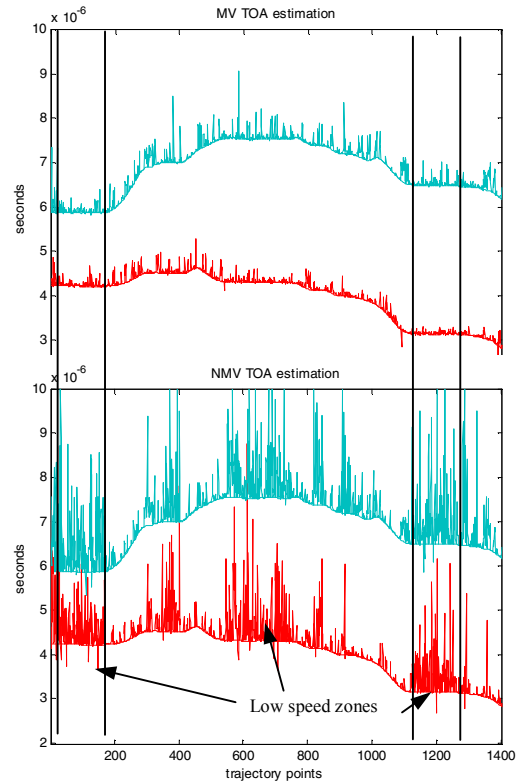


Figure 5. Same plot as in figure 4 for one single sensor used at the mobile terminal. Errors are larger than the observed in figure 3 with two uncorrelated sensors. MV seems to be more robust to this situation.

VI. APPLICATION TO MOBILE POSITIONING

The methods proposed have been used to provide measurements to a positioning TDOA system based on Kalman tracking [17]. The position errors obtained are shown in Figure 6 and compared with the position error obtained using the TOA estimated by the Early-Late method (mainly based on the maximum of the impulse response). It can be observed the improvement in location accuracy achieved by using the MV and NMV proposed TOA estimation methods. These seem to be good approaches for bias reduction due to multipath.

On the other hand, bias in TOA is also due to the NLOS situation, which cannot be completely spotted by a high-resolution method if the direct arrival has very low power or is not observable at all. In this case, the following strategy is chosen within the Kalman algorithm: the variance of the measurement noise is changed according to the differences between the TOA measurement and the forecast measurement computed from the forecast position. In Figure 7, a significant reduction of the position error is observed, being negligible the increase of the computational cost. Finally, in Figure 8, it can be observed the robustness of the Kalman tracker to the coherence measurement problems. Comparing the position error obtained with one or two uncorrelated sensors in the mobile unit, it can be concluded that the behavior is similar although the obtained TOA measurements are slightly more

accurate with two uncorrelated sensors than in the single sensor case.

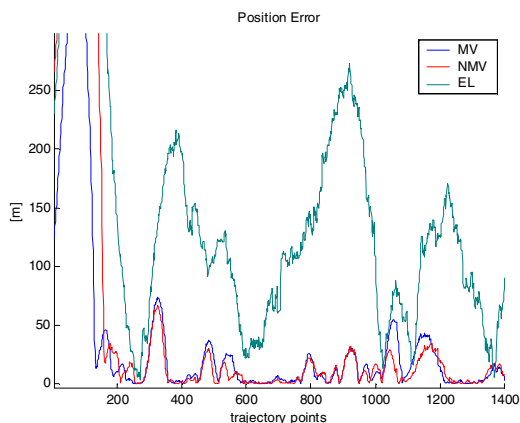


Figure 6. Position error obtained with Kalman tracking using the TOA estimated with the proposed techniques (MV and NMV) and with the Early-Late method.

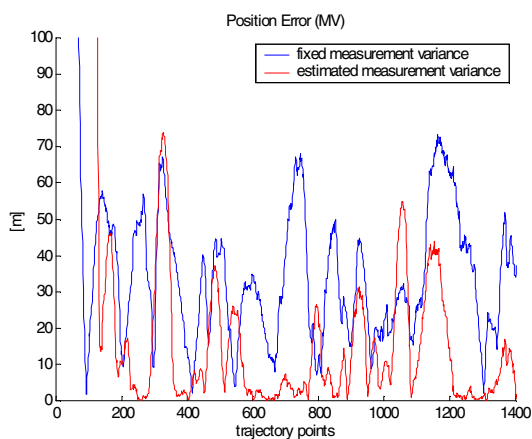


Figure 7. Position error using the error measurement at each trajectory point computed internally by the Kalman tracking and comparison with the error obtained assuming a fixed measurement noise covariance.

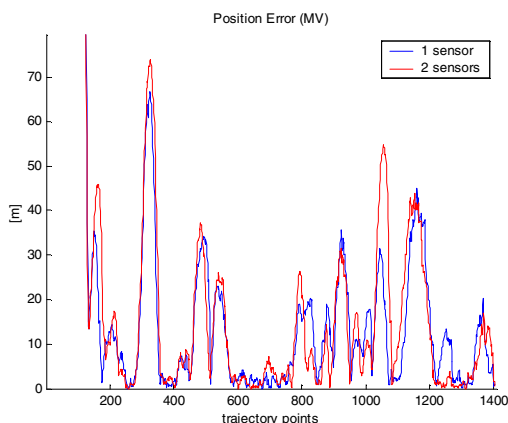


Figure 8. Comparison of the position error using one or two uncorrelated sensors at the mobile terminal.

VII. CONCLUSIONS

We have tackled the problem of mobile positioning in multipath and NLOS situations. According to the results, important improvements in the TOA estimation accuracy are obtained using (low cost) MV methods instead of the Early-Late estimator for multipath bias mitigation. To mitigate the NLOS situation, the estimation of the measurement variance can be efficacely computed internally by the Kalman algorithm yielding significantly better performance of the tracking position. Final errors demonstrate that positioning accuracy may well be improved through this combined approach.

REFERENCES

- [1] Josep Vidal et al, "Positioning Limits for UMTS Mobiles in Delay and Angular Dispersive Channels", *International Symposium on Location Based Services for Cellular Users (LOCELLUS)*, Munich, February 2001.
- [2] René Játiva et al, "Cramer Rao Bounds in Time of Arrival Estimation for a Distributed Source", *IST Mobile Communication Summit*, Sitges, Spain, September 2001.
- [3] Yi-Pin Eric Wang, and Tony Ottosson, "Cell Search in W-CDMA", *IEEE Journal on Selected Areas in Communications*, August 2000.
- [4] Sven Fischer, Hans Grubeck, et al, "Time of Arrival Estimation of Narrowband TDMA Signals for Mobile Positioning", *Personal, Indoor and Mobile Radio Communications*, PIMRC 1998.
- [5] Raviv Raich et al, "Bearing Estimation for a Distributed Source", *IEEE Transactions on Signal Processing*, Vol. 48, February 2000.
- [6] J. Soubielle, I. Fijalkow, P. Duvaut, "GPS Positioning in a Multipath Environment", *IEEE Trans. Signal Processing*, vol. 50, no. 1, January 2002.
- [7] J. Capon, "High resolution frequency-wavenumber spectrum analysis", *Proc. Of the IEEE*, vol. 57, August 1969, pp. 1408-1418.
- [8] M. A. Lagunas, A. Gasull, "An Improved Maximum Likelihood Method for Power Spectral Density Estimation", *IEEE Trans ASSP*, vol 32, Feb 1984, pp. 170-172.
- [9] A. L. Swindlehurst, "Time Delay and Spatial Signature Estimation Using Known Asynchronous Signals", *IEEE Trans. Signal Processing*, vol. 46, No. 2, Feb 1998.
- [10] R. O. Schmidt, "A Signal Subspace Approach to Multiple Emitter Location and Spectral Estimation", *Ph. D. dissertation*, Stanford University, Stanford, CA, Nov. 1981.
- [11] A. Paulraj, R. Roy, T. Kailath, "A Subspace Rotation Approach to Signal Parameter Estimation", *Proc. IEEE*, pp. 1044-1045, July 1986.
- [12] M. Cabrera, J. Vidal, O. Muñoz, "Time Evolutionary Wideband Propagation Channel Model for User Positioning in UMTS", *VTC Fall 2001*, 7-11 Oct. 2001, Atlantic City, USA
- [13] S. U. Pillai, B. H. Kwon, "Forward/Backward Spatial Smoothing Techniques for Coherent Signal Identification", *IEEE Trans on ASSP*, vol. 37, no. 1, pp. 8-15, Jan 1989.
- [14] J. Vidal, R. Játiva, "First Arriving Path Detection for Subscriber Location in Mobile Communication Systems", *Proc. ICASSP 2002*, 13-16 May 2002, Orlando, USA.
- [15] J. Vidal et al. *Location Based Services Performance Evaluation (Location techniques)*, Deliverable 621, IST-1999-10322 SATURN, www.ist-saturn.org.
- [16] L. Greenstein et al., "A New Path-Gain/Delay-Spread Propagation Model for Digital Cellular Channels", *IEEE Trans. Veh. Technol.*, vol. 46, no. 2, May 1997.
- [17] M. Nájár, J. Vidal, A. Kjellström, "Kalman Tracking for UMTS Mobile Location", *IST Mobile Communication Summit*, Sitges, Spain, September 2001.

René Játiva, E. Garzón and J. Vidal, “Space-Time Diversity for NLOS Mitigation in TDOA-Based Positioning Systems”, IEEE International Engineering Summit, II Cumbre Internacional de las Ingenierías, March 2016. DOI: 10.1109/IESummit.2016.7459771.

ATTENTION!

Pages 321 to 326 of the thesis are available at the editor’s web
<http://ieeexplore.ieee.org/document/7459771/>

René Játiva E., Diego Ortiz, Pablo Venegas and Josep Vidal, “Selection of the reference anchor node by using SNR in TDOA-based positioning”, IEEE Ecuador Technical Chapters Meeting (ETCM 2016), October 2016.

ATTENTION!

Pages 328 to 332 of the thesis are available at the editor’s web

<http://ieeexplore.ieee.org/document/7750813/>

Esteban Garzón, Santiago Valdiviezo, René Játiva E. and Josep Vidal, “Fast Computation of Cramer-Rao Bounds for TOA – An application to network-based positioning simulations”, Latin American Conference on Computational Intelligence, November 2016.

ATTENTION!

Pages 334 to 339 of the thesis are available at the editor’s web

<http://ieeexplore.ieee.org/document/7885716/>